PAGE REPLACEMENT GUIDE FOR

AMENDMENT 56

CLINCH RIVER BREEDER REACTOR PLANT

PRELIMINARY SAFETY ANALYSIS REPORT

(DOCKET NO. 50-537)

Transmitted herein is Amendment 56 to the Clinch River Breeder Reactor Plant Preliminary Safety Analysis Report, Docket 50-537. Amendment 56 consists of new and replacement pages for the PSAR text.

Vertical lines on the right hand side of the page are used to identify question response information and lines on the left hand side are used to identify new or changed design information.

The following attached sheets list Amendment 56 pages and instructions for their incorporation into the Preliminary Safety Analysis Report.

AMENDMENT 56

PAGE REPLACEMENT GUIDE

REMOVE THESE PAGES		INSERT THESE PAGES
	Chapter 1	
1.1-15, 16		1.1-15, 16
1.2-7, 8		1.2-7, 8
1.2-16 thru 103		1.2-16 thru 104
1.3-11, 12		1.3-11, 12
	Chapter 2	
2.4-49, 49a		2.4-49, 49a
	Chapter 3	
3.1-57, 58		3.1-57, 58
-		3.2-9a
3.2-16, 17		3.2-16, 17
3.7-15, 15a, 16		3.7-15, 16
3A.1-9a, 9b		3A.1-9a, 9b
3A.4-5, 4-6		3A.4-5, 4-6
	Chapter 4	
4.2-60, 61		4.2-60, 61
4.2-76, 77		4.2-76, 77
4.2-242, 243		4.2-242, 243
4.2-518, 519		4.2-518, 519
4.3-15, 16		4.3-15, 16
4.3-35, 36		4.3-35, 36
4.3-39 thru 50		4.3-39 thru 50
4.3-53 thru 56		4.3-53 thru 56
4.3-59, 60		4.3-59, 60
4.3-63, 64		4.3-63, 64
4.3-67 thru 88		4.3-67 thru 88
4.3-94, 95		4.3-94, 95
4.3-106, 107		4.3-106, 107
4.3-110 thru 119		4.3-110 thru 119
4.3-122 thru 125		4.3-122 thru 125
4.3-128 thru 131		4.3-128 thru 131
4.3-144, 145		4.3-144, 145

REMOVE THESE PAGES	INSERT THESE PAGES
Chapter 4 (Cont'd.)	
4.3-148, 149	4.3-148, 149
4.3-174, 175	4.3-174, 175
4.3-178, 179	4.3-178, 179
4.3-202, 203	4.3-202, 203
4.4-31, 32	4.4-31, 32
4.4-39, 40	4.4-39, 40
4.4-81 thru 86	4.4-81 thru 86
4.4-91 thru 94	4.4-91 thru 94
4.4-119, 120	4.4-119, 120
4.4-135, 136	4.4-135, 136
4.4-153, 154	4.4-153, 154
Chapter 5	
5-xv thru xviii	5-xv thru xviii
5-xix, xixa	5-xix, xixa
5-xxi, xxia, xxib	5-xxi, xxia, xxib
5.1-12, 13	5.1-12, 13
5.2-1, 1a	5.2-1, 1a
5.2-4a, 4b	5.2-4a, 4b
5.2-6, 6b	5.2-6, 6a
5.2-14, 14a	5.2-14, 14a
5.3-9, 10	5.3-9, 10
5.3-28, 28a	5.3-28, 28a
5.3-30, 31	5.3-30, 31
5.3-39b, 39c	5.3-39b, 39c
5.3-71, 71a	5.3-71, 71a
5.3-74a, 74b	5.3-74a, 74b
5.3-75, 75a, 75b, 75c	5.3-75, 75a, 75b, 75c
5.3-88 thru 94	5.3-88, 89
5.3-98 thru 109	5.3-98 thru 109
5.3-123 thru 133	5.3-123
5.3-136 thru 141	5.3-136 thru 141
5.4-10, 11	5.4-10, 11
Chapter 7	
7.5-18a, 18b, 19, 19a, 20 thru 25	7.5-18a, 18b, 19, 19a, 20 thru 25
7.5-40, 41	7.5-40, 41
7.5-45, 46	7.5-45, 46
Chapter 9	
9.8-14, 15, 16	9.8-14, 15, 16
9.13-47, 48	9.13-47, 48

REMOVE THESE PAGES		INSERT THESE PAGES
	Chapter 15	
15.3-50, 51		15.3-50, 51
15.6-41, 42		15.6-41, 42
	Chapter 17	
17E-33, 34		17E-33, 34
17J-3, 4		17J-3, 4
17J-38, 39		17J-38, 39

AMENDMENT 56

QUESTION/RESPONSE SUPPLEMENT

This Question/Response Supplement contains an Amendment 56 tab sheet to be inserted following the Q-i (Amendment 55, June 1980) page. Page Q-i (Amendment 56, August 1980) is to follow the Amendment 56 tab.

There are no new or updated Question/Response pages included in this Amendment.

	No.	Title	Rev.	Discussed Further in PSAR Section(s)
56 56	1.38	Quality Assurance Requirements for Packaging, Shipping, Receiving, Storage & Handling of Items for Water-Cooled Nuclear Power Plants (5/77)	2	17.1, Question 411.2
	1.39	Housekeeping Requirements for Water-Cooled Nuclear Power Plants (3/16/73)	-	17.1, Question 411.2
	1.40	Qualification Tests of Continuous-Duty Motors Installed Inside the Containment of Water-Cooled Nuclear Power Plants (3/16/73)	0	7.1.2 (Tables 7.1-2 and 7.1-3) 8.3
	1.41	Preoperational Testing of Redundant On-Site Electric Power Systems to Verify Proper Load Group Assignments (3/16/73)	0	8.3
	1.42	Interim Licensing Policy and As Low As Practicable for Gaseous Radio-iodine Releases from Light-Water-Cooled Nuclear Power Reactors (6/73)	-	This Guide has been withdrawn by the NRC.
	1.43	Control of Stainless Steel Weld Cladding of Low-Alloy Steel Components (5/73)	0	Note 3
	1.44	Control of the Use of Sensitized Stainless Steel (5/73)	-	NA
	1.45	Reactor Coolant Pressure Boundary Leakage Detection System (5/73)	-	NA
	1.46	Protection Against Pipe Whip Inside Containment (5/73)	-	NA
44	1.47	Bypassed and Inoperable Status Indication for Nuclear Power Plant Safety Systems (5/73)	0	7.1.2.9

TABLE I (Continued)

No.	Title	Rev.	Discussed Further in PSAR Section(s)
1.48	Design Limits and Loading Combinations for Seismic Category I Fluid System Components (5/73)	0	3.9.1.5
1.49	Power Levels of Nuclear Power Plants	1	Due to the Power Levels of CRBRP, this Guide has no impact.
1.50	Control of Preheat Temperature for Welding of Low-Alloy Steel (5/73)	0	Note 4
1.51	Inservice Inspection of ASME Code Class 2 and 3 Nuclear Power Plant Components (5/73)	-	This Guide has been withdrawn by the NRC.

44

25

the secondary shutdown system is arranged using a general coincidence logic. These logics are described in Section 7.2.1. Primary and secondary systems are electrically and mechanically isolated. Sufficient redundancy is included within each system to assure that single random failures will not degrade protection by either system.

1.2.7 Auxiliary Systems

The Auxiliary Liquid Metal System provides the facilities for receipt, storage and purification of all liquid metal used in the CRBRP. It also provides the capability for controlling reactor sodium level variations, accommodates primary sodium volumetric changes, provides cooling for the core components stored in the Ex-Vessel Storage Tank (EVST),and by means of the Direct Heat Removal Service (DHRS) gives a means of long term reactor decay heat removal that is independent of the
26 intermediate heat transport system and steam generator system loops.

The Compressed Gas System processes ambient air to provide compressed dry air for pneumatic instruments, maintenance systems, unloading devices, tooling, and miscellaneous cleaning and inspection services. This system provides for sodium removal systems and as required for plant usage.

The Recirculating Gas Cooling System provides cooling service to cells and equipment located in the Reactor Containment Building and the Reactor Service Building.

15 The Chilled Water Systems provide heat removal capability from certain equipment and areas in the Reactor Containment Building and the Reactor Service Building.

The Inert Gas Receiving and Processing System (IGRPS) provides inert gases as required by other systems of the CRBRP, including cover gas, cell inerting atmosphere, valve actuation gas in inerted cells, cooling gas, gas for certain seals, gas for fire-control blanketing, for component cleaning and other services, and vacuum for out-gassing and gas-collection purposes. In addition, the IGRP System provides for the control of reactor cover gas radioactivity and for the processing of gases to be released from the system to remove their contained radioactivity.

The Impurity Monitoring and Analysis System provides for the sampling, monitoring, and analysis of the sodium, NaK, and argon cover gas systems in the plant, and acceptance sampling and analysis of incoming
56 sodium, NaK, argon, and nitrogen.

The Treated Water System includes the domestic (potable) water system, the closed cooling water system, water (makeup) treatment system and the cooling water makeup system.

The River Water Service System handles and treats river water for the plant. The system includes the river water pumps and piping, intake filtration equipment and the plant service water system.

The Heat Rejection System provides the heat sink using the main
cooling tower for waste heat loads from the turbine condensers, and from the
various plant auxiliary and service systems such as sodium pump oil coolers,
air conditions, air compressors, pump coolers and the turbine oil coolers.
41 44 The Emergency Plant Service Water System emergency cooling tower structure pro-
vides the heat sink for the safety related components listed in Table 9.9-3. De-
33 tails of the auxiliary system are given in Chapter 9.

1.2.8 Refueling System

The reactor core is designed to be refueled annually. Under
equilibrium conditions, all fuel and inner blanket assemblies are replaced
as a batch every two years, with a planned mid-term interchange of 6 inner
41 blanket assemblies for 6 fresh fuel assemblies designed to add sufficient
20 excess reactivity to the system to complete the (550 fpd) burnup. The
radial blanket assemblies in the first and second rows are replaced as a
batch at 4 and 5 year intervals, respectively. No fuel or blanket
51 44 shuffling is planned.

The In-Vessel Handling Subsystem (IVHS) provides for the transfer of
44 core assemblies in the reactor vessel, between their normal positions in the
41 reactor core and storage positions outside the core accessible by the Ex-
vessel Transfer Machine. The major equipment comprising the IVHS are the In-
Vessel Transfer Machine (IVTM), Auxiliary Handling Machine (AHM), AHM Floor
Valves (FV), IVTM Port Adaptors, and associated maintenance and storage facili-
ties and equipment. The IVTM is installed in the small rotating plug in the
reactor head after reactor shutdown. The machine raises or lowers core
44 assemblies by means of a grapple. Translation to a new position is by rota-
41 tion of the reactor head rotatable plugs. The AHM is used to install and re-
44 move the control rod drivelines, port plugs, and in-vessel section of the IVTM
in the reactor. The port adaptors and floor valves provide a means for closure
of the reactor and storage ports during the time the port plugs are removed for
refueling operations.

The Ex-Vessel Handling Subsystem (EVHS) provides for the transfer
of core assemblies between the reactor, the Ex-Vessel Storage Tank (EVST),
41 44 and the Fuel Handling Cell (FHC) located in the Reactor Service Building (RSB). The
system consists of the Ex-Vessel Transfer Machine (EVTM) mounted on a Gantry-
44 Trolley (G-T), EVTM Floor Valves (FV), Core Component Pots (CCP), port plugs
and adaptors, and associated maintenance and storage equipment and facilities.

The Ex-Vessel Storage Subsystem (EVSS) consists of the Ex-Vessel
Storage Tank (EVST), and the associated maintenance equipment. The EVST is a
44 sodium-filled tank used to store and cool spent fuel prior to shipment off-
site, and preheat new core assemblies. The capacity of the EVST is about 650
41 assemblies.

44

41

20

Amend. 51

Sept. 1979

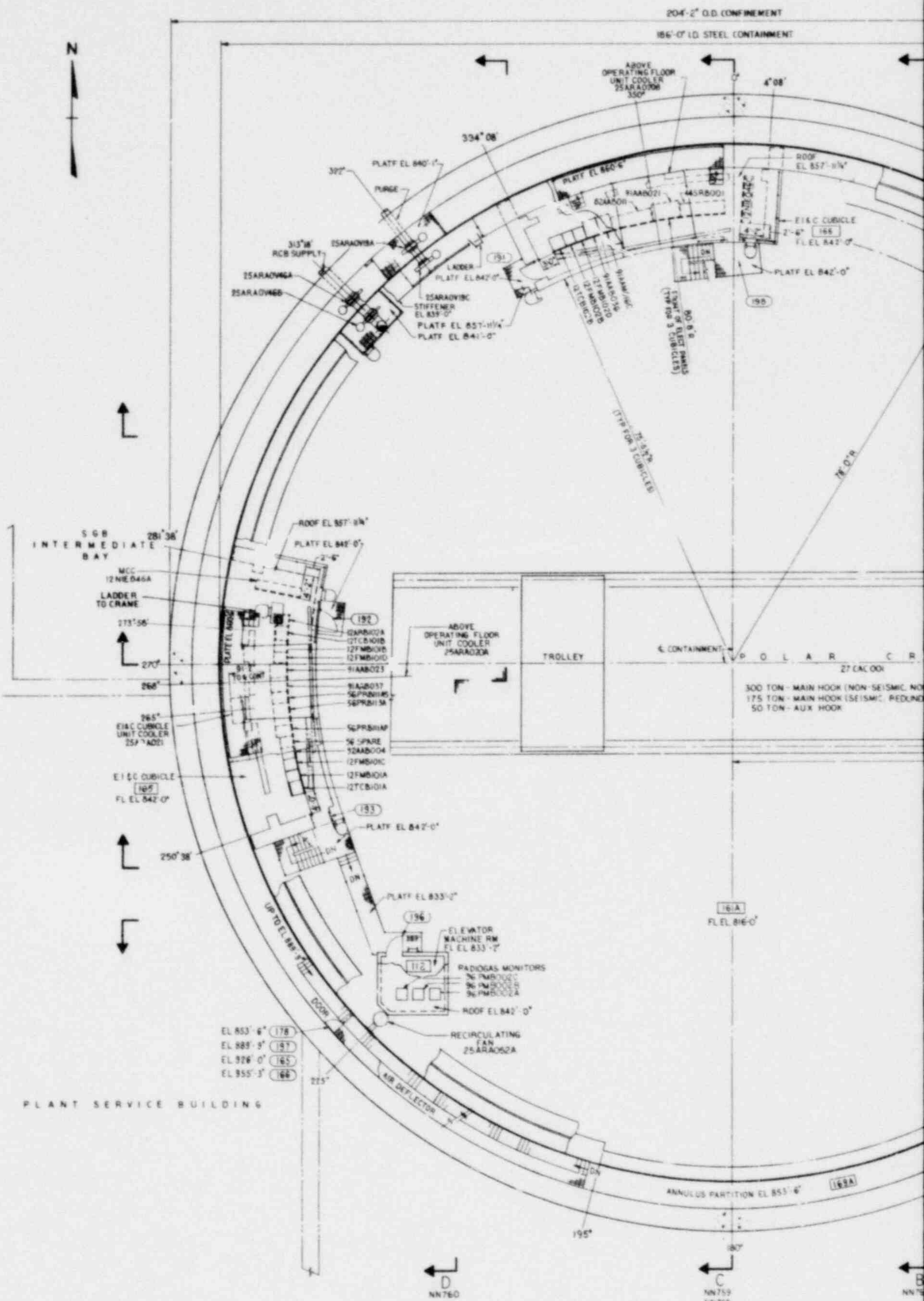

PLAN ABOVE EL. 842'-0"

NN750-12

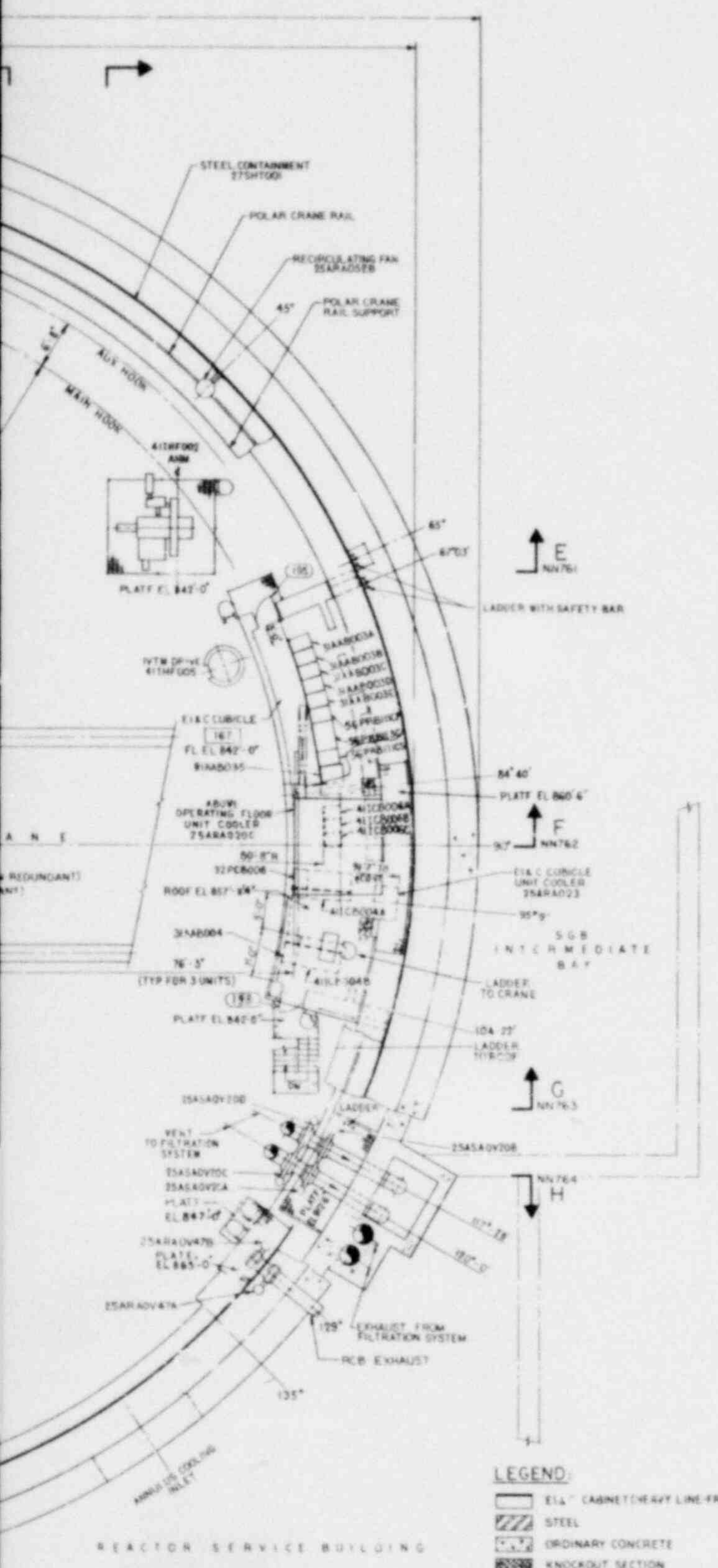

GENERAL NOTES

1. FOR RADIATION ZONING, SEE "DESIGN RADIATION DOSE RATES"

REFERENCE DRAWINGS

NN751	RCB - GEN. ARRGT - PLAN ABOVE EL 816'-0"
NN752	EL 794'-0"
NN753	EL 780'-0"
NN754	EL 766'-0"
NN755	EL 752'-8"
NN756	EL 733'-0"
NN757	SECTION A-A & A1-A1
NN758	B-B & B1-B1
NN759	C-C
NN760	D-D & D1-D1
NN761	E-E
NN762	F-F
NN763	G-G
NN764	H-H
NN765	OF DOME ABOVE EL 899'-0"

GRAPHIC SCALE

0 4 8 12 16 20 24

LEGEND:

- E & C CABINET (HEAVY LINE-FRONT)
- STEEL
- ORDINARY CONCRETE
- KNOCKOUT SECTION
- REMOVABLE CONCRETE NEUTRON SHIELDING
- CHECKERED PLATE
- GRATING
- 131 CELL NUMBER
- TBD TO BE DETERMINED
- 196 DOOR NUMBER
- SLAB BLOCK REMOVABLE PANEL SHIELD DOORS

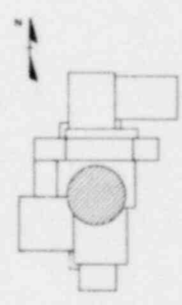

KEY PLAN

Figure 1.2-5
General Arrangement
Reactor Containment Building
Plan El. 842'-0"

Amend. 56
Aug. 1980

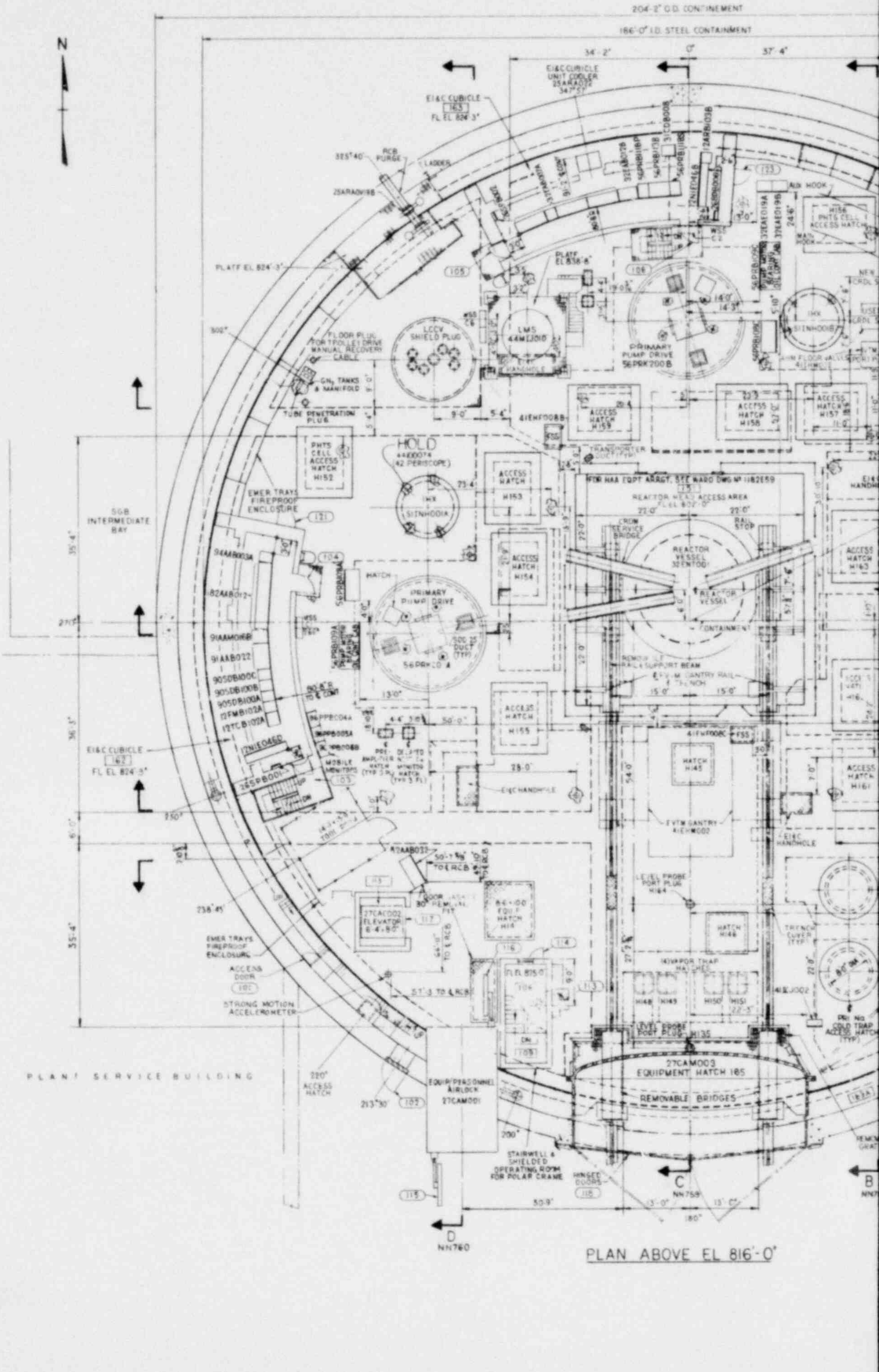

PLAN ABOVE EL 816'-0"

NN751-14

GENERAL NOTES

1. FOR GENERAL NOTES & LEGEND, SEE DWG NN750

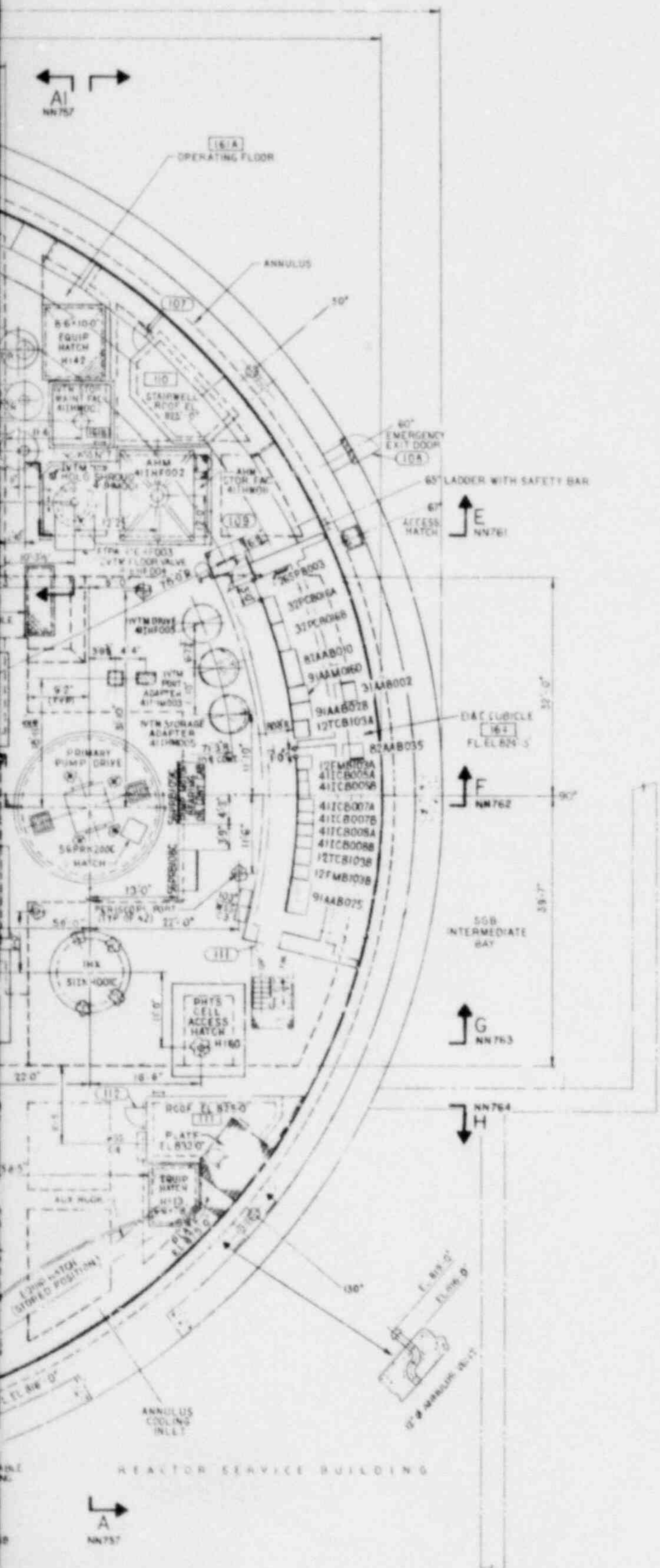

REFERENCE DRAWINGS

1. SEE REFERENCE DWGS. - DWG. NN750

GRAPHIC SCALE

0 4' 8' 12' 16' 20' 24'

1/8" = 1'-0"

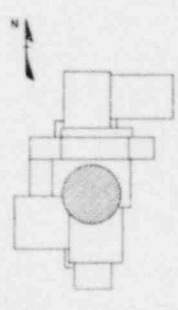

KEY PLAN

Figure 1.2-6
General Arrangement
Reactor Containment Building
Plan El. 816'-0"

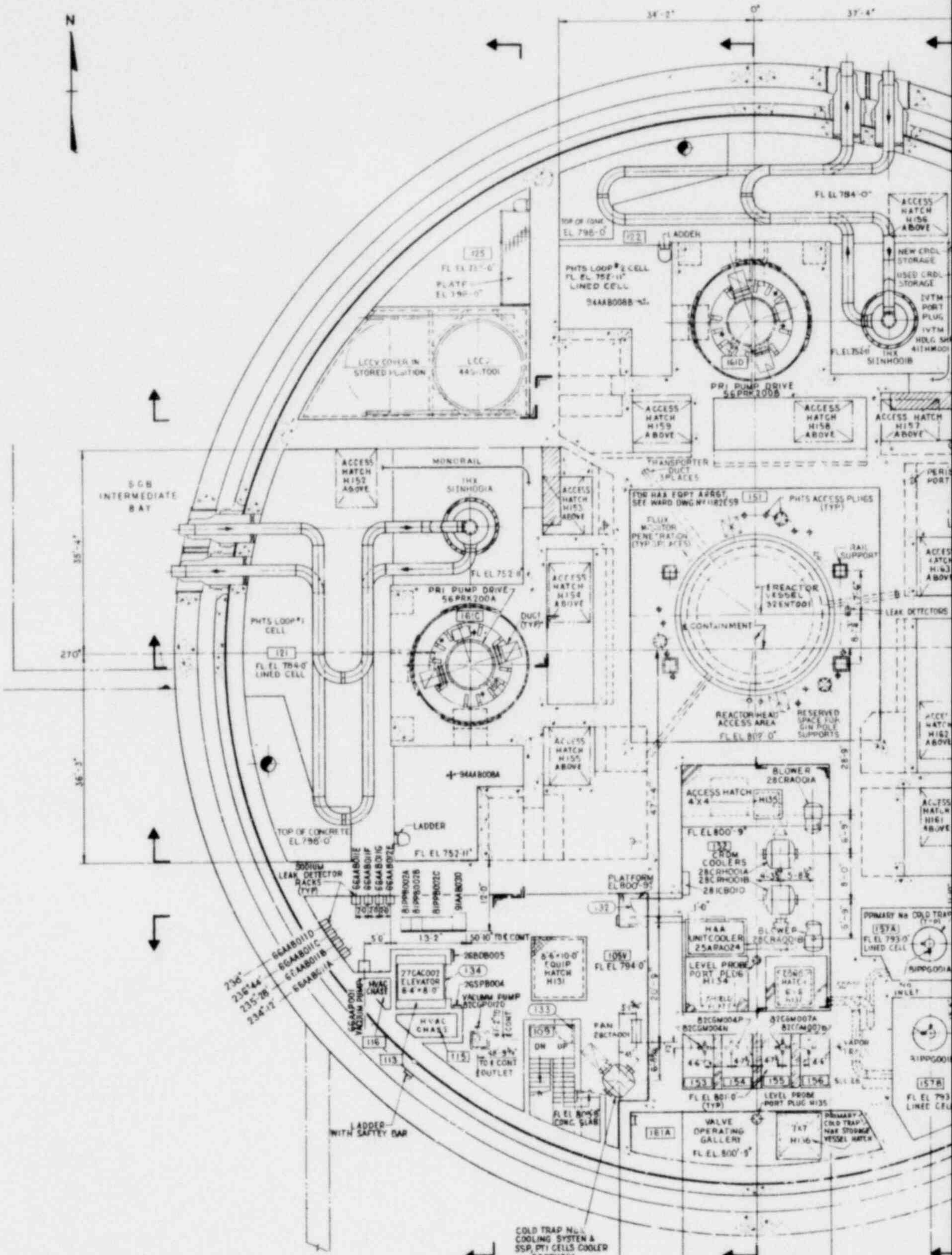

PLAN ABOVE EL. 794'-0"

GENERAL NOTES

1. FOR GENERAL NOTES & LEGEND, SEE DWG NN750

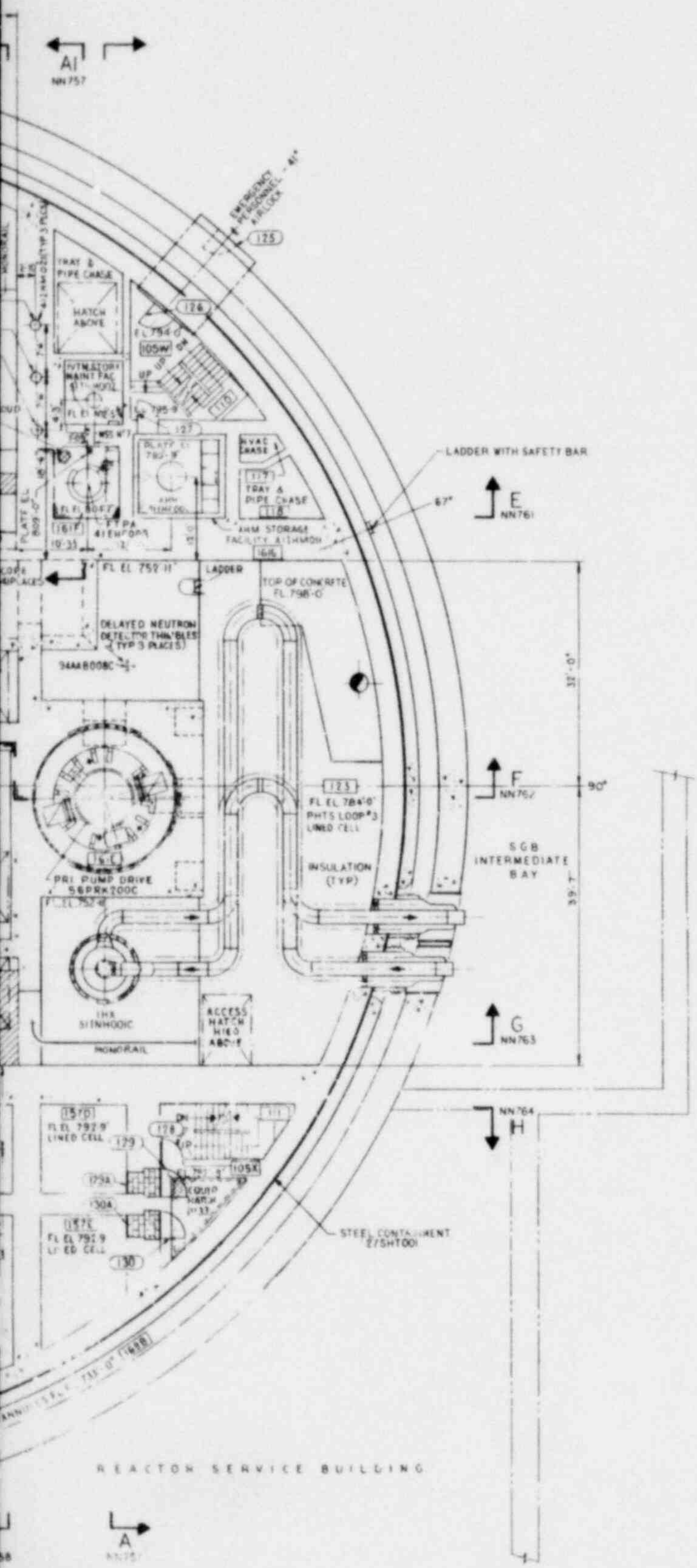

REFERENCE DRAWINGS

1. SEE REFERENCE DWGS.- DWG. NN750

GRAPHIC SCALE

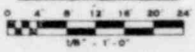

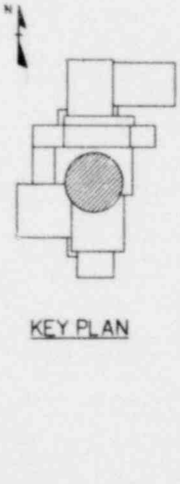

KEY PLAN

Figure 1.2-7
General Arrangement
Reactor Containment Building
Plan El. 794'-0"

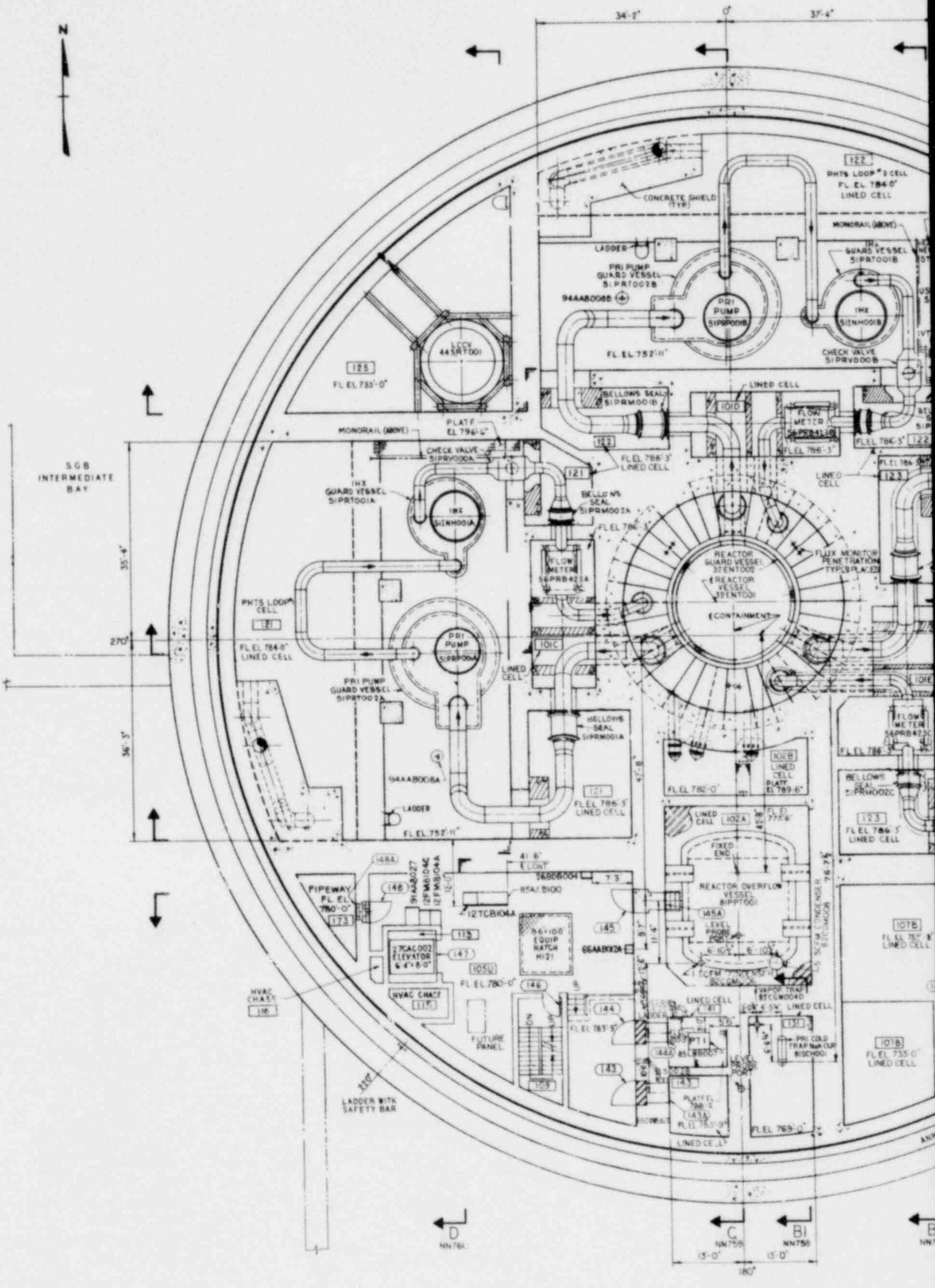

PLAN ABOVE EL. 780'-0"

NN753-14

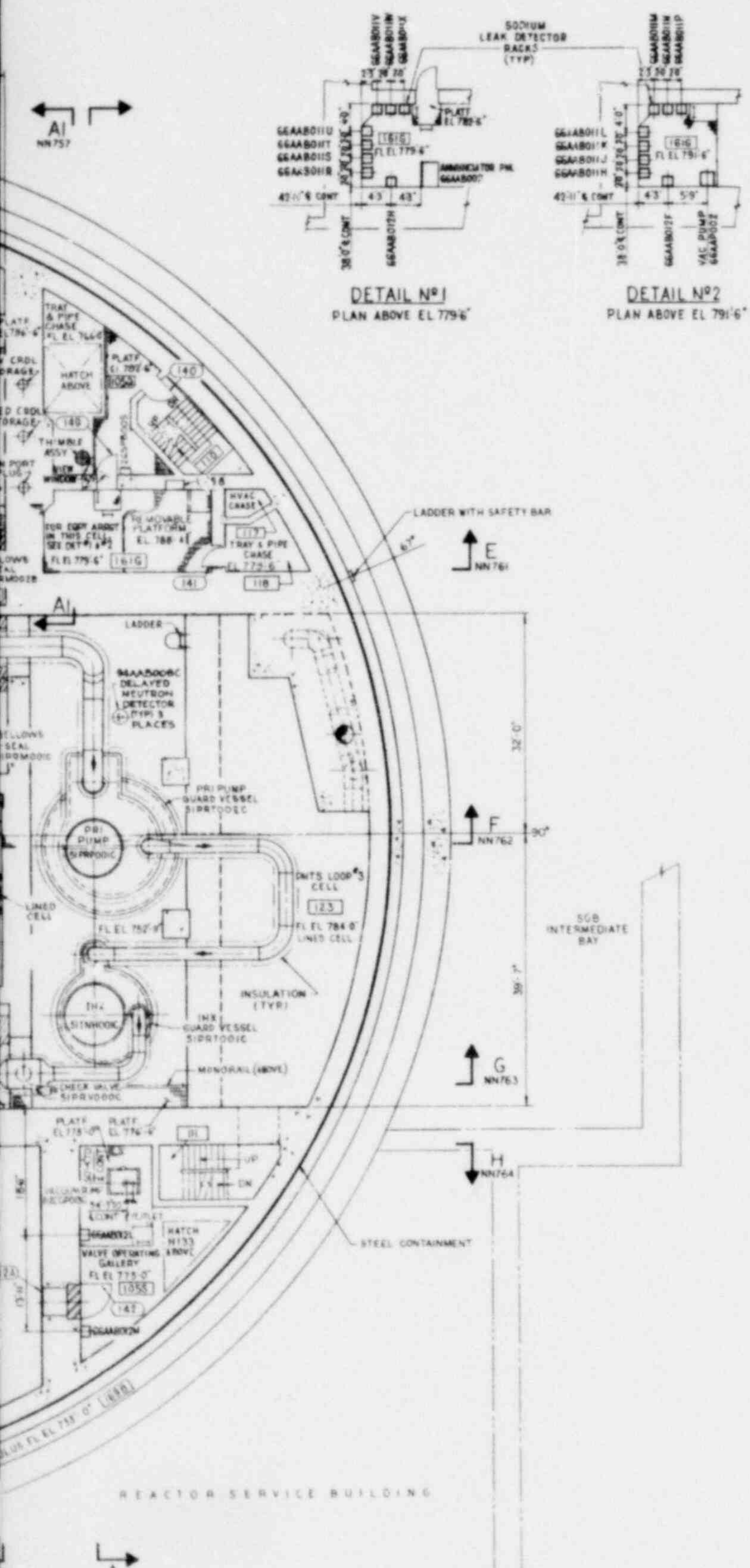

GENERAL NOTES

1. FOR GENERAL NOTES & LEGEND, SEE DWG NN750

REFERENCE DRAWINGS

1. SEE REFERENCE DWGS - DWG NN750

GRAPHIC SCALE

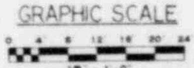

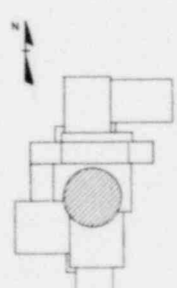

KEY PLAN

Figure 1.2-8
General Arrangement
Reactor Containment Building
Plan El. 780'-0"

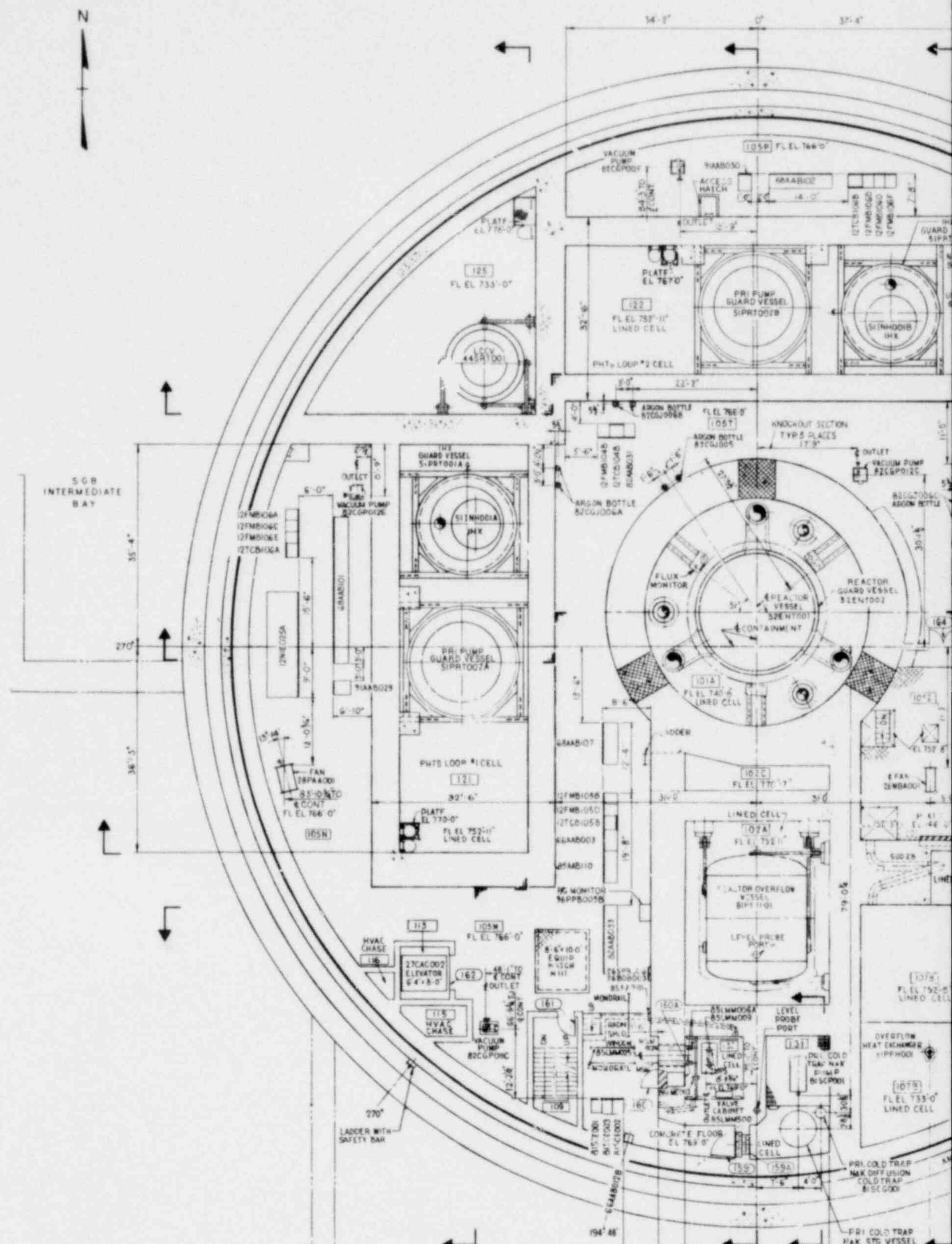

PLAN ABOVE EL. 766'-0"

NN754-14

GENERAL NOTES

1. FOR GENERAL NOTES & LEGEND SEE DWG NN750

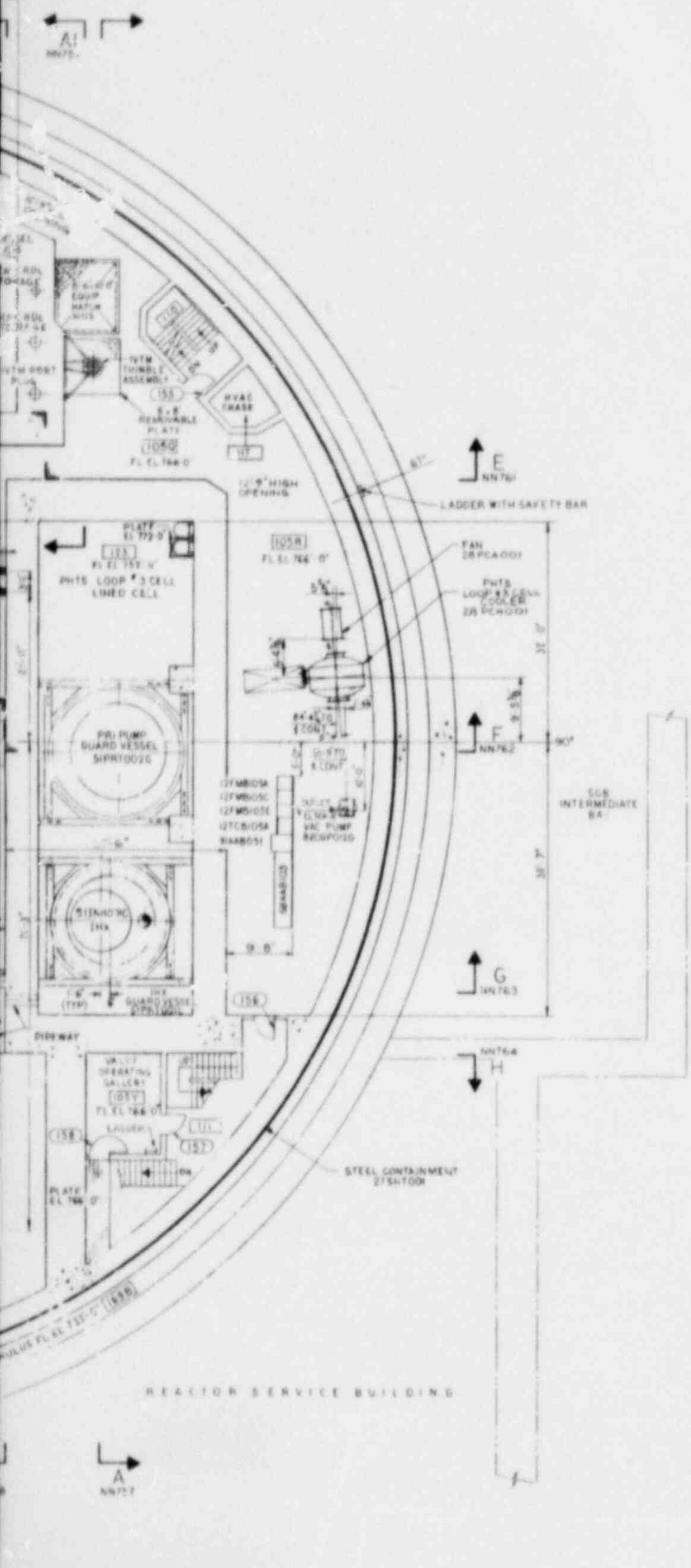

REFERENCE DRAWINGS

1. SEE REFERENCE DWGS. - DWG. NN750

GRAPHIC SCALE

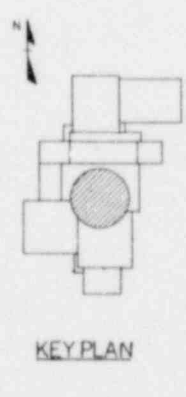

KEY PLAN

Figure 1.2-9
General Arrangement
Reactor Containment Building
Plan El. 766'-0"

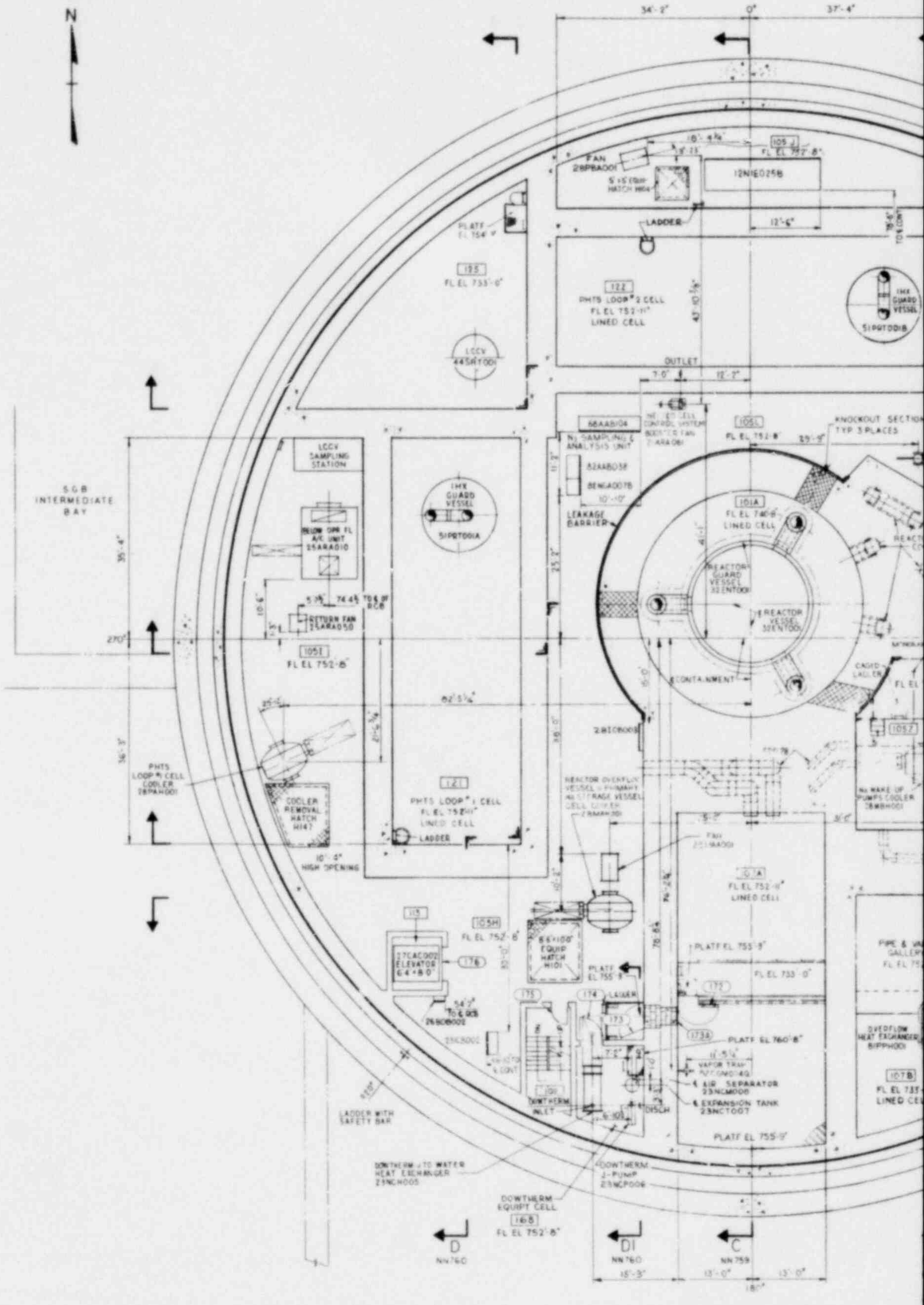

PLAN ABOVE EL. 752'-8"

NN755-14

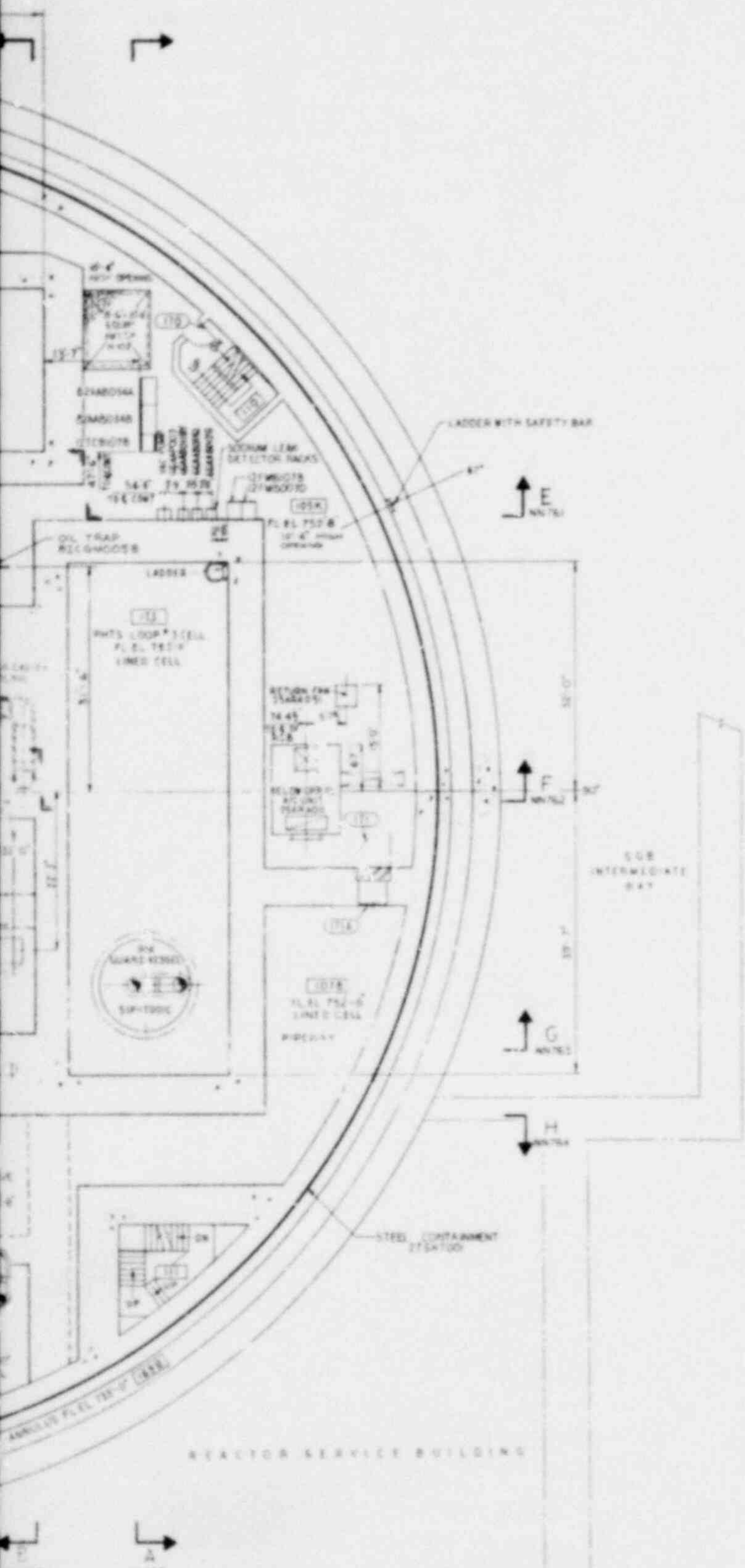

GENERAL NOTES

1. FOR GENERAL NOTES & LEGEND, SEE DWG NN750

REFERENCE DRAWINGS

1. SEE REFERENCE DWGS.-DWG. NN750

GRAPHIC SCALE

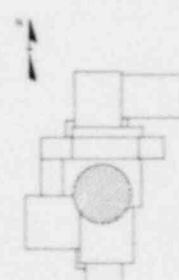

KEY PLAN

Figure 1.2-10
General Arrangement
Reactor Containment Building
Plan El. 752'-8"

Amend. 56
Aug. 1980

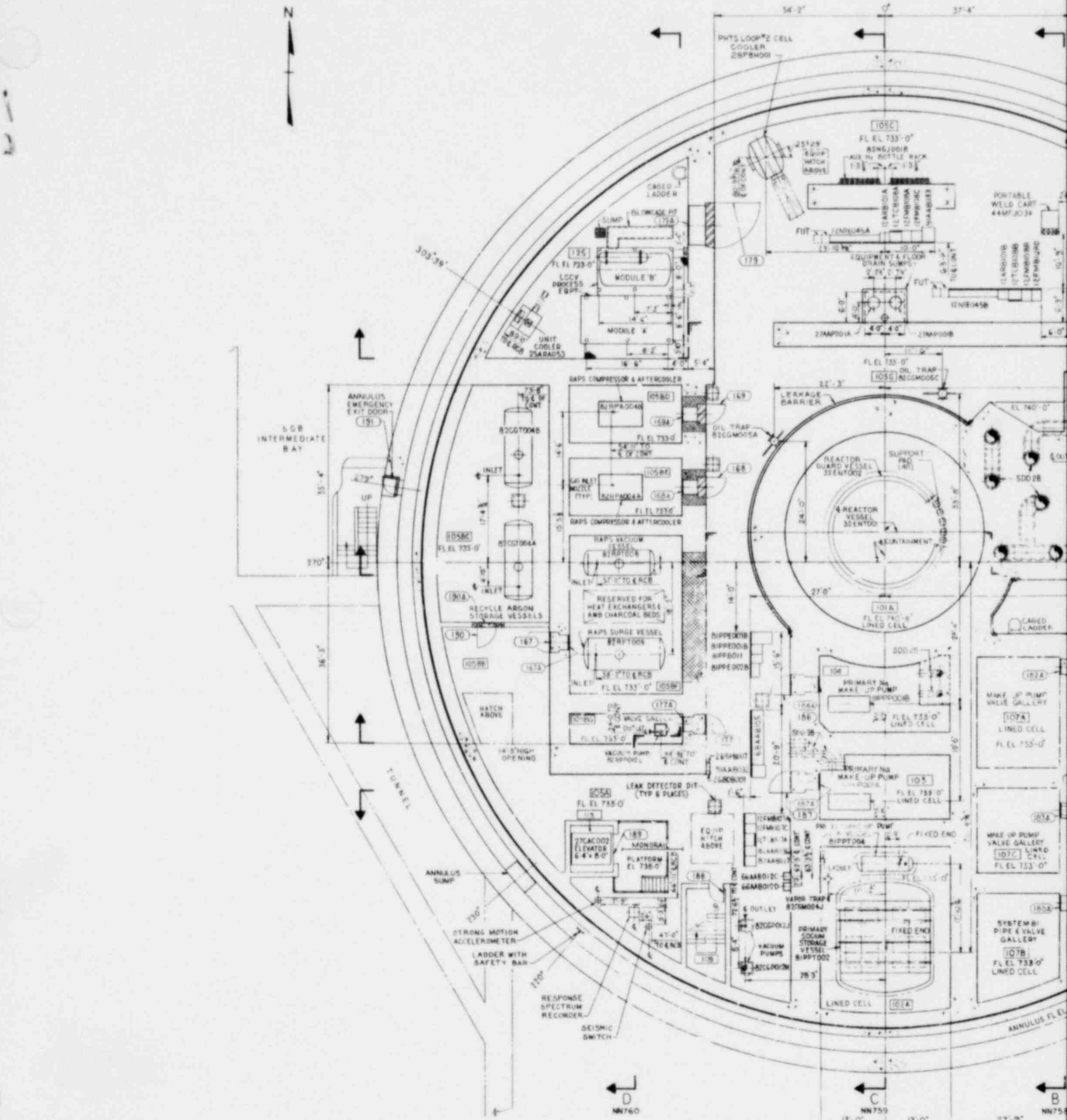

PLAN ABOVE EL. 733'-0"

NN756-14

GENERAL NOTES

1. FOR GENERAL NOTES & LEGEND, SEE DWG NN750

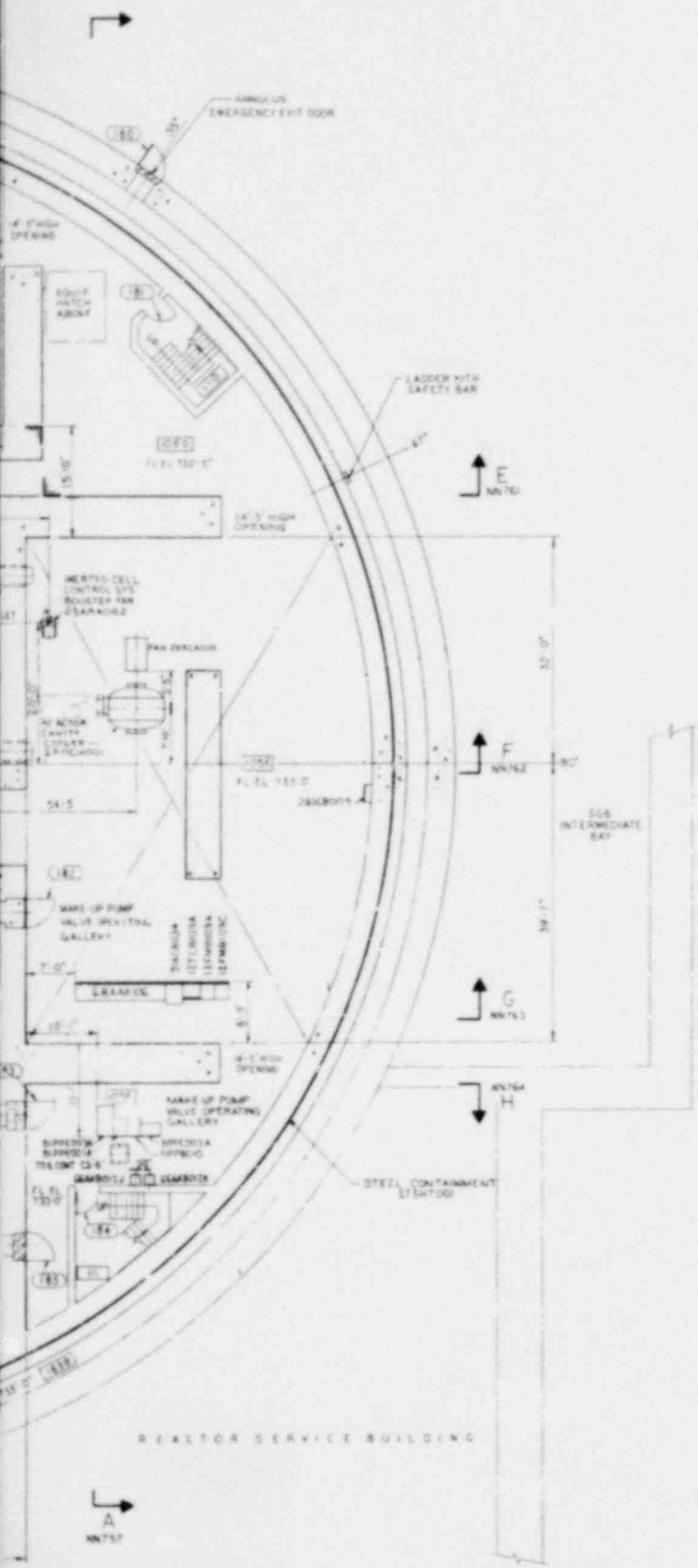

REFERENCE DRAWINGS

1. SEE REFERENCE DWGS. - DWG. NN750

GRAPHIC SCALE

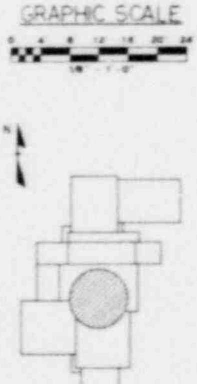

KEY PLAN

Figure 1.2-11
General Arrangement
Reactor Containment Building
Plan El. 733'-0"

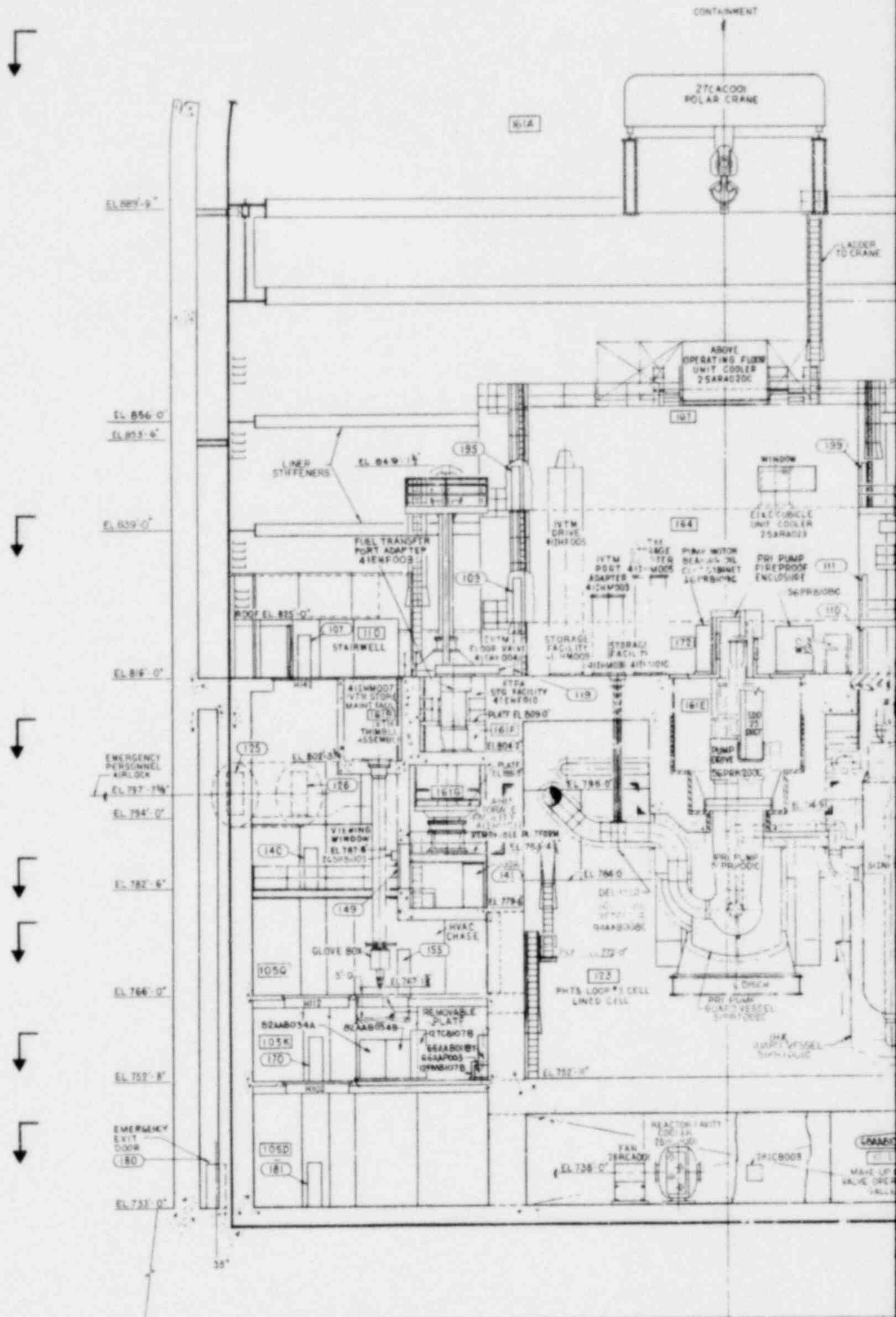

SECTION A-A

NN757-13

GENERAL NOTES

1. FOR GENERAL NOTES & LEGEND, SEE DWG NN750

REFERENCE DRAWINGS

1. SEE REFERENCE DWGS. - DWG. NN750

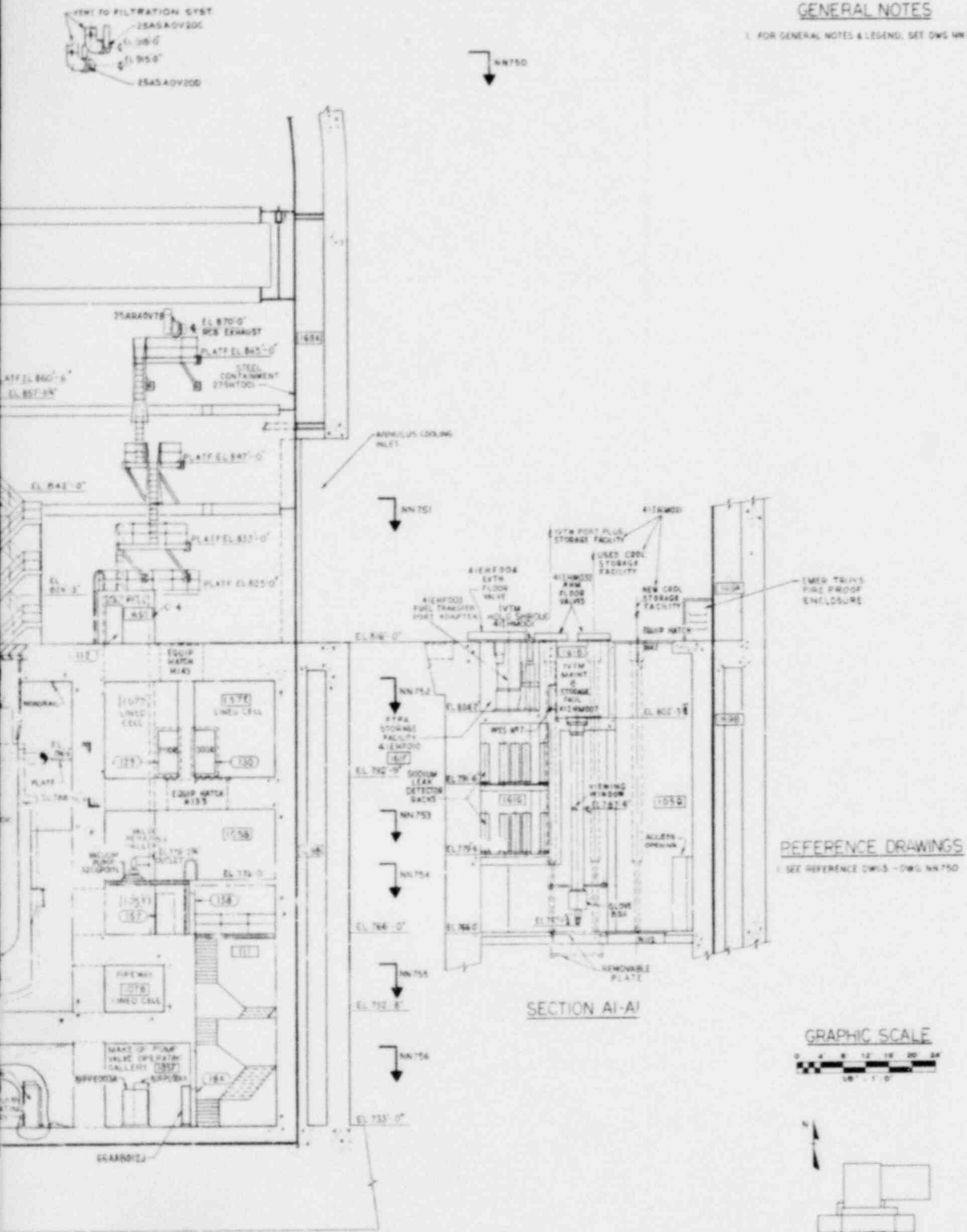

Figure 1.2-12
General Arrangement
Reactor Containment Building
Section A-A and A1-A1

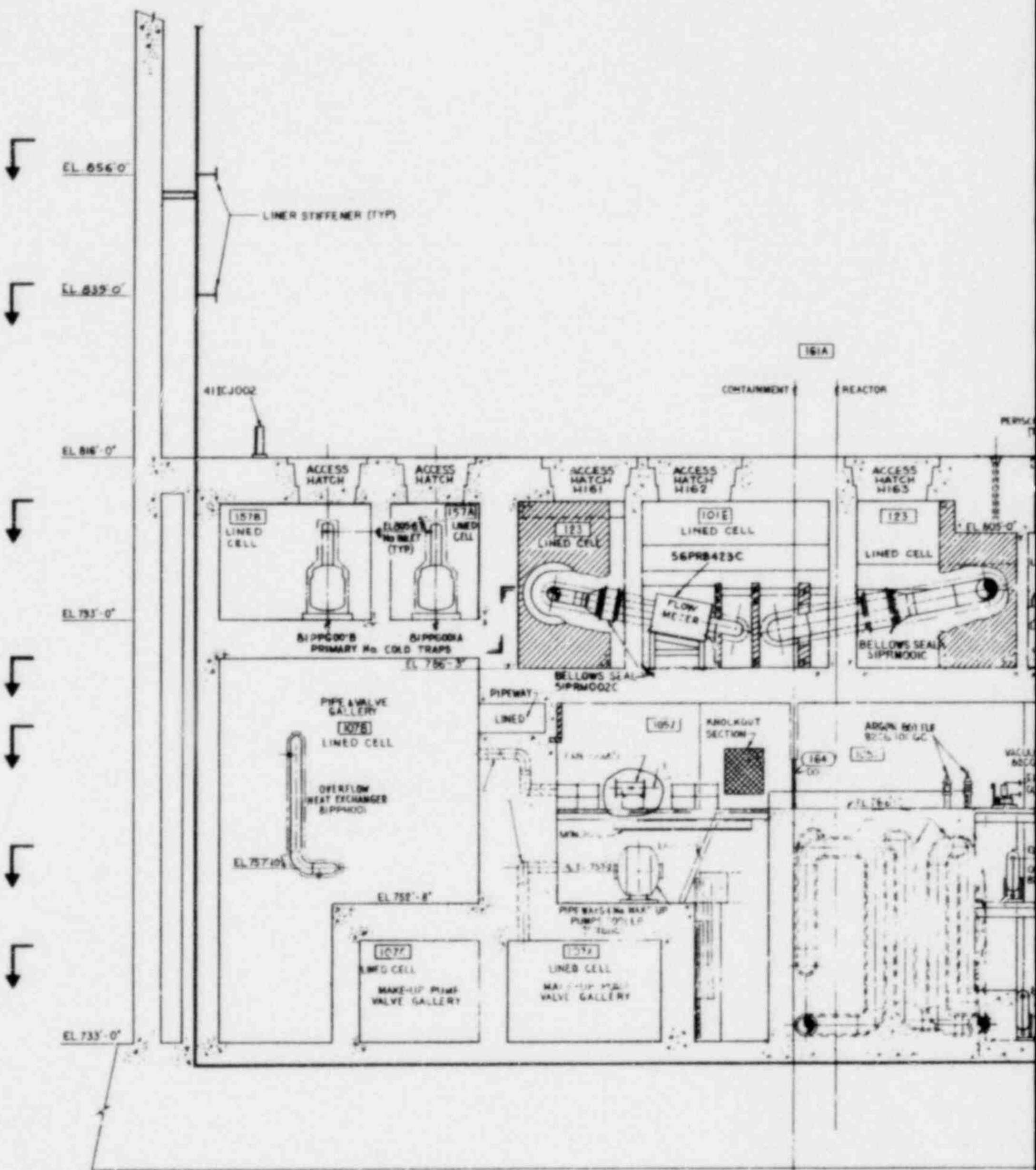

SECTION B-B

NN758-14

GENERAL NOTES

1. FOR GENERAL NOTES & LEGEND, SEE DWG NN750

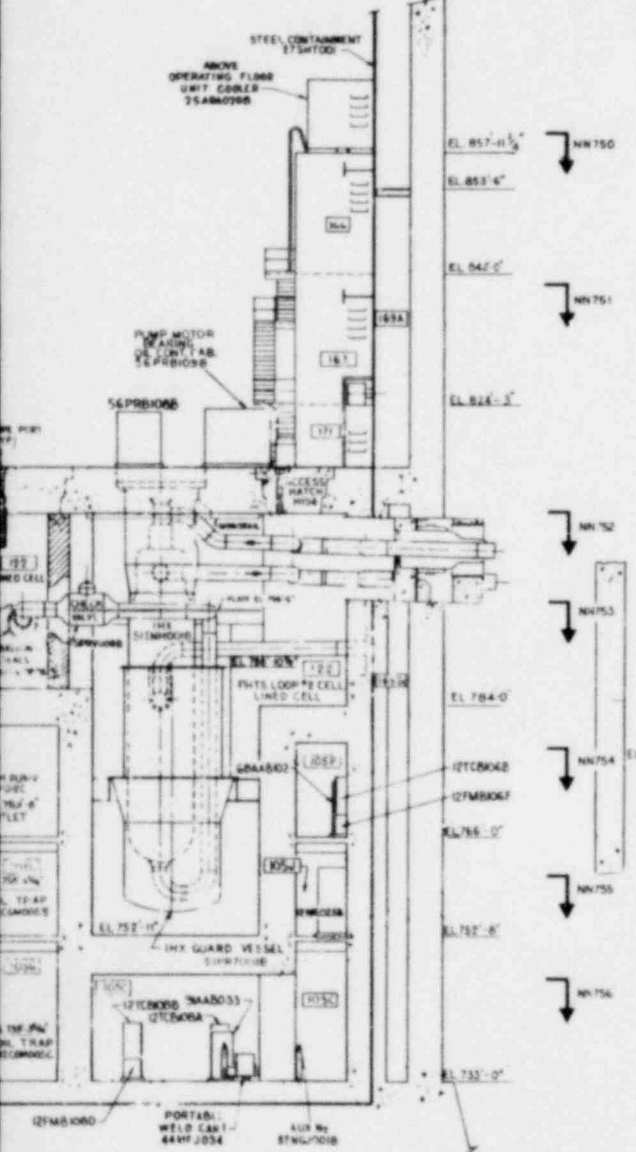

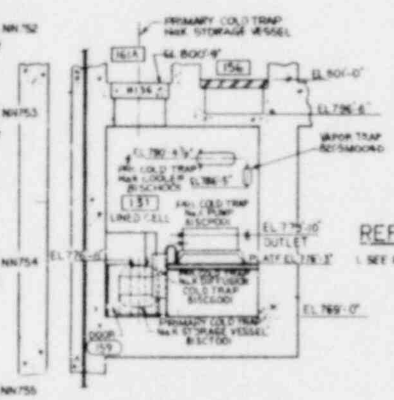

SECTION B1-B1

REFERENCE DRAWINGS

1. SEE REFERENCE DWGS - DWG NN750

GRAPHIC SCALE

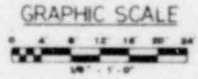

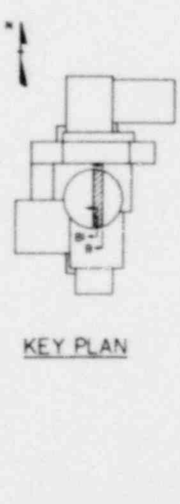

KEY PLAN

Figure 1.2-13
General Arrangement
Reactor Containment Building
Section B-B and B1-B1

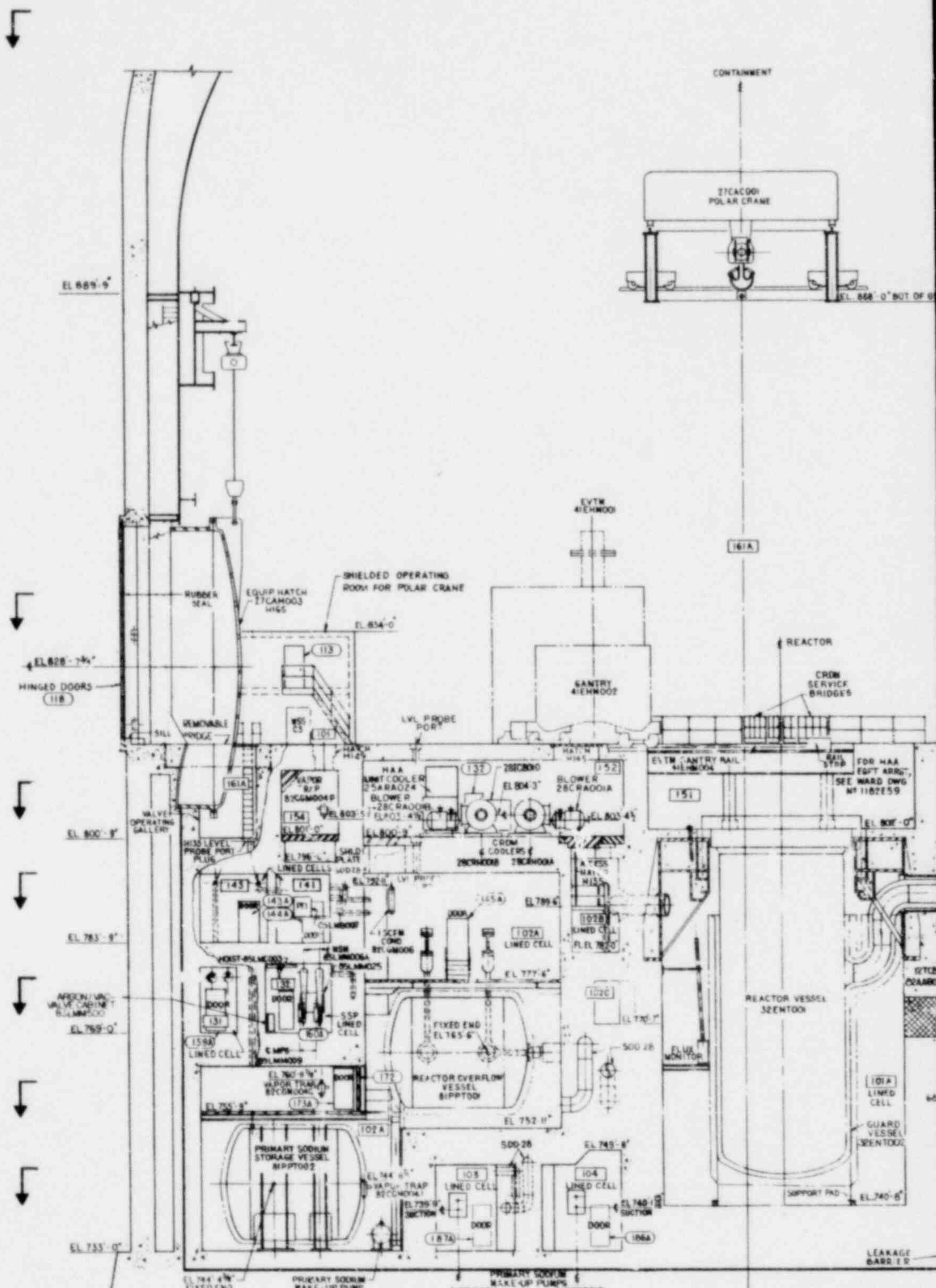

SECTION C-C

NN759-14

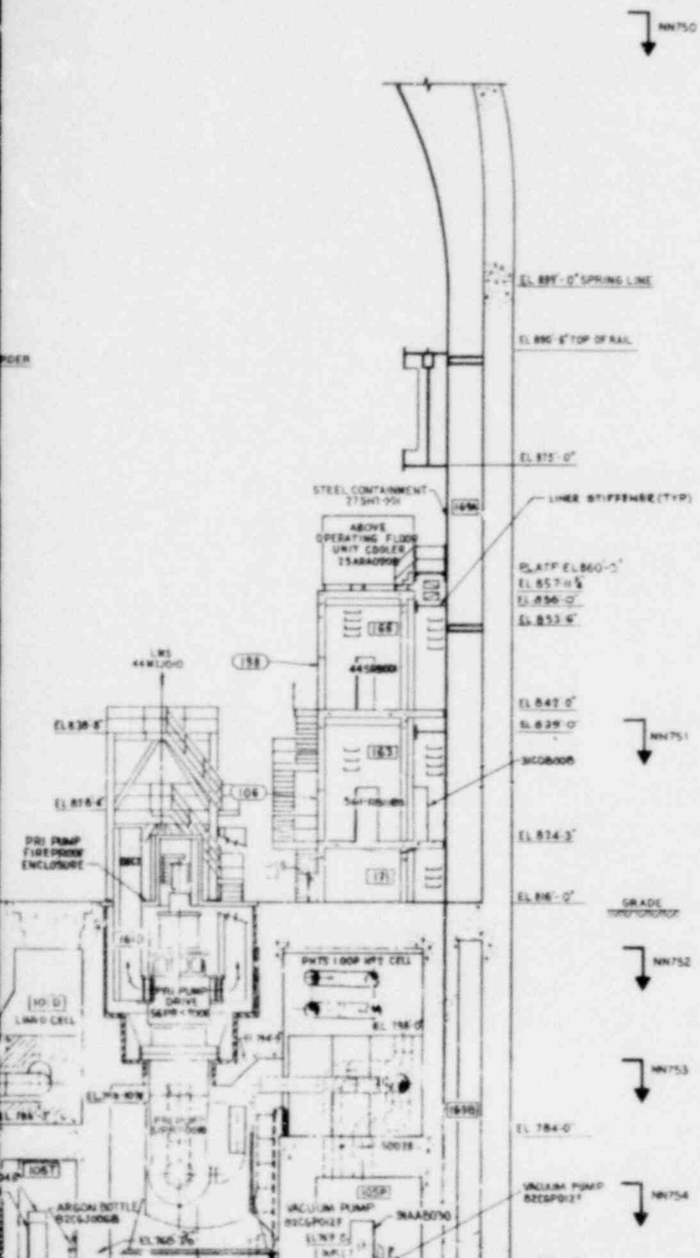

GENERAL NOTES

1. FOR GENERAL NOTES & LEGEND, SEE DWG NN750

REFERENCE DRAWINGS

1. SEE REFERENCE DWGS. - DWG. NN 750

GRAPHIC SCALE

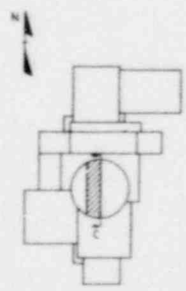

KEY PLAN

Figure 1.2-14
General Arrangement
Reactor Containment Building
Section C-C

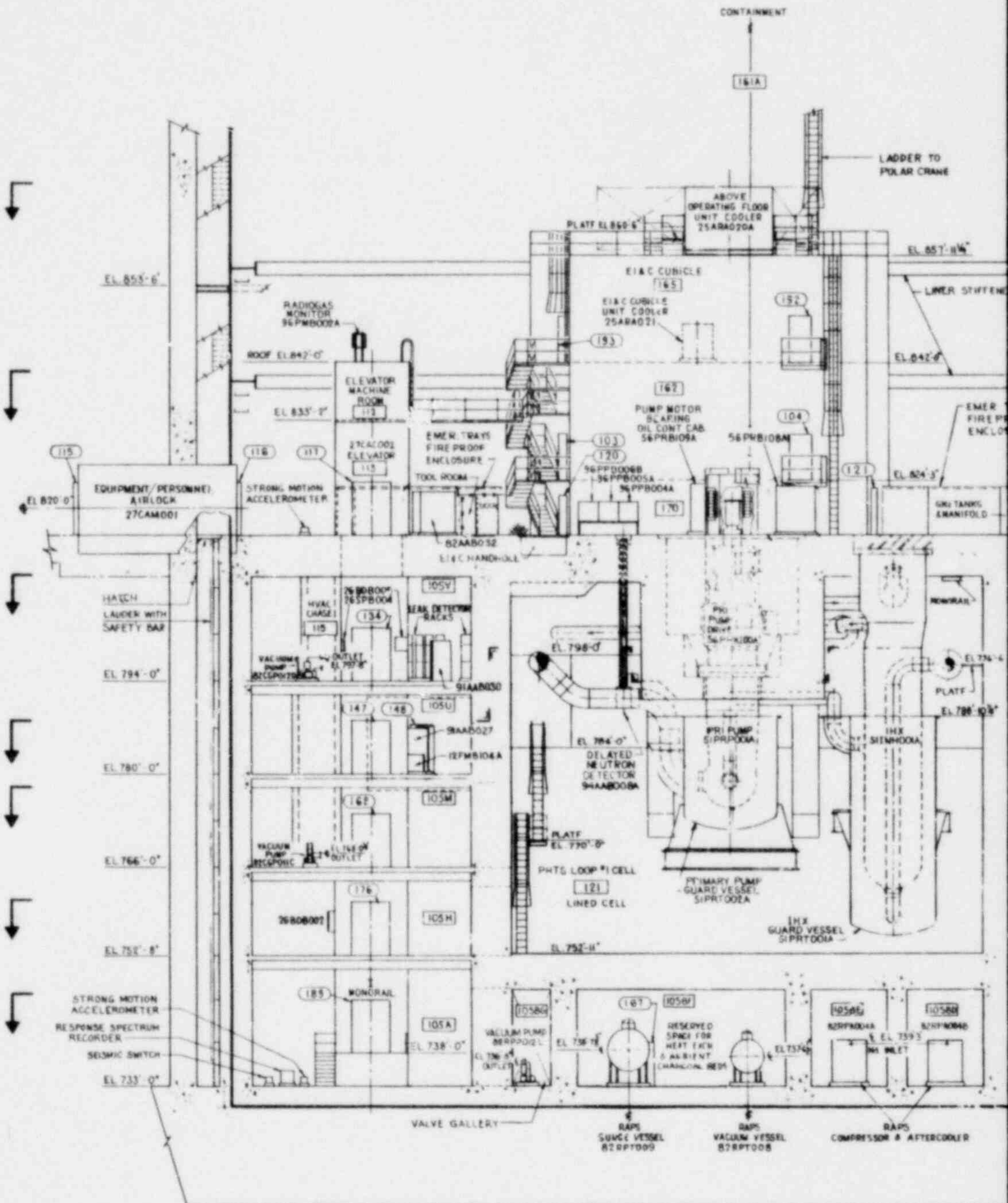

SECTION D-D

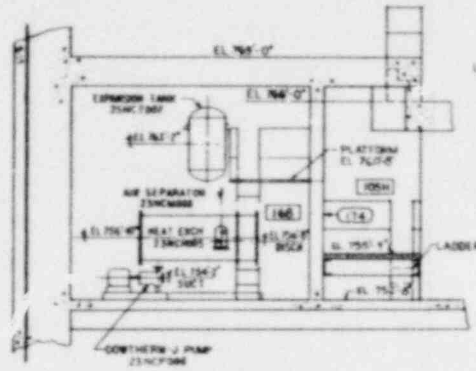

SECTION D1-D1

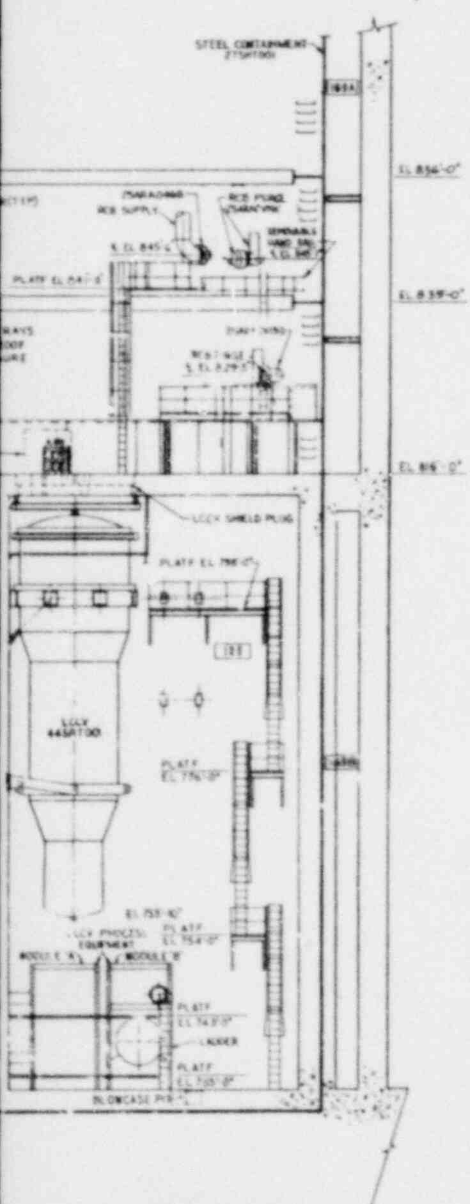

GENERAL NOTES

1. FOR GENERAL NOTES & LEGEND, SEE DWG NN750

REFERENCE DRAWINGS

1. SEE REFERENCE DWGS. - DWG. NN 750

GRAPHIC SCALE

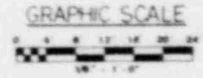

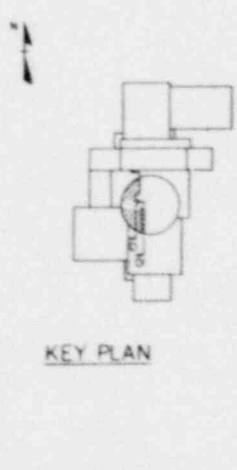

KEY PLAN

Figure 1.2-15
General Arrangement
Reactor Containment Building
Section D-D and D1-D1

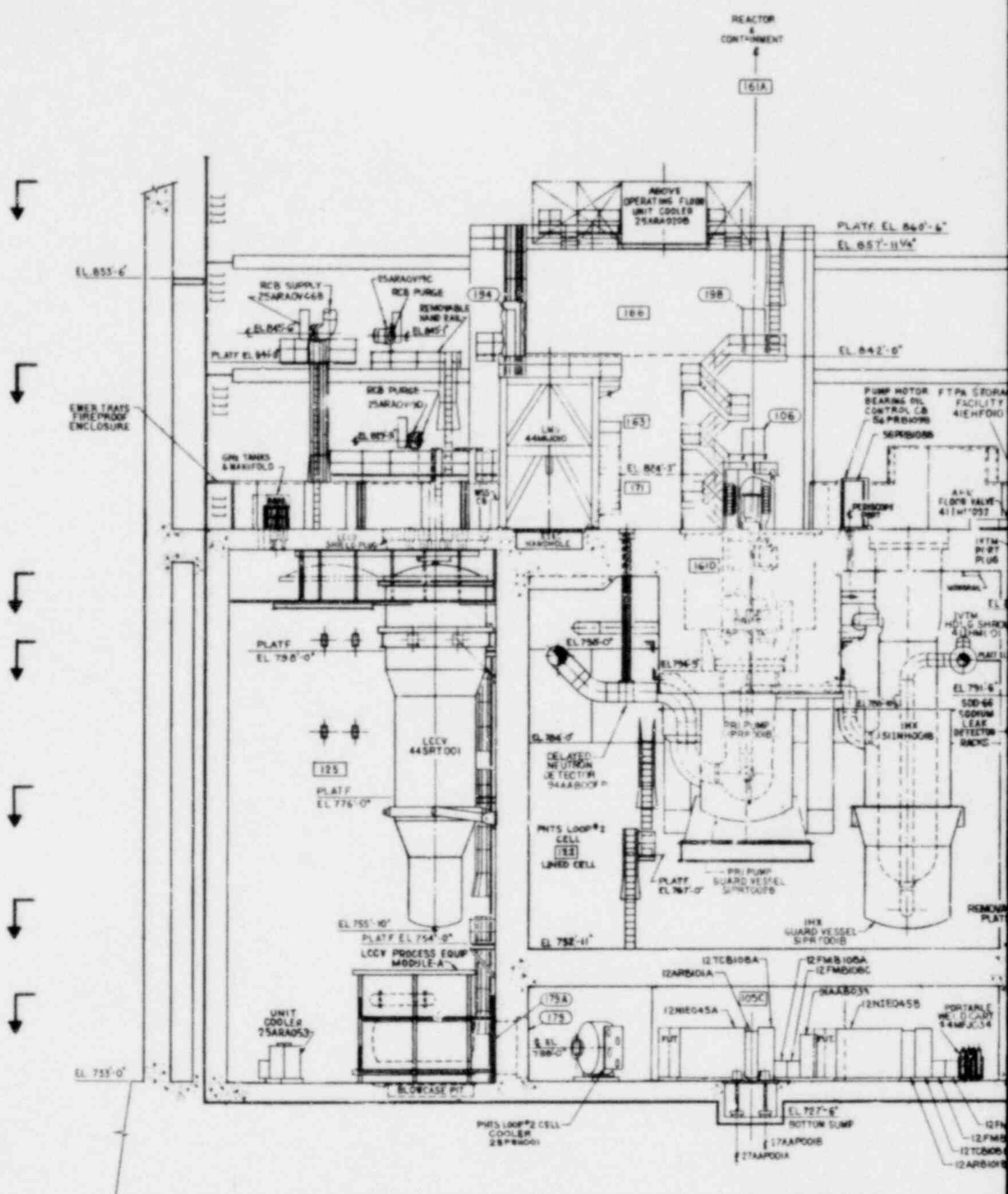

SECTION E-E

NN761-13

GENERAL NOTES

1. FOR GENERAL NOTES & LEGEND, SEE DWG NN750

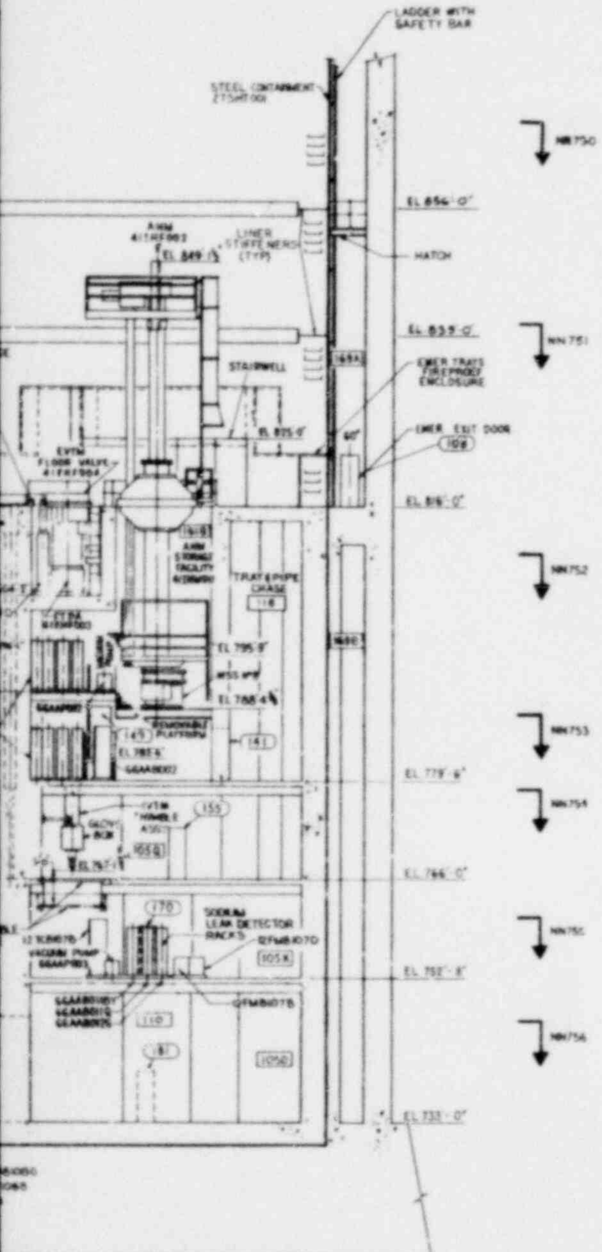

REFERENCE DRAWINGS

1. SEE REFERENCE DWGS - DWG NN750

GRAPHIC SCALE

KEY PLAN

Figure 1.2-16
General Arrangement
Reactor Containment Building
Section E-E

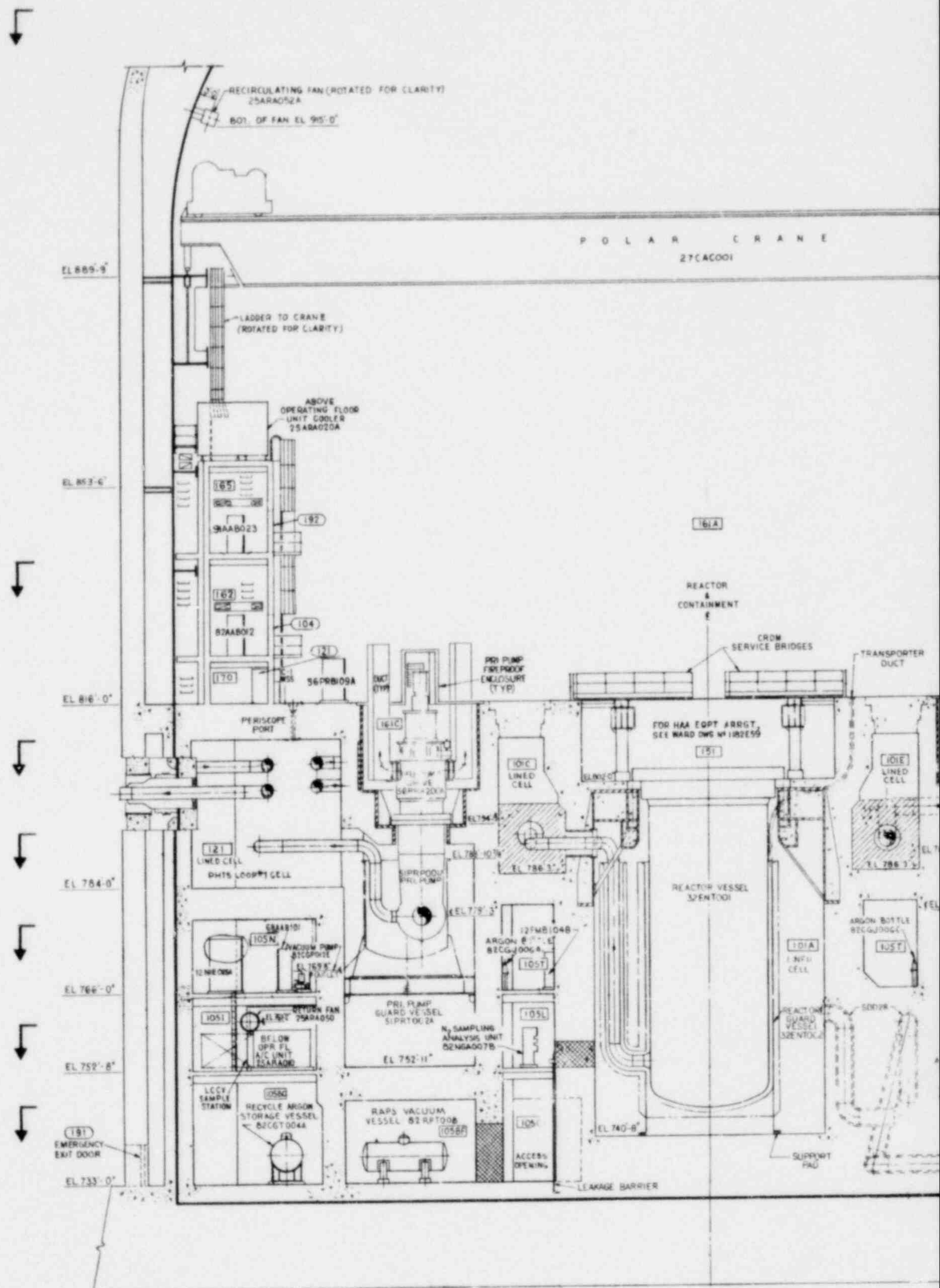
RECIRCULATING FAN (ROTATED FOR CLARITY) 25ARA052A
BOT. OF FAN EL 915'-0"
POLAR CRANE
27CAC001
EL 889'-9"
LADDER TO CRANE (ROTATED FOR CLARITY)
ABOVE OPERATING FLOOR UNIT COOLER 25ABA020A
EL 853'-6"
165
91AAB023
192
161A
162
82AAB012
104
REACTOR & CONTAINMENT ℄
CRDM SERVICE BRIDGES
TRANSPORTER DUCT
121
170
56PRB109A
PRI PUMP FIREPROOF ENCLOSURE (TYP)
EL 816'-0"
PERISCOPE PORT
161C
FOR HAA EQPT ARRGT, SEE WARD DWG Nº 1182E59
151
101C LINED CELL
101E LINED CELL
121 LINED CELL
PHTS LOOP #1 CELL
EL 786'-3"
EL 784'-0"
REACTOR VESSEL 32ENT001
105N
ARGON BOTTLE
105T
101A
EL 766'-0"
PRI PUMP GUARD VESSEL
105L
105I
RETURN FAN 25ARA050
BELOW OPR FL A/C UNIT
N₂ SAMPLING ANALYSIS UNIT 82NGA007B
REACTOR GUARD VESSEL 32ENT002
EL 752'-8"
EL 752'-11"
LCCV SAMPLE STATION
105G
RECYCLE ARGON STORAGE VESSEL 82CGT004A
RAPS VACUUM VESSEL 82RPT008
105F
105C
ACCESS OPENING
191
EMERGENCY EXIT DOOR
EL 740'-8"
SUPPORT PAD
EL 733'-0"
LEAKAGE BARRIER

SECTION F-F

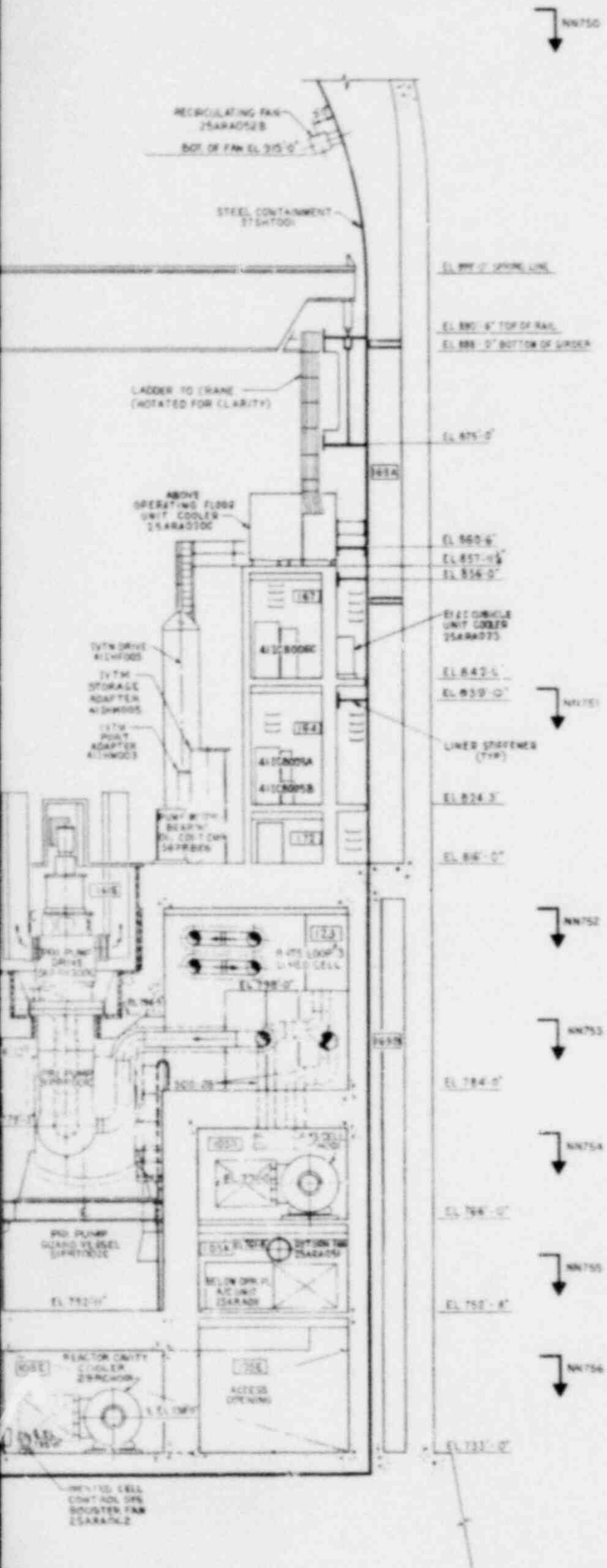

GENERAL NOTES

1. FOR GENERAL NOTES & LEGEND, SEE DWG NN750

REFERENCE DRAWINGS

1. SEE REFERENCE DWGS. - DWG. NN750

GRAPHIC SCALE

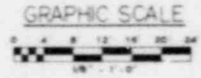

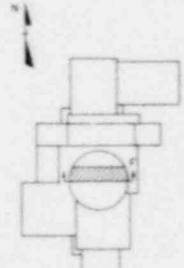

KEY PLAN

Figure 1.2-17
General Arrangement
Reactor Containment Building
Section F-F

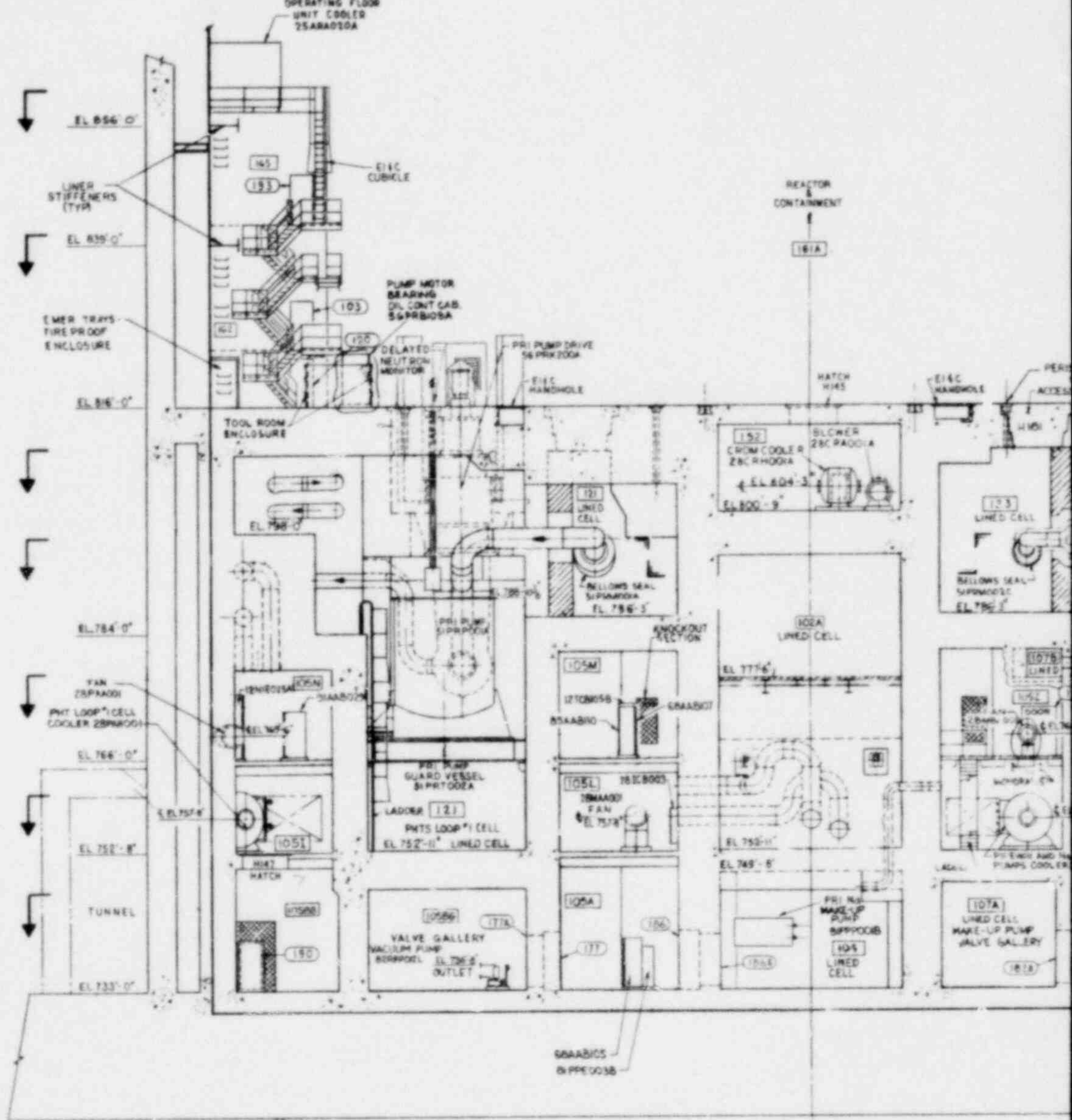

ABOVE OPERATING FLOOR UNIT COOLER 25ARA010A
EL 856'-0"
LINER STIFFENERS (TYP)
EL 835'-0"
EMER TRAYS FIRE PROOF ENCLOSURE
EL 816'-0"
EL 784'-0"
EL 766'-0"
EL 752'-8"
TUNNEL
EL 733'-0"
REACTOR CONTAINMENT
TOOL ROOM ENCLOSURE
LINED CELL
VALVE GALLERY
HATCH

SECTION G-G

GENERAL NOTES

1. FOR GENERAL NOTES & LEGEND, SEE DWG NN750

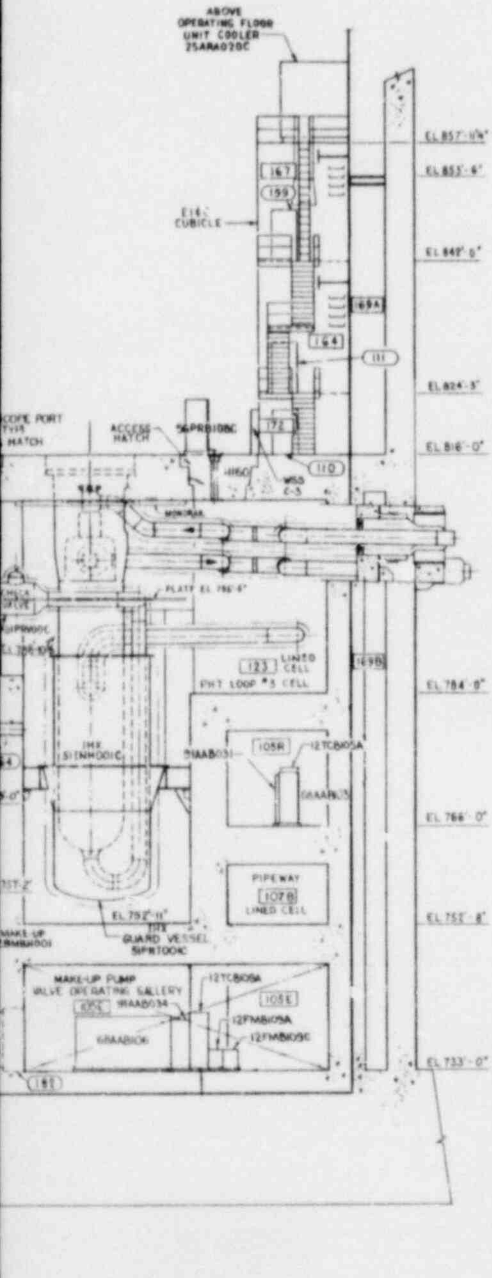

REFERENCE DRAWINGS

1. SEE REFERENCE DWGS. - DWG NN 750

GRAPHIC SCALE

0 4 8 12 16 20 24

1/8" = 1'-0"

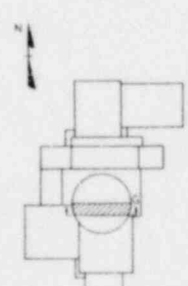

KEY PLAN

Figure 1.2-18
General Arrangement
Reactor Containment Building
Section G-G

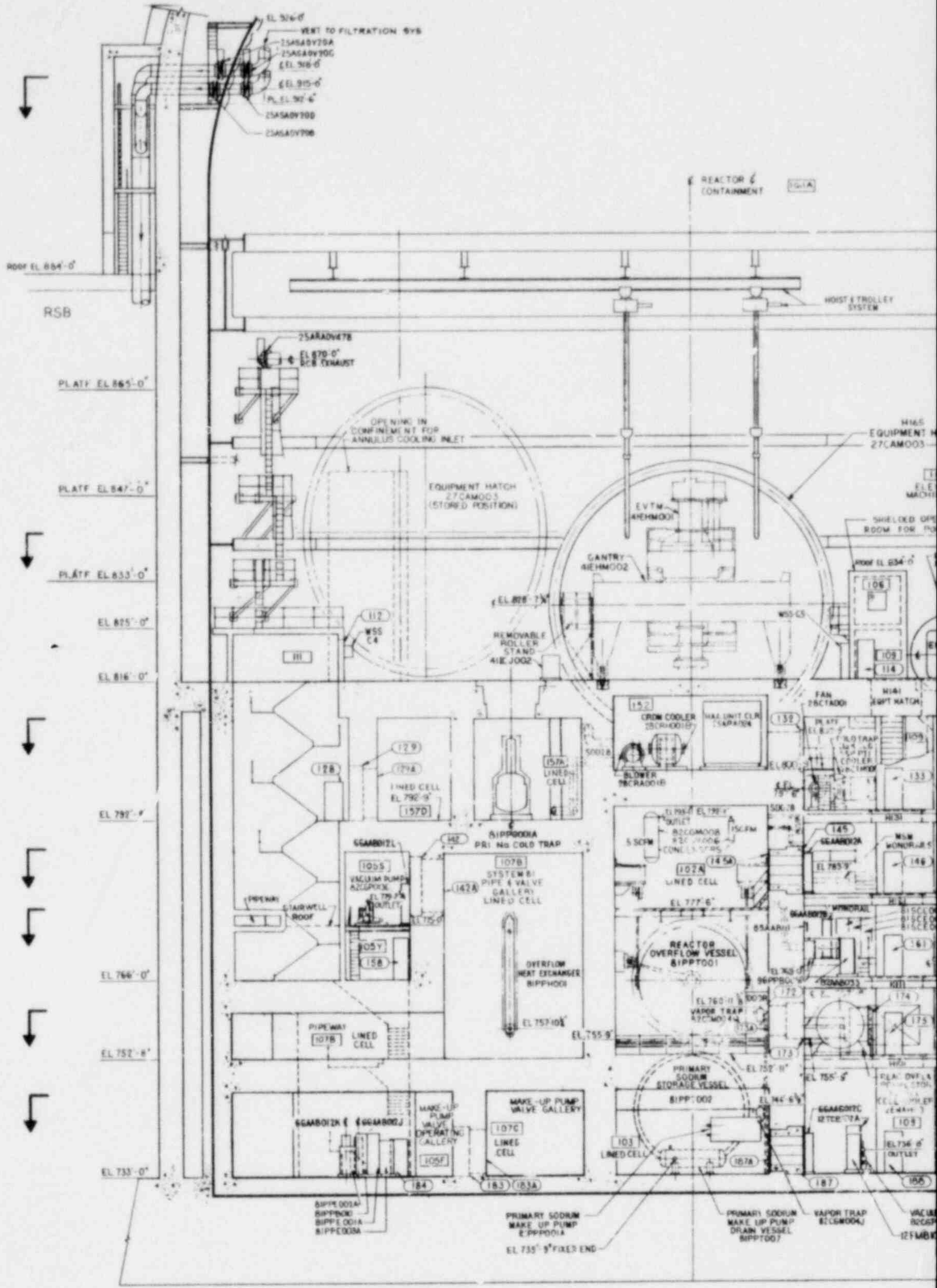

SECTION H-H

NN764-14

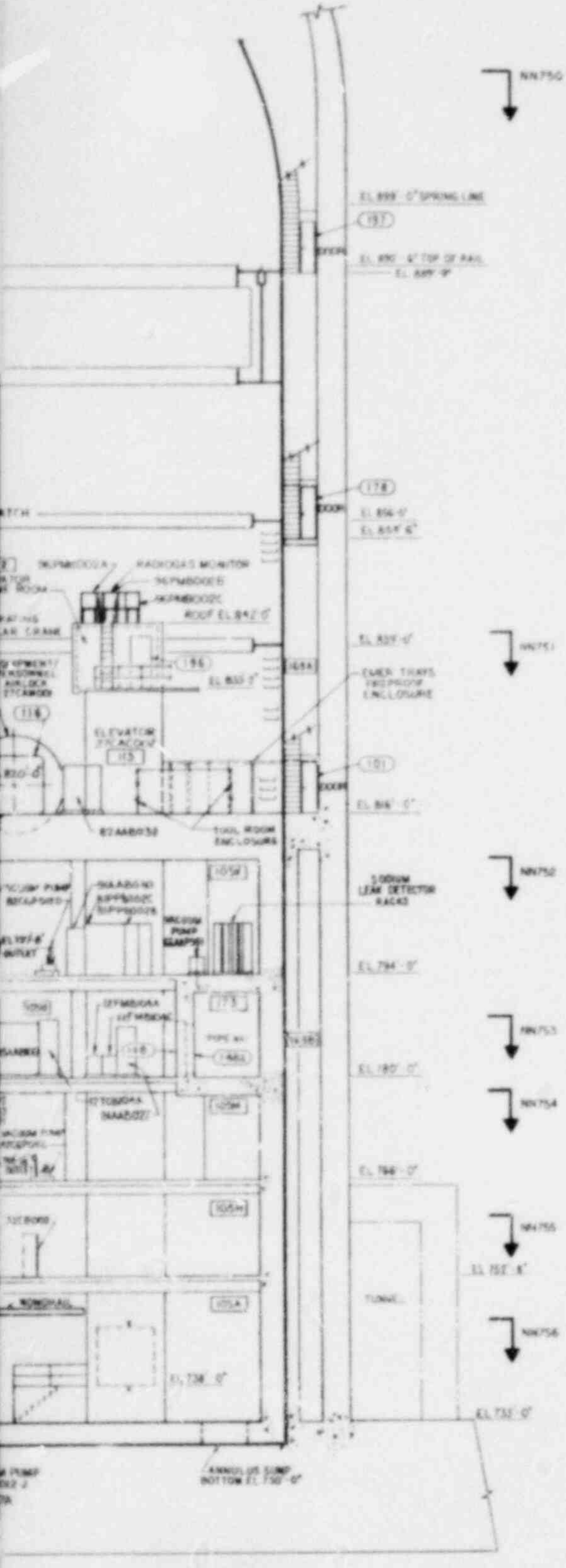

GENERAL NOTES

1. FOR GENERAL NOTES & LEGEND, SEE DWG NN750

REFERENCE DRAWINGS

1. SEE REFERENCE DWGS - DWG NN750

GRAPHIC SCALE

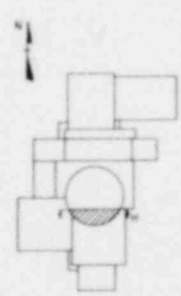

KEY PLAN

Figure 1.2-19
General Arrangement
Reactor Containment Building
Section H-H

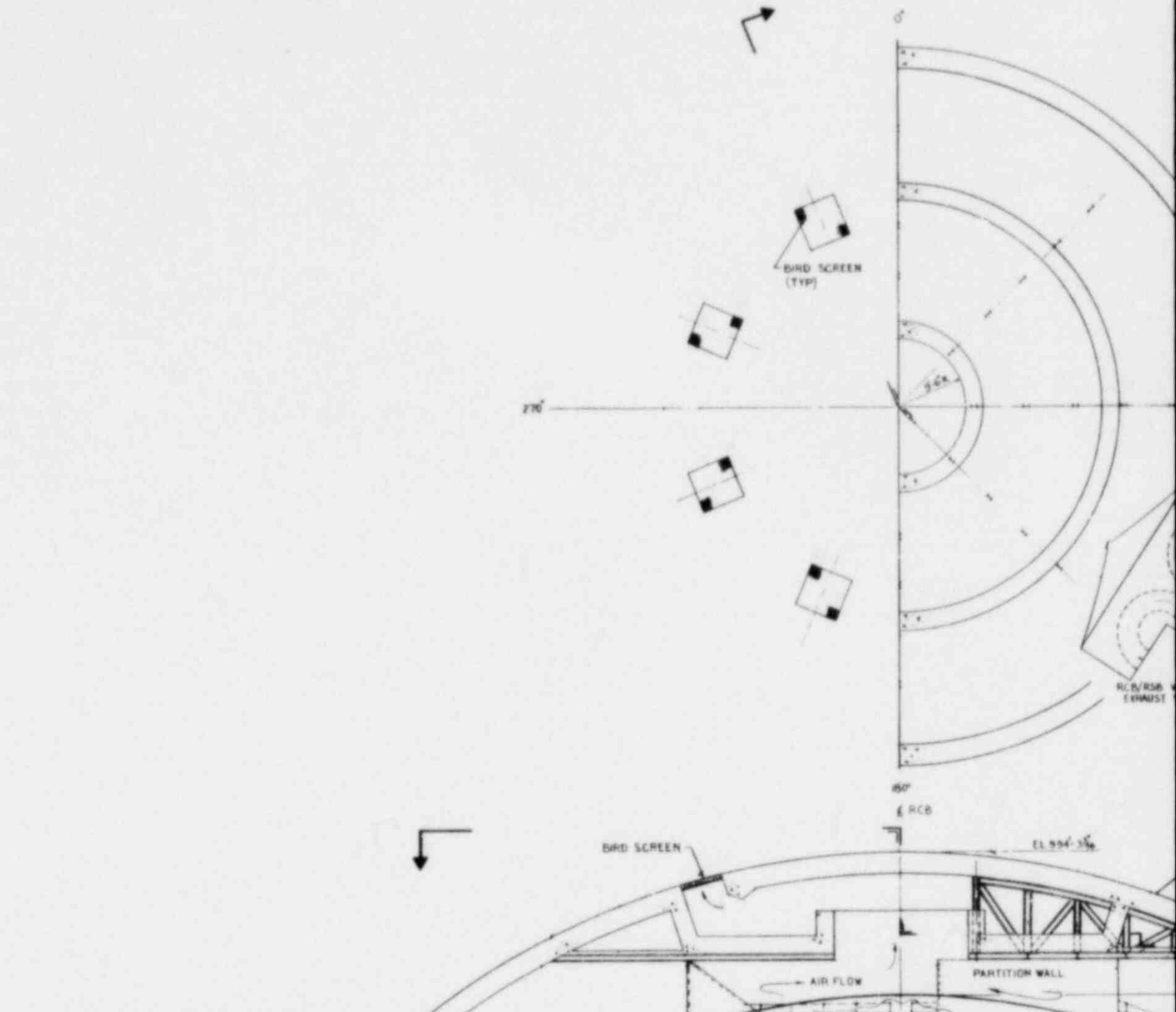

SECTION OF DOME

NN765-2

GENERAL NOTES

1. FOR GENERAL NOTES & LEGEND, SEE DWG NN750

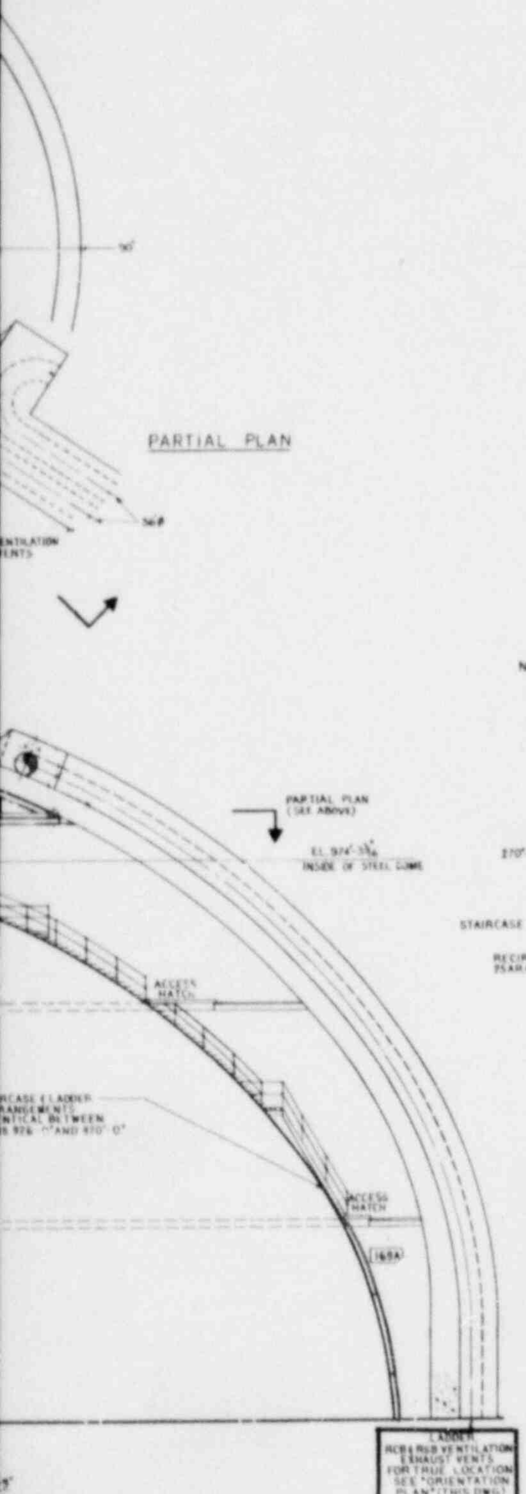

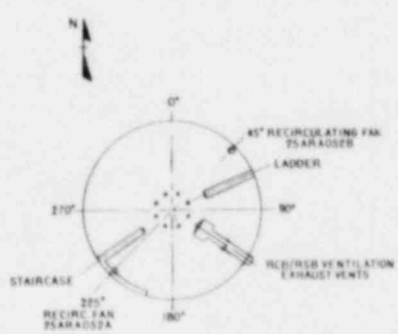

ORIENTATION PLAN
NOT TO SCALE

REFERENCE DRAWINGS

1. SEE REFERENCE DWGS - DWG NN750

GRAPHIC SCALE

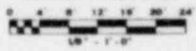

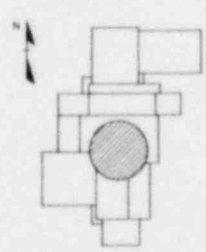

KEY PLAN

Figure 1.2-20
General Arrangement
Reactor Containment Building
Section C-C
above plan, El. 899-0"

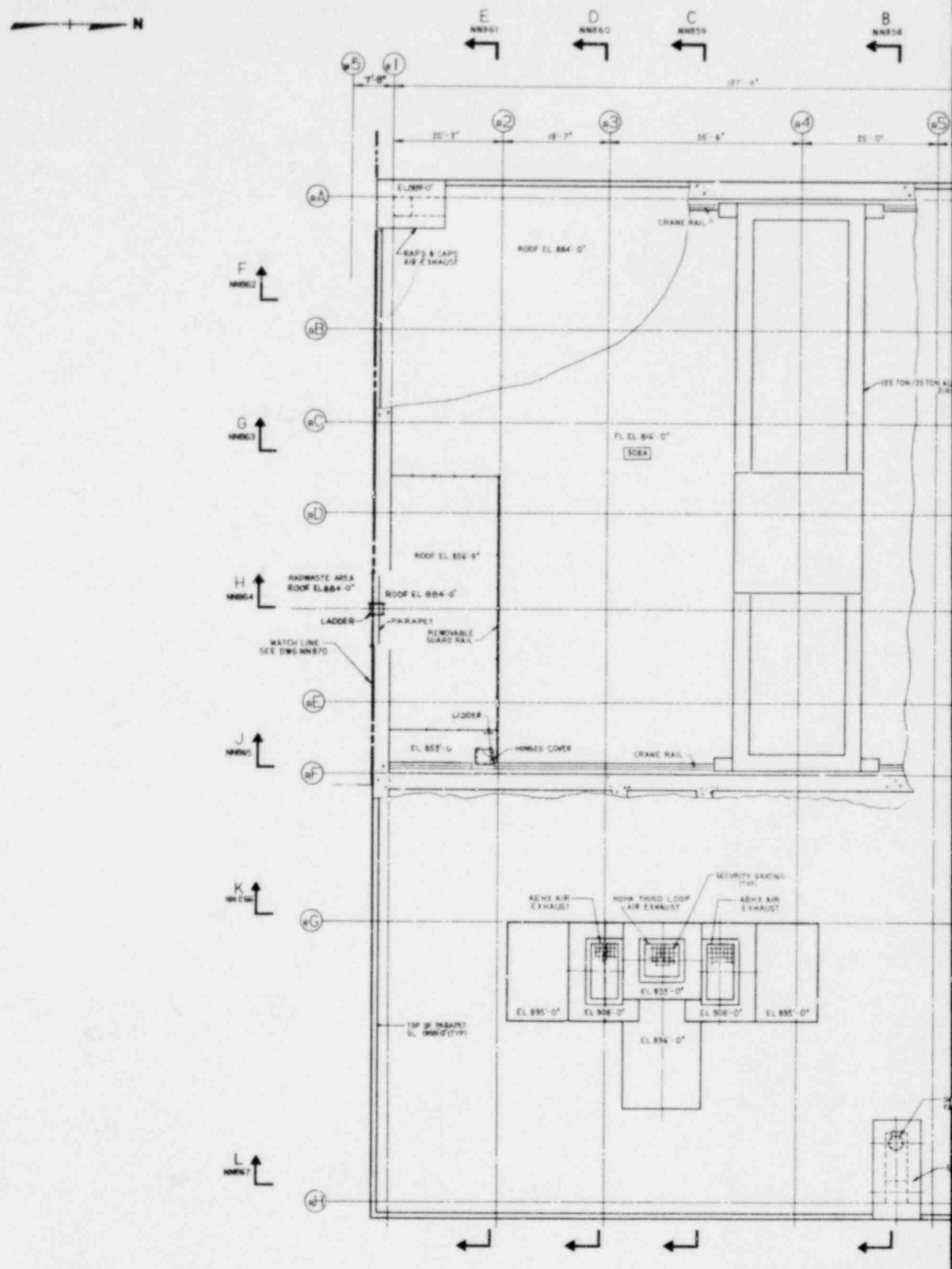

PLAN ABOVE EL. 858-0

NN850-8

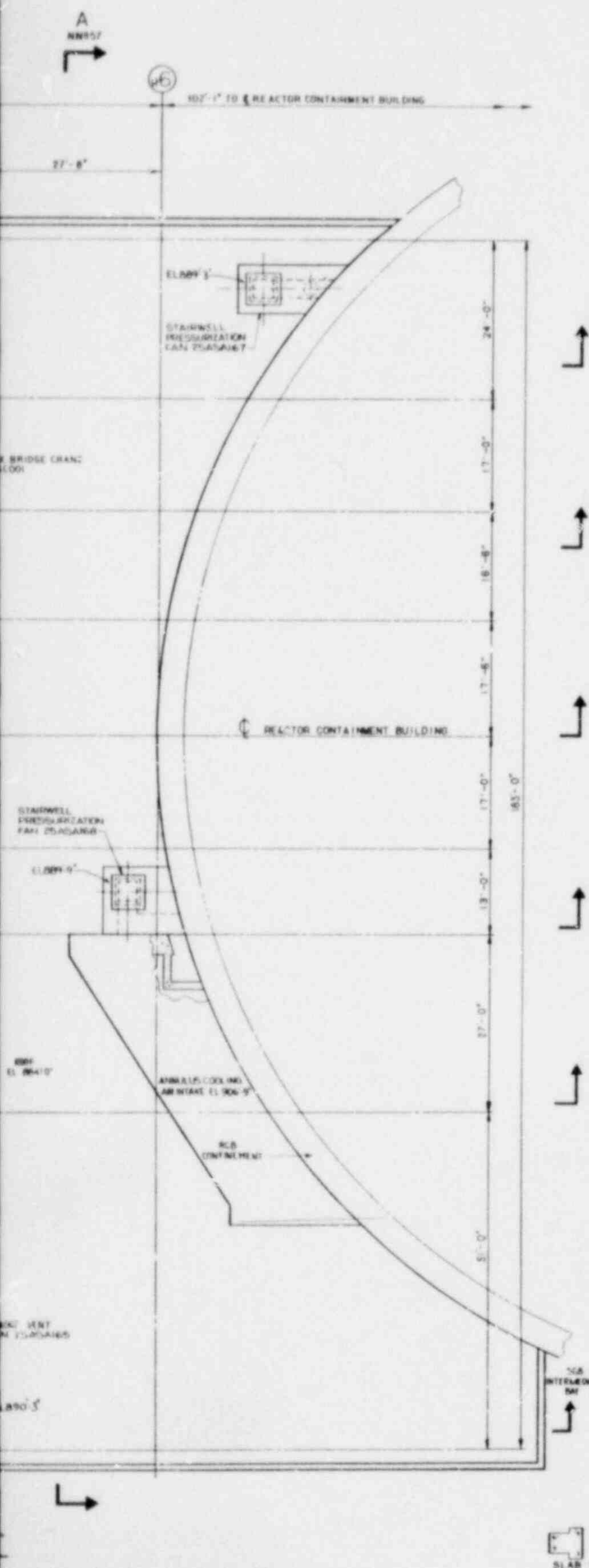

GENERAL NOTES

1. ALL HATCH DIMENSIONS ARE CLEAR OPENING SIZE
2. ALL EQUIPMENT/ACCESS HATCHES WILL BE PROVIDED WITH REMOVABLE GUARD RAILS FOR PERSONNEL SAFETY

REFERENCE DRAWINGS

NN851 RSB-GEN ARRGT-PLAN ABOVE EL 816'-0"
NN852 EL 792'-0"
NN853 EL 779'-0"
NN854 EL 755'-0"
NN855 PARTIAL EL 749'-0"
EL 840'-0"
EL 864'-6"
NN856 -PLAN ABOVE EL 733'-0"
NN857 SECTION A-A
NN858 B-B
NN859 C-C
NN860 D-D
NN861 E-E
NN862 F-F
NN863 G-G
NN864 H-H
NN865 J-J
NN866 K-K
NN867 L-L
NN870 RSB-GEN ARRGT-PLAN ABOVE EL 867'-0"
RADWASTE AREA & EL 838'-0"
NN871 EL 816'-0"
& EL 795'-0"
NN872 EL 775'-0"
NN873 SECTION A-A
NN874 B-B
NN875 C-C
NN876 D-D
NN877 E-E & F-F
NN878 G-G & H-H

GRAPHIC SCALE

0 4' 8' 12' 16' 20' 24'
1/8" - 1'-0"

LEGEND

- EI&C CABINET (HEAVY LINE FRONT)
- HIGH DENSITY CONCRETE
- KNOCKOUT SECTION
- STEEL
- ORDINARY CONCRETE
- CHECKERED PLATE
- GRATING
- 301 CELL NUMBER
- CONCRETE BLOCK
- 200 DOOR NUMBER
- CATCH PAN GRATING
- SLAB / BLOCK REMOVABLE PANEL SHIELD DOORS

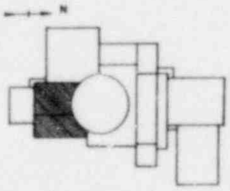

KEY PLAN

Figure 1.2-21
General Arrangement
Reactor Service Building
El. 858'-0"

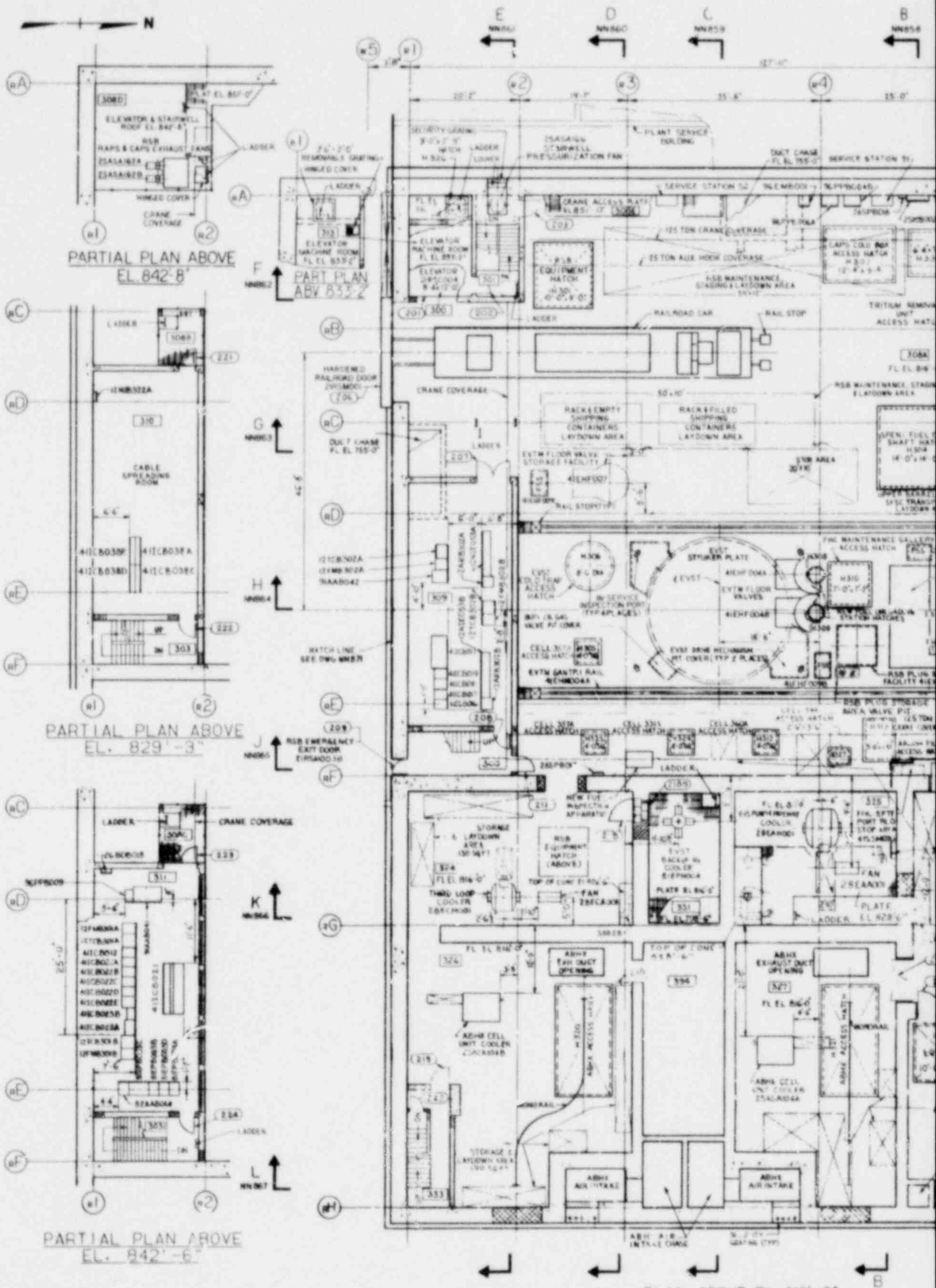

PARTIAL PLAN ABOVE EL. 842-8'

PARTIAL PLAN ABOVE EL. 829'-3"

PARTIAL PLAN ABOVE EL. 842'-6"

PLAN ABOVE EL. 816'-0"

NN851-13

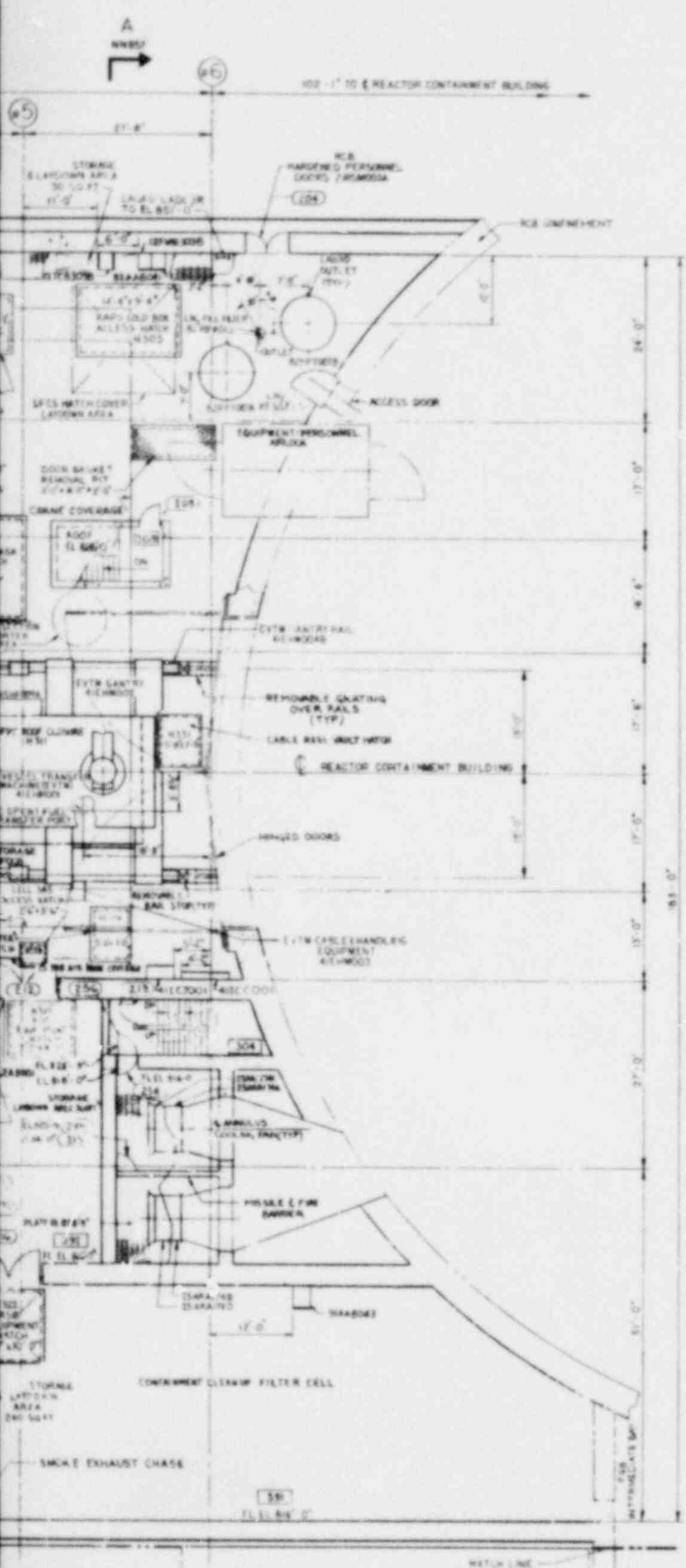

REFERENCE DRAWINGS

GRAPHIC SCALE

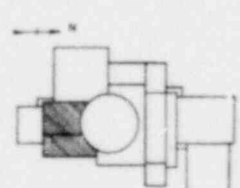

KEY PLAN

Figure 1.2-22
General Arrangement
Reactor Service Building
El. 816'-0"

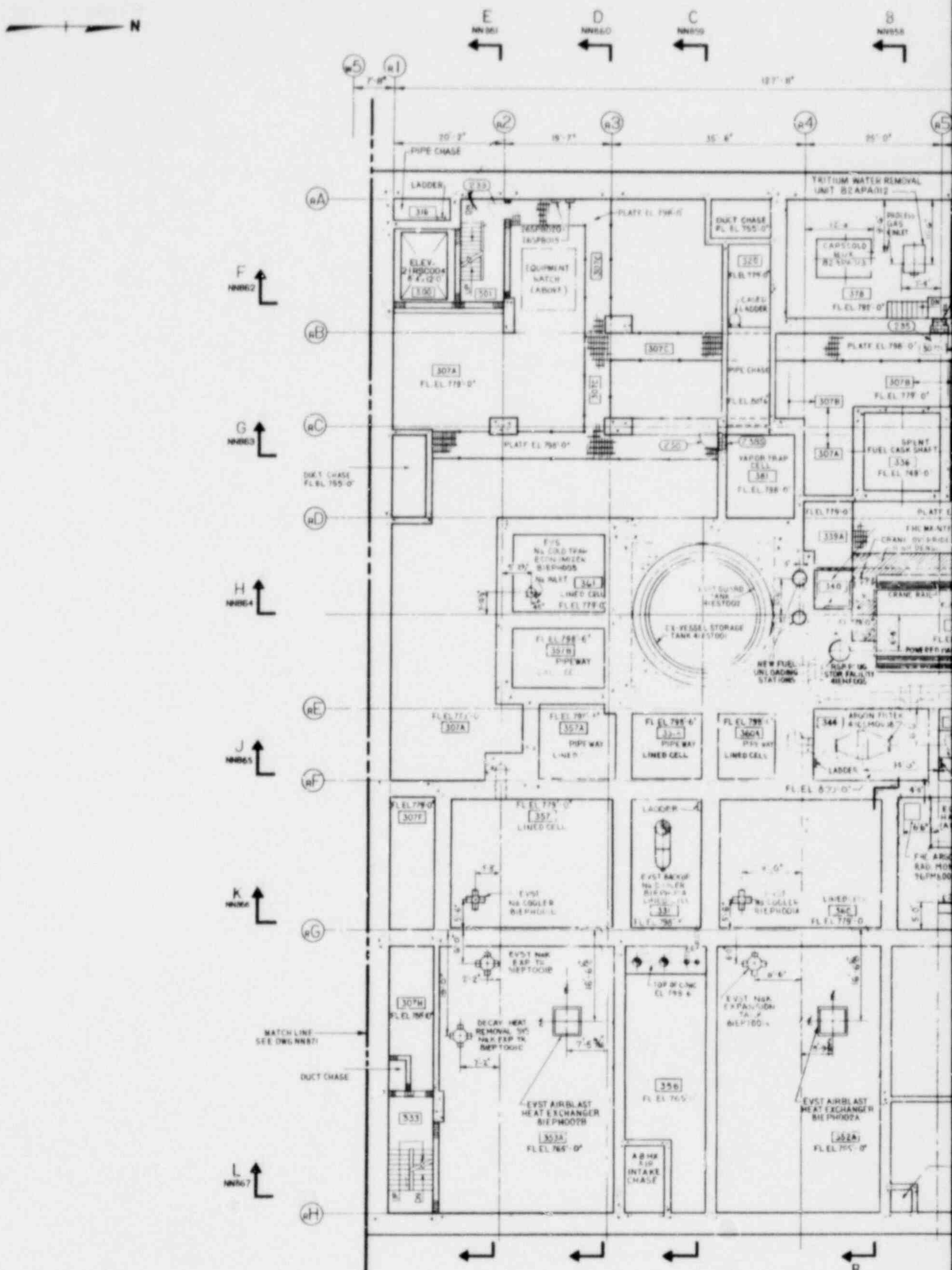

PLAN ABOVE EL. 792-

NN852-12

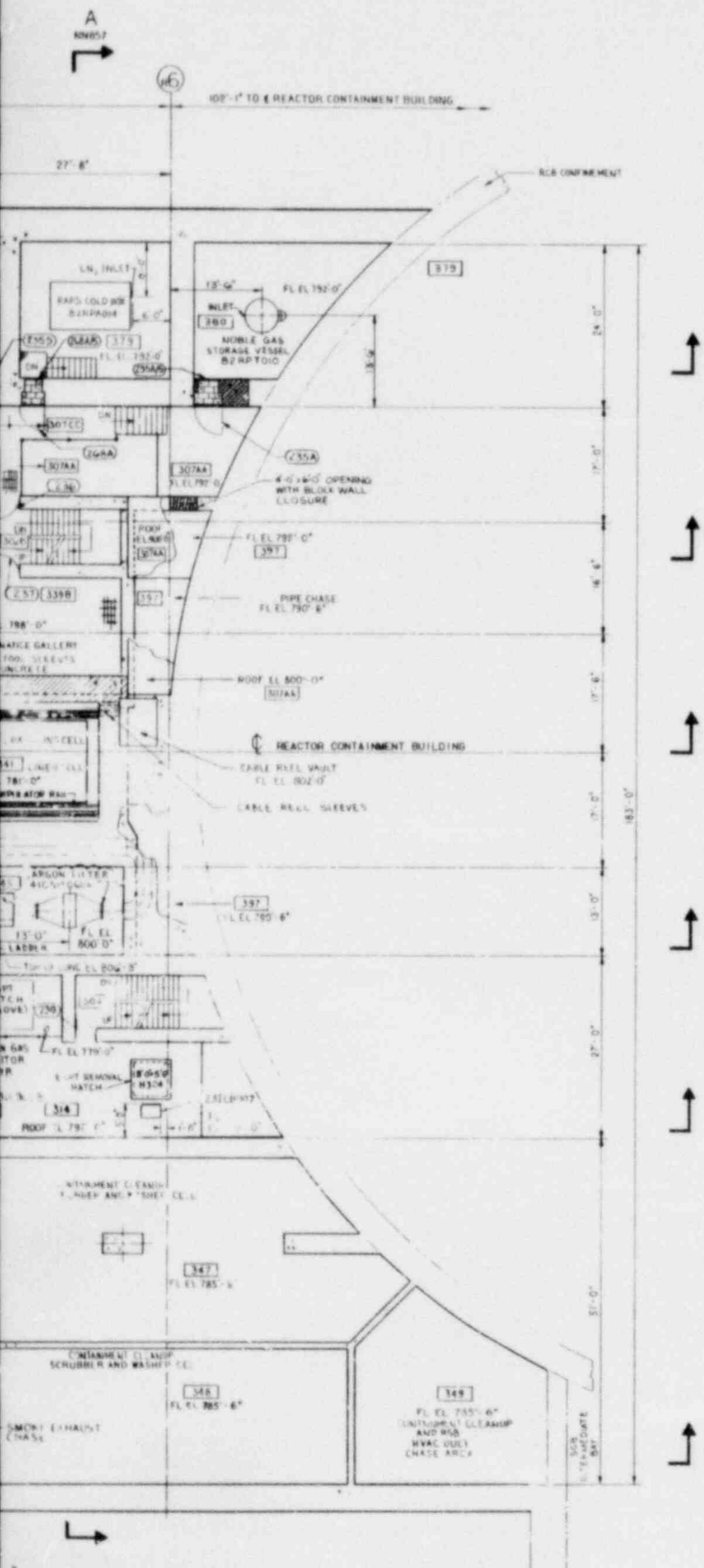

REFERENCE DRAWINGS

1. SEE REFERENCE DWGS - DWG NN850

GRAPHIC SCALE

KEY PLAN

Figure 1.2-23
General Arrangement
Reactor Service Building
El. 792'-0"

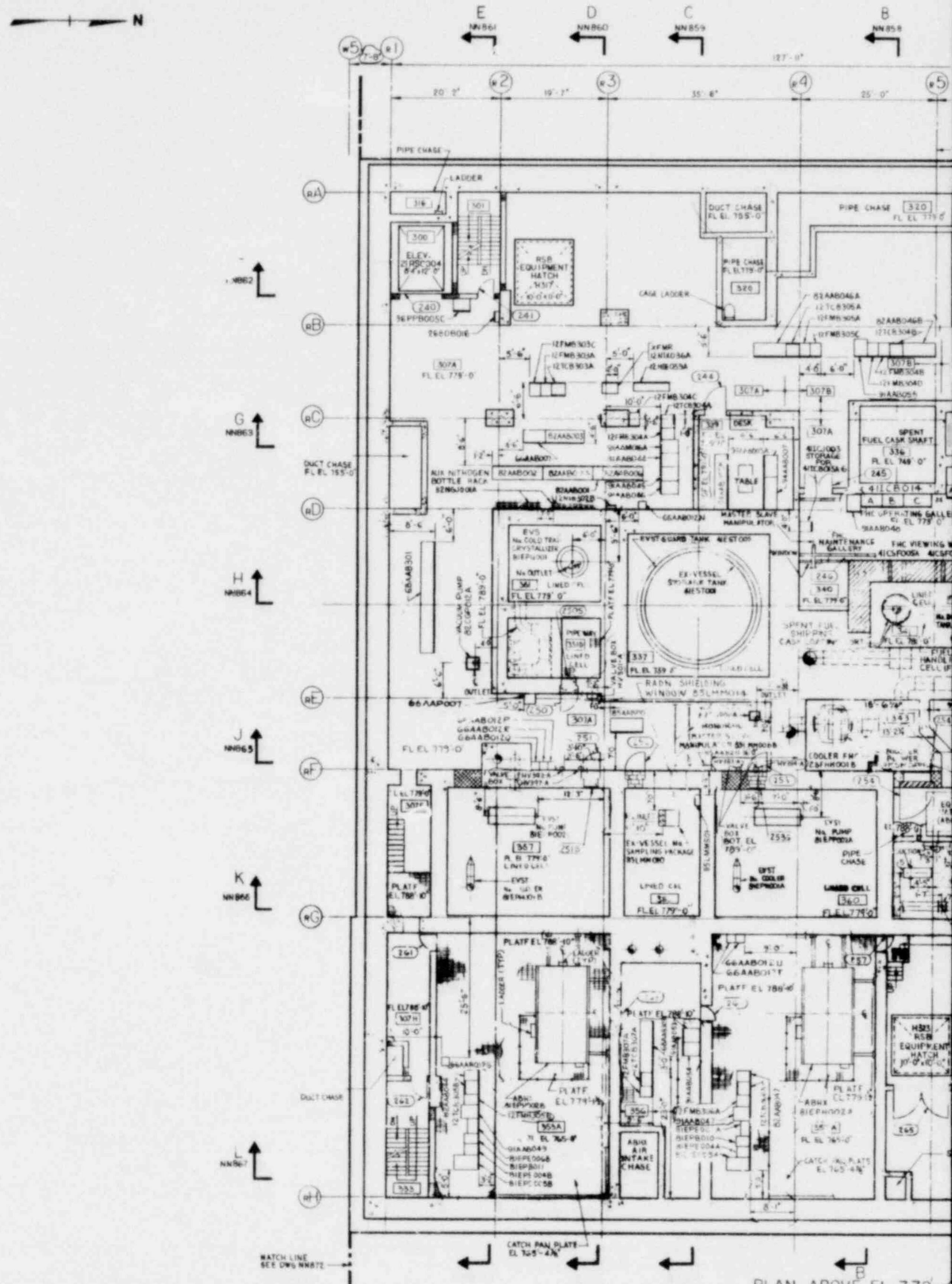

PLAN ABOVE EL 779'-0"

NN853-13

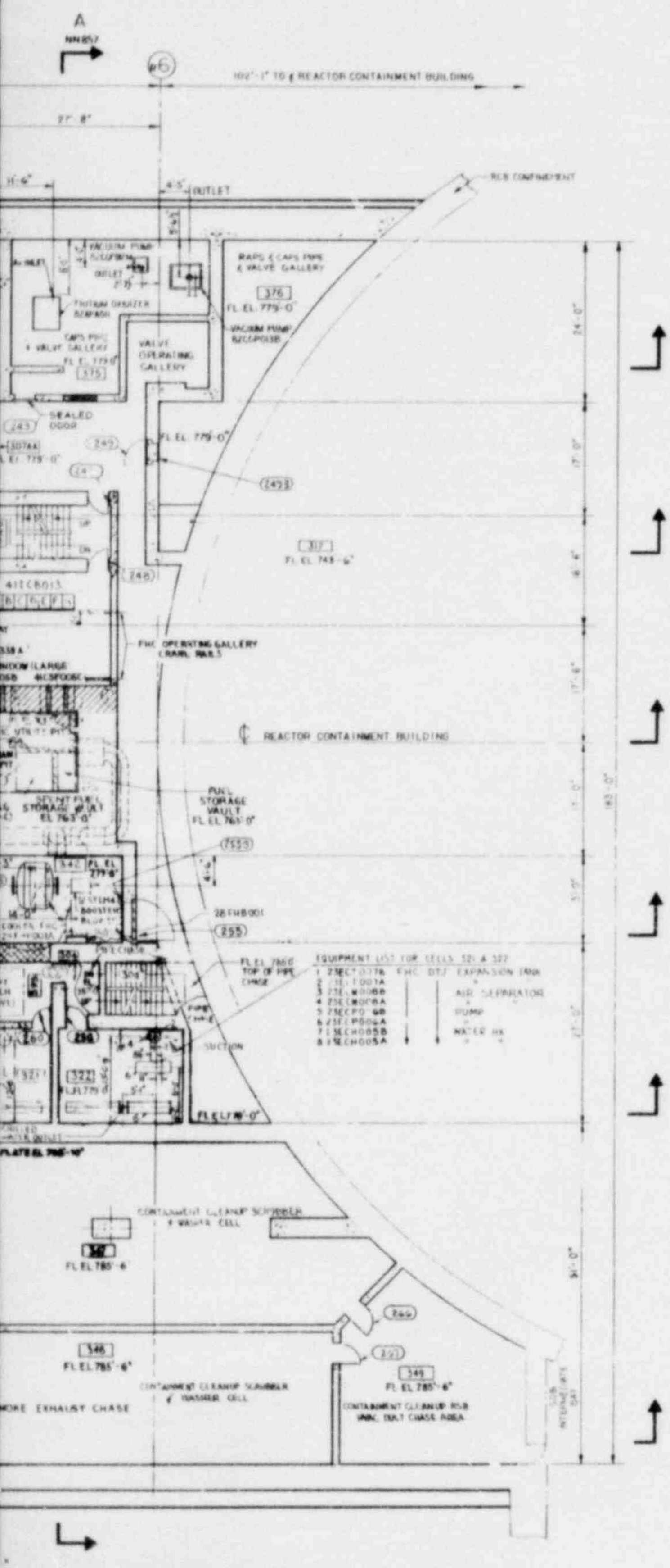

REFERENCE DRAWINGS

1. SEE REFERENCE DWGS - DWG NN850

GRAPHIC SCALE

KEY PLAN

Figure 1.2-24
General Arrangement
Reactor Service Building
El. 779'-0"

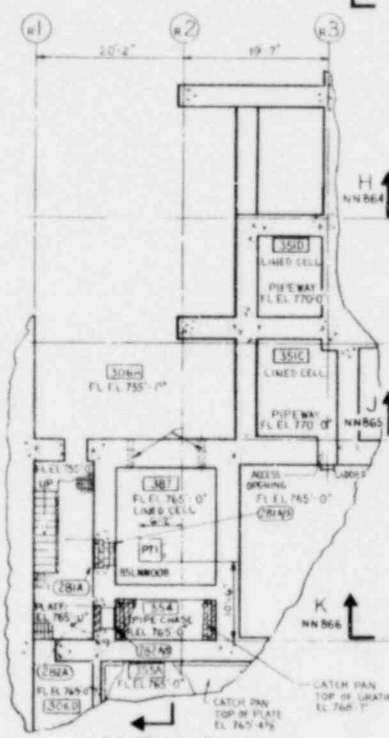

PARTIAL PLAN
ABOVE EL765-0" & EL770-0"

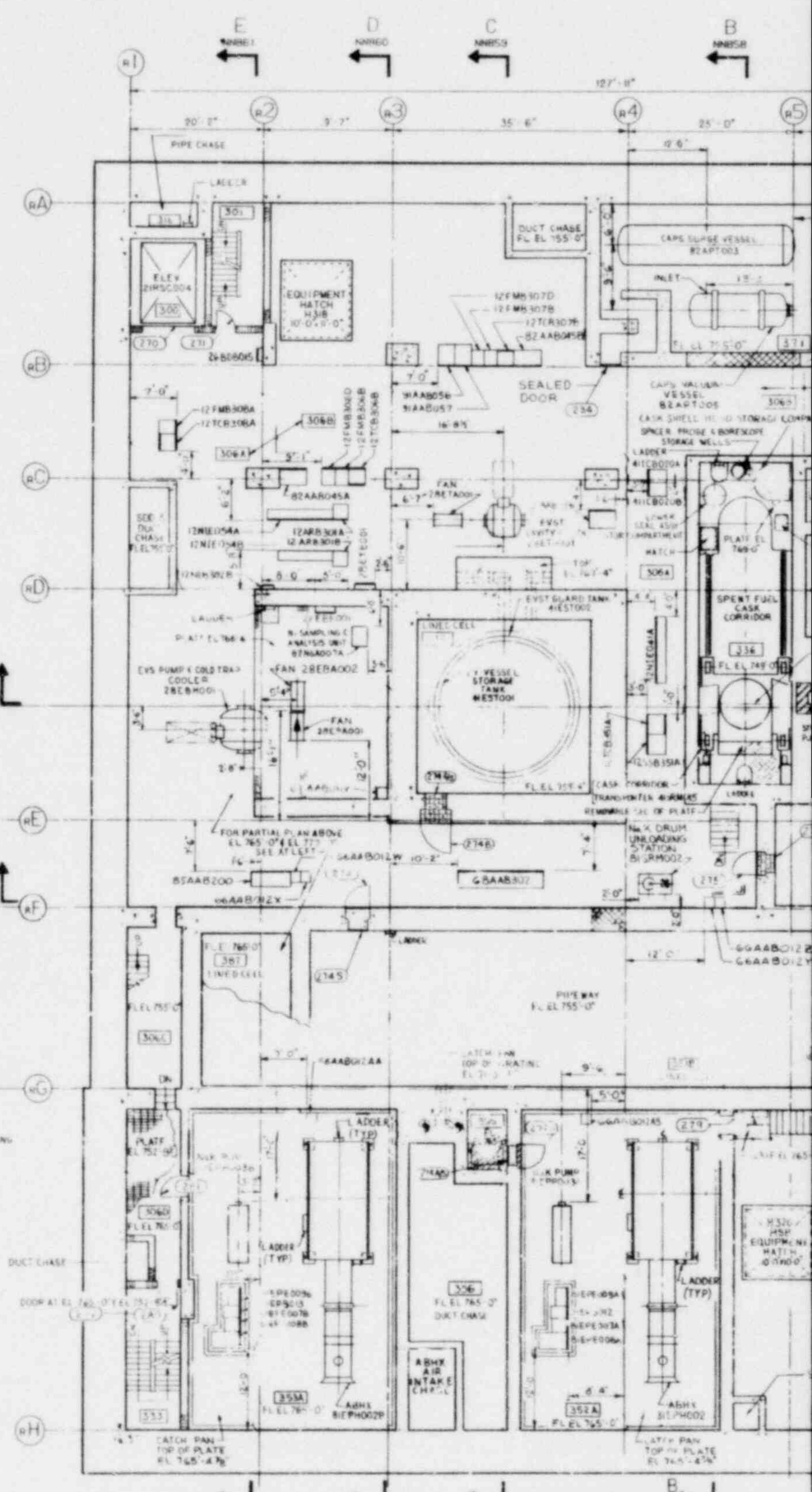

PLAN ABOVE EL. 755'-

NN854-13

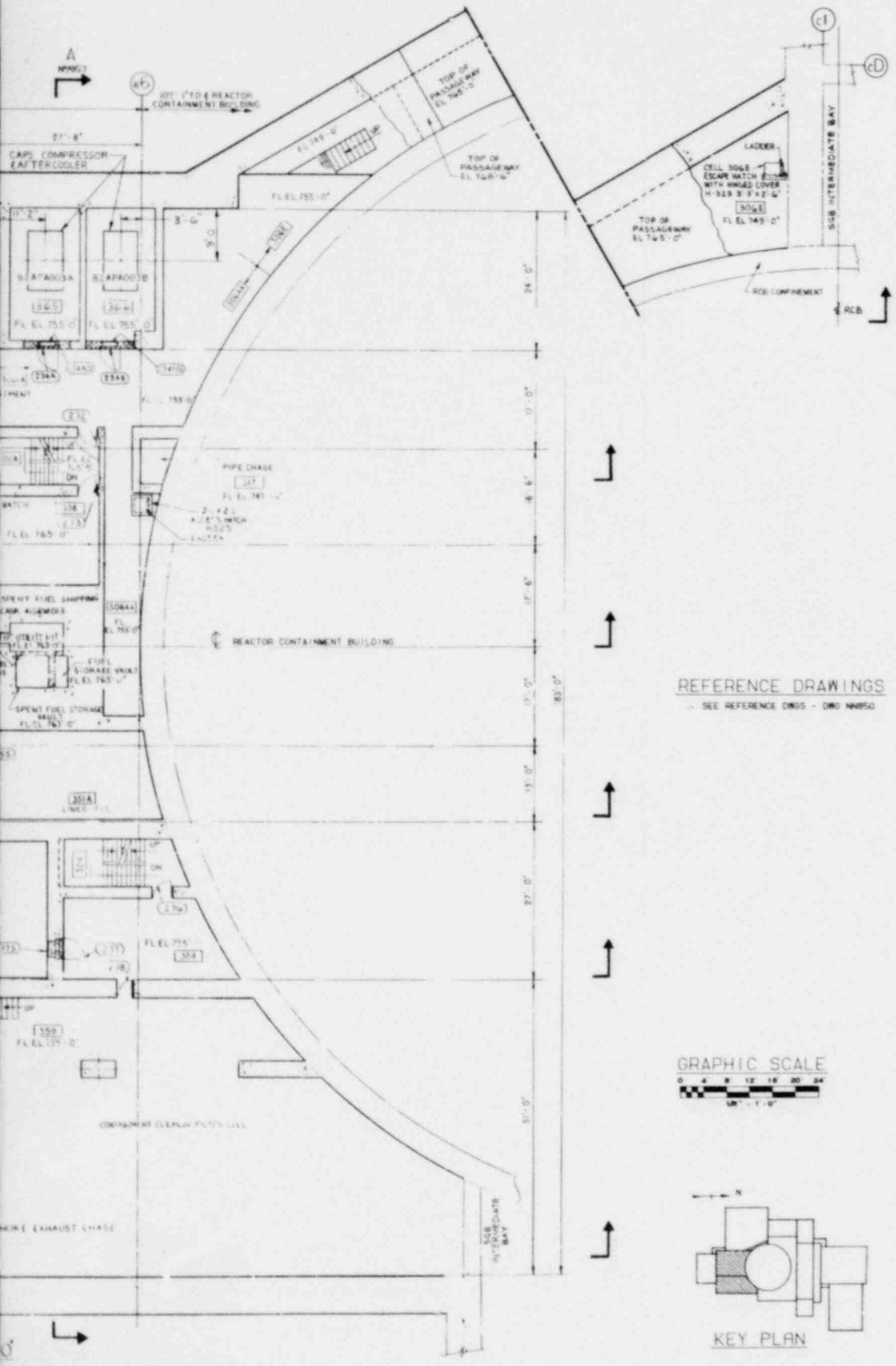

Figure 1.2-25
General Arrangement
Reactor Service Building
El. 755'-0"

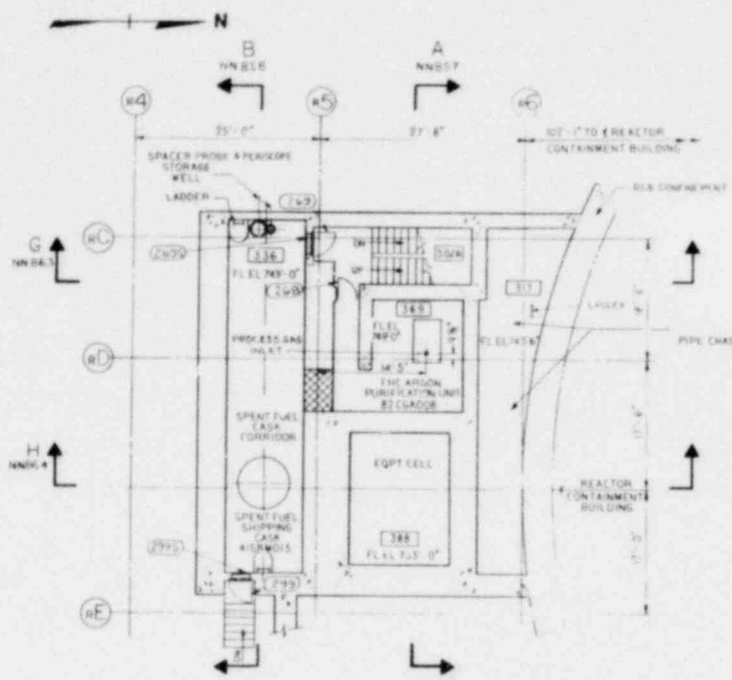

PARTIAL PLAN ABOVE EL 749-0"

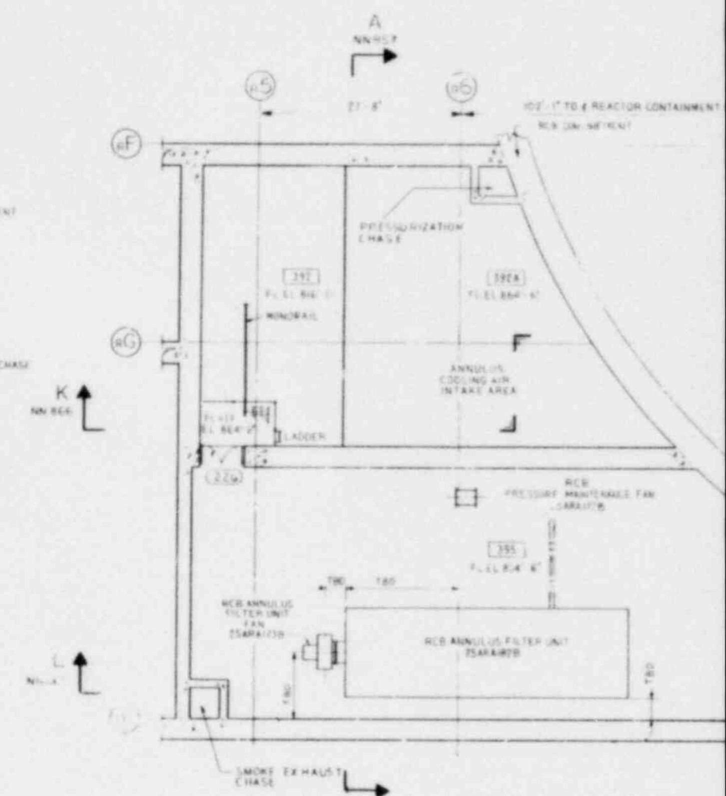

PARTIAL PLAN ABOVE EL 864-6"

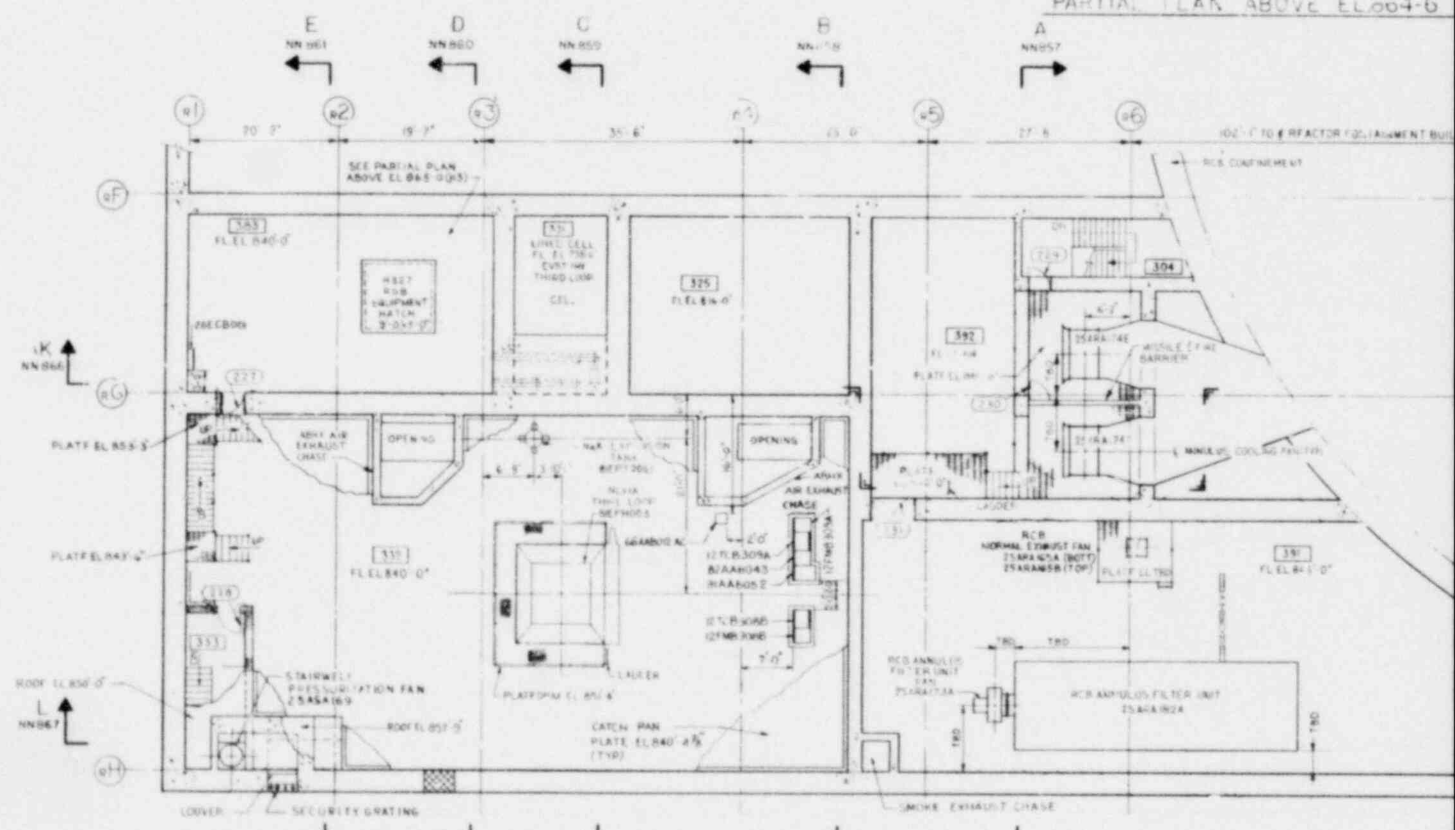

PARTIAL PLAN ABOVE EL 840'-0"

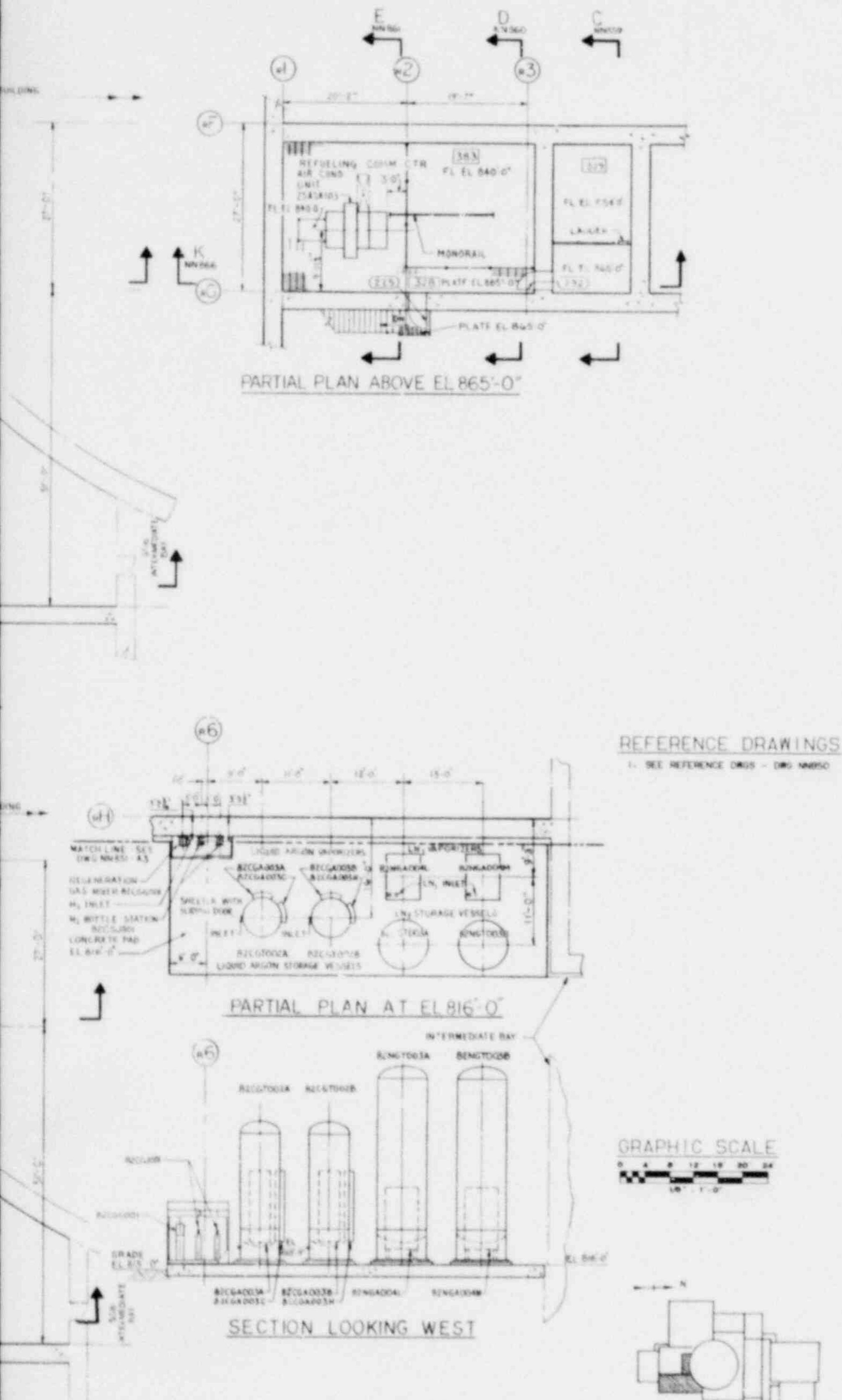

Figure 1.2-26
General Arrangement
Reactor Service Building
Above El. 749'-0", El. 840'-0"
and 864'-6"

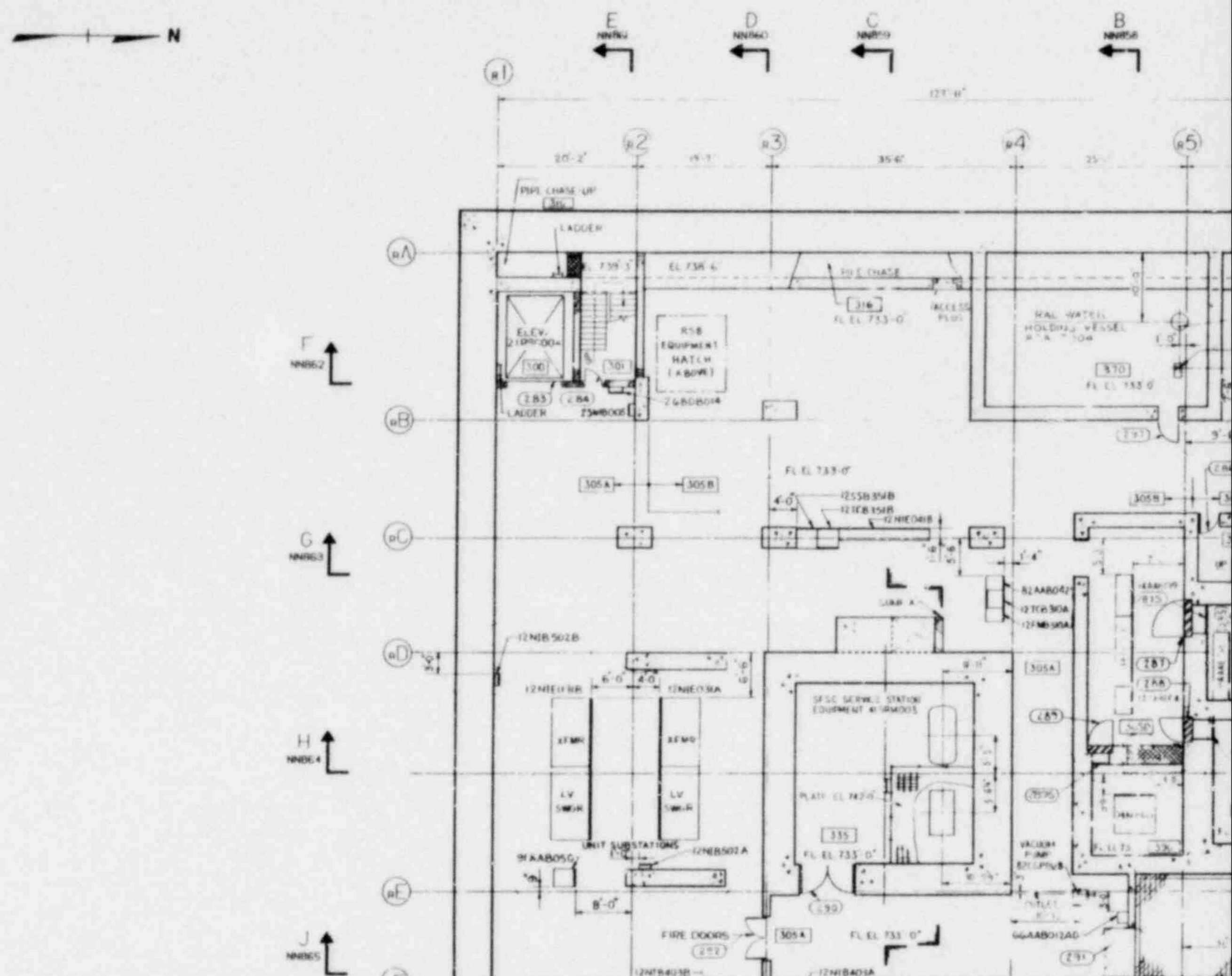

PLAN ABOVE EL 733'-0"

NN856-12

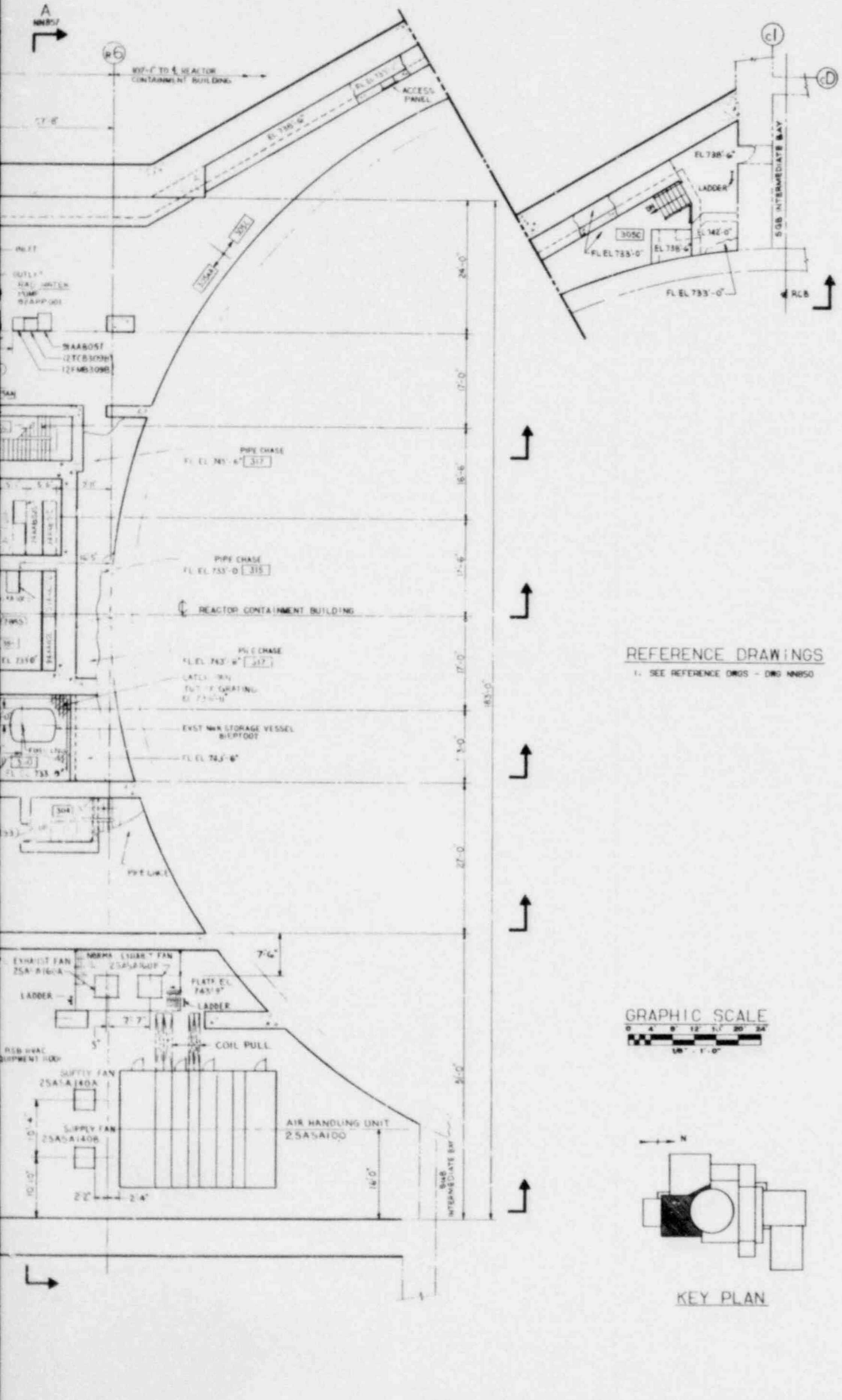

Figure 1.2-27
General Arrangement
Reactor Service Building
El. 733'-0"

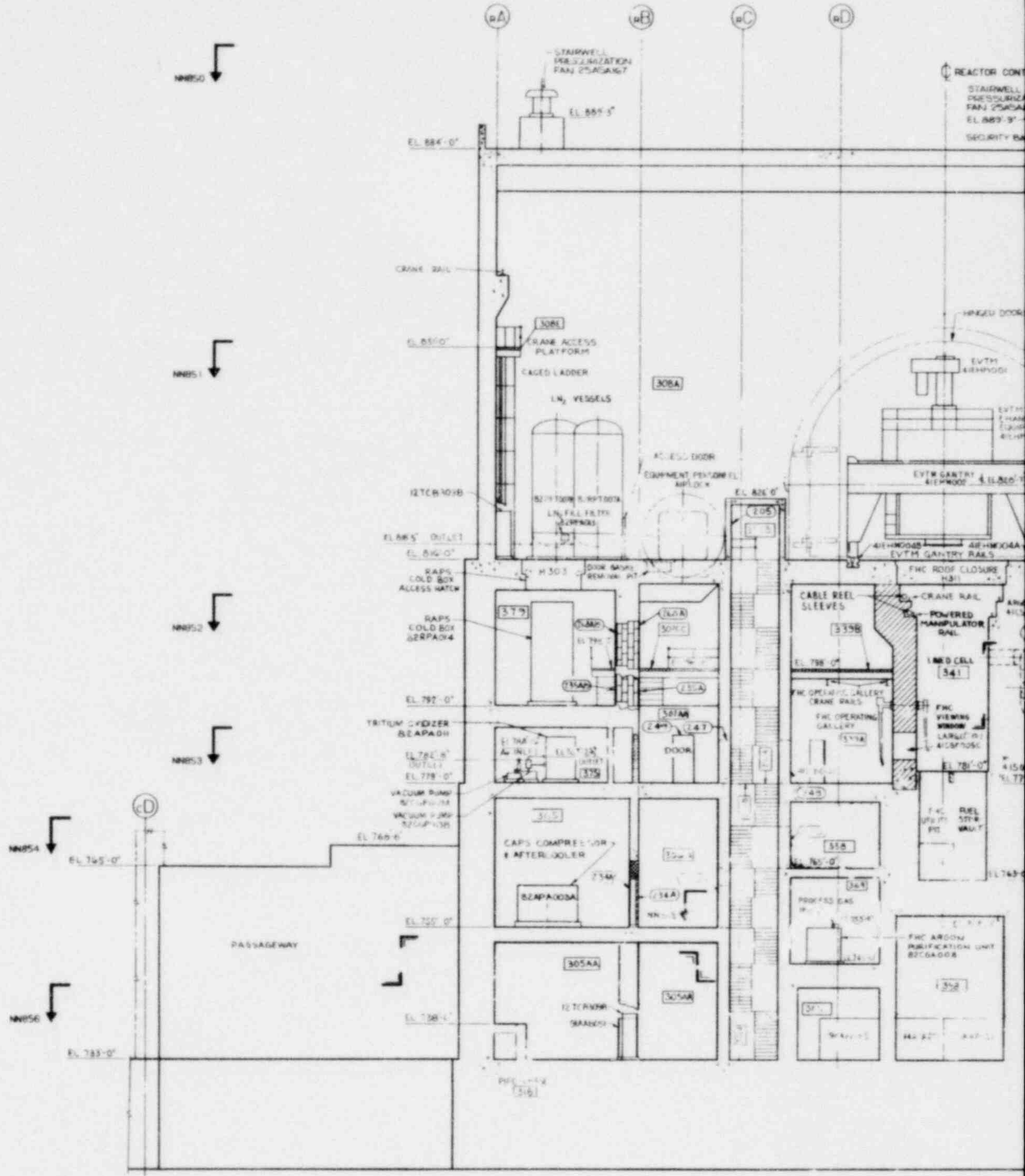

STAIRWELL PRESSURIZATION FAN 25ASA167
CRANE RAIL
CRANE ACCESS PLATFORM
CAGED LADDER
LN2 VESSELS
308A
CABLE REEL SLEEVES
POWERED MANIPULATOR RAIL
PASSAGEWAY
CAPS COMPRESSOR & AFTERCOOLER
82APA003A
RAPS COLD BOX 82RPA014
TRITIUM OXIDIZER 82APA011
SECTION A-A

NN857-13

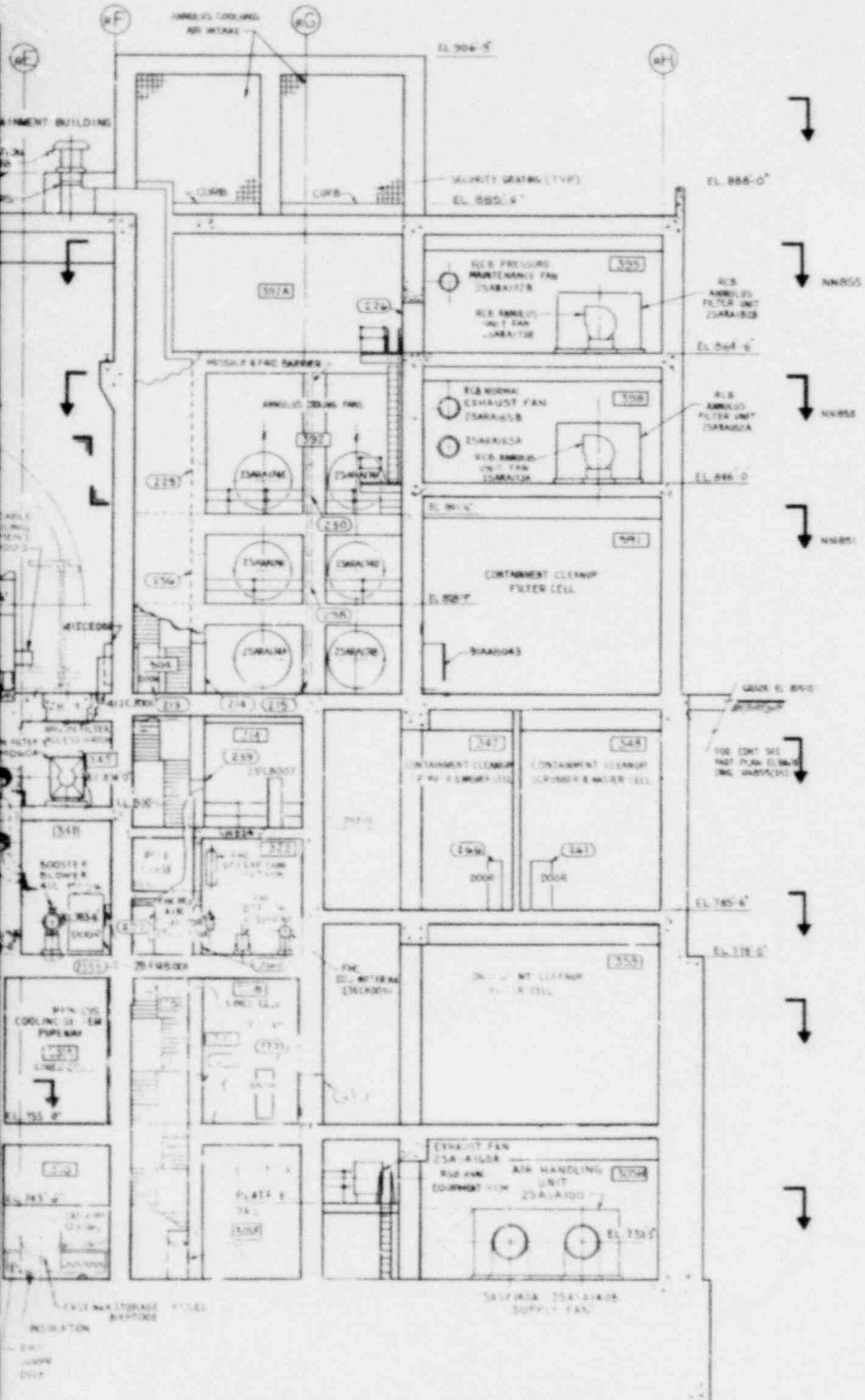

REFERENCE DRAWINGS

1. SEE REFERENCE DWGS - DWG NN850

GRAPHIC SCALE

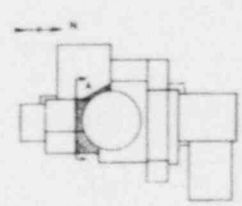

KEY PLAN

Figure 1.2-28
General Arrangement
Reactor Service Building
Section A-A

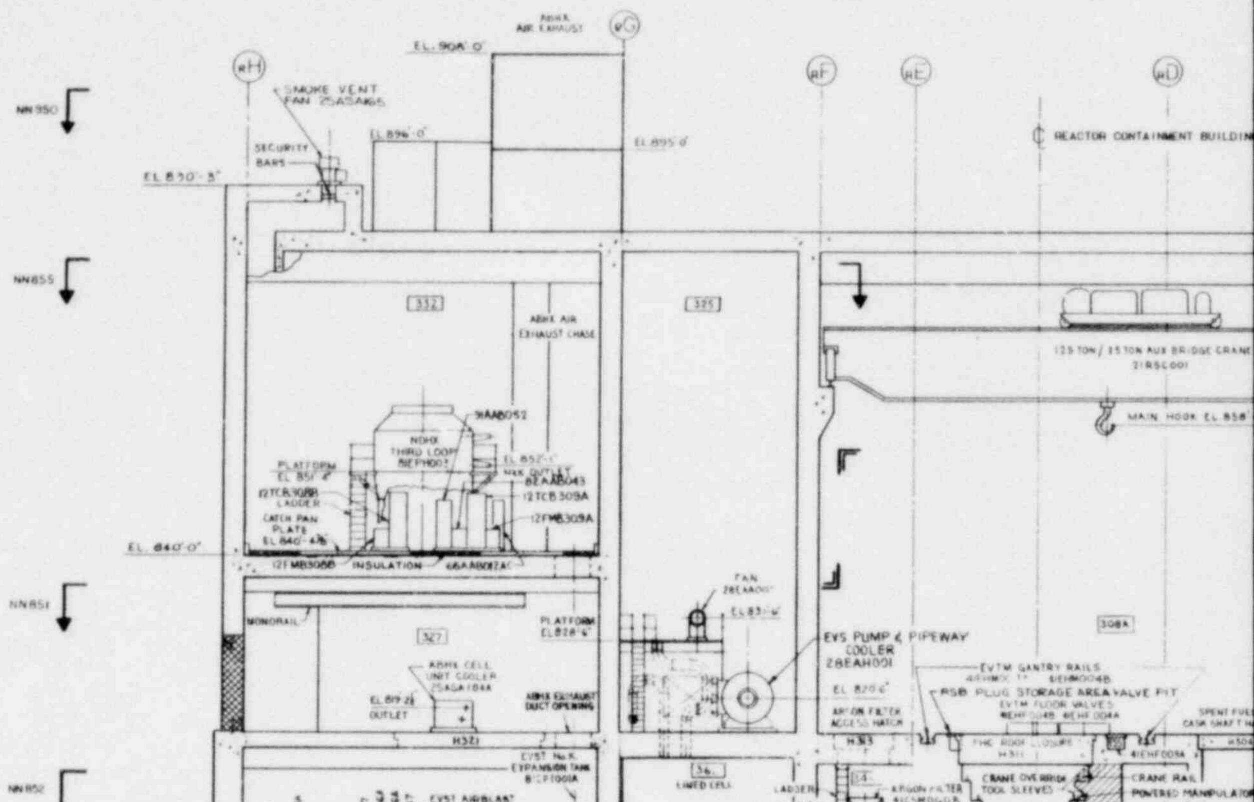

SECTION B-B

NN858-13

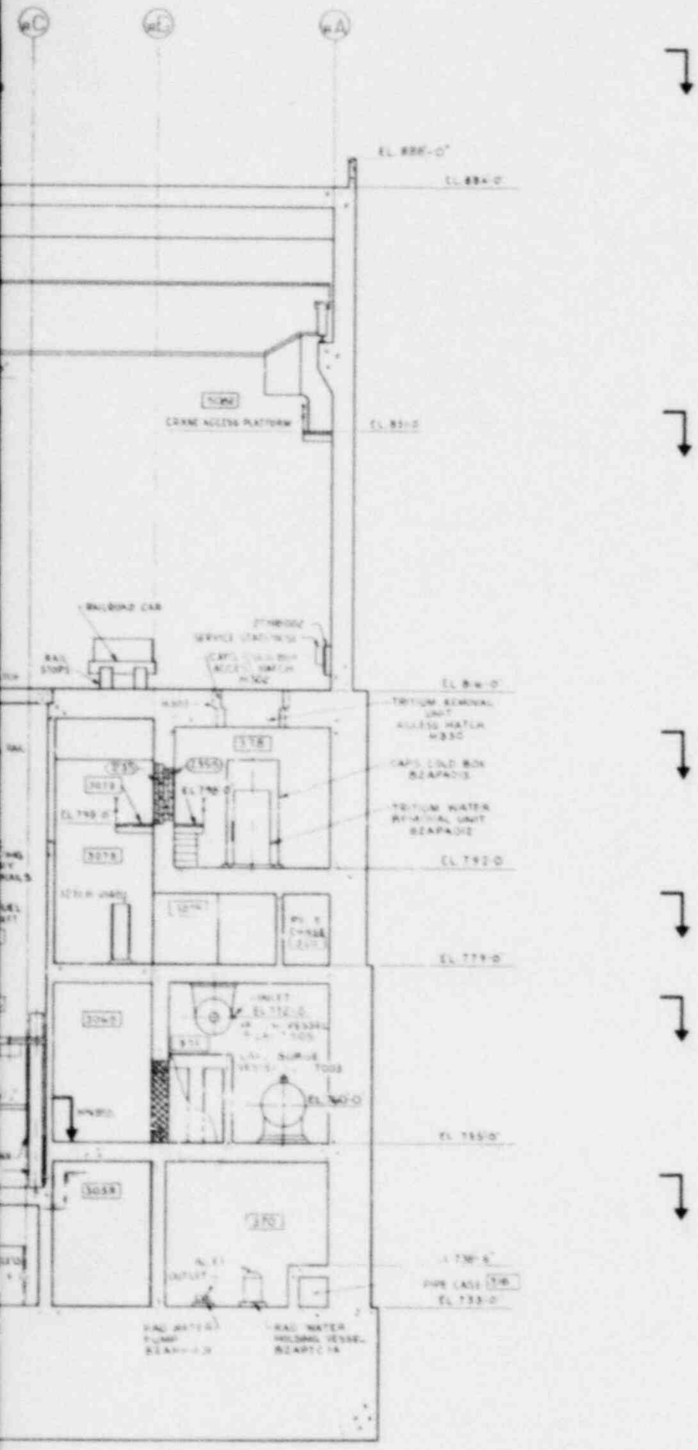

REFERENCE DRAWINGS

GRAPHIC SCALE

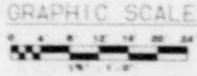

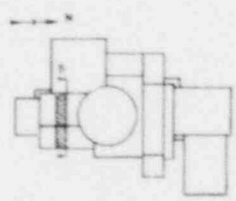

KEY PLAN

Figure 1.2-29
General Arrangement
Reactor Service Building
Section B-B

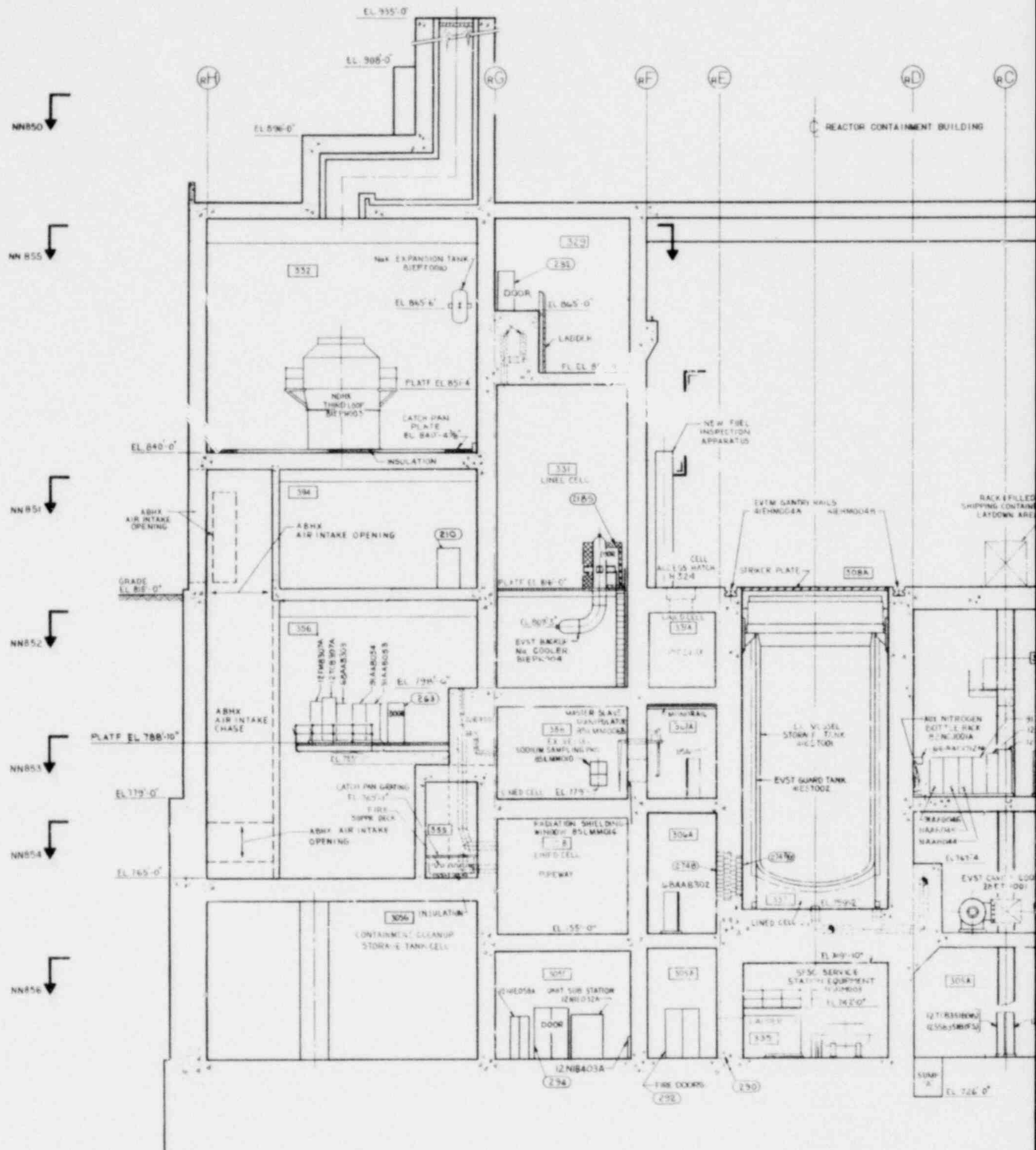

SECTION C-C

NN859-13

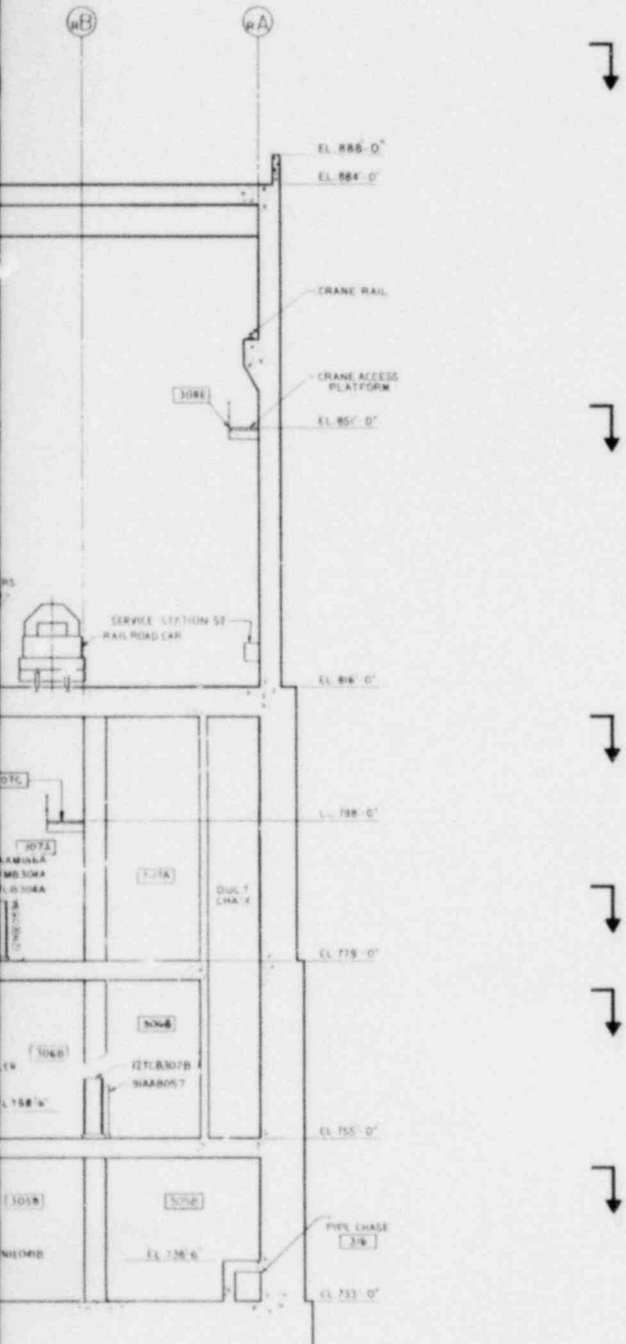

REFERENCE DRAWINGS

1. SEE REFERENCE DWGS - DWG NN850

GRAPHIC SCALE

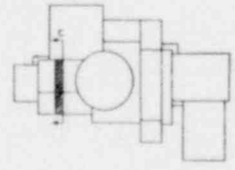

KEY PLAN

Figure 1.2-30
General Arrangement
Reactor Service Building
Section C-C

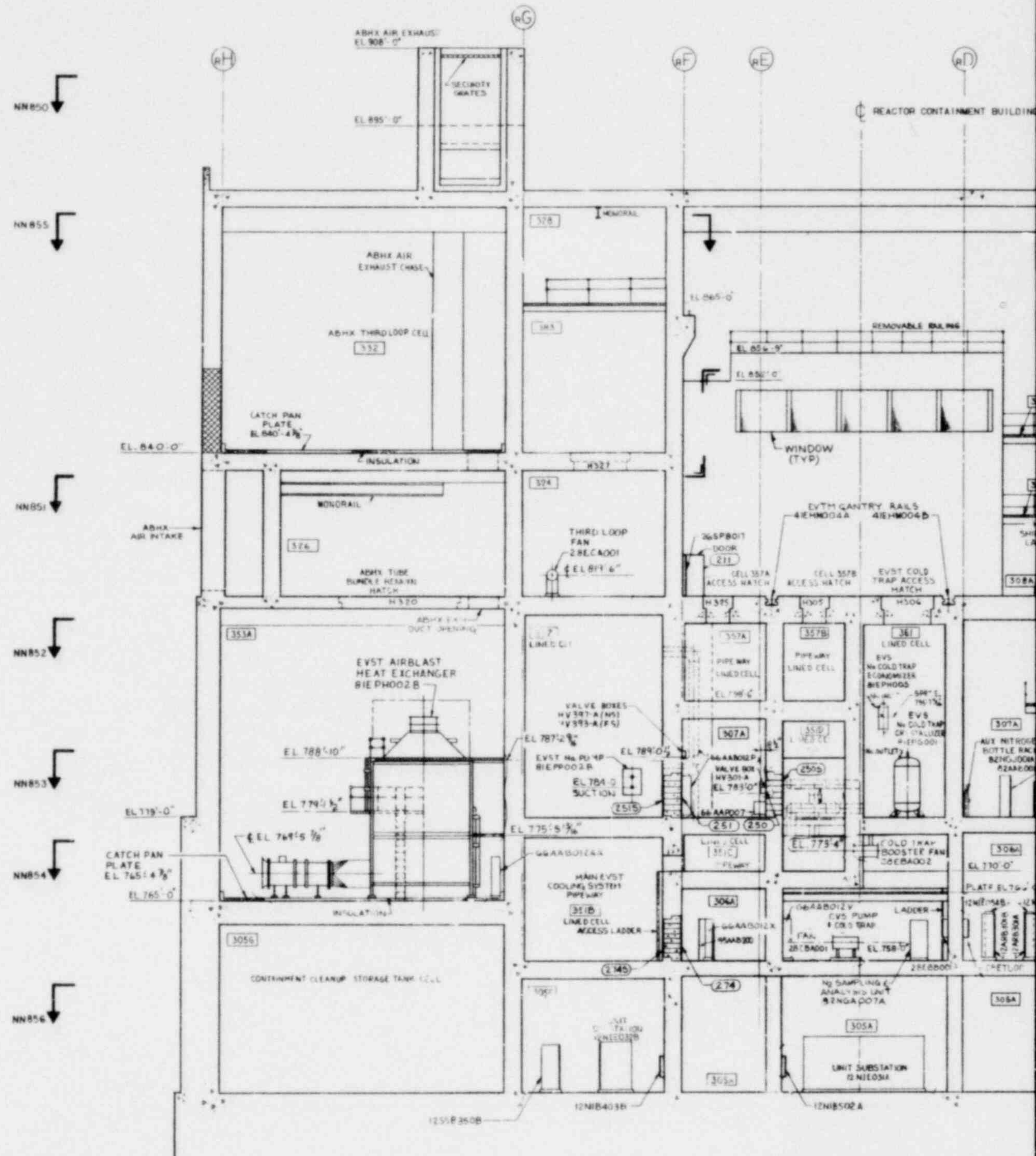

SECTION D-D

NN860-13

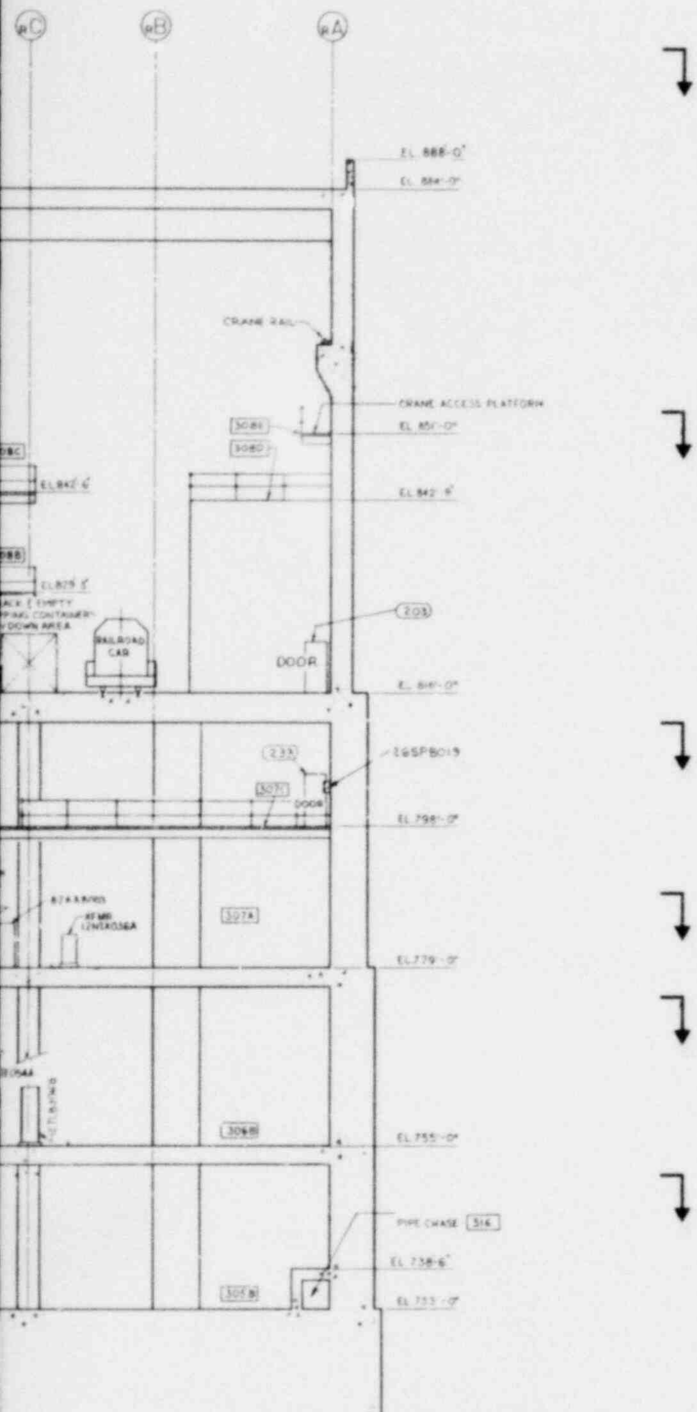

REFERENCE DRAWINGS

1. SEE REFERENCE DWGS - DWG NN850

GRAPHIC SCALE

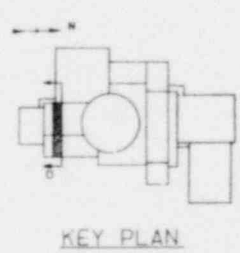

KEY PLAN

Figure 1.2-31
General Arrangement
Reactor Service Building
Section D-D

Amend. 56
Aug. 1980

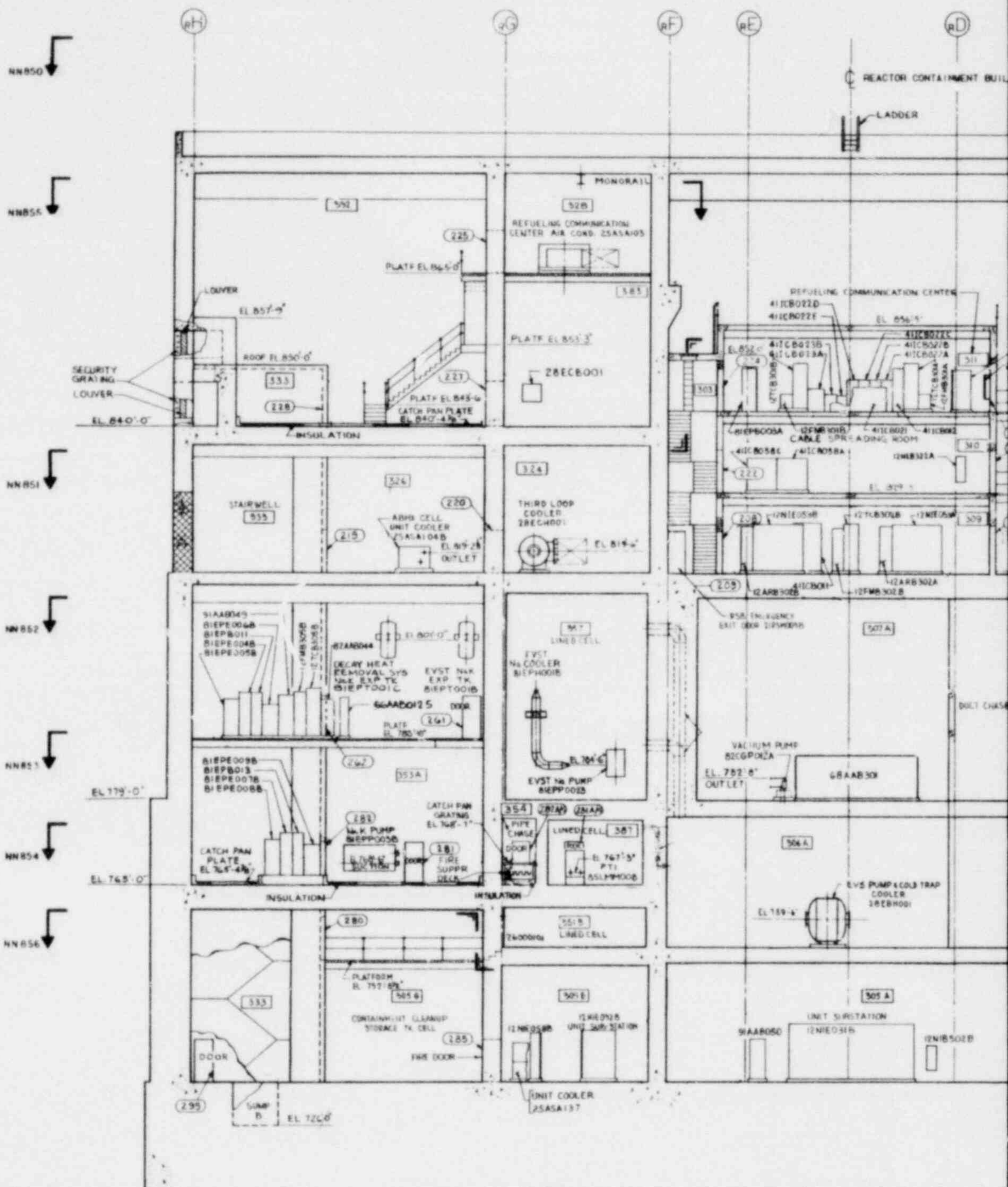

REACTOR CONTAINMENT BUIL
LADDER
MONORAIL
REFUELING COMMUNICATION CENTER AIR COND. 25ASA105
PLATF EL 865'-0"
LOUVER
SECURITY GRATING
LOUVER
ROOF EL 850'-0"
PLATF EL 853'-3"
28ECB001
REFUELING COMMUNICATION CENTER
CABLE SPREADING ROOM
EL 840'-0"
INSULATION
STAIRWELL
THIRD LOOP COOLER 28ECH001
OUTLET
DECAY HEAT REMOVAL SYS NaK EXP TK 81EPT001C
EVST NaK EXP TK 81EPT001B
LINED CELL
EVST Na COOLER 81EPH001B
VACUUM PUMP
OUTLET
DUCT CHASE
EVST Na PUMP 81EPP001B
EL 779'-0"
CATCH PAN GRATING
NaK PUMP 81EPP005B
FIRE SUPPR DECK
PIPE CHASE
DOOR
LINED CELL
CATCH PAN PLATE
EL 765'-0"
INSULATION
EVS PUMP & COLD TRAP COOLER 28EBH001
LINED CELL
PLATFORM
CONTAINMENT CLEANUP STORAGE TK CELL
FIRE DOOR
UNIT SUBSTATION
UNIT COOLER 25ASA137
DOOR
SUMP B
EL 720'-0"
NN850
NN855
NN851
NN852
NN853
NN854
NN856

SECTION E-E

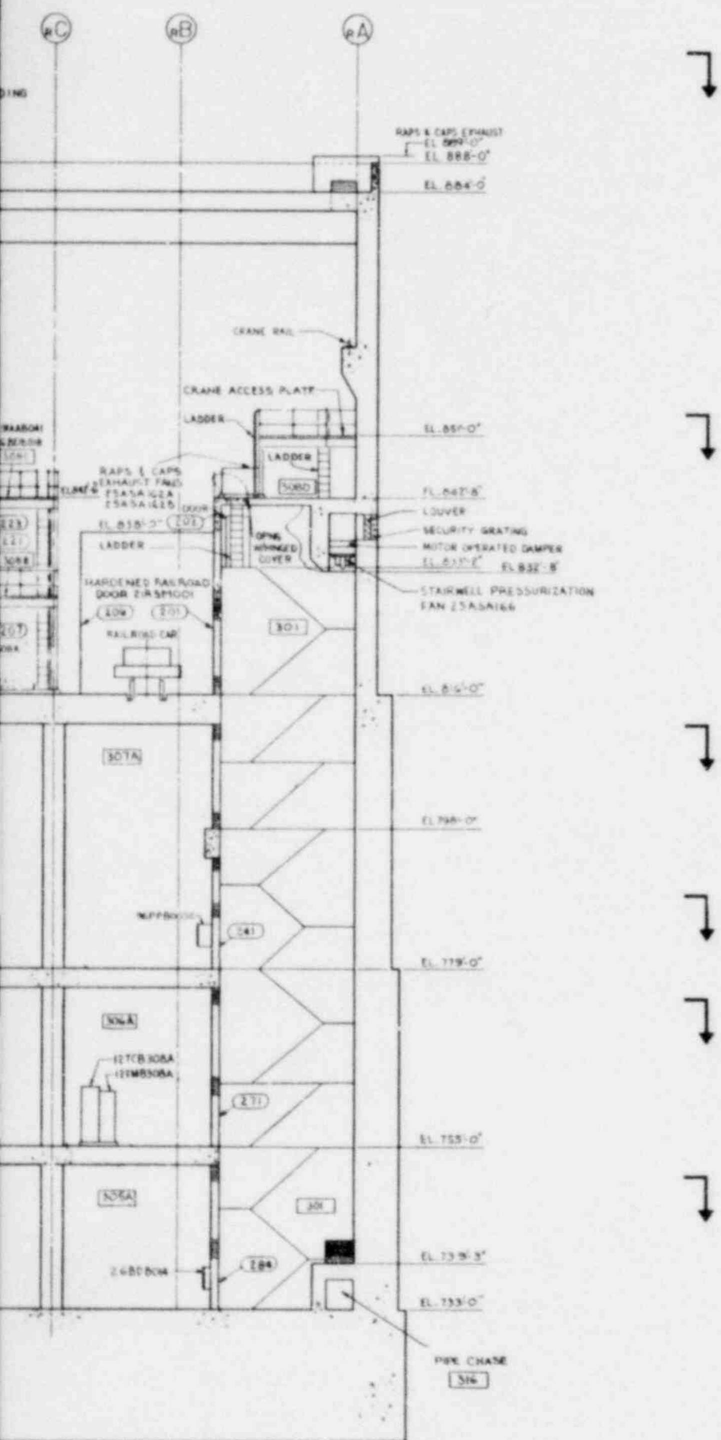

REFERENCE DRAWINGS

1. SEE REFERENCE DWGS - DWG NN850

GRAPHIC SCALE

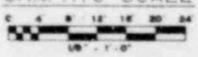

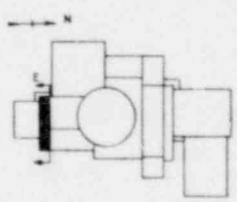

KEY PLAN

Figure 1.2-32
General Arrangement
Reactor Service Building
Section E-E

Amend. 56
Aug. 1980

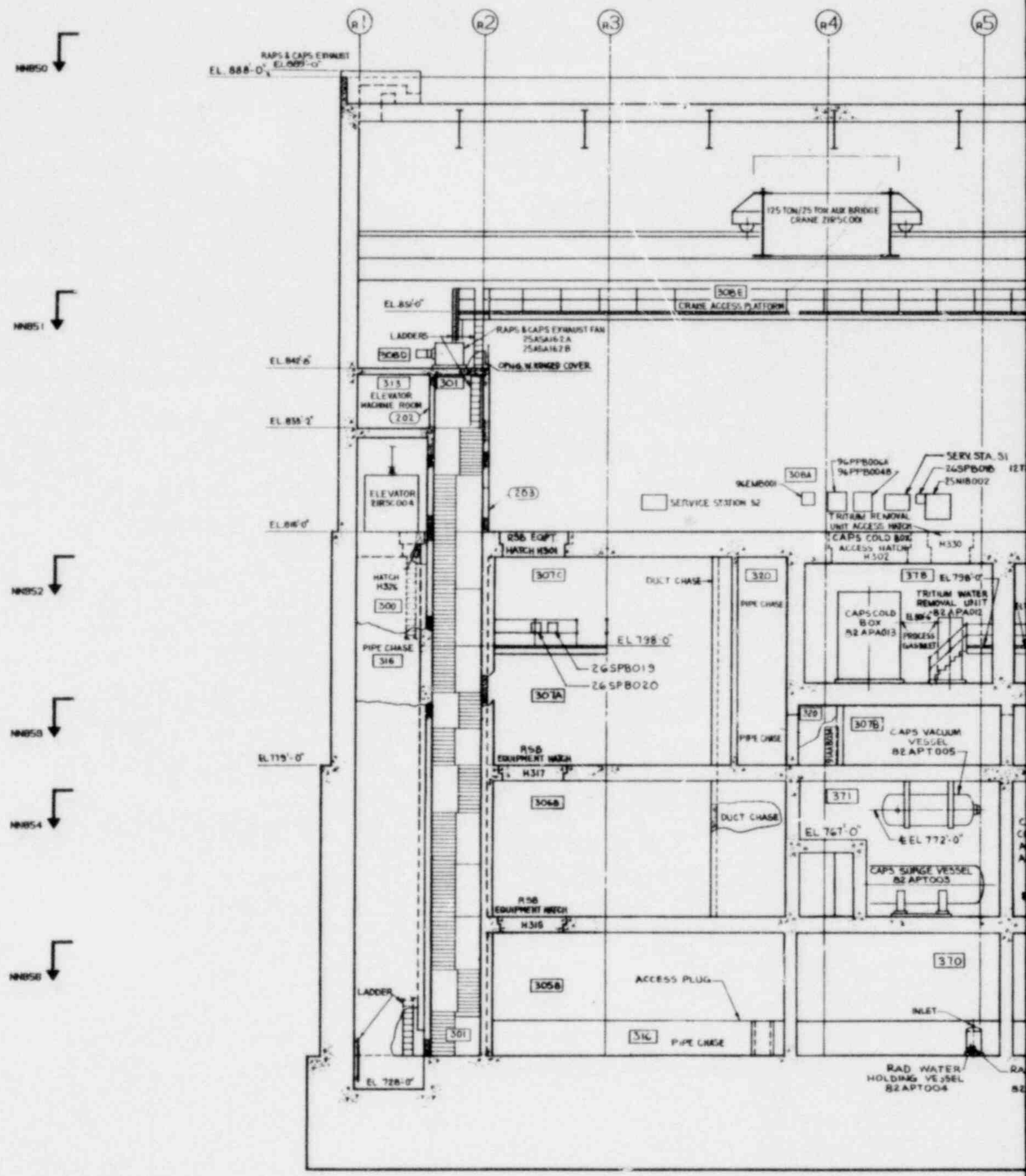

SECTION F-F

NN862-11

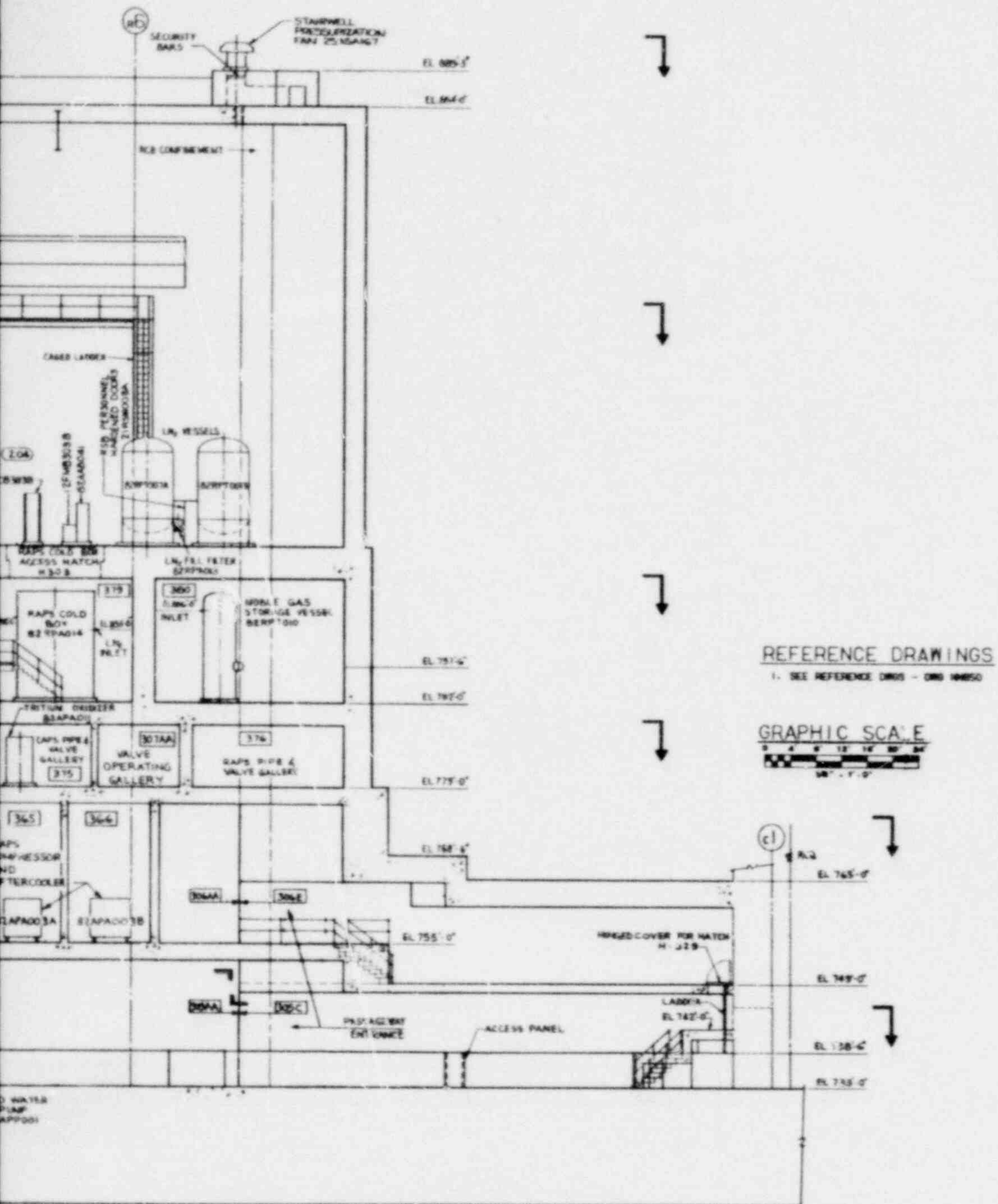

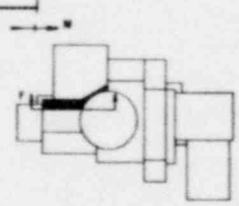

KEY PLAN

Figure 1.2-33
General Arrangement
Reactor Service Building
Section F-F

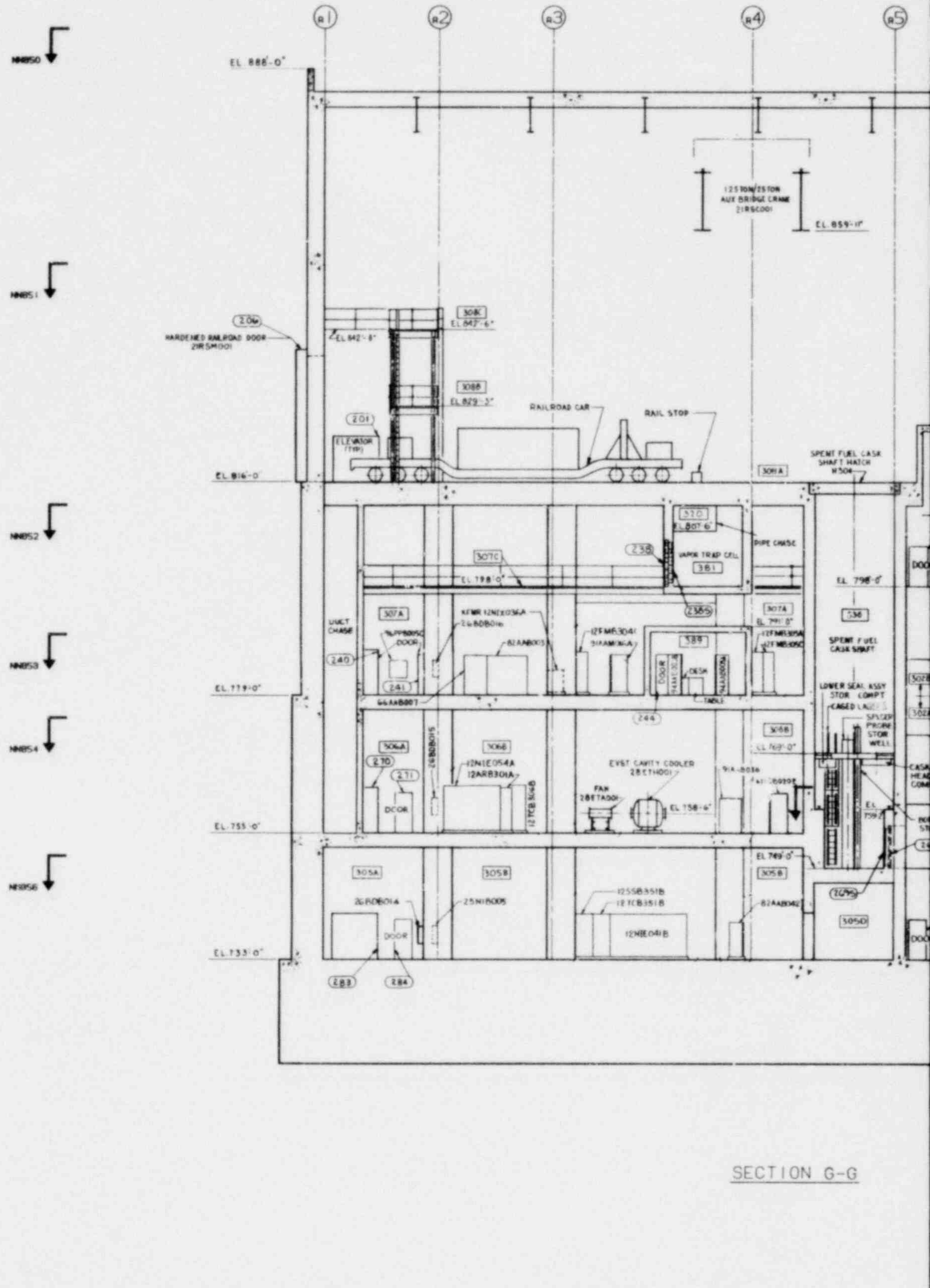
EL. 888'-0"
EL. 859-11"
HARDENED RAILROAD DOOR
RAILROAD CAR
RAIL STOP
ELEVATOR (TYP)
EL. 816'-0"
SPENT FUEL CASK SHAFT HATCH
VAPOR TRAP CELL
PIPE CHASE
EL. 798'-0"
DUCT CHASE
SPENT FUEL CASK SHAFT
DOOR
DESK
TABLE
EL. 779'-0"
EVST CAVITY COOLER
FAN
DOOR
EL. 755'-0"
DOOR
EL. 733'-0"

SECTION G-G

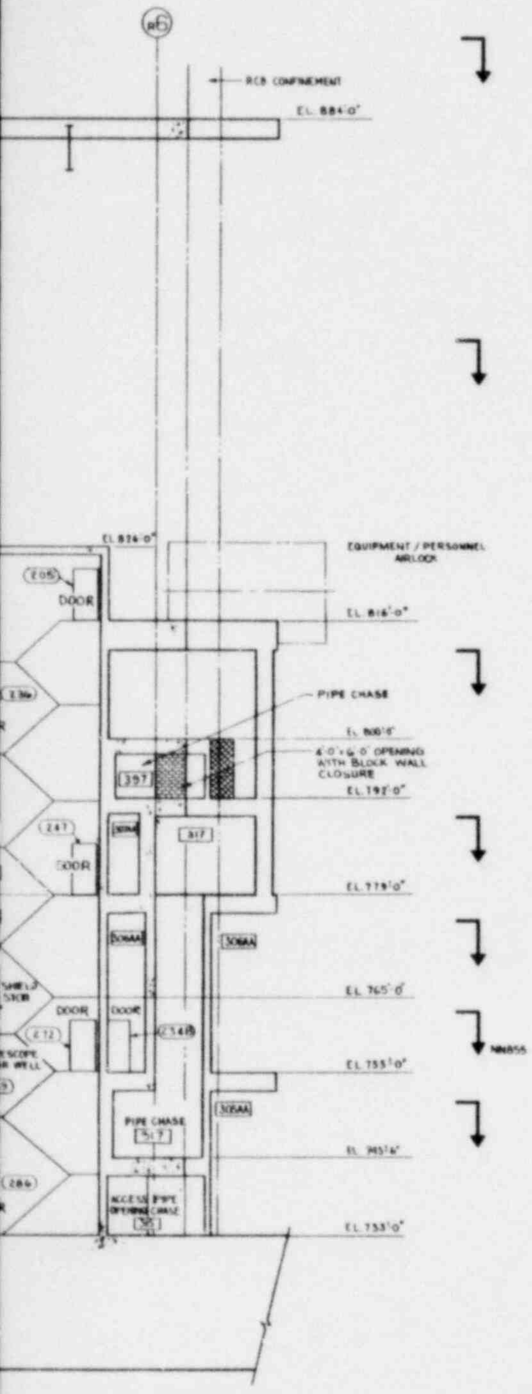

GRAPHIC SCALE

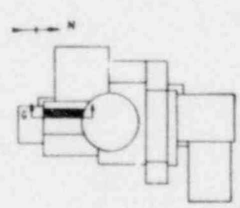

KEY PLAN

Figure 1.2-34
General Arrangement
Reactor Service Building
Section G-G

Amend. 56
Aug. 1980

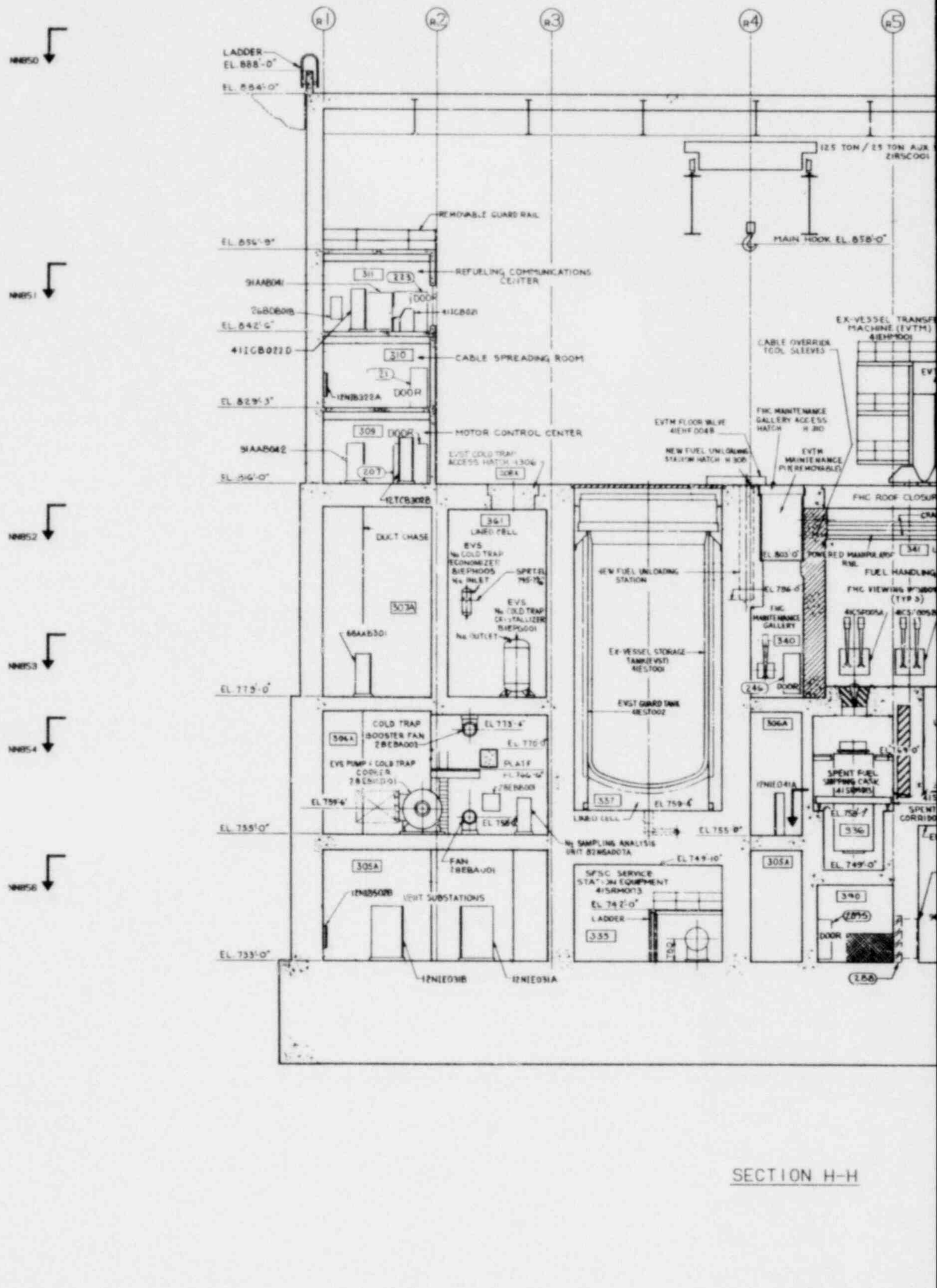

SECTION H-H

NN864-11

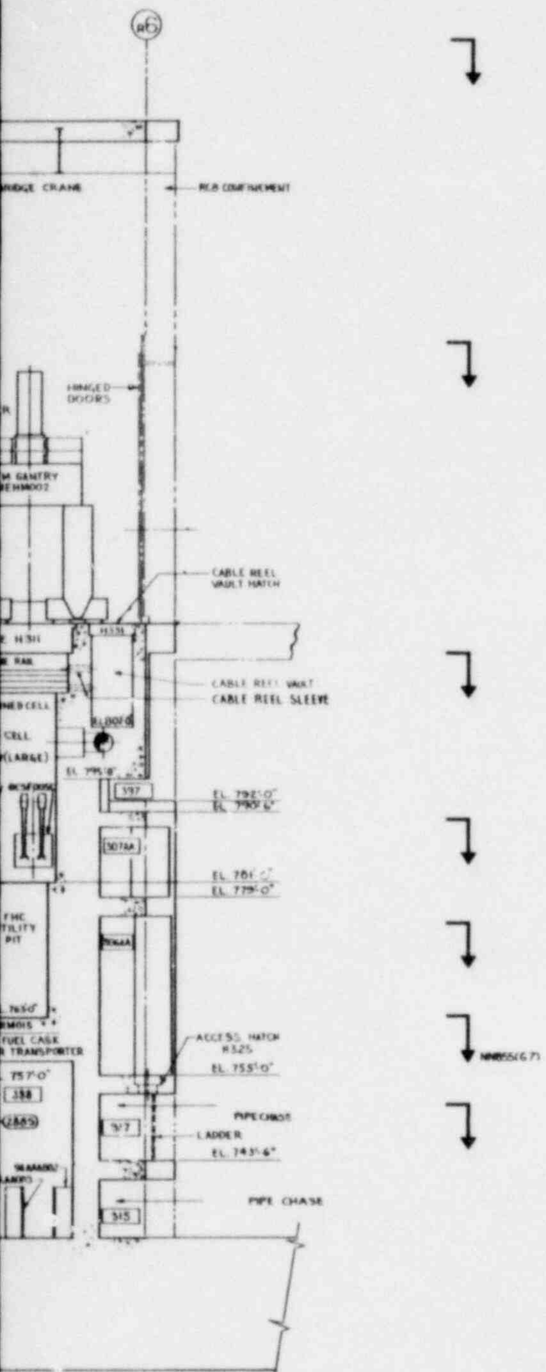

REFERENCE DRAWINGS

1. SEE REFERENCE DWGS - DWG NN850

GRAPHIC SCALE

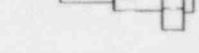

KEY PLAN

Figure 1.2-35
General Arrangement
Reactor Service Building
Section H-H

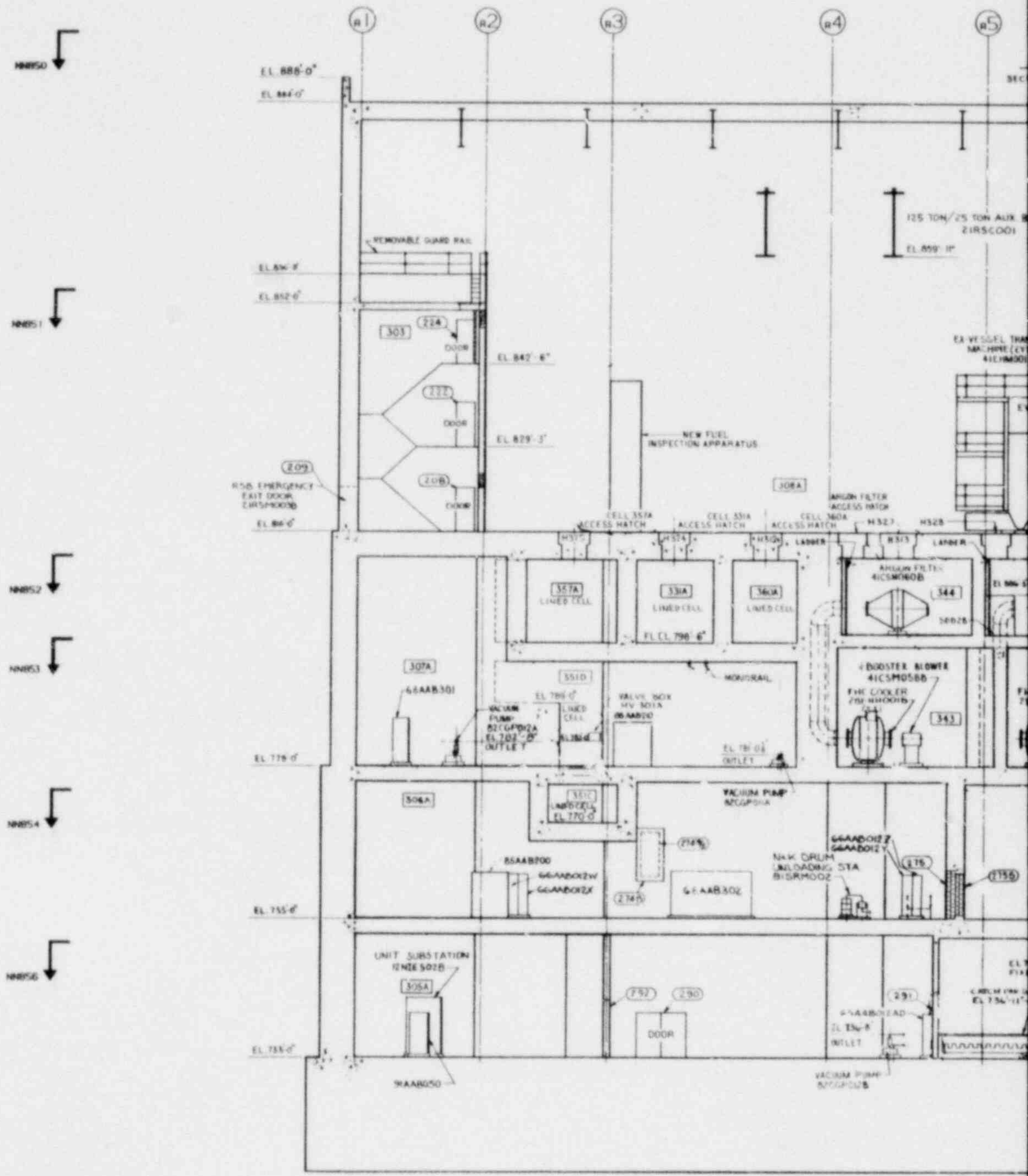

NN850
NN851
NN852
NN853
NN854
NN856
EL 888'-0"
EL 884'-0"
REMOVABLE GUARD RAIL
EL 852'-0"
EL 842'-6"
EL 829'-3"
RSB EMERGENCY EXIT DOOR
NEW FUEL INSPECTION APPARATUS
125 TON/25 TON AUX
21RSC001
EL 859'-11"
CELL 357A ACCESS HATCH
CELL 331A ACCESS HATCH
CELL 360A ACCESS HATCH
ARGON FILTER ACCESS HATCH
LADDER
LINED CELL
ARGON FILTER 41CSM060B
BOOSTER BLOWER 41CSM058B
MONORAIL
VALVE BOX
VACUUM PUMP 82CGP01A
66AAB301
66AAB302
85AAB200
N&K DRUM UNLOADING STA 81SRM002
EL 779'-0"
EL 755'-0"
EL 733'-0"
UNIT SUBSTATION
DOOR
91AAB050
VACUUM PUMP 82CGP02B

SECTION J-J

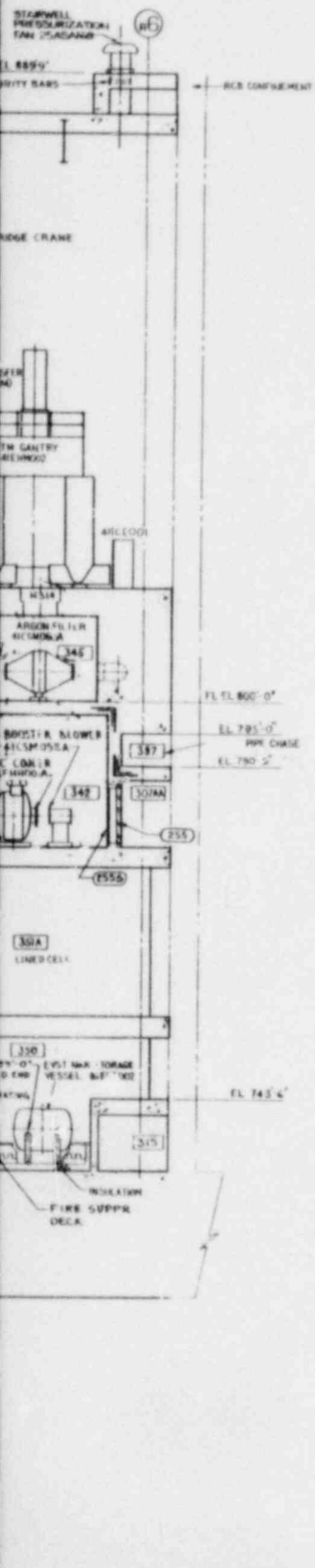

REFERENCE DRAWINGS

1. SEE REFERENCE DWGS - DWG NN850

GRAPHIC SCALE

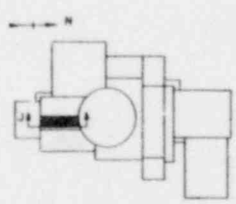

KEY PLAN

Figure 1.2-36
General Arrangement
Reactor Service Building
Section J-J

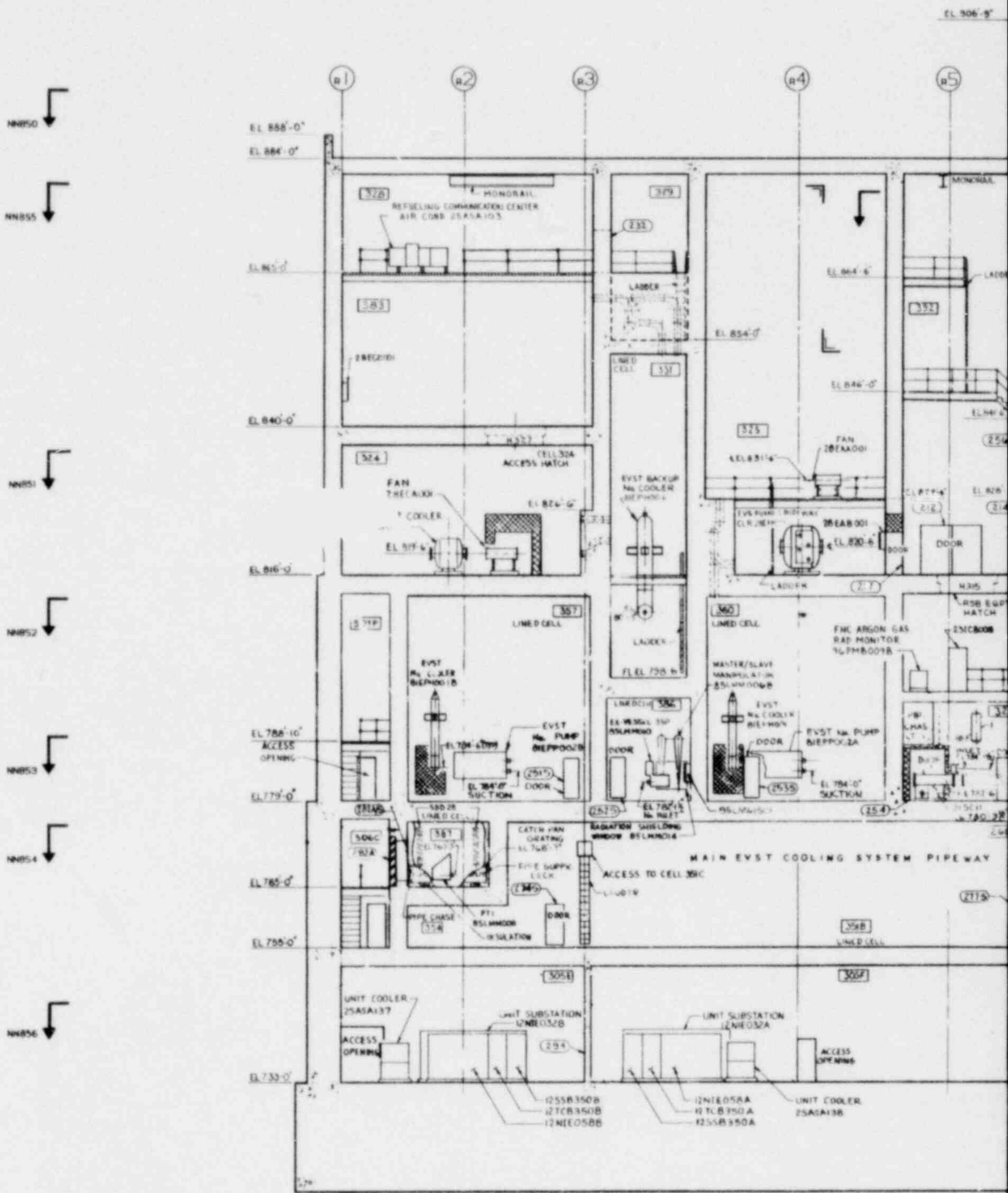
NN850
NN855
NN851
NN852
NN853
NN854
NN856
EL 888'-0"
EL 884'-0"
EL 865'-0"
EL 840'-0"
EL 816'-0"
EL 788'-10"
ACCESS OPENING
EL 779'-0"
EL 765'-0"
EL 755'-0"
EL 733'-0"
328
MONORAIL
REFUELING COMMUNICATION CENTER AIR COND 25ASA103
383
329
LADDER
EL 854'-0"
LINED CELL
331
EL 864'-6"
EL 846'-0"
325
FAN 28EAA001
324
CELL 32A ACCESS HATCH
FAN
EL 824'-6"
EVST BACKUP Na COOLER
DOOR
357
LINED CELL
360
LINED CELL
FHC ARGON GAS RAD MONITOR
LADDER
FL EL 798'-6"
MASTER/SLAVE MANIPULATOR
EVST Na COOLER
EVST Na PUMP
EVST Na PUMP 81EPP002A
DOOR
EL 784'-0" SUCTION
RADIATION SHIELDING WINDOW 85LMM014
MAIN EVST COOLING SYSTEM PIPEWAY
ACCESS TO CELL 351C
PIPE CHASE
INSULATION
DOOR
358
LINED CELL
305E
305F
UNIT COOLER 25ASA137
ACCESS OPENING
UNIT SUBSTATION 12NIE032B
UNIT SUBSTATION 12NIE032A
ACCESS OPENING
12SSB350B
12TCB350B
12NIE058B
12NIE058A
12TCB350A
12SSB350A
UNIT COOLER 25ASA138

SECTION K-K

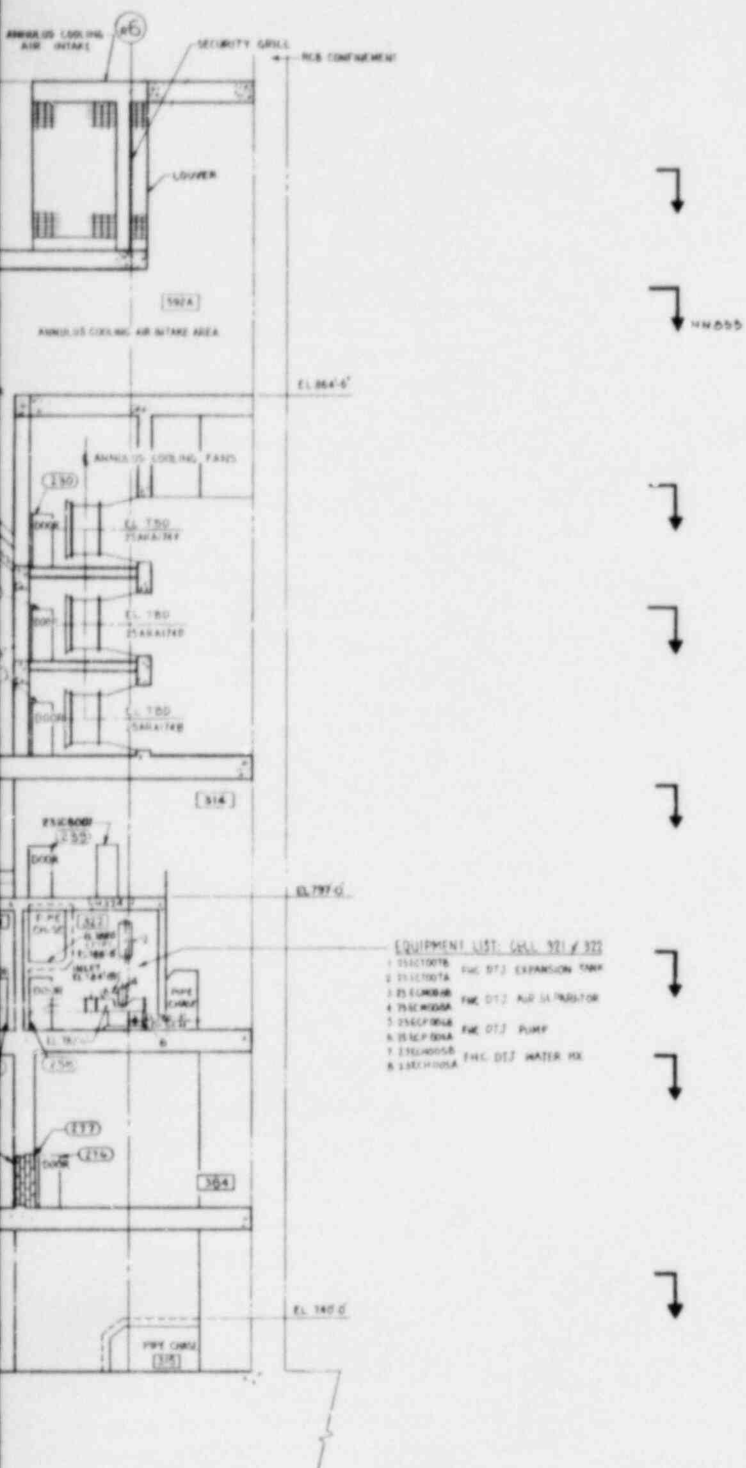

REFERENCE DRAWINGS

1. SEE REFERENCE DWGS - DWG NNR50

GRAPHIC SCALE

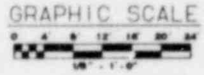

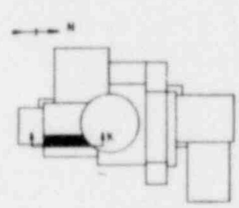

KEY PLAN

Figure 1.2-37
General Arrangement
Reactor Service Building
Section K-K

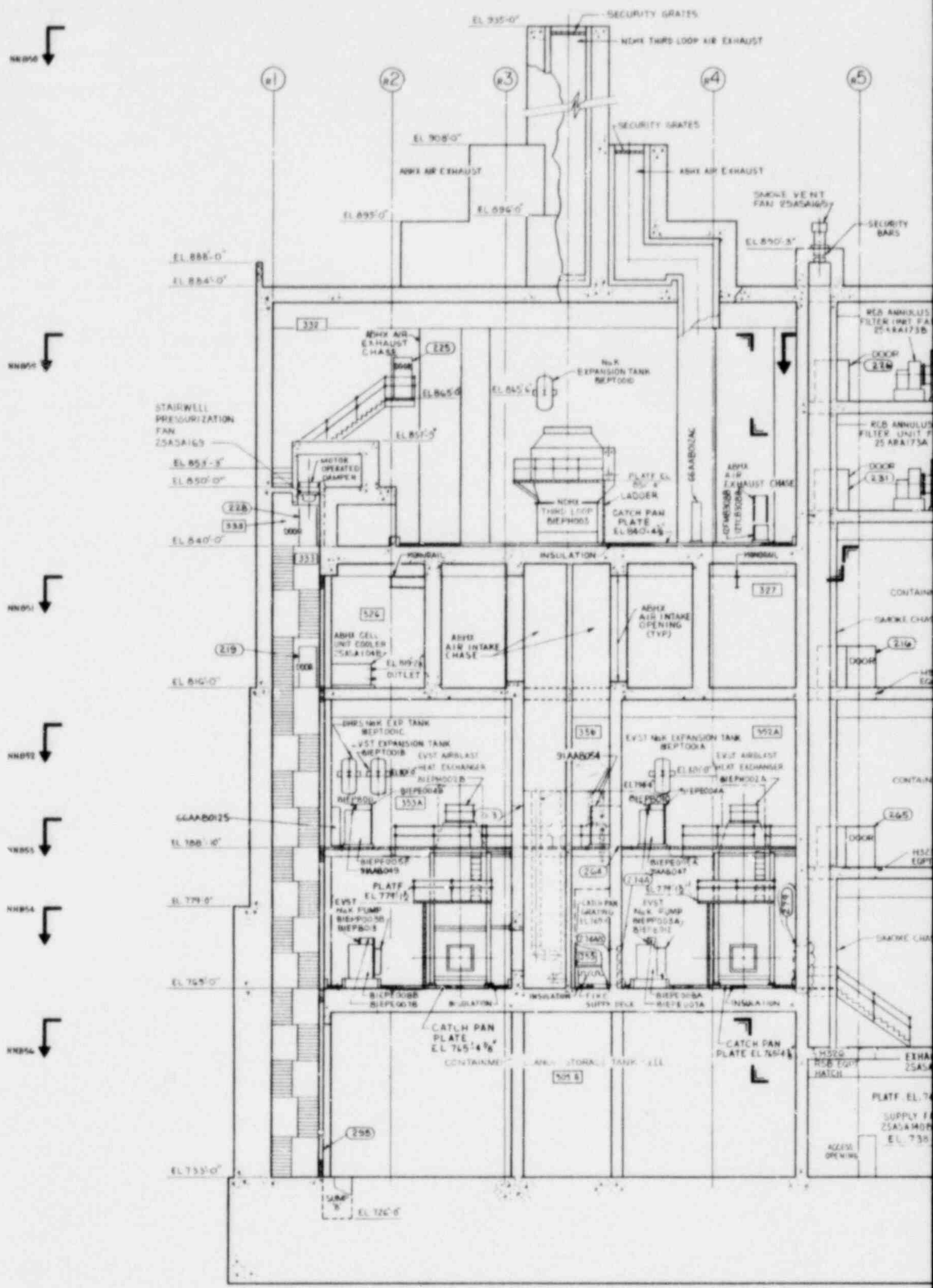

SECTION L-L

NN867-9

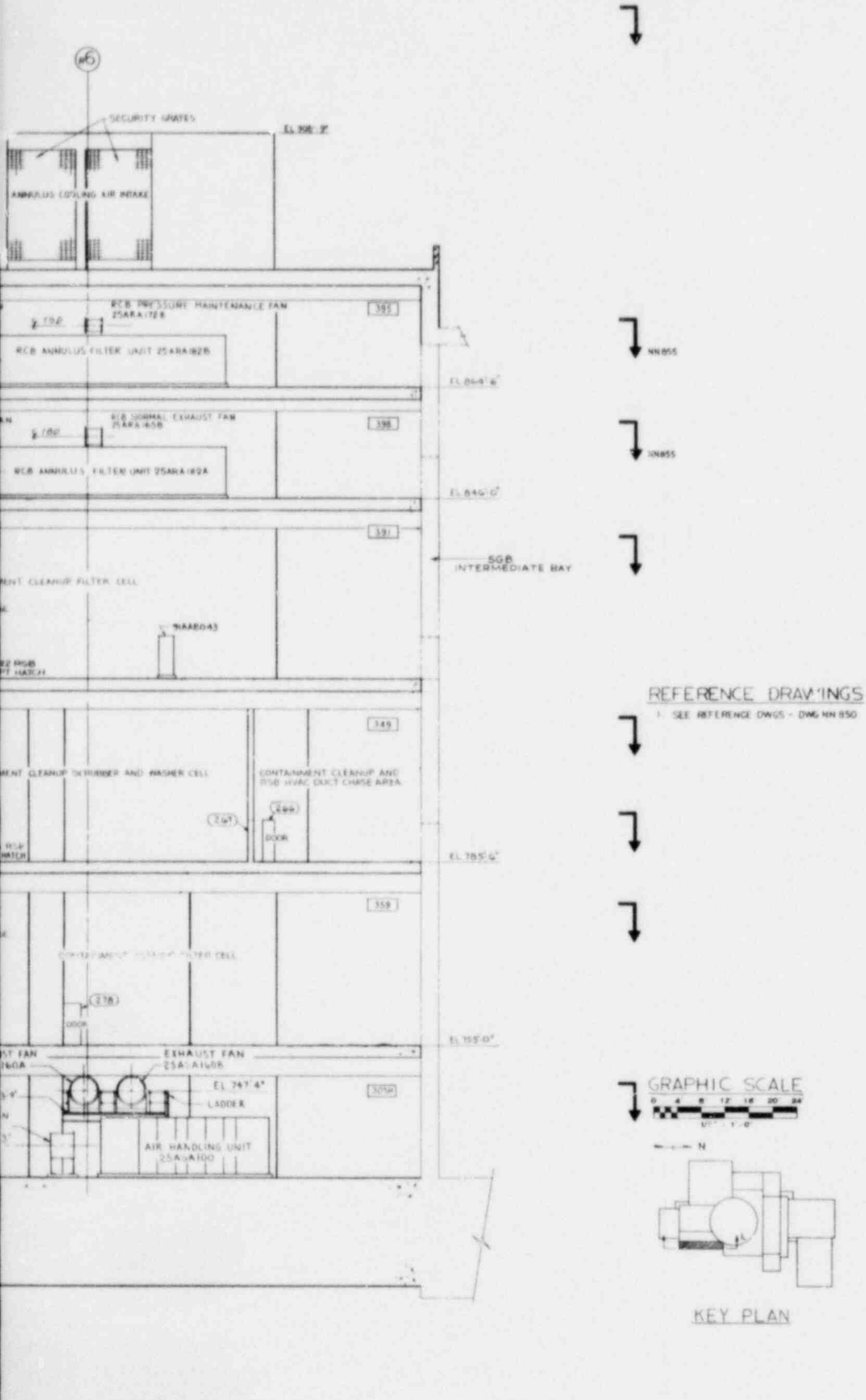

Figure 1.2-38
General Arrangement
Reactor Service Building
Section L-L

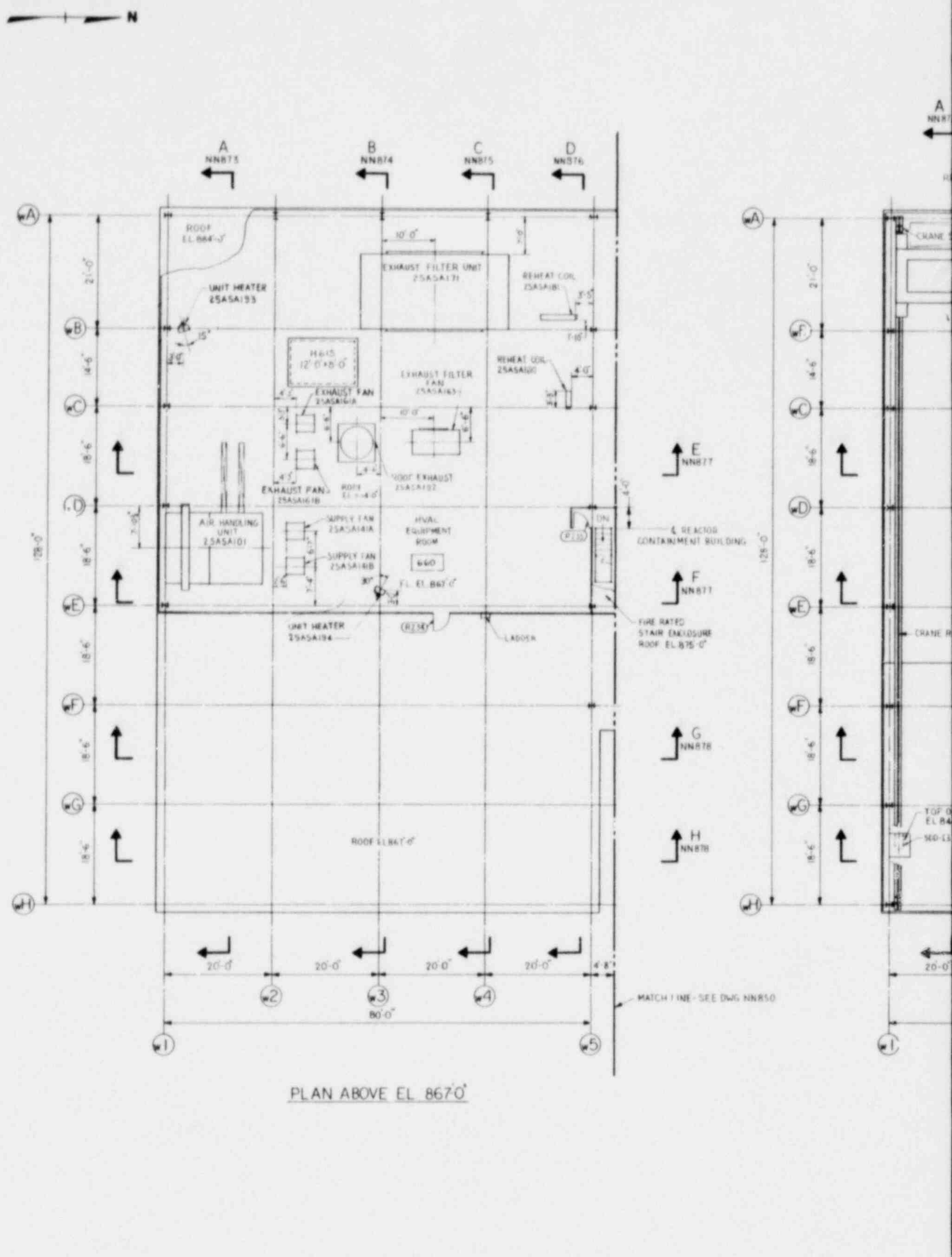

PLAN ABOVE EL 867'-0"

NN870-7

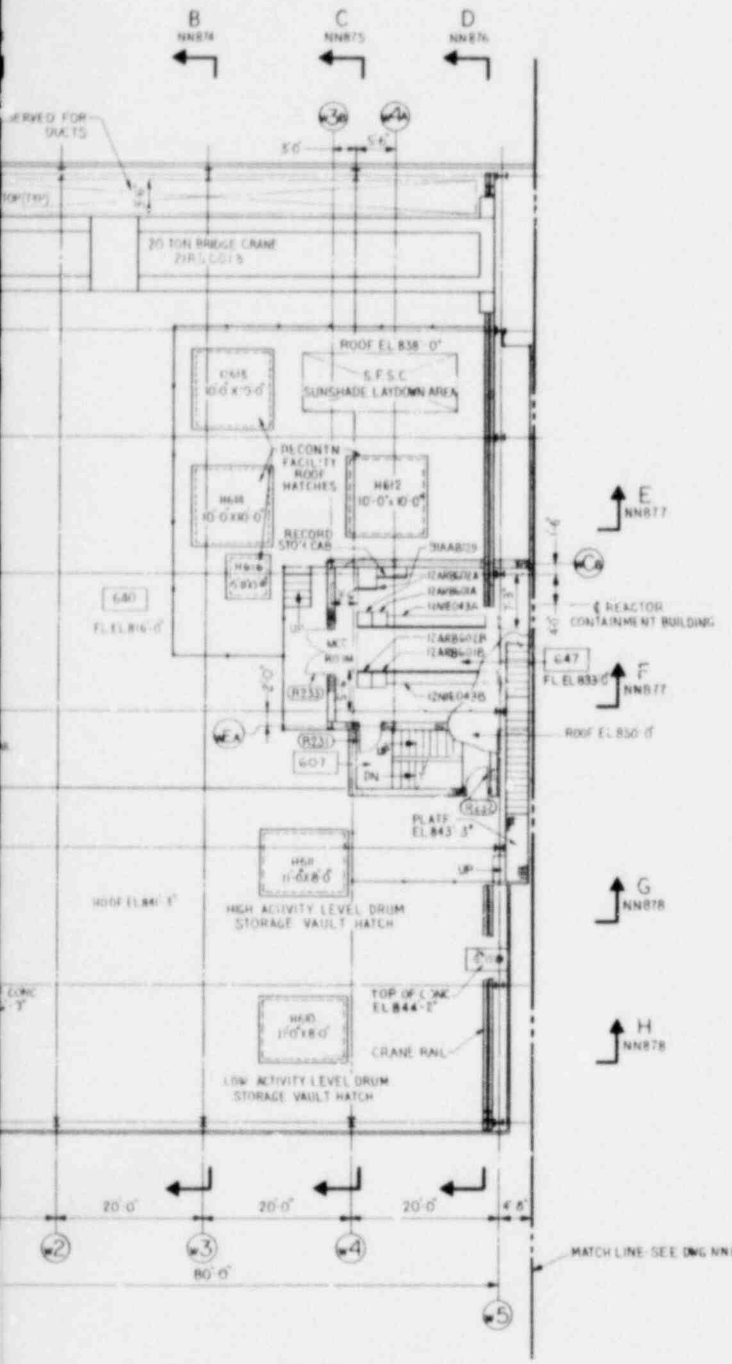

PLAN ABOVE EL 838'-0"

REFERENCE DRAWINGS
1. SEE REFERENCE DRAWINGS-DWG NN850

GRAPHIC SCALE

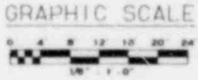

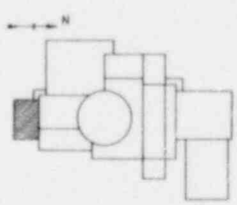

KEY PLAN

Figure 1.2-39
General Arrangement
Reactor Service Building
Radwaste Area
El. 867'-0" and 838'-0"

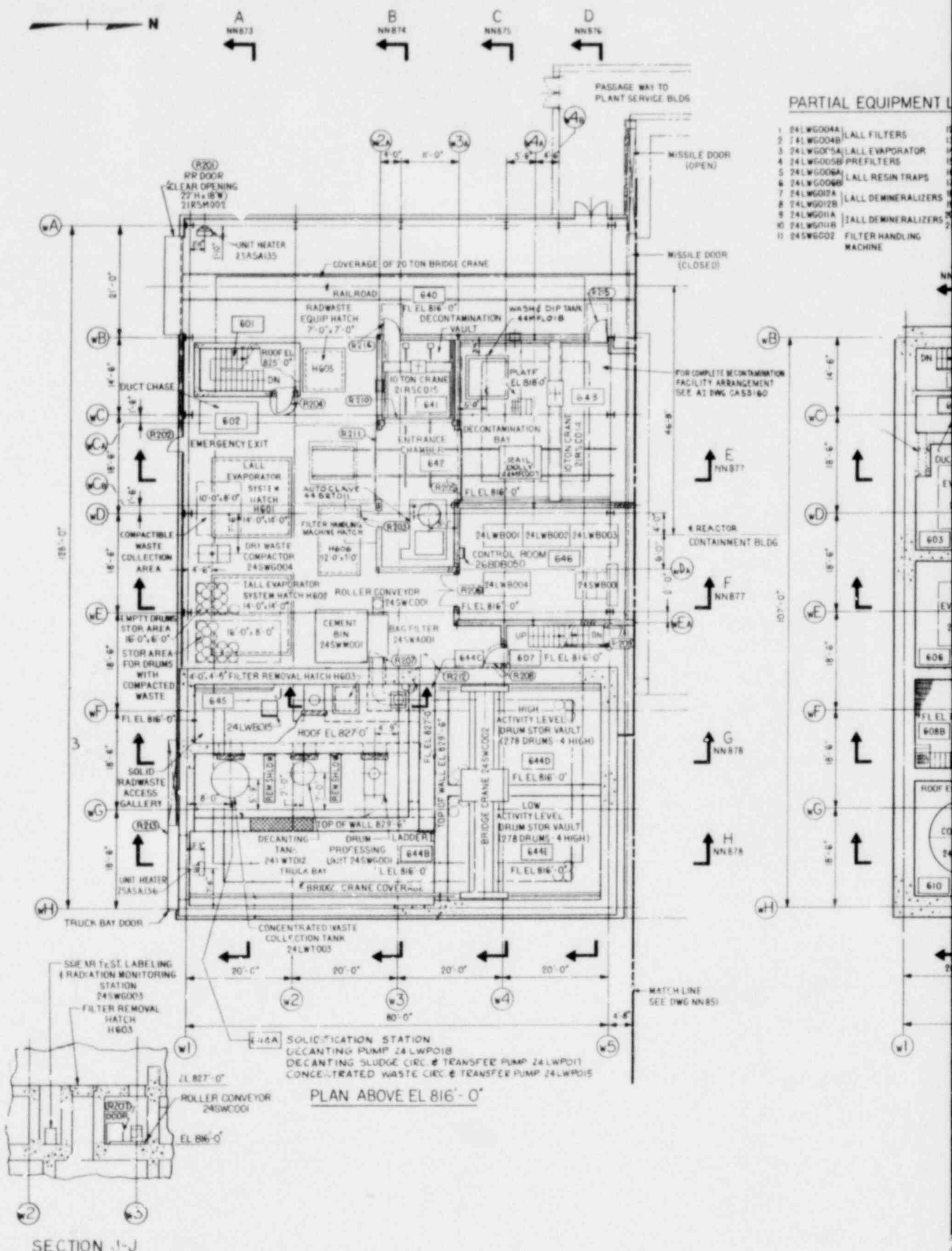

PLAN ABOVE EL 816'-0"
SECTION J-J
PARTIAL EQUIPMENT L
1 24LWG004A LALL FILTERS
2 24LWG004B
3 24LWG005A LALL EVAPORATOR
4 24LWG005B PREFILTERS
5 24LWG006A LALL RESIN TRAPS
6 24LWG006B
7 24LWG012A LALL DEMINERALIZERS
8 24LWG012B
9 24LWG011A
10 24LWG011B
11 24SWG002 FILTER HANDLING MACHINE
PASSAGE WAY TO PLANT SERVICE BLDG
MISSILE DOOR (OPEN)
MISSILE DOOR (CLOSED)
R/R DOOR CLEAR OPENING 22'H x 18'W 21R5M002
UNIT HEATER 23ASA135
COVERAGE OF 20 TON BRIDGE CRANE
RAILROAD
RADWASTE EQUIP HATCH 7'-0" x 7'-0"
DECONTAMINATION VAULT
WASHE DIP TANK 44MFL018
FOR COMPLETE DECONTAMINATION FACILITY ARRANGEMENT SEE AI DWG CA58160
DUCT CHASE
ROOF EL 825'-0"
10 TON CRANE 21RSC015
ENTRANCE CHAMBER
DECONTAMINATION BAY
10 TON CRANE 21RSC014
EMERGENCY EXIT
LALL EVAPORATOR SYSTEM HATCH H601
AUTOCLAVE 44SAT011
FILTER HANDLING MACHINE HATCH
COMPACTIBLE WASTE COLLECTION AREA
DRY WASTE COMPACTOR 24SWG004
CONTROL ROOM 26BDB050
REACTOR CONTAINMENT BLDG
IALL EVAPORATOR SYSTEM HATCH H602 14'-0" x 14'-0"
ROLLER CONVEYOR 24SWC001
EMPTY DRUMS STOR AREA 16'-0" x 6'-0"
STOR AREA FOR DRUMS WITH COMPACTED WASTE
CEMENT BIN 24SWM001
BAG FILTER 24SWA001
4'-0" x 4'-6" FILTER REMOVAL HATCH H603
HIGH ACTIVITY LEVEL DRUM STOR VAULT (278 DRUMS - 4 HIGH)
LOW ACTIVITY LEVEL DRUM STOR VAULT (278 DRUMS - 4 HIGH)
ROOF EL 827'-0"
SOLID RADWASTE ACCESS GALLERY
TOP OF WALL 829'-6"
BRIDGE CRANE 24SWC002
DECANTING TANK 24LWT012
DRUM PROCESSING UNIT 24SWG001
TRUCK BAY
BRIDGE CRANE COVERAGE
UNIT HEATER 25ASA136
TRUCK BAY DOOR
CONCENTRATED WASTE COLLECTION TANK 24LWT003
SHEAR TEST LABELING & RADIATION MONITORING STATION 24SWG003
FILTER REMOVAL HATCH H603
MATCH LINE SEE DWG NN851
644A SOLIDIFICATION STATION
DECANTING PUMP 24LWP018
DECANTING SLUDGE CIRC. & TRANSFER PUMP 24LWP017
CONCENTRATED WASTE CIRC. & TRANSFER PUMP 24LWP015
EL 827'-0"
ROLLER CONVEYOR 24SWC001
EL 816'-0"

NN871-7

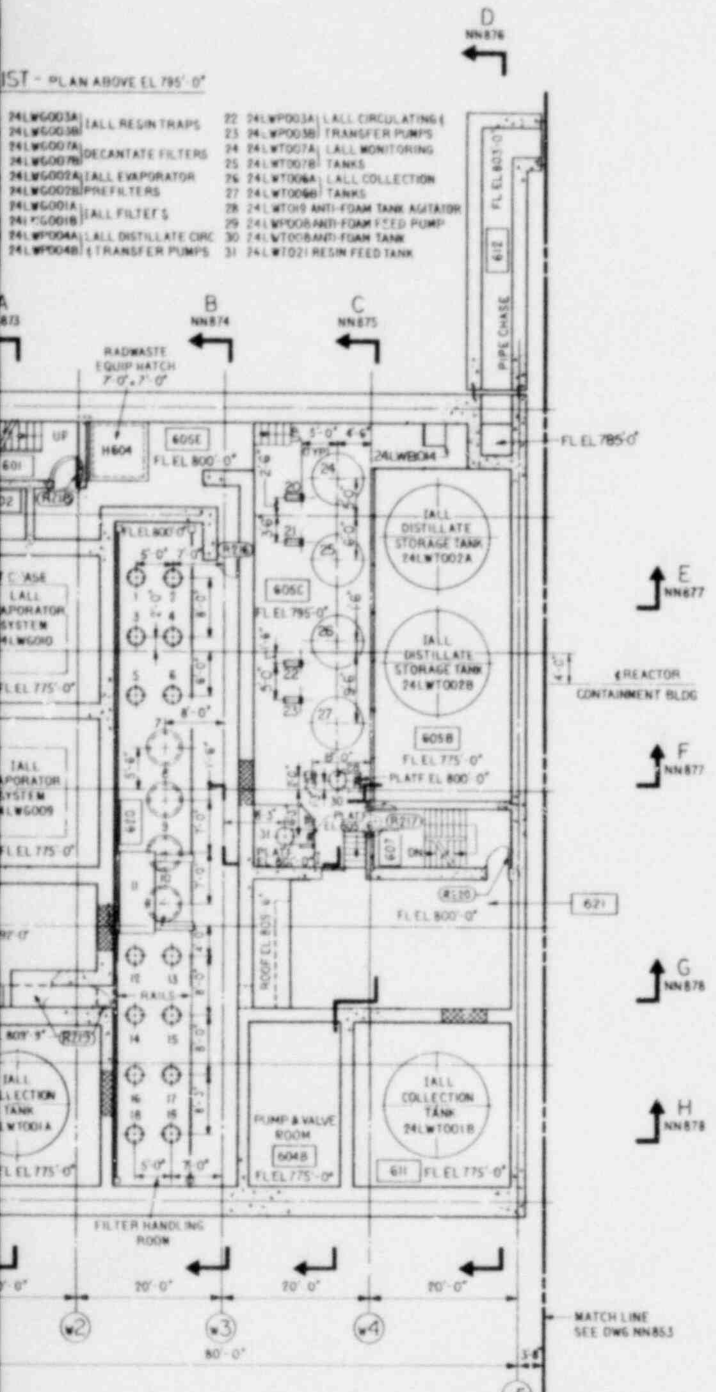

REFERENCE DRAWINGS
1. SEE REFERENCE DRAWINGS-DWG NN850

GRAPHIC SCALE

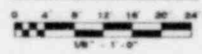

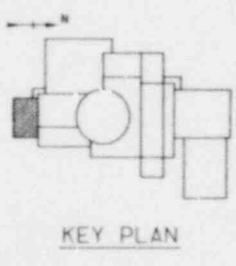

KEY PLAN

Figure 1.2-40
General Arrangement
Reactor Service Building
Radwaste Area
El. 816'-0" and 795'-0"

Amend. 56
Aug. 1980

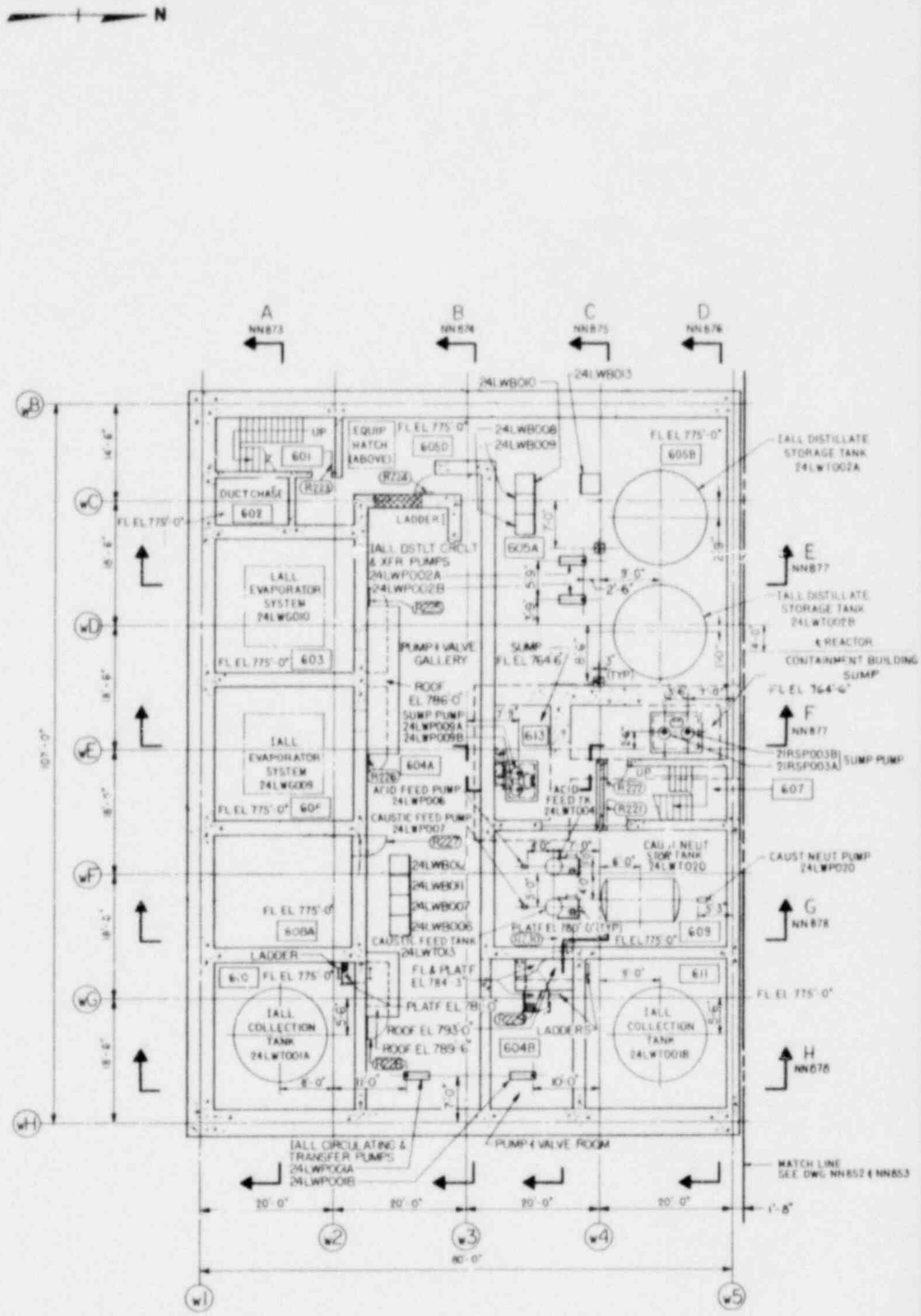

PLAN ABOVE EL 775'-0"

NN872-6

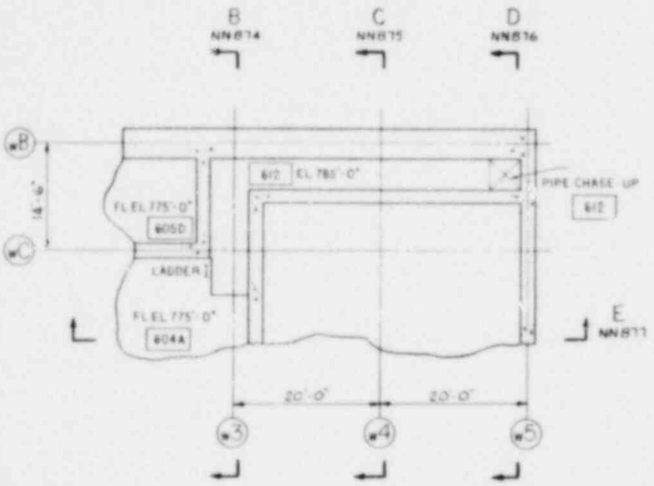

PARTIAL PLAN ABOVE EL785'-0"

REFERENCE DRAWINGS

1. SEE REFERENCE DRAWINGS-DWG NN850

GRAPHIC SCALE

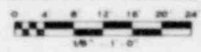

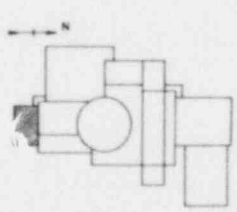

KEY PLAN

Figure 1.2-41
General Arrangement
Reactor Service Building
Radwaste Area
Plan El. 775'-0"

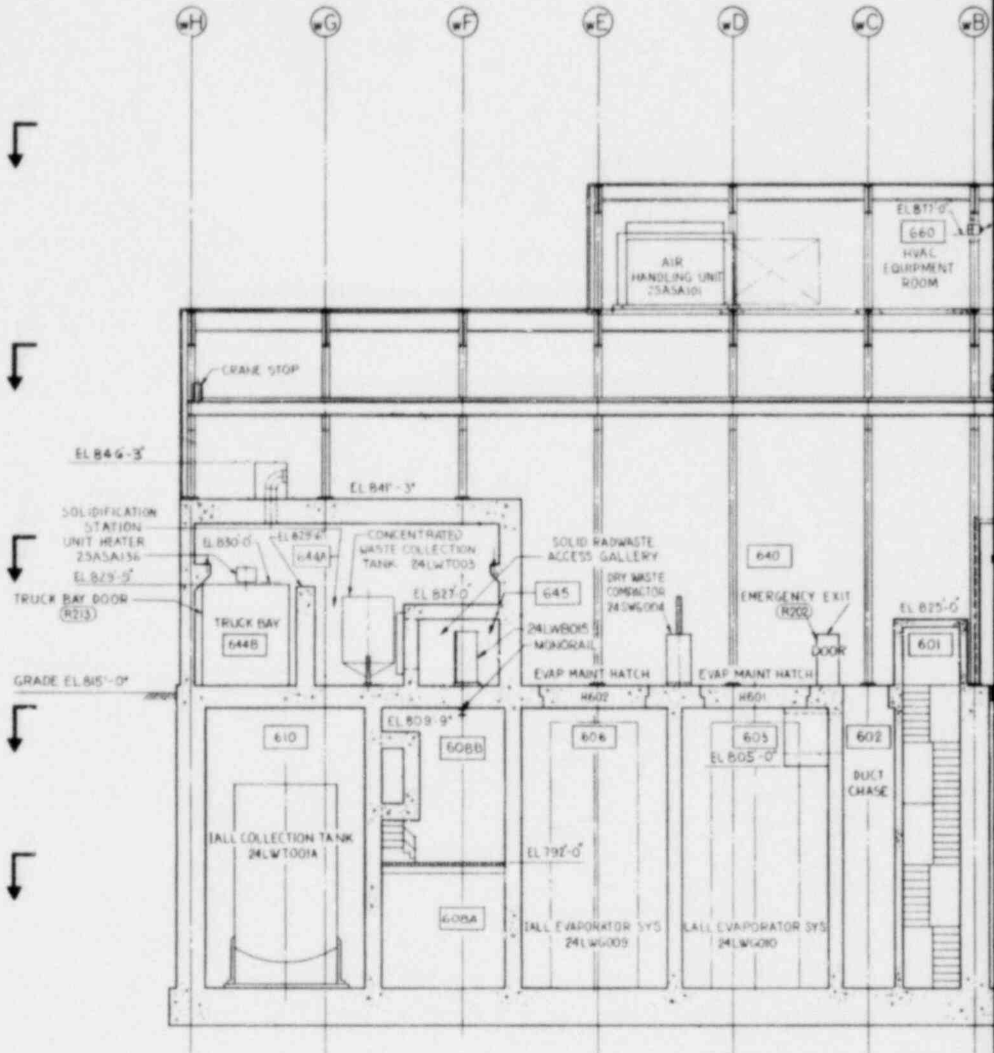

H
G
F
E
D
C
B
AIR HANDLING UNIT 25ASA101
660
HVAC EQUIPMENT ROOM
CRANE STOP
EL 846'-3"
EL 841'-3"
SOLIDIFICATION STATION
UNIT HEATER 25ASA136
EL 829'-9"
TRUCK BAY DOOR (R213)
TRUCK BAY
644B
644A
CONCENTRATED WASTE COLLECTION TANK 24LWT003
SOLID RADWASTE ACCESS GALLERY
645
24LWB015
MONORAIL
DRY WASTE COMPACTOR 24SWG004
640
EMERGENCY EXIT (R202)
DOOR
601
GRADE EL 815'-0"
EVAP MAINT HATCH
H602
H601
610
EL 809'-9"
608B
606
605
EL 805'-0"
602
DUCT CHASE
IALL COLLECTION TANK 24LWT001A
EL 791'-0"
608A
IALL EVAPORATOR SYS 24LWG009
LALL EVAPORATOR SYS 24LWG010

SECTION A-A

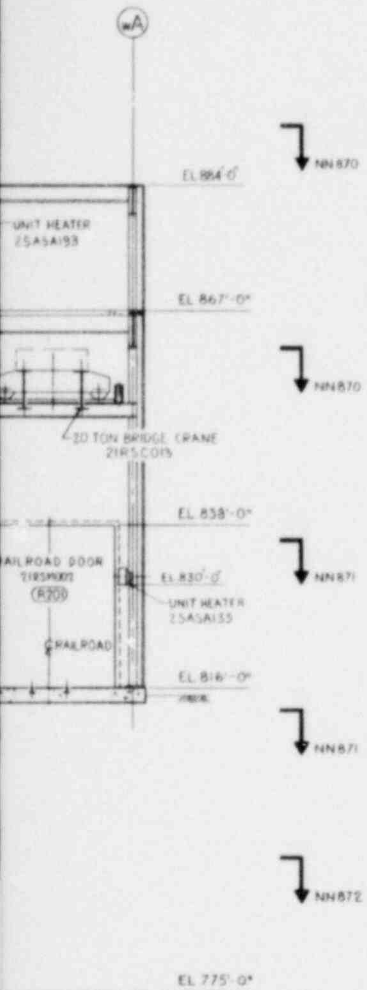

REFERENCE DRAWINGS

1. SEE REFERENCE DRAWINGS-DWG NN850

GRAPHIC SCALE

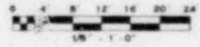

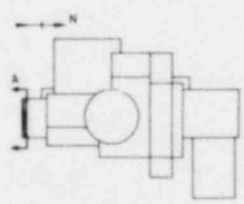

KEY PLAN

Figure 1.2-42
General Arrangement
Reactor Service Building
Radwaste Area
Section A-A

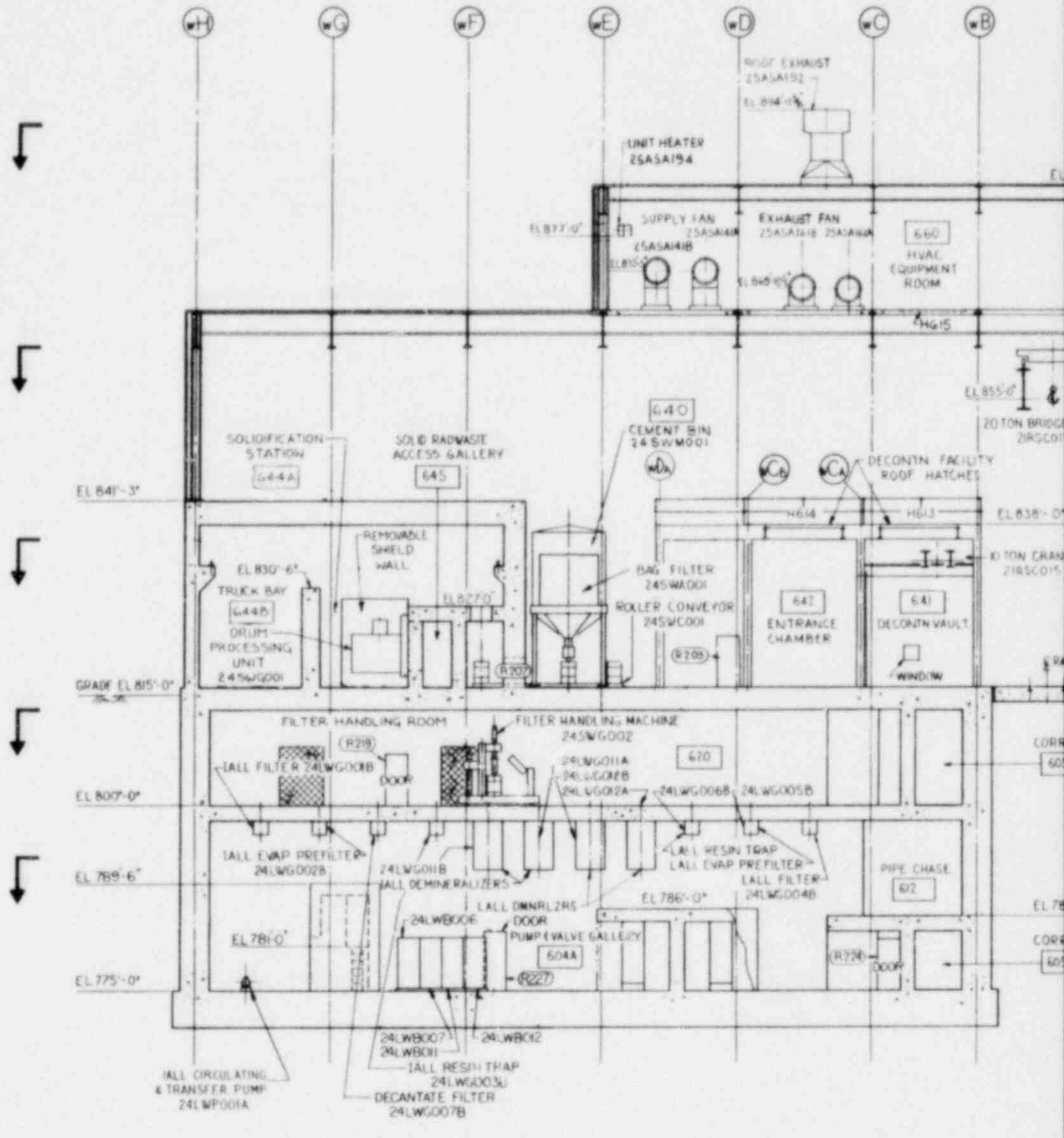

ROOF EXHAUST
25ASA192
UNIT HEATER
25ASA194
SUPPLY FAN
25ASA141B
EXHAUST FAN
660
HVAC EQUIPMENT ROOM
H615
EL 877'-0"
EL 855'-0"
20 TON BRIDGE
640
CEMENT BIN
24SWM001
SOLIDIFICATION STATION
644A
SOLID RADWASTE ACCESS GALLERY
645
DECONTN FACILITY ROOF HATCHES
H614
H613
EL 841'-3"
EL 838'-0"
REMOVABLE SHIELD WALL
EL 830'-6"
TRUCK BAY
644B
DRUM PROCESSING UNIT
24SWG001
EL 827'-0"
BAG FILTER
24SWA001
ROLLER CONVEYOR
24SWC001
642
ENTRANCE CHAMBER
641
DECONTN VAULT
WINDOW
R207
R206
GRADE EL 815'-0"
FILTER HANDLING ROOM
FILTER HANDLING MACHINE
24SWG002
R218
1ALL FILTER 24LWG001B
DOOR
620
24LWG011A
24LWG012B
24LWG012A
24LWG006B
24LWG005B
EL 800'-0"
1ALL EVAP PREFILTER
24LWG002B
24LWG011B
1ALL DEMINERALIZERS
LALL RESIN TRAP
LALL EVAP PREFILTER
LALL FILTER
24LWG004B
PIPE CHASE
612
EL 789'-6"
LALL DMNRLZRS
EL 786'-0"
24LWB006
DOOR
PUMP & VALVE GALLERY
604A
R227
R224
DOOR
EL 781'-0"
EL 775'-0"
24LWB007
24LWB011
24LWB012
1ALL RESIN TRAP
24LWG003U
DECANTATE FILTER
24LWG007B
1ALL CIRCULATING & TRANSFER PUMP
24LWP001A

SECTION B-B

GENERAL NOTES
1. SEE GENERAL NOTES-DWG NN850
2. SEE LEGEND-DWG NN850

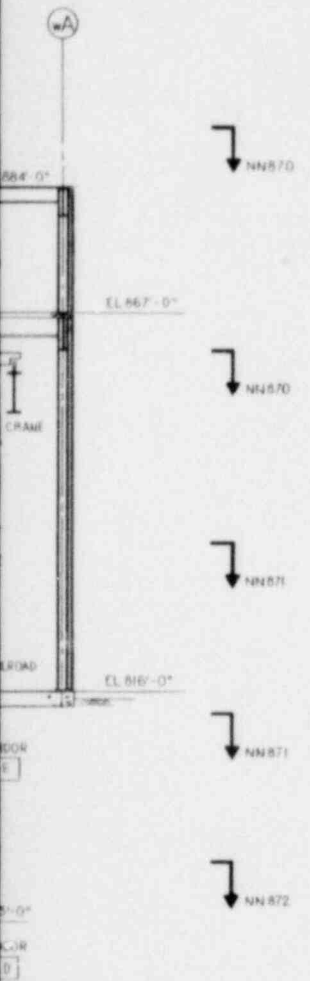

REFERENCE DRAWINGS
1. SEE REFERENCE DRAWINGS-DWG NN850

GRAPHIC SCALE
0 4 8 12 16 20 24
1/8" = 1'-0"

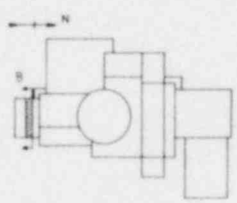

KEY PLAN

Figure 1.2-43
General Arrangement
Reactor Service Building
Radwaste Area
Section B-B

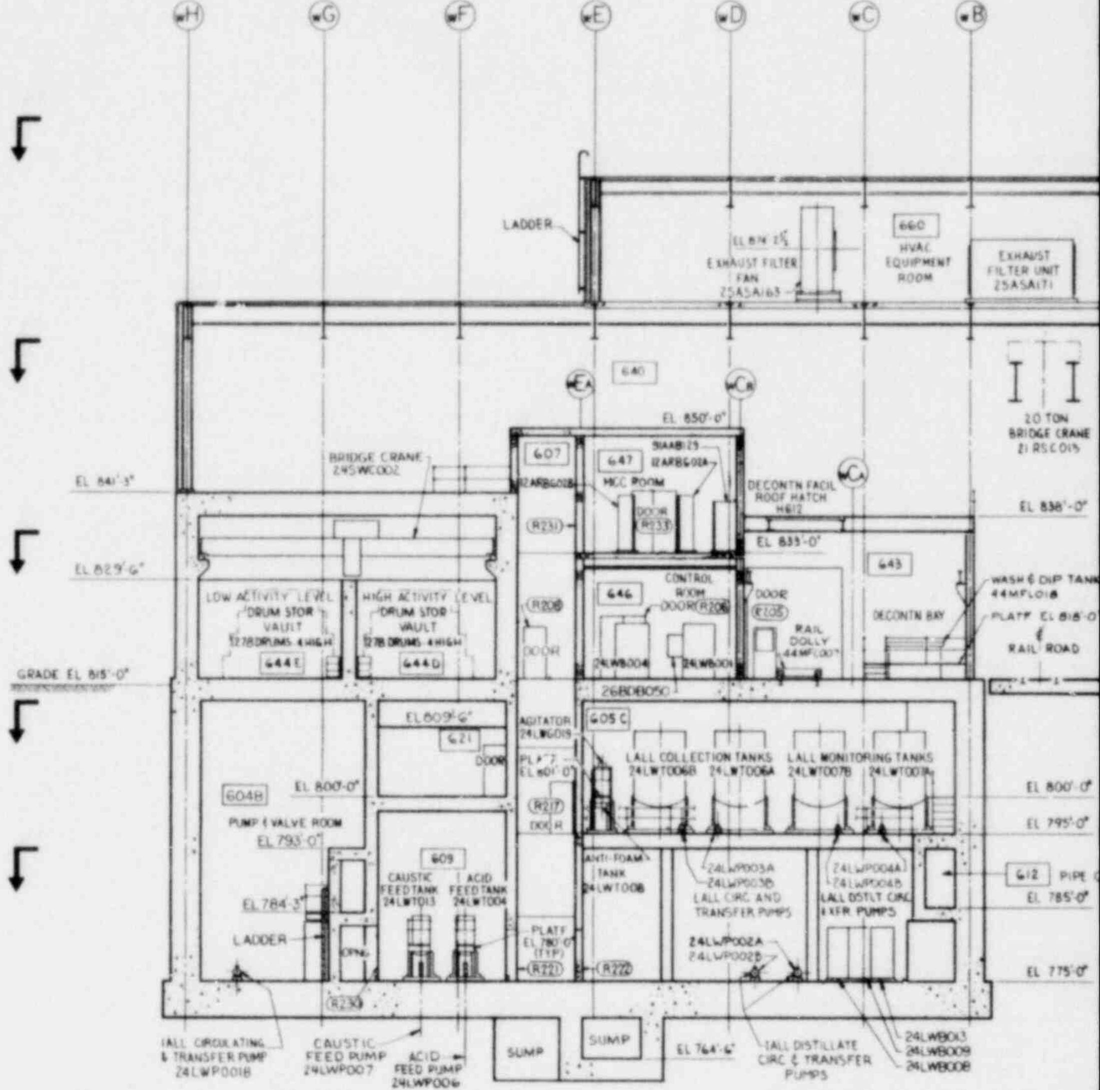

SECTION C-C

NN875-7

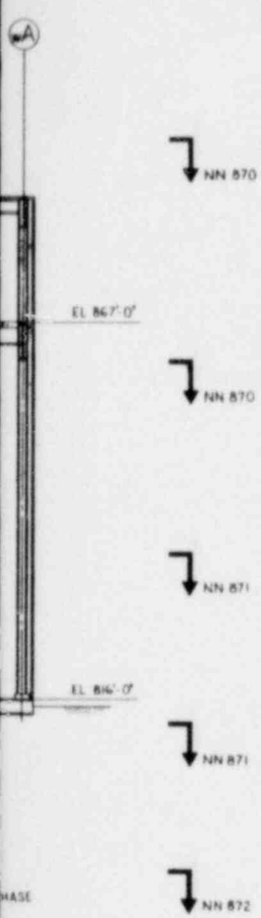

REFERENCE DRAWINGS

1. SEE REFERENCE DRAWINGS-DWG NN850

GRAPHIC SCALE

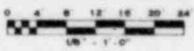

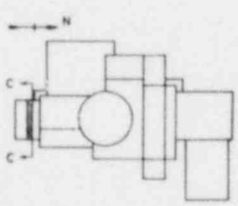

KEY PLAN

Figure 1.2-44
General Arrangement
Reactor Service Building
Radwaste Area
Section C-C

Amend. 56
Aug. 1980

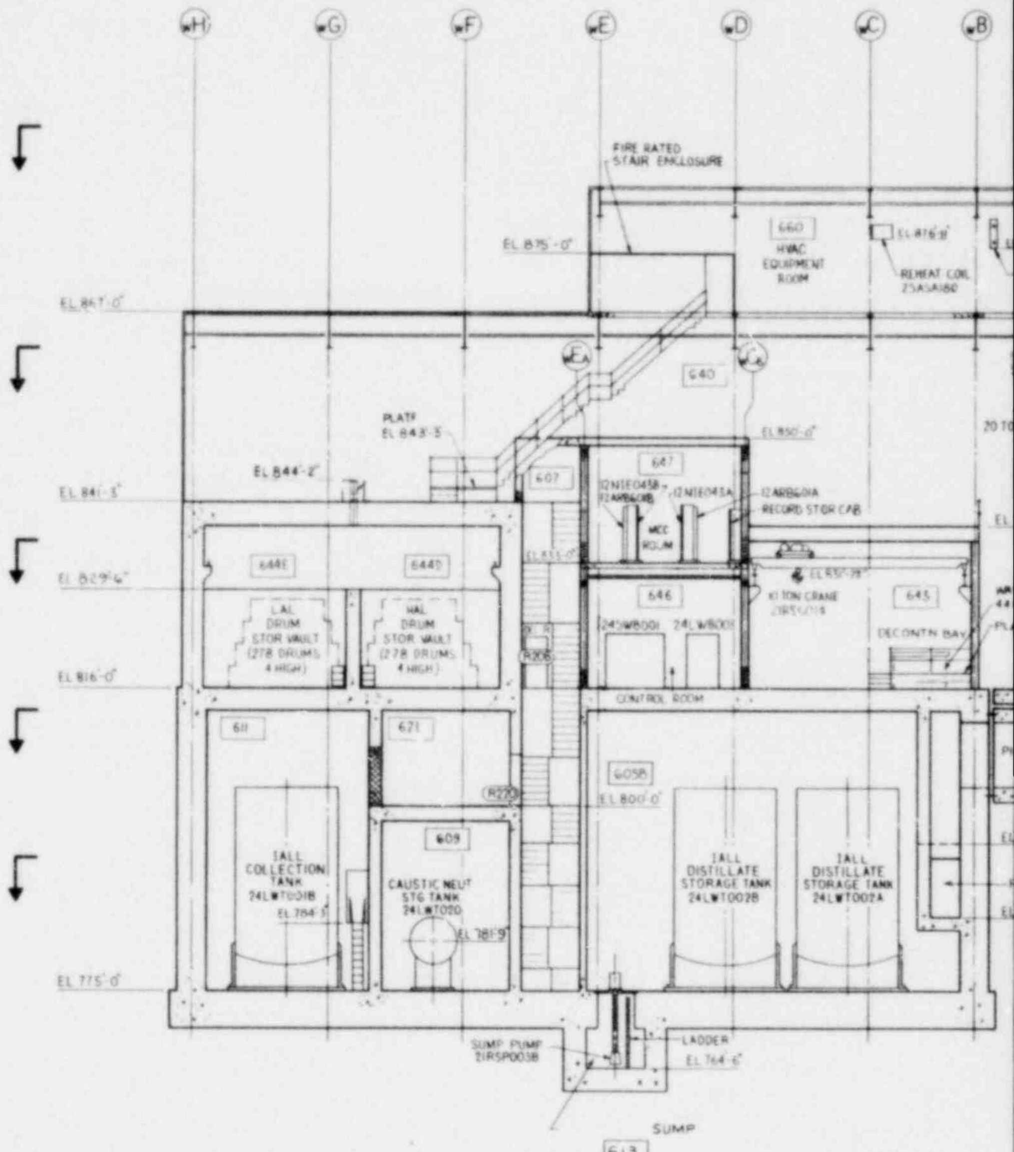

FIRE RATED STAIR ENCLOSURE
EL 875'-0"
660
HVAC EQUIPMENT ROOM
REHEAT COIL 25ASA180
EL 867'-0"
640
PLATF EL 843'-5"
EL 850'-0"
EL 844'-2"
EL 841'-5"
607
647
MCC ROOM
12ARB601A
RECORD STOR CAB
EL 829'-6"
644E
644D
LAL DRUM STOR VAULT (278 DRUMS 4 HIGH)
HAL DRUM STOR VAULT (278 DRUMS 4 HIGH)
646
645
DECONTN BAY
CONTROL ROOM
EL 816'-0"
611
621
605B
EL 800'-0"
609
TALL COLLECTION TANK 24LWT001B
CAUSTIC NEUT STG TANK 24LWT020
TALL DISTILLATE STORAGE TANK 24LWT002B
TALL DISTILLATE STORAGE TANK 24LWT002A
EL 775'-0"
SUMP PUMP 21RSP003B
LADDER
EL 764'-6"
SUMP
613

SECTION D-D

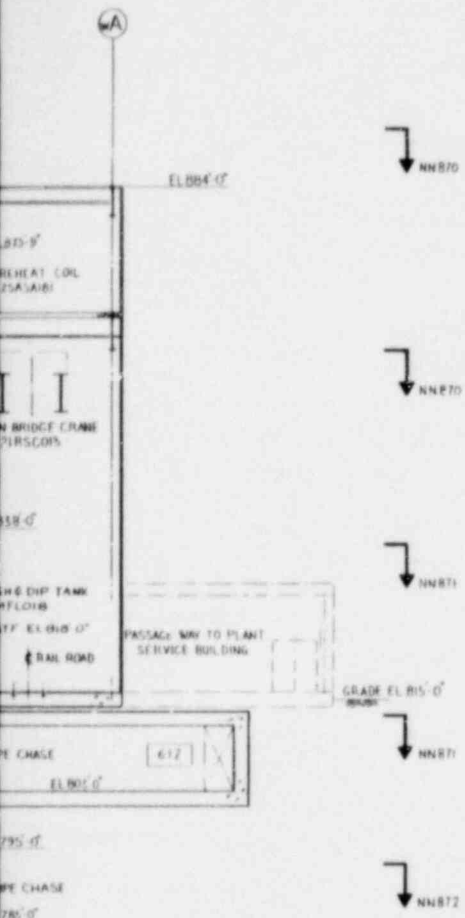

REFERENCE DRAWINGS

1. SEE REFERENCE DRAWINGS-DWG NN850

GRAPHIC SCALE

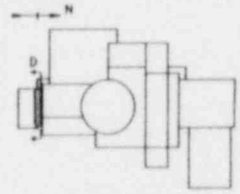

KEY PLAN

Figure 1.2-45
General Arrangement
Reactor Service Building
Radwaste Area
Section D-D

Amend. 56
Aug. 1980

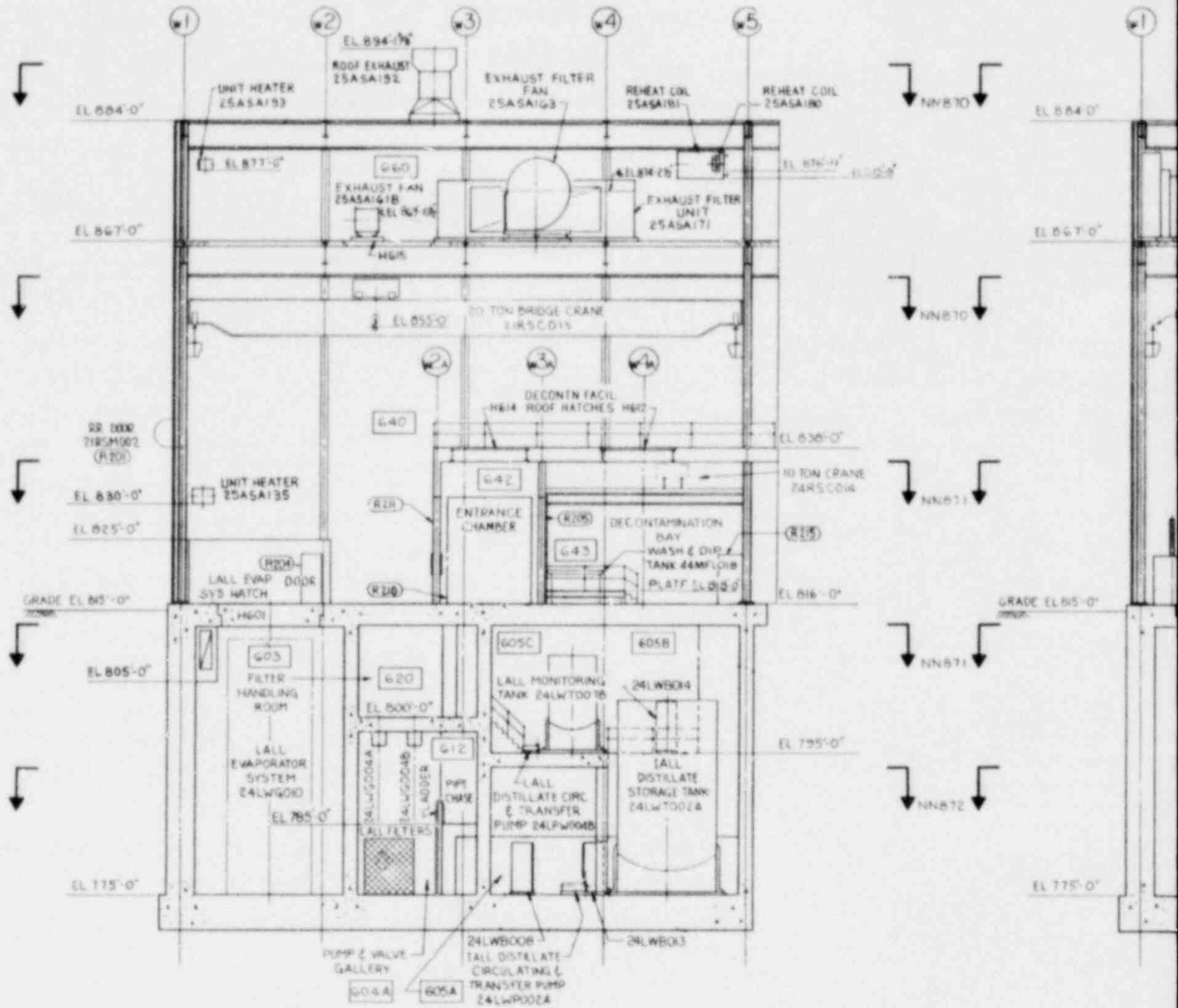

SECTION E-E

NN877-7

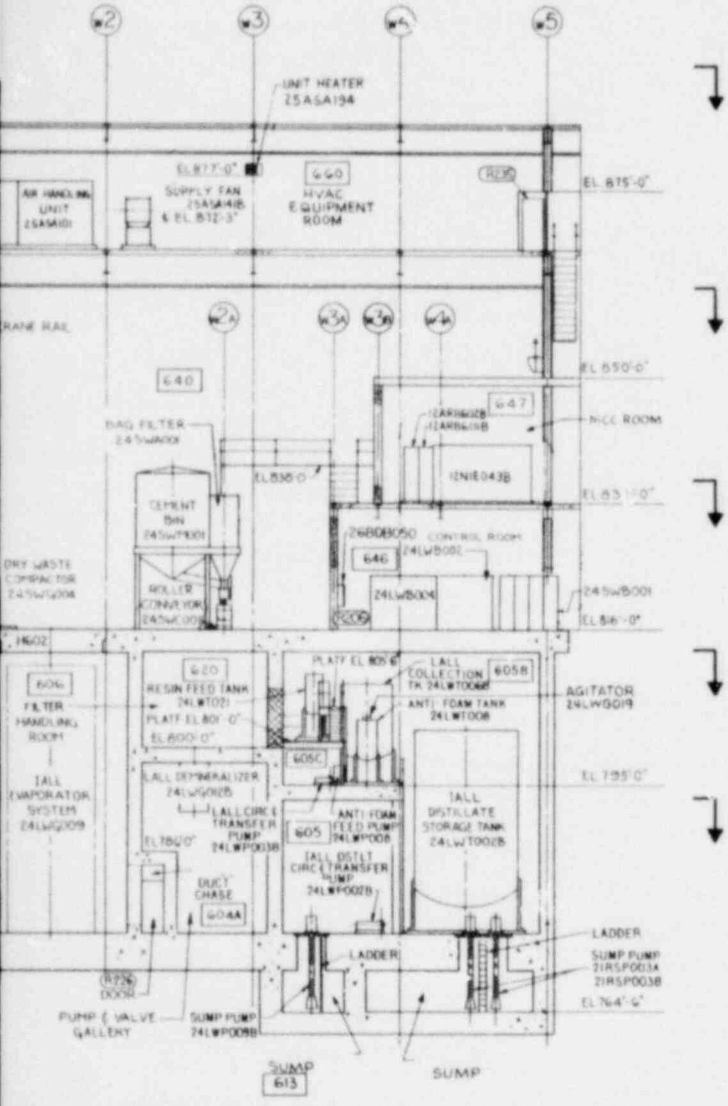

SECTION F-F

REFERENCE DRAWINGS

1. SEE REFERENCE DRAWINGS-DWG NN850

GRAPHIC SCALE

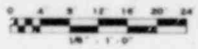

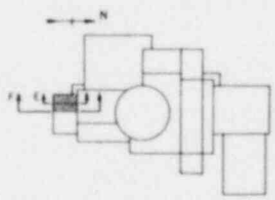

KEY PLAN

Figure 1.2-46
General Arrangement
Reactor Service Building
Radwaste Area
Section E-E and F-F

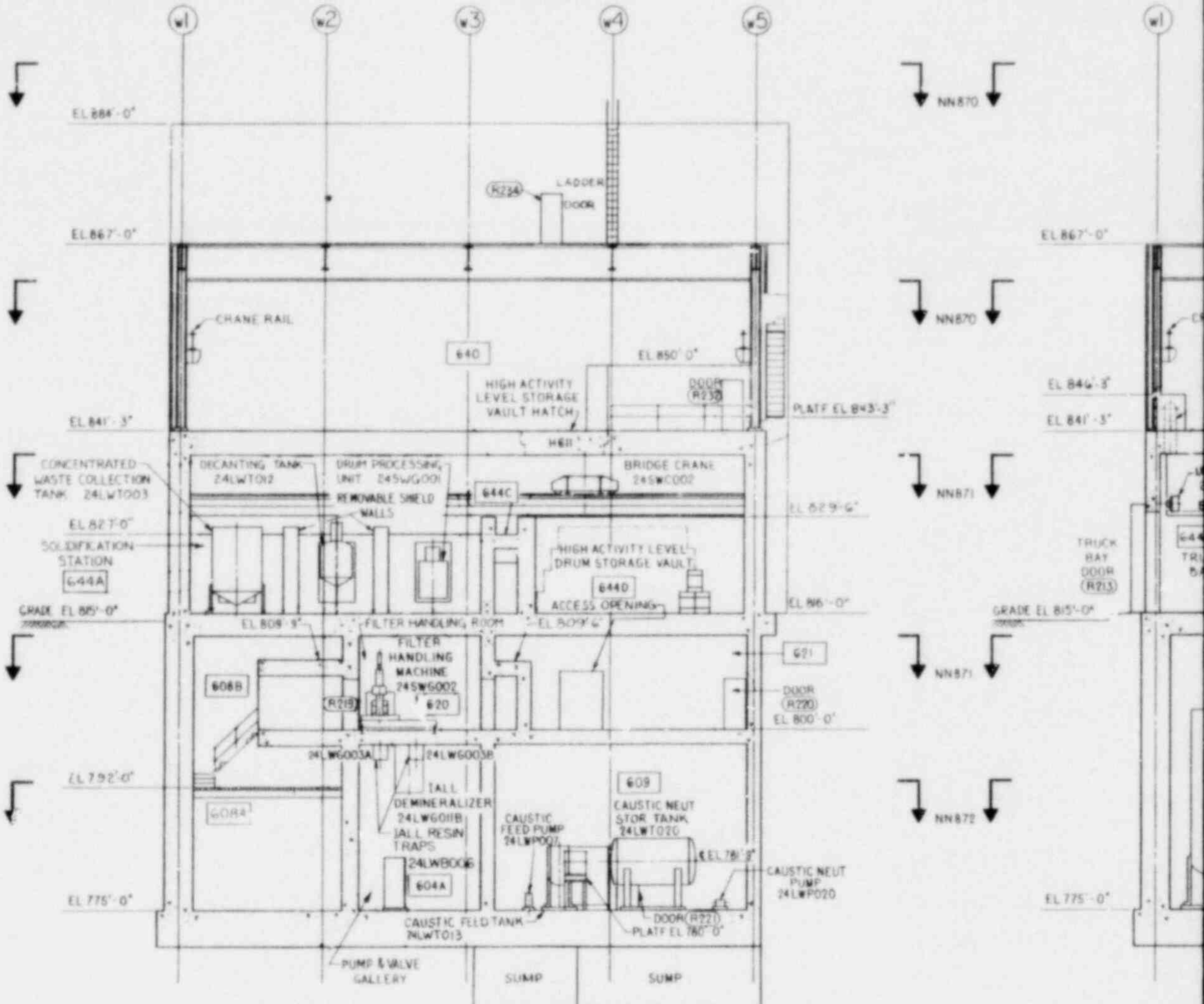

SECTION G-G

NN878-7

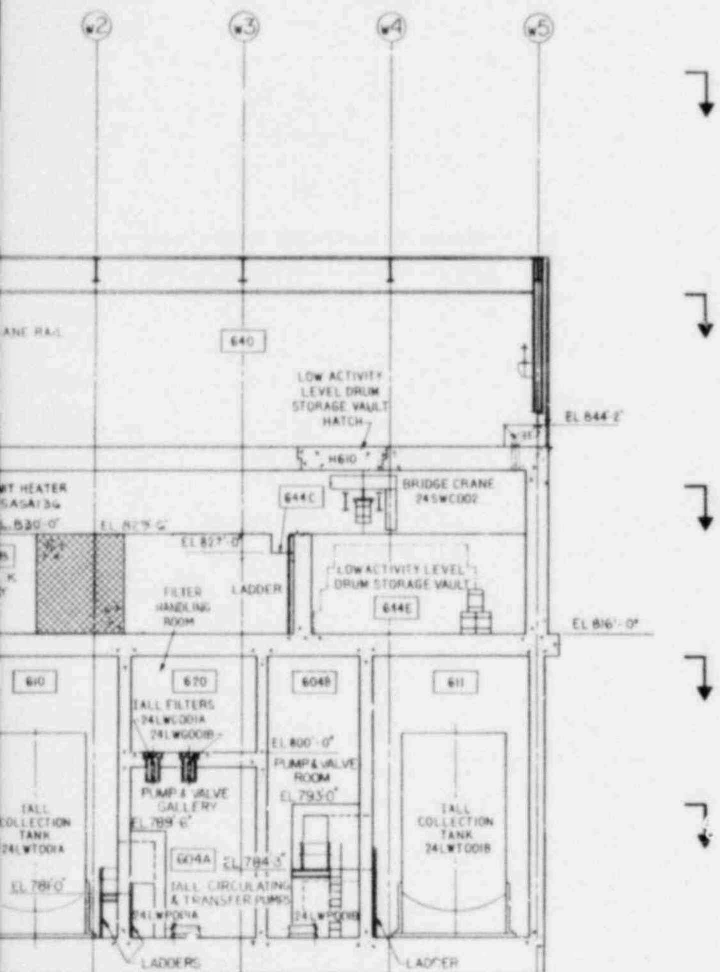

SECTION H-H

REFERENCE DRAWINGS

1. SEE REFERENCE DRAWINGS-DWG NNBSC

GRAPHIC SCALE

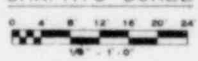

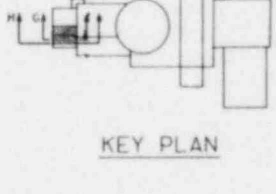

KEY PLAN

Figure 1.2-47
General Arrangement
Reactor Service Building
Radwaste Area
Section G-G and H-H

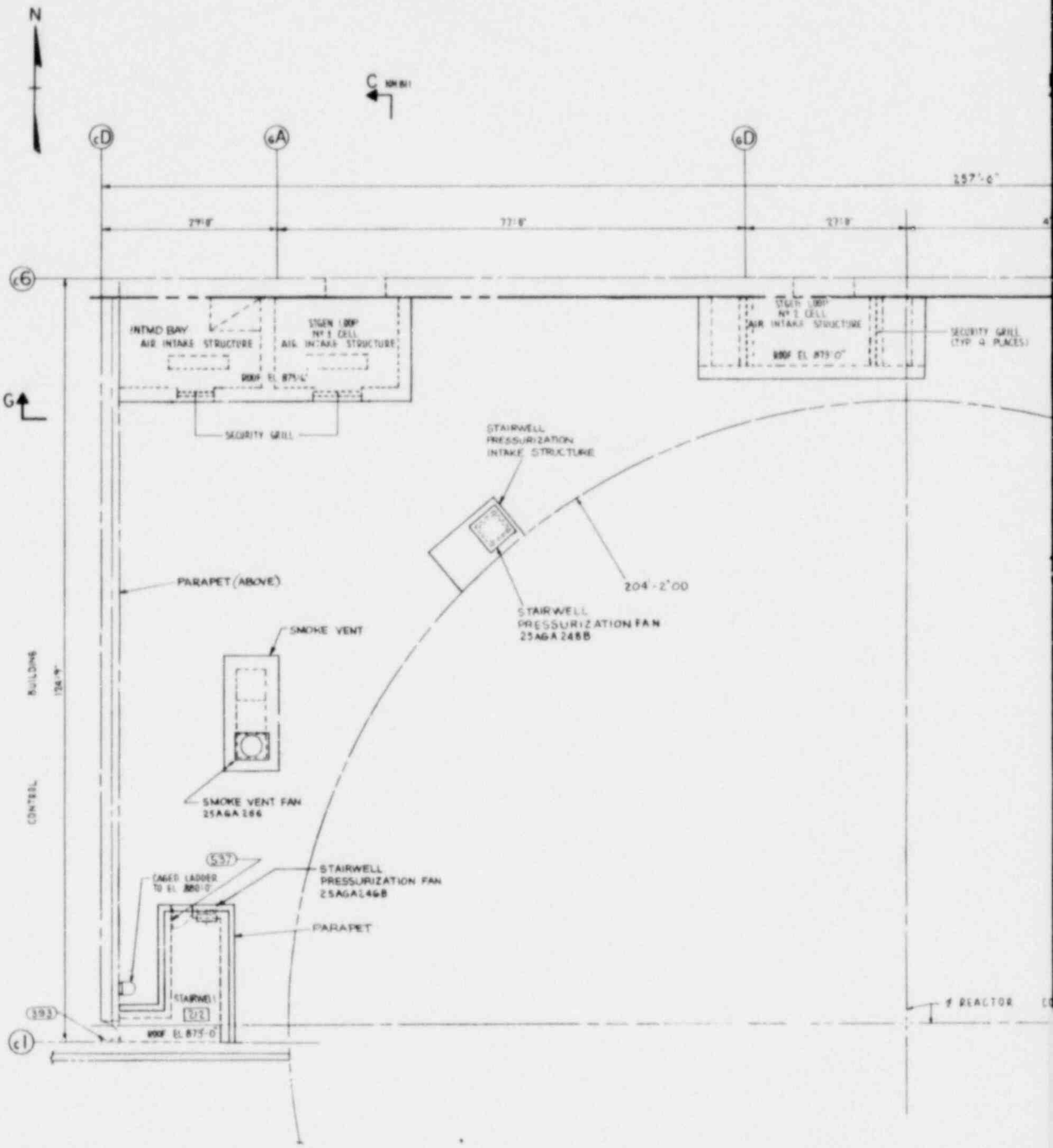

PLAN ABOVE EL 857'-6"

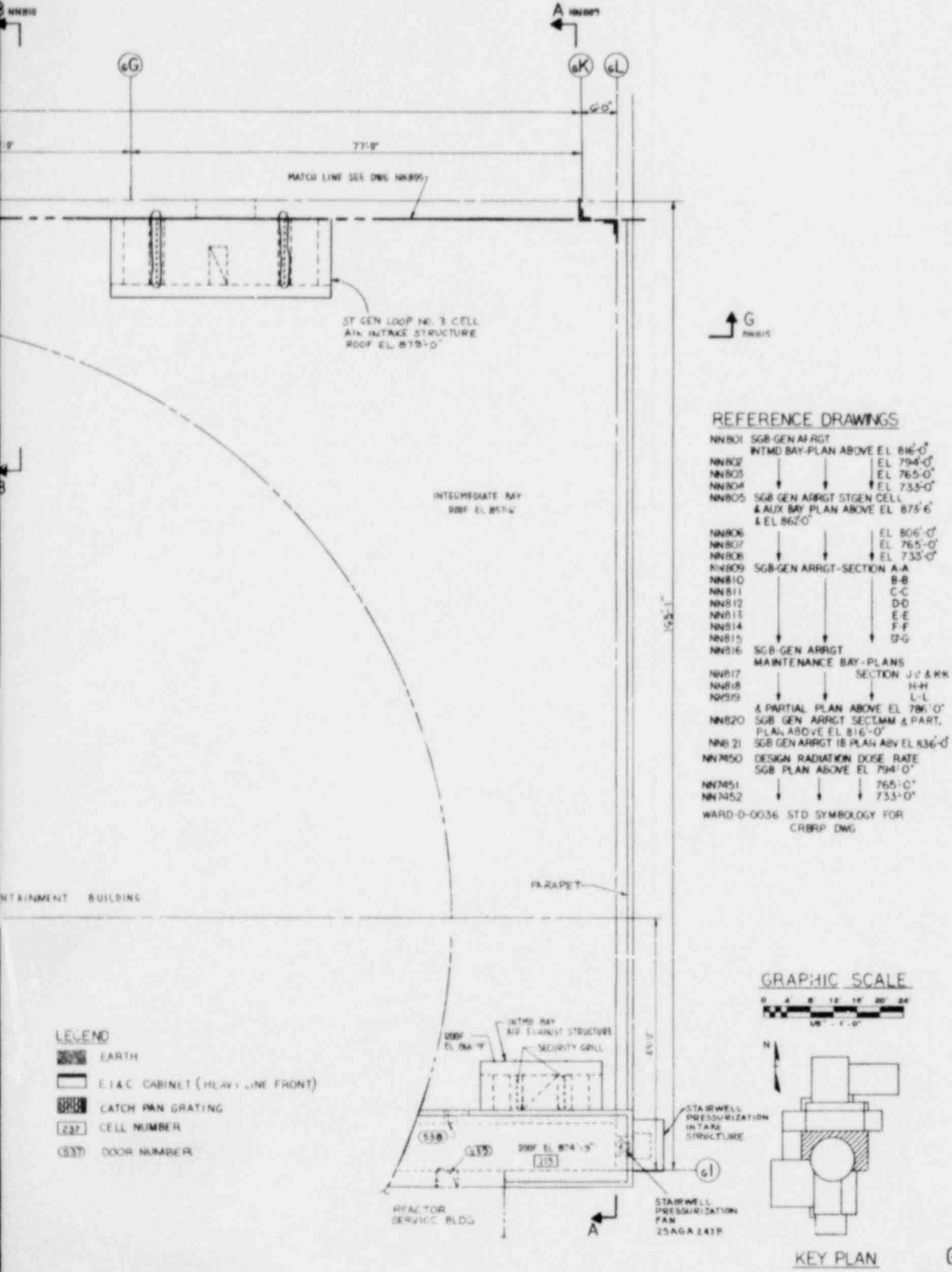

Figure 1.2-48
General Arrangement
Steam Generator Building
Plan El. 857'-6"

Amend. 56
Aug. 1980

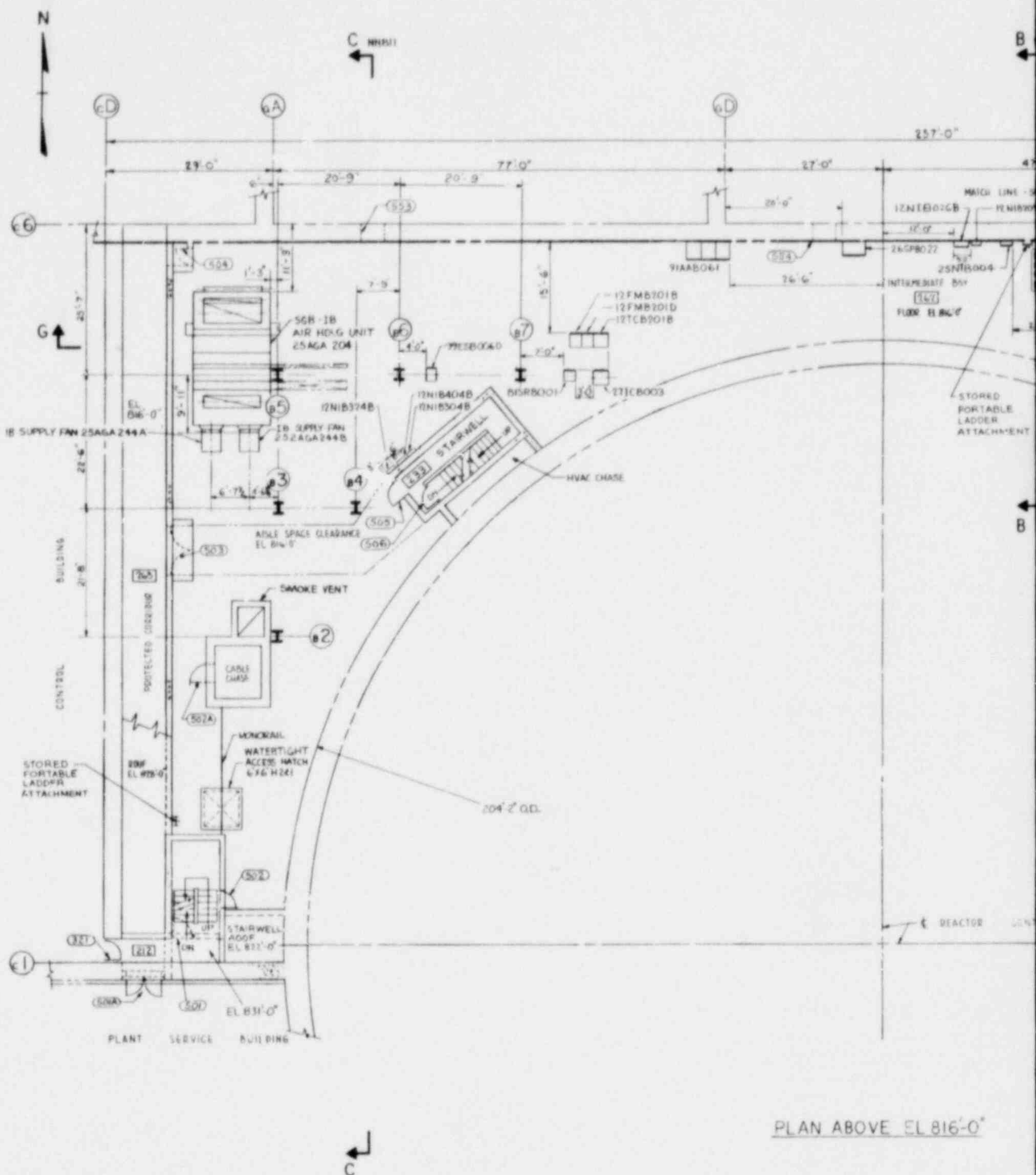

PLAN ABOVE EL 816'-0"

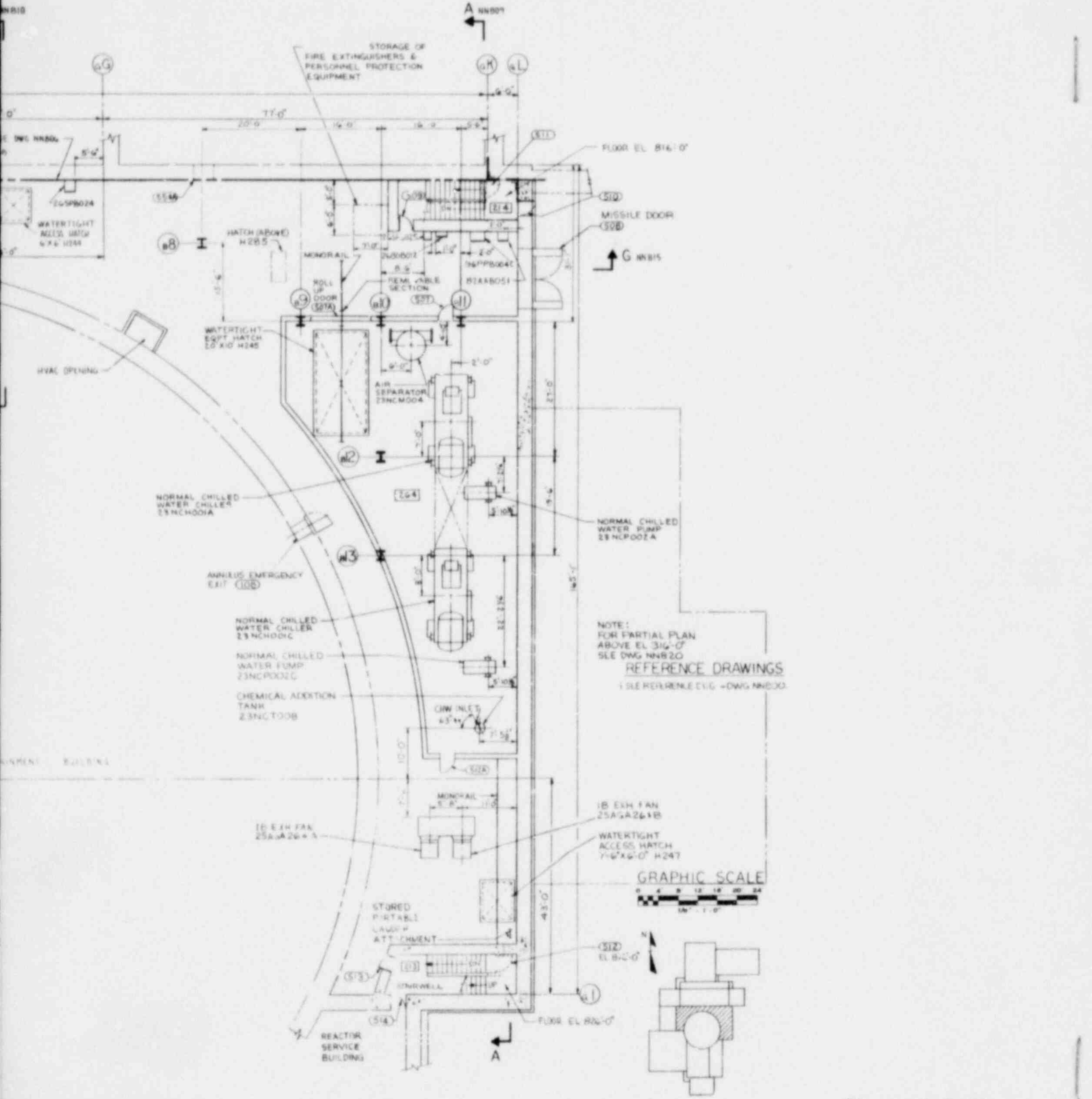

Figure 1.2-49
General Arrangemert
Steam Generator Building
Plan El. 816'-0"

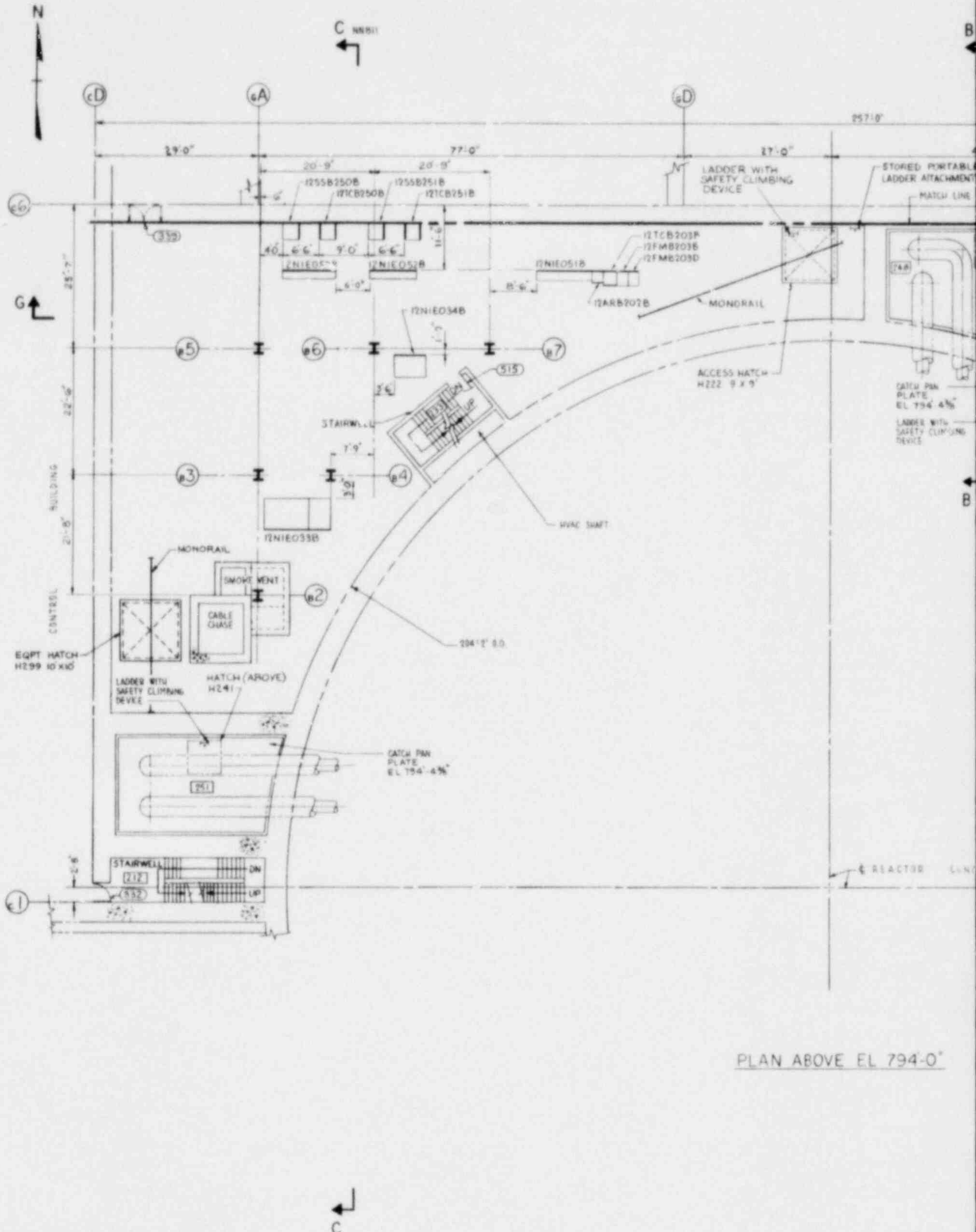

PLAN ABOVE EL 794'-0"

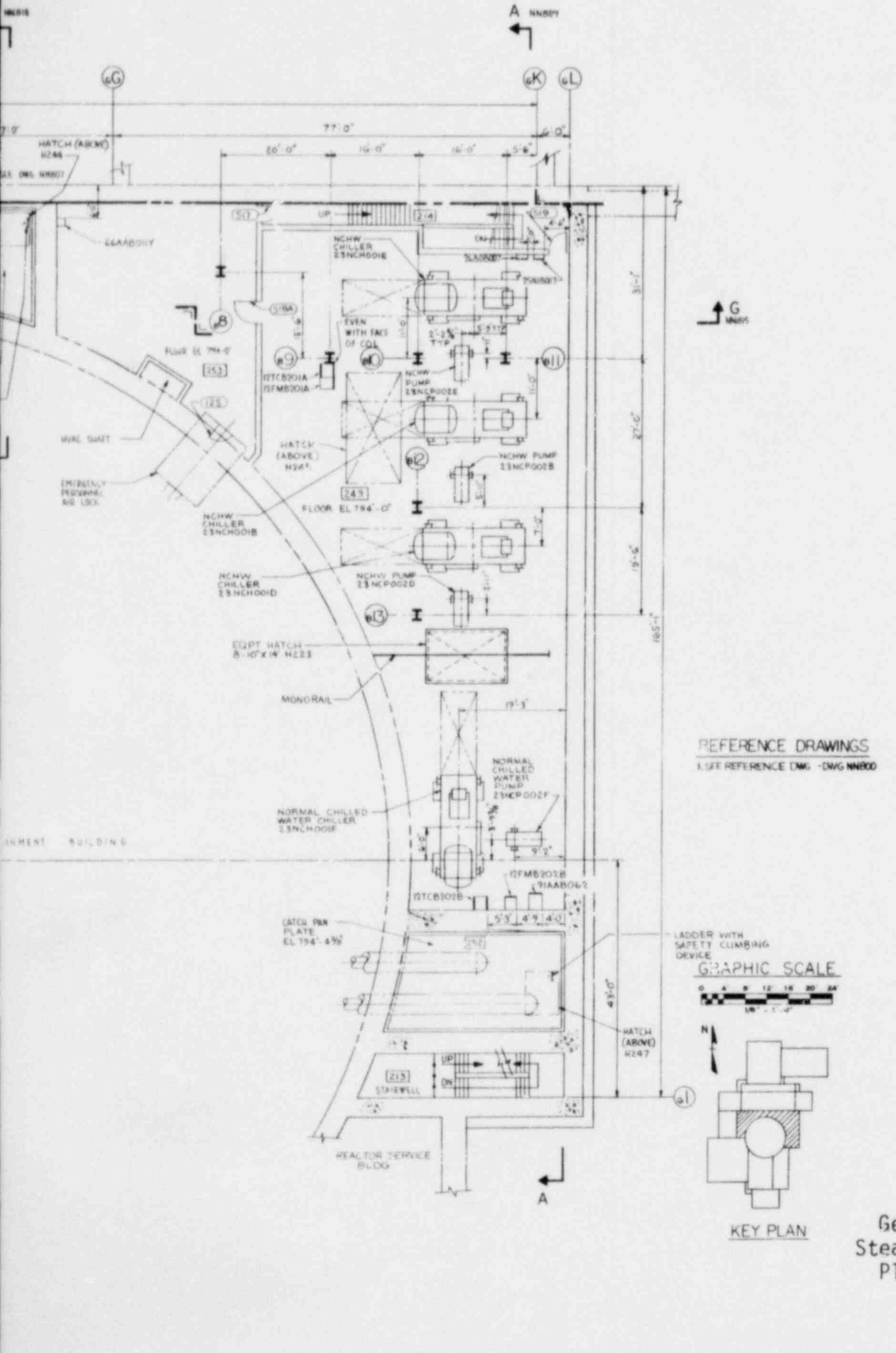

Figure 1.2-50
General Arrangement
Steam Generator Building
Plan El. 794'-0"

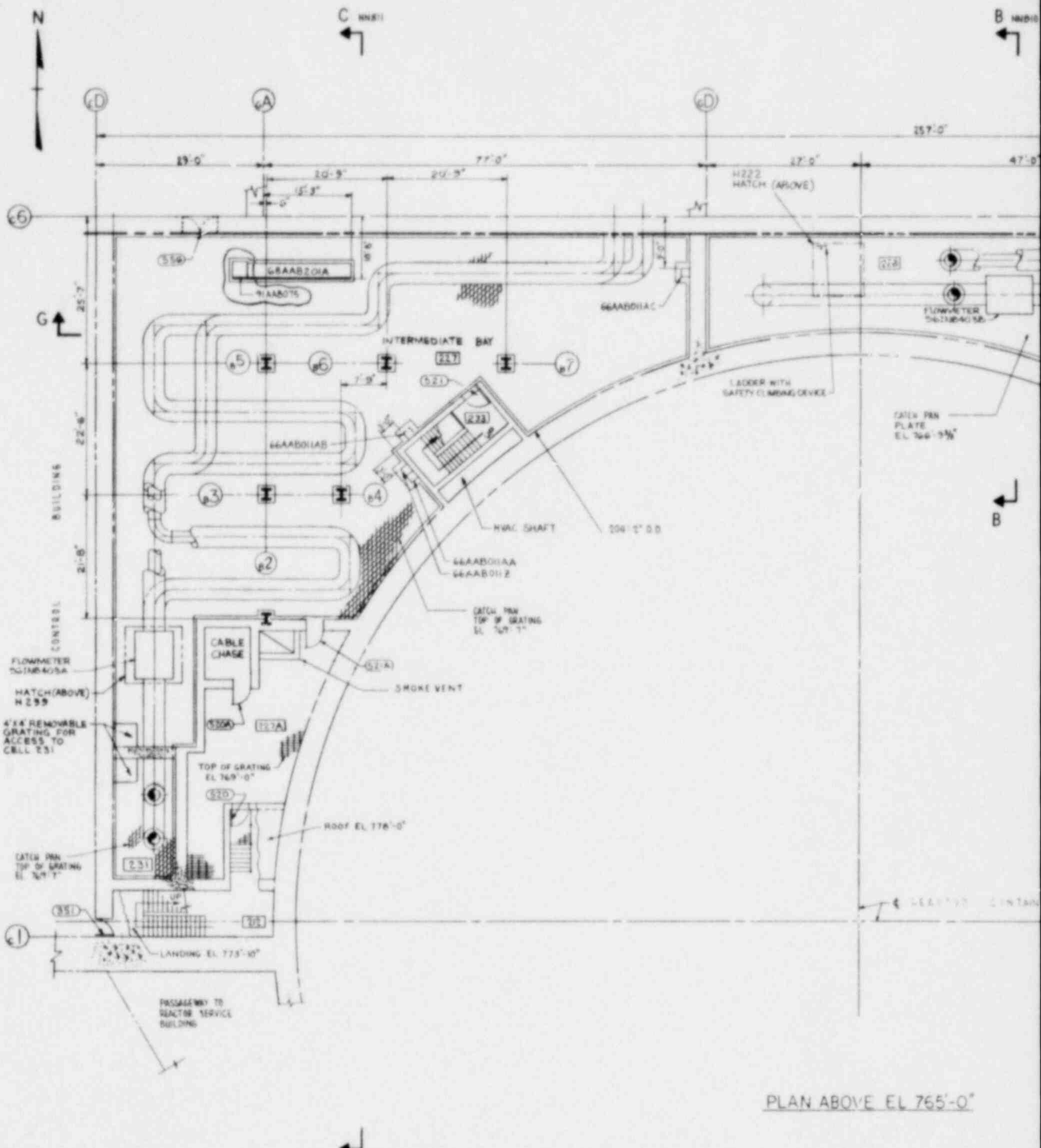

PLAN ABOVE EL 765'-0"

NN803-12

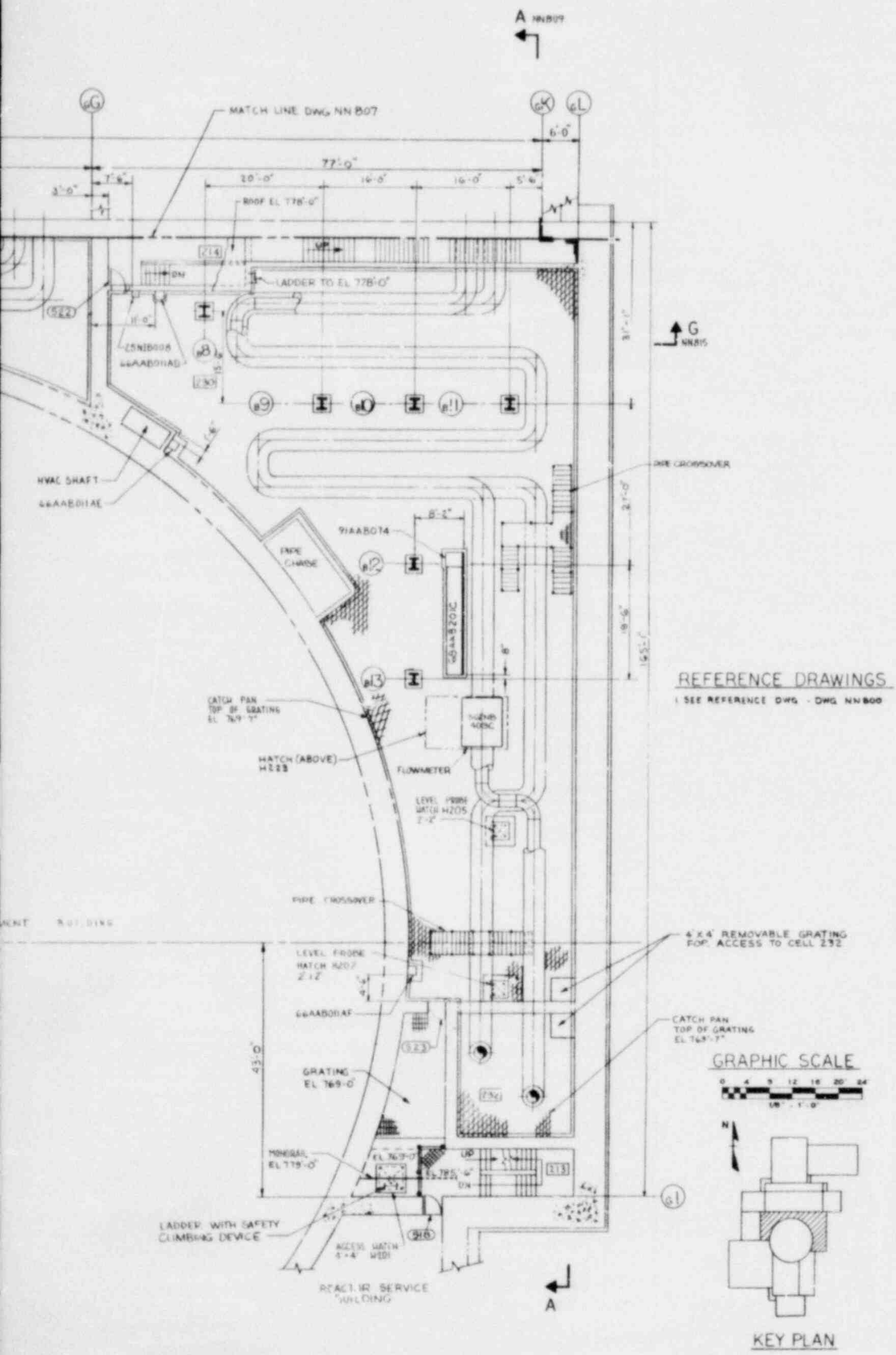

Figure 1.2-51
General Arrangement
Steam Generator Building
Plan El. 765'-0"

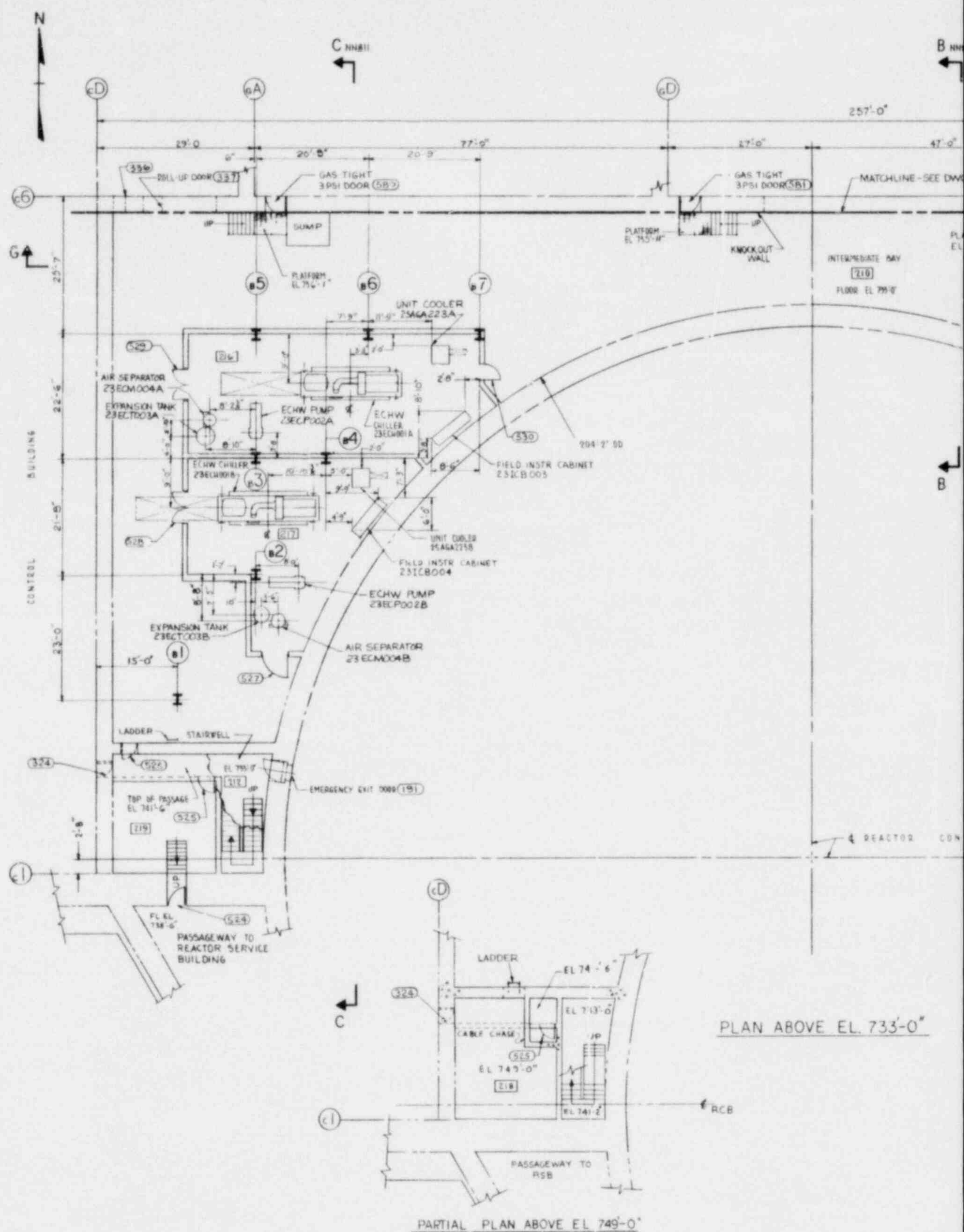

N
C NN811
B
257'-0"
29'-0
20'-8"
20'-9"
77'-0"
27'-0"
47'-0"
ROLL-UP DOOR
GAS TIGHT
3 PSI DOOR
MATCHLINE - SEE DWG
SUMP
PLATFORM
KNOCKOUT WALL
INTERMEDIATE BAY
UNIT COOLER
AIR SEPARATOR
23ECM004A
EXPANSION TANK
23ECT003A
ECHW PUMP
23ECP002A
ECHW CHILLER
FIELD INSTR CABINET
23ICB003
ECHW CHILLER
FIELD INSTR CABINET
23ICB004
ECHW PUMP
23ECP002B
EXPANSION TANK
23ECT003B
AIR SEPARATOR
23ECM004B
CONTROL BUILDING
15'-0"
LADDER
STAIRWELL
EMERGENCY EXIT DOOR
TOP OF PASSAGE
PASSAGEWAY TO
REACTOR SERVICE
BUILDING
REACTOR
C
PLAN ABOVE EL. 733'-0"
LADDER
CABLE CHASE
PASSAGEWAY TO
RSB
RCB
PARTIAL PLAN ABOVE EL 749'-0"

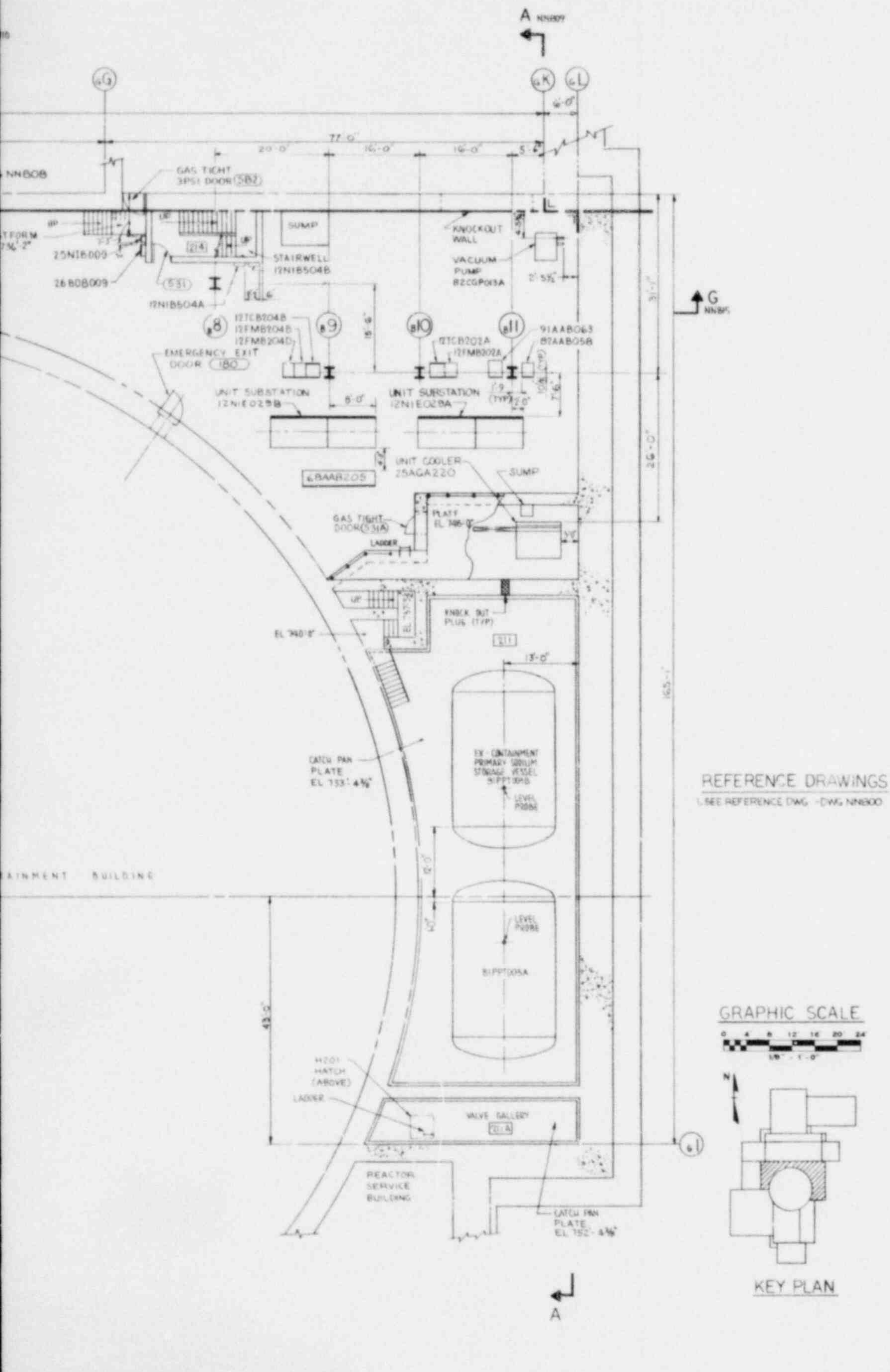

Figure 1.2-52
General Arrangement
Steam Generator Building
Plan El. 733'-0"

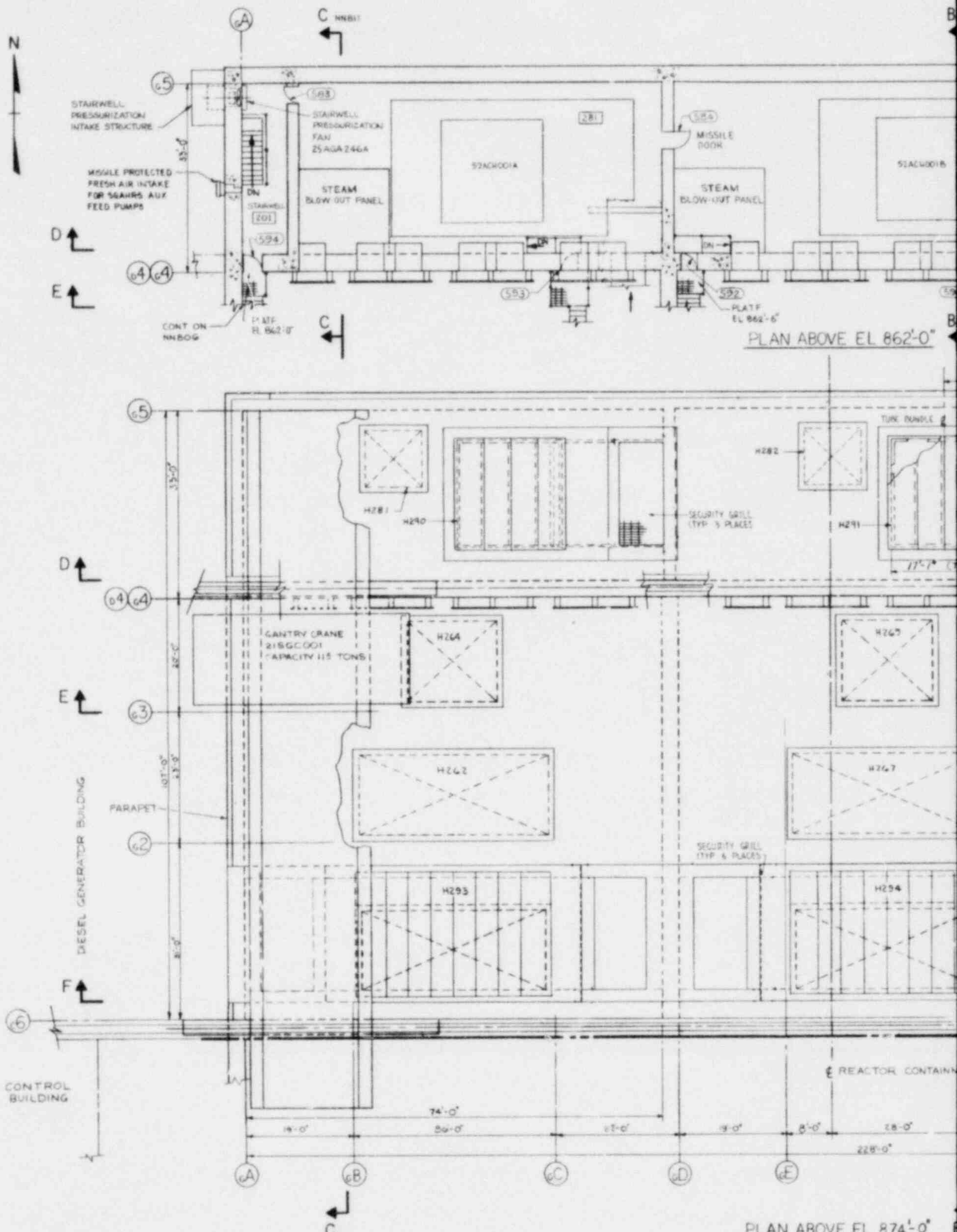
C
N
STAIRWELL PRESSURIZATION INTAKE STRUCTURE
MISSILE PROTECTED FRESH AIR INTAKE FOR 56AHRS AUX FEED PUMPS
STAIRWELL PRESSURIZATION FAN
DN
STAIRWELL
201
281
STEAM BLOW OUT PANEL
MISSILE DOOR
STEAM BLOW-OUT PANEL
D
E
594
593
592
CONT ON NN809
PLATF EL 862'-0"
PLATF EL 862'-6"
PLAN ABOVE EL 862'-0"
TUBE BUNDLE
H282
H281
H290
H291
SECURITY GRILL (TYP 3 PLACES)
GANTRY CRANE 21SGC001 CAPACITY 115 TONS
H264
H267
H262
H267
PARAPET
DIESEL GENERATOR BUILDING
SECURITY GRILL (TYP 6 PLACES)
H293
H294
F
CONTROL BUILDING
REACTOR CONTAINM
74'-0"
228'-0"
PLAN ABOVE EL 874'-0"

NN805-12

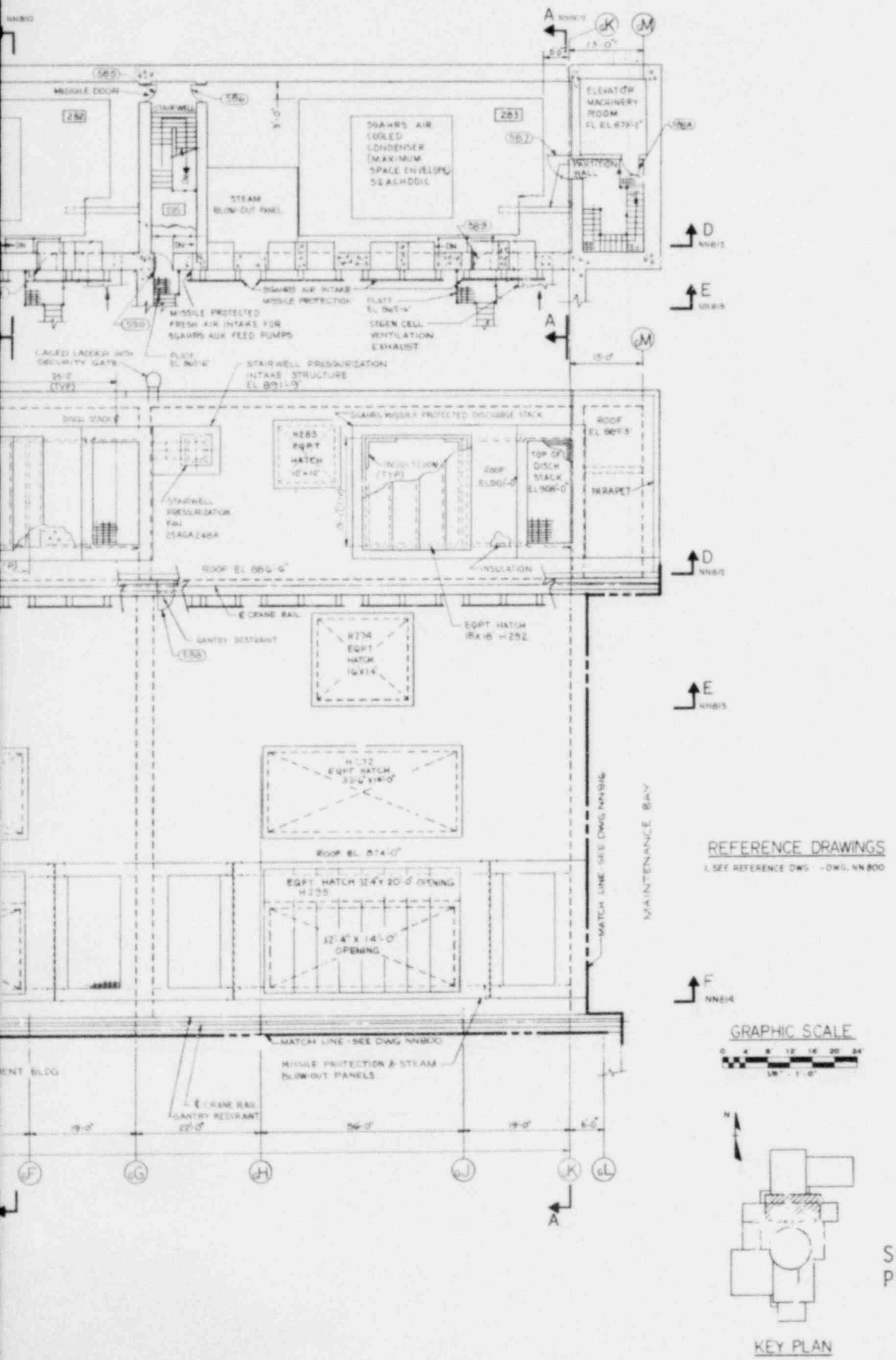

Figure 1.2-53
General Arrangement
Steam Generator Building
Plan El. 874'-0" and
El. 862'-0"

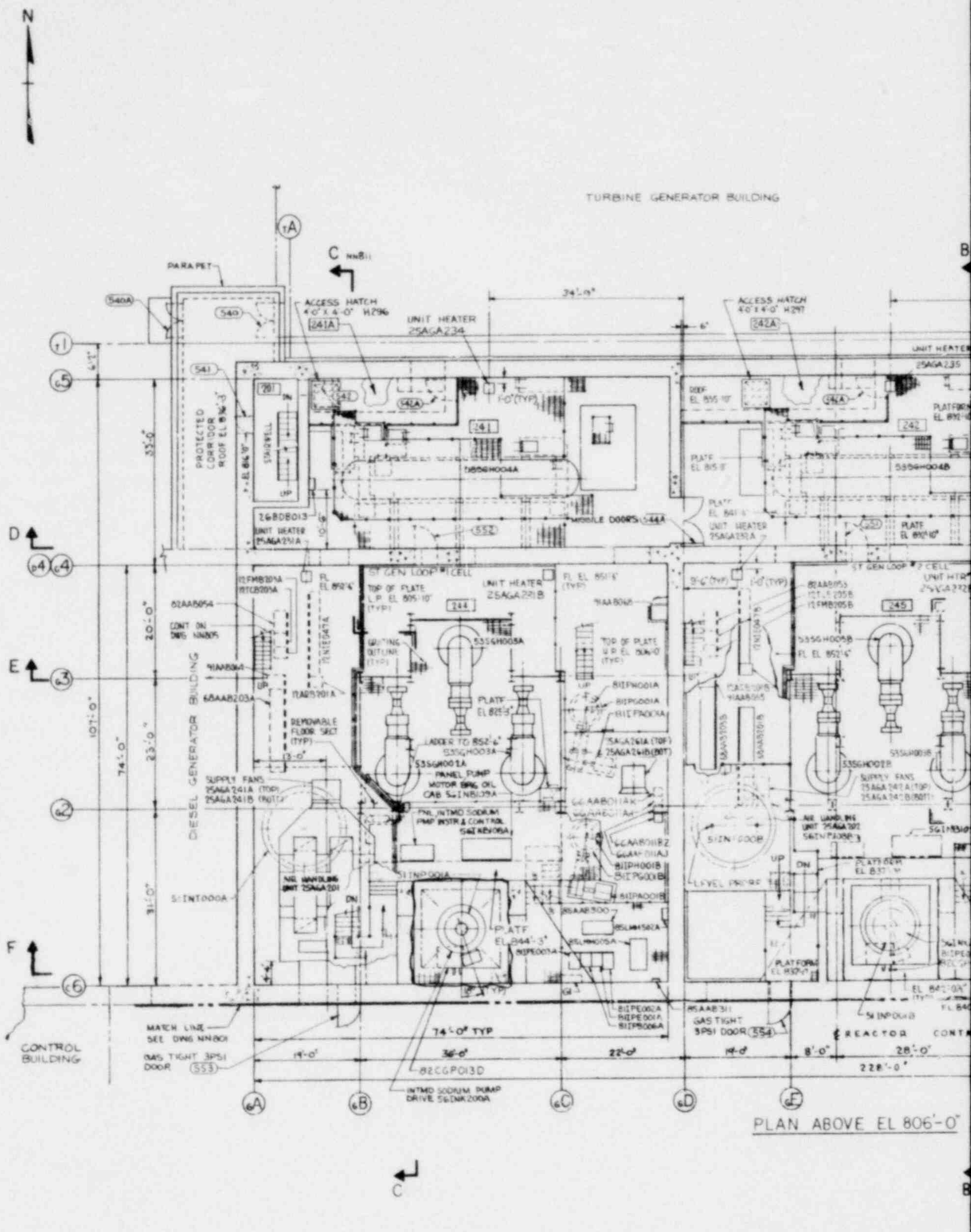

PLAN ABOVE EL 806'-0"

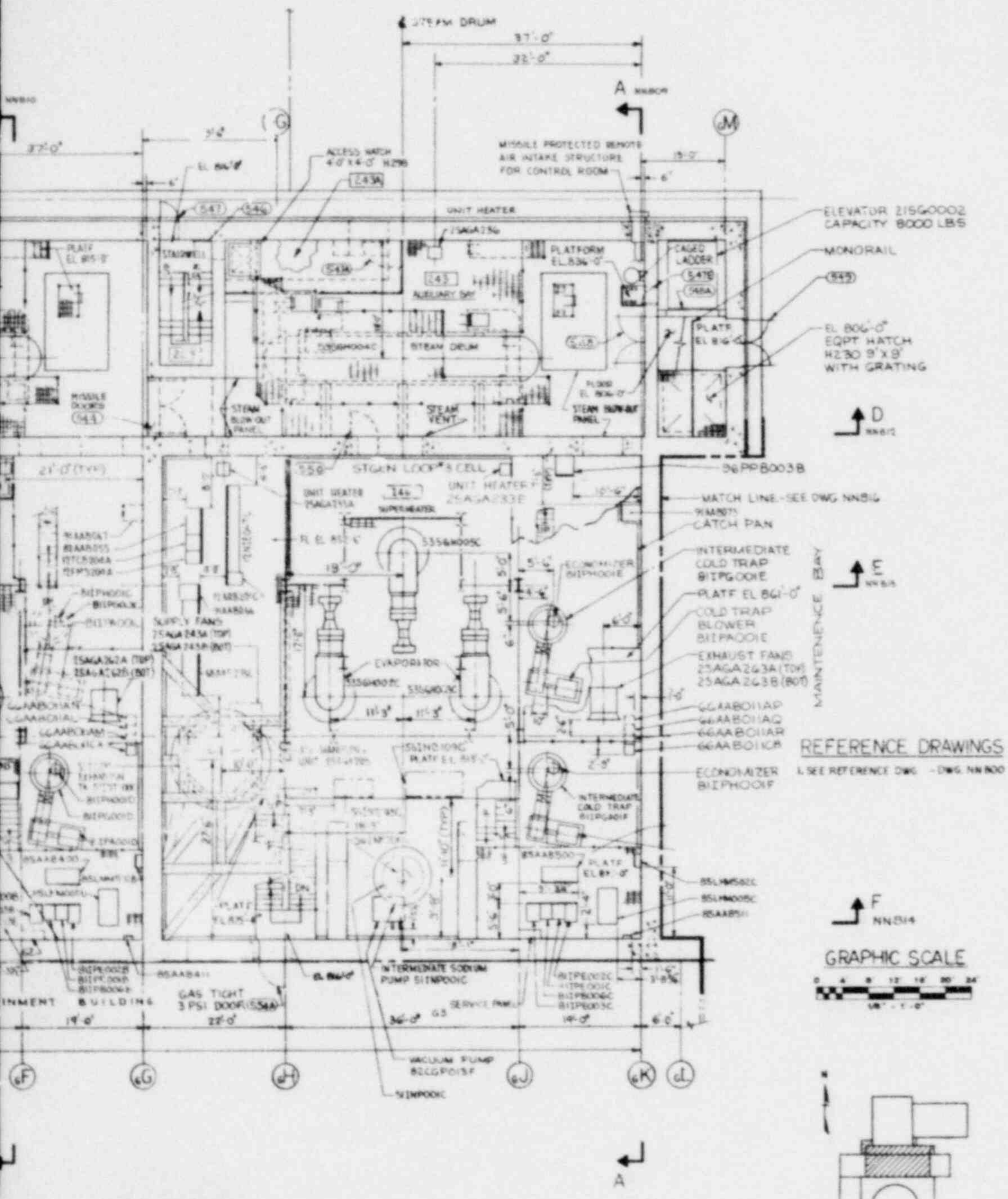

KEY PLAN

Figure 1.2-54
General Arrangement
Steam Generator Building
Plan El. 806'-0"

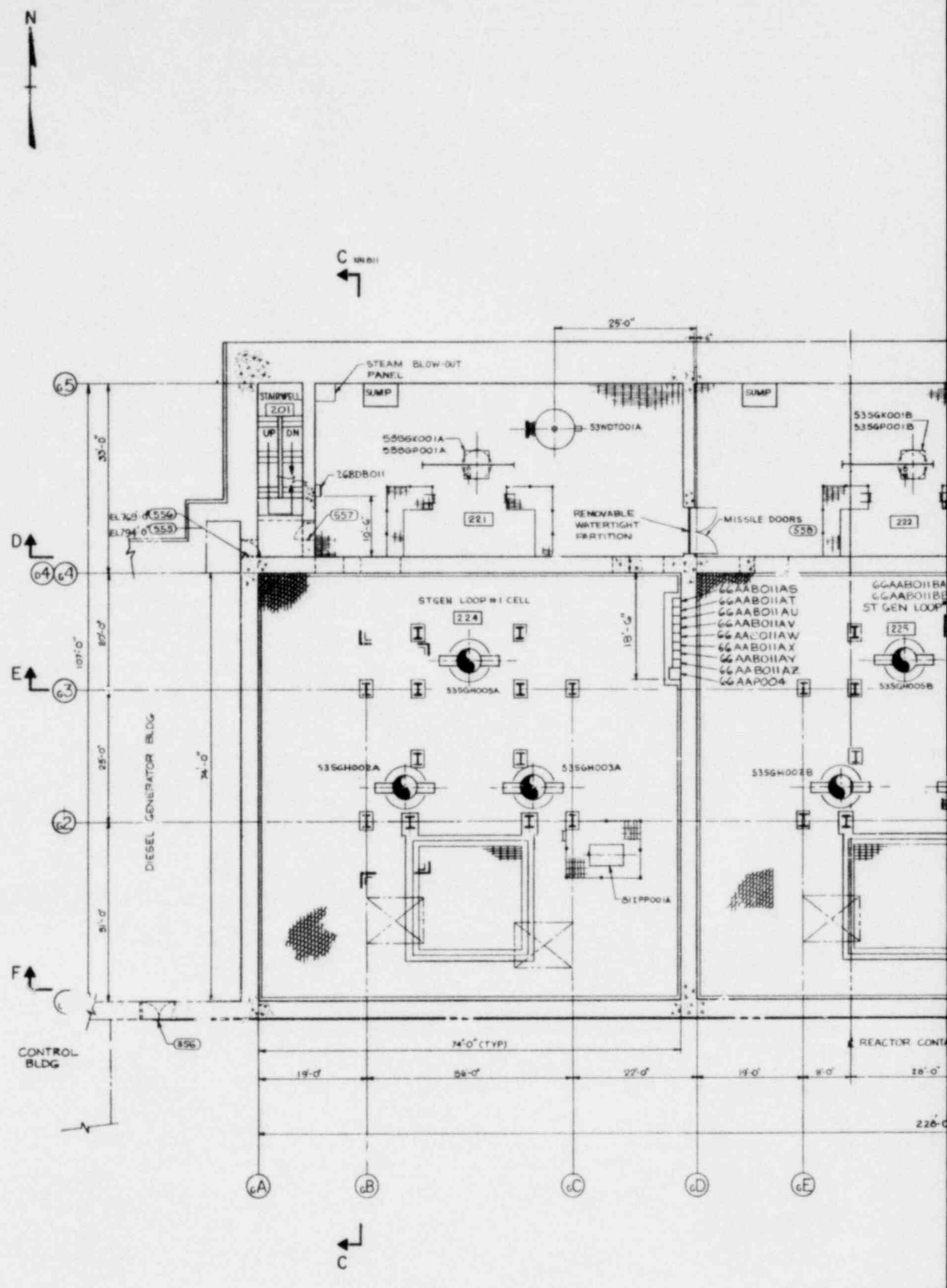
N
C NN811
25'-0"
STEAM BLOW-OUT PANEL
STAIRWELL
201
UP
DN
SUMP
53WDT001A
58BGK001A
58BGP001A
2GBDB011
557
EL 769'-0" 556
EL 794'-0" 555
221
REMOVABLE WATERTIGHT PARTITION
MISSILE DOORS
558
SUMP
53SGK001B
53SGP001B
222
STGEN LOOP #1 CELL
224
66AAB011AS
66AAB011AT
66AAB011AU
66AAB011AV
66AAB011AW
66AAB011AX
66AAB011AY
66AAB011AZ
66AAP004
ST GEN LOOP
225
53SGH005A
53SGH005B
53SGH002A
53SGH003A
53SGH002B
81IPP001A
DIESEL GENERATOR BLDG
35'-0"
20'-0"
107'-0"
25'-0"
51'-0"
74'-0"
18'-6"
10'-6"
D
E
F
CONTROL BLDG
856
74'-0" (TYP)
19'-0"
36'-0"
22'-0"
19'-0"
REACTOR CONT
228'-0
C
PLAN ABOVE EL 765

NN807-12

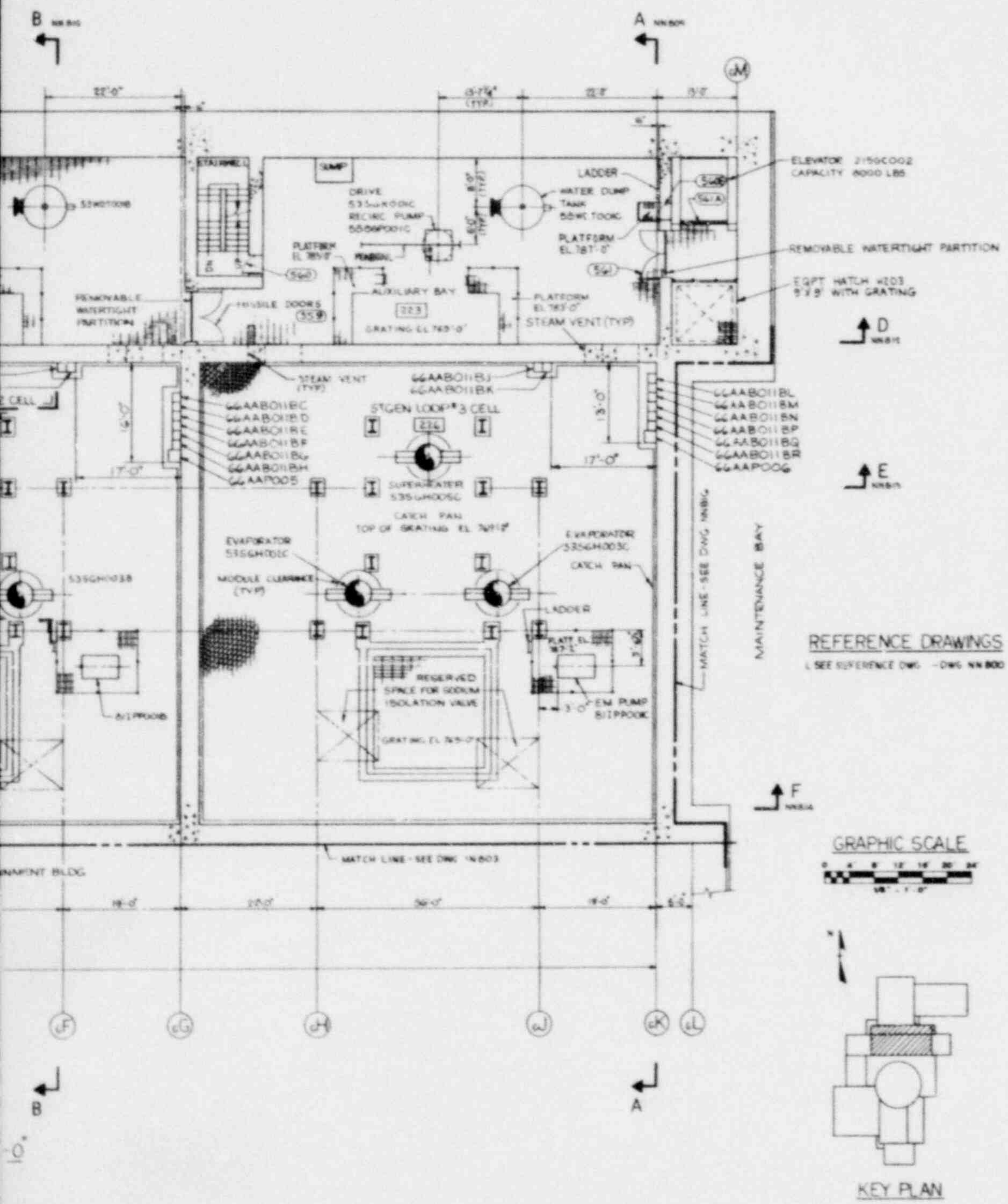

Figure 1.2-55
General Arrangement
Steam Generator Building
Plan 765'-0"

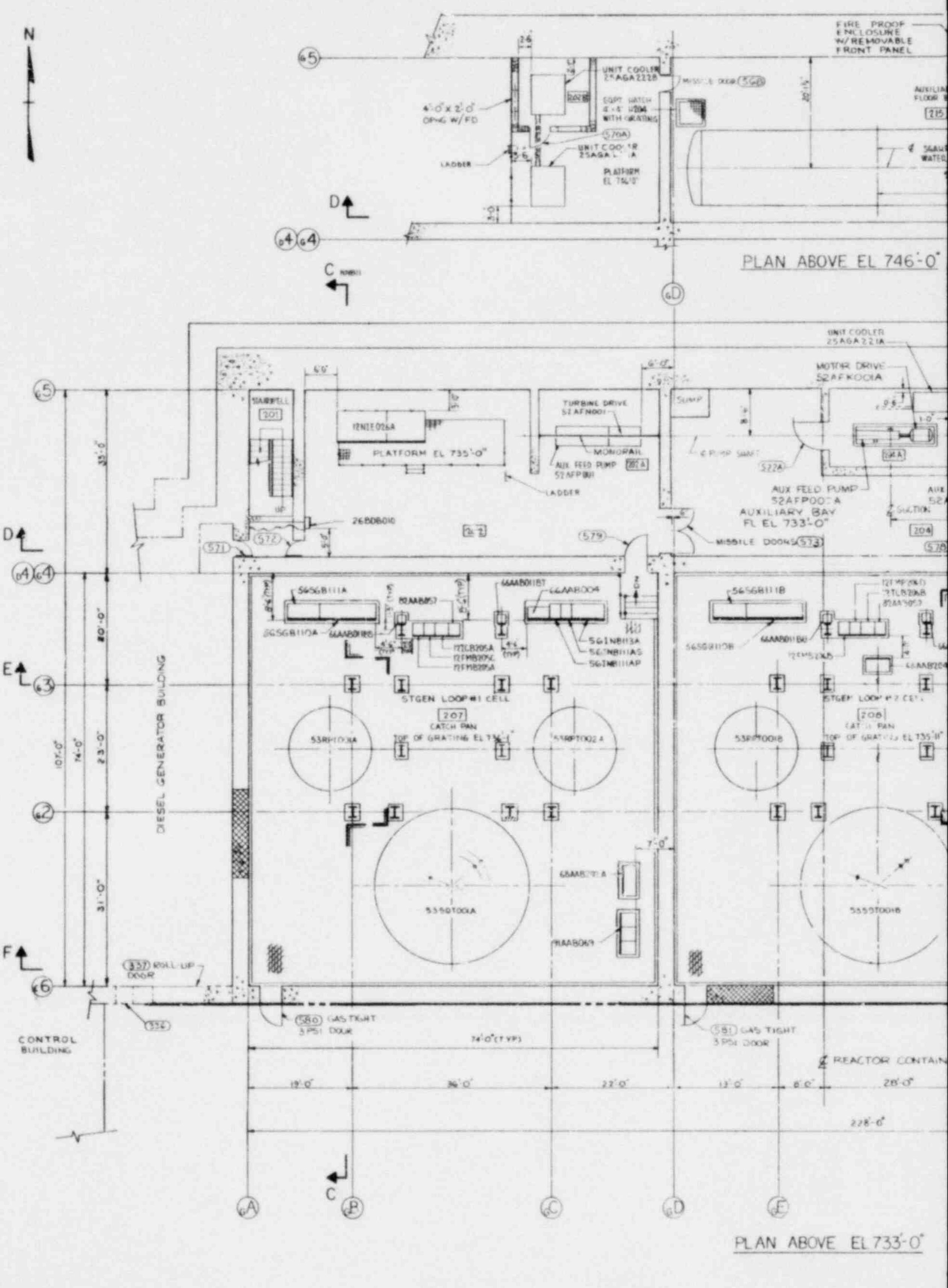

PLAN ABOVE EL 746'-0"
FIRE PROOF ENCLOSURE W/REMOVABLE FRONT PANEL
UNIT COOLER 25AGA222B
4'-0" X 2'-0" OPNG W/FD
LADDER
PLATFORM
STAIRWELL
201
PLATFORM EL 735'-0"
TURBINE DRIVE
MONORAIL
AUX FEED PUMP
LADDER
UNIT COOLER 25AGA221A
MOTOR DRIVE 52AFK001A
SUMP
AUX FEED PUMP 52AFP001A
AUXILIARY BAY
FL EL 733'-0"
204
MISSILE DOORS 573
26BDB010
571
572
579
DIESEL GENERATOR BUILDING
STGEN LOOP #1 CELL
207
CATCH PAN
208
53RPT001A
53RPT002A
53RPT001B
555OT001A
555OT001B
56SGB111A
56SGB111B
66AAB004
STGEN LOOP #2 CELL
337 ROLL-UP DOOR
580 GAS TIGHT 3 PSI DOOR
581 GAS TIGHT 3 PSI DOOR
334
CONTROL BUILDING
74'-0" (TYP)
REACTOR CONTAIN
19'-0"
36'-0"
22'-0"
13'-0"
6'-0"
28'-0"
228'-0"
107'-0"
74'-0"
23'-0"
31'-0"
33'-0"
80'-0"
7'-0"
6'-0"
PLAN ABOVE EL 733'-0"

NN808-13

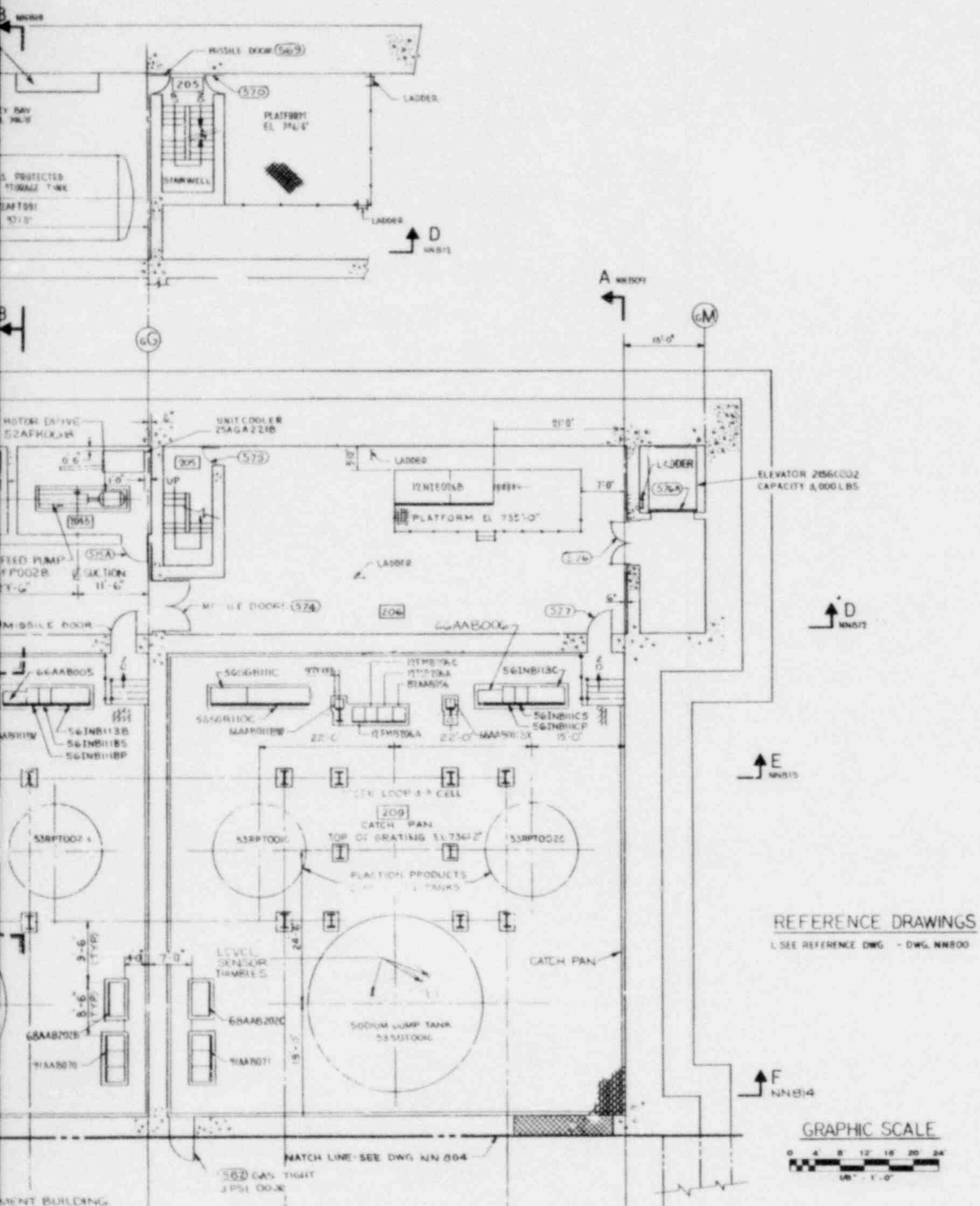

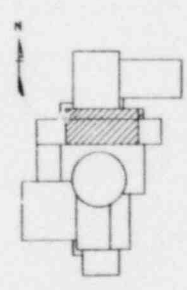

KEY PLAN

Figure 1.2-56
General Arrangement
Steam Generator Building
Plan 733'-0" and
El. 746'-0"

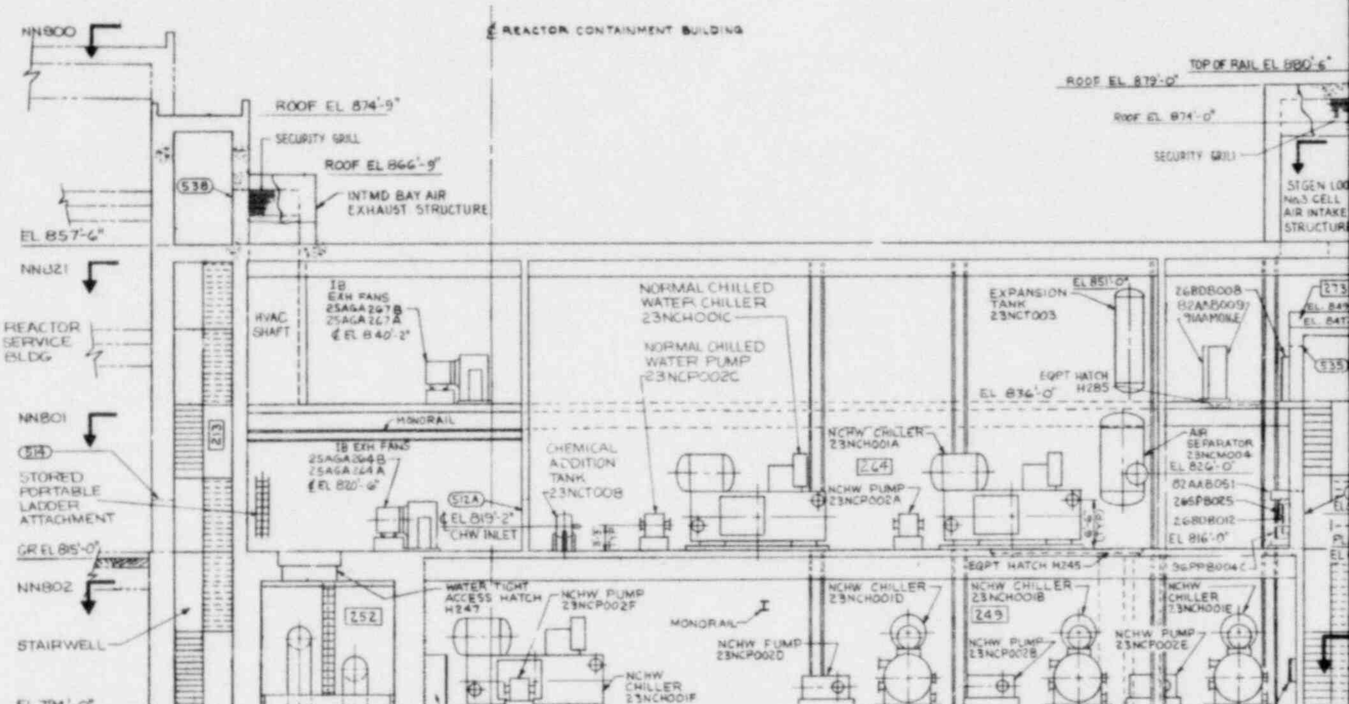

℄ REACTOR CONTAINMENT BUILDING
NN800
ROOF EL 874'-9"
SECURITY GRILL
ROOF EL 866'-9"
INTMD BAY AIR EXHAUST STRUCTURE
EL 857'-6"
NN821
REACTOR SERVICE BLDG
NN801
STORED PORTABLE LADDER ATTACHMENT
GR EL 815'-0"
NN802
STAIRWELL
EL 794'-0"
NN803
MONORAIL
ACCESS HATCH H201
EL 769'-0"
NN804
VALVE GALLERY
CATCH PAN
HVAC SHAFT
MONORAIL
NORMAL CHILLED WATER CHILLER 23NCH001C
NORMAL CHILLED WATER PUMP 23NCP002C
CHEMICAL ADDITION TANK 23NCT008
CHW INLET
WATER TIGHT ACCESS HATCH H247
NCHW PUMP 23NCP002F
NCHW CHILLER 23NCH001F
NCHW PUMP 23NCP002D
CATCH PAN
EQPT HATCH H223
LEVEL PROBE PULL SPACE
PIPE CROSSOVER
FIRE SUPPRESSION DECK
CATCH PAN
INSULATION
LEVEL PROBE PULL SPACE
LEVEL PROBE HATCH H202
LEVEL PROBE HATCH H205
81PPT003A
81PPT003B
SLOPE ⅛"/FT
KNOCKOUT PLUGS
2⅛" GROUTING (TYP)
CATCH PAN
EX CONTAINMENT PRIMARY SODIUM STORAGE VESSEL
EXPANSION TANK 23NCT003
EQPT HATCH H285
NCHW CHILLER 23NCH001A
NCHW PUMP 23NCP002A
EQPT HATCH H245
NCHW CHILLER 23NCH001D
NCHW CHILLER 23NCH001B
NCHW PUMP 23NCP002B
NCHW PUMP 23NCP002E
NCHW CHILLER 23NCH001E
PIPE CHASE
HVAC SHAFT
PIPE CROSSOVER
LADDER
PLATE EL 738'-0"
UNIT COOLER 25AGA220
SUMP
GAS TIGHT DOOR
UNIT SUBSTATION 12N1E029A
VACUUM PUMP 82CCP013A
TOP OF RAIL EL 880'-6"
ROOF EL 879'-0"
ROOF EL 874'-0"
SECURITY GRILL
STGEN LOOP No.3 CELL AIR INTAKE STRUCTURE
AIR SEPARATOR 23NCM004

NN809-14

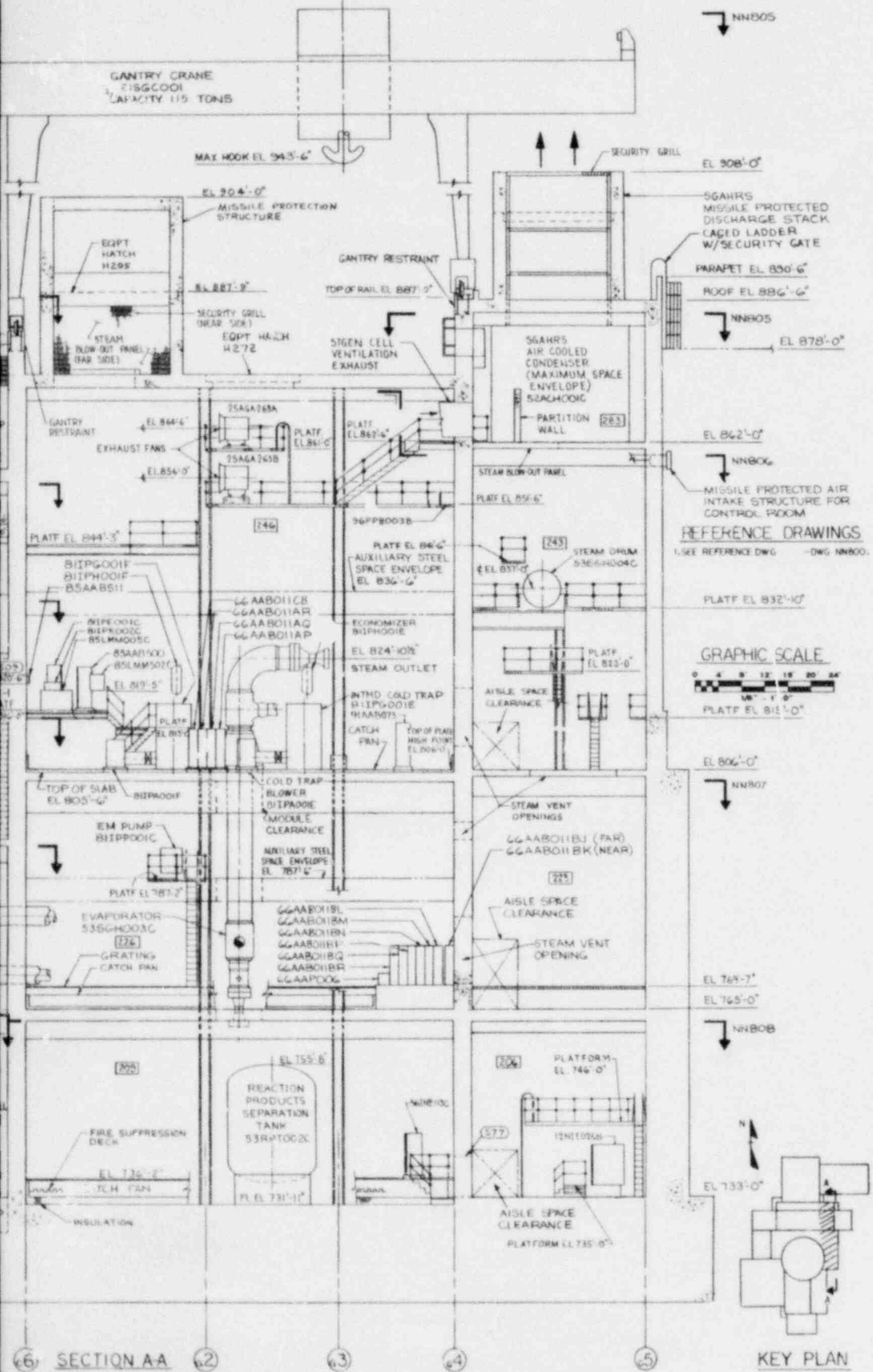

Figure 1.2-57
General Arrangement
Steam Generator Building
Section A-A

Amend. 56
Aug. 1980

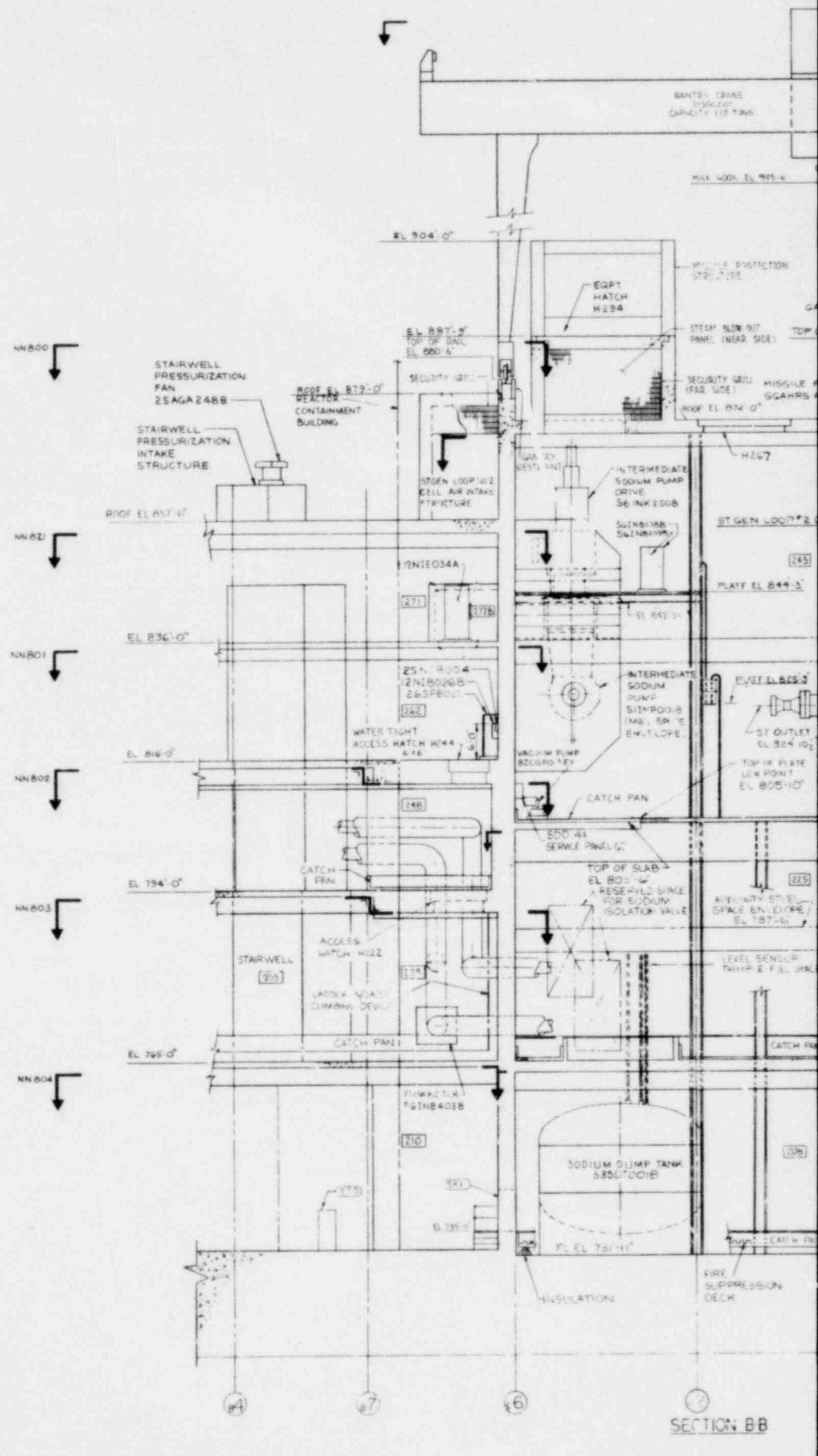
GANTRY CRANE
MAX HOOK EL
EL 904'-0"
EQPT HATCH H294
MISSILE PROTECTION STRUCTURE
EL 897'-9" TOP OF RAIL
EL 880'-6"
STEAM BLOW OUT PANEL (NEAR SIDE)
SECURITY GRILL (FAR SIDE)
ROOF EL 874'-0"
NN800
STAIRWELL PRESSURIZATION FAN 25AGA248B
STAIRWELL PRESSURIZATION INTAKE STRUCTURE
ROOF EL 879'-0" REACTOR CONTAINMENT BUILDING
SECURITY GRILL
ST GEN LOOP NO 2 CELL AIR INTAKE STRUCTURE
H267
INTERMEDIATE SODIUM PUMP DRIVE 56INK200B
ROOF EL 857'-0"
NN821
ST GEN LOOP #2
PLATF EL 844'-3"
EL 836'-0"
NN801
25NI8004
12NI8026B
26SPB021
INTERMEDIATE SODIUM PUMP
WATER TIGHT ACCESS HATCH H244
VACUUM PUMP
ST OUTLET
TOP OF PLATE LOW POINT EL 805'-10"
EL 816'-0"
NN802
CATCH PAN
SERVICE PANEL
TOP OF SLAB EL 805'-6"
RESERVED SPACE FOR SODIUM ISOLATION VALVE
CATCH PAN
EL 794'-0"
NN803
AUXILIARY STEEL SPACE ENVELOPE EL 787'-6"
ACCESS HATCH H222
STAIRWELL
LADDER W/ AUX CLIMBING DEVICE
LEVEL SENSOR THIMBLE FILL SPACE
CATCH PAN
EL 765'-0"
NN804
SODIUM DUMP TANK
INSULATION
FIRE SUPPRESSION DECK
SECTION BB

NN810-14

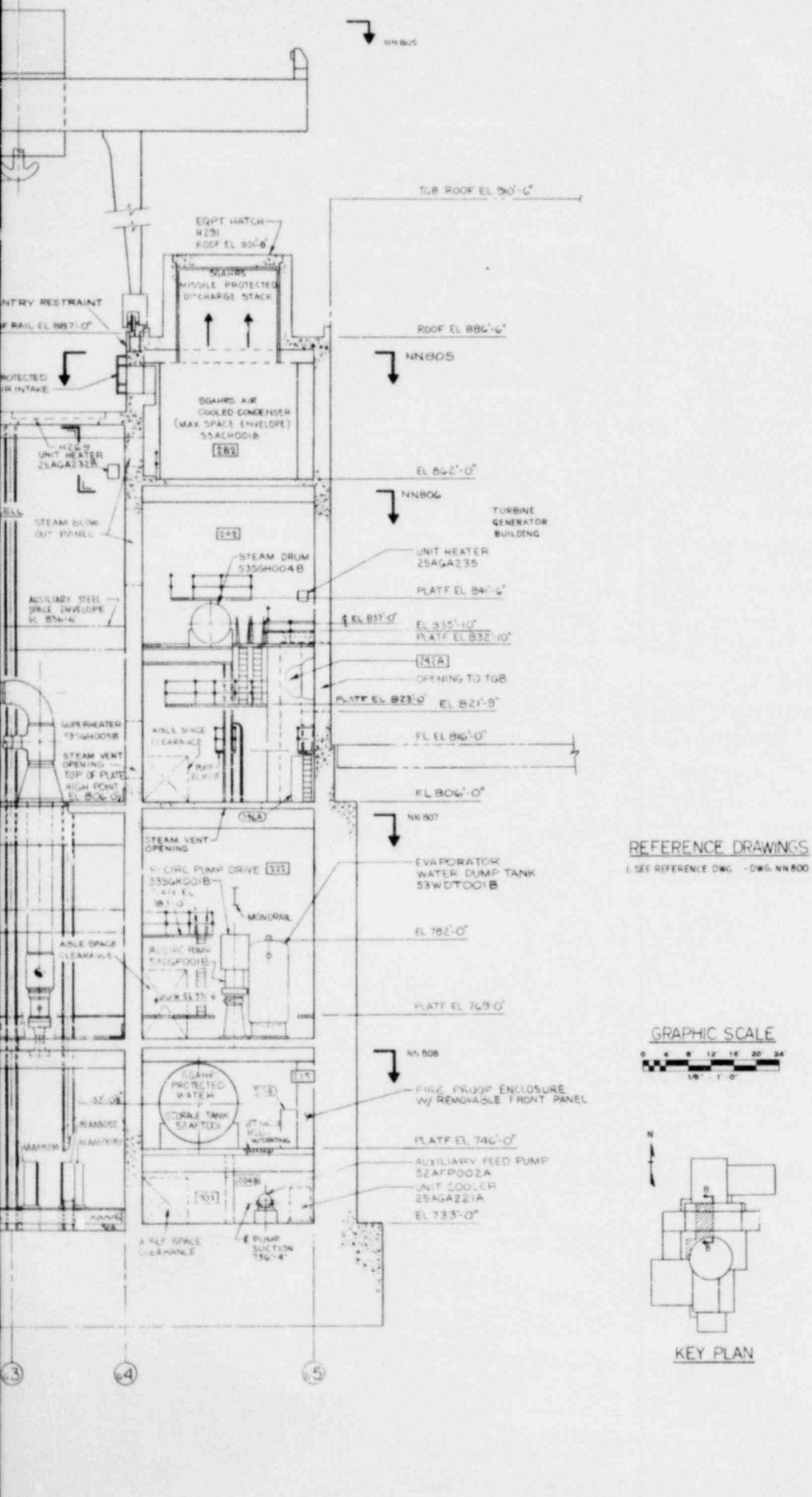

Figure 1.2-58
General Arrangement
Steam Generator Building
Section B-B

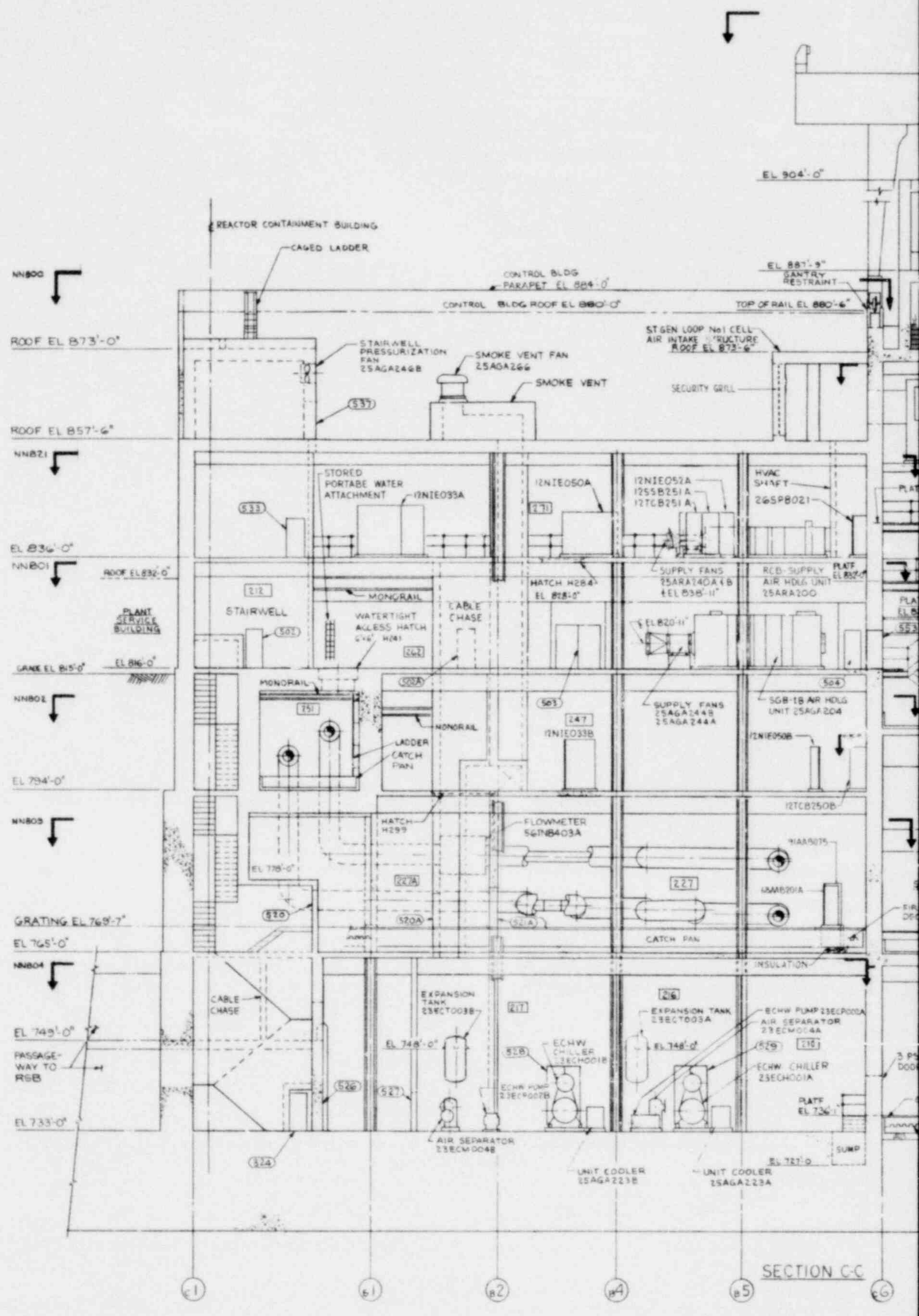
REACTOR CONTAINMENT BUILDING
CAGED LADDER
CONTROL BLDG PARAPET EL 884'-0"
CONTROL BLDG ROOF EL 880'-0"
EL 904'-0"
EL 887'-9" GANTRY RESTRAINT
TOP OF RAIL EL 880'-6"
ST GEN LOOP No1 CELL AIR INTAKE STRUCTURE ROOF EL 873'-6"
ROOF EL 873'-0"
ROOF EL 857'-6"
STAIRWELL PRESSURIZATION FAN 25AGA249B
SMOKE VENT FAN 25AGA266
SMOKE VENT
SECURITY GRILL
STORED PORTABE WATER ATTACHMENT
12NIE033A
12NIE050A
12NIE052A
12SSB251A
12TCB251A
HVAC SHAFT
26SPB021
EL 836'-0"
ROOF EL 832'-0"
STAIRWELL
MONORAIL
WATERTIGHT ACCESS HATCH
CABLE CHASE
HATCH H284 EL 818'-0"
SUPPLY FANS 25ARA240A & B EL 838'-11"
RCB SUPPLY AIR HDLG UNIT 25ARA200
PLANT SERVICE BUILDING
GRADE EL 815'-0"
EL 816'-0"
MONORAIL
LADDER
CATCH PAN
12NIE033B
SUPPLY FANS 25AGA244B 25AGA244A
SGB-1B AIR HDLG UNIT 25AGA204
12NIE050B
EL 794'-0"
12TCB250B
HATCH H299
FLOWMETER 56INB403A
EL 778'-0"
GRATING EL 769'-7"
EL 765'-0"
CATCH PAN
INSULATION
CABLE CHASE
EXPANSION TANK 23ECT003B
EXPANSION TANK 23ECT003A
ECHW CHILLER
ECHW PUMP 23ECP002A
AIR SEPARATOR 23ECM004A
ECHW CHILLER 23ECH001A
EL 749'-0"
EL 748'-0"
PASSAGE-WAY TO RSB
EL 733'-0"
AIR SEPARATOR 23ECM004B
UNIT COOLER 25AGA223B
UNIT COOLER 25AGA223A
SUMP
SECTION C-C

NN811-12

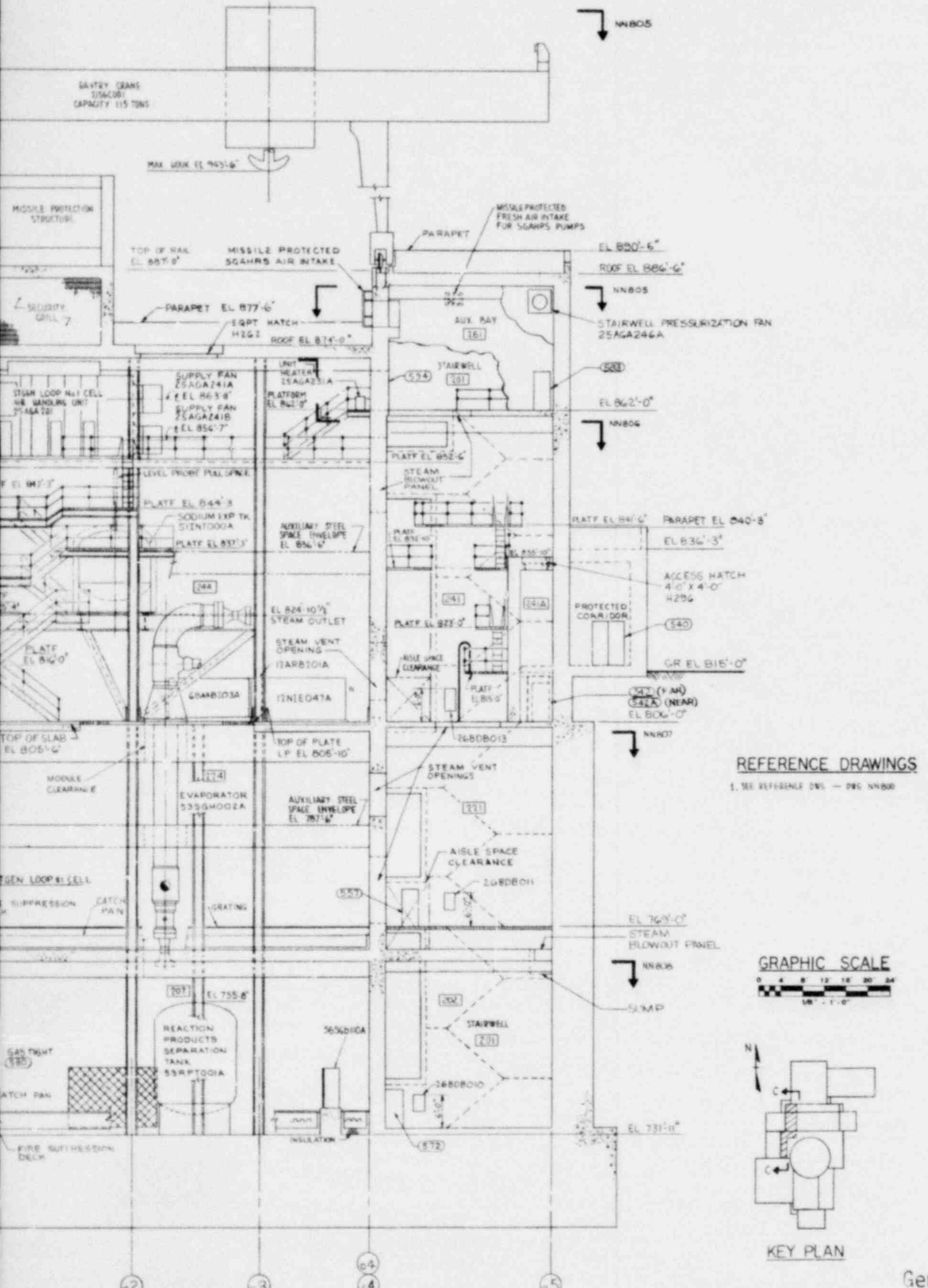

Figure 1.2-59
General Arrangement
Steam Generator Building
Section C-C

Amend. 56
Aug. 1980

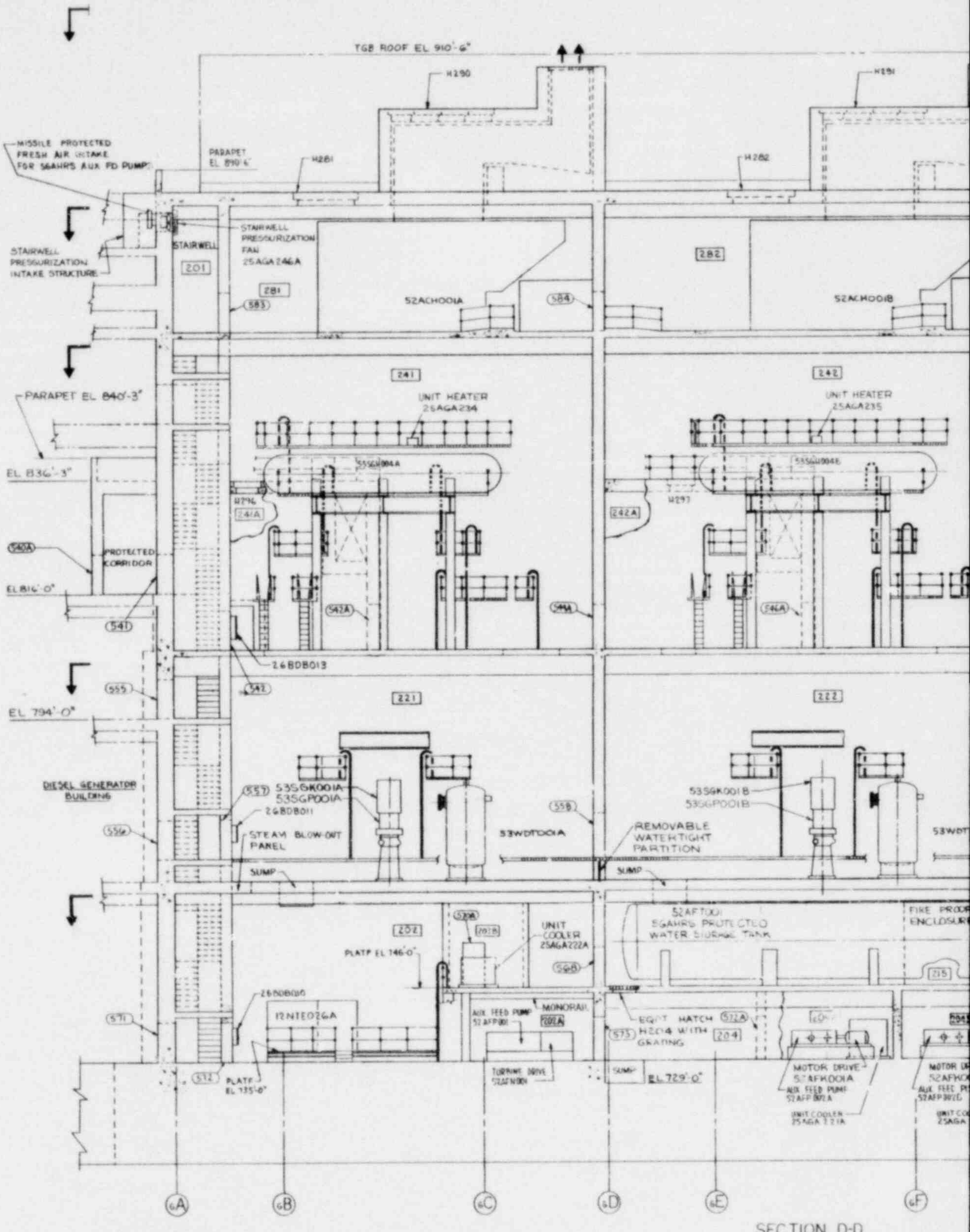

SECTION D-D

NN812-13

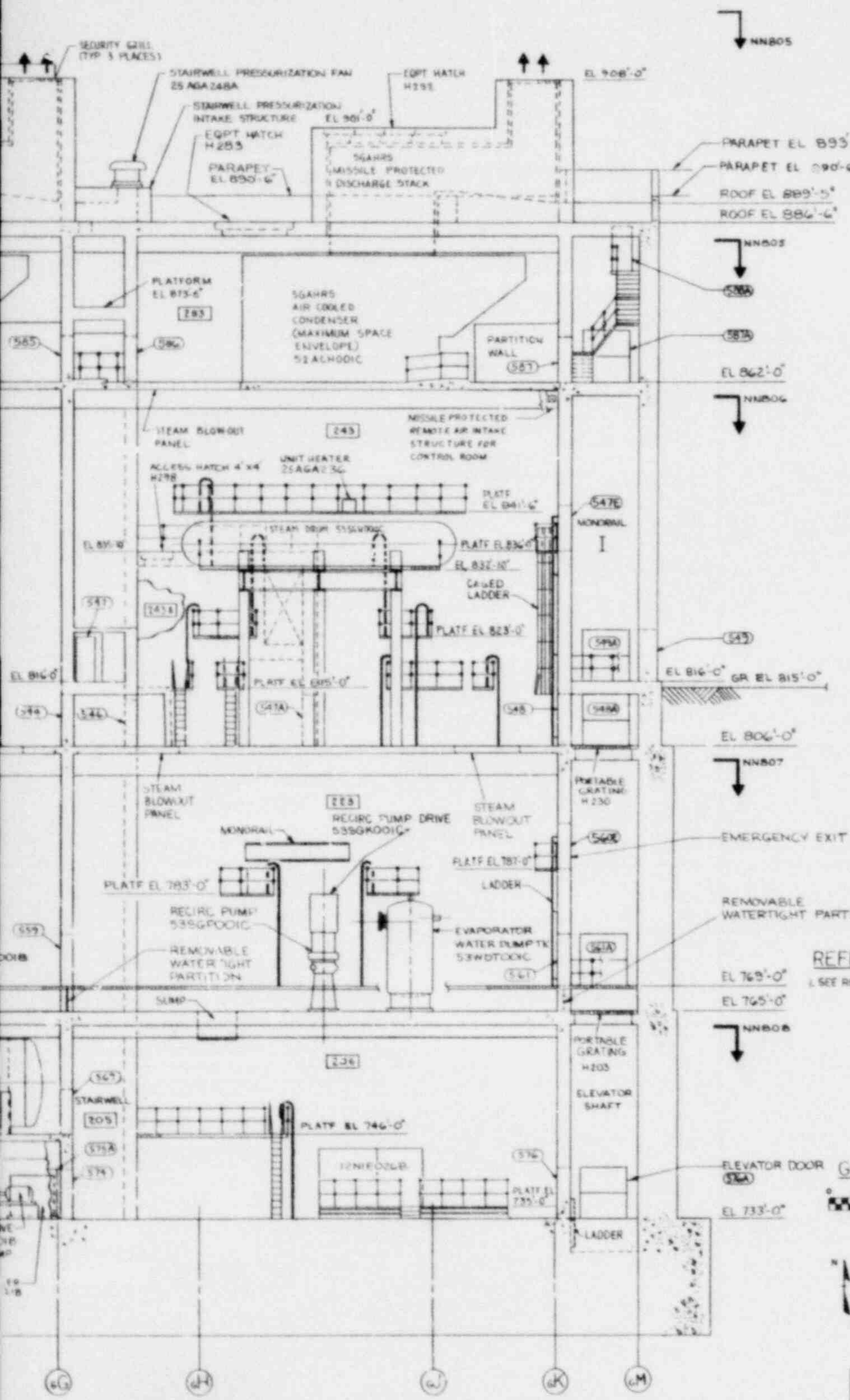

REFERENCE DRAWINGS

GRAPHIC SCALE

KEY PLAN

Figure 1.2-60
General Arrangement
Steam Generator Building
Section D-D

Amend. 56
Aug. 1980

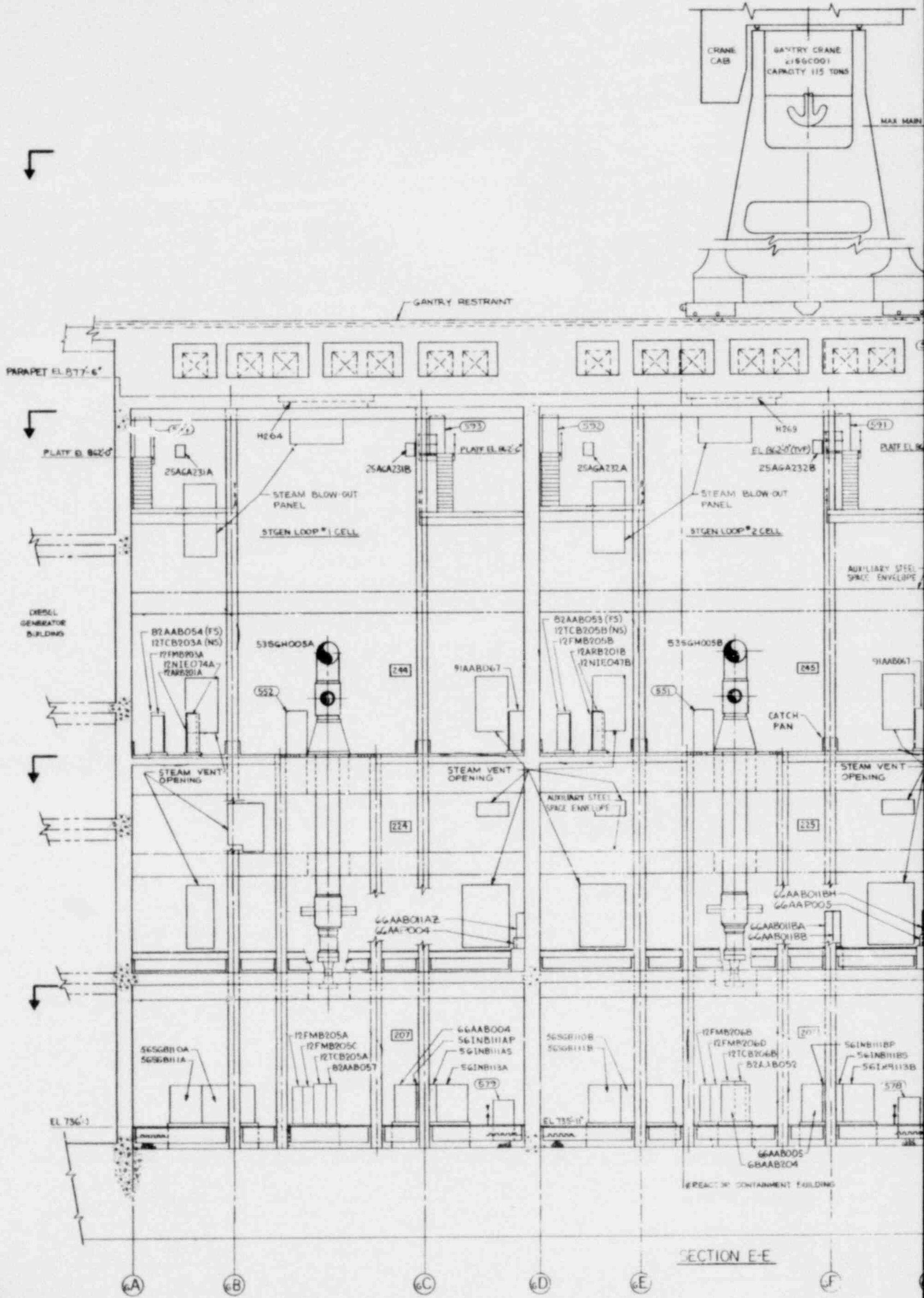

CRANE CAB
GANTRY CRANE
CAPACITY 115 TONS
MAX MAIN
GANTRY RESTRAINT
PARAPET EL 877'-6"
PLATF EL 862'-0"
H264
H269
25AGA231A
25AGA231B
25AGA232A
25AGA232B
STEAM BLOW-OUT PANEL
STGEN LOOP #1 CELL
STGEN LOOP #2 CELL
AUXILIARY STEEL SPACE ENVELOPE
DIESEL GENERATOR BUILDING
82AAB054 (FS)
12TCB203A (NS)
82AAB053 (FS)
12TCB205B (NS)
12FMB205B
12ARB201B
12NIE047B
53SGH005A
53SGH005B
91AAB067
CATCH PAN
STEAM VENT OPENING
66AAB011AZ
66AAP004
66AAB011BH
66AAP005
66AAB011BA
66AAB011BB
12FMB205A
12FMB205C
12TCB205A
82AAB057
66AAB004
56INB111AP
56INB111AS
56INB113A
12FMB206B
12FMB206D
12TCB206B
82AAB052
56INB111BP
56INB111BS
56INB113B
66AAB005
68AAB204
REACTOR CONTAINMENT BUILDING
EL 736'-1"
552
551
244
245
224
225
207
579
578
593
592
591
6A
6B
6C
6D
6E
6F
SECTION E-E

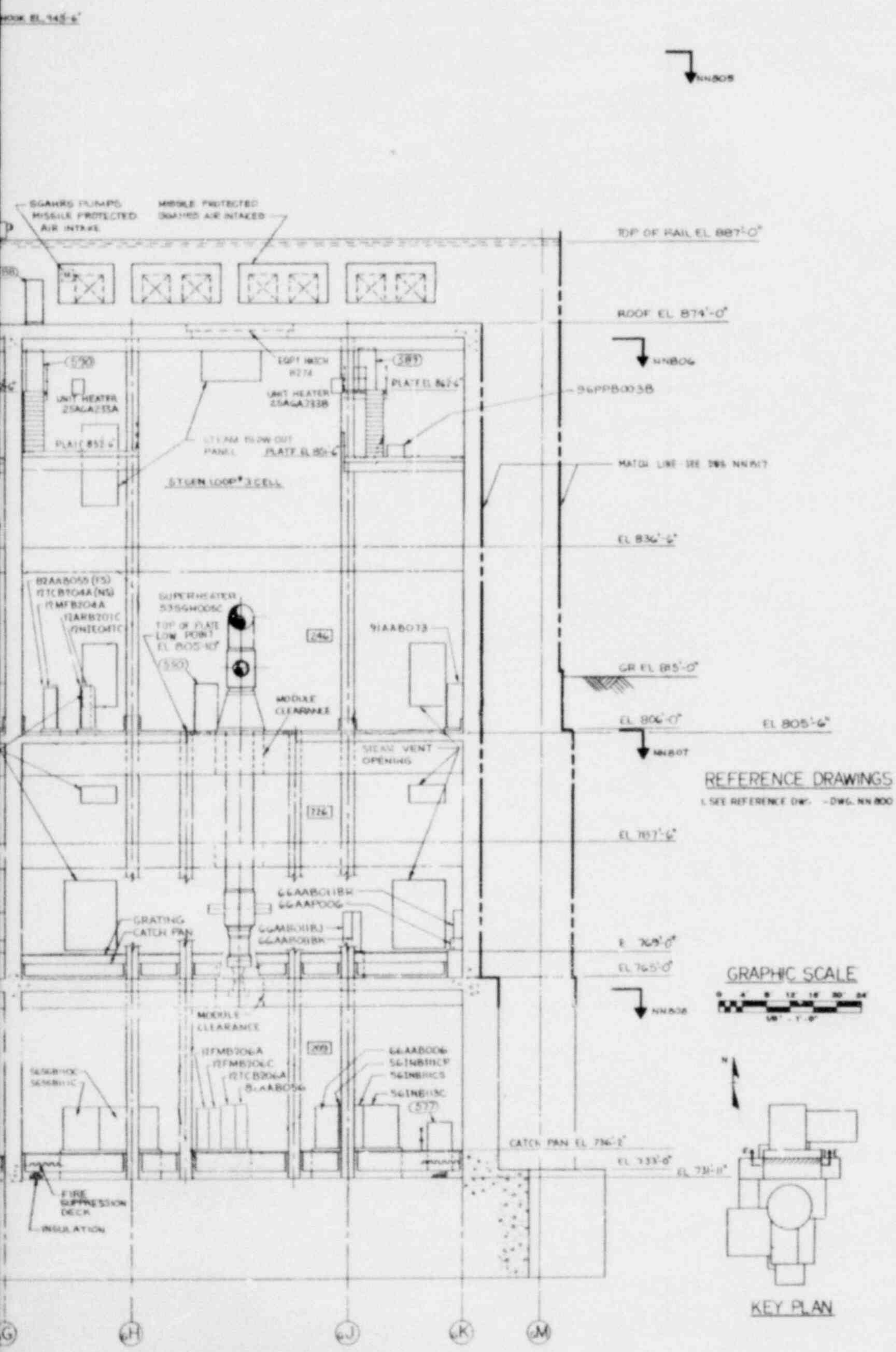

Figure 1.2-61
General Arrangement
Steam Generator Building
Section E-E

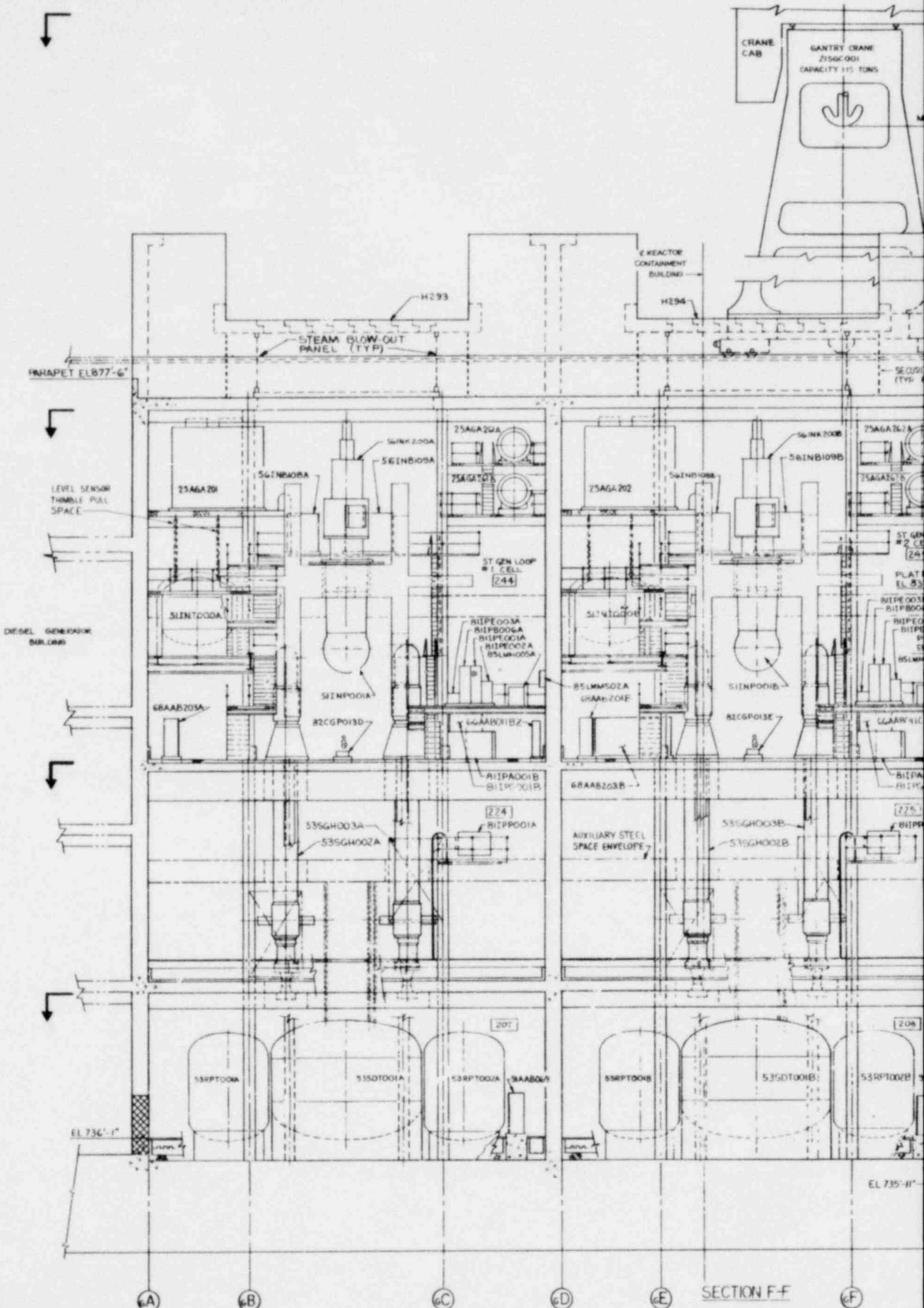

SECTION F-F

NN814-14

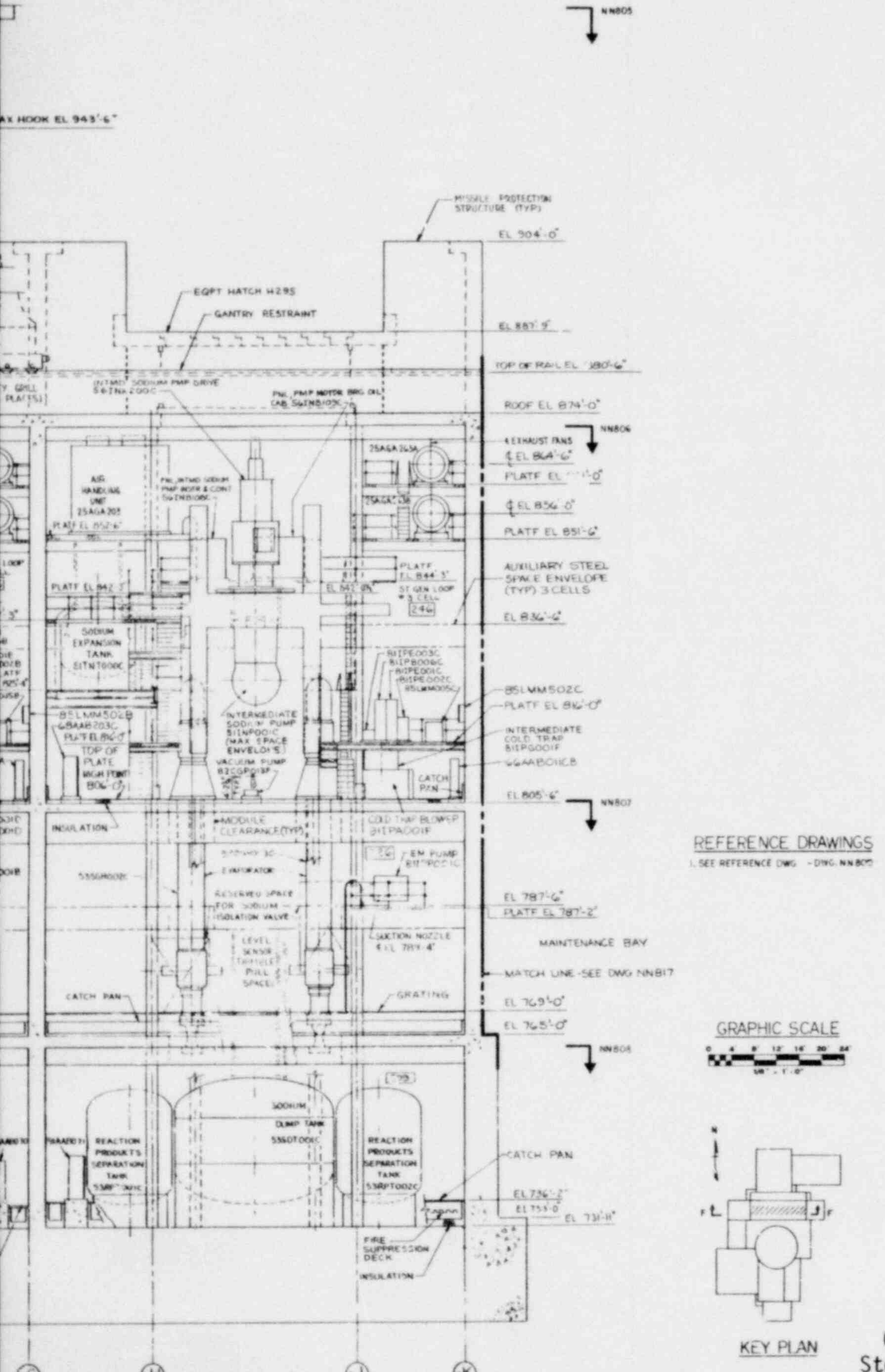

Figure 1.2-62
General Arrangement
Steam Generator Building
Section F-F

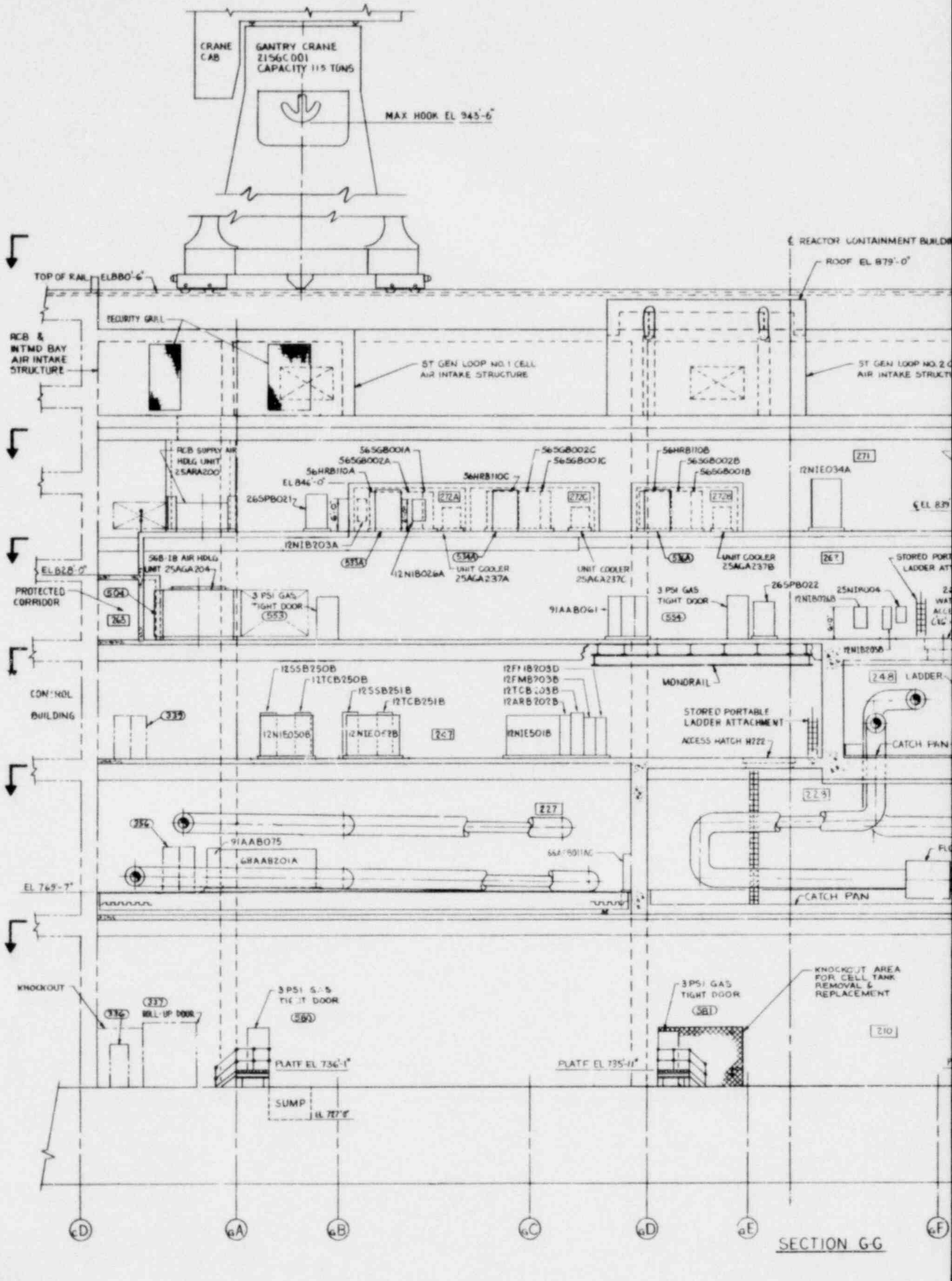
CRANE CAB
GANTRY CRANE 21S6C001 CAPACITY 115 TONS
MAX HOOK EL 945'-6"
℄ REACTOR CONTAINMENT BUILDING
ROOF EL 879'-0"
TOP OF RAIL EL880'-6"
SECURITY GRILL
RCB & INTMD BAY AIR INTAKE STRUCTURE
ST GEN LOOP NO.1 CELL AIR INTAKE STRUCTURE
ST GEN LOOP NO.2 AIR INTAKE STRUCTURE
RCB SUPPLY AIR HDLG UNIT 25ARA200
56SGB001A
56SGB002A
56HRB110A
EL 846'-0"
26SPB021
56HRB110C
56SGB002C
56SGB001C
56HRB110B
56SGB002B
56SGB001B
12NIE034A
12NIB203A
12NIB026A
UNIT COOLER 25AGA237A
UNIT COOLER 25AGA237C
UNIT COOLER 25AGA237B
STORED PORT LADDER ATT
EL 828'-0"
56B-1B AIR HDLG UNIT 25AGA204
PROTECTED CORRIDOR
3 PSI GAS TIGHT DOOR
91AAB061
3 PSI GAS TIGHT DOOR
26SPB022
25NIP004
12NIB205B
MONORAIL
12SSB250B
12TCB250B
12SSB251B
12TCB251B
12NIE050B
12NIE072B
12NIE501B
12FMB203D
12FMB203B
12TCB203B
12ARB202B
CONTROL BUILDING
STORED PORTABLE LADDER ATTACHMENT
ACCESS HATCH H222
LADDER
CATCH PAN
91AAB075
68AAB201A
EL 769'-7"
CATCH PAN
KNOCKOUT
ROLL-UP DOOR
3 PSI GAS TIGHT DOOR
PLATF EL 736'-1"
SUMP
EL 727'-8"
PLATF EL 735'-11"
3 PSI GAS TIGHT DOOR
KNOCKOUT AREA FOR CELL TANK REMOVAL & REPLACEMENT
227
267
248
224
271
210
SECTION G-G

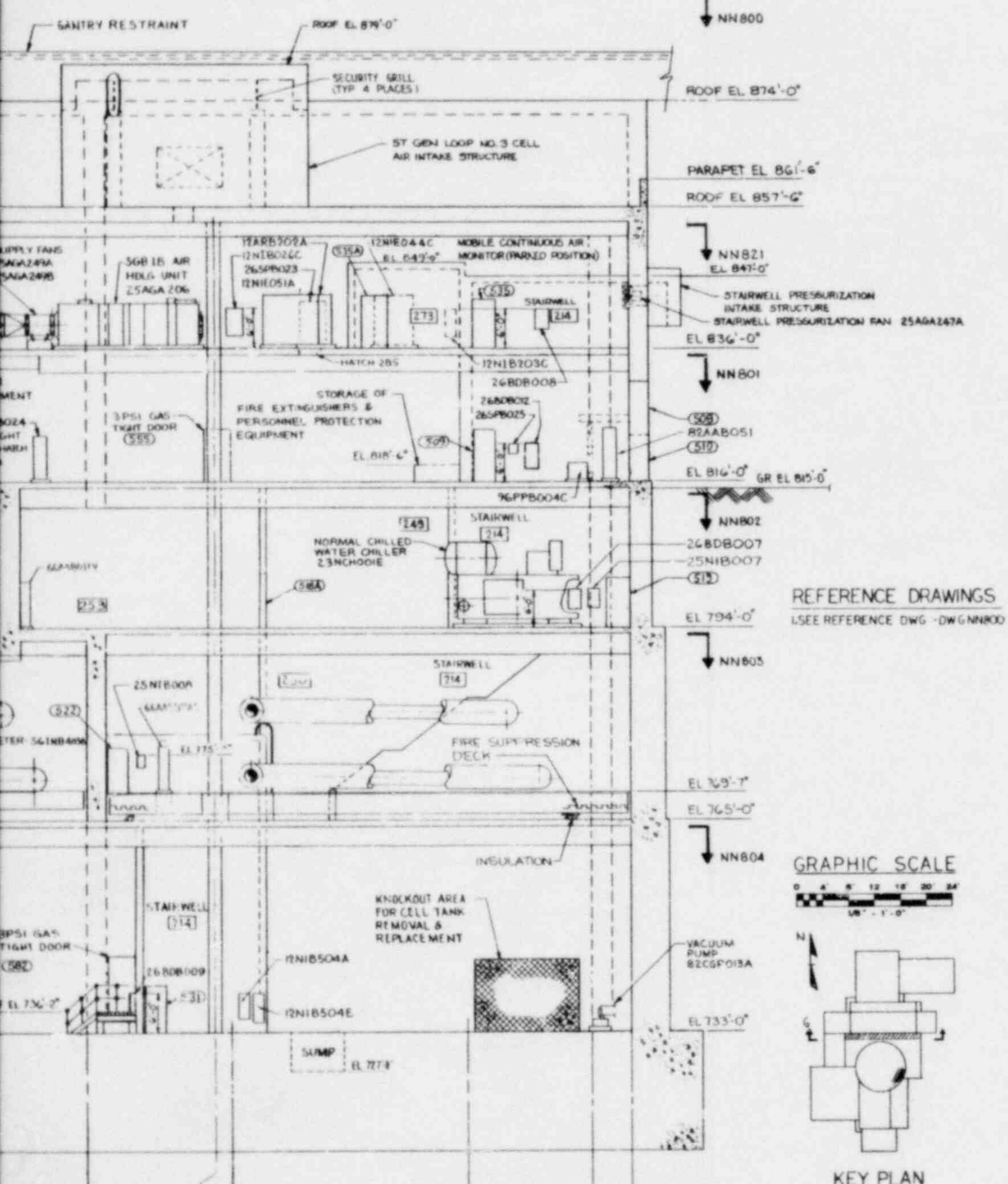

Figure 1.2-63
General Arrangement
Steam Generator Building
Section G-G

Amend. 56
Aug. 1980

IMAGE EVALUATION
TEST TARGET (MT-3)

6"

IMAGE EVALUATION
TEST TARGET (MT-3)

6"

IMAGE EVALUATION
TEST TARGET (MT-3)

6"

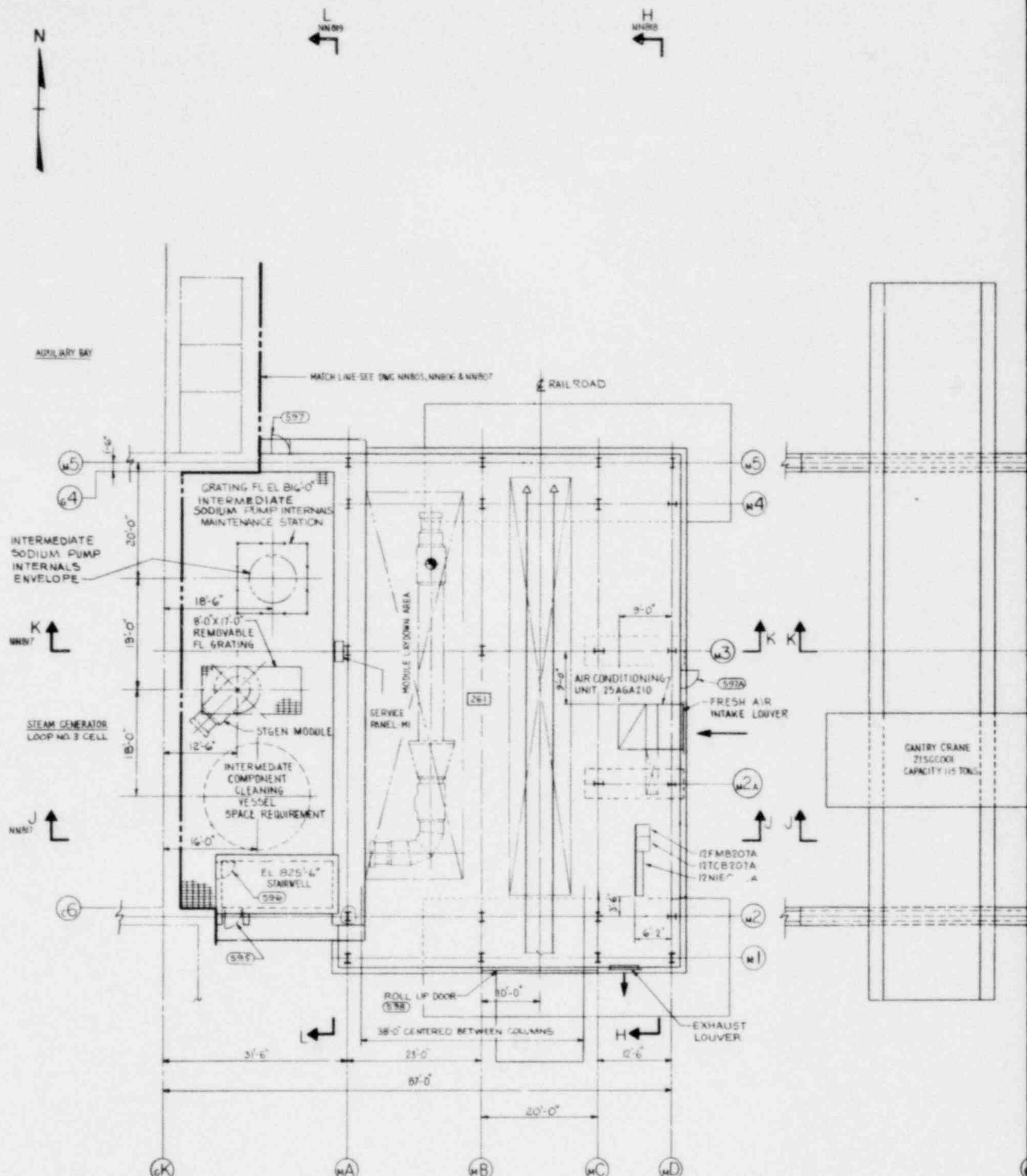

PLAN ABOVE EL 816'-0"

NN816-10

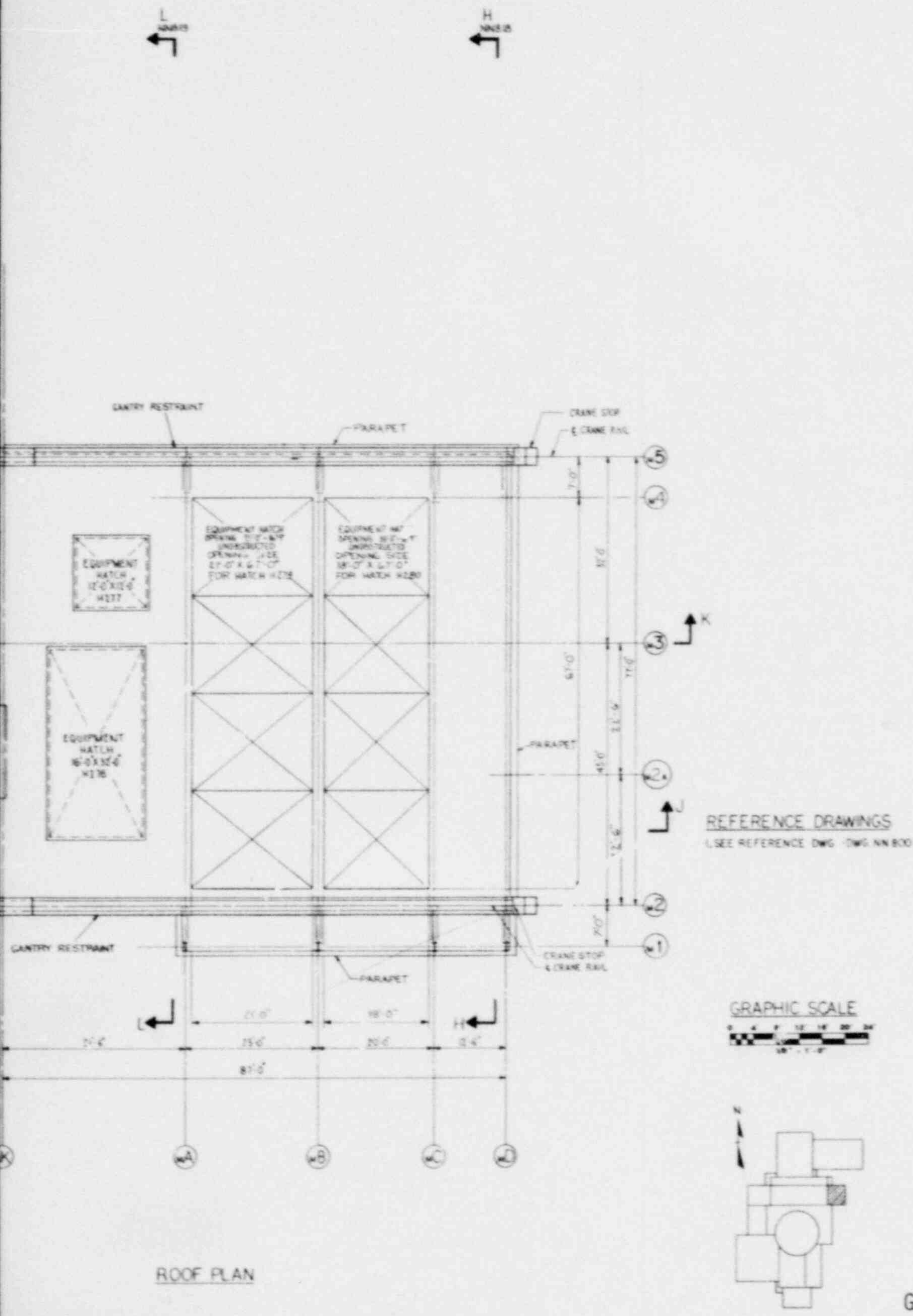

ROOF PLAN

KEY PLAN

Figure 1.2-64
General Arrangement
Steam Generator Building
Plan El. 816'-0" and Roof Plan

Amend. 56
Aug. 1980

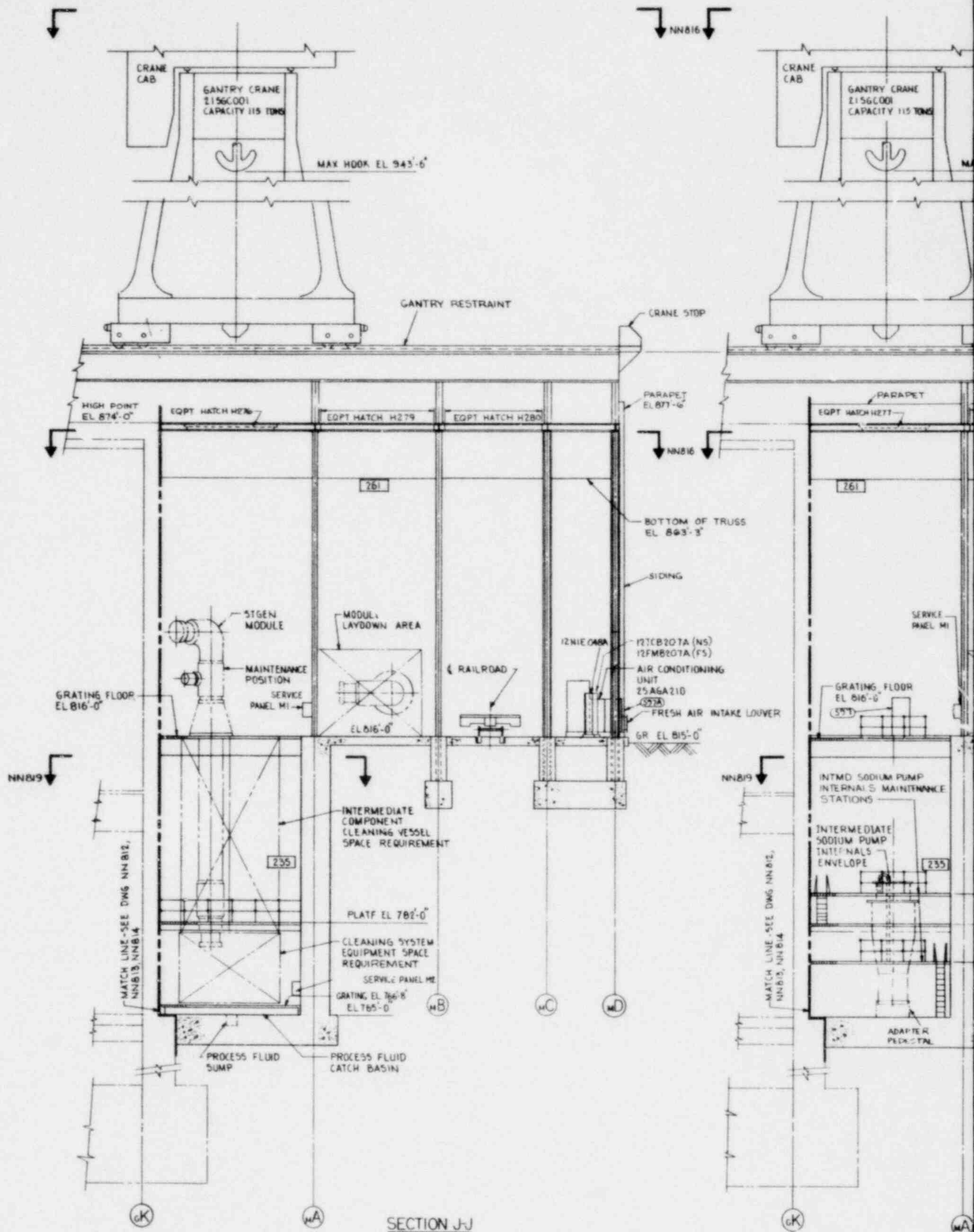

SECTION J-J

NN817-11

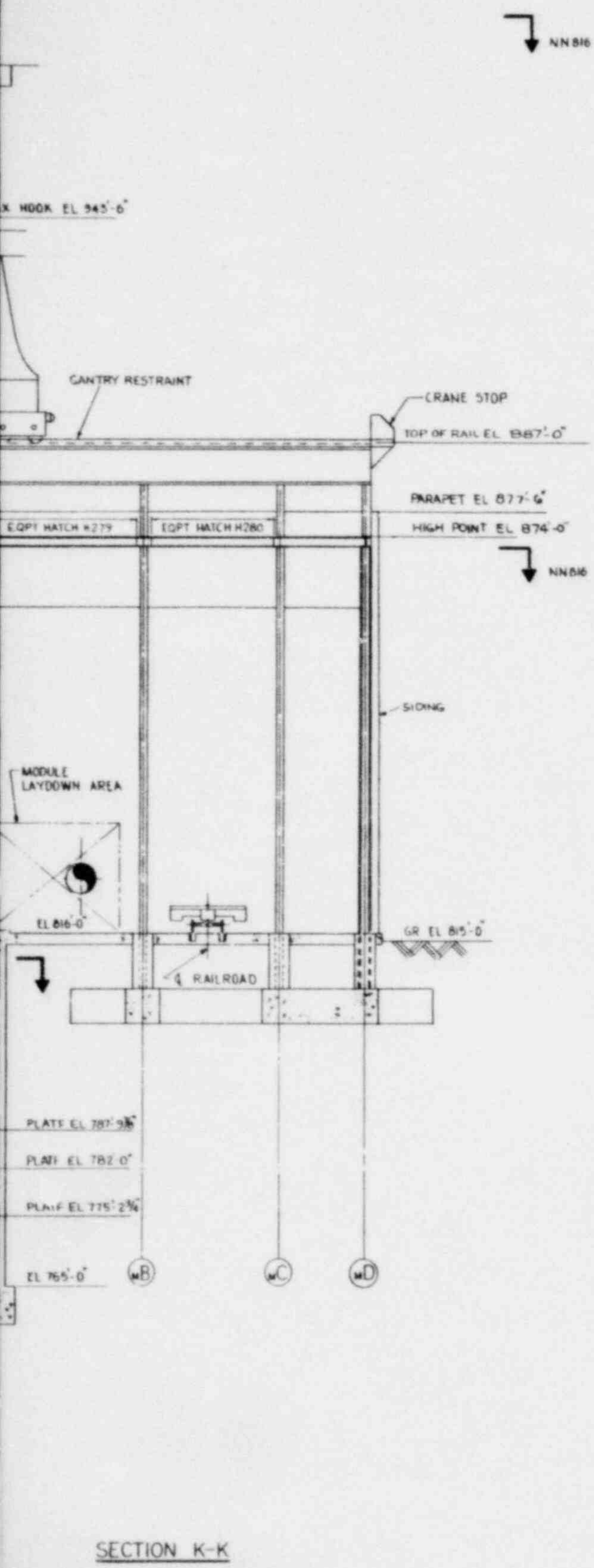

SECTION K-K

REFERENCE DRAWINGS
1 SEE REFERENCE DWG -DWG NN 800

GRAPHIC SCALE

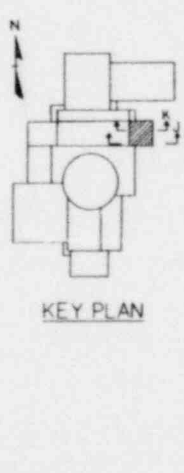

KEY PLAN

Figure 1.2-65
General Arrangement
Steam Generator Building
Section J-J and K-K

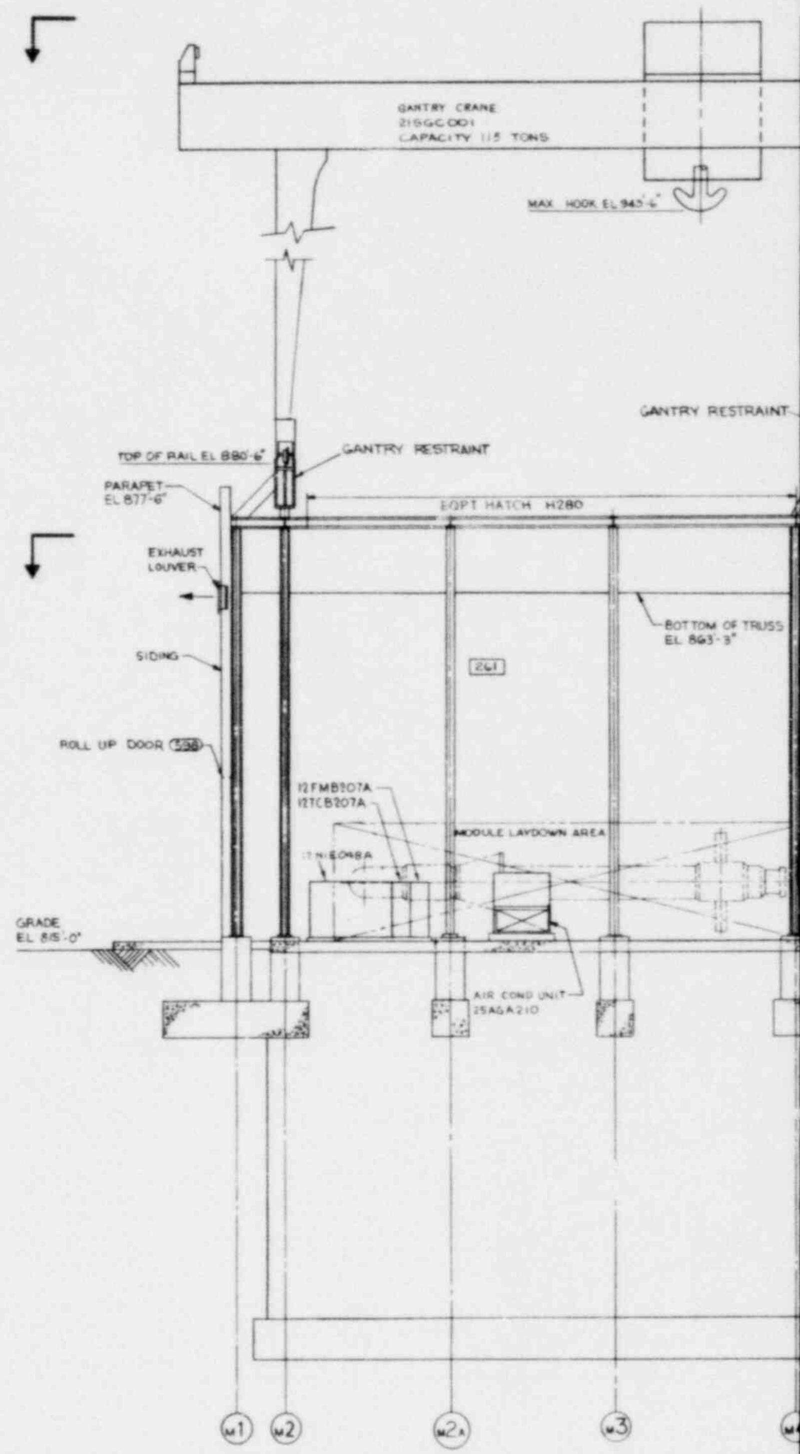

GANTRY CRANE
21SGC001
CAPACITY 115 TONS
MAX HOOK EL 943'-6"
GANTRY RESTRAINT
TOP OF RAIL EL 880'-6"
GANTRY RESTRAINT
PARAPET
EL 877'-6"
EQPT HATCH H280
EXHAUST
LOUVER
BOTTOM OF TRUSS
EL 863'-3"
SIDING
261
ROLL UP DOOR
12FMB207A
12TCB207A
MODULE LAYDOWN AREA
GRADE
EL 815'-0"
AIR COND UNIT
25AGA210
M1
M2
M2A
M3

NN818-11

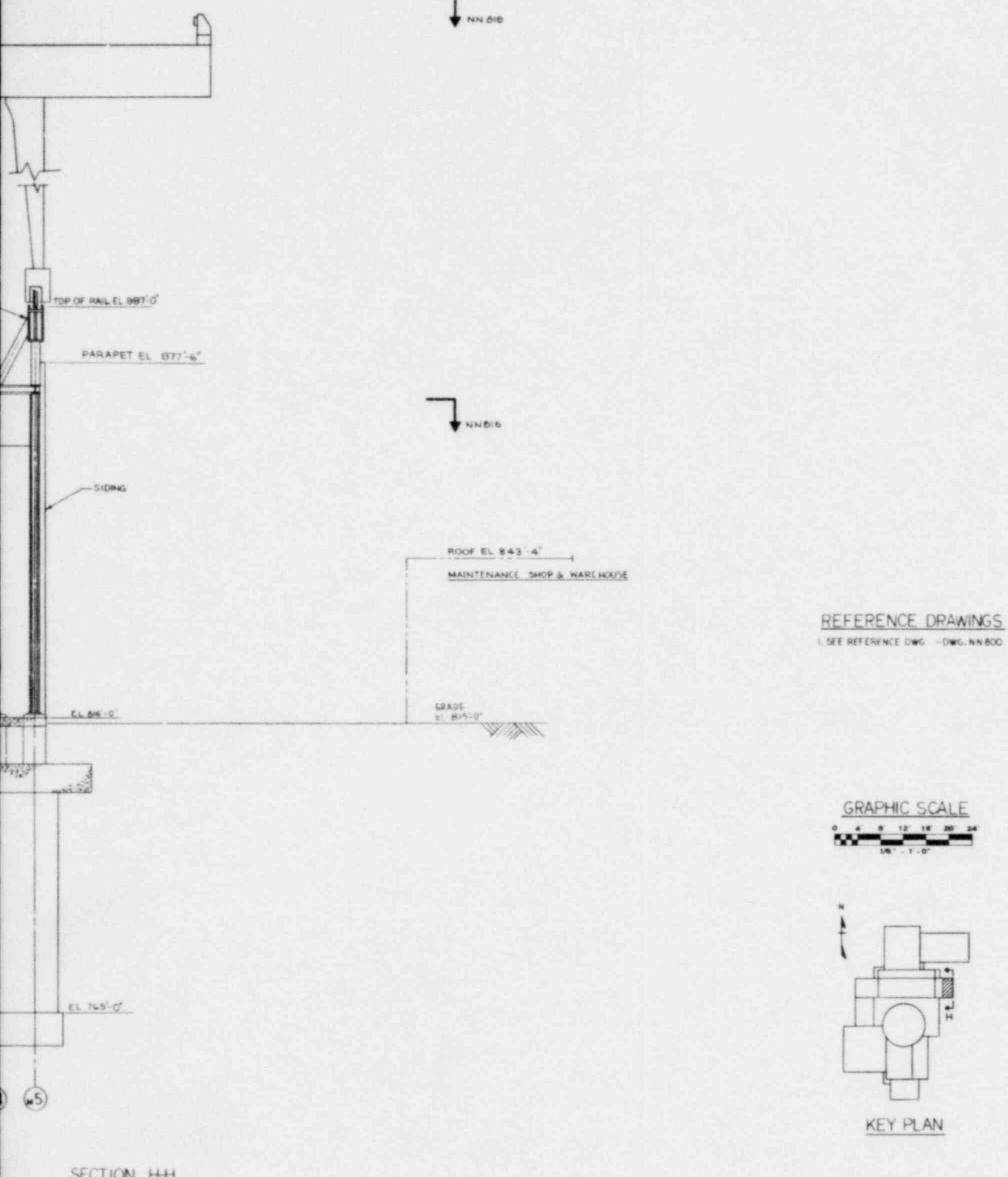

Figure 1.2-66
General Arrangement
Steam Generator Building
Section H-H

Amend. 56
Aug. 1980

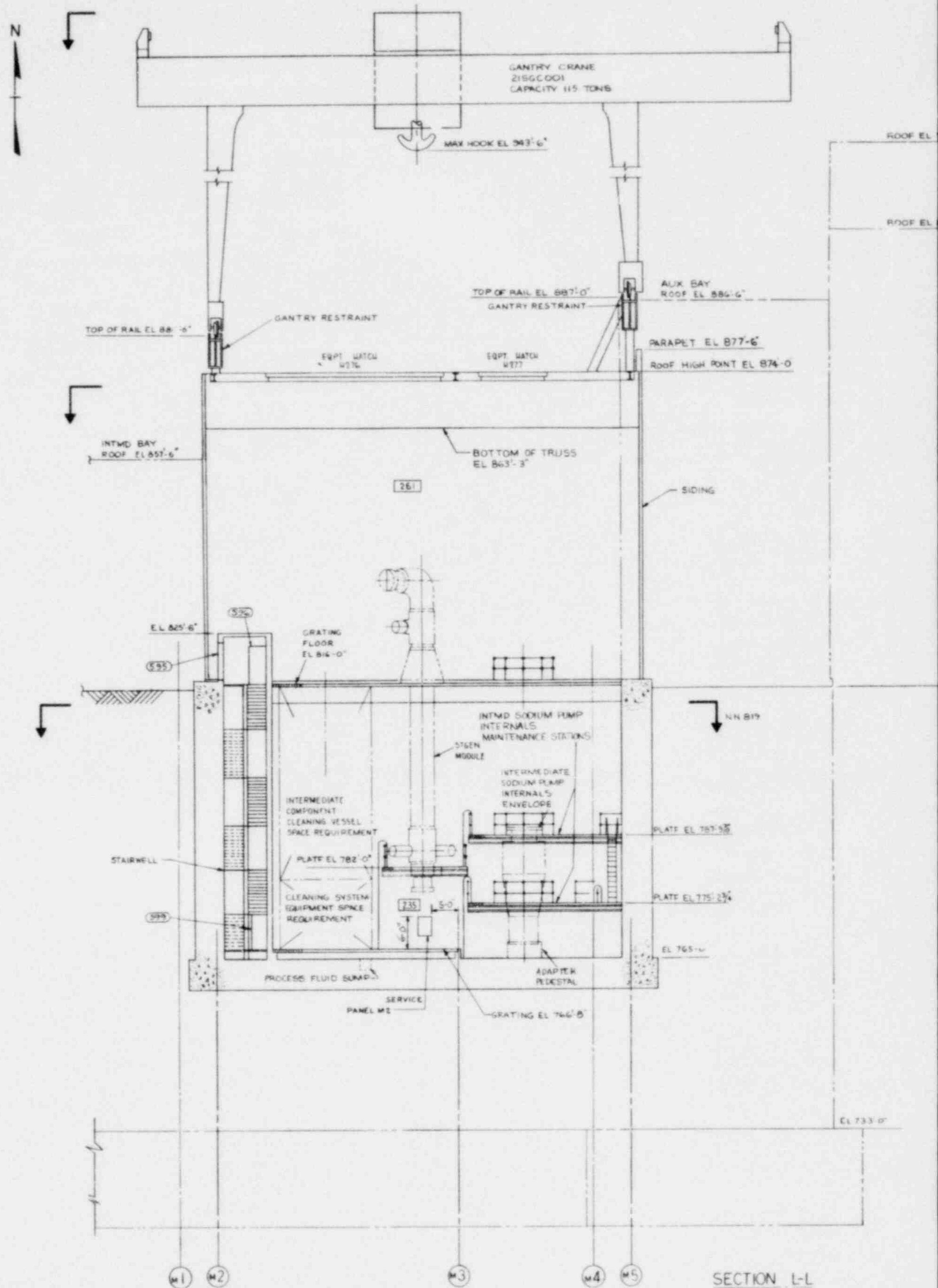

SECTION L-L

NN819-10

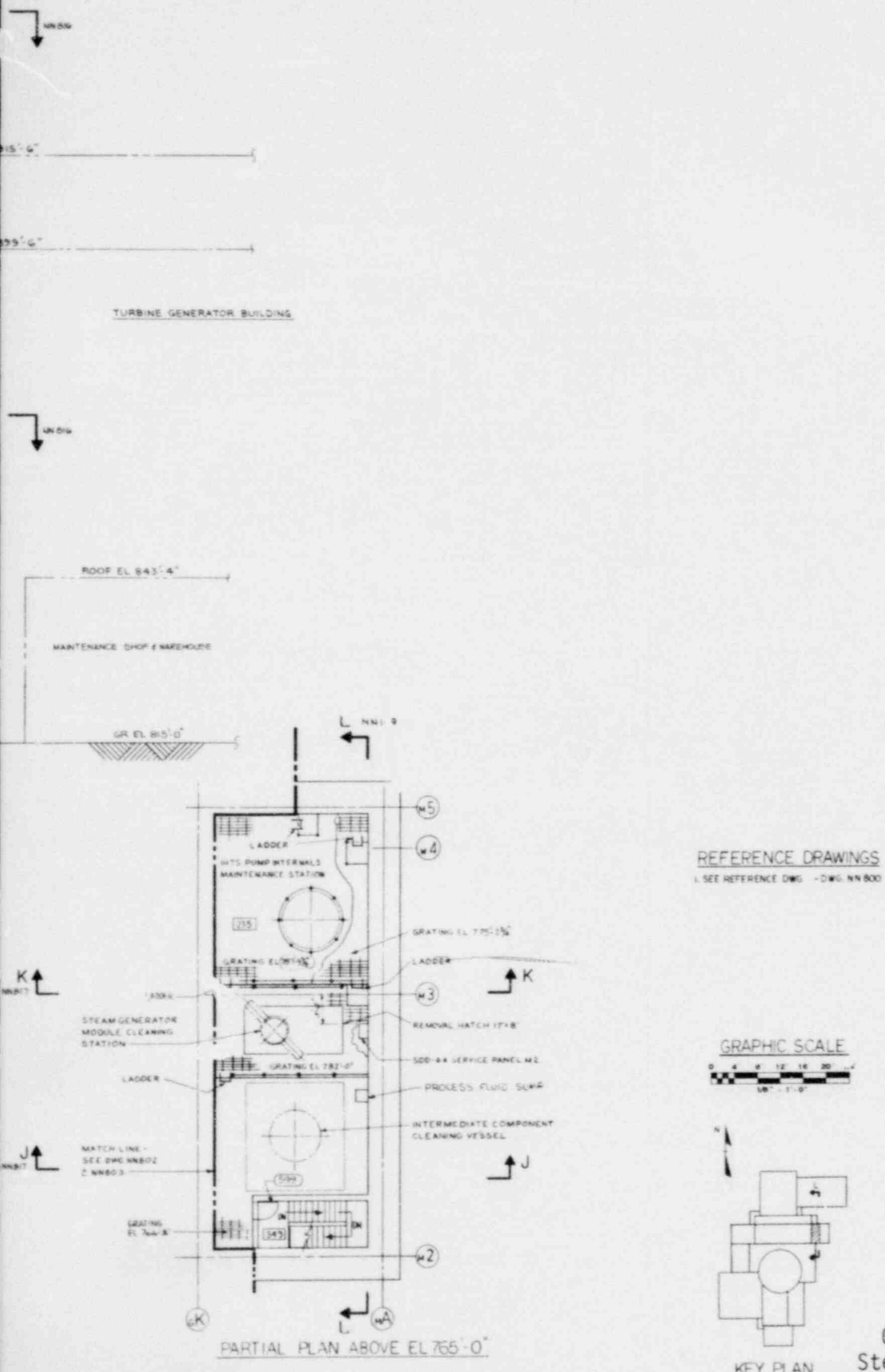

Figure 1.2-67
General Arrangement
Steam Generator Building
Section L-L Part Plan
El. 765'-0"

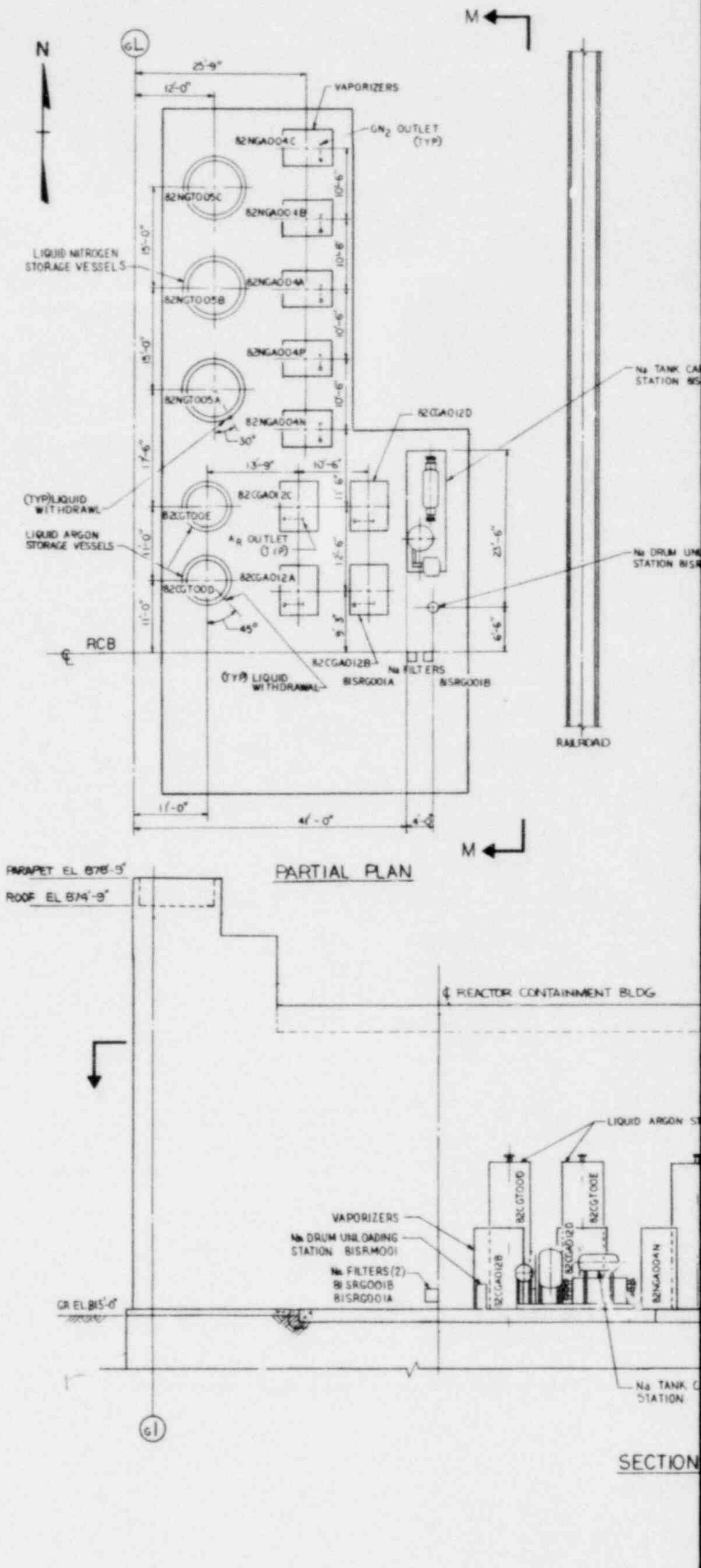

VAPORIZERS
LIQUID NITROGEN STORAGE VESSELS
LIQUID ARGON STORAGE VESSELS
(TYP) LIQUID WITHDRAWL
RCB
Na FILTERS
RAILROAD
PARTIAL PLAN
PARAPET EL 878'-9"
ROOF EL 874'-9"
REACTOR CONTAINMENT BLDG
Na DRUM UNLOADING STATION 81SRM001
Na FILTERS (2) 81SRG001B 81SRG001A
GR EL 815'-0"
SECTION

NN820-9

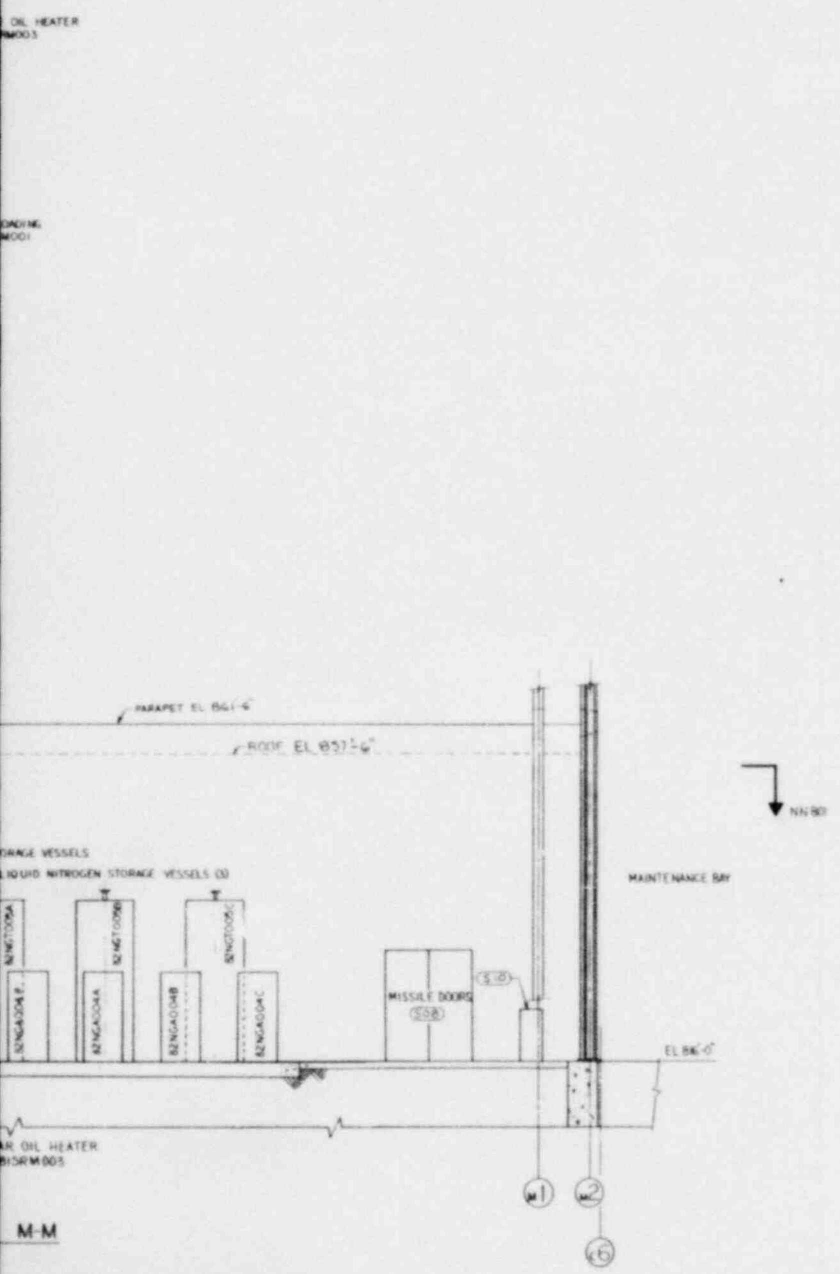

REFERENCE DRAWINGS

GRAPHIC SCALE

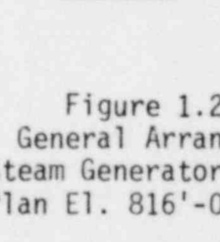

KEY PLAN

Figure 1.2-68
General Arrangement
Steam Generator Building
Plan El. 816'-0" and 840'-0"

Amend. 56
Aug. 1980

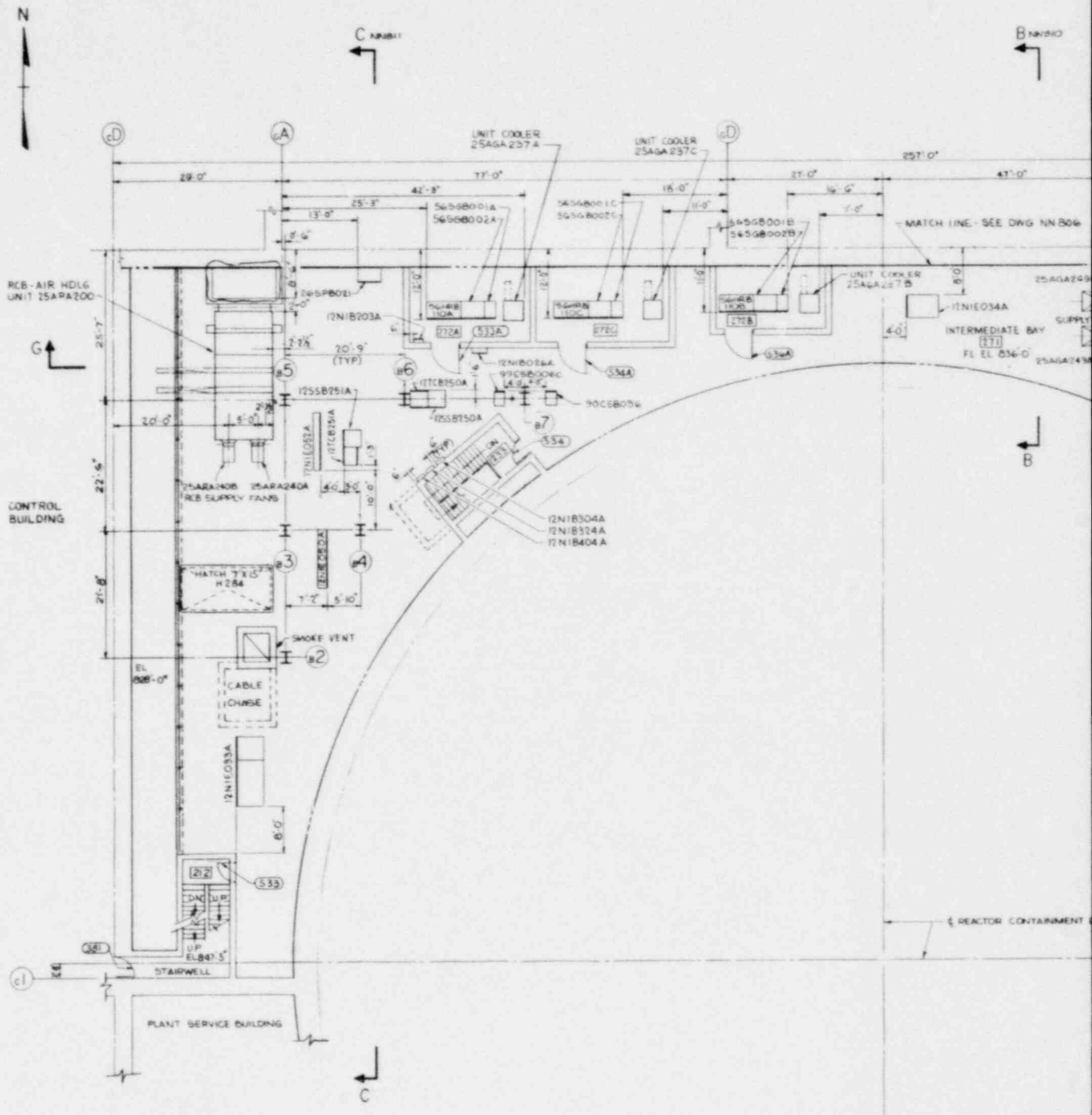

PLAN ABOVE EL 836'-0"

NN821-8

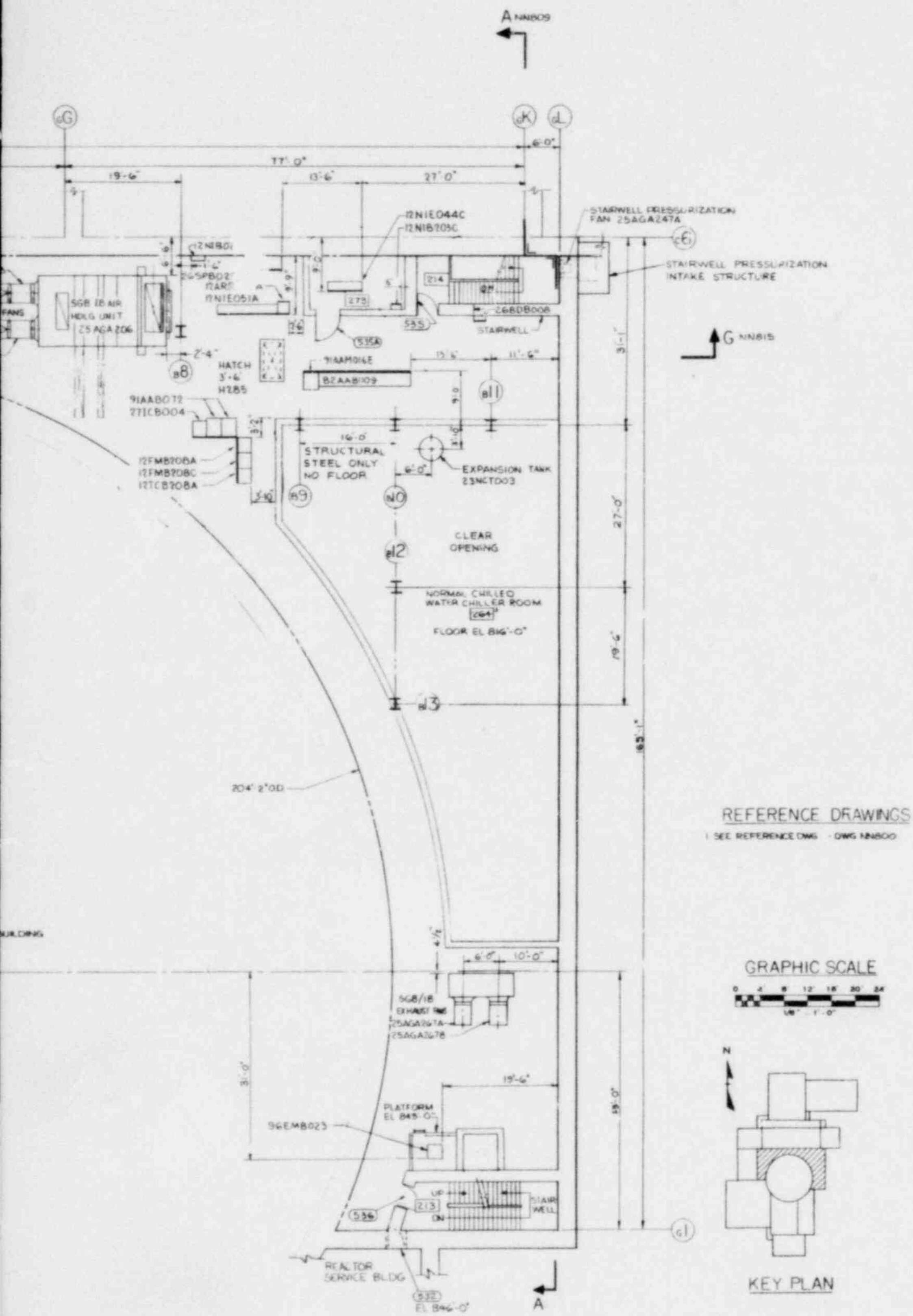

Figure 1.2-69
General Arrangement
Steam Generator Building
Intermediate Bay
El. 836'-0"

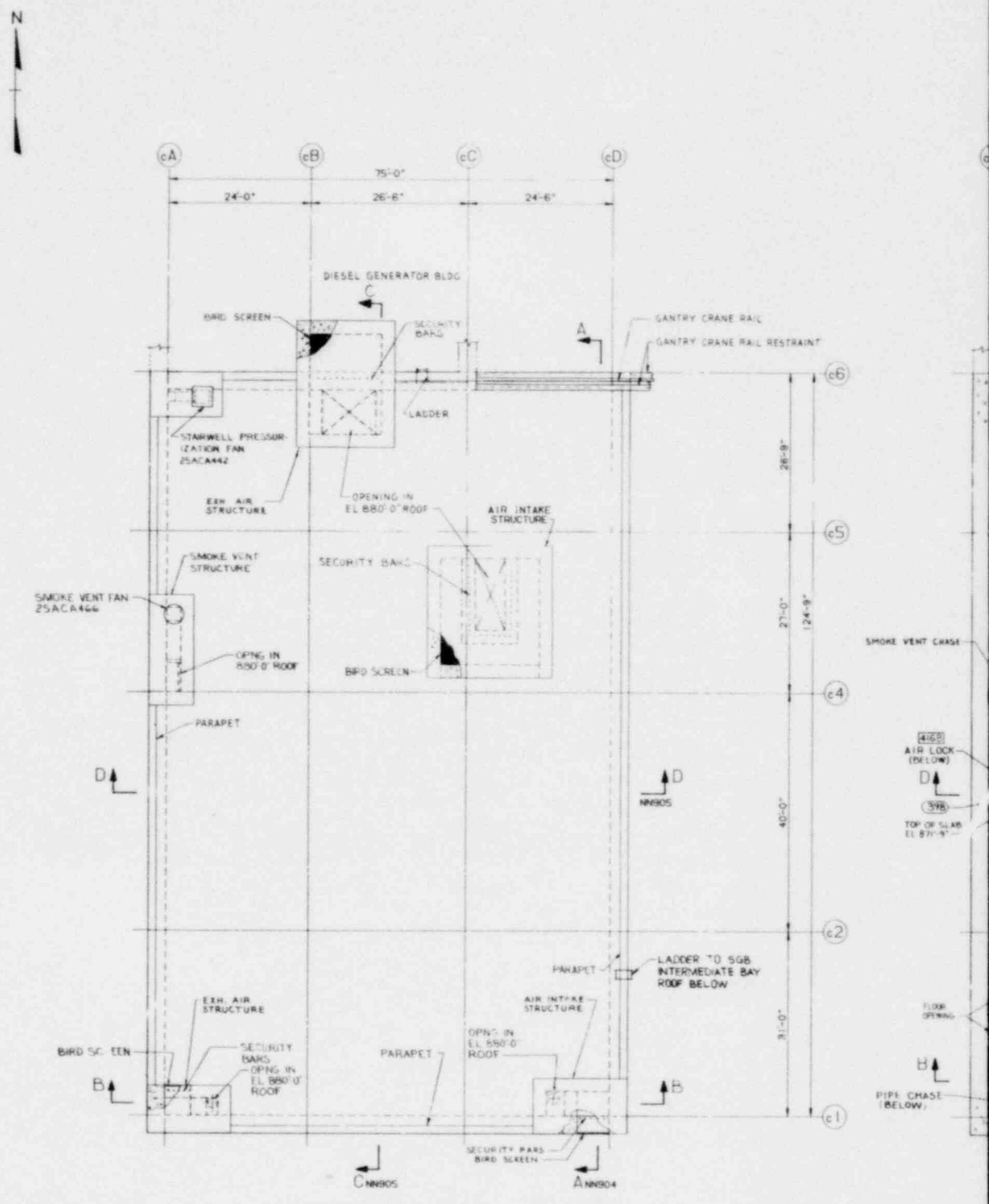

ROOF PLAN ABOVE EL 880'-0"

NN900-11

GENERAL NOTES

1. SYMBOLS AND ABBREVIATIONS WARD DOC. D-0034
2. ALL PARTITION WALLS ON EL 765'-0" & EL 733'-0" ARE FIREWALLS.

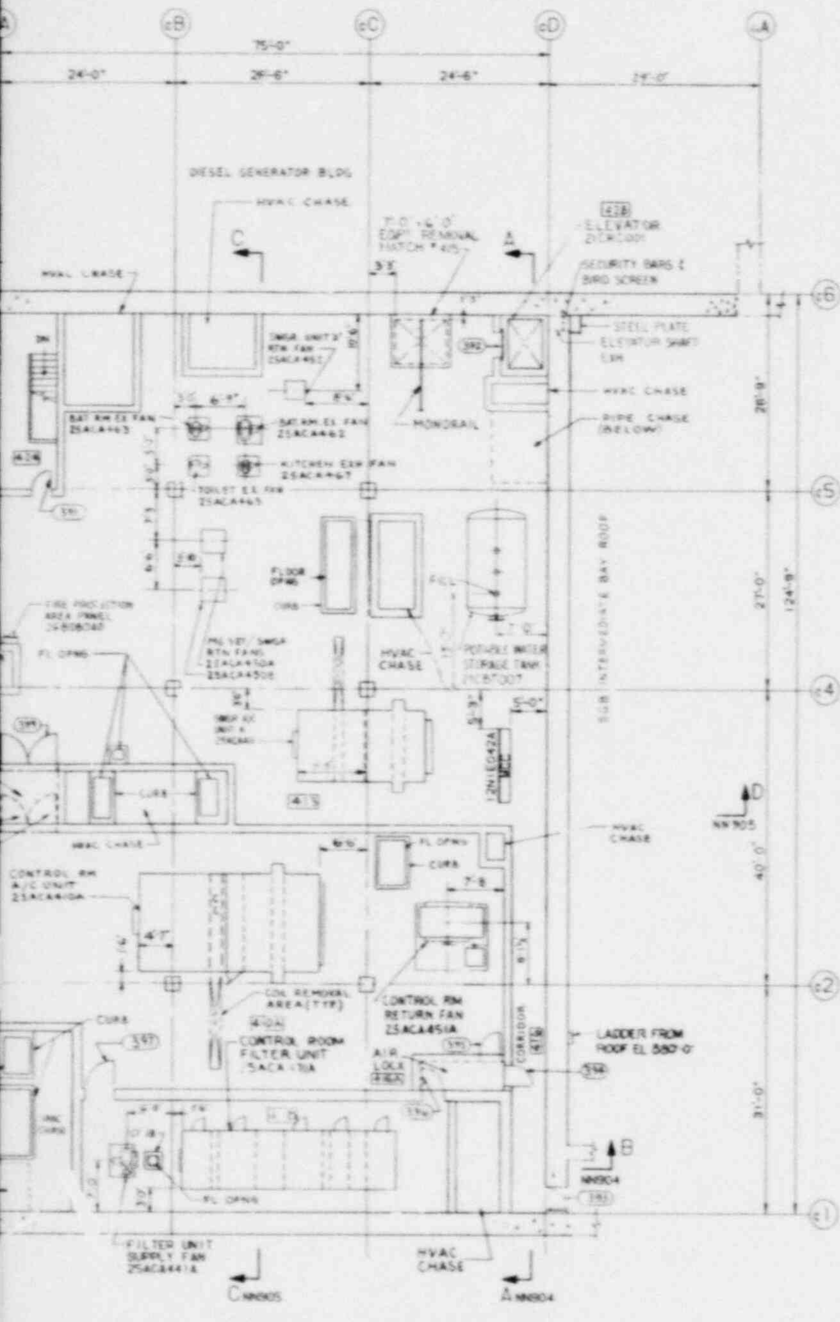

PLAN ABOVE EL 863'-3"

REFERENCE DRAWINGS

NN901-CB GENERAL ARRANGEMENT PLAN ABOVE EL 847'-3" & EL 831'-0"
NN902-CB GENERAL ARRANGEMENT PLAN ABOVE EL 816'-0" & EL 794'-0"
NN903-CB GENERAL ARRANGEMENT PLAN ABOVE EL 765'-0" & EL 733'-0"
NN904-CB GENERAL ARRANGEMENT SECTION A-A & B-B
NN905-CB GENERAL ARRANGEMENT SECTION C-C & D-D

LEGEND

- E/I/C CABINET SWGR (HEAVY LINE FRONT)
- GRATING
- 410 CELL NUMBER
- KNOCKOUT SECTION
- CONCRETE
- 794 DOOR NUMBER

GRAPHIC SCALE

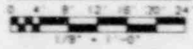

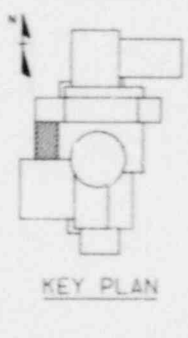

KEY PLAN

Figure 1.2-70
General Arrangement
Control Building
El. 880'-0" and 863'-3"

Amend. 56
Aug. 1980

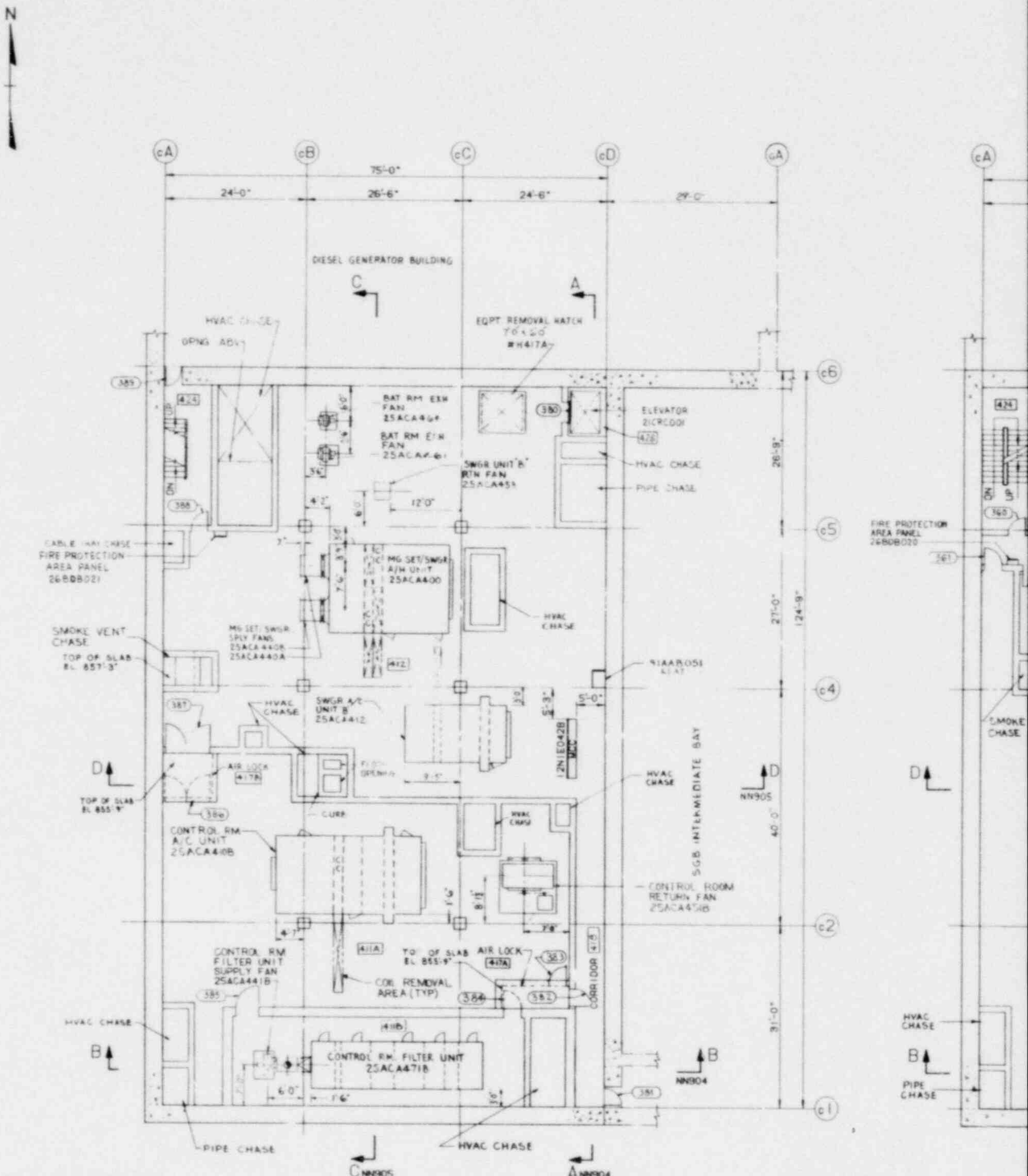

PLAN ABOVE EL 847'-3"

NN901-12

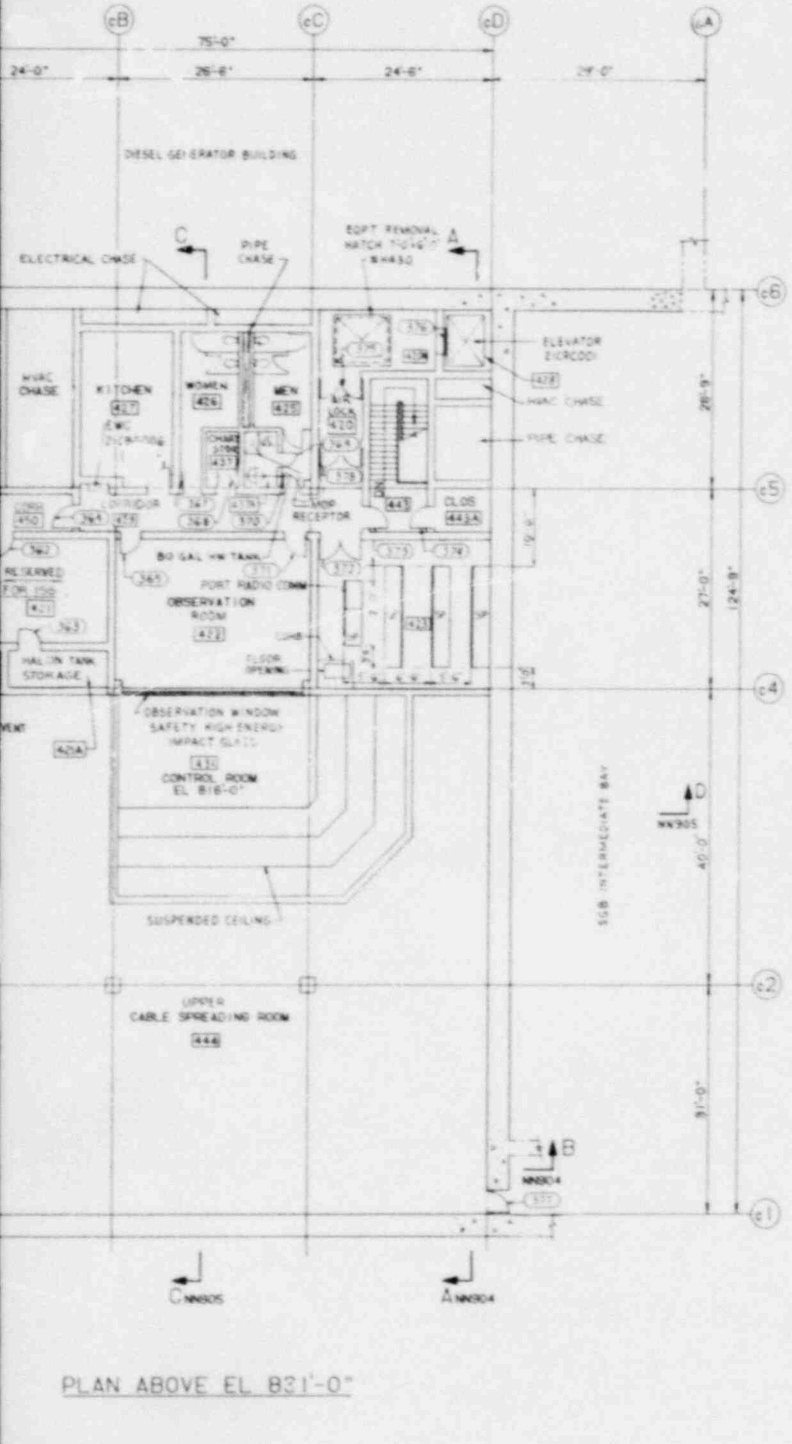

REFERENCE DRAWINGS

SEE DRAWING NN900

GRAPHIC SCALE

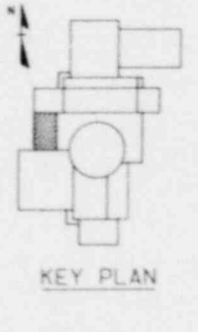

KEY PLAN

Figure 1.2-71
General Arrangement
Control Building
El. 847'-3" and 831'-0"

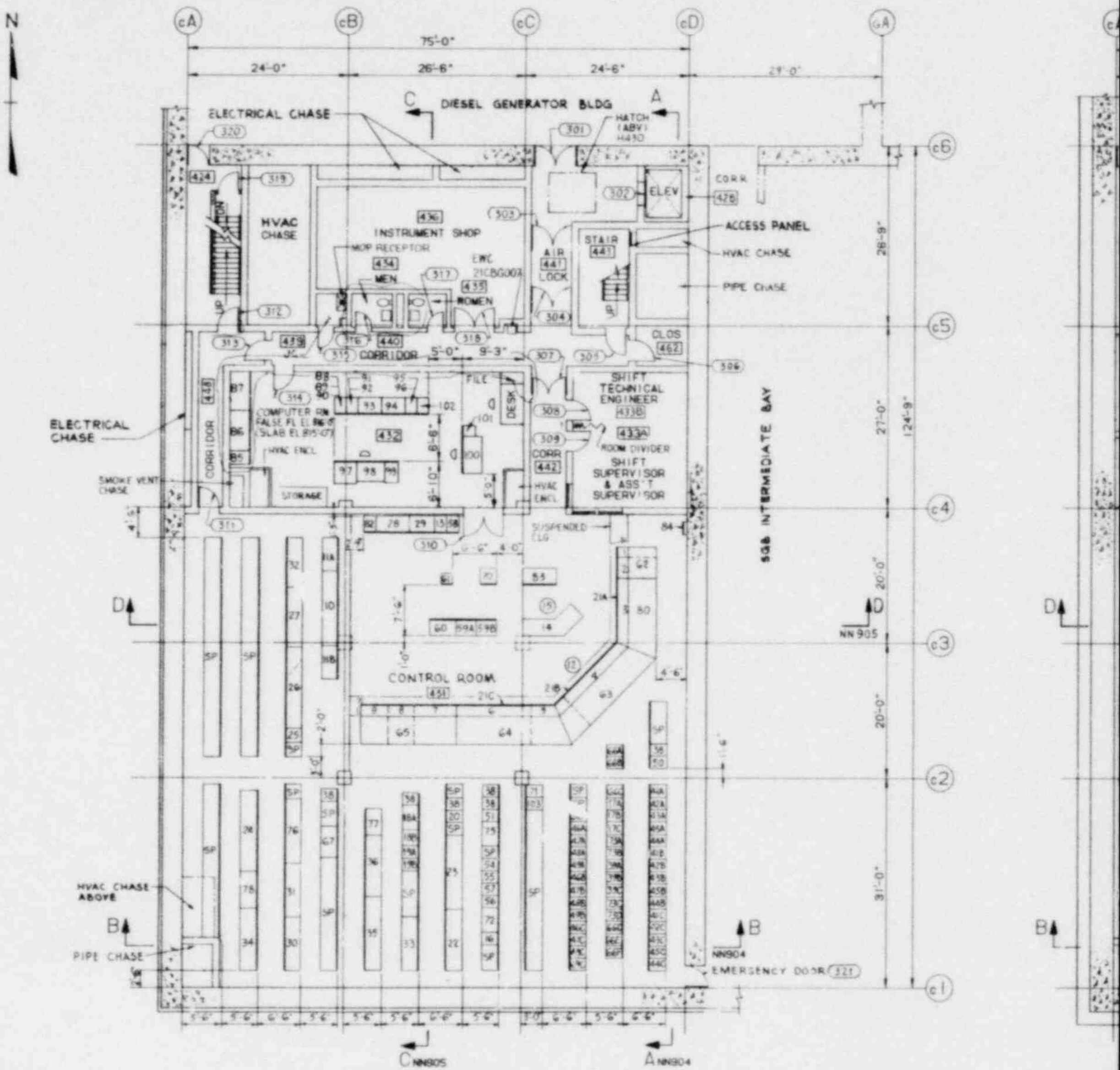

PLAN ABOVE EL 816'-0"

ITEM	DESCRIPTION	EQUIPMENT NO	ITEM	DESCRIPTION	EQUIPMENT NO	ITEM	DESCRIPTION	EQUIPMENT NO
1	REACTOR SUPPORT SYSTEMS	90CSB016	22	HVAC SYS RECIRC AIR [illegible]	59AAB001	43A	PRIMARY PPS COMPARATOR PNL	99PSB00
2	REACTOR SUPPORT SYSTEMS	90CSB016	23	HVAC CONTROL RACK	59AAB002	43B	PRIMARY PPS COMPARATOR PNL	99PSBC0
3	ENGINEERED SAFETY SYSTEMS	90CSB016	24	GEN PROTECTION	12NIB002	43C	PRIMARY PPS COMPARATOR PNL	99PSB00
4	REACTOR PRI HEAT TRANSPORT SYSTEMS	90CSB016	25	TURB GEN SUPERVISORY PANEL	69AAB025	44A	PRIMARY PPS LOGIC RACK	99PSB003
5	INTMD Na HEAT TRANSPORT SYSTEMS	90CSB016	26	TURB EHC EQUIPMENT BAYS	69AAB028	44B	PRIMARY PPS LOGIC RACK	99PSB003
6	STEAM GEN & ASSOCIATED SYSTEMS	90CSB016	27	BOP AUXILIARIES	69AAB024	44C	PRIMARY PPS LOGIC RACK	99PSB003
7	TURBINE SYSTEMS	90CSB016	28	NON SODIUM FIRE PROTECTION PANEL	26BDB042	45A	PRIMARY PPS ISOLATION RACK	99PSB003
8	GENERATOR SYSTEMS	90CSB016	29	SODIUM FIRE PROT Z-IND PANEL	26SPB015	45B	PRIMARY PPS ISOLATION RACK	99PSB003
9	SYNC & MAIN UNIT CONTROL	90CSB016	30	HEAT REMOVAL & CONDTN LGC RACK	56PRB020	45C	PRIMARY PPS ISOLATION RACK	99PSB003
10	SWYD & STA ELEC DISTR	12NIB02C	31	STEAM GEN LGC RACK	56SGB100	46A	SECONDARY PPS BUFFER	99PSB002
11A	EMER DIESEL GEN PANEL	12NIB010	32	CHILLED WATER CONTROL CABINET	23ICB001	46B	SECONDARY PPS BUFFER	99PSB002
11B	EMER DIESEL GEN PANEL	12NIB019	33	AUX LIQ METAL CONTROL CABINET	81AAB018	46C	SECONDAFY PPS BUFFER	99PSB002
12	REACTOR OPERATOR	———	34	REMOTE ANNUNCIATOR CABINETS	90CSB019	47A	SECONDARY PPS TERMINATION CAB	99PSB002
13	SODIUM LEAK DETECTOR PANEL	66AAB008	35	STEAM PLANT CONDITIONING RACK	69AAB026	47B	SECONDARY PPS TERMINATION CAB	99PSB002
14	DESK	———	36	STEAM PLANT LOGIC RACK	69AAB027	47C	SECONDARY PPS TERMINATION CAB	99PSB002
15	CHAIR	———	37			48A	SECONDARY PPS COMPARATOR CAP	99PSB002
16	SEISMIC INSTRUMENT PANEL	27ICB001	38	TERMINATION RACKS	90CSB015	48B	SECONDARY PPS COMPARATOR CAB	99PSB002
17A	FLUX MONITORING	95AAB001A	39A	PPS CONTAINMENT ISOL INSTR RACK	99ESB005A	48C	SECONDARY PPS COMPARATOR CAB	99PSB002
17B	FLUX MONITORING	95AAB001B	39B	PPS CONTAINMENT ISOL INSTR RACK	99ESB005B	49A	SECONDARY PPS SOLENOID DRIVE	99PSB004
17C	FLUX MONITORING	95AAB001C	39C	PPS CONTAINMENT ISOL INSTR RACK	99ESB005C	43B	SECONDARY PPS SOLENOID DRIVE	99PSB004
18A	CR RAD MON PRINTER	96AAB002A				49C	SECONDARY PPS SOLENOID DRIVE	99PSB004
18B	CR RAD MON CONSOLE	96AAB001A				50	PPS MONITOR RACK	99AAB001
19A	CLASS 1E PANEL A	96AAB003A	41A	PRIMARY PPS BUFFER	99PSB001[illegible]	51	PRIMARY ROD CONTROL & INSTR	90CSB010
19B	CLASS 1E PANEL A	96AAB003B	41B	PRIMARY PPS BUFFER	99PSB001D			
20	WEATHER STATION SPACE		41C	PRIMARY PPS BUFFER	99PSB001G	53	DESK TOP RADIO	———
21A	PAX TELEPHONE		42A	PRIMARY PPS TERMINATION CAB	99PSB001B	54	REACTOR CONTROL PANEL	90CSB013
21B	PAIC		42B	PRIMARY PPS TERMINATION CAB	99PSB001E	55	SUPERVISORY CONTROL PANEL	90AAB005
21C	COMMUNICATIONS JACK & SWITCH		42C	PRIMARY PPS TERMINATION CAB	99PSB001H	56	FLOW CONTROL PANEL	90CSB011

NN902-13

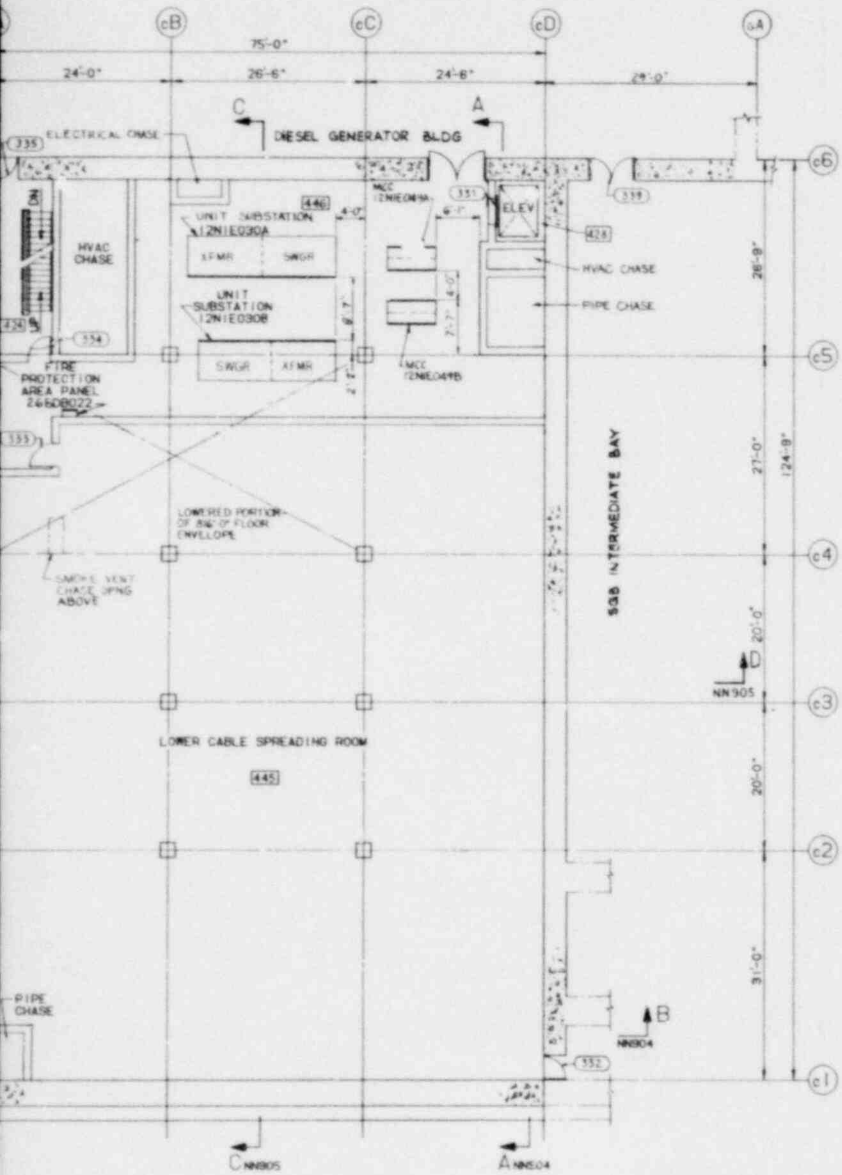

PLAN ABOVE EL 794'-0"

REFERENCE DRAWINGS
SEE DRAWING NN800

NO	ITEM	DESCRIPTION	EQUIPMENT NO	ITEM	DESCRIPTION	EQUIPMENT NO
	57	LOAD DISPATCH PANEL	90CSR005B	76	HEAT REMOVAL & CONDTN LOC RACK	56HRB020
	58	FAILED FUEL READOUT PANEL	94AAB012	77	PDH & DS REM DATA ACQ TERM	91AAB036
	59A	COMPUTER TYPEWRITER	91AAM015A	78	REMOTE ANNUNCIATOR CABINETS	67NIB003A
	59B	COMPUTER TYPEWRITER	91AAM015B	79	MANUAL TEL SWBD & PAIC HAND SET	
	60	COMPUTER LINE PRINTER/PLOTTER	91AAM013	80	CRT DISPLAY & KEYBOARD	91AAM001F
	61	CRT DISPLAY & KEYBOARD	91AAM001A	81		
	62	CRT DISPLAY & KEYBOARD	91AAM001B	82	BLDG FIRE PROTECTION PANEL	26BDB023
	63	CRT DISPLAY & KEYBOARD	91AAM001C	83	PLANT SECURITY	21CBC002
	64	CRT DISPLAY & KEYBOARD	91AAM001D	84	PATCH PANEL	
	65	CRT DISPLAY & KEYBOARD	91AAM001E	85	CABINET CARD STORAGE	91AAJ003
	66A	PDH & DS REM DATA ACQ TERM	91AAB051A	86	CABINET PAPER STORAGE	91AAJ002
	66B	PDH & DS REM DATA ACQ TERM	91AAB051B	87	CABINET MAGNETIC TAPE STORAGE	91AAJ001
	66C	PDH & DS REM DATA ACQ TERM	91AAB051C	88	MAGNETIC TAPE UNIT NO 3	91AAM010C
	66D	PDH & DS REM DATA ACQ TERM	91AAB055A	89	SERIAL LINE INTERFACE	91AAB005
	66E	PDH & DS REM DATA ACQ TERM	91AAB055B	90	FLEXIBLE DISC	91AAM014
	66F	PDH & DS REM DATA ACQ TERM	91AAB055C	91	FIXED HEAD DISC	91AAM008B
	67	RECIRCULATING GAS CONTROL CAB	28ICB001	92	MAGNETIC TAPE NO 2	91AAM010B
	68			93	CENTRAL PROCESSOR UNIT NO 1	91AAB002A
	69			94	CENTRAL PROCESSOR UNIT NO 2	91AAB002B
	70	SECURITY SURVEILLANCE STATION	21CBC003	95	FIXED HEAD DISC	91AAM008A
	71	CONTAINMENT INSTRUMENTATION	27ICB002	96	MAGNETIC TAPE UNIT NO 1	91AAM011A
	72	PCS SWITCHING LOGIC	90CSB014	97	CARD PUNCH WITH KEY BOARD	91AAM012
	73A	PPS AUX EQUIPMENT ISOLATION & LOGIC	99PSB005A	98	LINE PRINTER	91AAM009
	73B	PPS AUX EQUIPMENT ISOLATION & LOGIC	99PSB005B	99	CARD READER	91AAM005
	73C	PPS AUX EQUIPMENT ISOLATION & LOGIC	99PSB005C	100	RADIOGRAMMER CONSOLE	91AAB001
	73D	PPS AUX EQUIPMENT ISOLATION & LOGIC	99PSB005D	101	COLOR CRT DISPLAY UNIT	91AAM001F
	74	PORTABLE RADIO COMMUNICATION	TBD	102	MAGNETIC TAPE UNIT NO 4	91AAM010D
	75	SEC ROD CONTROL CABINET	TBD	103	CONTAINMENT INSTRUMENTATION DIVISION II	27ICB005

GRAPHIC SCALE
0 4' 8' 12' 16' 20' 24'
1/8" = 1'-0"

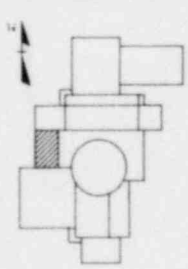

KEY PLAN

Figure 1.2-72
General Arrangement
Control Building
El. 816'-0" and 794'-0"

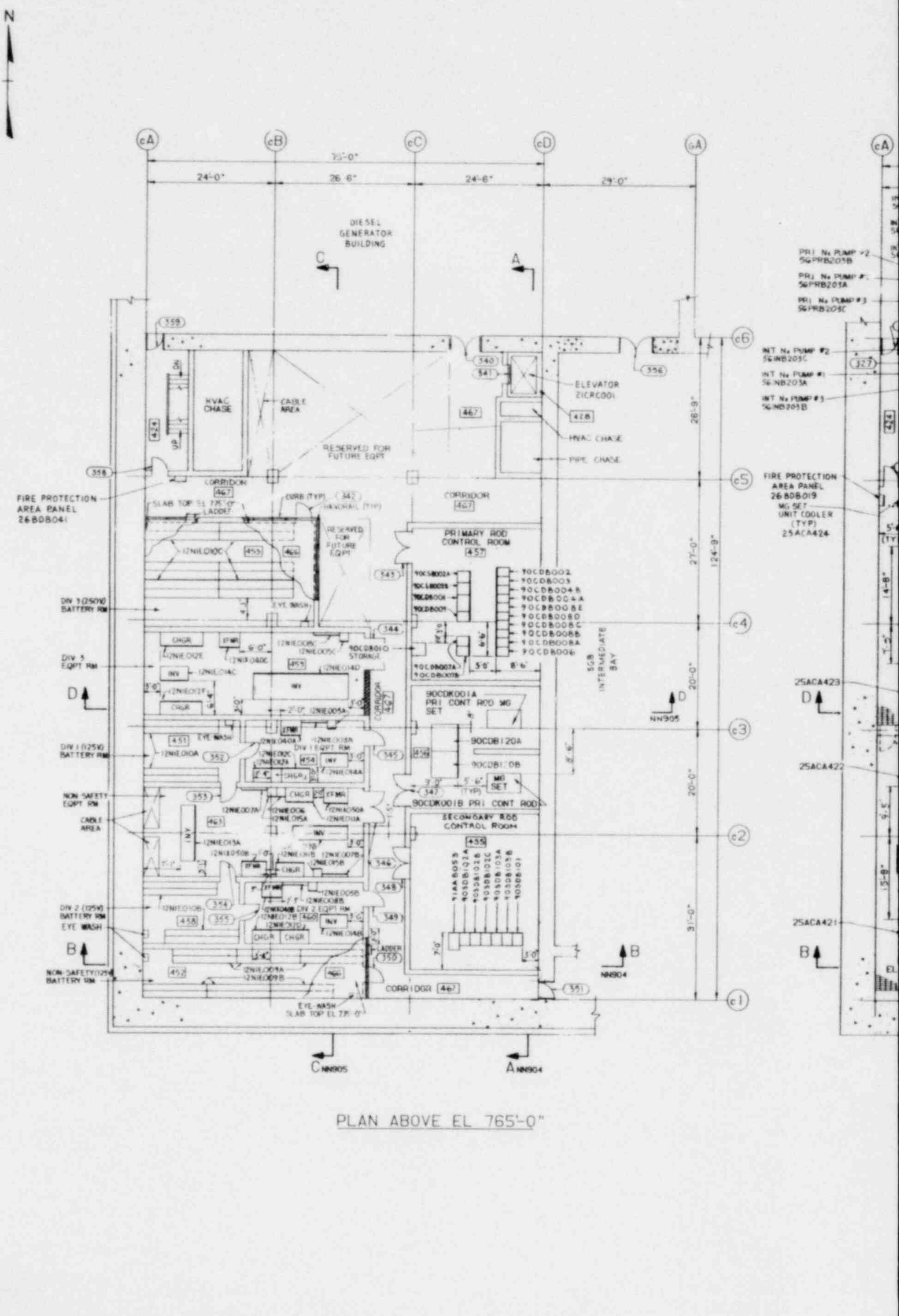

PLAN ABOVE EL 765'-0"

NN903-14

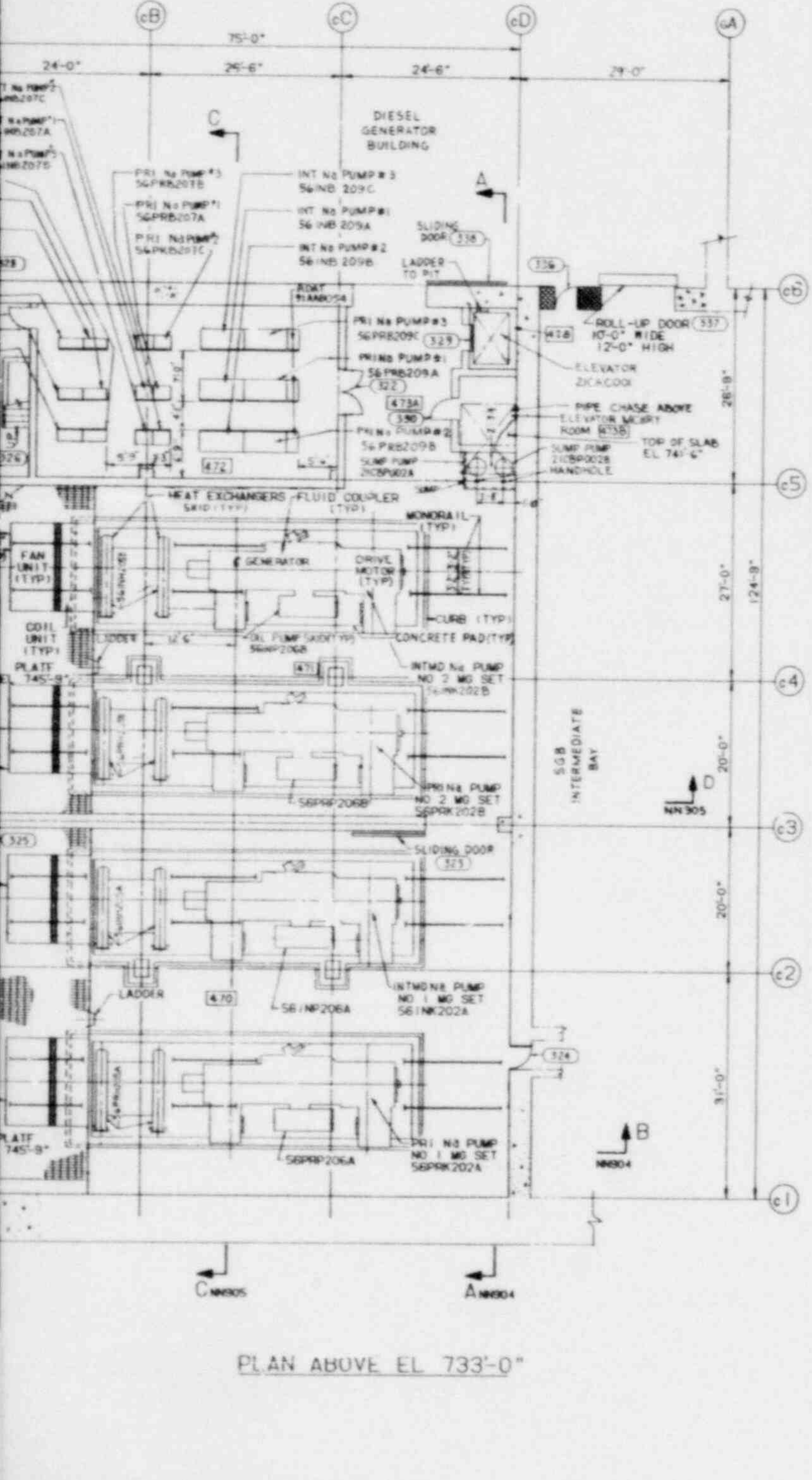

REFERENCE DRAWINGS
SEE DRAWING NN900

GRAPHIC SCALE
0 4' 8' 12' 16' 20' 24'
1/8" = 1'-0"

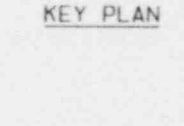

KEY PLAN

Figure 1.2-73
General Arrangement
Control Building
El. 765'-0" and 733'-0"

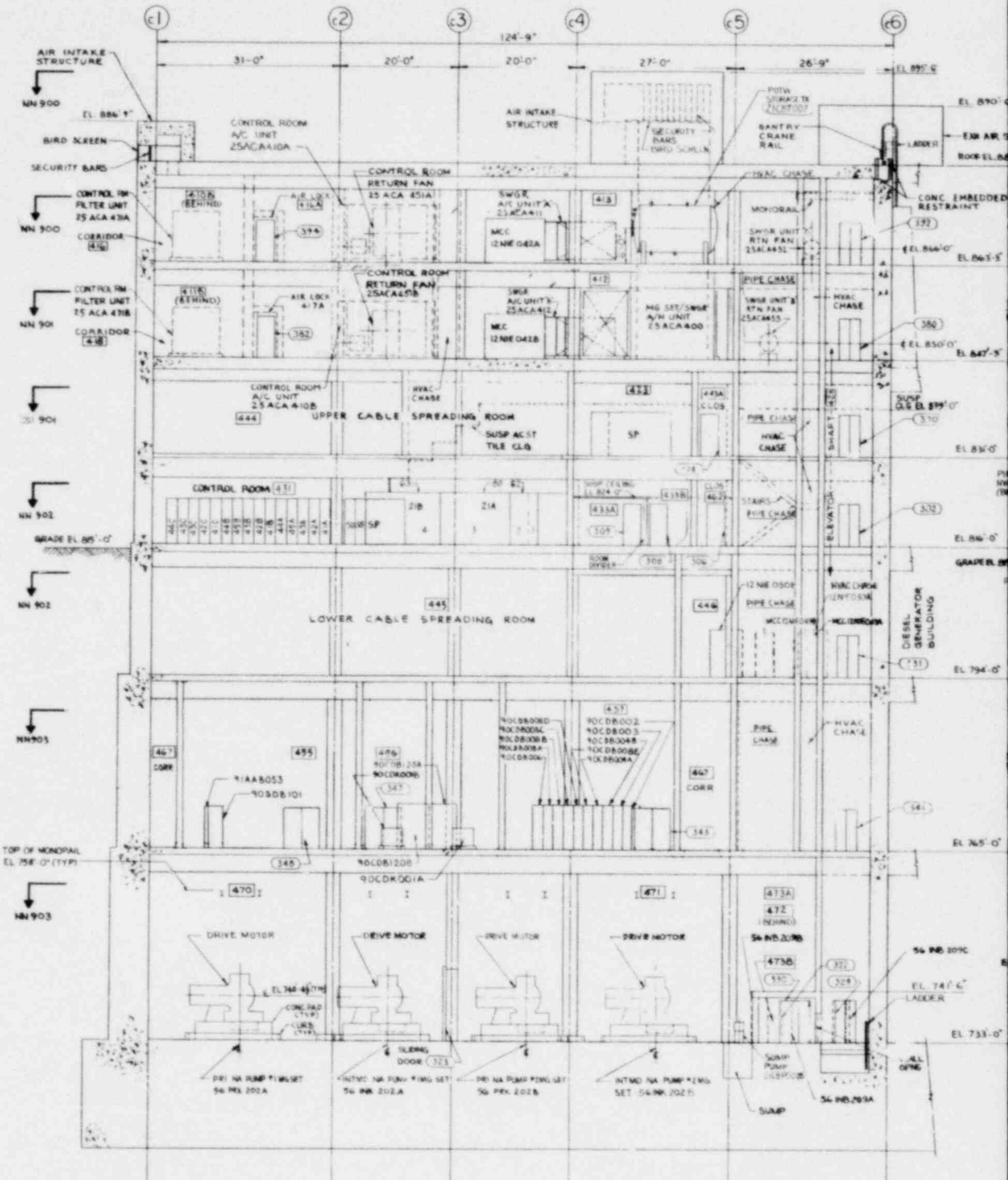
124'-9"
31'-0"
20'-0"
20'-0"
27'-0"
26'-9"
AIR INTAKE STRUCTURE
BIRD SCREEN
SECURITY BARS
CONTROL ROOM A/C UNIT 25ACA410A
CONTROL ROOM RETURN FAN 25 ACA 451A
CONTROL ROOM RETURN FAN 25ACA451B
CONTROL ROOM A/C UNIT 25ACA410B
UPPER CABLE SPREADING ROOM
SUSP ACST TILE CLG
CONTROL ROOM
LOWER CABLE SPREADING ROOM
DRIVE MOTOR
HVAC CHASE
PIPE CHASE
ELEVATOR
SHAFT
MONORAIL
GANTRY CRANE RAIL
LADDER
CONC. EMBEDDED RESTRAINT
DIESEL GENERATOR BUILDING
SUMP
SLIDING DOOR
GRADE EL 815'-0"
TOP OF MONORAIL EL 758'-0" (TYP)
NN 900
NN 901
NN 902
NN903

SECTION A-A

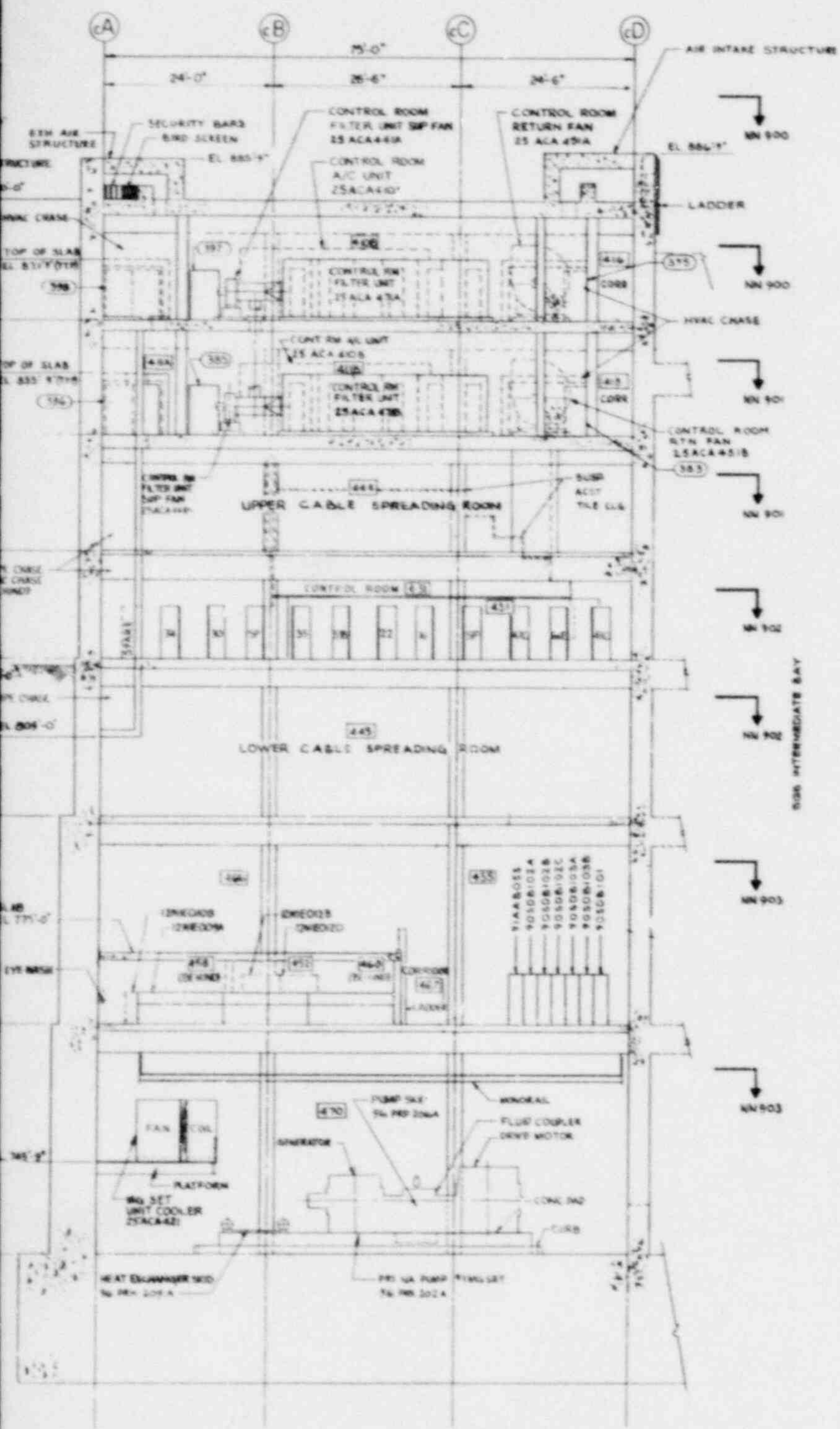

SECTION B-B

REFERENCE DRAWINGS

SEE DRAWING NN 900

GRAPHIC SCALE

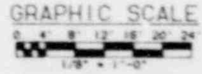

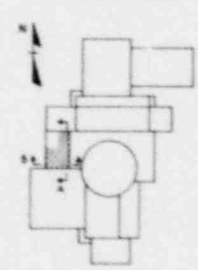

KEY PLAN

Figure 1.2-74
General Arrangement
Control Building
Section A-A and B-B

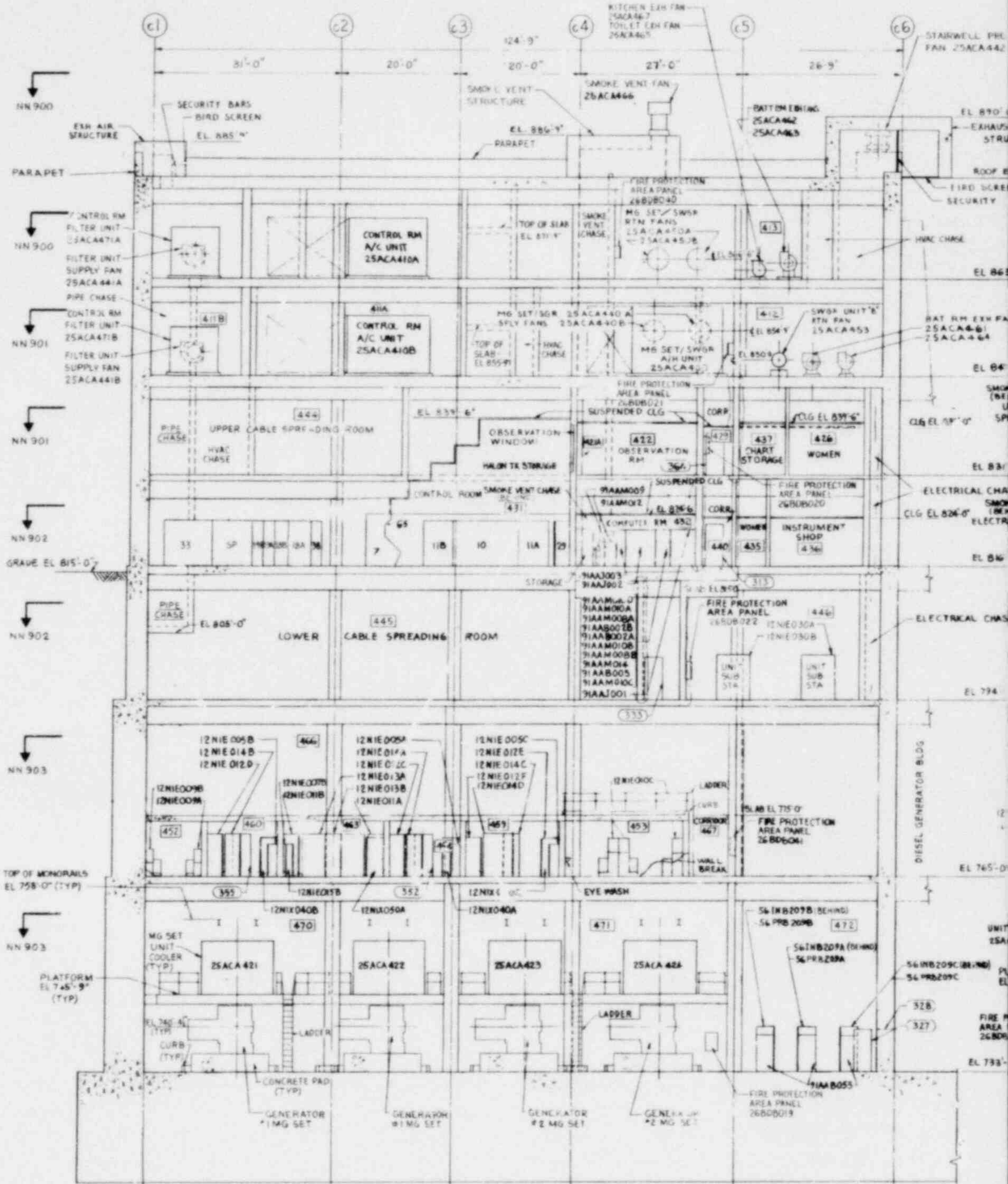

124'-9"
31'-0"
20'-0"
20'-0"
27'-0"
26'-9"
NN 900
NN 901
NN 902
NN 903
SECURITY BARS
BIRD SCREEN
EXH AIR STRUCTURE
PARAPET
SMOKE VENT STRUCTURE
SMOKE VENT FAN 26ACA466
KITCHEN EXH FAN
TOILET EXH FAN
STAIRWELL PRES FAN 25ACA442
CONTROL RM A/C UNIT 25ACA410A
CONTROL RM A/C UNIT 25ACA410B
UPPER CABLE SPREADING ROOM
OBSERVATION WINDOW
HALON TK STORAGE
OBSERVATION RM
CHART STORAGE
WOMEN
CONTROL ROOM
COMPUTER RM
INSTRUMENT SHOP
ELECTRICAL CHASE
GRADE EL 815'-0"
PIPE CHASE
LOWER CABLE SPREADING ROOM
FIRE PROTECTION AREA PANEL
UNIT SUB STA
DIESEL GENERATOR BLDG
TOP OF MONORAILS EL 758'-0" (TYP)
EYE WASH
MG SET UNIT COOLER (TYP)
25ACA421
25ACA422
25ACA423
25ACA424
PLATFORM EL 745'-9" (TYP)
LADDER
CURB (TYP)
CONCRETE PAD (TYP)
GENERATOR #1 MG SET
GENERATOR #2 MG SET

SECTION C-C

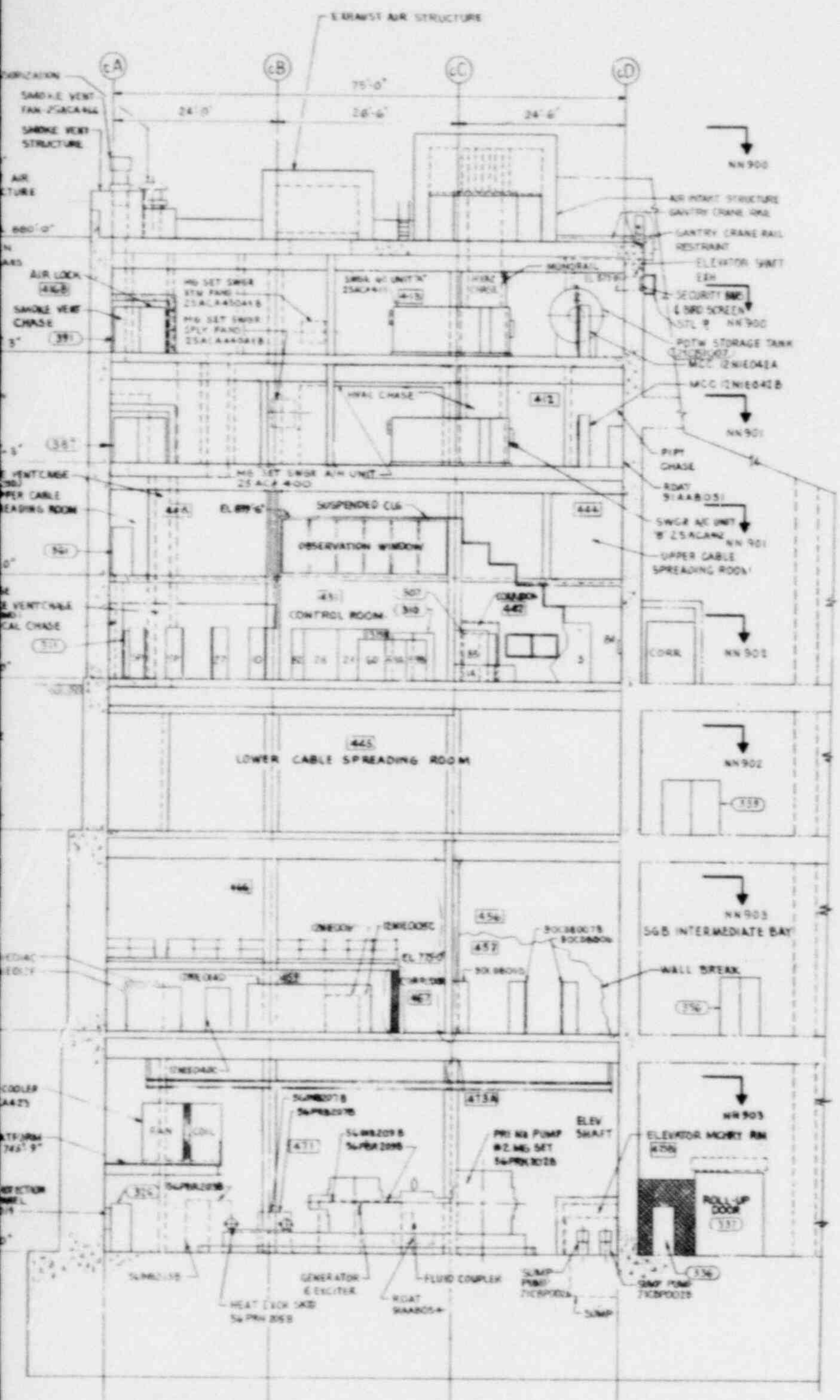

SECTION D-D

REFERENCE DRAWINGS
SEE DRAWING NN800

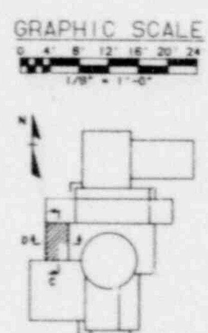

KEY PLAN

Figure 1.2-75
General Arrangement
Control Building
Section C-C and D-D

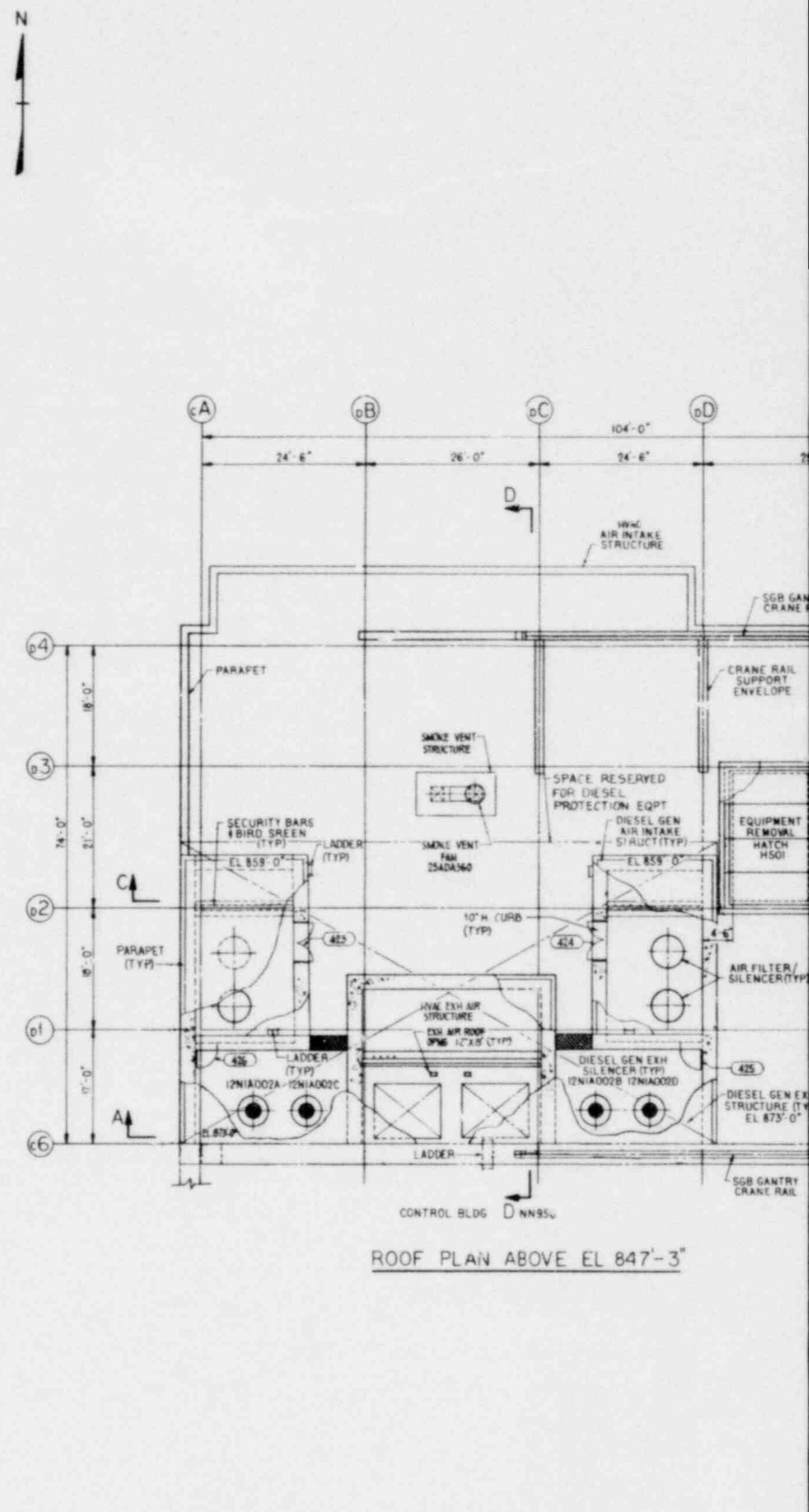

ROOF PLAN ABOVE EL 847'-3"

NN952-9

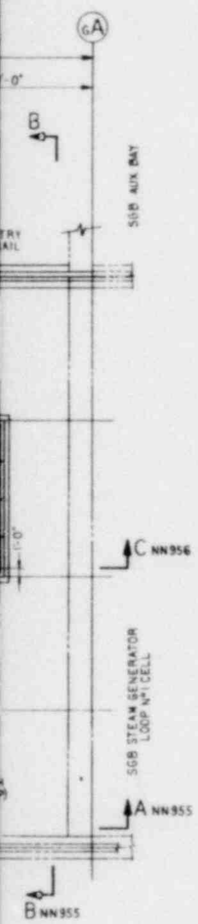

GENERAL NOTES

1. SYMBOLS & ABBREVIATIONS PER WARD DOC D-0036
2. ALL LEVELS IN THIS BUILDING ARE CLASSIFIED AS "UNRESTRICTED RADIATION ZONE"
3. EQUIPMENT REMOVAL HATCH WILL BE SERVICED BY THE EXTENSION OF THE SGB GANTRY CRANE

REFERENCE DRAWINGS

NN953 DGB GENERAL ARRANGEMENT - PLAN ABOVE EL 816'-0" & EL 794'-0"

NN954 DGB GENERAL ARRANGEMENT - PLAN ABOVE EL 765'-0" & EL 733'-0"

NN955 DGB GENERAL ARRANGEMENT SECTION A-A & B-B

NN956 DGB GENERAL ARRANGEMENT SECTION C-C & D-D

LEGEND

- EI&C CABINET, SWGR (HEAVY LINE FRONT)
- GRATING
- 410 CELL NUMBER
- KNOCKOUT SECTION
- CONCRETE
- CONCRETE BLOCK
- CHECKERED PLATE
- 400 DOOR NUMBER

GRAPHIC SCALE

0 4' 8' 12' 16' 20' 24'

1/8" = 1'-0"

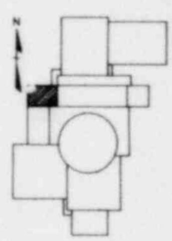

KEY PLAN

Figure 1.2-76
General Arrangement
Diesel Generator Building
El. 847'-3"

Amend. 56
Aug. 1980

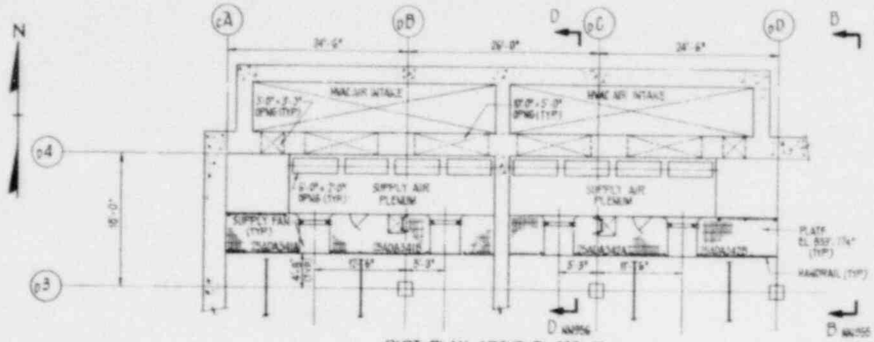

PART PLAN ABOVE EL 832'-0"

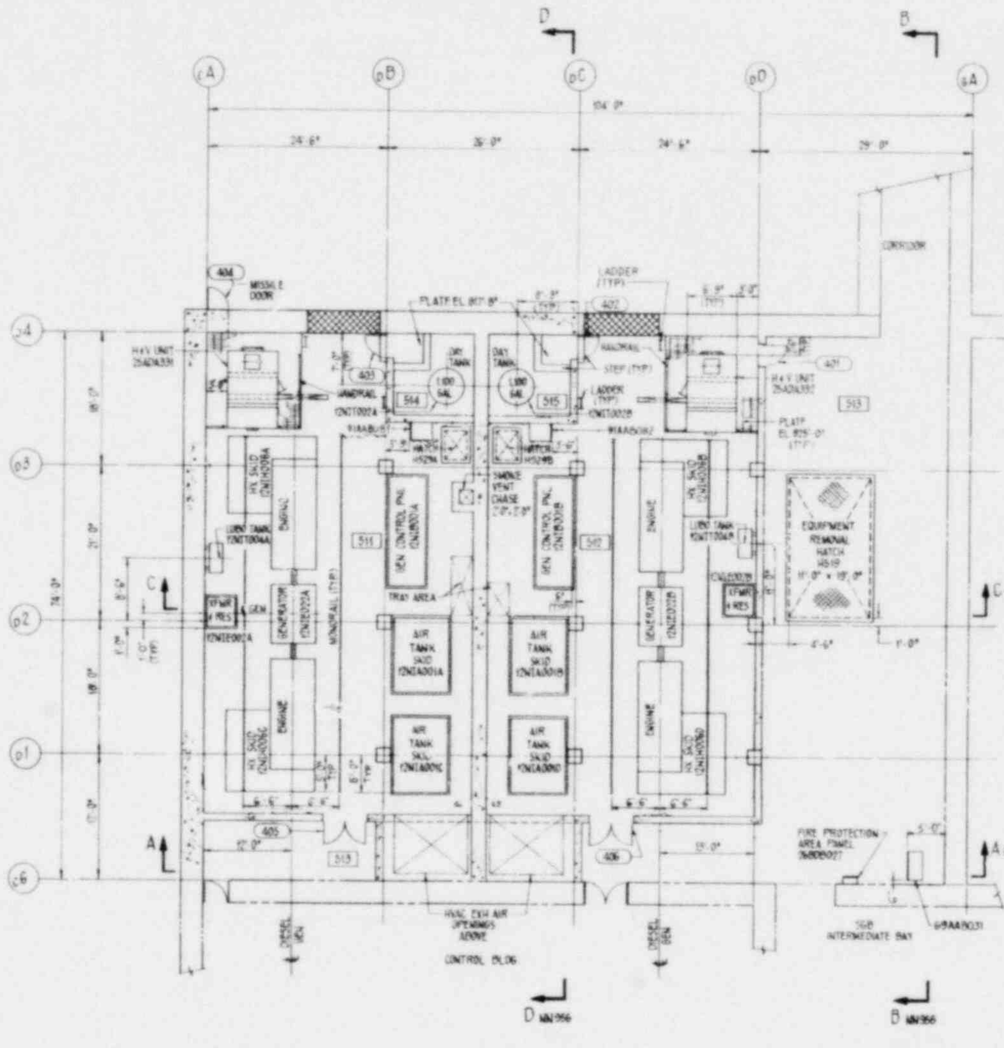

PLAN ABOVE EL 816'-0"

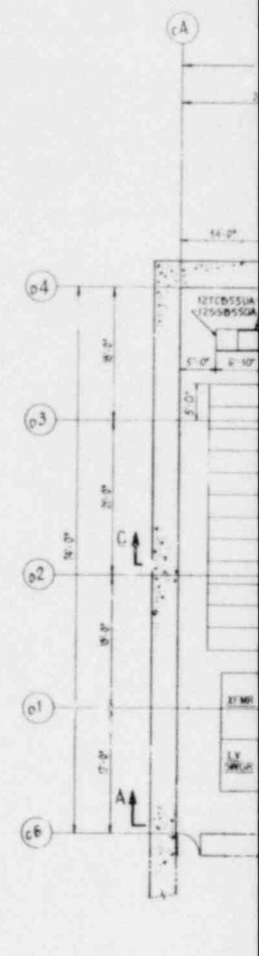

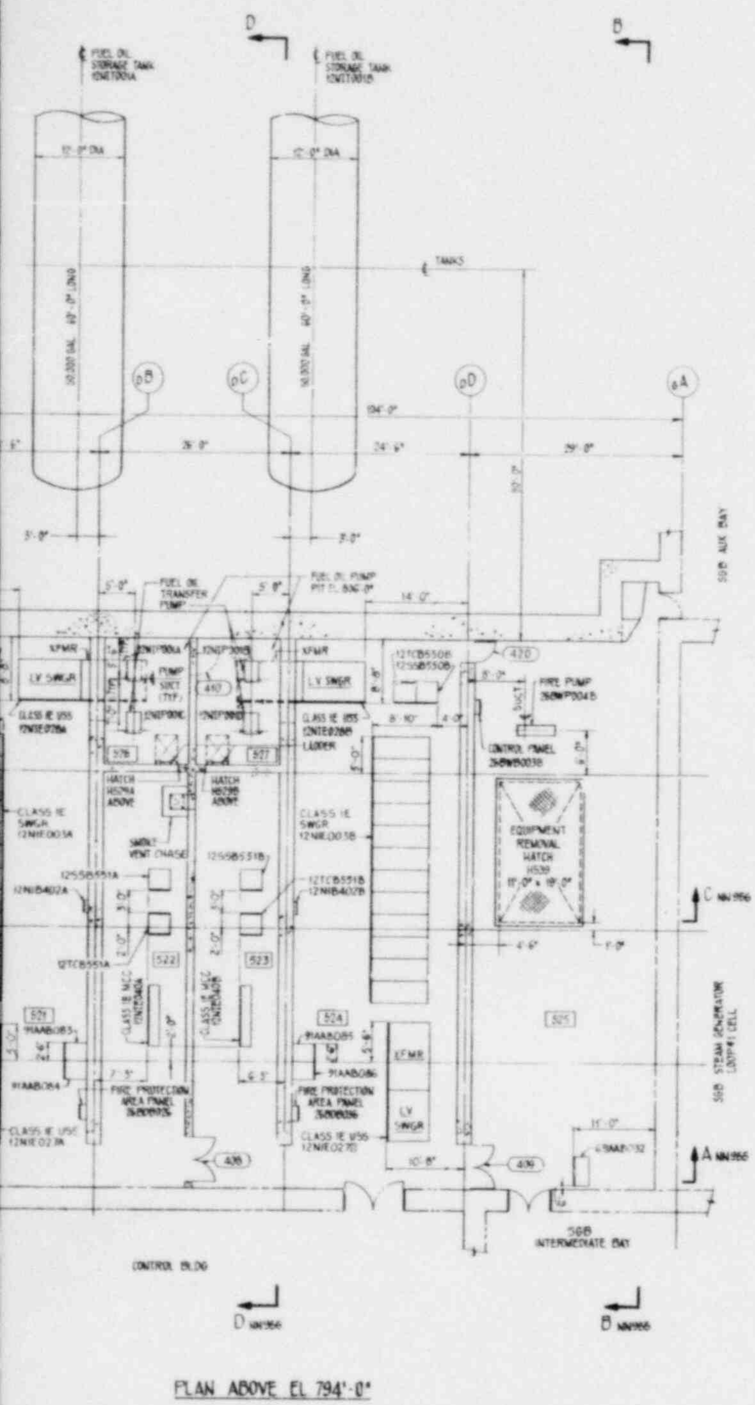

PLAN ABOVE EL 794'-0"

REFERENCE DRAWINGS

SEE DRAWING NN952

GRAPHIC SCALE

1/8" = 1'-0"

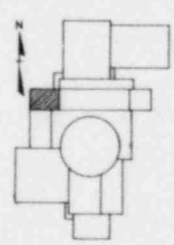

KEY PLAN

Figure 1.2-77
General Arrangement
Diesel Generator Building
El. 816'-0" and 794'-0"

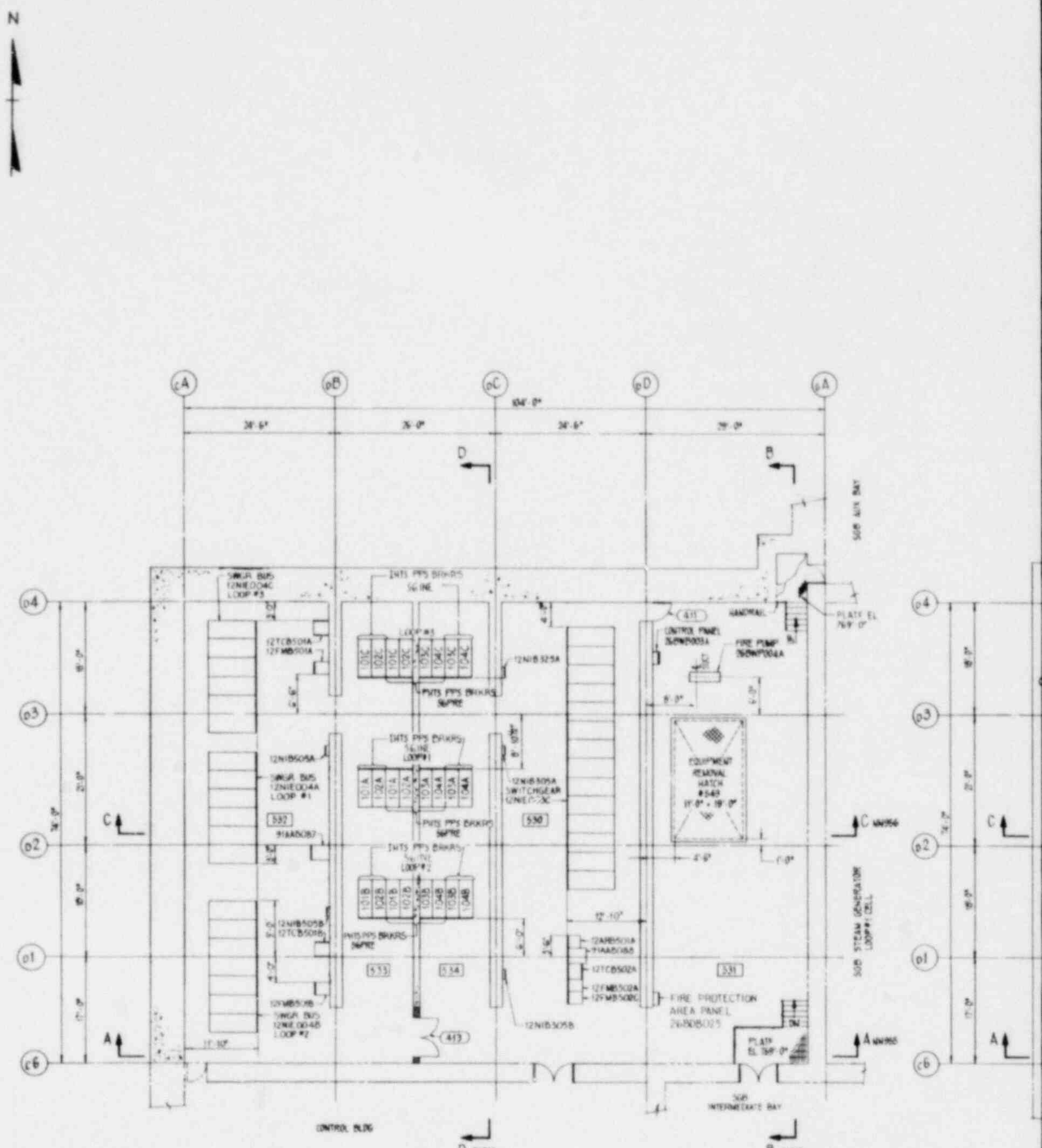

PLAN ABOVE EL 765'-0"

NN954-7

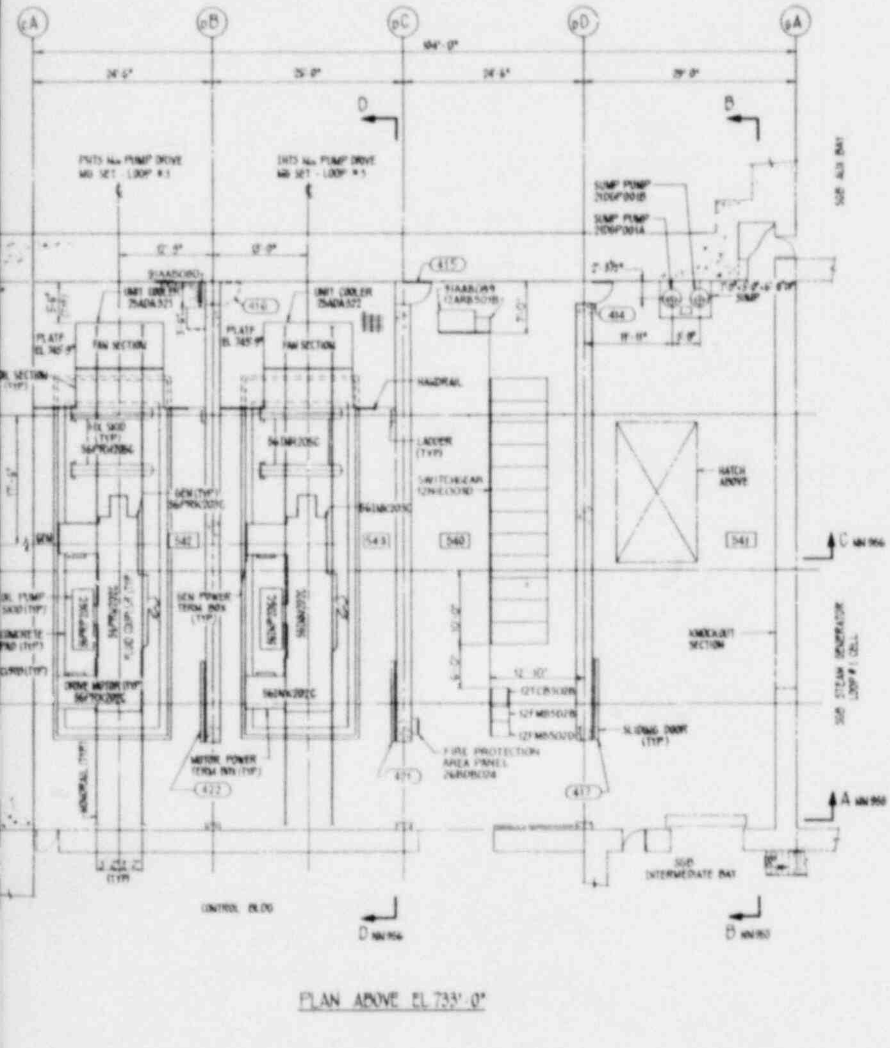

REFERENCE DRAWINGS

SEE DRAWING NN952

GRAPHIC SCALE

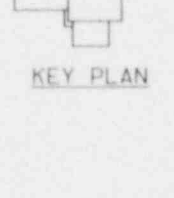

KEY PLAN

Figure 1.2-78
General Arrangement
Diesel Generator Building
El. 765'-0" and 733'-0"

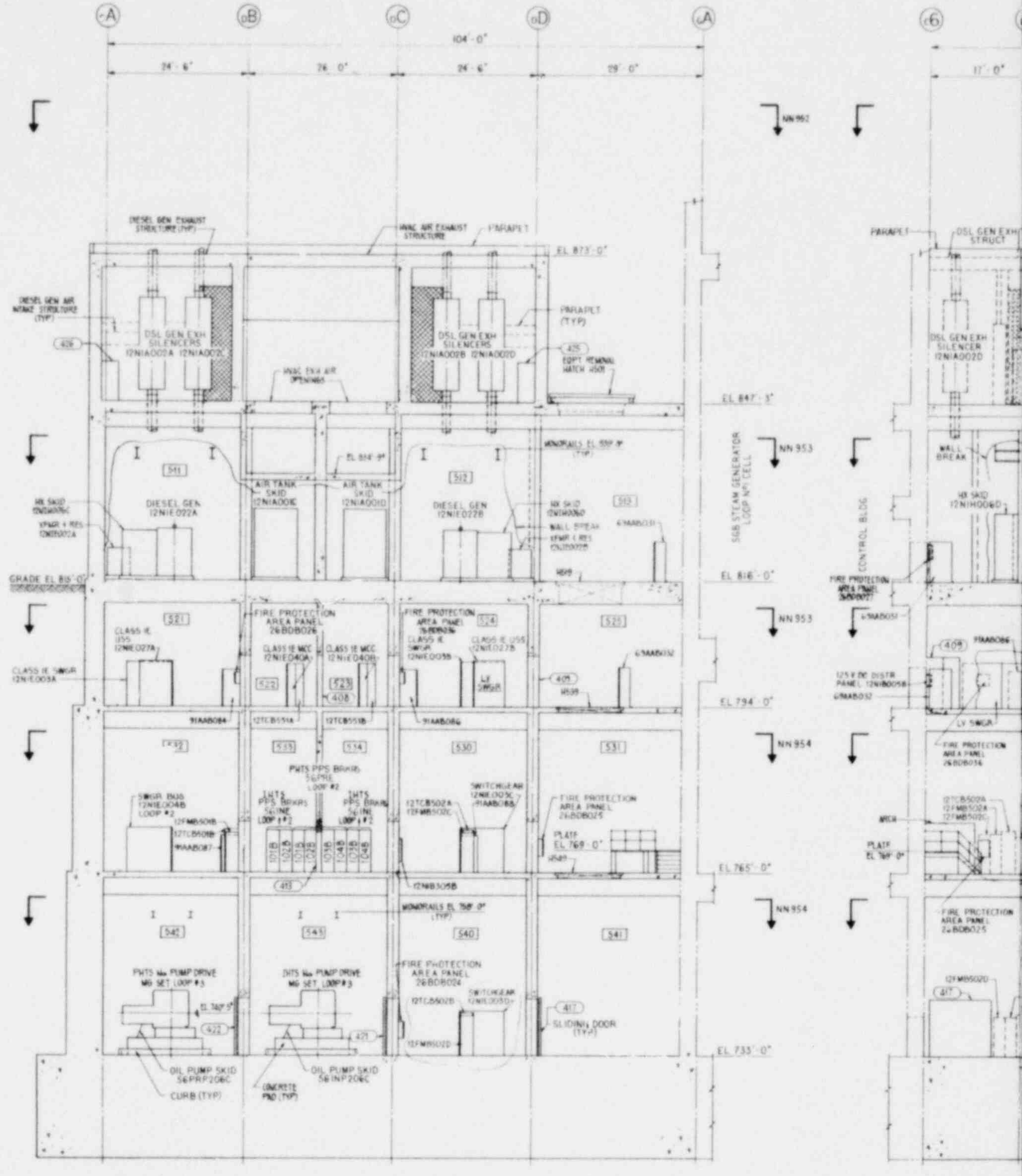

SECTION A-A

NN955-7

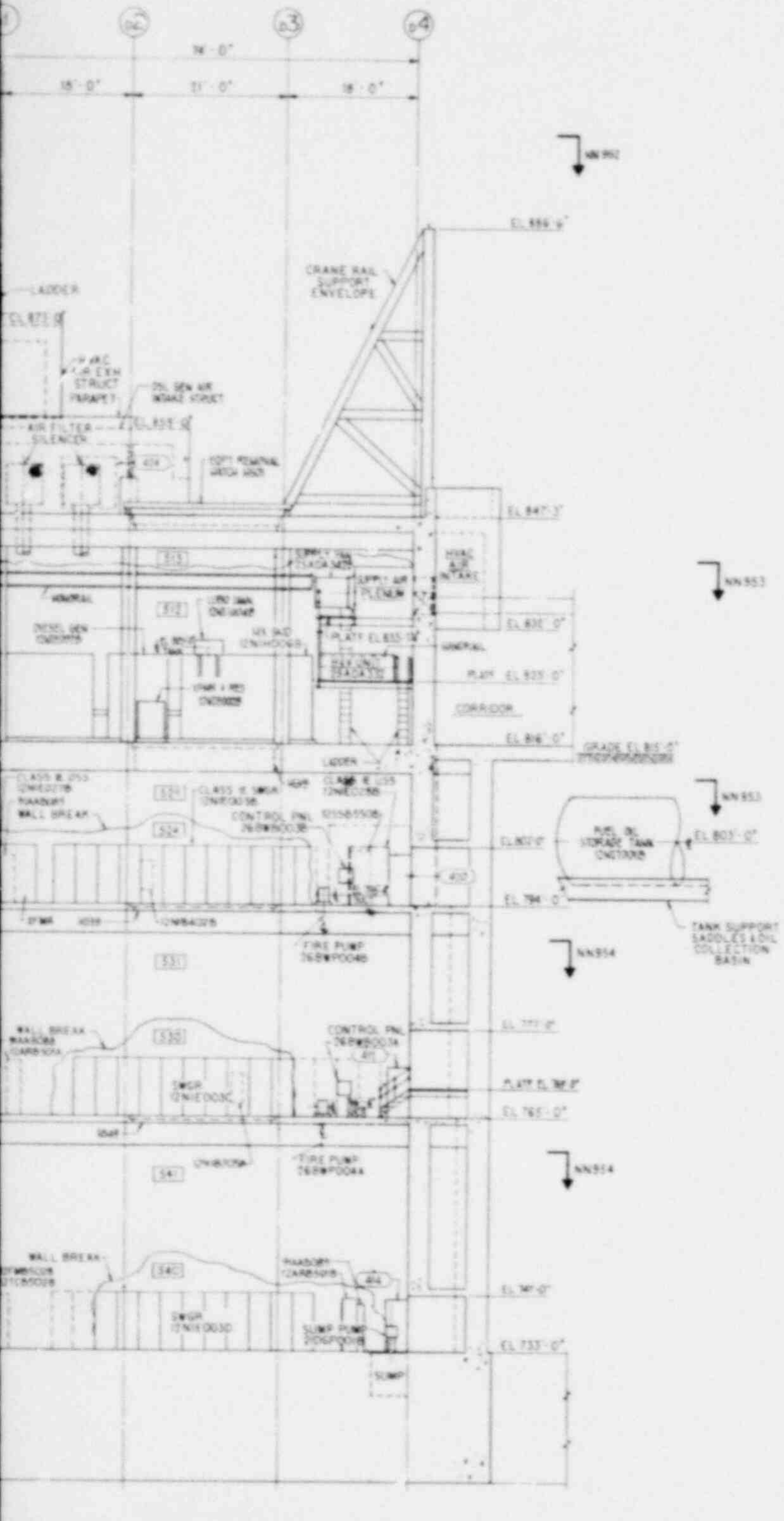

SECTION B-B

REFERENCE DRAWINGS

SEE DRAWING NN952

GRAPHIC SCALE

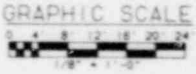

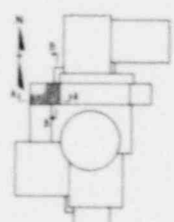

KEY PLAN

Figure 1.2-79
General Arrangement
Diesel Generator Building
Section A-A and B-B

Amend. 56
Aug. 1980

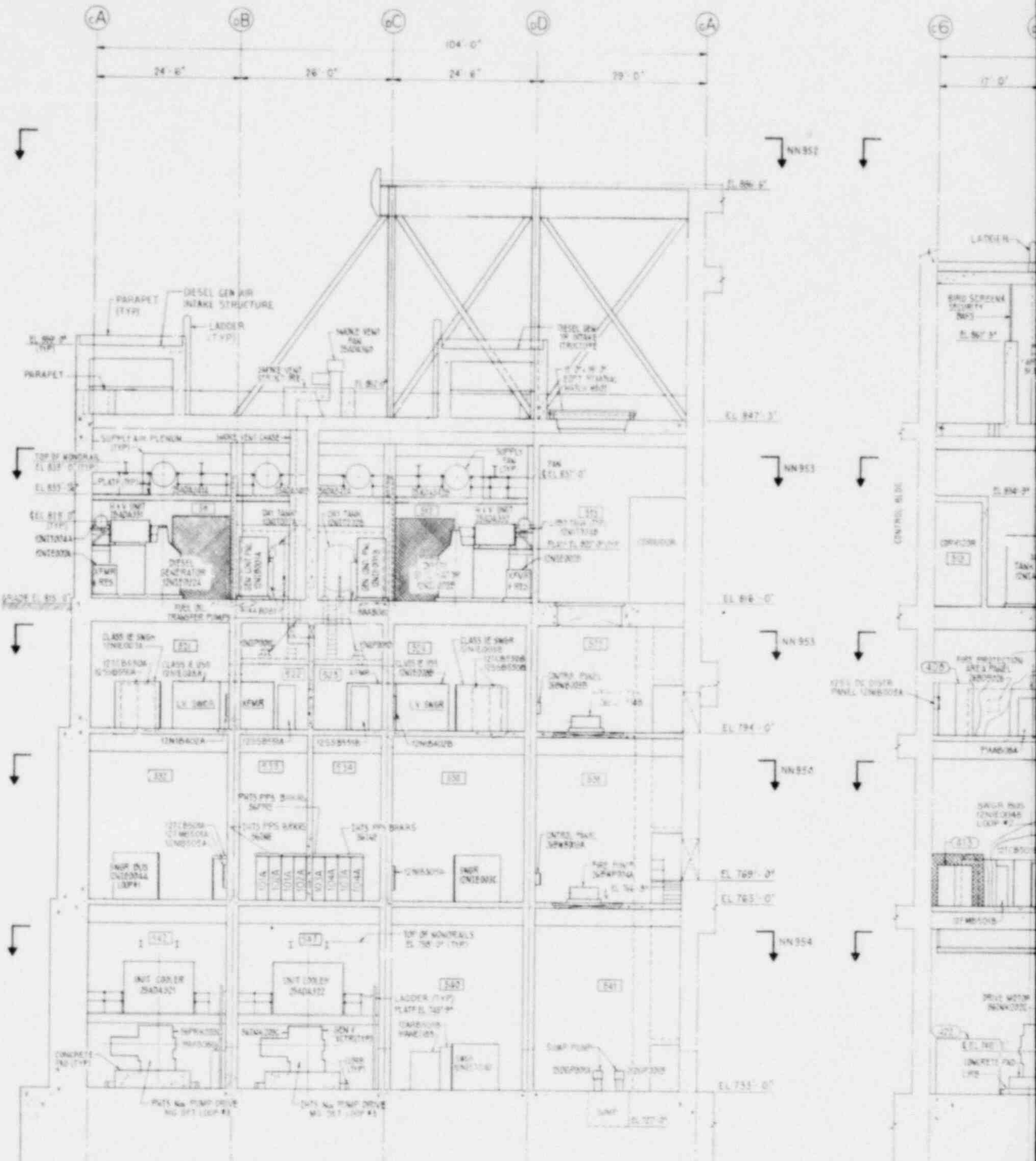

SECTION C-C

NN956-7

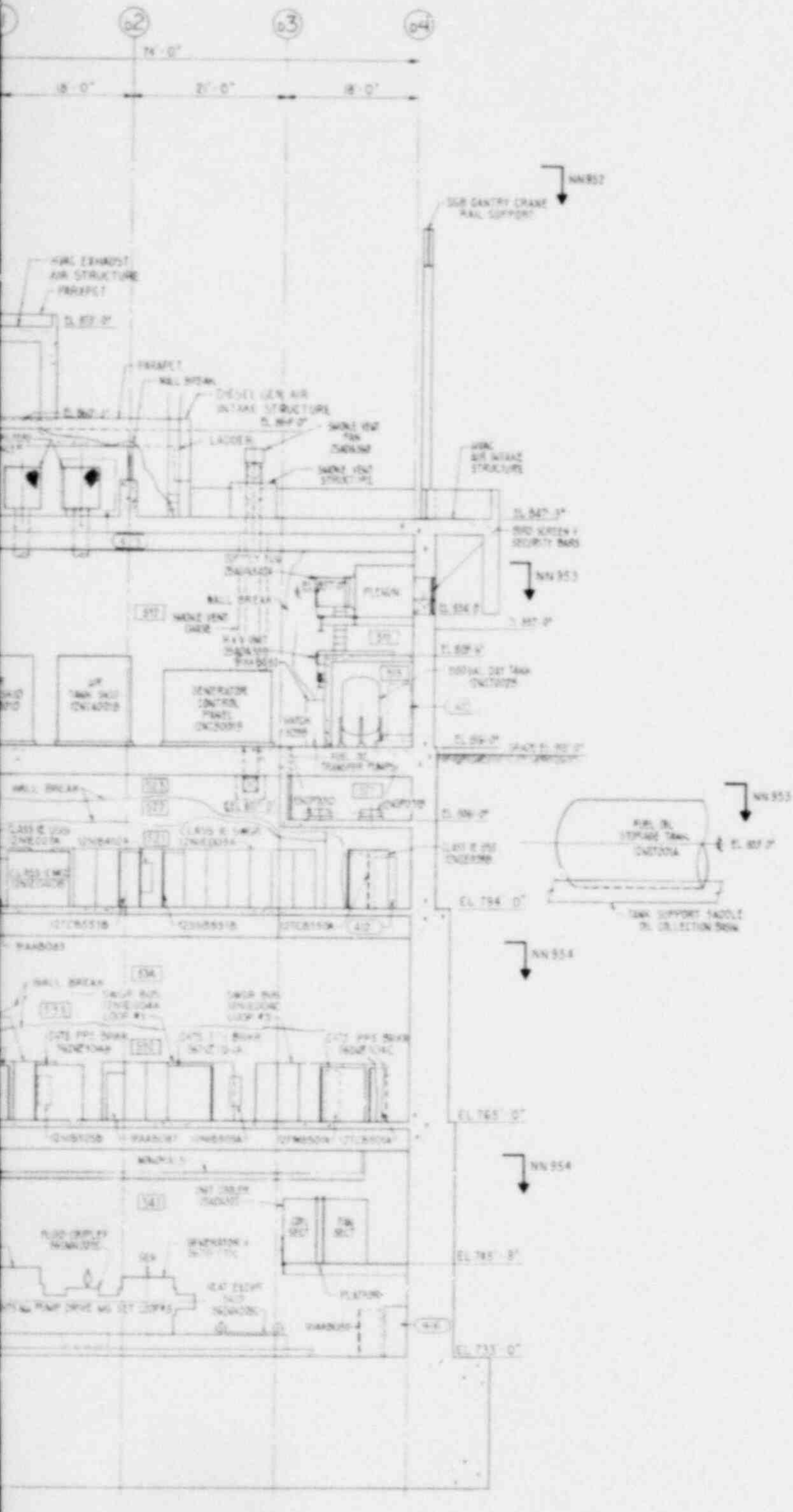

SECTION D-D

REFERENCE DRAWINGS

SEE DRAWING NN952

GRAPHIC SCALE

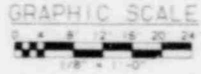

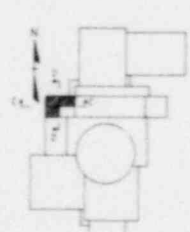

KEY PLAN

Figure 1.2-80
General Arrangement
Diesel Generator Building
Section C-C and D-D

Amend. 56
Aug. 1980

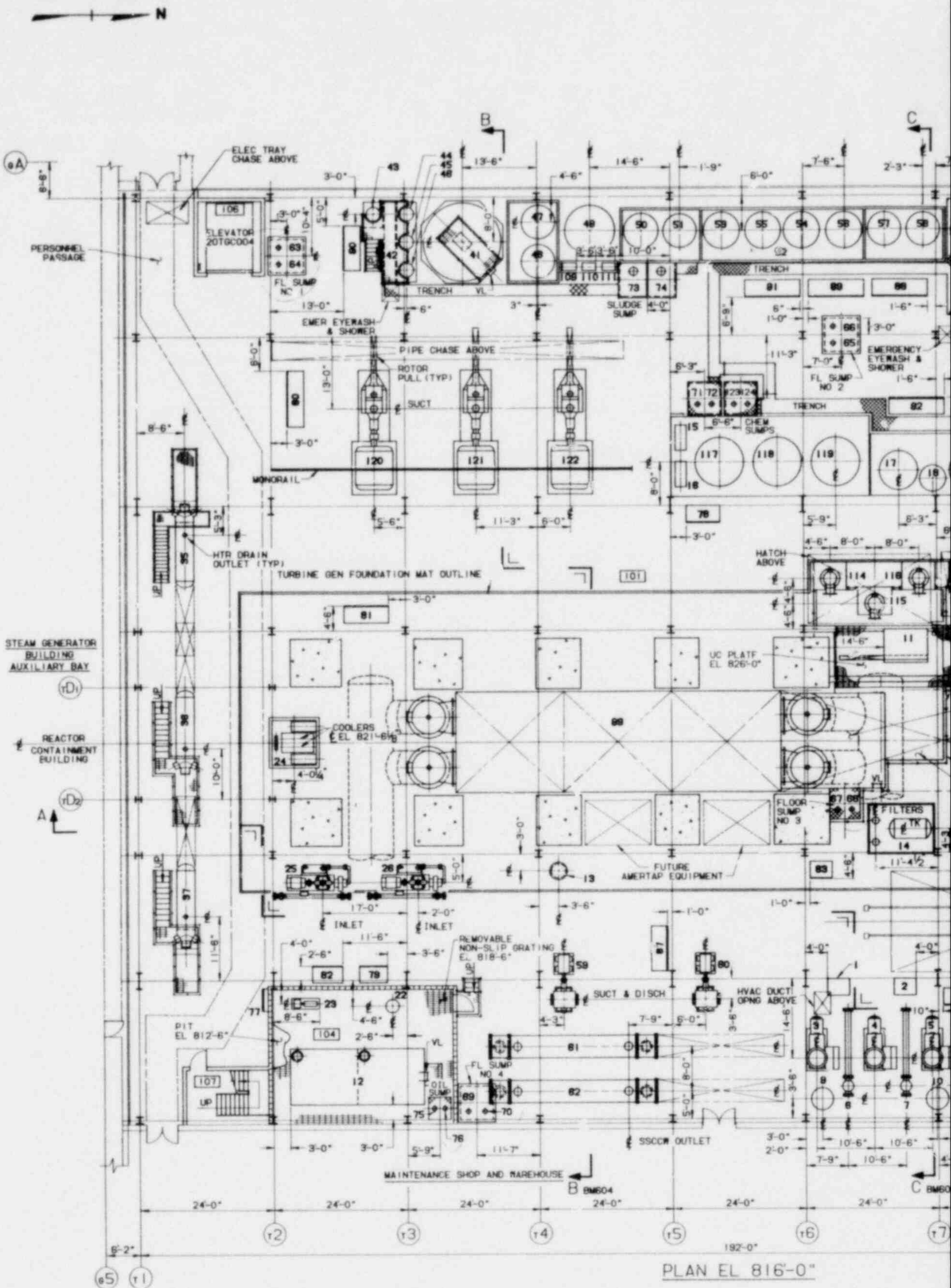

PLAN EL 816'-0"

BM600-4

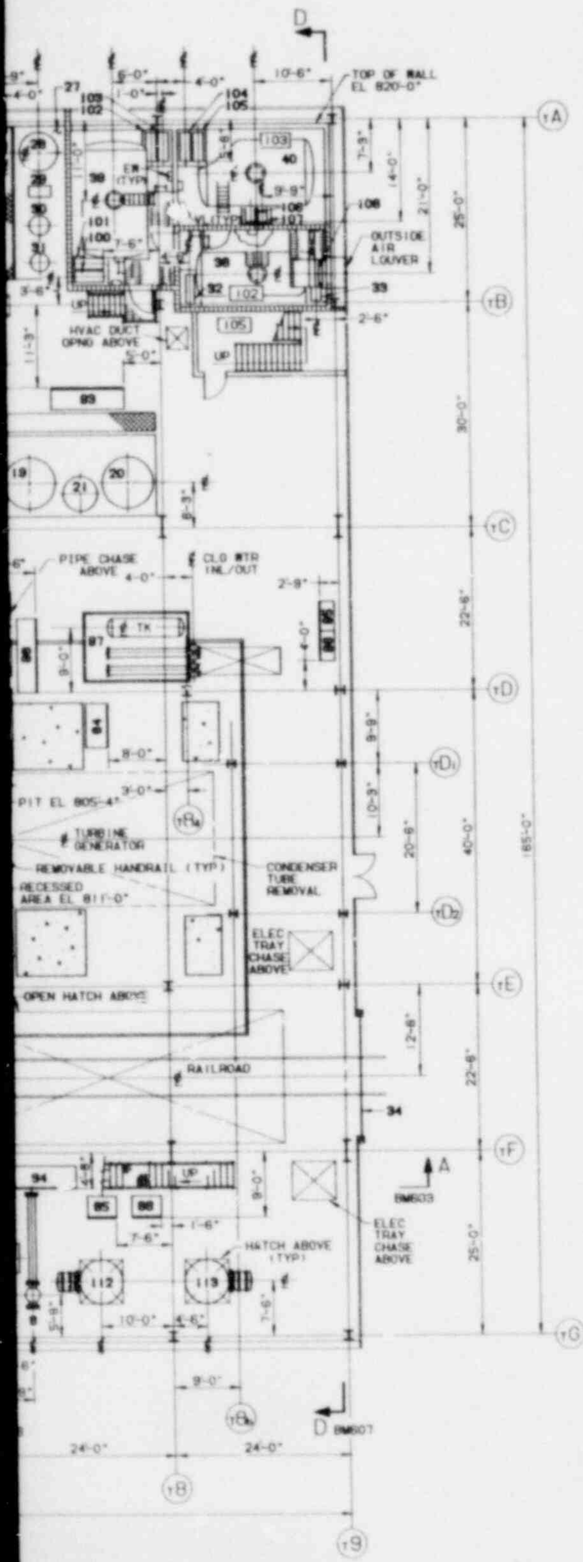

EQUIPMENT LEGEND

ITEM NO	ZONE	EQUIPMENT NUMBER	DESCRIPTION
1	C5	221AA001A	SERVICE & INSTRUMENT AIR DRYERS
2	C5	221AA001B	
3	B5	22SAA001A	SERVICE & INSTRUMENT AIR COMPRESSORS
4	B5	22SAA001B	
5	B5	22SAA001C	
6	B5	22SAA002A	SERVICE & INSTRUMENT AIR AFTERCOOLER & SEPARATORS
7	B5	22SAA002B	
8	B4	22SAA002C	
9	B5	22SAT001A	SERVICE & INSTRUMENT AIR RECEIVERS
10	B5	22SAT001B	
11	E5	25BGA321	UNIT COOLER
12	B7	72TST001	LUBE OIL STORAGE TANK
13	D6	71CDH008	DRAIN COOLER
14	D5	72TAM003	HYDROGEN SEAL OIL SUPPLY UNIT
15	G6	71CPP001A	CONDENSATE POLISHERS RECYCLE PUMPS
16	G6	71CPP001B	
17	G5	71CPT002	CATION TANK
18	G5	71CPT003	ANION TANK
19	G4	71CPT004	MIXED RESIN STORAGE TANK
20	G4	71CPT005	AMMONIA RECLAIM TANK
21	G4	71CPT006	HOT WATER TANK
22	C7	72TSM001	LUBE OIL PURIFIER
23	C7	72TSP001	LUBE OIL TRANSFER PUMP
24	E7	72TAM004	EHC HYD FLUID POWER UNIT
25	D7	73CEM100A	VACUUM PUMP UNITS
26	D7	73CEM100B	
27	H4	75CF0001	CONDENSATE CHEMICAL FEED
28	J4		HOT WATER TANK
29	H4		BLOWER
30	H4		AMMONIA TANK
31	H4		HYDRAZINE TANK
32	H4	75CFP001A	AMMONIA STORAGE TANK METERING PUMPS
33	H4	75CFP001B	
34	C3	20TGC001	ROLL-UP DOOR
35	F8	71FWH007A	TOPPING HEATER
36	E8	71FWH007B	
37	C8	71FWH007C	
38	H4	75CFT001	AMMONIA STORAGE TANK
39	H4	75CFT002	ACID STORAGE TANK
40	H4	75CFT003	CAUSTIC STORAGE TANK
41	H6	75MUG001	CLARIFIER
42	H7	75MUG002	CLARIFIER CHEMICAL FEED
43	J7		CAUSTIC TANK
44	J7		HYPOCHLORITE TANK
45	H7		COAGULANT TANK
46	H7		ALUM TANK
47	J6	75MUG003A	CLARIFIER FILTERS
48	H6	75MUG003B	
49	J6	75MUG004	CLEARWELL
50	J6	75MUG005A	ACTIVATED CARBON FILTERS
51	J6	75MUG005B	
52	H5	75MUG006	MAKE UP DEMINERALIZERS
53	J5		A CATION TANKS
54	J5		B
55	J5		A ANION TANKS
56	J5		B
57	J5		A MIXED BED TANKS
58	J5		B
59	C6	75SWP001A	SEC SVCE CL CLG WTR PUMP
60	C6	75SWP001B	
61	B6	75SWH001A	SEC SVCE CL CLG WTR HT EXCH
62	B6	75SWH001B	
63	H7	76WDP001A	FLOOR DRAIN SUMP PUMPS
64	H7	76WDP001B	
65	G4	76WDP002A	
66	G4	76WDP002B	
67	D5	76WDP003A	
68	D5	76WDP003B	
69	B6	76WDP004A	
70	B6	76WDP004B	
71	G6	76WDP005A	CHEMICAL SUMP PUMPS
72	G6	76WDP005B	
73	H6	76WDP008A	SLUDGE SUMP PUMPS
74	H6	76WDP008B	
75	B7	76WDP009A	LUBE OIL SUMP PUMPS
76	B7	76WDP009B	
77	C7	26BDB032	LOCAL FIRE PROTECTION PANEL
78	F5	69AAB003	INSTRUMENT RACKS
79	C7	69AAB004C	
80	G7	69AAB006	
81	F7	69AAB008A	
82	C7	69AAB008B	
83	D5	69AAB008D	
84	E4	69AAB008E	
85	B4	69AAB010A	
86	B4	69AAB010B	
87	C6	69AAB011	
88	H5	69AAB013A	
89	H5	69AAB013B	
90	H7	69AAB013C	
91	H5	69AAB013D	
92	G5	69AAB014A	
93	G4	69AAB014B	
94	C4	69AAB016	

EQUIPMENT LEGEND

ITEM NO	ZONE	EQUIPMENT NUMBER	DESCRIPTION
95	F3	69AAB018	INSTRUMENT RACKS
96	F3	69AAB019	
97	F4	72TAM001	STATOR WINDING CLG UNIT
98	F4	69AAB008F	HYDROGEN & STATOR COOLING WATER CABINET
99	E6	73CWH001	CONDENSER
100	H4	71CPP002A	ACID STORAGE TANK METERING PUMPS
101	H4	71CPP002B	
102	H4	75MUP007A	
103	H4	75MUP007B	
104	H4	71CPP003A	CAUSTIC STORAGE TANK METERING PUMPS
105	H4	71CPP003B	
106	H4	75MUP008A	
107	H4	75MUP008B	
108	H4	25BGA003	HEAT & VENTILATING UNIT
109	H6	75MUP001A	CLEARWELL PUMPS
110	H6	75MUP001B	
111	H6	75MUP001C	
112	B4	72ASH001A	AUXILIARY BOILERS
113	B4	72ASH001B	
114	F5	71CDP001A	CONDENSATE PUMPS
115	F5	71CDP001B	
116	F5	71CDP001C	
117	G5	71CPT001A	CONDENSATE POLISHERS
118	[illegible]	71CPT001B	
119	[illegible]	71CPT001C	
120	G7	71FWP001A	STEAM GENERATOR FEED PUMPS
121	G6	71FWP001B	
122	G6	71FWP001C	
123	[illegible]	76WDP005C	CHEMICAL SUMP PUMPS
124	G5	76WDP005D	

REFERENCE DRAWINGS

SEE DRAWING BM801

GRAPHIC SCALE

0 4' 8' 12' 16' 20' 24'

1/8" = 1'-0"

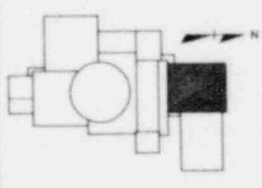

KEY PLAN

Figure 1.2-81
General Arrangement
Turbine Generator Building
Plan El. 816'-0"

Amend. 56
Aug. 1980

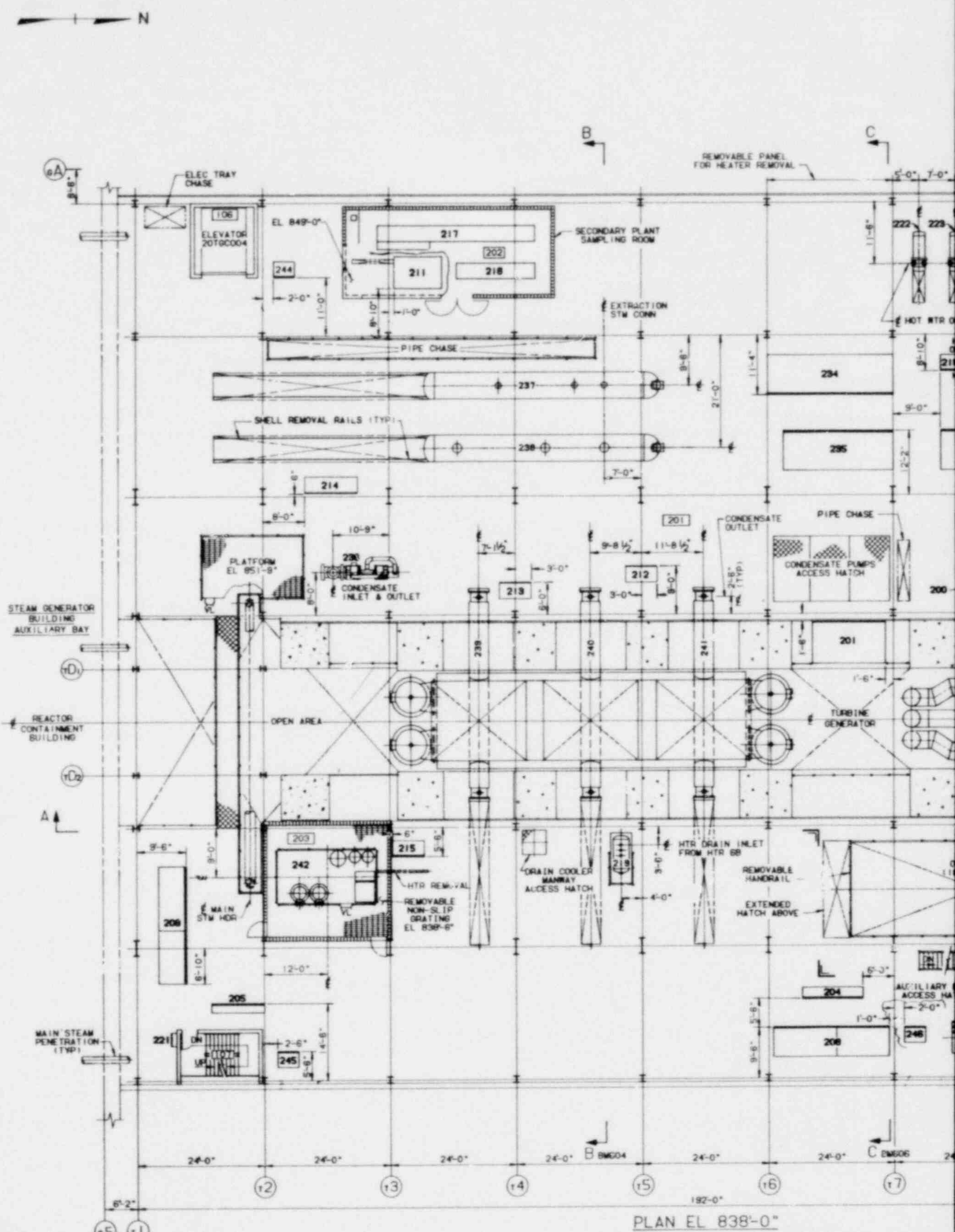

PLAN EL 838'-0"

BM601-3

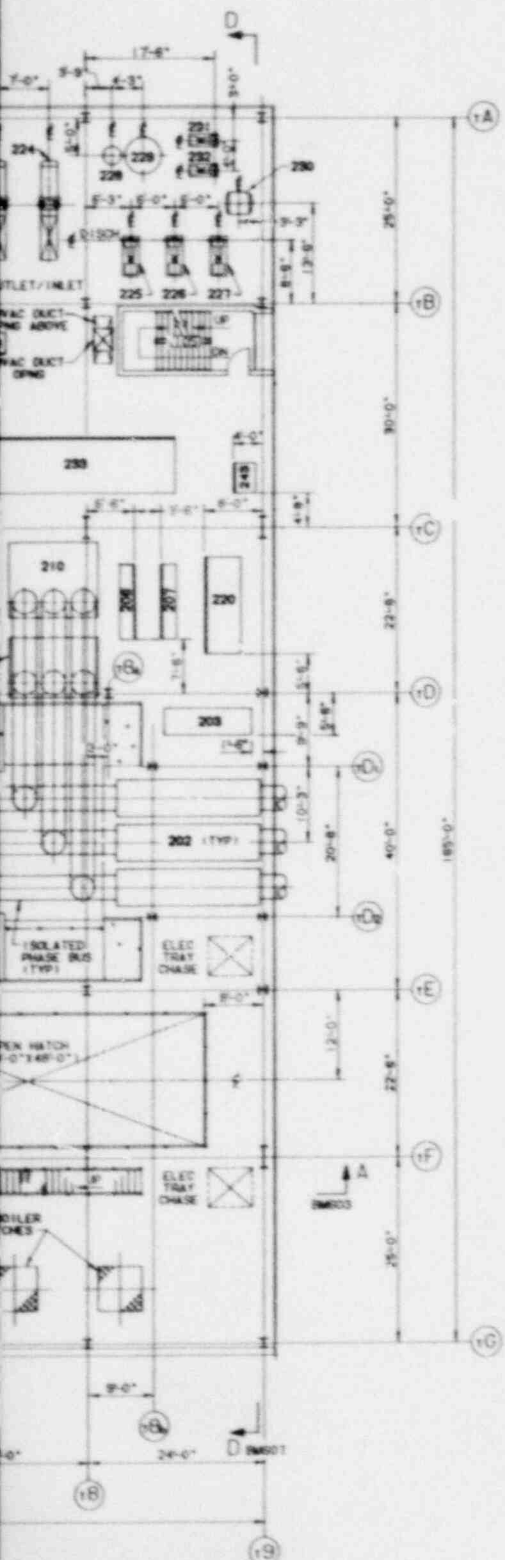

EQUIPMENT LEGEND

ITEM NO.	ZONE	EQUIPMENT NUMBER	DESCRIPTION
200	F4	11AAE008	PT & SURGE PROTECTION CUBICLE
201	E5	11AAE009	TURBINE GENERATOR ... XFMR & RES
202	E4	11AAE012	GENERATOR LOAD BREAK SWITCH
203	E4	11AAE013	COMPRESSOR LOAD BREAK SWITCH
204	B5	12BPE006A	MOTOR CONTROL CENTERS
205	B8	12BPE006B	
206	F4	12BPE007A	
207	F4	12BPE007B	
208	B5	12BPE022A	UNIT SUBSTATION
209	C8	12BPE022B	
210	F4	11AAH001	ISOLATED PHASE BUS HEAT EXCHANGER
211	H7	25B0A322	UNIT COOLER
212	F6	69AAB004A	INSTRUMENT RACKS
213	F6	69AAB004B	
214	D7	69AAB007A	
215	D7	69AAB008C	
216	H6	69AAB022	MONITORING PANEL
217	H7	69AAB023	SAMPLE PANEL
218	H4	69AAB030	INSTRUMENT RACK
219	D6	71DVT001	DRAIN TANK
220	F4	72TAM006	EXCITATION CUBICLE
221	B8	26BDB031	LOCAL FIRE PROTECTION PNL
222	H4	72ASH002A	HOT WATER HEAT EXCHANGERS
223	H4	72ASH002B	
[illegible]	H4	72ASH002C	
22[illegible]	H4	75HMP001A	CIRCULATING WATER PUMPS
226	H4	75HMP001B	
227	H4	75HMP001C	
228	H4	75HMM002	AIR SEPARATOR
229	H4	75HMT001	EXPANSION TANK
230	H4	75HMH001	MAKEUP WATER HEATER
231	H4	75HMP002A	MAKEUP WATER PUMPS
232	H4	75HMP002B	
233	D4	12BPE001A	SWITCHGEAR
234	D5	12BPE001B	
235	D5	12BPE001D	
236	F7	72TAH001	STEAM PACKING EXHAUSTER
237	D6	71CDH004	LP FEEDWATER HEATERS
238	D6	71CDH005	
239	E8	71CDH006A	
240	E5	71CDH006B	
241	E5	71CDH006C	
242	C7	72TAM002	LUBE OIL RESERVOIR
243	D4	91AAB074	REMOTE DATA ACQUISITION TERMINALS
244	H7	91AAB073	
245	B7	91AAB071	
246	B4	91AAB072	

GENERAL NOTES

1. FOR LEGEND AND SYMBOLS, UNLESS OTHERWISE NOTED, REFER TO WARD DOCUMENT DOC-0038-STANDARD SYMBOLOGY FOR CPNPP DRAWINGS
2. HEAVY LINE DENOTES FRONT OF UNIT
3. REMOVABLE HANDRAILS SHALL BE PROVIDED FOR ALL COVERED HATCHES
4. ACCESS AND MAINTENANCE PLATFORMS TO BE PROVIDED WHERE REQUIRED PENDING DEVELOPMENT OF PIPING AND EQUIPMENT DETAILS
5. EW-EYE WASH
6. 104 ROOM NUMBER

REFERENCE DRAWINGS

BM600 GENERAL ARRANGEMENT TURBINE GENERATOR BUILDING FIRST FLOOR PLAN EL 810'-0"

BM602 GENERAL ARRANGEMENT TURBINE GENERATOR BUILDING OPERATING FL PLAN EL 862'-0"

BM603 GENERAL ARRANGEMENT TURBINE GENERATOR BUILDING SECTION A-A

BM604 GENERAL ARRANGEMENT TURBINE GENERATOR BUILDING SECTION B-B

BM605 GENERAL ARRANGEMENT TURBINE GENERATOR BUILDING PARTIAL PLAN EL 862'-0" & SECTION E-E

BM606 GENERAL ARRANGEMENT TURBINE GENERATOR BUILDING SECTION C-C

BM607 GENERAL ARRANGEMENT TURBINE GENERATOR BUILDING SECTION D-D

GRAPHIC SCALE

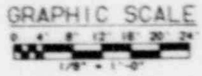

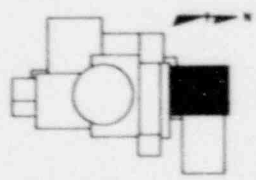

KEY PLAN

Figure 1.2-82
General Arrangement
Turbine Generator Building
Plan El. 838'-0"

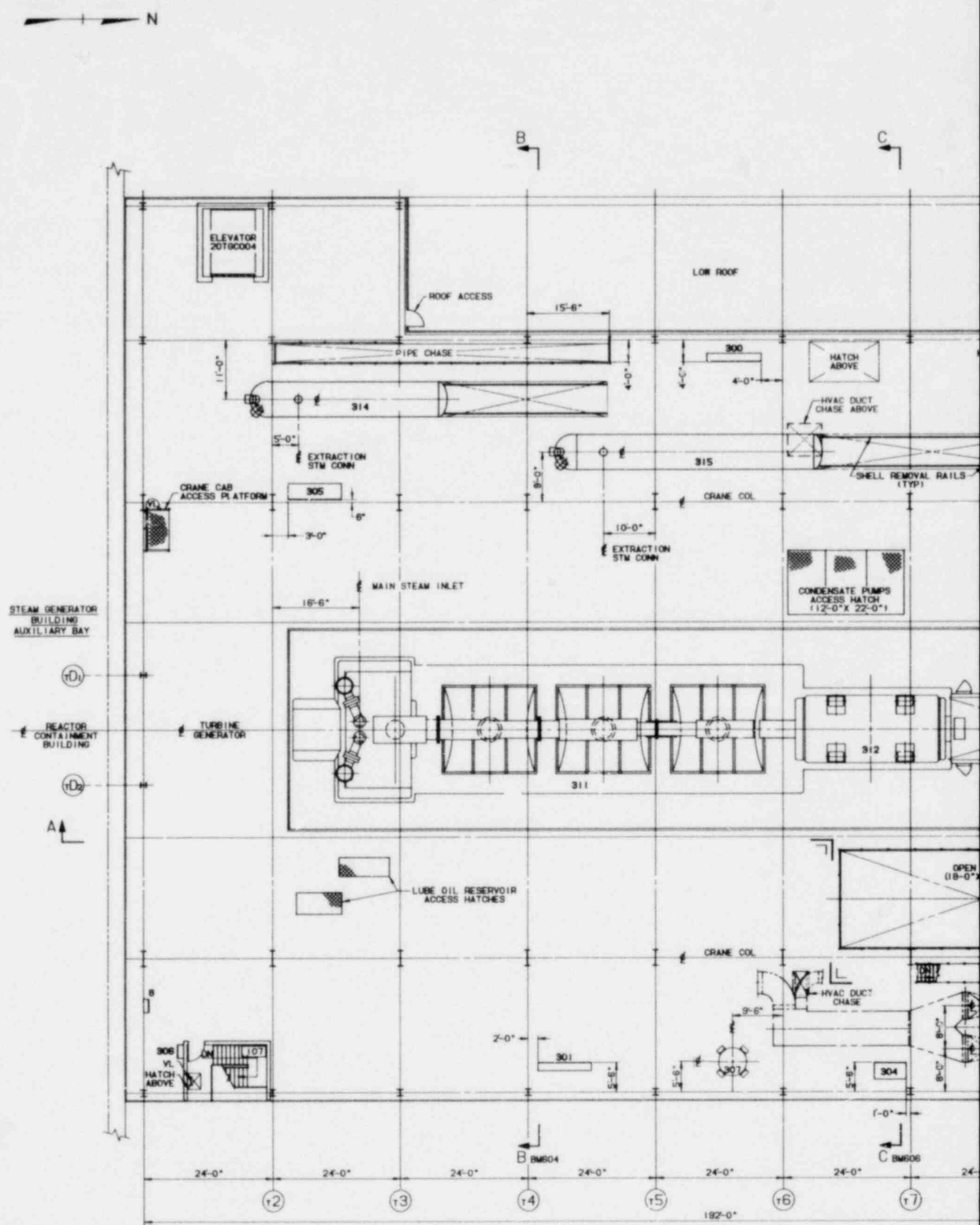

PLAN EL 862'-0"

BM602-3

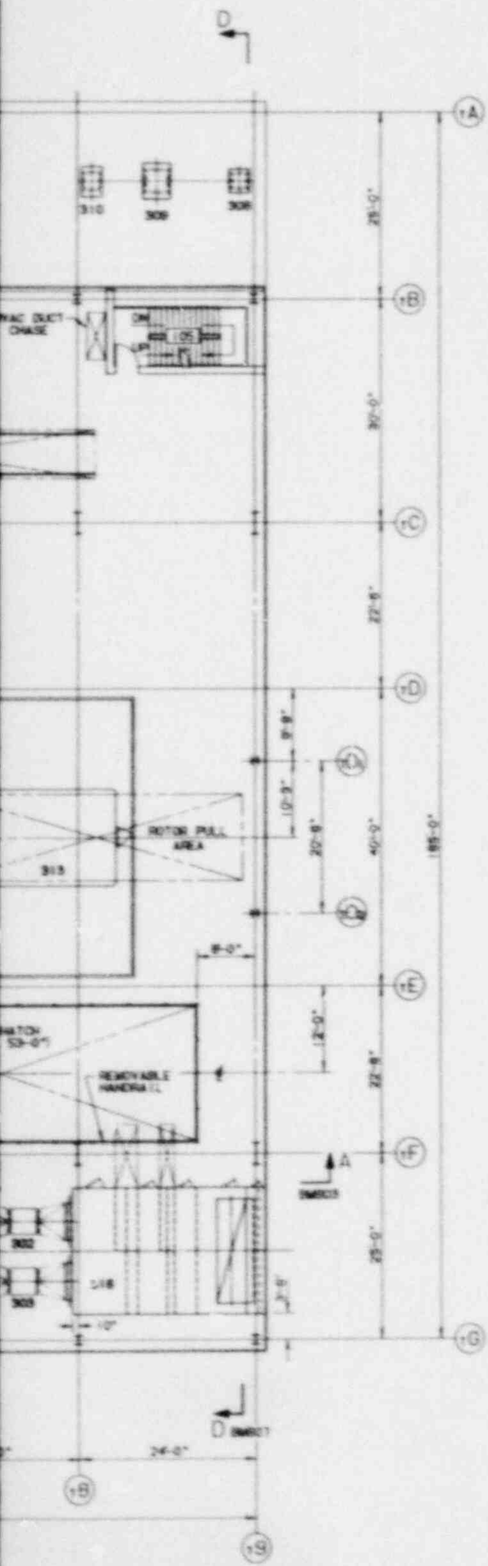

EQUIPMENT LEGEND			
[illegible]	ZONE	EQUIPMENT NUMBER	DESCRIPTION
300	H5	128PE005A	MOTOR CONTROL CENTERS
301	H6	128PE005B	
302	B4	25B0A241A	AIR HANDLING UNIT
303	B4	25B0A241B	SUPPLY FANS
304	B5	25BP8001B	INSTRUMENT RACKS
305	F7	59AA8007B	
306	B8	26BDB030	LOCAL FIRE PROTECTION PNL
307	B5	75BMT001	SSCCW SURGE TANK
308	H4	25B0A162	
309	H4	25B0A163	EXHAUST FANS
310	H4	25B0A361	
311	E6	72TBM001	TURBINE
312	E5	72TBM002	GENERATOR
313	E4	72TAM005	ALTERNATOR
314	G7	71FMW001	H.P. FEEDWATER HEATERS
315	G5	71FMW002	
316	B4	25B0A002	AIR HANDLING UNIT

REFERENCE DRAWINGS
SEE DRAWING [illegible]

GRAPHIC SCALE

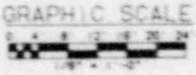

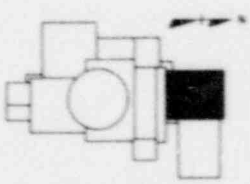

KEY PLAN

Figure 1.2-83
General Arrangement
Turbine Generator Building
Plan El. 862'-0"

Amend. 56
Aug. 1980

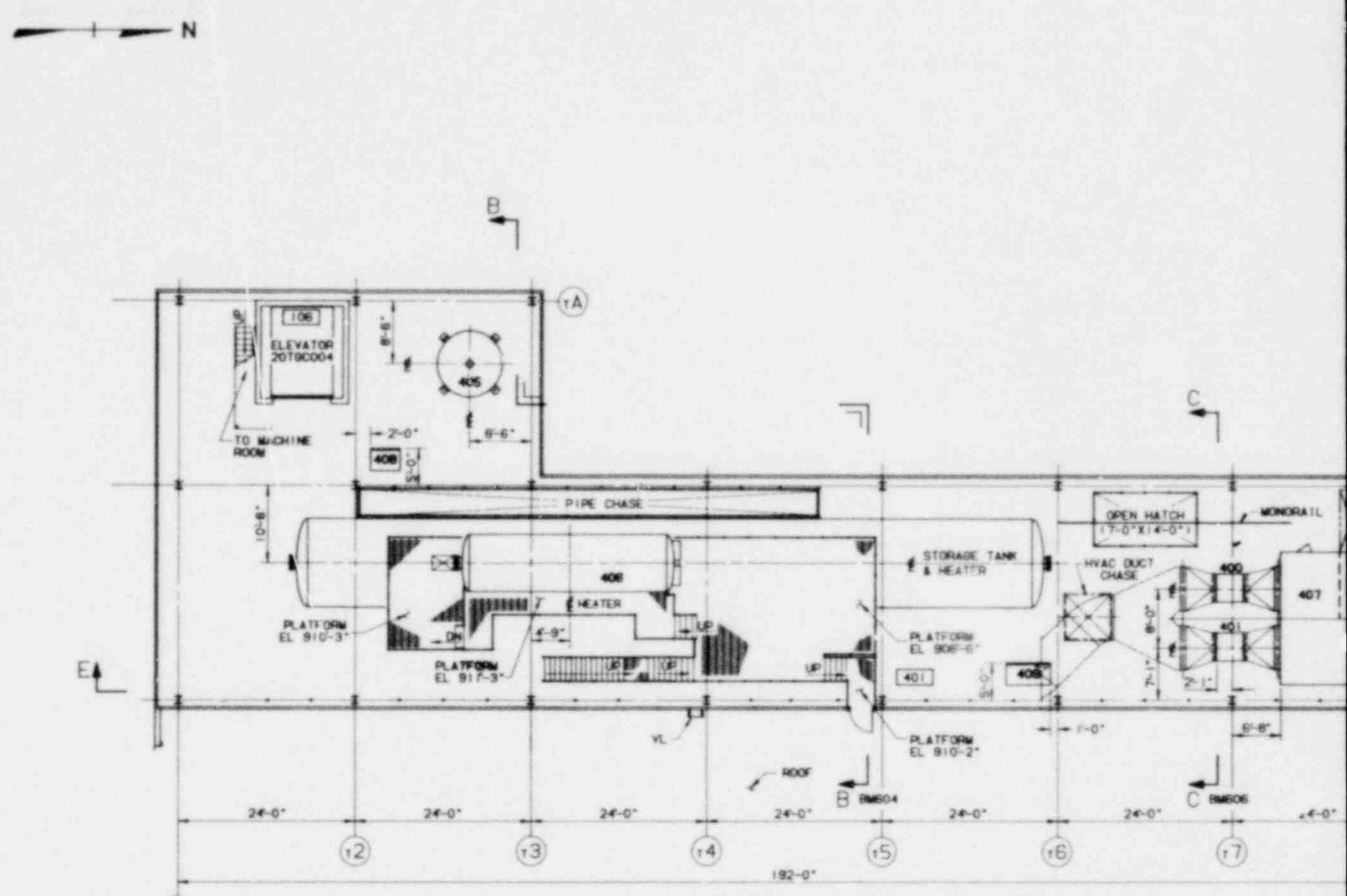

PARTIAL PLAN EL 892'-0"

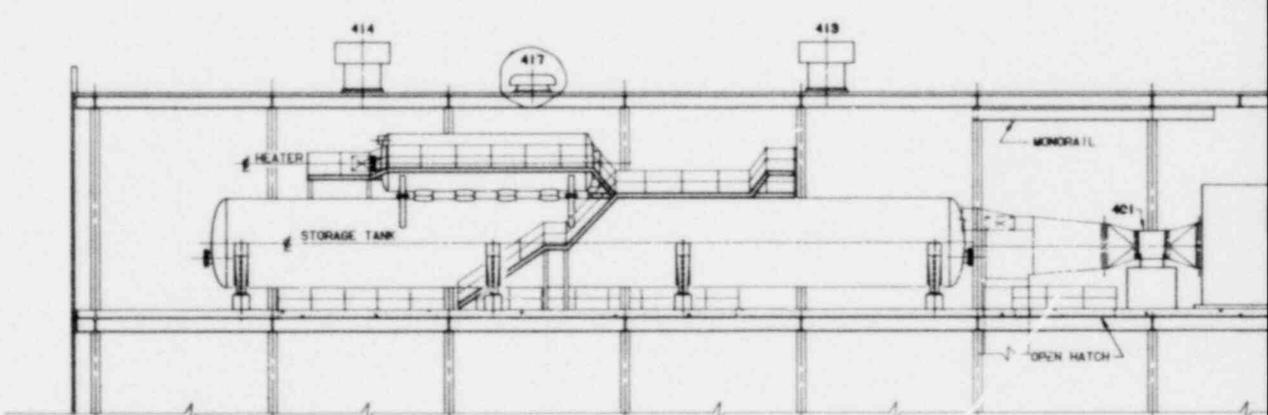

SECTION "E-E"

BM605-4

EQUIPMENT LEGEND

ITEM NO	ZONE	EQUIPMENT NUMBER	DESCRIPTION
400	G4	25BAA141A	AIR HANDLING UNIT
401	G4	25BGA141B	SUPPLY FANS
413	C6	25BGA161A	EXHAUST FANS
414	C7	25BGA151B	
417	C6	25BGA111	RELIEF HOOD
405	H7	71DVT062	FLASH TANK
406	G6	71FMH003	DEAERATOR HEATER
407	G4	25BGA001	AIR HANDLING UNIT
408	H7	69AAB029	INSTRUMENT RACKS
409	G5	25BPB001A	

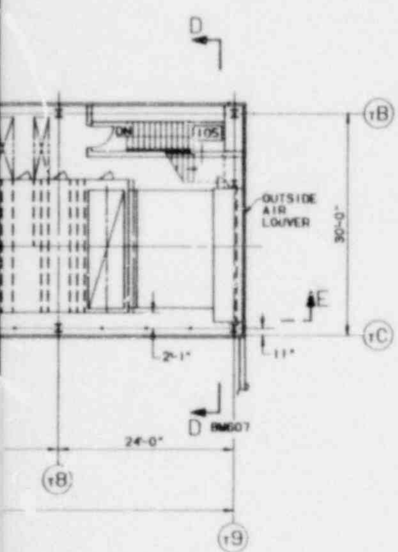

REFERENCE DRAWINGS
SEE DRAWING BM601

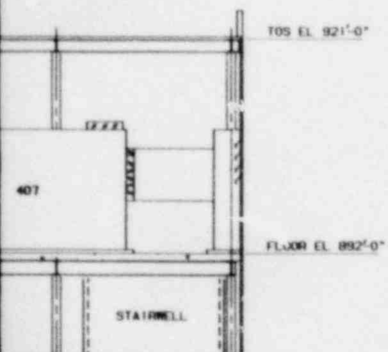

GRAPHIC SCALE

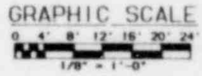

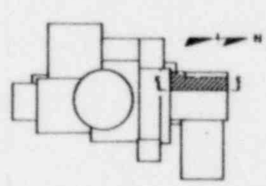

KEY PLAN

Figure 1.2-84
General Arrangement
Turbine Generator Building
Partial Plan and Section E-E

Amend. 56
Aug. 1980

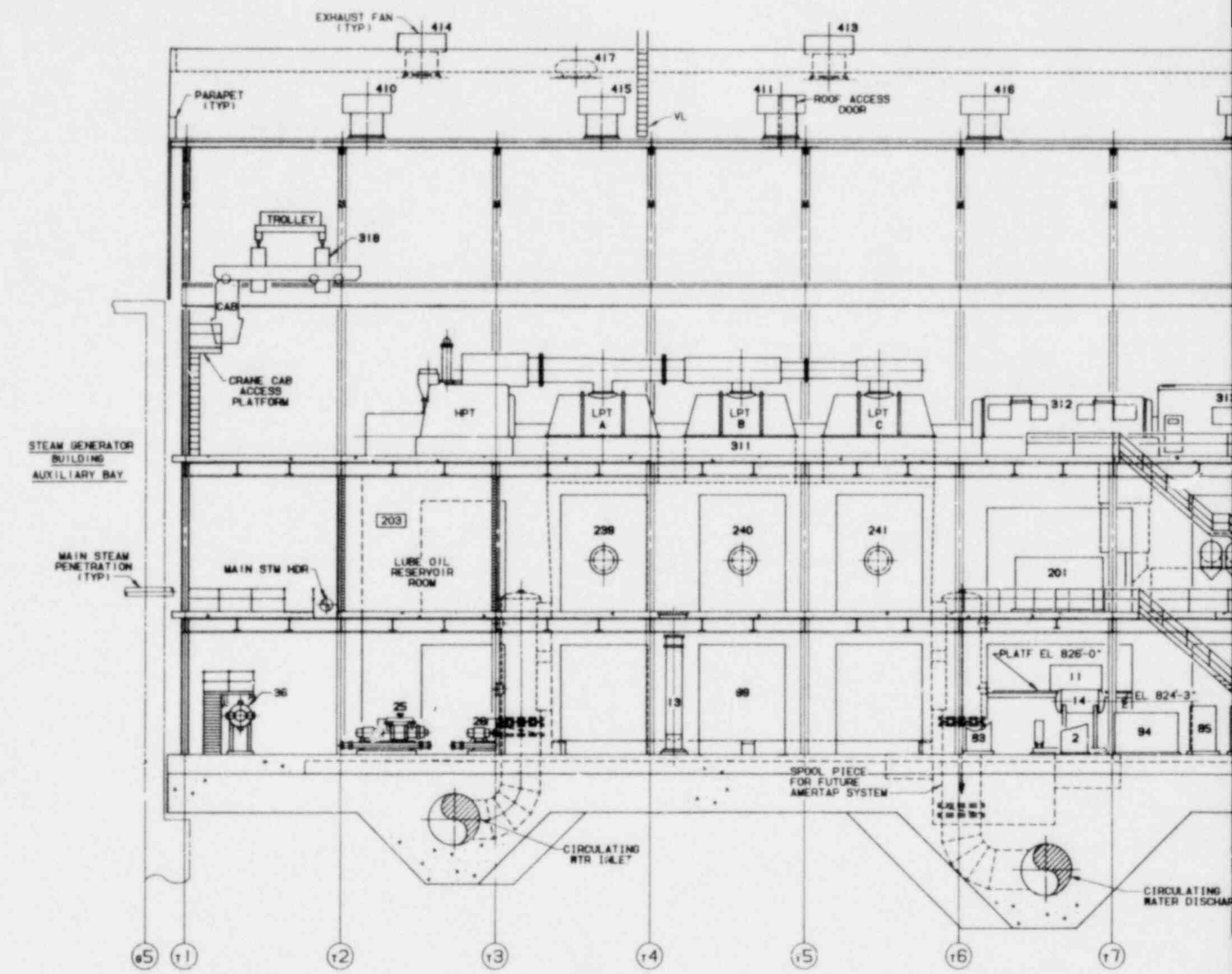

SECTION "A-A"

BM603-4

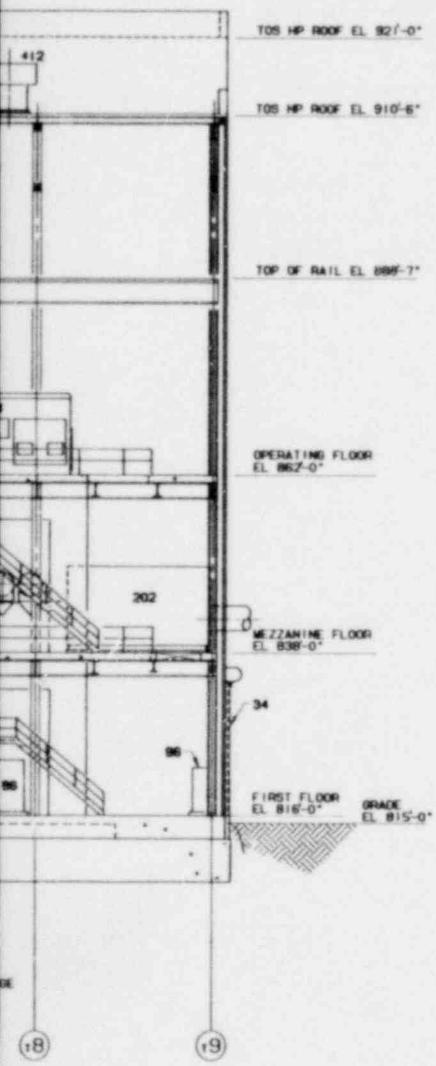

EQUIPMENT LEGEND

ITEM NO.	ZONE	EQUIPMENT NUMBER	DESCRIPTION
2	D5	221AA001B	AIR DRYER
11	D5	25BCA321	UNIT COOLER
13	D6	71CDH008	DRAIN COOLER
14	D5	72TAM003	HYDROGEN SEAL OIL SUPPLY UNIT
25	D7	73CEM100A	VACUUM PUMP UNITS
26	D7	73CEM100B	
34	D3	20TGC001	ROLL-UP DOOR
36	D8	71FWH007B	TOPPING HEATER
83	D5	69AAB008D	
85	D4	69AAB001A	
86	D4	69AAB001B	INSTRUMENT RACKS
94	D4	69AAB016	
96	D4	69AAB017	
99	D6	73CWH001	CONDENSER
201	E5	11AAE009	TURBINE GENERATOR GND XFMR & RESISTOR
202	E4	11AAE012	GENERATOR LOAD BREAK SWITCH
239	E6	71CDH006A	
240	E6	71CDH006B	LP FEEDWATER HEATERS
241	E5	71CDH006C	
311	F6	72TGM001	TURBINE
312	F5	72TGM002	GENERATOR
313	F4	72TAM005	ALTERNATOR
313	G7	20TGC003	CRANE BRIDGE
410	H7	25BGA261A	
411	H6	25BGA261B	
412	H4	25BGA261C	
413	H6	25BGA161A	EXHAUST FANS
414	H7	25BGA161B	
415	H7	25BGA161C	
416	H5	25BGA161D	
417	H6	25BRA111	RELIEF HOOD

REFERENCE DRAWINGS

SEE DRAWING BM601

GRAPHIC SCALE

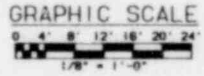

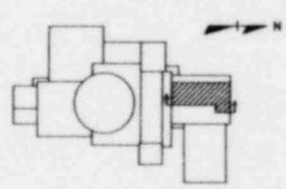

KEY PLAN

Figure 1.2-85
General Arrangement
Turbine Generator Building
Section A-A

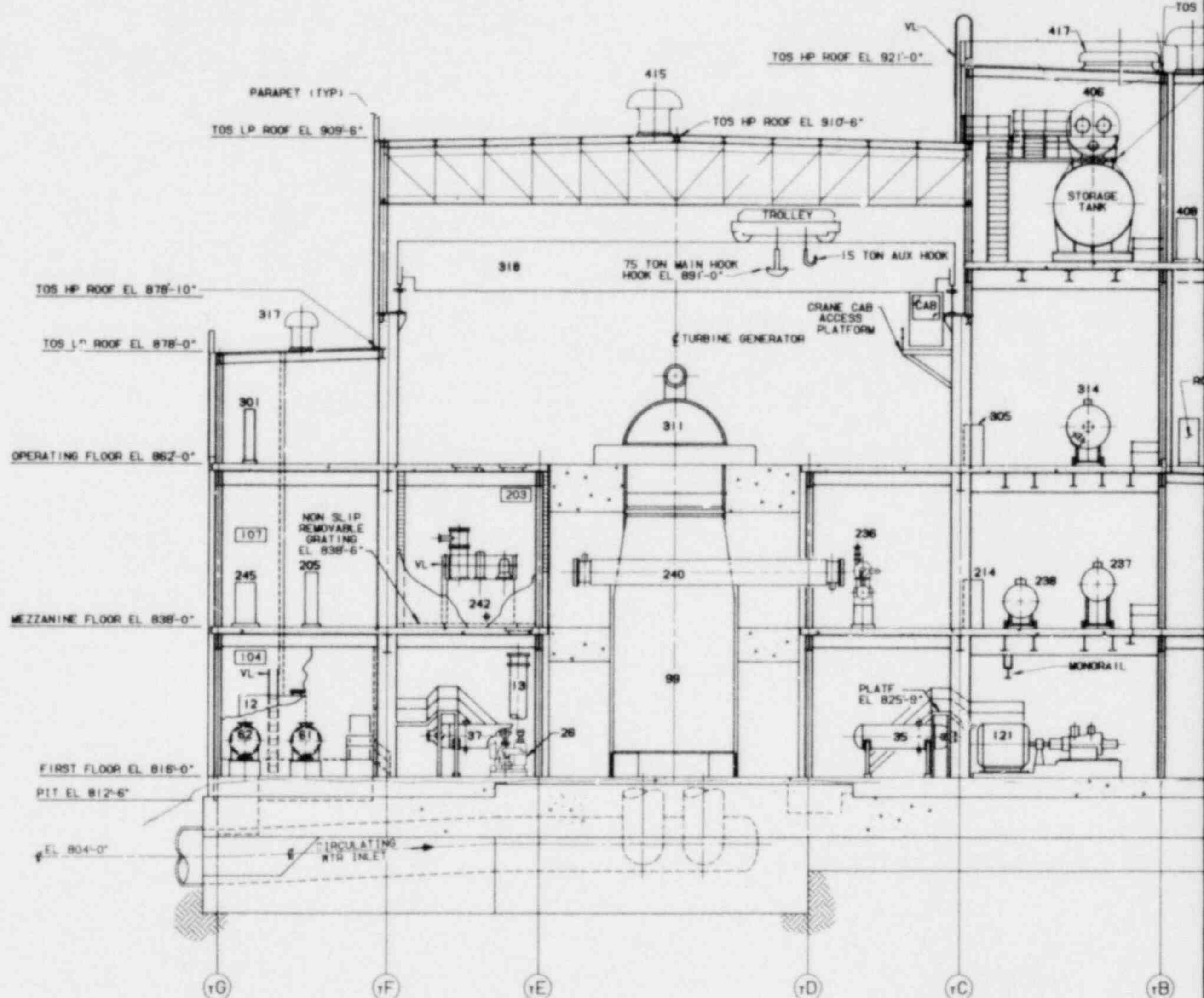

SECTION "B-B"

BM604-4

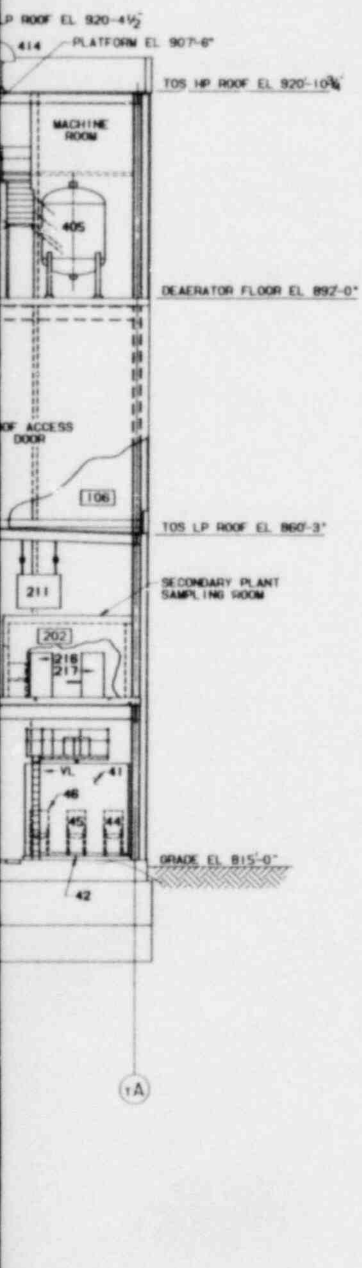

EQUIPMENT LEGEND

ITEM NO.	ZONE	EQUIPMENT NUMBER	DESCRIPTION
12	D7	72TST001	LUBE OIL STORAGE TANK
13	D6	71CDH008	DRAIN COOLER
26	D6	73CEM1008	VACUUM PUMP UNIT
35	D5	71FWH007A	TOPPING HEATERS
37	D6	71FWH007C	
41	D4	75MUG001	CLARIFIER
42	D4	75MUG002	CLARIFIER CHEMICAL FEED
44	D4		HYPOCHLORITE TANK
45	D4		COAGULANT TANK
46	D4		ALUM TANK
61	D7	75SCH001A	SEC SVCE CLOSED CLG WTR HEAT EXCHANGERS
62	D7	75SCH001B	
99	D6	73CWH001	CONDENSER
121	D5	71FWP001B	STEAM GENERATOR FEED PUMP
205	E7	128PE006B	MOTOR CONTROL CENTER
211	E4	25BGA322	UNIT COOLER
214	E5	63AAB007A	INSTRUMENT RACK
216	E4	69AAB022	MONITORING PANEL
217	E4	69AAB023	SAMPLE PANEL
236	E5	72TAH001	STEAM PACKING EXHAUSTER
237	E5	71CDH004	LP FEEDWATER HEATERS
238	E5	71CDH005	
240	E6	71CDH006B	
242	E7	72TAM002	LUBE OIL RESERVOIR
245	E7	91AAB071	REMOTE DATA ACQUISITION TERMINAL
301	F7	128PE005B	MOTOR CONTROL CENTER
305	F5	69AAB007B	INSTRUMENT RACK
311	F6	72TGM001	TURBINE
314	F5	71FWH001	HP FEEDWATER HEATER
317	F7	25BGA262	EXHAUST FAN
318	G6	20TGC003	CRANE BRIDGE
405	G4	71DVT002	FLASH TANK
406	H5	71FWH003	DEAERATOR HEATER
408	G4	69AAB029	INSTRUMENT RACK
414	H4	25BGA161B	EXHAUST FANS
415	H6	25BGA161C	
417	H4	25BGA111	RELIEF HOOD

REFERENCE DRAWINGS

SEE DRAWING BM601

GRAPHIC SCALE

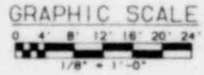

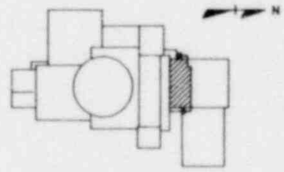

KEY PLAN

Figure 1.2-86
General Arrangement
Turbine Generator Building
Section B-B

Amend. 56
Aug. 1980

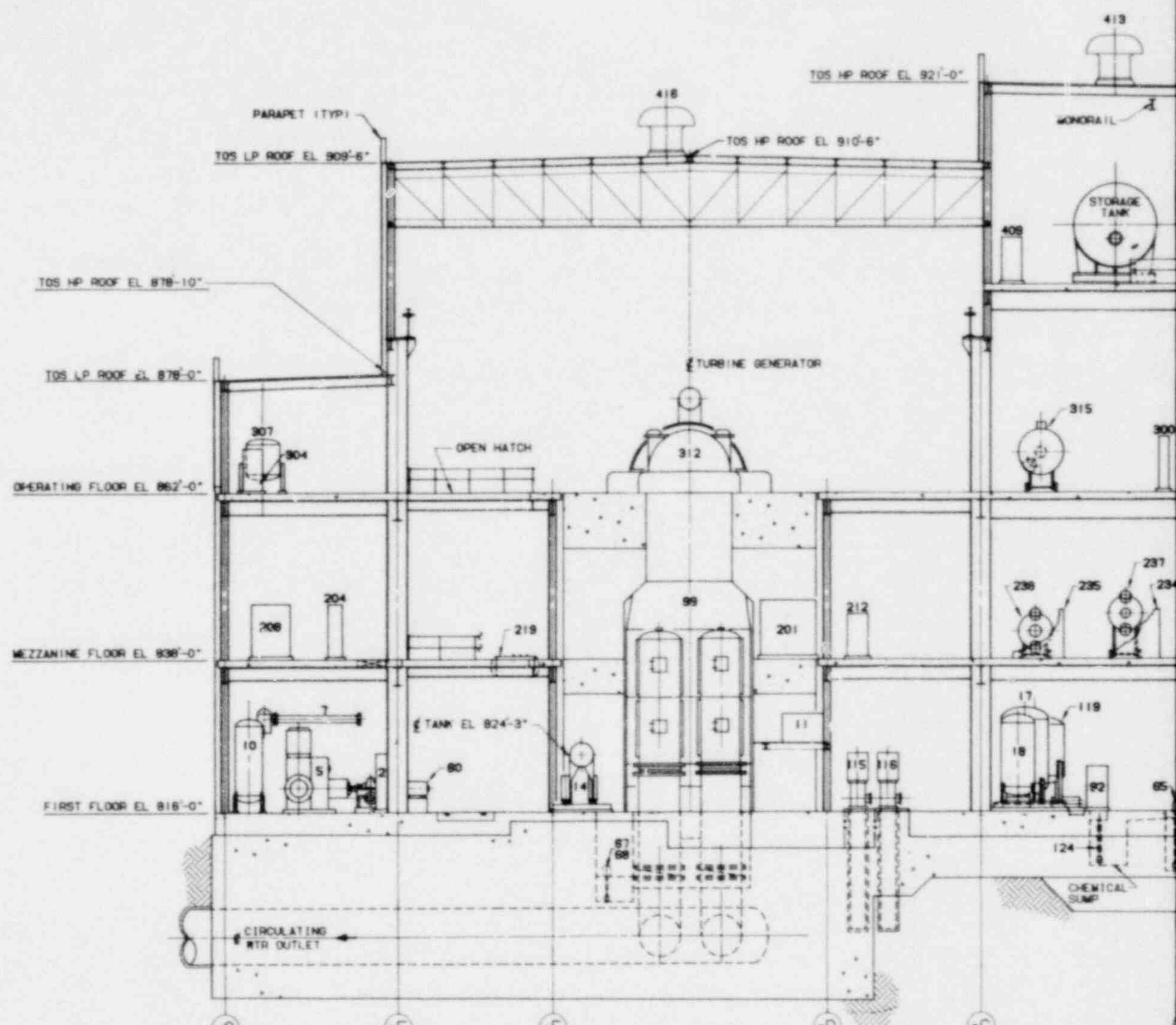

SECTION "C-C"

BM606-5

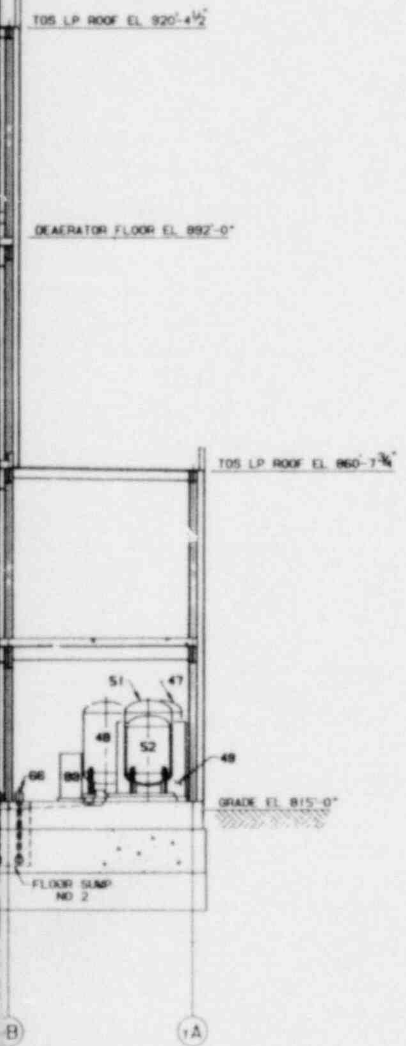

EQUIPMENT LEGEND

ITEM NO	ZONE	EQUIPMENT NUMBER	DESCRIPTION
2	D7	221AA001B	SERVICE & INSTRUMENT AIR DRYER
5	D7	225AA001C	SERVICE & INSTRUMENT AIR COMPRESSOR
7	D7	225AA002B	SERVICE & INSTRUMENT AIR AFTERCOOLER & SEPARATOR
10	D7	225AT001B	SERVICE & INSTRUMENT AIR RECEIVER
11	E6	258GA321	UNIT COOLER
14	E6	72TAM003	HYDROGEN SEAL OIL SUPPLY UNIT
17	E5	71CPT002	CATION TANK
18	D5	71CPT003	ANION TANK
47	D4	75MUG003A	CLARIFIER FILTERS
48	D4	75MUG003B	
49	D4	75MUG004	CLEARWELL
51	D4	75MUG005B	ACTIVATED CARBON FILTER
52	D4	75MUG006	MAKEUP DEMINERALIZER
60	D7	75SWP001B	SEC SVCE CL CLG WTR PUMP
65	D4	76MDP002A	FLOOR DRAIN SUMP PUMPS
66	D4	76MDP002B	
71	D5	76MDP005A	CHEMICAL SUMP PUMP
88	D4	69AAB013A	INSTRUMENT RACKS
92	D5	69AAB014A	
99	F6	73CMH001	CONDENSER
115	D5	71CDP001B	CONDENSATE PUMPS
116	D5	71CDP001C	
119	D5	71CPT001C	CONDENSATE POLISHER
124	D4	76MDP005D	CHEMICAL SUMP PUMP
201	E6	11AAE009	TURBINE GENERATOR GND XFMR & RESISTOR
204	E7	12BPE006A	MOTOR CONTROL CENTER
208	E7	12BPE022A	UNIT SUBSTATION
212	E5	69AAB004A	INSTRUMENT RACK
219	E7	71DVT001	DRAIN TANK
234	E5	12BPE001B	SWITCHGEAR
235	E5	12BPE001D	
237	E5	71CDH004	LP FEEDWATER HEATERS
238	E5	71CDH005	
300	F4	12BPE005A	MOTOR CONTROL CENTER
304	F7	25BPB001B	INSTRUMENT RACK
307	F7	75SWT001	SEC SVCE CL CLG WATER SURGE TANK
312	F6	72TGM002	GENERATOR
315	F5	71FWH002	HP FEEDWATER HEATER
413	H5	25BGA161A	EXHAUST FANS
416	H6	25BGA161D	
409	G5	25BPB001A	INSTRUMENT RACK

REFERENCE DRAWINGS
SEE BM601

GRAPHIC SCALE
0 4' 8' 12' 16' 20' 24'
1/8" = 1'-0"

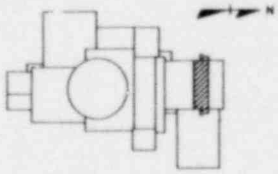

KEY PLAN

Figure 1.2-87
General Arrangement
Turbine Generator Building
Section C-C

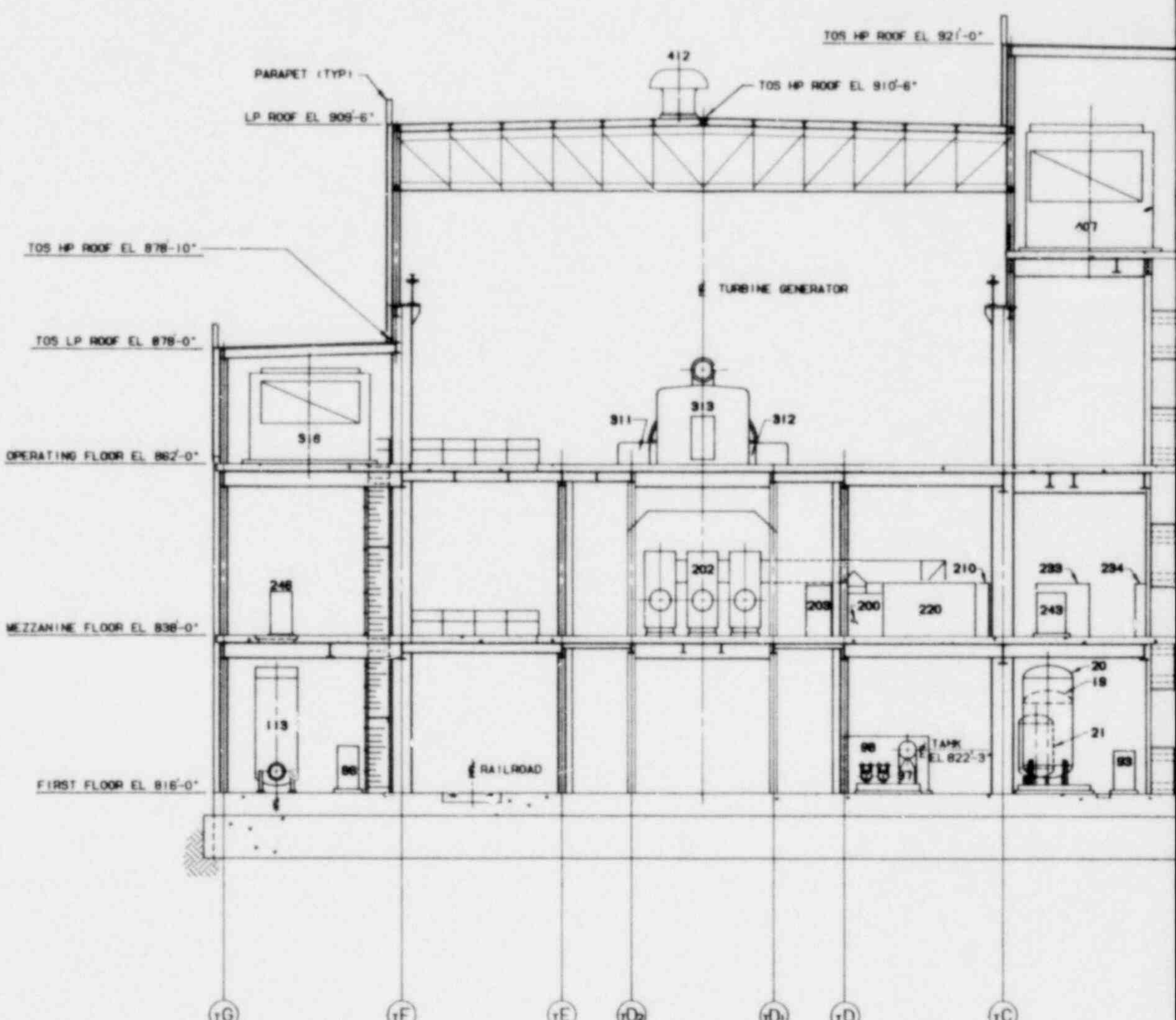

SECTION "D-D"

BM607-4

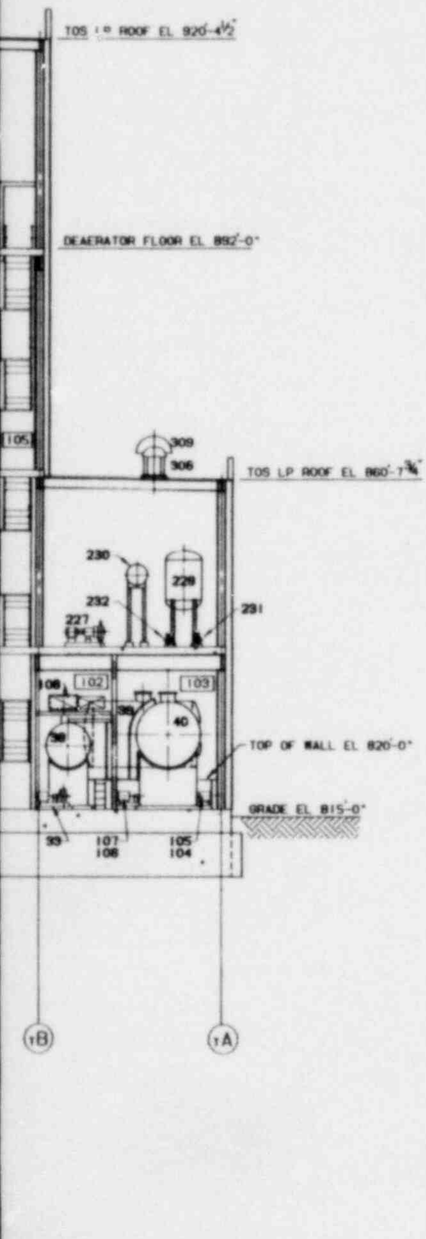

EQUIPMENT LEGEND

ITEM NO.	ZONE	EQUIPMENT NUMBER	DESCRIPTION
19	D5	71CPT004	MIXED RESIN STORAGE TANK
20	D5	71CPT005	AMMONIA RECLAIM TANK
21	D5	71CPT006	HOT WATER TANK
33	D4	75CFP001B	AMMONIA STORAGE TANK METERING PUMP
38	D4	75CFT001	AMMONIA STORAGE TANK
39	D4	75CFT002	ACID STORAGE TANK
40	D4	75CFT003	CAUSTIC STORAGE TANK
86	D7	69AAB010B	INSTRUMENT RACKS
93	D5	69AAB014B	
97	D5	72TAM001	STATOR WINDING CLG UNIT
98	D5	69AAB008F	HYDROGEN & STATOR COOLING WATER CABINET
104	D4	71CCP003A	CAUSTIC STORAGE TANK METERING PUMPS
105	D4	71CPP003B	
106	D4	75MUP008A	
107	D4	75MUP008B	
108	D4	25BGA003	HEAT & VENTILATING UNIT
113	D7	72ASH001B	AUXILIARY BOILER
200	E5	11AAE008	PT & SURGE PROTECTION CUBICLE
202	E6	11AAE012	GENERATOR LOAD BREAK SWITCH
203	E6	11AAE013	COMPRESSOR LOAD BREAK SWITCH
210	E5	11AAH001	ISOLATED PHASE BUS HEAT EXCHANGER
220	E5	72TAM006	EXCITATION CUBICLE
227	E4	75HWP001C	HOT WTR CIRCULATING PUMP
229	E4	75HWT001	EXPANSION TANK
230	E4	75HWH001	MAKEUP WATER HEATER
231	E4	75HWP002A	MAKEUP WATER PUMPS
232	E4	75HWP002B	
233	E5	12BPE001A	SWITCHGEAR
234	E5	12BPE001B	
213	E5	91AAB074	REMOTE DATA ACQUISITION TERMINALS
246	E7	91AAB072	
308	F4	25BGA182	EXHAUST FANS
309	F4	25BGA183	
311	F6	72TGM001	TURBINE
312	F6	72TGM002	GENERATOR
313	F6	72TAM005	ALTERNATOR
316	F7	25BGA002	AIR HANDLING UNIT
407	G5	25BGA001	AIR HANDLING UNIT
412	H6	25BGA261C	EXHAUST FAN

REFERENCE DRAWINGS

SEE BM601

GRAPHIC SCALE

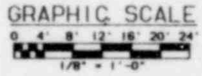

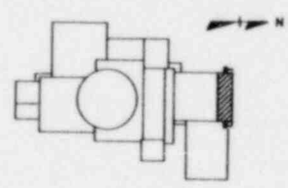

KEY PLAN

Figure 1.2-88
General Arrangement
Turbine Generator Building
Section D-D

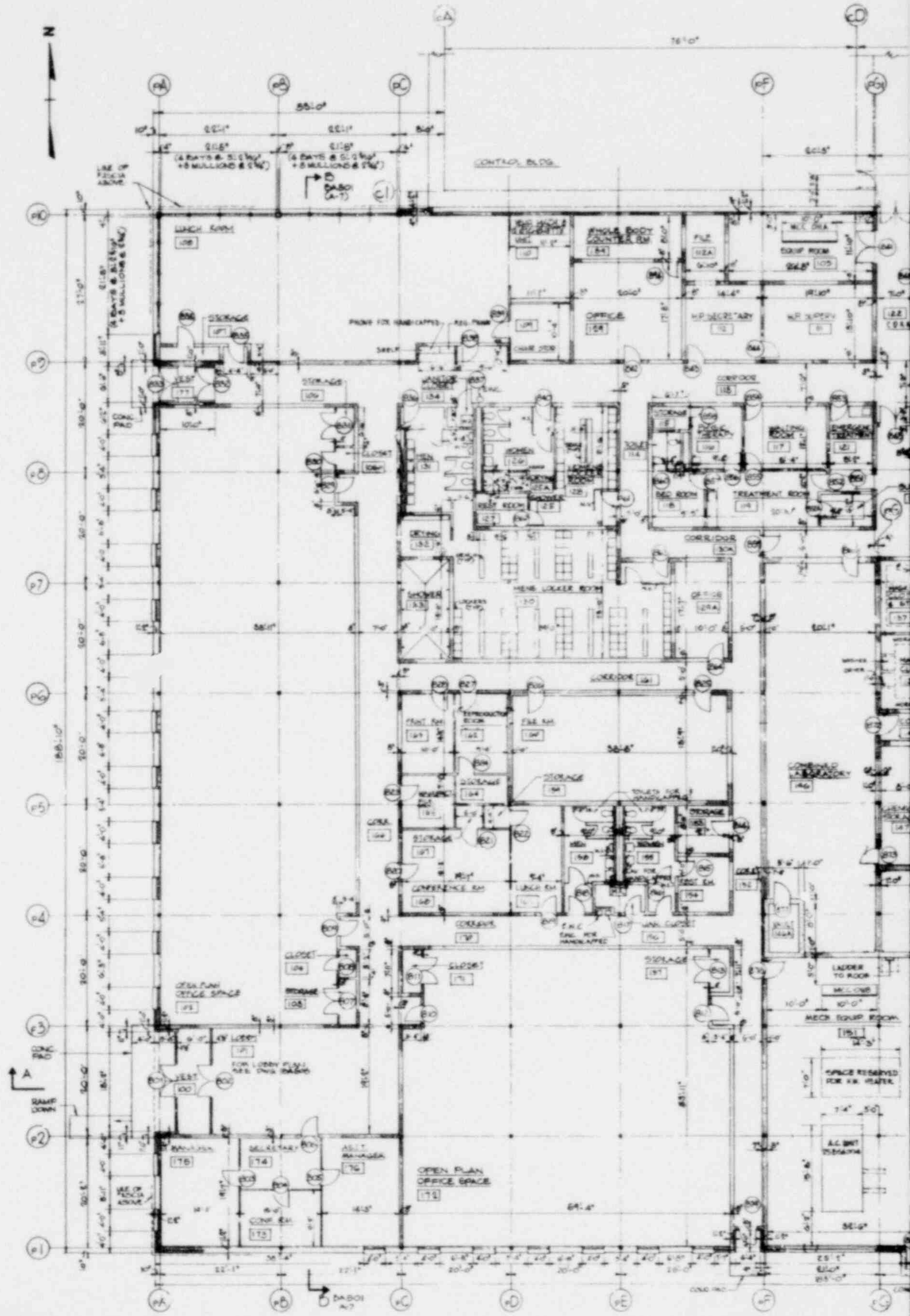

N
CONTROL BLDG.
LUNCH ROOM
STORAGE
OFFICE
CORRIDOR
SHOWER
CORRIDOR
CLOSET
FILE RM
CONFERENCE RM
LUNCH RM
OPEN PLAN OFFICE SPACE
LOBBY
VEST
SECRETARY
CONF. RM
ASS'T. MANAGER
OPEN PLAN OFFICE SPACE
LADDER TO ROOF
MECH EQUIP ROOM
RAMP DOWN
CONC PAD

BA500-4

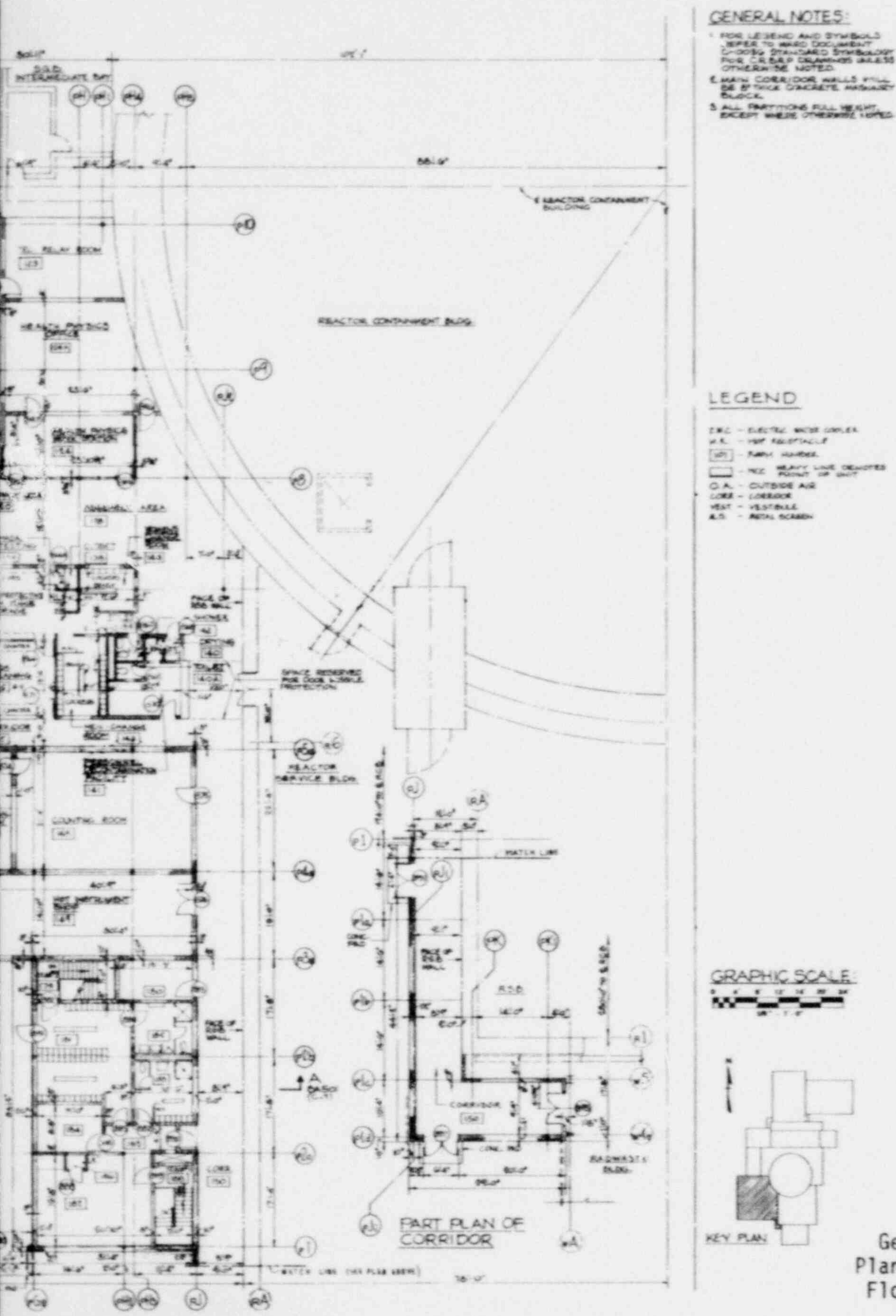

Figure 1.2-89
General Arrangement
Plant Service Building
Floor Plan El. 816'-0"

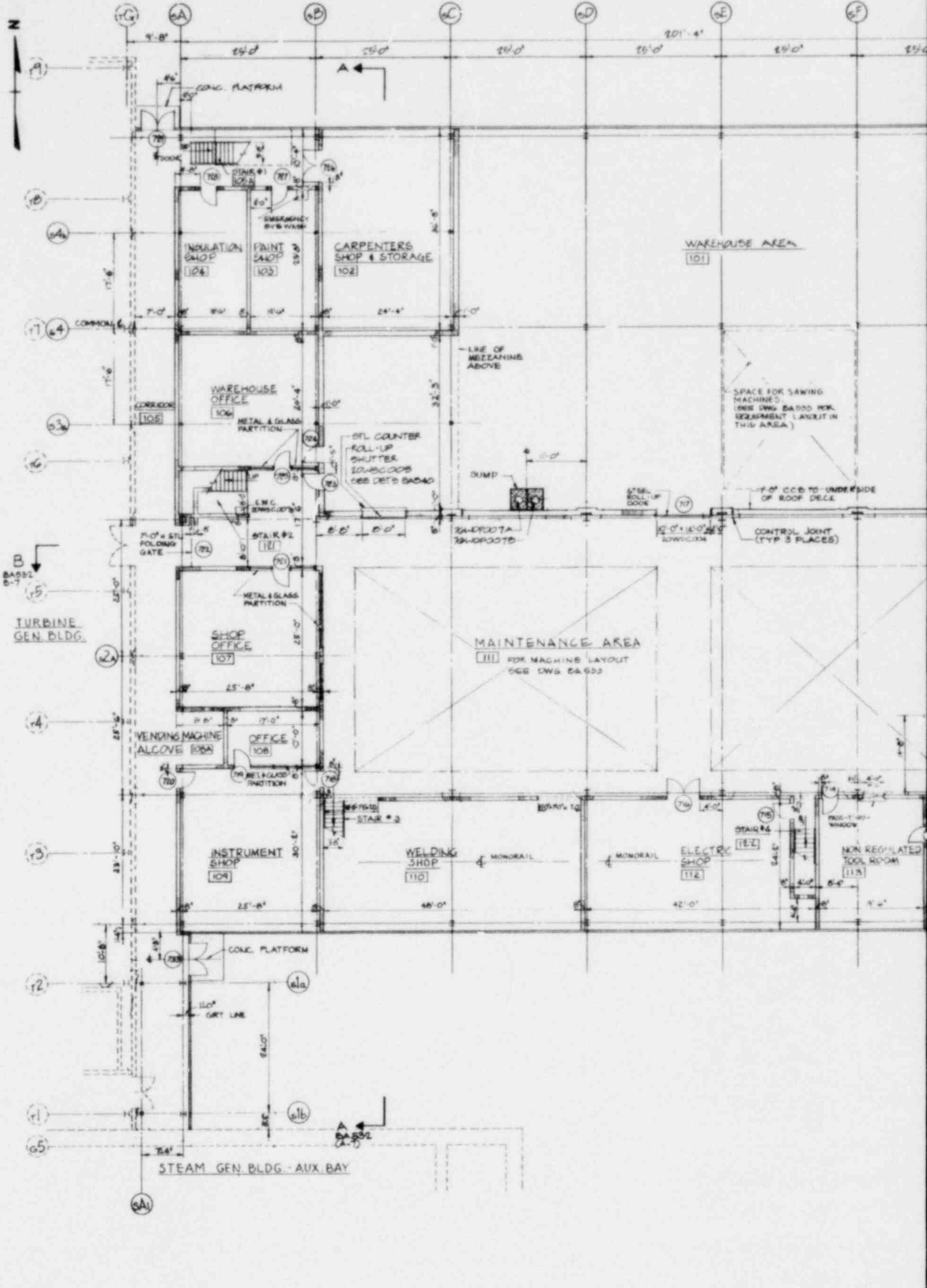
WAREHOUSE AREA
101
CARPENTERS
SHOP & STORAGE
102
PAINT
SHOP
103
INSULATION
SHOP
104
CORRIDOR
105
WAREHOUSE
OFFICE
106
SHOP
OFFICE
107
OFFICE
108
VENDING MACHINE
ALCOVE 108A
INSTRUMENT
SHOP
109
WELDING
SHOP
110
MAINTENANCE AREA
111
FOR MACHINE LAYOUT
SEE DWG BA533
ELECTRIC
SHOP
112
NON REGULATED
TOOL ROOM
113
STAIR #2
121
STAIR #3
STAIR #4
122
CONC. PLATFORM
LINE OF
MEZZANINE
ABOVE
METAL & GLASS
PARTITION
STL COUNTER
ROLL-UP
SHUTTER
SUMP
STEEL
ROLL-UP
DOOR
CONTROL JOINT
(TYP 3 PLACES)
SPACE FOR SAWING
MACHINES
EMERGENCY
EYE WASH
MONORAIL
GIRT LINE
TURBINE
GEN BLDG.
STEAM GEN BLDG. - AUX BAY
201'-4"

BA530-4

GENERAL NOTE:

1. FOR LEGEND AND SYMBOLS, UNLESS OTHERWISE NOTED, REFER TO WARD D-0056 STANDARD SYMBOLOGY FOR CRBRP DRAWINGS.

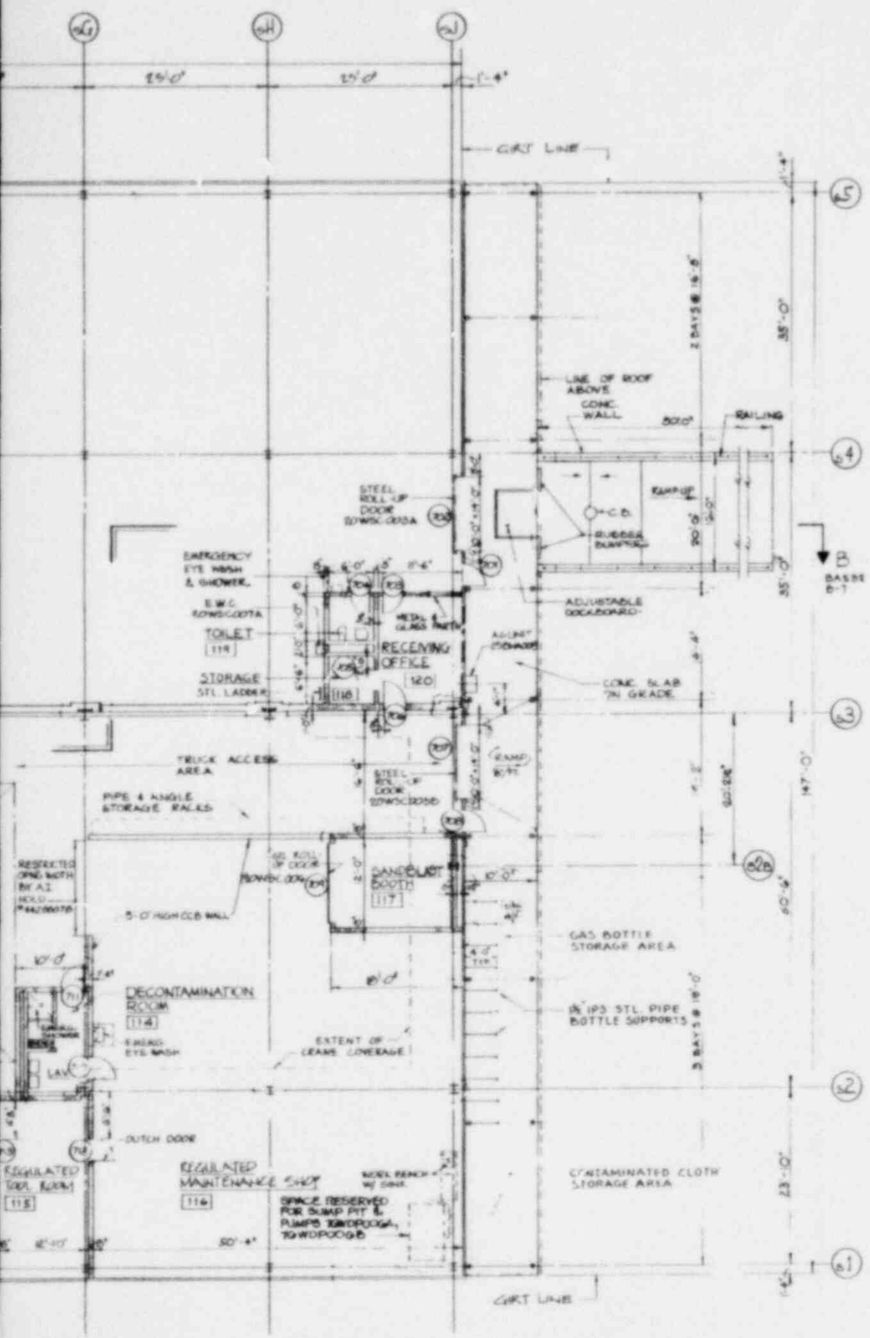

FLOOR PLAN EL. 816'-0"

LEGEND

AIR COND.	-	AIR CONDITION
CCB	-	CONCRETE BLOCK
CONC.	-	CONCRETE
ELEC	-	ELECTRIC
E.W.C.	-	ELECTRIC WATER COOLER
F.A.I.	-	FRESH AIR INTAKE
LVR.	-	LOUVER
MET	-	METAL
M.O.	-	MASONRY OPENING
OPNG.	-	OPENING
T.O.	-	TRIMMED OPENING
WTR.	-	WATER
	-	M.C.C. (HEAVY LINE FRONT)
	-	ROOM NO.

GRAPHIC SCALE:

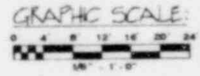

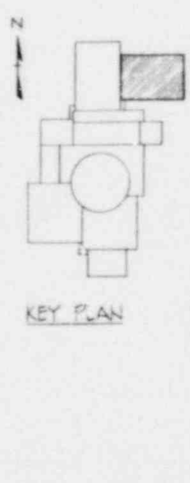

KEY PLAN

Figure 1.2-90
General Arrangement
Maintenance Shop and Warehouse
First Floor Plan El. 816'-0"

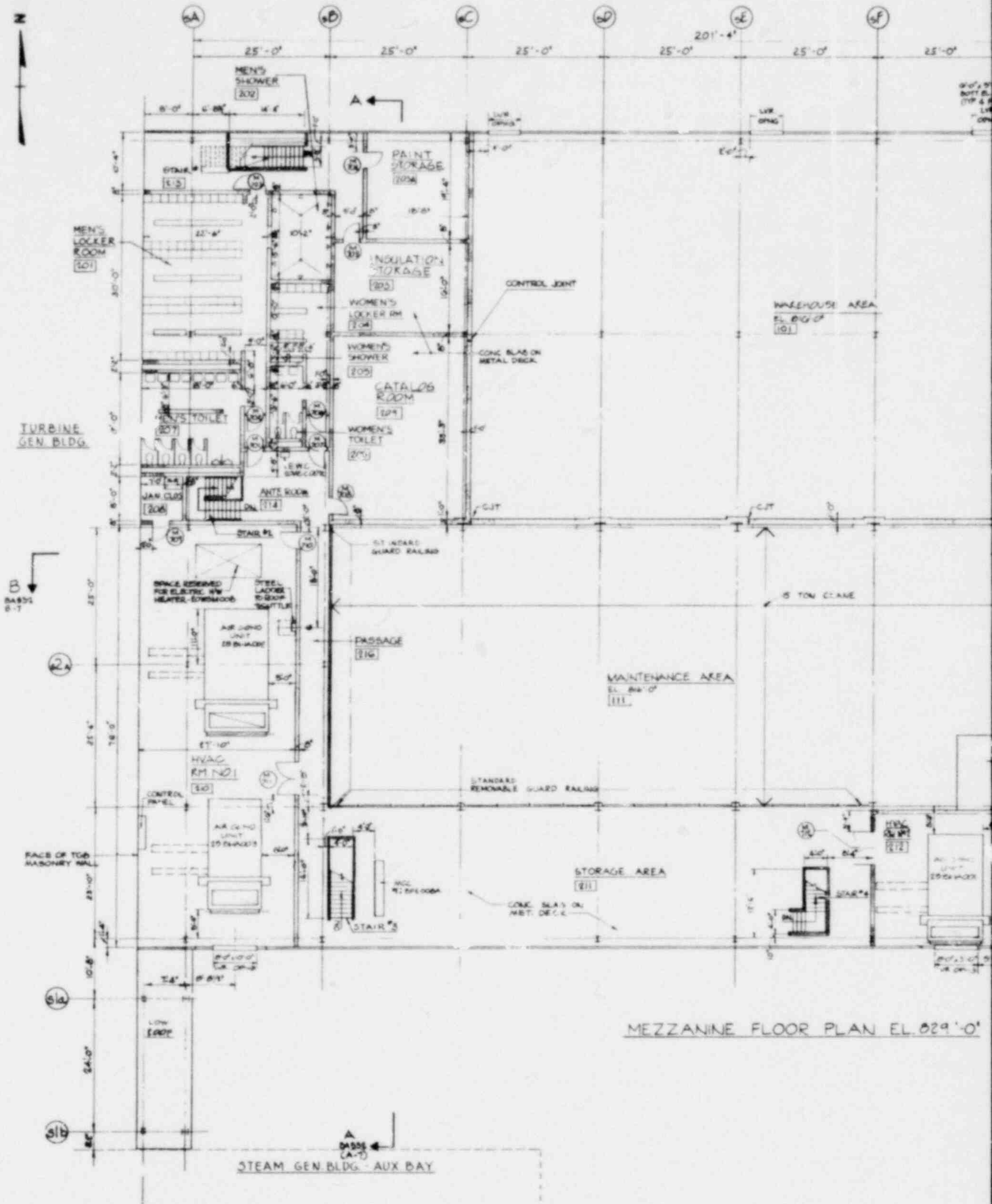

201'-4"
25'-0"
MEN'S SHOWER 202
A
PAINT STORAGE 206
MEN'S LOCKER ROOM 201
INSULATION STORAGE
CONTROL JOINT
WAREHOUSE AREA
WOMEN'S LOCKER RM 204
WOMEN'S SHOWER 205
CONC SLAB ON METAL DECK
CATALOG ROOM
WOMEN'S TOILET
TURBINE GEN BLDG
JAN CLOS 208
ANTE ROOM 214
B
PASSAGE
15 TON CRANE
MAINTENANCE AREA
HVAC RM NO1
STANDARD REMOVABLE GUARD RAILING
CONTROL PANEL
FACE OF TGB MASONRY WALL
STORAGE AREA
STAIR #3
MEZZANINE FLOOR PLAN EL. 829'-0"
STEAM GEN BLDG - AUX BAY

BA531-3

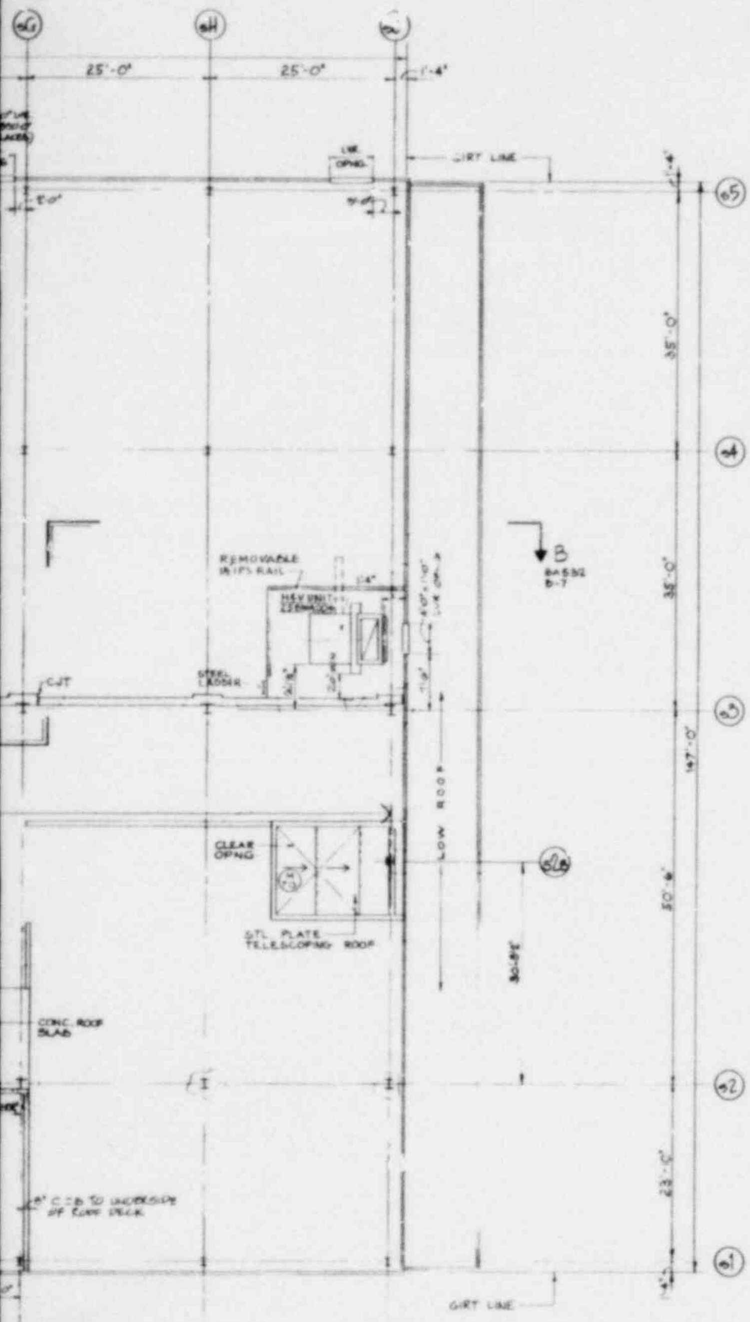

REFERENCE DRAWINGS:
SEE DRAWING 8A 550

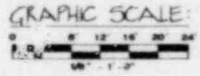

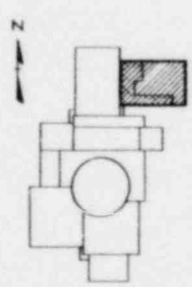

KEY PLAN

Figure 1.2-91
General Arrangement
Maintenance Shop and Warehouse
Mezzanine Plan El. 829'-0"

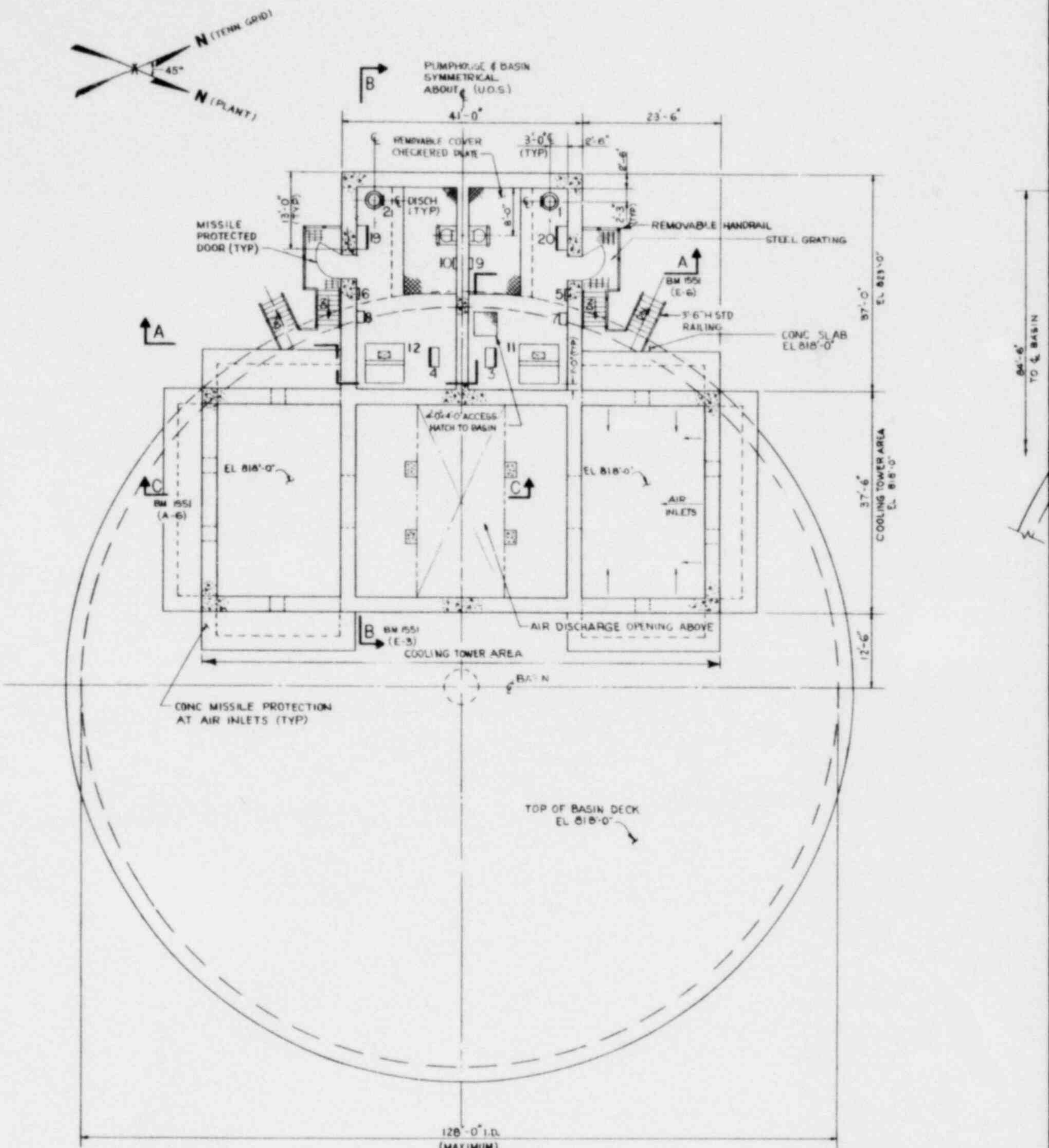

PLAN EL 823'-0"
U.O.S.

BM1550-1

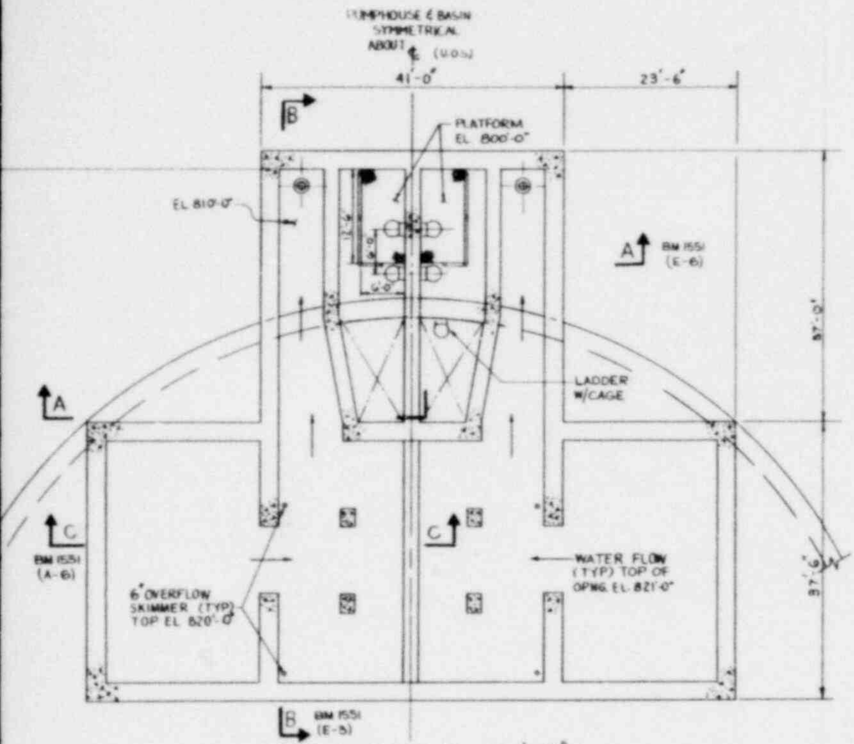

PARTIAL PLAN EL 818'-0" (U.O.S.)

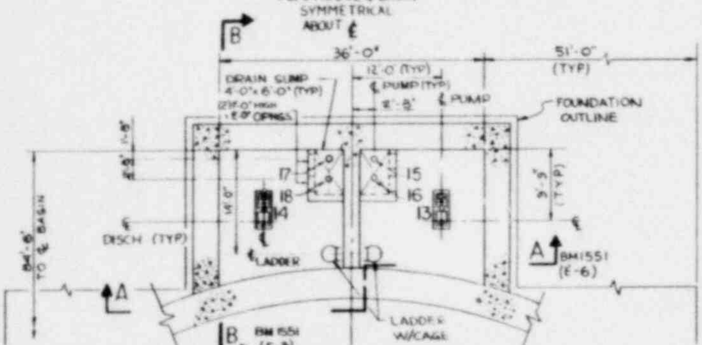

PARTIAL PLAN EL 771'-0"

EQUIPMENT LEGEND			
ITEM NO.	ZONE	EQUIPMENT NUMBER	DESCRIPTION
1 2	J6 J7	75EPP001B 75EPP001A	EMER PLANT SVCE WTR PUMPS
3 4	H6 H7	12NIE060B 12NIE060A	MOTOR CONTROL CENTERS
5 6	H6 H7	12NIB039B 12NIB039A	LIGHTING PANELS
7 8	H6 H7	12NIX039B 12NIX039A	TRANSFORMERS
9 10	H6 H6	12NIB040B 12NIB040A	DISTRIBUTION PANELS
11 12	H6 H7	25BEA100B 25BEA100A	AIR HANDLING UNITS
13 14	D3 D3	75EPP003B 75EPP003A	EMER PLANT SVCE WTR MKUP PMPS
15 16 17 18	D3 D3 D3 D3	20ECP002A 20ECP002B 20ECP001A 20ECP001B	DRAIN SUMP PUMPS
19 20	J7 J6	69AAB033 69AAB034	INSTRUMENT RACKS

GENERAL NOTES

1. FOR LEGEND AND SYMBOLS, UNLESS OTHERWISE NOTED, REFER TO WARD DOCUMENT DOC D-0036 STANDARD SYMBOLOGY FOR CRBRP DRAWINGS.
2. [box] HEAVY LINE DENOTES FRONT OF UNIT.

EMERGENCY COOLING TOWERS AND THEIR STRUCT SUPPORTS, INCLUDING AIR INTAKE MISSILE PROTECTION ARE ON HOLD # 20-000044 PENDING RECEIPT OF VENDOR INFORMATION

REFERENCE DRAWINGS

BM1551 GENERAL ARRANGEMENT EMER. COOLING TOWER PUMPHOUSE AND BASIN SECTIONS

GRAPHIC SCALE

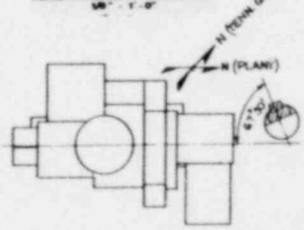

KEY PLAN

Figure 1.2-92
General Arrangement
Emergency Cooling Tower
Pumphouse and Basin Plan

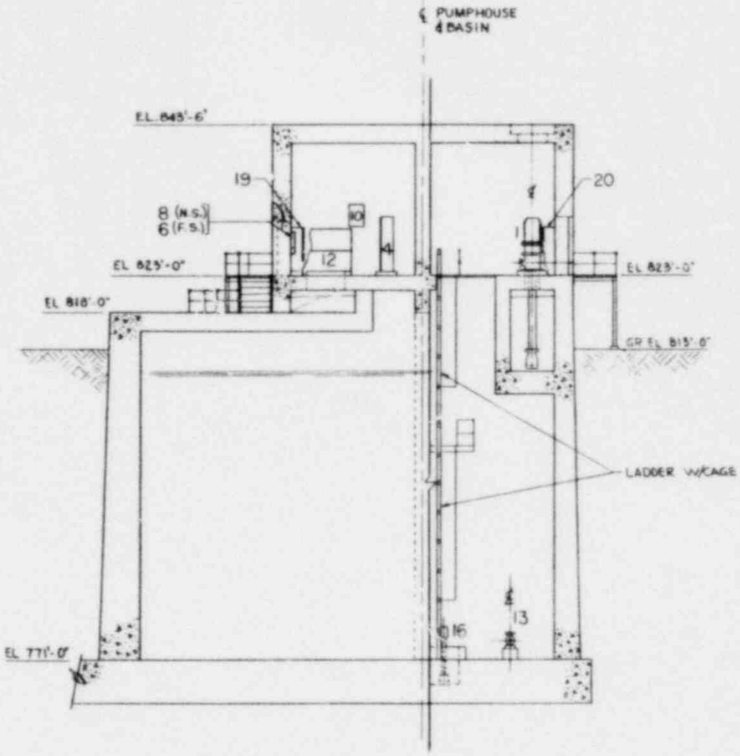

SECTION "A-A"

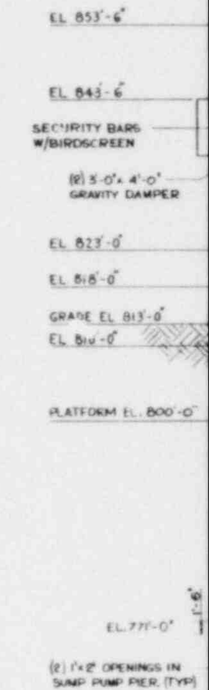

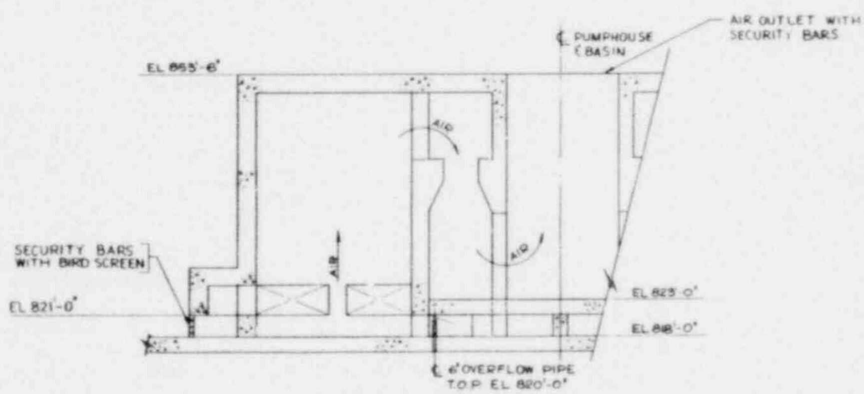

SECTION "C-C"

BM1551-1

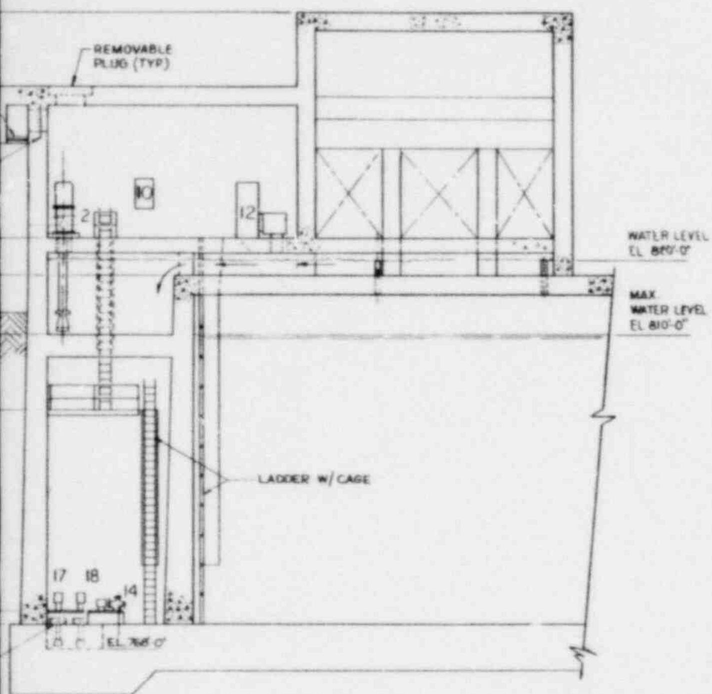

SECTION "B-B"

REFERENCE DRAWINGS

BM1550 GENERAL ARRANGEMENT EMER. COOLING TOWER PUMPHOUSE AND BASIN PLAN

EQUIPMENT LEGEND			
ITEM NO.	ZONE	EQUIPMENT NUMBER	DESCRIPTION
1 2	H6 H4	75EPP001B 75EPP001A	EMERGENCY PLANT SERVICE WATER PUMPS
4	H7	12NIE060A	MOTOR CONTROL CENTER
6	H7	12NIB039A	LIGHTING PANEL
8	H7	12NIX038A	TRANSFORMER
10	H6	12NIB040A	DISTRIBUTION PANEL
12	H5 H6	25BEA00A	AIR HANDLING UNIT
13 14	F6 F4	75EPP009B 75EPP009A	EMERGENCY PLANT SERV. WATER MAKEUP PUMPS
17 18	F4 F4	20ECP001A 20ECP001B	SUMP PUMPS
19 20	H6 H6	69AAB033 69AAB034	INSTRUMENT RACKS

GRAPHIC SCALE

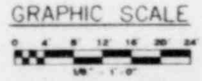

Figure 1.2-93
General Arrangement
Emergency Cooling Tower
Pumphouse and Basin Plan Sections

		CRBRP - 975 Mwt	FFTF - 400 Mwt	CRBRP PSAR Section
41	Fire Protection	Catch pans, oxygen suppression equipment, nitrogen flooding equipment, isolation devices.	Catch pans, oxygen suppression equipment, nitrogen flooding equipment, isolation devices, water prohibited from containment.	9.13
	Emergency Water Service	Provides water to systems essential for plant in safe shut-down condition, in event normal water distribution system is unavailable. Seismic design Category I cooling tower has 30-day supply of evaporative water.	No similar system.	9.9
56	Impurity Monitoring and Analysis	Provides for the sampling monitoring and analysis of sodium, NaK and argon cover gas systems in the plant and acceptance sampling and analysis of incoming sodium, NaK, argon, and nitrogen.	Same as CRBRP except that the argon cover gas sampling is an on-line subsystem.	9.8

TABLE 1.3-3

DETAILED COMPARISON BETWEEN CRBRP, FFTF, and MONJU

	CRBRP - 975 Mwt	FFTF 400 Mwt	MONJU*- 714 Mwt	PSAR Section
1. Reactor Core				
Number Assemblies				
Core Zone 1	156	28	108	4.3
Core Zone 2	NA	45	88	
Inner Blanket	82	NA	NA	
Radial Blanket	132	NA	174	
Removable Radial Shield	306	NA	316	
Primary Control	9	3	12	
51 Secondary Control	6	6	7	
Radial Reflector	NA	108	-	
Core Barrel Inner Diameter (in.)	150	140	-	
Active Core Ht. (in.)	36	36	35.4	
51 Active Core Equiv. Dia. (in.)	79.50	47.23	70.08	
2. Reactor Engineering Parameters				
Thermal Power Rating (mw)	975	400	714	4.3
Gross Electrical Rating (mw)	380	NA	300	
Gross Plant Efficiency (%)	39	NA	42	
Maximum Power (% of Rated Power)	115	115	116	4.4
Maximum Clad Temp.; Hot Channel, 100% Rated Power, T & H Design Condition, Beginning of Assembly Life, (2σ, except where noted)	1350	1180 (600°F Reactor Inlet Temp.) 1380 (800°F Reactor Inlet Temp.)	1209 (nominal)	

51

51 *Notation "-" reflects data not available.
"NA" = not applicable

8

in these two figures coincides with the area of deepest weathering and lies about one-third of the way upslope from the topographic low towards the crest of the ridge to the northwest.

Water levels were measured at 33 of the observation wells shown
in Figure 2.4-67 on a regular basis from December 19, 1973 through April
55 1, 1974. The water levels in some of the wells changed as much as
20 feet during the period of observation. The rainfall recorded at Melton Hill Dam (Reference 45), about six miles from the site, is shown in Figure 2.4-71. Watts Bar headwater levels during the same period are listed in Figure 2.4-72.

Water levels measured subsequent to the site investigation indi-
cate fluctuations which comprise an annual cycle, with the maximum water
levels occurring during the months of January and February, decreasing to
low values recorded during the months of October and November. Water
level fluctuations due to rainfall conditions are shown for fifteen
56 55 12 selected wells in Figure 2.4-70a through 2.4-70o.

The rapid response of the water levels to precipitation is indicative of rapid recharge, which occurs largely in areas of exposed rock and small sinkholes along the northwest and southeast ridges which bound the Plant Island. The large fluctuations in the groundwater table on the topographic highs and the quick response to precipitation are likely due to the proximity of these areas to recharge areas.

Eleven piezometers were installed in nests of twos and threes near borings 6, 7, 12, and 40 to supplement the information obtained from the observation wells described above. A typical piezometer installation is shown in Figure 2.4-73 and the locations of the piezometers are shown in Figure 2.4-74.

The water levels at the piezometers were also recorded at regular
monthly intervals after the completion of the site investigation work until
47 the suspension of the groundwater monitoring program. They were measured
on a regular basis during the investigation from the beginning of February
55 12 1974 to April 1, 1974 and groundwater fluctuations in selected piezometers
are plotted in Figures 2.4-75a through 2.4-75f. The piezometric head decreased with depth in the piezometers located on topographic highs, indicating downward flow and thus confirming that these areas are recharge areas. The piezometric head increase with depth in those piezometers located in the groundwater trough around boring 27. The upward piezometric gradient indicates that this is an area of upward flow and, thus, is a discharge area.

Amend. 56
Aug. 1980

2.4.13.2.3 Movement of Groundwater

In general, movement of groundwater occurs in a direction normal to the groundwater contours. At the site, movement is generally from topographically high areas to topographic lows; however, this pattern is modulated by the extent of weathering of the bedrock aquifers. Ultimately, the Clinch River acts as a sink to which all groundwater at the site migrates. Reference 33 lists instances in carbonate rock terraines in which weathering in topographically high areas is so deep that interchanges between adjacent valleys separated by these topographic highs may occur. Such situations are conducive to important reversals of groundwater flow. No evidence of such deep weathering action has been encountered at the site. Sound rock was encountered in the core of the ridges at elevations higher than the adjacent valley floors. Thus, at the site, the major ridges may be regarded as approximate locations of groundwater divides. Reversals in direction of flow which may occur because of the rather large fluctuations of the groundwater table will be local in extent and will not represent a diversion of groundwater from one major groundwater basin to another.

The Clinch River itself may act as a source of recharge during those periods when the river is subject to a rapid increase in stage. During such periods, water will flow from the river into the aquifer. This reverse flow will occur until a new condition of dynamic equilibrium within the groundwater system is established.

2.4.13.2.4 Effects of Plant Construction and Operation on Groundwater System

The groundwater environment at the site will be substantially changed by the construction of the Nuclear Island. The foundation of the Nuclear Island Structures is to be placed generally at elevation 715.
55 Excavation for the Nuclear Island foundation will be concurrent with dewatering. Due to the proximity of the

Amend. 55
June 1980

2) Tornadoes - tornado protection is provided by ensuring the integrity of the RCB and SGB.

3) Missiles - missile protection is provided by ensuring the integrity of the RCB and SGB and the individual cells within the RCB and SGB.

4) Earthquakes - protection from earthquake induced damage is provided by ensuring the structural adequacy of the RCB and SGB, the individual cells within the RCB and SGB, the components and the components supports of the IHTS.

32 5) Fires - fire protection is provided by both the conventional fire protection system and the sodium fire protection system.

Criterion 33 INSPECTION AND SURVEILLANCE OF INTERMEDIATE COOLANT BOUNDARY

Components which are part of the intermediate coolant boundary shall be designed to permit (1) periodic inspection of areas and features important to safety, to assess their structural and leaktight integrity, and (2) appropriate material surveillance program for the intermediate coolant boundary. Means shall be provided for detecting intermediate coolant leakage.

Response:

33 A Liquid Metal-to-Gas Leak Detector System is provided to detect and identify the location of Liquid Metal-to-Gas leaks for the purpose of continuous surveillance of the intermediate system boundaries.

The major portion of the intermediate boundary is in readily accessible areas, facilitating in-service inspection by visual methods. An in-service inspection program for the IHTS will be implemented and conducted in accordance with the intent of the ASME Boiler and Pressure Vessel Code, Section XI, Rules for Inservice Inspection of Nuclear Reactor Coolant System. The inservice inspection program will include all IHTS components such as pressure vessels, piping, pumps and valves.

To facilitate the inspection program, it is a design goal that all IHTS sodium welds be accessible for inspection after insulation and heater removal. Where necessary, hand held optical aids or remote devices such as periscopes will be used for inspection.

The need to monitor austenitic stainless steel toughness changes (due to carburization, plastic creep straining and the thermal environment) will be assessed as part of an ongoing program. These studies will be performed in parallel with design. If fracture toughness surveillance is determined, by ongoing programs, to be required, then the surveillance program will be designed in accord with the philosophy of Appendix H to CFR Part 50.

Criterion 34 REACTOR COOLANT AND COVER GAS PURITY CONTROL

Systems shall be provided to monitor and maintain reactor and intermediate coolant and cover gas purity within specified design limits. These limits shall be based on consideration of (1) chemical attack, (2) fouling and plugging of passages and (3) radioisotone concentrations and (4) detection of sodium-water reactions.

Response:

Plugging temperature indicators are used to monitor the saturation temperature of the total impurities in the primary sodium, the EVST coolant, and the Intermediate Heat Transfer System (IHTS) sodium. Additionally, sodium samples are taken from these systems for laboratory analysis of sodium impurities. Gas impurity analysis is performed periodically on reactor, EVST, FHC and IHTS cover gas samples by the gas chromatograph in the Plant Service Building laboratory. These monitoring systems are described in
32 56 Section 9.8.

TABLE 3.2-2 (Continued)

PRELIMINARY LIST OF SEISMIC CATEGORY I MECHANICAL SYSTEM COMPONENTS AND ASSIGNED SAFETY CLASSES(3)

20

Components	Safety Class(1)	Quality Group(11)	Location(2)
Impurity Monitoring and Analysis System			
Primary Plugging Temperature Indication Package	3	C	RCB
Primary Sodium Sampling Package	3	C	RCB
Ex-Vessel Plugging Temperature Indication Package	3	C	RSB
Ex-Vessel Sodium Sampling Package	3	C	RSB
56 IHTS Sodium Characterization Package(3)	3	C	SGB

Table 3.2-6

Preliminary Listing of Non-Seismic Category 1 Equipment in Containment

Compressed Air System (non-safety related)
Pump Seal Oil Control System
Primary Sodium Impurity Monitoring System - 1/4 T Hoist
56 Master-slave Manipulator
Primary Sodium Removal and Decontamination System
Leak Detection (Liquid Metal-to-Gas) System
Primary Cold Trap NaK Cooling System
Refueling System - AHM
IVTM
Adapters
Floor Valves
Control Equipment
Electric Heating System - Control Panels
Electrical System - Non-class IE Motor Control Centers
Fire Protection System - Portable Equipment
Area Panels
Radiation Monitoring System - Area Monitors
HVAC System - Below floor air conditioning units
Below floor return fan
HAA Heaters
HAA Ducts

Communication System
Inservice Inspection Equipment
Maintenance Equipment and Supplies
Closure Head Plug Drive System
HAA Cable Handling Units and Personnel Platforms
Dip Seal Control Panel
DHDS - Remote Terminals
Delayed Neutron Detectors

TABLE 3.2-7

INVOKED RDT STANDARDS TO ASME CODE SECTION III COMPONENTS

Standard Number, Revision	Standard Title	Application
E15-2NB, (NC, ND)T	Class 1, (2,3) Nuclear Components	All ASME Section III Components which perform liquid metal service with a Design Temperature above 800°F or other severe conditions
F9-4T	Requirements for Construction of Nuclear System Components at Elevated Temperatures	
F2-2	Quality Assurance Program Requirements	See PSAR Chapter 17
F3-6T	Nondestructive Examination	All ASME Section III Components which perform liquid metal service
F6-5T	Welding & Brazing Qualifications	

54

upper shroud tube is attached to the intermediate rotating plug and pilots over the lower shroud tube. The CRDM nozzle extension and seismic support structure are rigidly attached to the intermediate rotating plug.

The PCRS is included in the reactor system model in somewhat simplified form. The gap locations where the translating assembly is intended to be guided within surrounding components (i.e., CRDM bushings and absorber wear pads) are replaced by pin connections. Thus, for purposes of determining reactor system motions, we have a coupled model which includes both system and linearized subsystem. The stiffness and mass of the PCRS (and SCRS) are therefore included in the reactor system model. Note, however, that this linearized model cannot provide the detailed gap force data that is required from this analysis.

The detailed nonlinear PCRS model is decoupled from the reactor system model to make it practical economically to analyze both system and subsystem. The reactor system model is used for many time history and response spectrum cases for operating, refueling and preparation for refueling cases. However, the PCRS model need only be run for the few worst seconds of the horizontal seismic events and for the operating configuration of the reactor system model only.

The loads on and motions of the PCR system (supported system) occur as a result of the relative motions of the core, the upper internals structure and the intermediate rotating plug (not by any forces applied directly to the PCRS system). The nonlinear model of Figure 3.7-18A. uses displacement time history input at the six locations indicated by the arrows. These displacement inputs are obtained from the reactor system model. A careful interpolation (on time) is made between reactor system results to obtain a fine time increment needed for the PCRS model.

The direct results obtained from the impact analysis are histories of gap forces and displacements. Displacement results can be used directly to obtain component loads and/or stresses. The gap force histories, however, are the results of most interest. Special total impact force results are prepared from the individual gap results for use in subsequent scram analyses. A typical plot of the total force is shown in Figure 3.7-18B.See Section 4.2.3 for the detailed discussion
46 of the seismic scram analysis.

46

3.7.4 Seismic Instrumentation Program

3.7.4.1 Comparison With NRC Regulatory Guide 1.12

Seismic instrumentation will be provided to determine promptly the seismic response of the plant features important to safety to permit comparison of such response with that used as the design basis. Such a comparison is needed to decide whether the plant can continue to be operated safely.

The instrumentation to be provided is described in Section 3.7.4.2 below and meets the requirements of Regulatory Guide 1.12 for
47 a Safe Shutdown Earthquake maximum foundation acceleration of 0.3g or greater.

3.7.4.2 Location and Description of Instrumentation

Preliminary information on seismic instrumentation for the CRBRP is summarized in the following. More detailed information on instrument locations, basis of the selection of the locations, the extent of planned utilization, etc. will be provided in the FSAR.

The seismic instrumentation as planned will consist of the following:

1. Triaxial Time - History Accelerograph

47 7 It will consist of four (4) strong motion triaxial sensors, one (1) triaxial seismic trigger, one (1) central recorder and control unit and one (1) tape playback unit.

The strong motion triaxial sensors will be installed at the following locations:

a) "Free field" at a distance away from plant large enough to record the undisturbed free field motion.
b) On the foundation mat of the Reactor Containment Building.

Amend. 47
Nov. 1978

TABLE 3A.1-3 (Continued)

CELL NO. (1)	TITLE	FLOOR ELEVATION	RADIATION OPERATION	ZONE (2) SHUTDOWN	DESIGN PRESS. (PSIG)	DESIGN (4) TEMP. (°F)	OPERATING TEMP. (°F)	NORMAL (3) ATMOS.	EQUIPMENT CONTAINED
104	Primary Na Makeup & Future Pump Cell	733'-0"	V	IV	10	180	120	N	Primary Na LM Make-up Pump
107A	Primary Na Makeup Pump Valve Gallery	733'-0"	V	V	10	180	120	N	Primary Na LM Make-up Piping & Valves
107B	Aux. LM Pipeway and Valve Gallery	733'-0"	V	V	10	180	120	N	Direct Heat Removal Service DHRS Cooler Sodium Piping & Valves
121	PHTS Loop #1 Cell **	752'-8"	V	V	10	180	120	N	Primary Na Pump & Guard Vessel, Intermediate Heat Exchanger & Guard Vessel, Cold Leg Check Valve, PHTS and IHTS Hot Leg & Cold Leg Sodium Piping
122	PHTS Loop #2 Cell **	752'-8"	V	V	10	180	120	N	"
123	PHTS Loop #3 Cell **	752'-8"	V	V	10	180	120	N	"
131	NaK Cooling Equip. Cell	769'-0"	III	III	10	180	120	N	NaK Storage Tank, NaK EM Pump, NaK Cooler
132	NaK Sampling Cell	769'-0"	V	V	10	180	120	N	Multipurpose Sample (MPS), MPS Valve Cabinet, Master Slave Manipulator, Sodium Piping, Radiation Shielding Window, Sodium Transfer tunnel

26
44
56
3

TABLE 3A.1-3 (Continued)

Sheet 3 of 3

CELL NO. (1)	TITLE	FLOOR ELEVATION	RADIATION OPERATION	ZONE (2) SHUTDOWN	DESIGN PRESS. (PSIG)	DESIGN (4) TEMP. (°F)	OPERATING TEMP. (°F)	NORMAL ATMOS. (3)	EQUIPMENT CONTAINED
141	PTI Cell	783'-9"	V	V	10	180	120	N	Plugging Temp. Indicator (PTI), PTI Valve Cabinet
143	PTI Cell	792'-0"	V	V	10	180	120	N	"
157A	Pri. Na Cold Trap Cell (A)	793'-0"	V	V	10	180	120	N	Pri. Na Cold Traps
157B	Pri. Na Cold Trap Cell (B)	792'-9"	V	V	10	180	120	N	Pri. Na Cold Traps
157D	Cold Trap Valve Gallery (A)	792'-9"	V	IV	10	180	120	N	Cold Traps Piping & Valves
157E	Cold Trap Valve Gallery (B)	792'-9"	V	IV	10	180	120	N	Cold Traps Piping & Valves

44

NOTES:
1) Alphabetical designations following cell nos. indicate sub-cells sharing a common atmosphere.
2) For definition of Radiation Zones see Table 12.1-1
3) N = Nitrogen
4) Liner Design Temperature

** These cells shall have a design capability of surviving a one time high temperature sodium spill of 1050°F.

3

3A.4.2.9 Auxiliary Liquid Metal

The Auxiliary Liquid Metal System provides the facilities for purification and cooling of the sodium in the ex-vessel storage tank (EVST). The EVST sodium storage is provided by the Primary Sodium Storage and Processing System of the Auxiliary Liquid Metal System. This is discussed in greater
46 detail in Section 9.1, 9.3.

The maximum activity in the EVST sodium (i.e., after 30 years of plant operation and with no EVST cold trapping) is given in Table 12.1-23.

3A.4.2.10 Inert Gas Receiving and Processing

Sections 9.5 and 11.3 present details of this system. The radioactive inventory, by isotope, present in the various cells within the RSB are given in Table 12.1-12 through 12.1-18.

3A.4.2.11 Impurity Monitoring and Analysis

The Impurity Monitoring and Analysis System provides for the sampling monitoring, and analysis of sodium and cover gas impurities in the CRBRP systems. The system provides the following areas of impurity monitoring and
46 sampling;

1) EVS cover gas sampling

2) Primary cover gas sampling

46 3) EVS sodium sampling

56 Section 9.8 presents more details of this system.

3A.4.2.12 Fuel Failure Monitoring

Section 7.5.4 presents details of this system. The isotopic gas activity in the sampling trap cell (gas tag analysis) and the cover gas monitor cell are presented in Table 12.1-20.

3A.4.3 Design Evaluation

The RSB is designed to house the various systems listed in Table 3A.4-1. Each of the systems containing radioactive fluids or components will be separately housed in their respective cells, that have thick concrete walls. These walls, in addition to providing radiation protection to operating personnel, will act as a confinement barrier. Accidents considered by the individual systems housed in the RSB are presented in Chapter 15.

3A.4.4 Tests and Inspection

A CRBRP Quality Assurance Program is established to assure that critical structures are built in accordance with specifications. This program is described in Chapter 17.

Principal Materials Used in the RSB - Concrete, reinforcing steel, steel liner plates, and structural steel - are manufactured in accordance with nationally recognized standards. User installation tests and inspections are detailed in construction specifications.

Conventional methods will be used to inspect the cell liners. These methods may include:

1) Visual inspection of welds

2) Dye penetrant

3) Vacuum box

Tests and inspection will be performed during construction of the RSB structure, to verify conformance with construction specifications and applicable parts of building codes.

The tests and inspection of systems within the RSB are discussed in detail in those sections of this report pertaining to the individual systems housed by the RSB (see Table 3A.4-1).

3A.4.5 Instrumentation Requirements

The RSB will be sufficiently instrumented to provide for the safety of both operating personnel and the general public. This instrumentation will include such items as neutron counters for EVST and the FHC area, radiation detectors in all accessible areas, exhaust monitors for the H&V System, etc. The specific instrumentation requirements for the various systems in the RSB will be the joint responsibility of the functional system and its corresponding instrumentation system. These pairs of systems, together with a brief discussion of their instrumentation requirements, are given in other sections of this PSAR (see Table 3A.4-1). The responsibility of providing general radiation monitoring (i.e., not within the jurisdiction of any functional system) will be the Radiation Monitoring System. Section 12.2.4 of this PSAR presents the requirement for radiation monitoring in the RSB.

has an incubation period in which the swelling rate is low. During this time the fuel swelling generally closes the fabricated fuel-clad gap and generates a fuel-clad interaction stress. After the incubation period the increased clad swelling relieves the interaction stress. Under certain conditions, this increased cladding swelling results in re-opening the fuel clad gap. This has been observed experimentally with solution treated cladding in EBR-II.

The code used in the ongoing calculations of cladding loads is LIFE, Reference 175, (see Appendix A). LIFE was developed by Argonne National Laboratory as a fuel performance code with the capability of following the reactor power history. The magnitude and duration of the fuel-cladding mechanical contact are calculated with the LIFE code. LIFE has been adopted as the national fuel pin modeling code and is undergoing further development at ANL, W-ARD, HEDL, AI and GE. Limitations on the current version of the LIFE code (LIFE-III) and the methodology by which it is app ied to fuel and blanket rod analysis is discussed in Section 4.2.1.1.3.5

Two types of rods were investigated for FCMI effects: those with the highest end-of-life damage due to fission gas loads, and those which experienced the highest percent increase in steady state power level between cycles. The first type of rods are the least capable of withstanding any additional loading of any variety. In the second type of rod, the power increase at middle-of-life could lead to FCMI due to fuel-cladding differential thermal expansion, particularly if previous conditions resulted in a closed fuel-cladding gap at the time of the power increase. For all rods, the axial locations which showed the most significant calculated FCMI loads
56 were analyzed in detail for cladding damage. A corewide map of end-of-life cladding steady state CDF for the hot spot of the hot rod in each assembly is given and discussed in Section 4.2.1.3.1.2. The hot rod of radial blanket assembly 201, which experiences a 12% power jump between cycles 2 and 3, was chosen for investigation of power jump effects. In addition to experiencing a relatively high power jump, this rod also has one of the higher cladding CDF values at end-of-life.

Steady state FCMI loads were calculated for the hot rods of fuel assemblies 10 and 14, inner blanket assembly 67, and radial blanket
53 assembly 201 (see Figure 4.2-10B). These rods were found to sustain the highest cladding damage due to fission gas pressure alone (see Section 4.2.1.3.1.2.1 below). Between cycles, a 10 hour drop to zero power followed by a 10 hour rise to full power was assumed. The FCMI pressure values calculated by LIFE III for the fuel rods were adjusted to account for the greater cladding wastage which is assumed in the CRBR for design evaluations.
51 For example, in the LIFE III calculations, the initial cladding thickness

of 15 mils typically decreased by a maximum of 2 mils at X/L = .75. In the fuel rod design code FRST (see Section 4.2.1.3.1.2.2 below), the initial cladding thickness of 13.5 mils typically decreased by 6 mils over the design lifetime at X/L = 75. To compensate for this effect, the FCMI loads calculated by LIFE for the fuel rods, were multiplied by the ratio of the average cladding thickness calculated by FRST to that calculated by LIFE III over the rod design lifetime for each rod and axial location considered. Pending calibration of the LIFE code for blanket rods, the blanket rod FCMI loads were not adjusted for cladding wastage when input to the design code for added conservatism.

The results of these calculations are shown in Figures 4.2-17A, 4.2-17B, 4.2-17C and 4.2-17D. These figures are plots of total internal cladding pressure (plenum gas pressure + FCMI pressure) at the three cladding axial locations under consideration. The straight line pressure histories are due to plenum gas pressure only while the non-linear portions of these pressure history plots indicate the occurrence of FCMI loading.

The effects of the mid-life power increase on FCMI in the hot rods of radial blanket assembly 201 was investigated with the LIFE-III code by varying the power ramp rate at the beginning of the third cycle. For this study, three third cycle startup programs were considered:

- Normal startup (3 loop operation)
- Fast startup (3% min.)
- Programmed startup

The three startup procedures used in the analysis are shown in Figure 4.2-16. The fast startup was based on the maximum possible ramp rate achievable in the reactor, i.e., 3% per minute. The programmed startup was based on an earlier fuel pin power-to-melt uncertainty analysis for CRBR (Section 4.4).

Figure 4.2-24 shows the maximum calculated FCMI loads during the third cycle startup for the three startup schemes described above. This figure demonstrates that the FCMI loading calculated by LIFE III due to mid-life power increases in radial blanket rods can be significantly altered by varying the rates at which these rods are brought up to power at the beginning of the cycle when the power increase occurs. The effects of these cladding loadings on rod lifetime, and the overall conclusions derived from these calculations are discussed in Section 4.2.1.3.1.2.

Based upon experience with FFTF and EBR-II fuel assembly design, the following mechanisms were expected to be of secondary importance with respect to cladding damage in CRBRP but important to overall fuel and
51 blanket rod performance.

From the data of Figure 4.2-27, the hot rods of outer blanket assembly 201, and inner blanket assembly 67 were calculated to have the highest end-of-life CDF values at the hot spot for each blanket type. These rods were analyzed for transient effects at the hot spot using the methods and assumptions previously described for the fuel rods. The results of these analyses are shown in Figure 4.2-28A and 4.2-28B. These results show that these blanket rods achieve the goal life with the transient limit curves at end-of-life lying above the peak transient cladding hot spot temperature. The cladding hot spot transient temperature margins
56 at end-of-life for the other blanket rods are greater than the hot spot margins for the hot rods of assemblies 201 and 67.

As noted in Section 4.2.1.1, the LIFE III code has not been calibrated for blanket rods. However, the magnitude of the calculated blanket rod FCMI loads as a function of rod power, temperature, etc., correlate well with the calculated fuel rod FCMI dependence on these parameters. This indicates the LIFE III models are mathematically capable of predicting blanket rod FCMI results. To compensate for the uncertainty in blanket rod FCMI magnitude due to lack of specific calibrations, the blanket rod wastage was assumed to equal the conservative design cladding wastage. This resulted in conservative calculated FCMI stresses.

The effects of these calculated steady state FCMI loads and the transient duty cycle on cladding lifetime at axial locations X/L = 0.46 and 0.62 were determined for the hot rods of outer blanket assembly 201 and inner blanket assembly 67. The cladding temperature assumptions and transient limit curve techniques utilized for these blanket rods are identical to those utilized for the fuel rods. The total cladding internal pressures are shown in Figures 4.2-17C and 4.2-17D for the axial locations considered. These calculations predict that at end-of-life, the steady state and transient CDF margins at these axial locations on both blanket rods exceed the CDF margins at
56 the hot spot location.

<u>Mid-Life Power Increase Effects</u>

As noted in Section 4.2.1.1, the LIFE III code has not been calibrated to calculate the magnitude of FCMI loads for this type of environment change. However, the code models are capable of predicting the qualitative physical relation between FCMI and power change rate over the periods of time typical of reactor startup. Thus, for this study, blanket rod cladding performance with these startup programs at the beginning of the third cycle were calculated and compared. These startup programs were described in detail in Section 4.2.1.3.1.1.

The cladding CDF due to the most severe startup loading (100% power at 3% per minute) was calculated with the FURFAN code. Results of these analyses are shown in Table 4.2-10. Steady state CDF values are shown for 878 EFPD (4 cycles of operation) with and without accounting for the power jump. Comparison of the results shows that even in the worst case the mid-life power jump, per se, has no significant deleterious effect on the steady
51 state performance capability (CDF) of the blanket rod.

4.2.1.3.1.2.2 Cladding Ductility Limited Strain

The FRST computer code (see Appendix A) was used to calculate fuel rod cladding ductility limited strain versus time. This code provides a means of calculating effects of time-varying cladding temperature, plenum pressure, cladding wastage, and fuel-cladding contact pressure on the cladding ductility limited strain as defined in Section 4.2.1.1.2.2. This is done by utilizing the cladding thermal and pressure loads which equal or envelope those of Section 4.4 in the solution annealed 316 SS thermal creep equation, referenced in Section 4.2.1.1. Cladding wastage and steady state fuel-cladding contact pressure effects are considered in the cladding load calculations. Irradiation creep and swelling strains are also calculated by FRST using the 20% cold worked 316 SS models. The FRST calculational procedure has been verified against both hand calculations and MINIGRO code results.

For conservatism, the FRST computer code used the material modeling assumptions presented in Section 4.2.1.1; all pertinent initial environmental conditions considered for the fuel rod cladding strain calculations are also described or referenced in this section.

A sub-routine to the FRST code which calculates the cladding plastic strain increment and thermal creep strain rate during the transient, was used to determine the effects of transients on cladding strain accumulation. For the cladding material, the solution annealed 316 SS thermal creep strain relation, specified in Section 4.2.1.1, and the stress-strain relationship
54| given in Figure 15.1.2-22, were assumed. Fission gas plenum pressure and FCMI at the time of transient occurrence is input to this sub-routine from the steady state analysis results. During a given transient, the sub-routine adjusts
54| this pressure to reflect increased fission gas pressure, transient fuel-cladding differential expansion, and the time varying cladding temperature. During the transient, the code calculates the cladding stress, and utilizes this stress and the cladding temperature in the solution annealed 316 SS thermal creep equation to calculate the cladding strain rate due to the transient. Whenever the cladding stress exceeds the material proportional elastic limit given by the stress-strain-temperature relation of Figure 15.1.2-22, the code uses the mathematical equation of this relation to calculate cladding plastic strain, and this value is added to the plastic strain to obtain the total cladding transient ductility limited strain. This technique, which is the same as used for FFTF, is described and verified in References 57 and 173.

A minimum beginning-of-life cladding thickness of 0.0135 inches was assumed, which allows for design tolerances and defect allowances. The cladding material wastage rates and mechanical properties are discussed in Section 4.2.1.2. The pertinent initial conditions used for these calculations were
51 previously described in this section.

is not fed back directly to the reactor control system, the operator utilizes the position data to evaluate the plant and to interpret reproducibility of reactivity control. The relative position indication accuracy of ±0.1 inch leads to reactivity reproducibility of approximately 1¢ for the highest worth rod in the primary system. In addition, the position indication is utilized for logic interlocks and alarm as described in Section 7.7.1.3.

4.2.3.1.5 Structural Requirements

Control Rod Drive Mechanisms

The primary and secondary control rod drive mechanisms are designed to the following classes of components:

1. ASME Boiler and Pressure Vessel Code, Section III, 1974 edition, Class 1. For the primary control rod system, the mechanism motor tube, motor tube hold-down ring, nozzle extensions and position indicator housing form a part of the pressure retaining boundary. For the secondary control rod system, the extension nozzle, the hold-down ring, the upper portion of the mechanism housing, and the connector plate form a portion of the pressure retaining boundary.

2. Seismic Category I. The control rod systems are required to remain functional and shutdown the reactor in the event of an SSE. (See Section 3.2.1 for detailed discussion).

3. Safety Class I. The control rod systems are categorized as Class I because of their control and shutdown functions. (See Section 3.2.2 for detailed discussion).

The primary control rod drive mechanisms shall be designed to the load conditions of Table 4.2-37. For these loading conditions, pressure boundary components shall meet the structural requirements of
51 Section III of the ASME Pressure Vessel Code together with applicable code cases and amendments to the code by RDT Standards. The portion of the Secondary Control Rod System that is coded in accordance with the ASME B&PV code and hence forms a part of the pressure retaining boundary shall be designed to the load conditions of Table 4.2-37. The structural requirements of Section III of the ASME Pressure Vessel Code together with applicable code cases and amendments to the code by RDT Standards shall be met.

The governing stresses in the mechanism are the time independent effects of primary mechanical loads, secondary thermal loads and fatigue. Use of the methods of these codes together with consideration of material effects such as carbon and nitrogen depletion, thermal aging, and environmental correction factors to account for material interaction with sodium leads to conservative structural designs of the mechanisms.

The primary and secondary control rod drive mechanisms shall have a design life of 30 years. This lifetime is consistent with the design lifetime of the reactor. Sufficient shielding shall be provided where appropriate to assure adequate strength to meet the structural criteria over the required lifetime. Interim maintenance will be required in order to achieve this lifetime.

The PCRDM and SCRDM shall remain structurally intact and attached to the reactor vessel, and shall not permit sodium leakage under Structural Margin Beyond the Design Base conditions. (See Reference
56 51 10a, Section 1.6). This requirement provides added margin of safety for an event for which no causative mechanism is known.

The PCRDM and SCRDM shall be designed such that no mechanical failure can result in any parts becoming missiles.

Control Rod Driveline

The primary control rod driveline (PCRD) and the secondary control rod driveline (SCRD) shall meet the intent of the structural requirements of Section III, ASME Pressure Vessel Code, together with applicable Code Cases (1592), and amendments by applicable RDT Standards. The stress and stability criteria for evaluation of the design shall be as specified in the above codes for all significant loading conditions including those identified in Table 4.2-37. Material physical property changes due to irradiation, thermal, and sodium environments shall be considered in evaluating the design.

The ASME Code specifies conservative allowable stresses for various loads and combinations of loads. The compressive load limit shall be no greater than 1/3 the buckling stability load of the driveline, and the design stress intensity limit shall be the lower of 1/3 ultimate or 2/3 yield stress. Satisfaction of the criteria assures that conservative margins exist for all conceivable loads including rod ejection for which no causative mechanism is known.

The design lifetimes of the primary and secondary drivelines shall be as shown in Table 4.2-38. The design lifetime requirements are conservative with regard to material considerations, taking into account the irradiation environments of these components (Table 4.2-39).

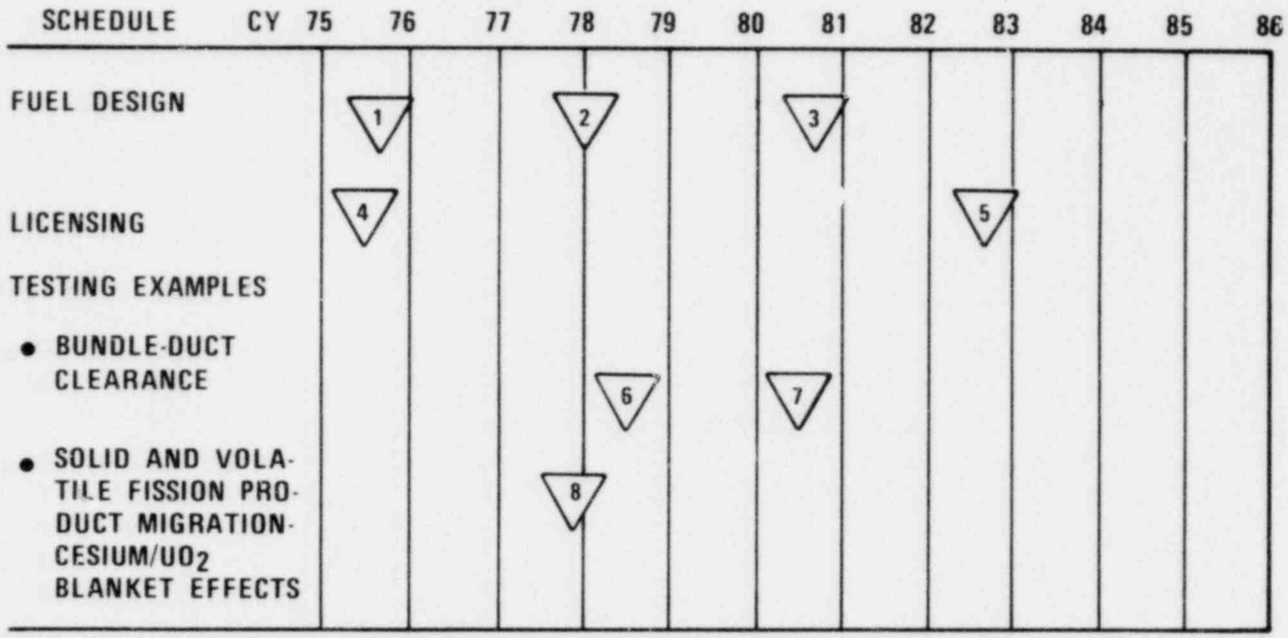

FALLBACK EXAMPLES

- BUNDLE-DUCT INTERACTION – CHANGE THE INITIAL POROSITY BY SMALL CHANGES IN WIRE WRAP DIAMETER AND/OR SELECTIVE ASSEMBLY
- CESIUM/UO_2 BKT. EFFECTS – FOR THE FIRST SEVERAL AXIAL BLANKET PELLETS AT EACH END, INCREASE THE DIAMETRAL GAP.

LEGEND:

- ▽1 PRELIMINARY DESIGN REVIEW
- ▽2 FINAL DESIGN REVIEW
- ▽3 RELEASE TO FABRICATION
- ▽4 PSAR SUBMITTAL
- ▽5 START FSAR
- ▽6 P13,P14 EXAMINATION COMPLETE
- ▽7 VALIDATE DESIGN FIX FOR BUNDLE VIBRATION AND WEAR
- ▽8 ESTABLISH EFFECT WITH LOW O/M FUEL

Figure 4.2-35A Design Fallback Positions

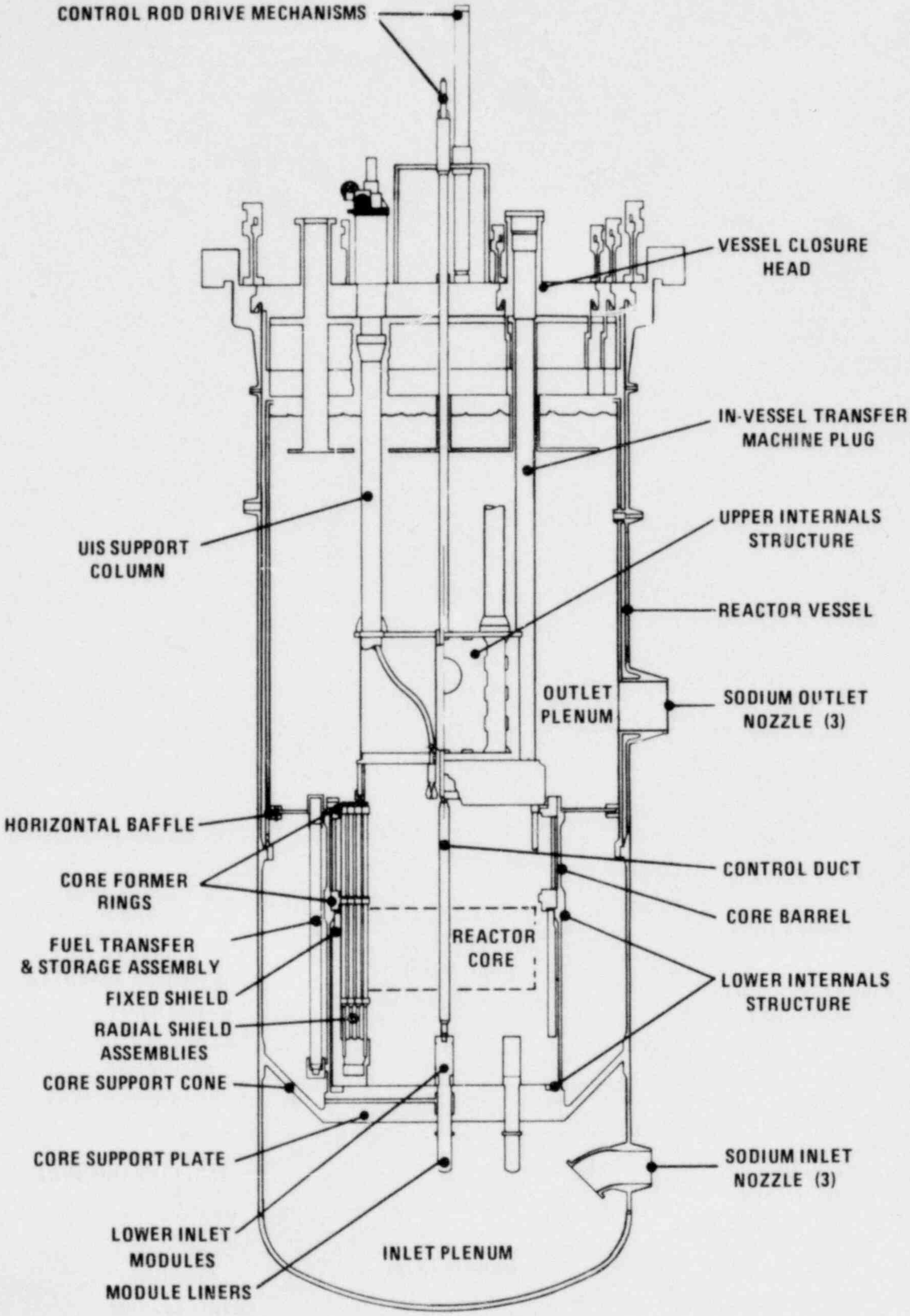

Figure 4.2-36. Reactor Elevation

1526-1a

Amend. 56
Aug. 1980

where

$$A_1 = \frac{1}{\beta} \sum_{i=1}^{M} \left[C_i'(t_1) - C_i'(t_0) \right]$$

$$A_2 = \frac{1}{\beta} \sum_{i=1}^{M} \left[C_i'(t_2) - C_i'(t_1) \right]$$

$$B_1 = \int_{t_0}^{t_1} CR(t)dt$$

$$B_2 = \int_{t_1}^{t_2} CR(t)dt$$

$$\Delta t_1 = t_1 - t_0$$

$$\Delta t_2 = t_2 - t_1$$

$$C_i'(t) = \frac{W\, C_i(t)}{\nu}$$

56 t_0 = a time slightly greater than t_s; $t_0 - t_s \cong 0.5$ seconds.

t_1 = a time greater than t_0 which occurs while the count rate transient is still decaying; $t_1 - t_s \cong 25$ seconds.

t_2 = a time near the end of the transient when the reactor is approaching its final steady-state condition; $t_2 - t_s \cong 240$ seconds.

The initial reactivity state ρ_0 is calculated by solving Equations (8) and (9) at steady-state, or

$$\rho_0 = -\frac{WS}{\nu\, CR(0)} \tag{12}$$

Substituting Equation (11) into Equation (12) we have

$$\rho_0 = -\left(\frac{B_1 A_2 - B_2 A_1}{B_1 \Delta t_2 - B_2 \Delta t_1}\right)\left(\frac{\beta}{CR(0)}\right) \tag{13}$$

Equations (10) and (13) are evaluated for the final, and initial subcritical reactivity states, respectively. The values for $C_i'(t)$ are based on a recursive solution of Equation (9); see Reference 3 for
51 details.

A study has been performed to assess the uncertainty in control rod worth as inferred from IKRD experiments due to the statistical uncertainty inherent in the observed count rate of the detector (Reference 4). The IKRD experiments were performed by ORNL personnel at the Southwest Experimental Fast Oxide Reactor. Two analytical methods were applied to the results from these experiments. First, a propagation of error analysis technique was applied to three-point IKRD subcritical measurements. The second verification method was an error analysis based on repeated rod-drops which were simulated from observed count rate vs. time data. In both cases, the assumption was made that the uncertainty in the reactivity estimate was due solely to the detection process itself. The reactivity uncertainties for various experimental rod-drop data sets were computed by both of these methods and the results were in good agreement. Both techniques yielded errors of approximately 0.6% in the initial and final reactivity states when control rods worth 1 to 2 dollars were inserted from a near critical state.

Additional analyses have been performed to determine the uncertainty in control rod worth as inferred from the IKRD technique which results from the uncertainty in the kinetics parameters β_i and λ_i (Reference 3). These analyses were based on rod-drop experiments performed on the Fast Flux Test Facility-Engineering Mockup Critical loaded into ZPR-9 at ANL. For this configuration, the uncertainty in the final reactivity measurement is 1.8% due to uncertainties in β_i and 0.6% due to uncertainties in λ_i. Similarly, the determination of the initial reactivity state is uncertain by as much as 3.0% due to uncertainties in β_i and as much as 2.0% due to uncertainties in λ_i. Adding together the β_i and λ_i related uncertainties and statistically combining the result with the 0.6% detector count rate uncertainty yields the following: the minimum uncertainty associated with the determination of the final reactivity state is 2.5%, and the minimum uncertainty associated with the determination of the initial reactivity state is 5.1% (minimum = theoretical, no systematic error included).

The precision of the IKRD technique depends to a large extent on systematic uncertainties, i.e., the ability to reproduce the same initial reactor conditions when a rod-drop experiment is to be repeated. Reference 4 discusses a particular rod-drop experiment that was repeated four times in SEFOR under nearly identical reactor conditions. The standard deviation (one σ error) for the control rod worth, which is based on the difference between ρ_f and ρ_o, is approximately 0.7%.

During refueling, the SRFM must provide a warning to the operator and thereby assure that the reactor does not approach criticality any closer than that level from which criticality could be attained by a single refueling error with adequate margin for the associated uncertainties. The uncertainties associated with the subcritical reactivity monitoring technique fall into three categories: (1) the uncertainty in the calcu-
51 lated reactivity worth of the single worst refueling error, (2) the

buildup, 2) the mid-term row 6 refueling, and 3) control rod bank withdrawal effects. Equivalent Doppler constants at the beginning-of-cycle one and at the end-of-cycle four in a sodium-voided environment are shown in Table 4.3-17. The effect of the removal of sodium is to harden the neutron energy spectrum and substantially reduce the magnitude of the Doppler constants.

Table 4.3-18 presents a typical nodal-average Doppler distribution in the fuel, inner, and radial blankets at the beginning-of-cycle one. Each region contains a total of seven axial nodes; five equal-volume nodes in the 36-inch high "fuel" region and one node each in the upper and lower blankets (extensions). The row 1 and row 2 radial blanket Doppler constants have been combined additively into a single region. This combination results in a slightly conservative (less negative) feedback reactivity due to temperature differences in the two rows of radial blankets.

Figures 4.3-27a and b show the distribution of Doppler constant by assembly in the 36-inch active fuel and inner blankets at the beginning of cycle one and the end of cycle four, respectively. The values in Figures 4.3-27a and b are condensed from three-dimensional (VENTURE) first-order perturbation theory calculations which were used to develop nodal feedback coefficient input to SAS analyses (see Chapter 15).

The temperature dependence of the Doppler constant is discussed in Reference 5. The Doppler contribution of the fissile material is a small positive effect, and generally follows a $T^{-3/2}$ dependence. However, the U-238 contribution is strongly negative and overrides the small positive contribution from the fissile nuclides. Calculations of the temperature dependence for a series of U-238 resonances result in a Doppler temperature relationship of T^{-1}. Self-shielding effects will tend to decrease the absolute value of the temperature exponent, but for a fast reactor having a fertile/fissile content similar to CRBRP, the overall Doppler constant has approximately a T^{-1} variation.

The temperature dependence of the Doppler reactivity constant
for CRBRP has been examined parametrically for a homogeneous core confi-
56 guration using FX-2. The code system used for generation of cross sections
is verified in Reference 6 and applied to the CRBRP model as explained
in Reference 7. FX-2 utilizes a three-term temperature-dependence for-
56 mula cross section curve fit (in terms of $T^{-1/2}$, T^{-1}, and T^{-2}) to four
points generated over the temperature range of interest from a theoretical
basis taking into account core design heterogeneity and self-shielding.
Using FX-2, the Doppler reactivity effect in changing the core tempera-
ture uniformly from 1000°K to other temperatures is tabulated in Table
56 4.3-19. A comparison is then made with a T^{-1} extrapolation of the
reactivity effect between 300°K and 1000°K. This comparison shows that
the more detailed temperature dependence in FX-2 agrees well with the
56 simple T^{-1} dependence. The maximum final average temperatures do not
51 exceed 4800°K.

At higher temperatures than those present in Table 4.3-19, other uncertainties make the comparison less meaningful. In SAS and VENUS calculations, the variations in Doppler associated with different postulated scenarios are large compared to the uncertainties associated with the temperature dependence of the Doppler constant. For example, in Section 4.4 of Reference 7 a $100/sec ramp rate was input to VENUS in a fully voided core. This condition corresponded to a Doppler constant of -0.00297. The resulting core average temperature at disassembly was 4802°K. A second case assumed some sodium remained in the core based on a somewhat different scenario. In this case, the effective Doppler constant was -0.00379, and the resulting core average temperature at disassembly was 4533°K. Consequently, large variations in Doppler have already been considered by considering different scenarios and the uncertainty in the Doppler temperature dependence is well within these other variations.

Doppler Uncertainty:

The uncertainty in the CRBRP Doppler Constant has been developed from the analysis of the SEFOR Core I and II experiments. The Southwest Experimental Fast Oxide Reactor (SEFOR) was constructed specifically to determine the LMFBR Core Doppler feedback through a series of power coefficient (¢/MWth) and sub- and super-prompt transient energy coefficient (¢/MWth.sec) measurements. SEFOR Core II had a material composition, resultant neutron energy spectrum and fuel temperature that was reasonably characteristic of that in CRBRP. The SEFOR experiments are described in, for example, Reference 8. The SEFOR Core II Doppler constant derived from these measurements (T dk/dT = -0.0060) is in good agreement with the value of -0.0062 calculated by GE in Reference 9. GE estimated the SEFOR Doppler constant uncertainty as $\pm$ 9% (1σ equivalent) in Reference 9. The principal contributions to this value, other than the direct measurement uncertainties themselves, are estimated uncertainties in the fuel temperature-power relationships (fuel to coolant thermal conductance and fuel specific heat) required to extract the Doppler constant, -T dk/dT, from the measured power and energy coefficients (¢/MWth and ¢/MWth.sec, respectively). Additional uncertainties in the extrapolation of the SEFOR power and energy coefficients to LMFBR power reactors are attributable to effects which are significantly different between the two reactors (uncertainties in fuel thermal properties, delayed neutron data, and the like are highly correlated between SEFOR and power reactors so that these uncertainties largely cancel in the normalization). The net extrapolated uncertainty in LMFBR power or energy coefficient was determined to be $\pm$ 11% (1σ) in Reference 9. This extrapolation accounted for differences in the SEFOR and LMFBR core composition and spectrum, fuel thermal property differences, and spatial temperature and importance weighting uncertainties. The neglect of spatial temperature and importance weighting (that is, the use of region Doppler constants
51 with average fuel temperatures) tends to (conservatively) underestimate

magnitude of the changes in sodium density reactivity with burnup are similar to those in the sodium void worth in Table 4.3-20. The uncertainty in the sodium density reactivity coefficient is taken to be the same as the sodium void worth uncertainty.

4.3.2.3.4 Expansion and Bowing Reactivity Coefficients

Physical changes in the overall reactor configuration will result in corresponding reactivity perturbations. The reactivity coefficients discussed in this section are: (1) uniform axial fuel expansion (fuel surface temperature dependent), (2) uniform radial core expansion (inlet coolant temperature dependent), and (3) relative radial motion of fuel assemblies (bowing) resulting from a combination of temperature gradients and long-term swelling, the latter being highly dependent on irradiation history.

a. Uniform Axial Expansion Coefficient

The axial expansion coefficient defines the relationship between reactivity and changes in the length of the active core (fuel pellet stack height). It should be noted that the axial expansion is assumed to be dependent on the temperature at the radial surface (shoulder) of the dished fuel pellets. Implicit in this definition of the uniform axial expansion coefficient is the assumption of free movement of the fuel pellets within the clad tubes. This assumption tends to yield the largest (magnitude) coefficient insofar as degradation of the fuel pellets under irradiation will significantly reduce the magnitude of this coefficient. This effect was noted in the RAPSODIE reactor (Ref. 13).

The reactivity feedback due to core axial expansion or contraction consists of worth components from fuel and blanket expansion, stainless steel expansion, and another component for relative core/control rod motion. The fuel and steel expansion worths are determined from a perturbation technique whereby the axial expansion worth is taken to be the difference between the uni-
56 form material worth over the 36-inch active core and the material worth at the core/axial blanket boundaries. These material worth distributions are determined from a first-order perturbation theory calculation in RZ geometry. Table 4.3-22 shows the distribution of the pellet and steel components of the uniform axial expansion coefficient (¢/mil of uniform expansion) in the fuel and blankets by radial "row" throughout the core at the beginning-of-cycle one and at the end-of-cycle four. Axial expansion of the fuel lowers the core density and removes reactivity from the system. The higher beginning of life fuel enrichment, and hence the relatively high fuel worth, results
51 in a larger fuel expansion worth in the fresh core at the beginning-of-cycle

one than in the burned core at the end-of-cycle four. Expansion of the blankets removes absorber from the core and thereby slightly increases reactivity, except in the case of the radial blankets where the predominant effect is to lower the reflective (scattering) worth of the blanket material. Expansion of either the fuel or inner blanket steel again removes absorber from the core and increases reactivity. In addition to the direct core expansion reactivity, there is an added effect of net movement of the core with respect to the partly inserted control rods.

The axial expansion coefficients in Table 4.3-22 can be converted to ¢/^{o}F using linearized material thermal expansion coefficients for fresh fuel pellet material (0.[illegible]81 mils/^{o}F) and for unirradiated stainless steel (0.425 mils/^{o}F). However, these material expansion coefficients are expected to be a function of accumulated burnup and fluence. In the case of fuel pellet material, the mechanism of thermal expansion may vary substantially from the fresh un-irradiated behavior due to pellet cracking. Consequently, the fuel expansion reactivity feedback can vary from a minimum of zero to the value calculated assuming free movement of the fuel column and thermal expansion driven by the pellet surface temperature. For this reason, fuel expansion negative reactivity feedback is generally not included in transient evaluations. At the other extreme, complete pellet-clad sticking could result in the fuel column growing axially according to the cladding temperature change. In this case, due to the higher thermal expansion coefficient for the steel cladding, the thermal growth of the fuel column in the startup transition from refueling temperature conditions to hot full power would increase approximately 20% (10¢ additional power defect) compared to the case of free-moving pellets. However, such global pellet-clad contact is unlikely to occur throughout the entire startup temperature transition, especially in fresh fuel where the axial expansion reactivity coefficients in Table 4.3-22 are highest. Therefore, pellet-clad sticking is not considered in the determination of the cold-to-hot temperature defect.

b. Uniform Radial Expansion Coefficient

The uniform radial expansion coefficient defines the relationship between reactivity and changes in the effective (equivalent circular) radius of the core (fuel/radial blanket boundary). The uniform radial expansion coefficient is dependent upon the change in dimensions of the lower core support structure which in turn depends on the inlet coolant temperature. This definition is convenient from a calculational standpoint since the detailed
51 mechanical motion of the fuel and inner blanket assemblies need not be known (this detailed mechanical motion is subsequently

Amend. 56
Aug. 1980

included in the bowing reactivity component). During the heat-up period between refueling and hot-standby temperature, the core is essentially isothermal and the uniform radial expansion coefficient is applicable.

Calculations of the uniform radial expansion coefficient for the CRBRP were performed in hexagonal geometry using the diffusion theory code 2DB with 9 energy groups. The pitch of all fuel, inner and radial blankets, primary and secondary control rods and removable radial shield assemblies is increased uniformly while at the same time the masses of structural and fuel materials are held constant. The mass of sodium necessarily increases in the expanded core. This calculational technique for the uniform radial expansion coefficient duplicates the results from three-dimensional calculations except for slight increases in axial leakage which accompany such expansions. The resulting values, expressed in terms of cents per mil of outward radial motion of the core/radial blanket boundary, are shown in Table 4.3-23 for various times-in-life. The beginning-of-cycle (hot standby startup conditions) are best characterized by the configuration with 6 Row 7 corner primary control rods inserted, whereas the end-of-cycle conditions are most nearly simulated by the all-control-rods-out configuration. The uniform radial expansion coefficients in Table 4.3-23 can be translated to units of ¢/°F change in coolant inlet temperature by multiplying by 0.415 mils/°F which is derived from the linearized stainless steel (lower core support plate) thermal expansion coefficient. At the beginning-of-cycle-one, the reactivity change from uniform core radial expansion between refueling temperature (400°F) and hot-full-power conditions (730°F inlet temperature) is -58.5¢.

c. Fuel Assembly Bowing Reactivity

In addition to structural reactivity changes associated with the uniform expansion of the fuel and blanket assemblies, additional reactivity contributions occur as a result of core assembly bowing during reactor startup and shutdown. Fuel and blanket assembly bowing is a complex function of both the local temperature and neutron flux irradiation. The temperature dependence is a function of the absolute temperature within and the temperature gradients across the assembly ducts and pins. The irradiation induced swelling and creep are complex functions of the flux
51 magnitude and spectrum, temperature and assembly residence time.

Radial bowing reactivity coefficients are calculated for each row of fuel and blanket assemblies at various axial nodes. First-order perturbation theory calculations in RZ geometry are used to determine the material worth gradients for fuel, steel, and coolant throughout the core. The radial bowing reactivity worth coefficients, expressed in units of ¢/inch of node displacement, are determined from differences in fuel, structural and coolant edge worths simulating row-by-row radial displacements.

The radial-row model for CRBRP is shown in Figure 4.3-30. Radial bowing reactivity coefficients were generated for Rows 2 through 12; the central (Row 1) blanket assembly and the six outermost radial blanket assemblies having a negligible reactivity contribution. Tables 4.3-24 and 4.3-25 give the radial bowing reactivity coefficients (¢/inch of inward radial motion) for two core configurations. The beginning-of-cycle one results (Table 4.3-24) model hot-standby (initial startup) conditions and are characterized by a clean core and blankets and six Row 7 corner primary control rods partially inserted. The end-of-cycle two results (Table 4.3-25) were calculated with burned fuel assemblies, bred plutonium in the blankets, and with all 15 control rods fully withdrawn.

The predicted mechanical bowing displacements, discussed in Section 4.2.2.4.1.8.3, are superimposed on the reactivity worth coefficients in Tables 4.3-24 and 4.3-25 to determine the total reactivity feedback associated with various bowed configurations experienced by the core during the approach to power.

d. Uncertainty in Expansion Reactivity Worth Coefficients

Core expansion reactivity effects are difficult to simulate experimentally. However, an indirect verification of the core expansion reactivity worth calculational technique, using small-sample reactivity worth profiles in the homogeneous ZPPR-5 configuration, is discussed in Reference 14. Worth profiles from an RZ reactivity worth map, synthesized from small-sample reactivity worth traverses for major reactor materials in the fuel and blankets, are integrated to represent the reactivity worth changes due to uniform core axial and radial expansion, and thereby to deduce the "experimental" expansion coefficients. First-order perturbation theory calculations of these same expansion coefficients were compared with the experimental values in order to assess the calculational uncertainty. The experimental simulation of uniform expansion using measured small-sample worth distributions was validated by using this same small-sample worth data to predict the measured axial expansion reactivity worth of a shimmed
51 oscillator fuel drawer in the inner and outer core zones.

Having accomplished the validation of the method for a measurable material rearrangement, the small sample traverses were used to determine an experimentally based (inferred) core expansion reactivity coefficient. First-order perturbation theory calculations of the reactor material worth distributions generally overestimated the magnitude of the worths themselves, consistent with the historically observed central worth discrepancy, but accurately predicted the shapes of the reactivity traverses upon which the expansion worth coefficients are based. The calculations of the measured expansion worth components resulted in calculation-to-prediction (C/P) ratios of 1.01 and 1.11 for axial and radial expansion, respectively. These differences are not only an indication of calculational uncertainty, but also an indication of the degree of accuracy in the measurement and integration techniques. In the expansion reactivity prediction from the small-sample traverses, two axial reactivity shapes were combined with the midplane radial worth measurements to create an RZ reactivity map from which the expansion coefficients were inferred by integration of the worth distributions over the fuel and blankets. The potential for systematic errors introduced by the approximations inherent in this technique was evaluated. The stainless steel contribution was found to be very sensitive to the location of the axial shape measurements and this was a substantial contributor to the estimated error in the radial expansion worth. In the case of the axial expansion worth coefficient, both positive and negative components were over-estimated resulting in compensating errors so that the calculation and measurement agreed very well (C/P = 1.01).

Based on the ZPPR-5 measurements and analysis, the uncertainty in the calculated expansion coefficient was estimated to be $\pm 15\%$ (1σ) in Reference 14 for a clean, homogenous core configuration. This uncertainty has been increased to $\pm$ 20% (1σ) for application to CRBRP expansion calculations to account for extrapolation effects.

4.3.2.3.5 Power and Startup Coefficients and Temperature Defect

a. Power Coefficient

The power coefficient relates the change in reactor power level to a change in reactivity in the power operating range (40 to 100 percent of full power). The power coefficient consists mainly of Doppler reactivity feedback. The average power coefficient incorporates slower acting feedback mechanisms such as uniform radial expansion (Section 4.3.2.3.4-b) and coolant density changes (Section 4.3.2.3.3), as well as the fast-acting fuel and blanket Doppler (Section 4.3.2.3.1) and
51 axial fuel expansion (Section 4.3.2.3.4.a). Between 40 percent

and 100% of full power, the average power coefficient is -0.18 ¢/MWt at the beginning-of-cycle one and -0.21 ¢/MWt at the end-of-cycle four. The increase in average power coefficient with fuel burnup is attributable primarily to the increase in Doppler feedback, particularly in the inner blankets.

The prompt power coefficient only incorporates the fast-acting feedback components: Doppler and axial fuel expansion. The Doppler reactivity feedback comes from both the fuel assemblies, where the fuel pellet temperature responds essentially instantaneously to changes in power and from the blanket assemblies where the feedback response is delayed due to the thermal inertia in the larger blanket rods. Fuel axial expansion, driven by the fuel pellet surface temperature, is considered as a fast-acting feedback response. The prompt power coefficient, averaged over the range of 40 to 100 percent of full power, is -0.15 ¢/MWt at the beginning-of-cycle one (-0.06 ¢/MWt when only fuel Doppler is considered) and -0.17 ¢/MWt at the end-of-cycle four (-0.05 ¢/MWt fuel Doppler only).

The hot-full-power prompt power coefficient provides the stabilizing, inherently negative, feedback mechanism in response to power level increases in the power operating range.

b. Startup Coefficient

The startup (shutdown) coefficient relates the change in power level to a change in reactivity in the startup and shutdown range from 0 to 40 percent of full reactor power. The startup coefficient includes the reactivity effect of fuel and blanket assembly bowing (Section 4.3.2.3.4-c) in addition to feedback from Doppler, uniform expansion, and coolant density changes as discussed in Item (a).

The startup profile (Appendix B) indicates that most of the core temperature gradients will be established during the interval when the reactor power is being incrementally increased from near zero to 40 percent at a constant coolant flow rate of 40 percent of full flow. Fuel and blanket assembly bowing occurs in response to the power-to-flow transitions as the core thermal gradients are established (Section 4.2.2.4.1.8.3). Above 40 percent power, the reactor power level and the coolant flow rate are increased simultaneously (power-to-flow ratio is maintained at a value of 1.0) so that no further assembly bowing occurs.

The reactor power ascent is initiated after the reactor coolant temperature has been raised isothermally from 400°F (refueling temperature) to 600°F (hot standby) using 100% primary flow
51 (i.e. using pump work) and minimum or no reactor power. During

this initial heat-up, Doppler, uniform core expansion and sodium density changes provide a negative reactivity feedback of about -90¢ which is compensated by control rod withdrawal. Beyond hot-standby conditions, as the reactor power is increased from near zero to 40 percent (at 40% primary coolant flow), the reactor coolant inlet temperature increases from 600°F to 635°F and the 265°F core ΔT is established. Table 4.3-26 summarizes the total feedback from Doppler, uniform radial and axial expansion, and sodium density changes between zero power (hot-standby conditions) and 40 percent power (40 percent flow). The largest negative feedback contribution in Table 4.3-26 is that from Doppler, ranging from -70.0¢ at the beginning-of-cycle one to -95.5¢ at the end-of-cycle four. The uncertainty in Doppler coefficient is $\pm$ 10% (1σ). When the Doppler coefficient uncertainty is combined in quadrature with the temperature change uncertainties, the total uncertainty in Doppler feedback in the 0 to 40 percent power range is $\pm$12% (1σ). Uniform radial expansion only contributes about -6¢ ($\pm$20% 1σ) based on the coolant inlet temperature change from 600°F to 635°F. Uniform axial expansion of -17.2¢ at the beginning-of-cycle one and -8.1¢ at the end-of-cycle four includes both a negative component from fuel pellet expansion and smaller positive contributions from blanket and steel expansion. The uncertainty in axial expansion reactivity is $\pm$20% from ZPPR -5 ($\pm$23% when combined in quadrature with thermal uncertainties at the 1σ level). Sodium coolant density changes contribute -1.4¢ ($\pm$30%) at the beginning of cycle one and +4.8¢ at the end of cycle four. The total negative feedback (excluding bowing) over the startup range from 0 to 40 percent power is therefore -94.8¢ (-76.0¢ minimum feedback with 2σ uncertainties)
56 at the beginning of cycle one and -105.3¢ (-81.7¢ minimum) at the end of cycle four.

The net bowing reactivity feedback is determined by superimposing the physical motion of the fuel and blanket assemblies (as described in Section 4.2.2.4.1.8.3) on the differential reactivity worth distributions (Section 4.3.2.3.4.c) throughout the core. The bowing reactivity response to the establishment of the core thermal gradients with increasing power-to-flow ratio (P/F) in the startup power range is characterized by an initial negative reactivity component as the assemblies bow outward and contact the TCLP (Top Core Load Pad). Further increases in P/F cause the fueled portion of the assemblies to be displaced inward toward the core centerline during which time reactivity is added to the system. The inward displacement continues until the assemblies again contact at the ACLP (Above Core Load Pad) in the upper axial blanket. From this point on, the assemblies assume an "S"-shape bowed configuration in which the fueled region of the core is again displaced radially outward and the
51 reactivity contribution is again negative. When worst case data

uncertainties (maximum positive bowing reactivity coupled with minimum compensating negative Doppler feedback) are combined with conservative core compaction assumptions, the overall net startup reactivity feedback is predicted to be positive over a limited power range. The significance of this limited positive startup coefficient to reactor control and transient response is evaluated in Section 4.3.2.8 (Reactor Stability), 7.7.1.2 (Reactor Control System), and 15.1.4.5 (Reactor Assembly Bowing Reactivity Considerations). In the power operating range, from 40-100 percent of full power, no additional bowing takes place and the reactivity feedback is dominated by the strongly negative Doppler.

c. Temperature Defect

The net reactivity loss between zero-power, isothermal hot-standby or refueling temperature conditions and steady-state, hot-full-power thermal conditions is called the power or temperature defect. The temperature defect reflects the negative feedback reactivity contributions from Doppler, uniform radial and axial core expansion, sodium density changes and net negative bowing. Table 4.3-27 shows the temperature defect components in CRBRP at the beginning of the first cycle. Table 4.3-28 summarizes the net temperature defect at the beginning and end of the first four cycles of operation. The temperature defect, in part, determines the primary and secondary control rod worth (shutdown) requirements discussed in Section 4.3.2.4. The uncertainties in the temperature defect components in Table 4.3-27 reflect the statistical combination of both reactivity coefficient and temperature difference uncertainties.

4.3.2.4 Control Requirements

The reactivity control systems in CRBR are designed in accordance with the General Safety Design Criteria given in Section 3.1 and the appropriate design bases discussed in Section 4.3.1. These criteria assure that acceptable fuel design limits are not exceeded as a result of any anticipated operational occurrence or for any single malfunction of the reactivity control system.

Two independent reactivity control systems are utilized in the CRBRP. The primary system serves both a safety and an operational function. This system must have sufficient worth at any time in the reactor operating cycle, assuming the failure of any single active component (i.e. a stuck rod), to shutdown the reactor from any planned operating condition and to maintain subcriticality over the full range of coolant temperatures expected during shutdown. Allowance must be
51 made for the maximum reactivity fault associated with any anticipated

occurrence. In addition, the primary control system is designed to meet the fuel burnup requirements for each cycle as well as to compensate for criticality and refueling uncertainties. The other reactivity control system, which is identified as the secondary system, must have sufficient worth at any time in the reactor cycle, assuming the failure of any single active component (i.e., a stuck rod), to shut down the reactor from any planned operating condition to the hot shutdown temperature of the coolant (hot standby conditions). Allowance must also be made for the maximum reactivity fault associated with any anticipated occurrence.

The primary and secondary control systems operate independently such that the capability of either system to fulfill its safety function is not dependent on the operation (or failure) of the other system. Design diversity and separation are provided to protect against common mode failures, as discussed in Section 4.2.3.

The aforementioned design criteria are interpreted to define the reactivity control requirements in terms of the minimum acceptable control capability under faulted conditions which will assure that the reactor power level can be brought down to zero at either the hot refueling temperature (in the case of the primary system) or the hot standby temperature (in the case of the secondary safety system). The faulted conditions are postulated to be the simultaneous failure of one system to scram, a stuck rod in the remaining system and a reactivity insertion resulting from the uncontrolled withdrawal of the highest worth control rod in the reactor.

The contributions to the control rod worth requirements are listed in Tables 4.3-29 and 30 for the primary and secondary systems, respectively, and are discussed in the paragraphs that follow.

a. Power Defect

The power defect (hot-full-power temperature defect) component of the control requirements compensates for the net positive reactivity insertion due to Doppler effect, radial and axial core contraction, bowing, and sodium density changes during reactor shutdown from hot-full-power to zero power isothermal temperature conditions as discussed in Section 4.3.2.3.5-c. The primary control system is designed to take the reactor temperature down from hot-full-power (including 3σ temperature uncertainties and 15% overpower) to 375°F (the hot refueling temperature, 400°F, less 25°F uncertainty). The secondary control system is designed to take the reactor temperature down from hot-full-power (including 3σ temperature uncertainties and 15% overpower) to 550°F (the hot-
56 | 51 stand by temperature, 600°F, less 50°F uncertainty). The

largest contribution to the power defect comes from Doppler feedback. The uncertainties in the hot-to-cold reactivity swing, at the 2σ level, are determined from the root-mean-square combination of hot-full-power and shutdown temperature uncertainties with $\pm$ 20% Doppler coefficient, $\pm$40% for each of the radial and axial expansion feedbacks, and $\pm$60% for the sodium density feedback. Also included is a worst-case uncertainty for assembly bowing which would lead to an additional positive reactivity component (core compaction) during shutdown.

b. Maximum Reactivity Fault

The maximum reactivity insertion in any anticipated operational occurrence is postulated to occur upon the withdrawal of the highest worth inserted control rod from its furthest inserted to the full out position. Although mechanical and electrical systems are provided to preclude this event, the resulting positive reactivity insertion envelopes other postulated operational faults and is, therefore, imposed on the shutdown requirements of both the primary and secondary control systems.

The maximum depth of insertion of the row 7 corner primary control bank is determined by the inserted worth required to compensate for the planned excess reactivity (excess fuel loading) for burnup requirements plus a combination of criticality and feedback uncertainties resulting in the highest anticipated excess reactivity in the system at any particular time-in-life. For example, at the beginning of cycle 5 (see Table 4.3-29), the excess fuel loading of 2.86% Δk plus the root-mean-square combination of minimum hot-to-cold feedback (0.29% Δk), maximum criticality prediction uncertainty (0.43% Δk), and maximum fissile content tolerance (0.28% Δk) results in a maximum anticipated excess reactivity of 3.45% Δk (2.86 + .59). This excess is compensated by an expected row 7 corner primary control rod bank insertion of about 16.7 inches (21.9 inches with minimum worths). The maximum reactivity fault is postulated to occur upon the withdrawal of one of these row 7 corner control rods from the furthest bank insertion (plus 1.5 inch out-of-bank tolerance). It will be shown in Section 4.3.2.6 that the worth of a single control rod withdrawn from an inserted row 7 corner bank is substantially larger than the "average" worth of the rods in the bank. This rod interaction effect for the banked conditions discussed above at the beginning of cycle 5, increases the worth of the rod runout approximately 66% over the average row 7 corner single rod worth in the bank. Consequently, at
51 the beginning of cycle 5, the maximum reactivity fault is taken

to be 0.98% Δk (3.45% Δk maximum excess reactivity divided equally among 6 row 7 corner inserted rods, increased by the out-of-bank tolerance, and then multiplied by a 1.66 rod interaction factor). The maximum reactivity fault values for other times-in-life are determined in a similar manner.

c. Reactivity Excess

The fuel enrichment requirements in CRBRP are based upon guaranteeing hot-full-power criticality at the end of each burnup cycle. Consequently, at times-in-life other than the end-of-cycle, some reactivity excess is present in the reactor. The primary control system (only) is designed to compensate this excess. Fuel burnup over the cycle is the largest reactivity margin which is included in the excess. Other reactivity effects, which include power defect uncertainties, fuel loading and core geometry tolerances, refueling worth, and criticality calculation uncertainties, are combined statistically and added to the nominal, resulting in a one-sided probability distribution which gives approximately 84% confidence (at the + 1σ level) that the fuel loadings will supply at least enough reactivity to meet the stated design fuel burnup lifetime requirements.

The criteria by which the reactivity excess is determined at any time-in-life is discussed in Section 4.3.2.1.1, "Fuel Enrichments and Loadings". The primary control rods must have sufficient worth at any time-in-life to suppress this excess reactivity.

d. Criticality Uncertainty

Control margin is included in the primary system (only) to compensate for the high-side of the 0.43% Δk (2σ) biased cold criticality prediction uncertainty. This value is derived from the analysis of ZPPR-7 critical experiments as the RMS sum of the 2σ ZPPR eigenvalue uncertainty and the uncertainty in the application of this bias to CRBRP.

e. Fissile Tolerance

Control margin is also included in the primary system (only) to compensate for the high-side of the 0.5% batch fissile content tolerance in the fuel. The batch fissile content tolerance results in a ± 0.28% Δk excess reactivity uncertainty.

51

f. Miscellaneous Uncertainties

Fuel pellet stack height and impurities uncertainties were included in the fuel enrichment (start-of-cycle excess reactivity) requirements discussed in Section 4.3.2.1.1 to assure that the fuel loadings provided sufficient excess reactivity to compensate for potential reactivity deficits from variations in fuel column height and axial alignment and from the presence of neutron-absorbing impurities in the system. However, it is not necessary to cover the other side of these same uncertainties in the control requirements. That is, the potential for too much excess reactivity from these particular sources is already included in the nominal calculations which consider the highest core reactivity state resulting from the most compact core (axially aligned pellet stacks) and no impurities.

Burnup reactivity swing uncertainties could affect the core reactivity state at times-in-life other than with a fresh core loading. The burnup reactivity swing uncertainty is, however, considered to be one-sided. That is, we do not consider the potential for the core to be in a higher-than-expected reactivity state at the end-of-life due to a gross overprediction of the burnup reactivity deficit.* Therefore, the burnup reactivity swing uncertainties are not included in the control requirements.

---

* The burnup reactivity swing uncertainty, which is included in the fuel enrichment (excess reactivity) requirement, accounts for 1) the expected underprediction of the lumped fission product worth, 2) the expected overprediction of core conversion ratio, 3) the expected irradiation-induced fuel swelling, and 4) the expected Np^{239} reactivity deficit at the end-of-life. All of these expected deviations from the nominal calculated burnup reactivity swing act more as biases rather than uncertainties, and they tend to make the nominal calculated burnup reactivity deficit smaller than expected (hence, the end-of-life reactivity state is already higher than expected which is conservative from the standpoint of control rod requirements but must be included in the fuel
51 enrichment requirements).

4.3.2.6 Control Rod Worths

The locations of the primary and secondary control rod banks are shown in Figure 4.3-1. The principal components and dimensions of the control assemblies are summarized in Table 4.3-1.

The available control worths in the primary and secondary systems were calculated for a variety of control configurations as a function of time-in-life. The analytical technique used in these calculations is summarized in Figure 4.3-31. Microscopic cross sections for the primary and secondary control rods were generated from ENDF/B-III data (Ref. 15) with the XSRES/1DX code (Appendix A) in a central control channel surrounded by fuel. The cross sections were resonance self-shielded and collapsed to 9 energy groups in the appropriate spectral zones. Nine-group macroscopic control assembly cross sections were homogenized over the full hexagonal subassembly. This was done by volume and transport flux-disadvantage weighting the microscopic cross sections in the rod bundle, the surrounding duct and sodium volumes using their respective atom densities. The resulting macroscopic control rod cross sections were used in coarse-mesh, two-dimensional (120 degree, hexagonal) direct eigenvalue difference calculations (2DB) to determine the reactivity worth of the inserted control banks. The axial neutron leakage used in these problems was modeled from a group-independent, zone-dependent buckling obtained from an RZ model of the reactor at this particular time-in-life.

The burnup-dependent spatial distributions of fuel and fission products were modeled explicitly in the control rod worth calculations. Additionally, the secondary control rod worths were determined for an initially critical core configuration with the row 7 corner primary control rod bank partially inserted.

The calculated primary and secondary control rod worths are shown in Tables 4.3-29 and 30, respectively.

The nominal calculated control rod worths may contain uncertainties attributable to methods and modeling approximations, cross section uncertainties, the use of few-group, coarse mesh, two-dimensional diffusion theory, and others. Consequently, the control rod worth analysis methods and data are biased using calculations and measurements of control rod worths in the ZPPR-7 and 8 critical experiments. ZPPR-7 and 8 are pre-EMC (Engineering Mockup Critical) mockups of the heterogeneous CRBRP core configuration. Control rod bank worth (R4, R7C, and R7F) measurements were performed in both beginning-of-life (clean blankets) and end-of-life (plutonium loaded in the inner blankets) configurations. In addition, extensive measurements were made of single and asymmetric-bank worths in order to assess the accuracy of first-in and first-out control rod interaction factors. The analysis of these experiments using CRBRP design methods
51 and cross-section data is summarized in Section 4.3.3.9.

For beginning-of-life conditions, the row 4 and 7 flat rod bank worths are systematically underpredicted by 10%, whereas the row 7 corner rod bank worth is only slightly underpredicted (1%) using standard few-group, coarse mesh diffusion theory. This difference is attributed to the observed tilt from the center of the core out toward the row 7 corner control channel in the calculation-to-experiment (C/E) ratios of both fission rates and small-sample reactivity worths. That is to say, the overall better agreement between calculated and measured R7C rod bank worths at beginning-of-life is most likely a result of at least partial cancellation of errors. At the end-of-life, with plutonium in the inner blankets, the rod bank worths are all consistently underpredicted by 10-12%. These biases differ markedly from the near-unity C/E ratios for rod bank worth predictions in the homogeneous-core (ZPPR-4) experiments. However, in contrast with the ZPPR-4 measurements where coarse mesh and diffusion-transport effects approximately canceled, the ZPPR-7 control rod worth calculations have been shown to be very sensitive to mesh structure. In fact, adjusting the aforementioned ZPPR-7 control rod worth biases for the difference between the ZPPR mesh structure (1 mesh per ZPPR-drawer or 4 meshes per "assembly") and the CRBRP mesh structure (6 meshes per assembly) lowers the bias factors about 4%, to 0.97 for the R7C rods at beginning-of-life and 1.05 to 1.06 for the remaining rod banks at the beginning or end-of-life. The worth-weighted primary control system (R4 + R7C) bias is, therefore, near unity; and the secondary control system bias is greater than unity indicating that the calculated control rod worths are conservatively underpredicted. The unbiased Root-Mean-Square (RMS) variation in the calculation-to-experiment ratios is about $\pm 4\%$. Considering that the systematic differences in these calculated control rod worths are not yet completely understood, it has been decided not to bias the calculated CRBRP control rod worths until final resolution of these values in the Engineering Mockup Critical (EMC) experiments. Rather, the minimum worths are determined from the unbiased calculated primary and secondary control rod worths, less uncertainty (2 x 4%) from above. It is well to note that the control rod worth biases have no direct impact on the minimum shutdown worth (which is set equal to the shutdown requirement). Rather, the control rod worth biases only enter into the determination of the minimum B^{10} loading (enrichment) required to satisfy the safe shutdown requirements. At the present stage of the CRBRP design, the primary and secondary control rod worths continue to be specified with fully enriched (92% B^{10}) B_4C, and the calculated worths exceed the shutdown requirements by a substantial ($\sim$10%) margin as indicated in Tables 4.3-29 and 30 (i.e., the "minimum" B^{10} loading is not being specified at this time).

The control rod worths, reported in Tables 4.3-29 and 30, represent expected configurations with symmetric bank insertion patterns. Significant rod interaction effects exist between the rods within a given bank and between banks due to flux redistribuion in the reactor in response to the insertion of the highly enriched poison. Table 4.3-31 summarizes various control rod interaction effects* for single

*Interaction defined as relative rod worth normalized to the "average" rod worth in a bank where, for example, the average rod worth in a
51 6-rod inserted bank is one-sixth of the total inserted bank worth.

rods inserted in a clean core, asymmetric banks inserted, etc., determined from a series of parametric two-dimensional rod worth calculations with a 360° full-core model. Of special significance is the higher worth of a single row 7 corner rod removed from an inserted bank (first-out effect) which directly impacts the maximum worth available in a rod runout event. Figure 4.3-32 shows the variation in first-out row 7 corner rod interaction factor with depth of bank insertion. The worth of single rods inserted in a clean (or symmetrically poisoned) core are significantly lower than the average in the bank (first-in effect). The minimum worth of 5-out-of-6 secondary control rods is strongly influenced by whether the stuck secondary control rod is adjacent to the faulted primary rod which has been withdrawn (in which case the stuck secondary rod occurs in a local flux peak and is worth nearly twice as much as the average secondary rod) or opposite to the faulted primary rod.

Control rod interactions and flux tilting effects were investigated in ZPPR-7G (Section 4.3.3.9) where it was shown that control rod interaction factors (ratios of single first-in or first-out rod worths or asymmetric rod cluster worths to average rod worths in a symmetric bank) can be calculated with an accuracy somewhat better than the rod bank worths themselves. For a large number of measurements in ZPPR-7G, the ratio of calculated to measured rod interaction factors was 0.99 ± .01 which is well within the ±4% control rod worth uncertainty.

The control requirements specify that each of the primary and secondary control systems must perform their stated safety functions assuming the failure of a single active component. This is interpreted to be the failure of the highest worth single control rod in the system to respond to the trip signal (i.e., a stuck rod).

In the primary system, the stuck rod is the highest of either a fully withdrawn row 4 rod or a partly inserted row 7 corner rod. If a row 4 rod is stuck, then by definition all the row 7 corner (plus the 2 remaining row 4) rods scram, including the rod which is running out, thereby removing the reactivity fault. If a row 7 corner rod fails (other than the faulted rod which is running out), then the rod running out scrams, again removing the reactivity fault. If, however, the rod running out is also the primary rod which fails to respond to the scram then one has the largest realizable net positive reactivity insertion which must be compensated by the negative reactivity insertion from the remaining primary rods. In no case can this net reactivity (run-out plus stuck rod) exceed the worth of one row 7 corner rod with the maximum (full-in to full-out) first-out rod interaction effect. Therefore, the highest stuck primary rod worth is determined by:

[worth of average row 7 corner rod * full first-out rod interaction factor] - rod run-out (requirement),

51

where the worth of the average row 7 corner rod is one-sixth of the total row 7 corner bank worth and the full first-out rod interaction factor, from Table 4.3-31, is 2.11 at beginning-of-cycle or 1.66 at end-of-cycle. It should be noted that this is an entirely self-consistent definition of reactivity fault and the stuck rod worth. That is, for any smaller reactivity fault within the allowed criticality uncertainty band width, the stuck rod worth would be proportionately larger, thereby maintaining the relationship between the worth and requirement in Table 4.3-29 such that the capability will always exist for the primary control system to satisfy the stated design safety function.

For the secondary control system in Table 4.3-30, the minimum shutdown capability occurs when the (highest worth) stuck secondary rod is adjacent to the faulted primary control rod which is running out at the beginning-of-life (interaction effect from Table 4.3-31 is 2.01). This is the value used at the start of each cycle in Table 4.3-30. Since the limiting secondary control rod capability (minimum shutdown margin) occurs at the beginning-of-life, and since the control rod interaction factor decreases with burnup as the primary control rod bank is withdrawn, this interaction factor is conservatively applied at all times-in-life in Table 4.3-30.

The minimum primary and secondary control rod worth capability is determined by reducing the nominal calculated rod worth by the 2σ (8%) uncertainty and subtracting the highest worth stuck rod from each system as described above. As shown in Tables 4.3-29 and 30, the minimum control rod worths exceed the maximum requirements at all times in life, which satisfies the safety design criteria.

It should be noted that these requirements are satisfied even under the extremely pessimistic, postulated accident assumptions that: the highest worth burnup and load-follow rod is uncontrollably withdrawn, one of the two independent, shutdown control systems fails to operate, and the highest worth control rod in the operating system remains stuck in the fully withdrawn position.

The integral rod worth characteristic curve, fraction of worth withdrawn vs. fraction of rod bank distance withdrawn, over the operating range of fully inserted to fully withdrawn is presented in Figure 4.3-33. The integral rod worth is well approximated by a $\sin^2$ function of rod bank height, with a slight downward skew (phase shift) resulting from the relatively low worth of the uppermost regions of the core caused by the parked control rods in the upper axial blanket.

The primary control rods serve both as a burnup operational control system and as the primary shutdown system. The fraction of the
51 total primary system reactivity worth which is available for shutdown

rod at a time. The nominal design rod withdrawal rate is 9 inches per minute, although a rod could be driven out of the core at maximum rate of 73 inches per minute in the event of a controller failure. Control rod outmotion in the unlatched condition is not considered credible, as is discussed in Section 4.2.3, and in any event would be limited by the out-motion pawl. An uncontrolled withdrawal of the highest worth control rod (the nominal calculated rod worth with the high side uncertainty, the maximum B-10 content and the highest rod interaction factor) at ramp runout rates of 9 and 73 inches per minute ("anticipated" and "unlikely" class accidents, respectively) would result in peak reactivity insertion rates of 4.1 and 32.9 ¢/sec, respectively at the highest point on the differential worth curve near the core midplane. The values corresponding to minimum shutdown margin conditions are 2.4 and 19.1 ¢/sec, respectively.

4.3.2.7 Criticality of Fuel Assemblies

Two aspects of the criticality of fuel assemblies are discussed in this section. First, the uncertainty in the prediction of the absolute eigenvalue for CRBRP is considered. This result has a direct impact on the calculation of the feed enrichments and the control shutdown margins for the first and equilibrium cycles. Second, the criticality of small bundles of fuel assemblies is discussed in detail. These results impact the safety related aspects associated with the determination of the minimum number of fuel assemblies required for criticality.

4.3.2.7.1 Reactor Eigenvalue Prediction

The uncertainty in the CRBRP eigenvalue prediction is obtained from analysis of zero power fast critical assemblies which mock-up the composition and geometry of the CRBRP core. One major difference between the experimental configuration and the CRBRP core is the use of fuel plates in a square lattice in place of the cylindrical fuel pins in a hexagonal array. Another difference is the extrapolation of the room temperature reactivity, obtained in the critical assembly, to that expected in the hot-full-power reactor.

The accuracy of design eigenvalue calculations is evaluated by a comparison of calculated and measured criticality in ZPPR. Table 4.3-33 lists selected measured and calculated room temperature eigenvalues (k_{eff}) for several ZPPR experiments modeling both homogeneous (ZPPR-4) and heterogeneous (ZPPR-7) core configurations. Using the CRBRP design method (coarse-mesh, XY diffusion theory
51 in this case) and data (ENDF/B-III cross sections in 9 energy groups)

results in a systematic underprediction of the reactor eigenvalue with an average C/E ratio of 0.996 ± 0.003 in the homogeneous systems and 0.990 ± 0.002 in the heterogeneous systems. The inverse of the average C/E ratio is applied as a bias in the calculation of CRBRP criticality (using the same calculational methods and data base) and the 1σ variation is included as an uncertainty in the start-of-cycle excess reactivity requirement. In order to use such an eigenvalue bias, one must consider the sensitivity of the eigenvalue to particular ZPPR parameters (plate heterogeneity correction as discussed in Reference 16, streaming and the like) which are not present in the power reactor and which may therefore introduce errors in the extrapolation of the ZPPR-bias to the power reactor. Consequently, an additional uncertainty of 0.2% Δk is included to account for potential systematic uncertainties in the k_{eff} bias arising from extrapolation of the heterogeneous plate-geometry ZPPR k_{eff} bias to the nearly homogeneous pin-geometry power reactor.

In order to establish the criticality of the hot-full-power CRBRP, a cold-to-hot temperature defect correction is applied to the cold-critical eigenvalue. The temperature defect accounts for the net reactivity loss from Doppler feedback, radial and axial core thermal expansion, sodium density changes, etc., in the escalation to hot-full-power conditions. The calculation of the temperature defect is discussed in Section 4.3.2.3.5. The uncertainty in the components of the temperature defect are combined statistically with the cold criticality uncertainty to establish the overall uncertainty in the hot-full-power reactor eigenvalue.

4.3.2.7.2 Minimum Critical Configuration

The highest expected fuel enrichment under equilibrium cycle conditions in CRBRP with low-240 grade plutonium fuel is 33.1 weight percent. Consideration of worst-case criticality uncertainties, highest fissile content tolerance, and simultaneous refueling of the entire core (including fuel, inner, and radial blankets) results in a 35.0 weight percent fuel enrichment envelope. A cluster of fresh fuel assemblies with the maximum fuel loading would contain a minimum number of assemblies required to achieve a critical configuration. Critical eigenvalue calculations were performed for various numbers of these maximum enrichment fuel assemblies in a regular hexagonal array spaced with a reactor pitch corresponding to refueling temperature. The assembly cluster was assumed to be immersed in a sodium pool with no control or blanket assemblies. One-dimensional S_4, Po, 21-group fundamental mode eigenvalue calculations were performed in ANISN to determine k_{eff} as a function of the number of fresh fuel assemblies in concentric annular rings. Axial leakage was modeled by buckling factors determined from two-dimensional, RZ
51 geometry, diffusion theory calculations.

The equations describing the temperature dependence in the reactor are a simplified version of the ones in the computer code DEMO (Appendix A). All coefficients are assumed constant at nominal full-power conditions. The average channel in the core is modeled with seven axial nodes, one each for upper and lower axial blankets and five evenly spaced nodes in the fuel region. Radially, three nodes are used; one in the fuel, one in the clad, and one for the sodium coolant temperature at the node exit. Inner and radial blankets are modeled with seven evenly spaced axial nodes. Radially, three nodes are used; one in the fuel, one in the clad and one for the sodium coolant temperature at the node exit. The equations described thus treat only internal reactivity feedback mechanisms. Specifically, the effect of control system response, operator intervention and plant system operation resulting in variation in inlet coolant temperature and flow, are not included.

The above set of linear first-order differential neutronic and thermal equations is mathematically expressed as:

$$\dot{\underline{X}} = \underline{A}\,\underline{X} + \underline{b}\,\delta k_e \qquad (8)$$

where A is a 70 x 70 matrix. The feedback network of this system is shown in Figure 4.3-41. The various reactivity coefficients used in the analysis are discussed in Section 4.3.2.3.

The criterion for absolute stability is based on Liapunov's "first method" (Ref. 17) which reduces the problem of determining the stability of the system to that of finding the eigenvalues of the matrix $\underline{A}$ of equation (8)*. If the real part of all roots is negative, the system is stable. Conversely, if the real part of any root is positive, the system is unstable. The GASA program (Appendix A) is used to determine the eigenvalues of matrix $\underline{A}$ of equation (8).

The GASA program is also used to generate transfer functions for various combinations of reactivity feedback coefficients. The transfer functions at beginning and end of equilibrium cycle are shown in Figures 4.3-42 through 44. Normalization is at 100 Hz to zero
56 decibels (DB) since at that frequency all feedback effects have negligible effect and the -20DB/decade roll-off due to the finite prompt neutron lifetime has not become apparent. The stability analysis was performed for an early version of the CRBRP heterogeneous core configuration in which the predominant negative Doppler feedback was slightly smaller than in the current design. The results of the stability

---

* The eigenvalues of matrix $\underline{A}$ are identical to the roots of the
51 characteristic equation of the system.

analysis presented herein are therefore somewhat conservative and the qualitative characteristics and the inherent reactor stability are valid. The interpretation of the transfer functions for the various reactivity feedback coefficient combinations is presented below.

a. Zero Power-Zero Feedback Transfer Function

The transfer function of the system at zero power with no feedback is shown in Figure 4.3-42, Curve A. The characteristic equation has one root equal to zero, which shows up in the -20DB/decade slope of the curve at low frequencies; i.e., the system acts as a pure integrator at low frequencies. Therefore, the system is unstable at zero frequency. This is expected since zero frequency corresponds to a constant reactivity insertion. In a system with no feedback, the power will increase indefinitely, thus invalidating the zero power transfer function. The utility of curve A is that it provides a basis to compare the stabilizing effect of feedback effects. A transfer function of lower magnitude than that of the zero power transfer function will be more stable and one of larger magnitude will be less stable at the particular frequencies where these differences occur.

b. Sodium Density Feedback

The transfer function of Figure 4.3-42, Curve B, results if credit is taken for the sodium density feedback only. The system is stable since all roots of the characteristic equation have negative real parts. This transfer function, which includes only the smallest negative feedback mechanism, already results in a noticeable improvement in stability as compared to the zero-power, zero-feedback transfer function.

c. Axial Expansion Feedback

Considering only the negative feedback due to axial expansion of the fuel (active core region only) results in the transfer function shown in Figure 4.3-42, Curve C. This feedback effect is noticeably stronger than the sodium expansion feedback.

d. Doppler Feedback

Curves D and E (Figure 4.3-42) depict transfer functions obtained when only the Doppler feedback is considered, with Curve D, representing the case where credit was taken for only half the nominal Doppler feedback, and Curve E, the case where the nominal Doppler feedback was used. It is apparent that the Doppler constant represents the strongest feedback mechanism, even
51 taken at half its nominal value.

FORE-2M reactor kinetics and feedback model. As a further conservatism a dynamic bowing reactivity function (Figure 4.3-45) was defined in order to envelope the dynamic uncertainties associated with thermal time constant differences between the fuel and blanket assemblies. The dynamic function applies during that portion of the transient when the fuel assembly duct temperatures are changing rapidly (on the order of $50^{o}F$/second). The static function applies during the portion of the transient when the fuel assembly duct temperatures are changing slowly (less than $5^{o}F$/second). The duct temperature used in the model was determined from the assembly coolant temperature as shown schematically in Figure 4.3-41.

Additional conservative features which were employed in the model were:

1. Minimizing the negative Doppler reactivity effect.
2. Evaluating the results at the hottest fuel, cladding and coolant locations in the reactor.
3. Neglecting the ~2 second delay of the duct temperature relative to the coolant.

Figures 4.3-46 through 49 illustrate key reactor responses during an inherent response transient (no control or PPS action) initiated at a reactor startup operating point (8% power; 40% flow) at which the reactivity insertion due to bowing would be maximum. The transient was initiated by a +2¢ step reactivity perturbation.

The responses illustrate that all parameters rise initially due to the dominance of positive bowing reactivity at low power/flow ratios. However, when the bowing reactivity coefficient becomes negative at higher power flow/ratios, all parameter responses change slowly and approach a new stable equilibrium state. The final values of the parameters are shown in Table 4.3-34 together with acceptability limits.

It is concluded that if the limits for acceptability (Table 4.3-34) are selected so as to remain below reactor parameter severity levels associated with a major incident (Table 15.1.2-1), and parameter responses remain below acceptability limits, the reactor is stable in the practical sense and inherent reactor protection shall have been demonstrated.

Additional reactor stability (inherent response) transients have been evaluated which were initiated at other operating states (i.e., reactor flow, reactor power, etc.). All of these indicate the response characteristics typically exhibited in Figures 4.3-46 through 4.3-49 and were bounded by the acceptability levels of
51 Table 4.3-34.

As a result of these studies, it is concluded that the reactor is stable given the bowing reactivity characteristics exhibited in
56 Figure 4.2-92a since all transient responses are bounded for a bounded input perturbation. Furthermore, the reactor is stable in the practical sense since the maximum values of key reactor variables are below levels which are considered acceptable for the reactor when responding to its inherent feedbacks. Therefore, reactor inherent protection is demonstrated and Criterion 9 is satisfied.

4.3.2.9 Vessel Irradiation

The spatial and energy dependent neutron flux distributions are utilized in obtaining the irradiated characteristics of the reactor structural materials and components. One application of this flux data is in determining the total and fast fluence received by both replaceable and non-replaceable reactor components. The neutron fluence must be limited so that the end-of-life ductility for structural materials exceeds the specified minimum requirements.

Assembly-by-assembly radial neutron flux distributions (assembly-average in the central 36-inch active core height) are given in Figures 4.3-50 and 51 for core conditions reflecting the beginning of cycle one with the six row 7 corner primary control rods partly inserted and with fresh fuel and clean blankets, and for the end of cycle four conditions with all control rods fully withdrawn and with plutonium burned out of the fuel and built up in the blankets. Values are shown in Figures 4.3-50 and 51 for both the total neutron flux and for the fraction of the flux with an energy greater than 0.11 MeV. The latter reflects the relative spectral behavior throughout the core. The shift in the critical flux shape toward the center of the core with increasing burnup, and the spectral hardening in the blankets, is evident by comparing the fluxes in Figure 4.3-50 at the beginning-of-life with the end-of-life fluxes in Figure 4.3-51. Figures 4.3-52 and 53 show typical axial distributions of the total flux and the fast flux fraction in the core. These axial distributions are normalized to 1.0 over the central 36-inch active core height such that the product of the axial shape factors in Figures 4.3-52 and 53 with the fluxes in Figures 4.3-50 and 51 results in the three-dimensional flux distribution throughout the central core and blankets. The total flux in Figure 4.3-52 exhibits the typical bell-shaped axial distribution. Figure 4.3-53 indicates that the neutron energy spectrum (as measured by the fraction of the flux with an energy greater than 0.11 MeV) is relatively flat throughout the central core and degrades rapidly through the axial blankets. These radial and axial flux and spectrum distributions were obtained from two-dimensional, 21-group diffusion calculations in hexagonal-planar and RZ geometry,
51 respectively.

The peak total and fast ($E > 0.11$ MeV) fluxes in CRBRP (5.5×10^{15} n/cm^2 sec and 3.4×10^{15} n/cm^2 sec, respectively) occur in the rows 7 and 8 fuel cluster around the row 7 corner primary control rods.

The peak total (fast) fluences in the fuel and inner blanket assemblies have been determined for cycles one and two (first core) and for the subsequent equilibrium cycles. The first-core peak total (fast) fluences for the fuel and inner blanket assemblies are 1.47×10^{23} (9.20×10^{22}) neutrons/cm^2 and 1.46×10^{23} (8.66×10^{22}) neutrons/cm^2, respectively. For the equilibrium core, the peak total (fast) fluences of the fuel and inner blanket assemblies are 2.38×10^{23} (1.45×10^{23}) neutrons/cm^2 and 2.29×10^{23} (1.35×10^{23}) neutrons/cm^2, respectively. The most conservative estimate of the neutron flux at the reactor vessel boundary is obtained at the beginning of equilibrium cycle. Later in life, the flux has shifted toward the center of the core and away from the core periphery in response to the inner blanket plutonium buildup, and therefore, the corresponding vessel fluxes would be somewhat lower. Table 4.3-35 summarizes the flux and spectrum data for the core, core and shield boundaries, core barrel, and the reactor vessel wall at the beginning of equilibrium cycle.

4.3.3 Analytical Methods

Each preceeding section described briefly the neutron data and computer codes used in the analysis. In most cases, calculational flow diagrams were presented for the particular analysis. This section describes the overall analytical techniques used in analysis of CRBRP and the supporting critical experiments performed in the ZPPR assemblies.

4.3.3.1 Analytical Approach

The CRBRP analytical methodology is summarized in Figure 4.3-54. Specific details about the development of particular nuclear characteristics were discussed in the preceeding subsections. The core mockup experiments in ZPPR are analyzed with the same CRBRP design methods and cross-section data as described in Figure 4.3-55.

The multigroup cross-section libraries for CRBRP (or for ZPPR) are developed using the Bondarenko formalism (Reference 20). A generalized cross-section file, consisting of infinitely dilute fine-group cross sections, inelastic scatter transfer matrices, and temperature dependent self-shielding factors as a function of
56 σ_0 (the total cross-section per atom), is obtained from the ENDF/B-III data file by way of the MINX* or ETOX* code. Using atom densities

51 * Appendix A contains computer code abstracts.

and cell models from the reactor or critical assembly, resonance self-shielding factors are calculated in the SPHINX* (XSRES) resonance module for each isotope as a function of temperature and non-resonant total cross-section (σ_0) using an iterative scheme whereby the self-shielding factors are used to calculate σ_0 for the mixture and σ_0 and temperature are then used to interpolate new self-shielding factors. A Dancoff correction is applied to the cross-sections using Sauer's approximation for a cylindrical fuel pin in a hexagonal lattice (reactor design calculations) or Bell's approximation for plate lattices (critical assembly calculations). The resulting cross-sections are corrected for elastic removal and collapsed (condensed) to the desired few-group structure (9 or 21 neutron energy groups are generally used in CRBRP nuclear design calculations) in the SPHINX* (1DX) diffusion module. Both the elastic removal correction and group condensation are performed over the local reactor spectrum obtained from a one-dimensional (cylindrical or slab) diffusion calculation. Due to the size of the fuel plates in the ZPPR criticals, these cross-sections are further corrected for the in-cell fine structure in the flux by applying spatial flux-weighted cell homogenization factors obtained from one dimensional SPHINX* (ANISN) transport calculations with P_0 scattering and S_{16} quadrature.

The resulting 9 and 21-group master cross-section libraries are employed in the W-2DB* code in both hexagonal-planar and cylindrical (RZ) geometry to determine critical reactor eigenvalue (k_{eff}), radial and axial power and flux distributions, and control rod worth parameters and to perform burnup (depletion) calculations. Reactor depletion and power distribution calculations are performed in two-dimensional hexagonal geometry with each of the fuel, inner and radial blanket assemblies modeled as a separate burnup zone in order to accurately model the spatial dependence of the fuel depletion, and blanket plutonium accumulation. Axial leakage in the hexagonal calculations is modeled as a DB^2-type absorption cross section with a region-dependent, group-independent buckling determined from an equivalent RZ geometry calculation at the beginning and end of each cycle. Using these depletion models, control rod worth parameters are determined using 2DB eigenvalue difference calculations for a variety of reactor configurations as a function of time in life. Reactivity feedback coefficients, such as Doppler constants and sodium void worth, are calculated using first-order perturbation theory (PERT-V)* and forward and adjoint flux distributions from RZ 2DB calculations.

51 * Appendix A contains computer code abstracts.

There are particular areas in the nuclear design process where the two-dimensional synthesis methods are known to be lacking
56 due to spatial inseparability. One of these areas is the prediction of the local power distribution in the vicinity of partly inserted control rods as described in Section 4.3.2.2. Another area is the determination of the sodium void worth distribution throughout the core for input to design-limiting (margin) safety analyses (Section 4.3.2.3.2). In these particular areas, three-dimensional methods with the VENTURE* code (Reference 21) have been employed for the analysis of benchmark design problems.

4.3.3.2 Neutron Cross Section Data

The cross section data used in the CRBRP nuclear design calculations is obtained from the ENDF/B-III data file. A description of the Evaluated Nuclear Data File/B Version III is given in Ref. 15. The ENDF/B-III pointwise data and resonance parameters were processed by the ETOX code (Appendix A) at HEDL and supplied as punched-card output in the Bondarenko format for final processing as described in the preceeding section. The 30 neutron energy group structure consists of basically 0.5 lethargy width groups with some subdivisions to handle the principal resonance structure of the diluents Na, Fe and O. Details of this group structure and that of the condensed 9- and 21-group sets are shown in Table 4.3-36.

The inclusion of axial and radial blankets is a primary design feature of LMFBR's. Therefore, the prediction of in-core gamma heating has become an important post-FFTF LMFBR design problem. LMFBR gamma heating is calculated for CRBRP by the neutron-gamma coupled diffusion method in which the coupling between neutron and gamma groups, which occurs due to gamma production by way of neutron interactions, is mathematically represented in the cross sections in the scattering matrix. The scattering matrix contains gamma energy yield data from fission, capture and inelastic scattering sources. The gamma energy yield cross-section matrix is developed and coupled with a neutron cross-section data set, producing an N plus G group master cross section library in a module of SPHINX*. The SPHINX neutron-gamma coupling libraries currently contain data from three basic sources:
56 (1) Westinghouse's local coupling library designed for use in the APPROPOS* code, (2) ENDF/B-IV coupling data processed through AMPX by ORNL, and (3) particle energy release data (MeV/fission) from M. F. James (Reference 22).

51 * Appendix A contains computer code abstracts.

4.3.3.3 Critical Experiments in Support of CRBRP

The LMFBR design methods and cross section data are verified by direct comparison of calculated parameters with integral measurements in critical mockup experiments. In the following sections, we will discuss the historical application of these integral experiments as benchmarks against which the accuracy of the design methods and data are evaluated and design bias factors and uncertainties are developed for application to the CRBRP (Reference 23).

4.3.3.4 ZPPR Assembly 2 and ZPR-6 Assembly 7

ZPPR Assembly 2 was the first demonstration plant benchmark critical assembly. It was designed in accordance with the general LMFBR design features envisioned by the major LMFBR contractors, including Atomics International, General Electric and Westinghouse Electric Corporation. The experimental program was developed by the Argonne National Laboratory for pin versus plate measurements in order to assess the influence of the critical assembly plate environment, which generates local heterogeneities that are significantly different than those found in the nearly homogeneous pin environment in power reactors. Special emphasis was placed on reactivity, reaction rate ratios, Doppler effects and sodium voiding. The ZPPR-2 program on pin versus plate experiments and analyses was essential to the verification of the general applicability of the plate critical experiments to the design analyses of pin geometry power reactors. Prior to the ZPPR-2 pin measurements, the only experimental data for testing heterogeneity estimates involved plate bunching experiments wherein reactivity effects of varying plate drawer arrangements were made. The pin replacement experiments provided a more direct test of heterogeneity effects even though the experimental pin cells are somewhat more heterogeneous than an LMFBR fuel assembly. Similar measurements were performed in ZPR-6-7 which is a large single-zone assembly with a cell structure and composition nearly identical to the inner core zone in ZPPR-2.

The pin versus plate measurements in ZPPR-2 and ZPR-6-7 were performed by replacing small regions of the normal plate core with pin calandria containing 16 fuel rods (0.410 and 0.348 inch cladding and mixed oxide fuel pellet diameters, respectively) within each approximately 2x2 inch drawer. Figure 4.3-56 shows a cross section view of the ZPPR-2 assembly which outlines the central pin region (69 matrix drawers) and the radial pin sector. Initial pin versus plate measurements were performed in the central 69 drawers and the pin calandria were then rearranged into the radial pin sector for later measurements. Figure 4.3-56 also shows cross sections of the
51 ZPPR-2 inner core zone plate arrangement and of the pin calandria.

In ZPR-6-7, the pin sector was comprised of 25 drawers. Axially, the ZPPR-2 pin region included the full 36 inch core height and extended 6-inches into the axial blankets, while the ZPR-6-7 pin region included only the central 24 inches of the 60 inch core height.

The evaluation and analysis of the pin versus plate ZPPR-2 measurements have been reported elsewhere (Ref. 16, 24, & 25). This data is summarized in Table 4.3-37. With the exception of the pin versus plate interchange reactivity effects, calculations at both ANL and ARD accurately reproduced the measured values for pin/plate ratios including sodium void, Doppler effect, reaction rate ratios and central Pu^{239} worth measurements (Ref.16). These results gave considerable confidence that biases and uncertainties derived for these quantities from the plate-critical integral experiments could be applied to the power reactor. However, there was a substantial discrepancy in the capability to calculate the pin versus plate interchange reactivity effect in ZPPR-2 compared to ZPR-6-7 (C/E
56 ratio of 1.64 in ZPPR-2 compared to 1.07 in ZPR-6-7). The axially longer region of pin versus plate replacement in ZPPR-2 (48 inches) compared with ZPR-6-7 (24 inches) was pointed out (Ref. 24) as a possible cause for the significant effects in ZPPR-2 due to rod/plate streaming differences. A difference of about 5-6% in diffusion coefficients between pin and plate environments was shown to be sufficient to explain the inconsistency between ZPPR-2 and ZPR-6-7 pin versus plate reactivity effects (Ref. 16 & 24). The direction-dependent streaming in the conventional pin versus plate reactivity analysis in ZPPR-2 has been confirmed by Zoltar, etc. (Ref. 26). Application of Benoist's streaming corrections (Ref. 27) to the analyses of ZPPR-2 and ZPR-6-7 put the two comparisons in reasonable consistency. The ratio of calculation to experiment for the pin versus plate fuel replacement reactivity is about 1.2 for ZPPR-2 and 1.07 for ZPR-6-7.

4.3.3.5 ZPPR Assembly 3

ZPPR-3 was a two enrichment zone assembly with each zone containing approximately 50% of the core volume. Axial and radial blankets surround the core. The drawer fuel loading pattern remained the same as ZPPR-2. The major difference between ZPPR-2 and ZPPR-3 was the simulation of a control system in ZPPR-3.

A series of critical experiments were performed in ZPPR Assembly 3 to investigate the effects of the control system on core nuclear characteristics as a part of the Demonstration Plant Benchmark Critical Program. The experimental configuration of ZPPR-3 (shown in Figure 4.3-57) was separated into 3 phases corresponding to the end-of-cycle (Phase 1B), middle-of-cycle (Phase 2), and beginning-
51 of-cycle (Phase 3) reactor control conditions. The principal reactor parameters experimentally studied in ZPPR-3 were power distri-

bution, control worth and sodium void reactivity effects. ZPPR-3 was used primarily to provide a preliminary estimate of the Demonstration Plant power and control rod worth uncertainties.

4.3.3.6 ZPPR-3 Modified Phase 3 Sodium Void Benchmark

The Modified Phase 3 configuration of ZPPR-3 was designed to more closely mockup the homogeneous core design of the CRBRP with seven inserted control rods. An extensive series of sodium void measurements were performed in ZPPR-3. The primary purpose of these experiments was to measure the reactivity effect of large sodium void zones with a number of control rods inserted. One of the measurement configurations, the 632 drawer reference void in the Modified Phase 3 configuration as shown in Figure 4.3-58, has been chosen to be the basis for the sodium void benchmark.

This series of experiments provided considerable insight into the ability of the design methodology and cross section data to predict the maximum positive sodium void reactivity worth in a CRBRP-size LMFBR. Sodium voiding was accomplished in ZPPR-3 by replacing a number of steel-clad sodium plates with empty steel cans such that only a change in sodium content occurred. The axial height of the voided zone was $\pm$ 12 inches about the core midplane which is approximately the void height which is predicted to result in the maximum positive reactivity effect. The sodium void reactivity worth was determined for void zones extending from the core centerline out to a total of 632 matrix drawers (approximately 80% of the core cross sectional area).

Figure 4.3-59 shows the two-dimensional RZ calculational model which was used for the analysis of the ZPPR-3 Modified sodium void worth experiments. First-order perturbation calculations were performed using 21-group ENDF/B-III cross section data. The results of this analysis are shown in Figure 4.3-60 for 228, 466, 510, and 632-drawer voided zones. Experimentally, the maximum positive void worth occurs at approximately 510 drawers voided where the ratio of the calculated void reactivity worth to the measured value is about 1.33. All of the calculated void worths lie within $\pm$ 50 percent of the measured values up to and including the point of maximum positive void worth, and in fact, the RZ calculation conservatively overpredicts the positive void reactivity worth. The experimental voiding patterns did not lend themselves particularly well to the cylindrical modeling in two dimensional RZ geometry. This was particularly evident in Figure 4.3-60 where the calculation-to-experiment ratios were somewhat divergent in the vicinity of the smeared row seven control ring. Consequently, a series of three-dimensional (VENTURE) perturbation calculations were performed for the sodium voiding experiments in both ZPPR-3 Phase 3 and Phase
51 3 Modified configurations. The results of these calculations are shown

in Figures 4.3-61 and 62, respectively. The three-dimensional calculations produced void reactivity worth results which were within ± 10 percent of the measured values for the Phase 3 experiments and ± 4 percent of the measured values for the Phase 3 Modified experiments. This overall good agreement suggests that the design method and data can indeed accurately predict the worth of large-scale sodium voiding so long as the void zone is confined to the strongly moderation-driven positive void worth regions of the core.

4.3.3.7 ZPPR-4 (Pre-Engineering Mockup Critical for Homogeneous CRBRP)

The primary objectives of the ZPPR-4 program were to verify the homogeneous CRBRP core nuclear characteristics including power margins for the first and equilibrium cycles, control rod worth characteristics and the effect of control insertion patterns on the core power distribution, and radial and axial blanket effects. The reference ZPPR-4 configuration is shown in Figure 4.3-63. The drawer fuel loadings and core layout of ZPPR-4 closely simulated the CRBRP first-core configuration.

The detailed results of the analysis of the ZPPR-4 experiments are presented in References 28 and 29. Table 4.3-38 summarizes the measured and calculated eigenvalues for the four phases of ZPPR-4. The calculations systematically underpredict the critical eigenvalue resulting in a k_{eff} bias of 1.0036 and an uncertainty of ± 0.0031 (1σ).

Foil activation measurements of Pu^{239} (n,f), U^{235} (n,f), U^{238} (n,f), and U^{238} (n,γ) (for the prediction of blanket plutonium buildup and core conversion ratio) reaction rates and TLD measurements of gamma heating rate support the determination of the power distribution uncertainty throughout the core and blankets. Foil and thermoluminescent dosimeter (TLD) irradiations are performed at a large number of locations throughout a symmetric core sector at both the core midplane and for axial distributions in selected fuel and blanket drawers. Special emphasis is placed on enrichment-zone, blanket and reflector interfaces, as well as regions surrounding inserted control rods. The pointwise foil data are corrected for cell fine-structure through a combination of cell calculations and drawer-averaging measurements, making the measured reaction rate data compatible with homogenized-drawer calculations. In order to avoid a first-order uncertainty in the normalization to ZPPR power level, the calculated reaction rates are normalized such that the total calculated Pu^{239} fission rate in the fuel is equal to the total measured value. This is nearly
51 equivalent to a power level normalization since Pu^{239} fission accounts

for 80-90% of the total reactor power. The remaining reaction rates are then compared based on this same power (flux level) normalization. Complete details of the analysis of the ZPPR-4 reaction rate measurements are given in References 28 and 29. Table 4.3-39 summarizes this analysis in terms of a mean or average calculation-to-experiment (C/E) ratio and a 1σ variation about this mean, with each calculated distribution being power (flux) normalized to the measured Pu^{239} fission rate as described above. The normalization factors indicate that U^{235} fission is overpredicted by about 2% relative to Pu^{239} fission, and U^{238} fission is unpredicted by nearly 7%, suggesting an underprediction of the high-energy fluxes in the few-group diffusion calculation. U^{238} capture is overpredicted by nearly 6% relative to Pu^{239} fission, indicating an overprediction of the end-of-life blanket plutonium content. Several general trends are noted in the data. Most importantly, it appears that the standard power reactor design calculational method does a good job of predicting the power distributions throughout a great majority of the core. The RMS variation in the C/E ratio for the important Pu^{239} fission rate is less than $\pm 2\%$. There does tend to be some degree of misprediction of the C/E ratios across the inner core/outer core boundary and the core/blanket interface. The largest differences show up in the radial blanket where the C/E ratios consistently fall off approximately 10 to 15% in the vicinity of the blanket/reflector interface which is generally a low power region. The normalized axial reaction rate distributions indicate a 2-3% overprediction of the midplane values with respect to the core-average, resulting in an overprediction of the axial peak-to-average ratio. Correspondingly, these same C/E ratios are low by about 5% in the vicinity of the core/axial blanket interface.

The ability to accurately and reliably predict the minimum available control rod worth in a variety of reactor configurations is clearly important in the design of reactors. Consequently, a substantial amount of effort has been expended in the recent ZPPR program, commencing with ZPPR-3 and 4, toward confirmation of control rod worth calculational methods and the establishment of calculational bias factors and uncertainties. The analysis of the ZPPR-4 control rod worth measurements is contained in References 28 and 29. Table 4.3-40 summarizes the results of ZPPR-4 control rod bank worth calculations using the standard power reactor coarse mesh, two-dimensional diffusion theory methods with 9-group ENDF/B-III data. Overall, the control rod bank worths were well predicted, confirming the adequacy of the design calculational method, with calculation-to-experiment ratios ranging from 0.95 to 1.04. There is a very slight tendency to underpredict the worth of the central and inner ring (row 4) rods. The average control rod worth bias (inverse of the calculation-to-experiment ratio),
51 based on 27 control rod worth measurements in all four phases of ZPPR-4 is 1.01 ± 0.02 (1σ). In addition to the determination of the control

rod worth bias and uncertainty, a number of special experiments were performed to investigate particular design problems. Among these special experiments were the determination of the worth as a function of B-10 enrichment (B_4C loading), the measurement of several data points on the integral worth curve for partly inserted rod banks (ZPPR-6), and the confirmation of the worth reduction associated with a tightly clustered control absorber bundle (ZPPR-4).

4.3.3.8 ZPPR-5 (HCDA Engineering Mockup Critical for Homogeneous CRBR)

Upon completion of the ZPPR-4 program, an Engineering Mockup Critical program for CRBRP was initiated. The program was to consist of measurements and analysis of two distinct configurations. The first, ZPPR-5, was designed to provide HCDA related measurements, and the second, ZPPR-6, was to provide measurements of basic design related parameters such as power distributions and control rod worths. Due to the implementation of the ZPPR-7 program for the heterogeneous core (Section 4.3.3.9), only the ZPPR-5 results are considered herein.

ZPPR-5 investigated such HCDA related parameters as sodium voiding, steel slumping, fuel slumping and Doppler feedback. The sodium voiding experiments encompassed portions of the core and the upper axial blanket in a sequence representative of a hypothetical power reactor voiding pattern. Two-dimensional RZ analysis indicated a non-statistical uncertainty of $\pm 20\%$ in regions of large positive voiding worths (central core regions). The error is much larger in the axial blankets due to the inability of the method to accurately predict neutron streaming in the plates. Three-dimensional (XYZ) perturbation theory analysis has been performed in the voiding sequence in ZPPR-5 but has indicated no significant improvement in the uncertainty. It should be noted that the voiding was not confined axially to $\pm$ 12 inches as was the case in the ZPPR-3 experiments but extended into the axial blankets in order to model a representative sodium voiding sequence. Voiding was performed in the axial blankets prior to the fuel height region. Consequently, the uncertainty in these predictions are larger than ZPPR-3 due to the enhanced neutron streaming. The neutron streaming effect due to plate heterogeneity in the criticals will not be so predominant in power reactors because
56 of their more homogeneous material distribution.

4.3.3.9 ZPPR-7 (Pre-Engineering Mockup Critical for CRBRP Heterogeneous Core)

The purpose of the ZPPR-7 program was to provide pre-EMC design support for the heterogeneous CRBRP core arrangement. Information
51 mation obtained from this program was used to validate and provide

preliminary design bias factors and uncertainties for the CRBRP heterogeneous core physics characteristics, and to affect the selection of the CRBRP core layout and fuel management scheme. The experimental program was divided into a number of phases, highlighted by a clean benchmark configuration with annular blanket rings and no control rod or control channel heterogeneities; simulations of both a clean, beginning-of-life, core with fresh blankets and a burned, end-of-life, core with depleted fuel and plutonium buildup in the internal blankets; and various simulations of control pattern effects on core characteristics. The initial ZPPR-7 configurations modeled an early version of the CRBRP heterogeneous core layout. These measurements were followed by a brief series of experiments which validated the earlier results in a mockup of the final CRBRP heterogeneous core configuration in Figure 4.3-1. The analysis and description of the ZPPR-7 measurements is contained in References 30 and 31. Figure 4.3-64 shows the core layouts for the principal ZPPR-7 configurations.

ZPPR-7A was a benchmark configuration with clean (no plutonium) annular blanket rings inside a single enrichment core with no control rods or control rod channels which was intended to isolate the characteristics of the heterogeneous core geometry. The principal experiments investigated criticality, key isotopic neutron reaction rate distributions and sodium void worth.

The Phase B core was rearranged to provide a better simulation of a CRBRP fresh core with 12 control rod channels (6 in row 4 and 6 in row 7 corner) and inner blanket islands in the outer fuel zones. The objectives of this configuration included an examination of criticality, control rod bank worths and fuel/blanket interchange worths, and isotopic fission and capture rate distributions in the fuel and blankets.

Many of the Phase B measurements were repeated in the Phase C configuration which simulated end-of-life core conditions with depleted fuel and plutonium loaded in the inner blankets. This series of experiments provided information on the flux and power shift associated with blanket plutonium buildup and its effect on criticality, reaction rate distributions, and control rod worth.

The Phase D configuration more closely simulated the CRBRP control pattern with a total of 15 control rods (6 row seven corner rods, 6 row seven flat rods, and 3 row 4 rods) in the end-of-life mockup. The Phase E configuration examined the effects of the inserted row seven corner control rod bank on the core power distribution.

After the completion of the ZPPR matrix expansion to 14 feet by 14 feet to accommodate larger core configurations, the ZPPR-7B configuration was reassembled as a normalization to the earlier
51 measurements (designated Phase F).

Amend. 56
Aug. 1980

Extensive control rod worth measurements were performed in Phase G. The Phase G core configuration was the same as that of Phase D with 15 control rods except that no plutonium was loaded in the blankets in order to simulate beginning-of-life clean core conditions. Control rod interactions and flux tilting effects were investigated through a series of symmetric and asymmetric rod-cluster and individual rod insertion measurements.

56 In Phase H, the row seven corner control rod bank was half inserted and extensive foil irradiations were performed in order to simulate the three-dimensional power perturbations encountered in a clean, beginning-of-life core with partial control rod insertion.

Following a series of non-CRBRP thorium-zone measurements in ZPPR-8, the Phase 8F configuration was assembled to simulate the final CRBRP heterogeneous core configuration at the beginning-of-life with fuel islands surrounding both the row seven corner and the row seven flat control rod banks (Figure 4.3-1). The experimental program was structured to verify the power shape and control rod worth biases and uncertainties which were determined in the earlier ZPPR-7 experiments. In addition, the power tilt associated with an out-of-bank control rod was measured as was the control rod/fuel assembly interchange worth in the shutdown configuration.

The ZPPR-7 Critical experiments provide a valuable integral data base against which the accuracy of the CRBRP design methods and cross section data can be evaluated for application to the heterogeneous core configuration. Because of differences in geometry, composition, size, and temperature between the zero power critical experiments and the CRBRP, the measured integral parameters obtained from the critical are not applied directly to the reactor design. Rather, the accuracy of the design calculational methods and cross section data are evaluated by comparing calculated and measured critical parameters. The resulting biases and/or uncertainties from this comparison are then applied to the calculation of these same parameters in the reactor design using the same calculational methods and data. In the paragraphs that follow, the development of the preliminary design bias factors and uncertainties from the ZPPR-7 and 8 data base will be summarized for application to the heterogeneous core configuration in the principal design areas of reactor eigenvalue prediction, power distribution accuracy, control rod worth uncertainty and sodium void worth. Complete details of the ZPPR-7
51 and 8 analysis are included in References 30 and 31.

ZPPR-7 and 8 Eigenvalue Prediction:

Table 4.3-41 summarizes the measured and calculated critical eigenvalues (k_{eff}) for ZPPR-7 and 8. In order to avoid mixing the control rod worth biases in with the development of the reactor eigenvalue bias, only the clean (unrodded) phases of ZPPR-7 and 8 are included in Table 4.3-41. The calculations systematically underpredict the critical eigenvalue, resulting in a k_{eff} bias of 1.0101 and an uncertainty of $\pm$ 0.19% Δk (1σ). Within the stated standard deviation in the calculation-to-experiment ratios in Table 4.3-41, there is no statistical difference between the eigenvalue bias in the beginning-of-life and end-of-life phases of ZPPR-7 and 8. The ZPPR-7 and 8 eigenvalue bias is included directly in the determination of the CRBRP critical loading and the 1σ variation is included as an uncertainty in the excess reactivity requirements for both the critical fuel loading and control rod worth requirements determinations.

Power Distribution:

The integral data from the ZPPR experiments supporting the power distribution analysis consists of foil activation measurements of Pu^{239} (n,f), U^{235}(n,f), U^{238}(n,f), and U^{238}(n,γ)(for the prediction of blanket plutonium buildup and core conversion ratio), and TLD measurements of gamma heating rate. Foil and TLD irradiations are performed simultaneously in a large number of locations throughout a symmetric core sector at the core midplane and axial distributions in selected fuel and blanket drawers. Special emphasis is placed on blanket and reflector interfaces as well as regions surrounding inserted control rods. The pointwise foil data are corrected for cell fine structure through a combination of cell calculations and drawer-averaging measurements, making the measured reaction rate data compatible with homogenized-drawer calculations. In order to avoid a first-order uncertainty in the normalization to ZPPR power level, the calculated reaction rates are normalized such that the average calculated Pu^{239} fission rate in the fuel is set equal to the average measured value. This is nearly equivalent to a power normalization since Pu^{239} fission accounts for between 80 and 90% of the total reactor power generation. The remaining reaction rates are then compared based on this same power (flux level) normalization.

Table 4.3-42 summarizes the analysis of the ZPPR-7 reaction rates in terms of an average calculation-to-experiment (C/E) ratio and a 1σ variation, with each calculated distribution being power (flux level) normalized to the measured Pu^{239} fission rate in the fuel as described above. The normalization factors indicate that U^{235} fission is overpredicted by about 4% relative to Pu^{239} fission in the heterogeneous critical assemblies. U^{238} fission is underpredicted
51 by nearly 20% in the fuel and about 6% in the inner blankets, indica-

ting both a general underprediction of the high energy fluxes and substantial errors in predicting the spectral gradients between the fuel and blanket assemblies with the coarse-mesh, few-group diffusion calculations. U^{238} capture is overpredicted by nearly 10% relative to Pu^{239} fission, indicating a general overprediction of the end-of-life blanket plutonium buildup, and hence, the end-of-life blanket power generation. The important Pu^{239} fission rate is, however, well predicted with the standard reactor design methods, with an RMS deviation of less than $\pm$ 2% in the C/E ratios throughout the core and blankets.

Figures 4.3-65 and 66 show the normalized distributions of the midplane Pu^{239} fission rate calculation-to-experiment ratios representing the general radial distribution trends at the beginning-(Phase B) and end-of-life (Phase C). In the beginning-of-life core (Phase B in Figure 4.3-65) with no plutonium in the blankets, the C/E ratios tend to be low in the central core regions and tilted toward 3-5% higher values around the outer ring fuel clusters especially around the row-seven corner control channels. The impact of refinements in the power distribution calculation methods, and the sensitivity of this tilted characteristic to cross section data variations is discussed in Reference 32. The CRBRP power predictions in comparable regions are biased downward 1-3% as described in Section 4.3.2.2.9 to compensate for this inherent overprediction. This tilt is not observed in the end-of-life (Phase C in Figure 4.3-66) simulation with a more homogeneous distribution of plutonium throughout the core.* The largest differences in both phases occur in the radial blanket where the C/E ratios consistently fall off 10-15% or more in the vicinity of the blanket/reflector interface (which is generally a low power region). This fall-off, which is similar to that observed in the homogeneous ZPPR-4 experiments, is included in the blanket uncertainty assessment in Section 4.3.2.2.9. The normalized axial reaction rate distributions indicate a 2% overprediction of the midplane reaction rates with respect to the channel-average and a corresponding 5% underprediction of the reaction rates at the core extremities in the vicinity of the core/axial blanket interface.

The power-normalized reaction rate biases and uncertainties (at the 3σ level) are applied in the reactor design, with appropriate weighting for the time and space dependent fraction of power attributable to each reaction type, in order to determine the limits of the power distribution in Section 4.3.2.2.10 for design margin and safety analyses.

---

51 * The Phase C configuration has plutonium loaded in the inner blankets and removed from selected fuel locations to simulate an end-of-life burned core.

Control Rod Worth:

A substantial amount of effort was expended in the ZPPR-7 and 8 program toward confirmation of the control rod worth calculational methods and the development of calculation bias factors and uncertainties supporting the minimum shutdown margin. Table 4.3-43 lists the results of control rod worth calculations in the heterogeneous ZPPR-7 mockup for both the beginning-of-life with a clean core and blankets and for an end-of-life simulation with plutonium loaded in the inner blankets. In contrast to the generally well predicted ZPPR-4 results in Section 4.3.3.7, the heterogeneous ZPPR-7 control rod worth calculation-to-experiment ratios exhibit a strong spatial bias in the beginning-of-life core (Phase B), varying between 0.91 in the inner ring (row 4) rod worths and 0.99 in the outer ring (row 7 corner) rod worths. The end-of-life worths (Phase C) are consistently underpredicted by nearly 10%. It would seem that the close prediction of the beginning-of-life row 7 corner rod worths is an anomaly associated with the calculated reaction rate tilt (overprediction) in this same region. Transport and mesh effects no longer compensate in the highly-loaded ZPPR-7 control rods as noted by the much closer overall agreement obtained with a finer mesh diffusion calculation in Table 4.3-43. The coarse-mesh (1 mesh per ZPPR drawer corresponding to 4 meshes per control assembly) control rod bias is therefore not directly applicable to the power reactor control rod worths, calculated with 6 triangular meshes per control assembly, without adjustment for mesh sensitivity. Although the consistent underprediction of control rod worths in ZPPR-7 may not be fully understood at this time, the experiments do seem to indicate that the unbiased power reactor calculated rod worths are probably conservatively low (that is, final resolution of a set of heterogeneous ZPPR-7 control rod worth biases will tend to raise the calculated power reactor rod worths).

Due to the importance of the control rod withdrawal event (reactivity fault) in the design of the heterogeneous CRBRP where flux shifting and control rod interactions have been found to be substantial, a series of experiments (ZPPR-7G) were performed in which a large number of asymmetric control rod insertion patterns were studied. These patterns included single and small clusters of rods inserted asymmetrically in the core, five-out-of-six rods inserted in a bank (simulating the stuck rod condition), and five-out-of-six secondary control rods inserted in a core containing five-out-of-six inserted primary rods (simulating the limiting condition where the stuck secondary control rod is adjacent to a faulted-withdrawn-primary control rod). The patterns produced substantial flux shifts in the reactor, resulting in control rod interaction factors* exceeding a factor of two. Pre-

---

* Control rod interaction factor is defined as the ratio of the rod worth in a particular asymmetric pattern to the average worth in a symmetric
51 bank.

liminary analysis of these experiments in Reference 30 indicates that the grossly asymmetric patterns (or control rod interactions) are predicted with approximately the same accuracy as the symmetric bank worths in Table 4.3-43 using the standard power reactor design method and a full-core two-dimensional calculation model, thereby confirming the adequacy of the maximum reactivity fault values used in the development of the heterogeneous power reactor control requirements.

Sodium Void Worth:

A series of sodium void worth measurements were performed in the clean benchmark ZPPR-7A configuration. The voiding was more confined to the central core regions than the HCDA simulation in ZPPR-5 (Section 4.3.3.8). The voided region extended stepwise from the central blanket out through the second fuel ring (see Figure 4.3-64) at a radius of about 50 cm, and the axial void included parts of the axial blanket ($\pm$ 60 cm from the core midplane) in the central blanket and first fuel ring, and only the central core regions ($\pm$30.5 cm) in the first blanket ring and the second fuel ring in Figure 4.3-64. Two-dimensional (RZ) first order perturbation theory calculations indicated that the positive (moderation) component of the void worth is reduced compared to the homogeneous ZPPR core values, confirming the lower positive sodium void worth characteristic of the heterogenous core, and the calculation-to-experiment ratios for the positive void worth regions were somewhat lower than the comparable ZPPR-3 and 5 values.

4.3.3.10 Computer Code Abstracts

Nine computer codes were used to support the nuclear analysis described in the previous sections. They are: ANISN-W, W-2DB, PERT-V,
56 ETOX, XSRES-WIDX, PUMA, SPHINX, VENTURE, and POWPIN. A brief abstract of each of these codes is found in Appendix A.

4.3.4 Changes

The design features of the Clinch River Breeder Reactor can be compared with at least four different sodium cooled, fast reactors built or currently under construction in the United States. These include: (1) the Experimental Breeder Reactor (EBR)-II, (2) the Enrico Fermi Atomic Power Plant, (3) the Southwest Experimental Fast Oxide Reactor (SEFOR), and (4) the Fast Flux Test Facility (FFTF). These four reactors were all designed to test and verify
51 specific features and components of fast breeder reactors.

The EBR-II was originally designed as a demonstration of the feasibility of operating an LMFBR power plant with integral closed fuel cycle provided by an on-site fuel reprocessing and refabrication plant. Although not specifically designed for the purpose, it was designated as the nation's principal fast flux irradiation facility. Samples are irradiated in high temperature sodium and high fast neutron flux environment. The reactor core employs metallic uranium fuel surrounded by radial and axial blankets and produces 62.5 MWt and 20 MWe.

The Fermi reactor was designed and built to serve as the first full-scale mockup of a large, sodium cooled, fast breeder reactor. More specifically, its objectives included the testing of such components as the steam generator, sodium pump and fuel handling equipment and to demonstrate the economic feasibility of the LMFBR to produce power on an electric utility grid. The Fermi reactor also employed metallic uranium fuel, radial and axial blanket assemblies. The rated power of the first core loading was 200 MWt.

SEFOR was a ceramic fueled, sodium cooled fast flux reactor intended to provide data in support of a test program to demonstrate
56 that fast power reactors could be designed with desirable operating
and safety characteristics. In particular, it was designed for the systematic determination of the Doppler coefficient of reactivity at temperatures up to the vicinity of fuel melting. SEFOR employed a mixed uranium-plutonium oxide fueled core with a nickel reflector and was rated at 20 MWt.

The FFTF, currently under construction, was designed to provide a fast neutron, sodium cooled environment typical of a large LMFBR. This reactor will act as a full size test bed for both current and advanced fast reactor fuel, absorber and structural materials. These samples will be irradiated in both open and closed test loop locations within the reactor core. The FFTF employs $(U\text{-}Pu)O_2$
56 fuel in two enrichment zones surrounded by a nickel reflector and
has a nominal power rating of 400 MWt.

The CRBRP has particular design objectives which set it apart from previous fast reactors built in the United States. Principal among these is the requirement that CRBRP must breed fissile plutonium with a breeding ratio in excess of 1.2 to demonstrate the potential for large scale commercial LMFBR operation. A second distinctive feature is the nominal power capability of 975 MWt which is more than twice as large as any of the four reactors described above. In addition, CRBRP is the first sodium-cooled LMFBR in the United States to incorporate
51 the heterogeneous core configuration.

These requirements imply that the fuel and blanket regions of the CRBR must be designed to maximize both the breeding of fissile material and the thermal power output. But at the same time the reactor must be maintained and operated in a safe and reliable manner throughout its thirty year design life. In the following discussion a detailed comparison will be made between the CRBRP and the FFTF designs with particular emphasis on safety related features and components.

Pertinent nuclear design features of the two reactors are compared in Table 4.3-44. It should be noted that the dimensions included in Table 4.3-44 are based on cold (room temperature) conditions.

For the initial core loading, the CRBRP fuel pin and fuel assembly designs take the maximum advantage of the FFTF fuel experience. Essentially, the same design has been employed with a slightly larger assembly pitch. Because of the increased power capability, the CRBRP fuel volume was increased by approximately 2.3 times compared to FFTF. Since the demonstration of breeding was not an FFTF design objective, axial and radial blankets were not employed.

The fuel enrichments, compositions and loadings are also compared in Table 4.3-44. In the early operating cycles the CRBRP fuel assemblies employ the same type of low-240 plutonium fuel as the FFTF. In later cycles the CRBRP may employ light water reactor discharge grade plutonium which has a fractionally lower relative amount of Pu-239 and larger concentrations of the higher plutonium isotopes. More than twice as much fissile plutonium is employed in the first core loading of the CRBRP as in FFTF.

The designs of the control rod systems for these two reactors are summarized in Table 4.3-44. Both the primary and secondary control systems in CRBRP and FFTF employ boron carbide as the neutron absorber. All CRBRP control assemblies are fully enriched in B-10 to meet the control requirements (see subsection 4.3.2.6 for details).

The operating conditions, including burnup limits, refueling, power distributions and peak flux for these two reactors are also listed in Table 4.3-44. The overall radial power peaking factors for the CRBRP are smaller than those quoted for FFTF. This is due to the larger core radius, different control rod patterns and the heterogeneous fuel and blanket arrangement.

The reactivity coefficients for the CRBRP are discussed in detail in subsection 4.3.2.3. Table 4.3-45 compares the different
51 reactivity coefficients of CRBRP and FFTF.

The Doppler effect in fast reactors with a large U-238 content provides a reliable, prompt negative reactivity feedback to mitigate the effects of reactivity transients which can lead to rapid power increases. Consequently, the magnitude of the Doppler coefficient has special significance in the safety analysis of fast reactors. The Doppler coefficients in Table 4.3-45 are listed by reactor zone for four different times in the life of the plant.

In all four cases the CRBRP Doppler coefficient summed over all core zones is at least 60% larger (more negative) than the FFTF value. The fuel and inner blanket Doppler constant is nearly 40% larger than the FFTF value. The fast-acting fuel Doppler contribution alone is about half the comparable FFTF value.

The remaining reactivity coefficients compared for these two
reactors are all associated with mechanical motion due to temperature
changes in the fuel, coolant and structure. The average sodium density
coefficients for the CRBRP and FFTF during the first cycle are given
in Table 4.3-45. These results are based on changing the density of
the coolant in all fueled zones, including the inner and radial
blankets in the CRBR. The sodium density coefficient is significantly
smaller (less negative) in the CRBRP because of the positive contribu-
56 tion from the fuel zone.

The uniform radial expansion coefficients for the two reactors during the first cycle are also shown in Table 4.3-45. These values are based on the expansion of the lower core support structure, which changes the average assembly pitch with changes in the coolant inlet temperature. The uniform radial expansion coefficient for CRBRP is smaller than the FFTF value because of the heterogeneous fuel and blanket arrangement in the CRBRP core. Radial bowing effects, including those imposed by the core restraint mechanism, are discussed in Section 4.3.2.3.4.

Finally, the uniform axial expansion coefficients for the two reactors at beginning-of-life are listed in Table 4.3-45. These results are based on the expansion of the fuel pellet stack with changes in the average surface temperature of the dished fuel pellets. It is assumed that the pellets move freely within the cladding tubes and that the axial motion is governed solely by the linear expansion coefficient of the mixed uranium-plutonium oxide. This assumption tends to yield the largest (magnitude) coefficients; fuel pellet sticking to the clad or degradation of the fuel pellets under irradiation will significantly reduce the magnitude of this coefficient.

Additional safety related features and components of the
51 CRBRP are compared with selected foreign built LMFBRs in Section 1.3.

REFERENCES FOR SECTION 4.3

1. R. L. Childs, F. R. Mynatt, L. S. Abbott, "Analyses of the TSF First-Fission Stored-Fuel and Ex-Vessel Low-Level Flux Monitor Experiments for the Clinch River Breeder Reactor", ORNL-TM-5057, March 1976 (Chapters 3, 4, and 5).

2. J. B. Bullock, M. V. Mathis, J. T. Michalczo, "Inverse Kinetics Rod Drop Measurements With a Mockup of the Clinch River Breeder Reactor Shields", ORNL-TM-4828, March 1976 (Chapters 5 and 6).

3. J. W. Allen, "Development and Application of a Three-Point Inverse Kinetics Rod Drop Technique for Subcriticality Determination", ORNL-TM-4758, November 1975.

4. J. W. Allen, J. C. Robinson and N. J. Ackerman Jr., "Statistical Errors in Subcritical Reactivity Inferred from Inverse Kinetics Rod-Drop Measurements Using the Three-Point Method", ORNL-TM-4101, July 1973.

5. Harry H. Hummel and David Okrent, "Reactivity Coefficients in Large Fast Power Reactors", Monograph Series on Nuclear Science and Technology, American Nuclear Society, 1970.

6. "National Topical Meeting on New Developments in Reactor Physics and Shielding", CONF-720901, September 12-15, 1972.

7. Bohl, et. al., "An Analysis of Transient Undercooling and Transient Overpower Accidents Without Scram in the Clinch River Breeder Reactor", ANL/RAS 75-29, July 1975.

8. L. D. Noble, G. Kussmaul and S. L. Derby, "Experimental Program Results in SEFOR Core II", GEAP - 13838, June 1972.

9. D. D. Freeman, "SEFOR Experimental Results and Application to LMFBRs", GEAP-13929, January 1973.

10. R. E. Kaiser and J. M. Gasidlo, "On the Effect of Core Configuration on U^{238} Doppler Measurements in ZPPR Assembly 2", New Developments in Reactor Physics and Shielding, CONF-720901, Sept. 12-15, 1972, p. 1006.

11. "Reactor Development Program Progress Report, Oct. 1973", RDP-21, Argonne National Laboratory.

12. S. L. Stewart, J. T. Hitchcock, and C. L. Cowan, "Critical Experiments and Analysis - Task 5 Quarterly", GEAP-13771-21, Oct.-Dec.
51 1976, p. A-39.

13. Proceedings of the International Symposium on Physics of Fast Reactors, October 16-23, 1973, Tokyo, Japan. Vol. 1, p. 19, Power Reactor and Nuclear Fuel Development Corp., Tokyo, Japan.

14. B. W. Lee, R. E. Kaiser, J. T. Hitchcock and C. S. Russell, "Thermal Expansion Worths for a Liquid Metal Fast Breeder Reactor Inferred from Small-Sample Reactivity Measurements", Nuclear Science Engineering, 65, pg. 429, 1978.

15. T. A. Pitterle, N. C. Paik, and C. Durston, "Evaluation and Integral Testing of Modifications to ENDF/B Version II Data", WARD-4210T1-1, December 1971.

16. N. C. Paik and T. A. Pitterle, "Analysis of ZPPR-2 Measurements Topical Report", WARD-3045T4B-5, February 1973. (Availability:
56 USDOE Technical Information Center).

17. A. M. Letov, Stability in Nonlinear Control Systems, Princeton University Press, Princeton, N.J. 1961.

18. "Modern Control Principles and Applications", Hsu and Meyer, McGraw Hill, New York, 1968, p. 131.

19. "Stability by Liapunov's Direct Method with Applications", LaSalle and Lefschetz, Academic Press, New York, 1961, p. 122.

20. I. Bondarenko, Group Constants for Nuclear Reactor Calculations, Consultants Bureau, New York, N. Y. 1964.

21. D. R. Vondy, T. B. Fowler and G. W. Cunningham, "VENTURE: A Code Block for Solving Multigroup Neutronics Problems Applying the Finite-Difference Diffusion-Theory Approximation to Neutron Transport", ORNL-5062, October 1975.

22. M. F. James, "Energy Released in Fission", J. Nuclear Energy, 23, p. 517, 1969.

23. R. A. Doncals, J. A. Lake, and N. C. Paik, "Use of Integral Data in the Development of Design Methods for Fast Reactors", from the Proceedings of the American Nuclear Society Topical Meeting on Advances in Reactor Physics, Gatlinburg, Tennessee, April 1978 (CONF-780401).

24. T. Pitterle and N. C. Paik, "Summary of Analyses of Plate vs. Pin Measurements Emphasizing Reactivity and Sodium Void Effects", presented at the National Topical Meeting on New Developments
51 in Reactor Physics and Shielding, September 12-15, 1972, Kiamesha Lake, New York.

TABLE 4.3-1 (Continued)

INNER/RADIAL BLANKET RODS (Cont)	UNITS	DESCRIPTION
Clad Material		20 Percent CW-Type 316 SS
Clad Thickness	MM	0.381
Pitch/Diameter Ratio		1.072
INNER/RADIAL BLANKET PELLETS		
Material		Depleted Uranium Oxide
Pellet Density (Percent of Theoretical)	%	95.6
56 Pellet Diameter	MM	11.938
Pellet Stack Height	M	1.626
CONTROL ROD ASSEMBLIES		
Geometry		Hexagonal
Number in Plant		15
Primary Rods (Startup, Burnup and Load Follow)		9
Secondary Rods (Safety)		6
Neutron Absorber		Enriched Boron Carbide
Fraction of Theoretical Density	%	92.0
B-10 Enrichment in Boron Carbide:		
1) Primary Rods (all cycles)	atom percent	92.0
2) Secondary Rods	atom percent	92.0

51

TABLE 4.3-1 (Continued)

CONTROL ROD ASSEMBLIES (Cont)	UNITS	DESCRIPTION
Rods Per Assembly		
Primary System		37
Secondary System		31
Clad Material		20 Percent CW-Type 316 SS
Clad Outside Diameter		
Primary System	MM	15.291
Secondary System	MM	14.036
Clad Thickness		
Primary System	MM	1.270
Secondary System	MM	0.699
Pellet Diameter		
Primary System	MM	11.659
Secondary System	MM	11.951
Pellet Stack Height	M	0.9144

51

TABLE 4.3-7

FUEL AND INNER BLANKET POWER FRACTION SUMMARY*

Time-In-Life	Fuel	INNER Blanket (36")
BOC1	.8603	.0720
EØC1	.8174	.0989
BOC2	.8208	.0967
EØC2	.7618	.1330
BOC3	.8308	.0683
EØC3	.7526	.1190
BOC4	.7623	.1129
EØC4	.6973	.1536
BOC5	.8351	.0690
EØC5	.7541	.1214
BOC6	.7895	.1195
EØC6	.7172	.1639

51 * fraction of full operating power in central 36 inch high region.

TABLE 4.3-8

AXIAL BLANKET, AXIAL EXTENSION POWER NORMALIZATION FACTORS

TIME IN LIFE: $\frac{\text{POWER IN CORE + LAB + UAB}}{\text{POWER IN CORE}} : \frac{\text{POWER IN CORE + LAB}}{\text{POWER IN CORE}}$

TIME IN LIFE	Fuel Assemblies	Inner Blankets		Radial Blankets	
		Rows 2,4	Rows 6,8	RB1	RB2
BOC1	1.0137:1.0079	1.13:1.07	1.11:1.07	1.11:1.06	1.17:1.09
EOC1	1.0176:1.0102	1.12:1.07	1.11:1.07	1.11:1.06	1.15:1.08
BOC2	1.0177:1.0105	1.12:1.07	1.11:1.07	1.11:1.06	1.15:1.08
EOC2	1.0247:1.0140	1.12:1.07	1.11:1.07	1.11:1.06	1.14:1.07
BOC3	1.0140:1.0081	1.13:1.07	1.11:1.07	1.11:1.06	1.13:1.07
EOC3	1.0224:1.0132	1.12:1.07	1.11:1.07	1.11:1.06	1.13:1.07
BOC4	1.0229:1.0143	1.12:1.07	1.11:1.07	1.11:1.06	1.13:1.07
EOC4	1.0329:1.0192	1.12:1.07	1.11:1.07	1.11:1.06	1.13:1.07
	(a)	(b)		(c)	(d)

(a) Cycles 5-6 and subsequent repeat cycles 3-4 for the fuel.

(b) Cycles 5-6 and subsequent repeat cycles 3-4 for the inner blankets.

(c) Cycles 5-8 and subsequent repeat cycles 1-4.

(d) Assume cycle 5 = 1.12:1.07. Cycles 6-10 and subsequent repeat
51 cycles 1-5.

Amend. 56
Aug. 1980

TABLE 4.3-11

RADIAL BLANKET POWER AND BURNUP HISTORY
HIGHEST POWER ASSEMBLY (#1)

	Average Rod		Peak Rod		Peak Power	Peak Burnup
	Power(kw)+	Burnup(a/o)+	Power(kw)+	Burnup(a/o)+	(kw/ft)	(a/o)
Initial:						
SOC1	10.78	0.0	16.55	0.0	6.37	0.0
EOC1 (128 fpd)	13.19	0.075	19.59	0.114	7.83	0.241
SOC2	13.37	0.075	19.86	0.114	7.94	0.241
EOC2 (200 fpd)	16.67	0.235	24.00	0.347	9.92	0.749
SOC3	17.96	0.235	25.68	0.347	10.58	0.749
EOC3 (275 fpd)	21.46	0.536	29.68	0.770	12.53	1.695
SOC4	20.03	0.535	27.62	0.770	11.66	1.695
EOC4 (275 fpd)	22.67	0.871	30.65	1.227	13.11	2.737
"Equilibrium":						
SOC5	10.89	0.0	16.44	0.0	6.33	0.0
EOC5 (275 fpd)	15.65	0.187	22.27	0.272	9.13	0.580
SOC6	14.45	0.187	20.89	0.272	8.57	0.580
EOC6 (275 fpd)	17.84	0.430	25.10	0.618	10.56	1.352
SOC7	20.97	0.430	29.60	0.618	12.43	1.352
EOC7 (275 fpd)	23.91	0.783	32.80	1.108	13.99	2.465
SOC8	22.31	0.783	30.50	1.108	13.01	2.465
EOC8 (275 fpd)	24.59	1.159	33.03	1.616	14.23	3.634

+ total power and burnup in full 64" blanket rod.

TABLE 4.3-12

AXIAL PEAK-TO-AVERAGE POWER FACTORS, F_Z^N

(Normalized to 1.0 Over 36-inch Active Core Height)

Time-in-Life	Peak F_Z^N					
	Clean Fuel[a]	Fuel With CR Influence[b]	Row 2, 4 Inner Blanket	Row 6, 8 Inner Blanket	Radial Blanket Row 1	Radial Blanket Row 2
BOC1	1.282	1.381	1.280	1.325	1.290	1.273
EOC1	1.255	1.309	1.340	1.377	1.331	1.331
BOC2	1.262	1.347	1.342	1.395	1.334	1.332
EOC2	1.210	1.210	1.371	1.370	1.344	1.353
BOC3	1.271	1.381	1.276	1.306	1.373	1.373
EOC3	1.230	1.269	1.365	1.377	1.376	1.387
BOC4	1.242	1.356	1.369	1.426	1.383	1.391
EOC4	1.186 (c)	1.193 (c)	1.375 (c)	1.360 (c)	1.359	1.378

(a) applicable to all core fuel assemblies excluding those directly adjacent to R7C control rods.

(b) applicable to those fuel assemblies directly adjacent to R7C control rods. Note, first year of life (i.e. cycles 1, 3,...) values should be applied to freshly refueled R6C fuel assemblies.

51

(c) cycles 5-6, and subsequent, assumed to repeat cycles 3-4 for the fuel and inner blankets.

TABLE 4.3-13

CRBRP POWER DISTRIBUTION UNCERTAINTY (%)
FUEL ASSEMBLIES

	CLEAN FUEL ZONES				FUEL ZONES ADJACENT TO INSERTED R7C CR			
	Peak Power Density	Power Density At Top Of Core	Rod Power	Assembly Power	Peak Power Density (near/far)[a]	Power Density at Top of Core (near/far)[a]	Rod Power (near/far)[a]	Assembly Power
STATISTICAL[b]								
Experimental (3σ)	±7	±7	±7	±7	±7	±7	±7	±7
Criticality	±1	±1	±1	±1	±4/±1	±0/±3	±4/±1	±2
Fissile Content (tolerance)	±3	±3	±3	±3	±3	±3	±3	±3
SUBTOTAL (RMS)	±7.7	±7.7	±7.7	±7.7	±8.6/±7.7	±7.6/±8.2	±8.6/±7.7	±7.9
NON-STATISTICAL (DIRECT)[c]								
Modeling	±2	±10	±2	±1	+3/-5[g]	±15[e]	+4/+1[g]	±2[g]
Control Rod Banking	±2	±2	±2	±2	±4/±2[g]	±1	±4/±2[g]	±3[g]
Power Level/Dead Band[d]	±3	±3	±3	±3	±3	±3	±3	±3
ZPPR-7 Tilt (BØL)	f	f	f	f	f	f	f	f

[a]near refers to side of F/A directly adjacent to inserted R7C CR; far refers to far side of F/A adjacent to R7C CR.

[b]statistical uncertainties combine by quadrature.

[c]non-statistical uncertainties combine directly .

[d]not applied simultaneously with 15% overpower.

[e]EØL value with substantial portion of R7C control rods withdrawn. BØL apply +25±5 on far side of F/A adjacent to R7C CR.

[f]direct bias power down 3% in F/A #s 9, 10, 13-17, 23, 25, 37, 38, 41-45, 51 and 53; bias power down 1% in F/A#s 8, 11, 19, 36, 39, 47, 65, 68, 101 and 104 (BØC1, BØC3, BØC5,..... only); bias power down 1% in F/A #62 at BØC2 and F/A #'s 62 and 98 at BØC4, BØC6,.....

[g] for EØC, use corresponding clean fuel zone uncertainty.

51

56 TABLE 4.3-14

CRBRP INNER BLANKET POWER DISTRIBUTION UNCERTAINTY (%)

	Beginning-Of-Life				End-Of-Life			
	Peak-Power Density	Power Density At Top Of Core (36")	Rod Power	Assy. Power	Peak-Power Density	Power Density At Top Of Core (36")	Rod Power	Assy. Power
56 NONSTATISTICAL (Direct)[a]								
Experimental	±10	+7 ±10	+2±10	+2 ±10	-5 ±5	+2 ±5	-2 ±5	-2 ±5
Heavy Metal Content	±1	±1	±1	±1	±1	±1	±1	±1
U-235 Content	±1	±1	±1	±1	-	-	-	-
Modeling	±7	±11	±6	±1	±4	±12	±2	±1
Criticality	±2	±2	±2	±2	±1	±1	±1	±1
Control Rod Banking	±2	±2	±2	±2	±2	±2	±2	±2
Reactor Power[b]	±3	±3	±3	±3	±3	±3	±3	±3
Non-Pellet Heating[c]	-5	-5	-5		-2.5	-2.5	-2.5	
TOTAL	-5±26	+2±30	-3±25	+2 ±20	-7.5±16	-0.5±24	-4.5±14	-2 ±13

(a) Nonstatistical uncertainties combine directly.

(b) Not applied simultaneous with 15% overpower.

(c) Gamma heating in clad, Na and duct. Apply only to calculation of pellet (stack) power density.

51

TABLE 4.3-15

CRBRP RADIAL BLANKET POWER DISTRIBUTION UNCERTAINTY (%)

	Beginning-Of-Life				End-Of-Life			
	Peak-Power Density	Power Density At Top Of Core (36")	Rod Power	Assy. Power	Peak-Power Density	Power Density At Top Of Core (36")	Rod Power	Assy. Power
56 NONSTATISTICAL (Direct)[a]								
Row 1:								
Experimental	+2±9	+9±9	+4±9	+4±9	-4±7	+3±7	-2±7	-2±7
Heavy Metal Content	±1	±1	±1	±1	±1	±1	±1	±1
U-235 Content	±1	±1	±1	±1	-	-	-	-
Modeling	±7	-3±5	-2±5	±2	±7	-3±8	-2±3	±2
Control Rod Banking	±2	±2	±2	±2	±2	±2	±2	±2
Reactor Power[b]	±3	±3	±3	±3	±3	±3	±3	±3
Non-Pellet Heating[c]	-5	-5	-5		-3	-3	-3	
TOTAL	-3±23	+1±21	-3±21	+4±18	-7 ±20	-3±21	-7±16	-2±15
Row 2:								
Experimental	+10±14	+18±14	+13±14	+13±14	+5 ±8	+13±8	+7 ±8	+7 ±8
Heavy Metal Content	±1	±1	±1	±1	±1	±1	±1	±1
U-235 Content	±1	±1	±1	±1	-	-	-	-
Modeling	±7	-6±5	-2±5	±2	±7	-6±8	-2±3	±2
Control Rod Banking	±2	±2	±2	±2	±2	±2	±2	±2
Reactor Power[b]	±3	±3	±3	±3	±3	±3	±3	±3
Non-Pellet Heating[c]	-5	-5	-5		-3	-3	-3	
TOTAL	+5±28	+7±26	+6±26	+13±23	+2 ±21	+4 ±22	+2±17	+7±16

a) Nonstatistical uncertainties combine directly.

b) Not applied simultaneous with 15% overpower.

c) Gamma heating in clad, Na and duct. Apply only to calculation of pellet (stack) power density.

51

TABLE 4.3-16

CRBRP DOPPLER CONSTANTS

($-T\ dk/dT * 10^4$)

	Fuel	Inner[(a)] Blankets	Radial[(a)] Blankets	Lower Axial Blanket	Upper Axial Blanket
BOC1	25.8	44.0	11.8	1.90	0.68
EOC1	25.8	47.6	12.4	2.10	0.74
BOC2	25.3	45.9	11.7	2.26	0.69
EOC2	25.8	49.3	12.0	2.38	0.88
BOC3	24.3	40.6	15.3	1.99	0.68
EOC3	24.6	47.7	14.9	2.32	0.83
BOC4	23.6	44.6	13.1	2.68	1.00
EOC4	24.2	45.9	12.8	2.56	1.16

51 (a) Includes axial extensions

TABLE 4.3-17

CRBRP VOIDED DOPPLER CONSTANTS

($-T\ dk/dT * 10^4$)

	Fuel	Inner[a] Blankets	Radial[a] Blankets	Lower Axial Blanket	Upper Axial Blanket
BOC1	16.6	35.4	9.9	1.6	0.6
EOC4	15.8	35.1	10.8	2.1	0.9

51 (a) Includes axial extensions

TABLE 4.3-18

NODAL DOPPLER CONSTANTS

BOC1

(T DK/DT)

	UPPER EXTENSION -.5110E-04	UPPER AXIAL BLANKET -.6780E-04	UPPER EXTENSION -.2359E-04
	INNER BLANKET -.4284E-03 -.7519E-03	Fuel -.2471E-03 -.4391E-03	RADIAL BLANKET -.1373E-03 -.2168E-03
56	-.1272E-02 -.1139E-02 -.6084E-03	-.7865E-03 -.7098E-03 -.3942E-03	-.3340E-03 -.2899E-03 -.1471E-03
51	LOWER EXTENSION -.1459E-03	LOWER AXIAL BLANKET -.1904E-03	LOWER EXTENSION -.3213E-04

TABLE 4.3-19

TEMPERATURE DEPENDENCE OF DOPPLER CONSTANT

	Uniform temperature of fueled core, ^{o}K	300	2000	3000	4000	5000
56	Reactivity change, Δk from $1000^{o}K$ core, as computed by FX-2 three-term temperature dependence formula	+.004727	-.002744	-.004331	-.005443	-.006296
56	Reactivity change, Δk* using T^{-1} extrapolation of data between $300^{o}K$ and $1000^{o}K$	+.004727	-.002721	-.004313	-.005443	-.006319

*Note that Δk is the integrated inverse temperature-dependent Doppler reactivity coefficient
51 such that $\Delta k = -.0.003926 \ln (T^{Final}/T^{Initial})$

TABLE 4.3-20

CRBRP REGIONWISE SODIUM VOID REACTIVITY

(\$)[a]

	Fuel	Inner[b] Blankets	Radial[b] Blankets	Lower Axial Blanket	Upper Axial Blanket	Maximum Positive Void Worth		
						Fuel	Inner Blankets	Total
BOC1	+0.02	+1.38	-0.79	-0.27	-0.15	1.51	1.40	2.91
EOC1	+0.28	+1.43	-0.72	-0.25	-0.16	1.60	1.46	3.06
BOC2	+0.51	+1.45	-0.67	-0.27	-0.15	1.76	1.48	3.24
EOC2	+0.82	+1.51	-0.58	-0.23	-0.17	1.89	1.55	3.44
BOC3	+0.28	+1.36	-0.81	-0.28	-0.15	1.60	1.36	2.96
EOC3	+0.79	+1.47	-0.63	-0.25	-0.16	1.77	1.49	3.26
BOC4	+1.20	+1.48	-0.56	-0.27	-0.15	2.10	1.50	3.60
EOC4	+1.56	+1.61	-0.46	-0.22	-0.20	2.31	1.64	3.95

(a) $\beta_{eff} = 0.0034$

51 (b) Includes axial extensions

TABLE 4.3-23

CRBRP UNIFORM RADIAL EXPANSION COEFFICIENTS

	Cents per Mil of Outward Radial Motion			
	BOC-1	EOC-2	BOC-3	EOC-4
All Control Rods Out	-0.461	-0.441(1)	-0.459	-0.448(1)
6 Row 7 Corner Rods In	-0.427(2)	--------	-0.426(2)	--------
All 15 Control Rods In	-0.422(3)	--------	--------	-0.390(3)

(1) Recommended values for end-of-cycle conditions.

(2) Recommended values for beginning-of-cycle conditions.

51 (3) Refueling conditions.

Amend. 51
Sept. 1979

TABLE 4.3-24

RADIAL MOTION REACTIVITY COEFFICIENTS
(BEGINNING OF CYCLE ONE -- HOT STANDBY)

AXIAL LOCATION (Inches above bottom of fuel assembly)		CENTS PER INCH OF INWARD RADIAL MOTION													
		Row 2	Row 3	Row 4	Row 5	Row6A	Row 6B	Row 7	Row 8A	Row 8B	Row 8C	Row 9	Row 10	Row 11	Row 12
		Blkt.	Fuel	Blkt.	Fuel	Blkt.	Refuel*	Fuel	Fuel	Fuel	Blkt.	Fuel	Fuel	Radial Blkt.	Radial Blkt.
Upper Axial Blanket	107.0	0.0	0.0	0.0	0.0	0.0	0.0	0.0	0.0	0.0	0.0	0.0	0.0	+0.01	0.0
	103.0	0.0	0.0	0.0	0.0	0.0	0.0	-0.01	0.0	+0.01	0.0	+0.01	+0.1	+0.11	0.0
	97.0	+0.01	-0.01	0.0	-0.01	-0.01	0.0	-0.07	0.0	+0.05	0.0	+0.08	+0.7	+1.10	+0.29
	93.0	+0.08	-0.18	-0.03	-0.39	-0.12	-0.07	-1.44	-0.08	+1.08	+0.19	+1.45	+10.5	+5.30	+1.13
Core Zone	87.0	+0.43	-0.59	-0.16	-1.34	-0.67	-0.47	-4.99	-0.29	+3.71	+1.51	+4.88	+36.0	+11.44	+2.56
	81.0	+0.91	-1.02	-0.35	-2.35	-1.48	-1.07	-9.27	-0.53	+6.79	+3.53	+8.68	+64.5	+15.27	+2.60
	75.0	+0.97	-1.03	-0.38	-2.43	-1.67	-1.21	-10.29	-0.58	+7.40	+4.03	+9.14	+67.6	+15.06	+3.42
	69.0	+1.02	-1.13	-0.40	-2.72	-1.87	-1.36	-11.88	-0.67	+8.52	+4.45	+10.34	+76.0	+19.14	+3.75
	63.0	+0.55	-0.73	-0.22	-1.79	-1.06	-0.75	-7.95	-0.45	+5.69	+2.34	+6.80	+49.1	+16.56	+3.78
	57.0	+0.14	-0.23	-0.06	-0.56	-0.31	-0.21	-2.50	-0.14	+1.85	+0.46	+2.24	+16.0	+8.76	+1.90
Lower Axial Blanket	50.0	+0.01	0.0	-0.01	0.0	-0.04	-0.02	0.0	0.0	+0.03	+0.03	+0.05	+0.5	+0.76	+0.19
	43.0	0.0	0.0	0.0	0.0	0.0	0.0	0.0	0.0	0.0	0.0	0.0	0.0	+0.02	0.0
Row Total		+4.12	-4.92	-1.61	-11.59	-7.23	-5.16	-48.40	-2.74	+35.13	+16.54	+43.67	+321.0	+93.53	+19.82

*Six refueling locations contain blanket assemblies in cycle one.

TABLE 4.3-25

RADIAL MOTION REACTIVITY COEFFICIENTS
(END OF CYCLE TWO -- ALL RODS OUT)

AXIAL LOCATION (Inches above bottom of fuel assembly)		CENTS PER INCH OF INWARD RADIAL MOTION													
		Row 2	Row 3	Row 4	Row 5	Row6A	Row 6B	Row 7	Row 8A	Row 8B	Row 8C	Row 9	Row 10	Row 11	Row 12
		Blkt.	Fuel	Blkt.	Fuel	Blkt.	Refuel*	Fuel	Fuel	Fuel	Blkt.	Fuel	Fuel	Radial Blkt.	Radial Blkt.
Upper Axial Blanket	107.0	0.0	0.0	0.0	0.0	0.0	0.0	0.0	0.0	0.0	0.0	0.0	0.0	+0.01	-0.01
	103.0	0.0	0.0	0.0	0.0	0.0	0.0	-0.01	+0.01	+0.01	0.0	+0.03	+0.1	+0.12	+0.01
	97.0	0.0	-0.01	0.0	-0.02	-0.01	+0.03	-0.07	+0.06	+0.08	-0.04	+0.19	+0.8	+1.22	+0.34
Core Zone	93.0	+0.03	-0.17	-0.05	-0.30	-0.11	+0.35	-0.92	+0.77	+1.20	+0.24	+2.78	+10.4	+5.93	+1.35
	87.0	+0.17	-0.55	-0.40	-0.95	-0.79	+0.82	-2.73	+2.31	+3.69	+3.33	+8.58	+32.9	+12.85	+3.02
	81.0	+0.33	-0.85	-0.79	-1.46	-1.52	+1.12	-4.06	+3.42	+5.51	+6.69	+13.08	+51.0	+17.31	+3.33
	75.0	+0.32	-0.80	-0.74	-1.37	-1.40	+1.05	-3.69	+3.12	+5.02	+5.98	+12.12	+47.5	+16.88	+4.06
	69.0	+0.34	-0.87	-0.81	-1.50	-1.52	+1.16	-4.06	+3.42	+5.50	+6.37	+13.22	+51.5	+18.05	+4.45
	63.0	+0.19	-0.58	-0.45	-1.01	-0.84	+0.86	-2.74	+2.31	+3.71	+3.24	+8.79	+33.7	+13.58	+4.50
	57.0	+0.05	-0.19	-0.12	-0.32	-0.23	+0.29	-0.89	+0.77	+1.25	+0.41	+2.97	+11.3	+6.92	+2.25
Lower Axial Blanket	50.0	+0.01	0.0	-0.02	0.0	-0.03	-0.01	-0.01	+0.02	+0.04	+0.02	+0.10	+0.4	+0.65	+0.23
	43.0	0.0	0.0	0.0	0.0	0.0	0.0	0.0	0.0	0.0	0.0	0.0	0.0	+0.01	-0.01
Row Total		+1.44	-4.02	-3.38	-6.93	-6.45	+5.57	-19.18	+16.21	+26.01	+26.24	+61.80	+239.6	+93.53	+23.52

51

56 *Six refueling locations contain three fuel and three blanket assemblies in cycle two.

TABLE 4.3-26

CRBRP INHERENT FEEDBACK REACTIVITY ($)

STARTUP FROM HOT-STANDBY CONDITIONS* TO 40% POWER/40% FLOW+

	Feedback ($)	
	BOC1	EOC4
Doppler		
Fuel	-0.385	-0.295
Axial Blankets	-0.008	-0.013
Inner Blankets	-0.259	-0.547
Radial Blankets	-0.048	-0.100
Total	-0.700 $\pm$ 0.084	-0.955 $\pm$ 0.115
Uniform Radial Expansion	-0.062 $\pm$ 0.012	-0.065 $\pm$ 0.013
Uniform Axial Expansion		
Fuel	-0.219	-0.126
Structure (FA)	+0.023	+0.021
Blankets	+0.020	+0.015
Structure (BA)	+0.004	+0.009
Total	-0.172 $\pm$ 0.040	-0.081 $\pm$ 0.019
Sodium Density	-0.014 $\pm$ 0.004	+0.048 $\pm$ 0.014
Total $\pm$ 1σ**	-0.948 $\pm$ 0.094	-1.053 $\pm$ 0.118

* 600°F isothermal

+ 635°F inlet temperature

51 **Uncertainty in net feedback includes both nuclear uncertainty in reactivity coefficient and thermal uncertainty.

56 | TABLE 4.3-29

CRBRP PRIMARY CONTROL SYSTEM REQUIREMENTS AND MINIMUM CONTROL WORTHS ($\frac{\%\Delta k}{k}$)

PCA Control Requirements	BOC1	EOC1	BOC2	EOC2	BOC3	EOC3
Hot-to-Cold*	0.99 ± .29	1.06 ± .30	1.04 ± .27	1.10 ± .32	0.98 ± .29	1.07 ± .32
Reactivity Fault	0.54	0.36	0.84	0.20	0.83	0.25
Excess Loaded	1.77	1.17	2.70	0.46	2.56	0.70
Criticality Uncertainty	± .43	± .43	± .43	± .43	± .43	± .43
Fissile Tolerance	± .28	± .28	± .28	± .28	± .28	± .28
Total	3.30 ± .59	2.59 ± .59	4.58 ± .58	1.76 ± .60	4.37 ± .59	2.02 ± .60
Maximum Requirement	3.89	3.18	5.16	2.36	4.96	2.62
Minimum PCA Control Worth (Calculated -2σ)**						
6-R7C	5.58	5.37	5.82	5.39	5.55	[illegible]
3-R4C	1.37	1.60	1.62	1.96	1.23	1.[illegible]6
Stuck Rod	-1.43	-1.44	-1.11	-1.45	-1.12	-1.36
Total	5.52	5.53	6.33	5.90	5.66	5.45

* Hot-full-power to refueling temperatures.

**σ = 4%, unbiased.

56 | 51 | $\$ = \frac{\Delta k}{k \cdot \beta eff}$, $\beta = 0.0034$

TABLE 4.3-29 (Continued)

56 CRBRP PRIMARY CONTROL SYSTEM REQUIREMENTS AND MINIMUM CONTROL WORTHS ($\% \frac{\Delta k}{k}$)

PCA Control Requirements	BOC4	EOC4	BOC5	EOC5	BOC6	EOC6
Hot-to-Cold*	1.00 ± .31	1.06 ± .32	0.98 ± .29	1.07 ± .32	1.00 ± .31	1.06 ± .32
Reactivity Fault	1.04	0.21	0.98	0.35	1.02	0.21
Excess Loaded	3.29	0.53	2.86	1.14	3.23	0.51
Criticality Uncertainty	± .43	± .43	± .43	± .43	± .43	± .43
Fissile Tolerance	± .28	± .28	+ .28	± .28	± .28	± .28
Total	5.[illegible] ± .60	1.80 ± .60	4.82 ± .59	2.56 ± .60	5.25 ± .60	1.78 ± .60
Maximum Requirements	5.93	2.40	5.41	3.16	5.85	2.38
Minimum PCA Control Worth (Calculated -2σ)**						
6-R7C	5.94	5.36	5.56	5.12	5.91	5.26
3-R4C	1.87	2.24	1.29	1.75	2.07	2.48
Stuck Rod	-0.82	-1.27	-0.98	-1.25	-0.83	-1.25
Total	6.99	6.33	5.87	5.62	7.15	6.49

* Hot-full-power to refueling temperatures.

** σ = 4%, unbiased.

56 51 $\$ = \frac{\Delta k}{k \cdot \beta_{eff}}$, β = 0.0034

TABLE 4.3-30

56 CRBRP SECONDARY CONTROL SYSTEM REQUIREMENTS AND MINIMUM CONTROL WORTHS (% $\frac{\Delta k}{k}$)

SCA Control Requirement	BOC1	ECC1	BOC2	EOC2	BOC3	EOC3
Hot-to-Cold*	0.67 ± .27	0.73 ± .29	0.71 ± .27	0.78 ± .30	0.66 ± .27	0.75 ± .30
Reactivity Fault	0.54	0.36	0.84	0.20	0.83	0.25
Total	1.21 ± .27	1.09 ± .29	1.55 ± .27	0.98 ± .30	1.49 ± .27	1.00 ± .30
Maximum Requirement	1.48	1.38	1.82	1.28	1.76	1.30
Minimum SCA Control Worth (Calculated -2σ)**						
6-R7F	4.01	4.17	4.17	4.30	3.82	4.09
Stuck Rod	-1.34	-1.40	-1.40	-1.44	-1.28	-1.37
Total	2.67	2.77	2.77	2.86	2.54	2.72

* Hot-full-power to standby temperature.

** σ = 4%, unbiased.

56 51 $\$ = \frac{\Delta k}{k \cdot \beta_{eff}}$, β = 0.0034

TABLE 4.3-30 (Continued)

56 CRBRP SECONDARY CONTROL SYSTEM REQUIREMENTS AND MINIMUM CONTROL WORTHS (% $\frac{\Delta k}{k}$)

SCA Control Requirements	SOC4	EOC4	SOC5	EOC5	SOC6	EOC6
Hot-to-Cold*	0.70 ± .29	0.76 ± .30	0.66 ± .27	0.75 ± .30	0.70 ± .29	0.76 ± .30
Reactivity Fault	1.04	0.21	0.98	0.35	1.02	0.21
Total	1.74 ± .29	0.97 ± .30	1.64 ± .27	1.10 ± .30	1.72 ± .29	0.97 ± .30
Maximum Requirement	2.03	1.27	1.91	1.40	2.01	1.27
Minimum SCA Control Worth (Calculated -2σ)**						
6-R7F	4.17	4.30	3.92	4.14	4.33	4.40
Stuck Rod	-1.40	-1.44	-1.31	-1.39	-1.45	-1.47
Total	2.77	2.86	2.61	2.75	2.88	2.93

* Hot-full-power to standby temperature.

** σ = 4%, unbiased

56 | 51 $\$ = \frac{\Delta k}{k \cdot \beta_{eff}}$, β = 0.0034

TABLE 4.3-43

ZPPR-7 CONTROL ROD WORTH CALCULATION-TO-EXPERIMENT RATIOS*

	Beginning-of-Life Phase B	End-of-Life Phase C
Row 4	0.916 (0.963)	0.906 (0.973)
Row 7 - Flat	0.898 (0.987)	0.887 (0.952)
Row 7 - Corner	0.992 (1.074)	0.905 (0.986)

* Calculated with standard two-dimensional (hexagonal planar geometry) coarse-mesh direct eigenvalue difference diffusion theory methods using 9-group ENDF/B-III data. Values in ( ) from four-mesh per ZPPR drawer diffusion calculations.

51

Amend. 51
Sept. 1979

TABLE 4.3-44

COMPARISON OF NUCLEAR PARAMETERS FOR CRBRP AND FFTF

	CRBRP	FFTF
LAYOUT		
Number of Fuel Assemblies	156	73
Inner Enrichment Zone		28
Outer Enrichment Zone		45
Number of Test Loop Locations	-	9
Number of In-Core Control Rods	15	9
Number of Inner Blanket Assemblies	82	-
Number of Radial Blanket Assemblies	150	-
Number of Radial Reflector Assemblies	-	108(1)
Number of Removable Radial Shields	306	-
DIMENSIONS		
Assembly Pitch (meters)	0.1209	0.1198
Core(2) Equivalent Diameter (meters)	2.019	1.200
Core(2) Cross-Sectional Area (meters)	3.203	1.131
Active Fuel Height (meters)	0.9144	0.9144
Height-to-Diameter Ratio	0.453	0.762
56 Axial Blkt. Height, Upper/Lower (meters)	0.3556/0.3556	-
Inner and Radial Blanket Height (meters)	1.6256	-
INITIAL CORE ENRICHMENTS AND FUEL MASSES		
Enrichments (Pu/U+Pu)		
Inner Enrichment Zone	0.328	0.224
Outer Enrichment Zone		0.274
Enrichment Ratio (Outer/Inner)	N/A	1.22
Isotopic Composition of Feed Plutonium		
Pu-238	0.0006	-
Pu-239	0.8604	0.864
Pu-240	0.1170	0.117
Pu-241	0.0200	0.017
Pu-242	0.0020	0.002

(1) Includes positions for as many as fifteen peripheral shim rods.

51 (2) "Core" includes fuel, inner blankets and in-core control rods.

Amend. 56
Aug. 1980

TABLE 4.3-44 (Continued)

	CRBRP	FFTF
Peak Neutron Flux [4] (neutrons/cm^2 sec)		
Fuel and Inner Blanket Zone		
Total Flux	5.5×10^{15}	8×10^{15}
Fast Flux (energy $\geq$ 0.1 MeV)	3.4×10^{15}	5×10^{15}
Radial Blanket Zone		
Total Flux	3.9×10^{15}	-
Fast Flux (energy $\geq$ 0.1 MeV)	2.4×10^{15}	-

51 (4) Maximum value attained at any time in life and at any point in the zone.

Amend. 56
Aug. 1980

TABLE 4.3-45

COMPARISON OF REACTIVITY COEFFICIENTS FOR CRBRP AND FFTF

		CRBRP	FFTF
Doppler Constant $(-T\frac{dk}{dT})$			
Initial Core, BOC1	Fuel	0.0026	0.0050
	Inner Blanket	0.0044	-
	Radial Blanket	0.0012	-
	Axial Blankets	0.0003	-
Initial Core, EOC2	Fuel	0.0026	0.0055
	Inner Blanket	0.0049	-
	Radial Blanket	0.0012	-
	Axial Blankets	0.0003	-
Equilibrium Core, BOL	Fuel	0.0024	0.0050
	Inner Blanket	0.0041	-
	Radial Blanket	0.0015	-
	Axial Blankets	0.0003	-
Equilibrium Core, EOL	Fuel	0.0024	0.0055
	Inner Blanket	0.0046	-
	Radial Blanket	0.0013	-
	Axial Blankets	0.0004	-
Core-Average Sodium Density Coefficients (cents/^{o}F)			
First Cycle		-0.006	-0.049
Uniform Radial Expansion Coefficient (cents/^{o}F)			
First Cycle		-0.177	-0.21
Uniform Axial Expansion Coefficient (cents/^{o}F)			
51 First Cycle		-0.038	-0.038

Amend. 56
Aug. 1980

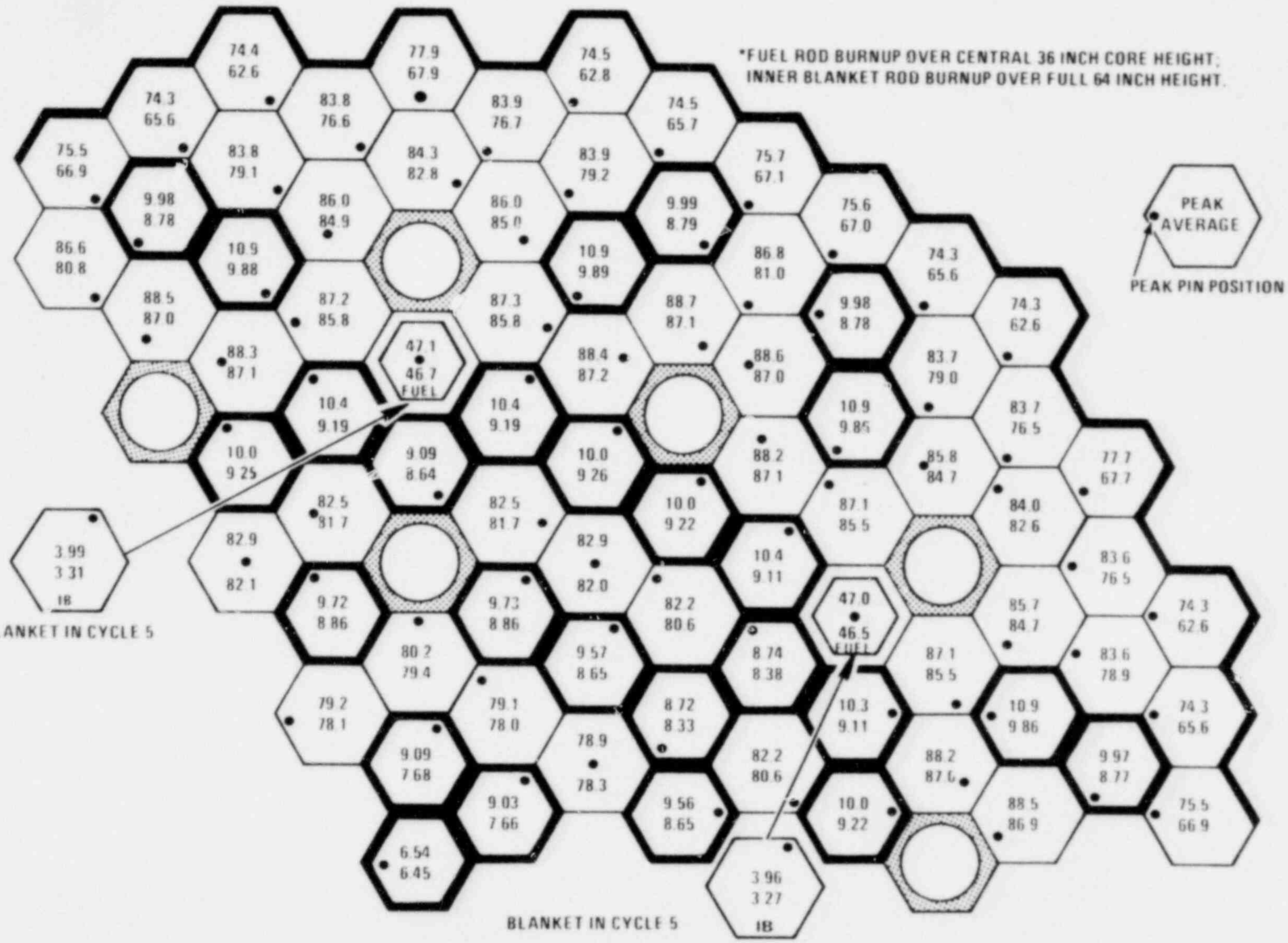

Figure 4.3-25. Peak and Average Rod Burnup* (MWD/KG) Cycles 5-6

Amend. 51
Sept. 1979

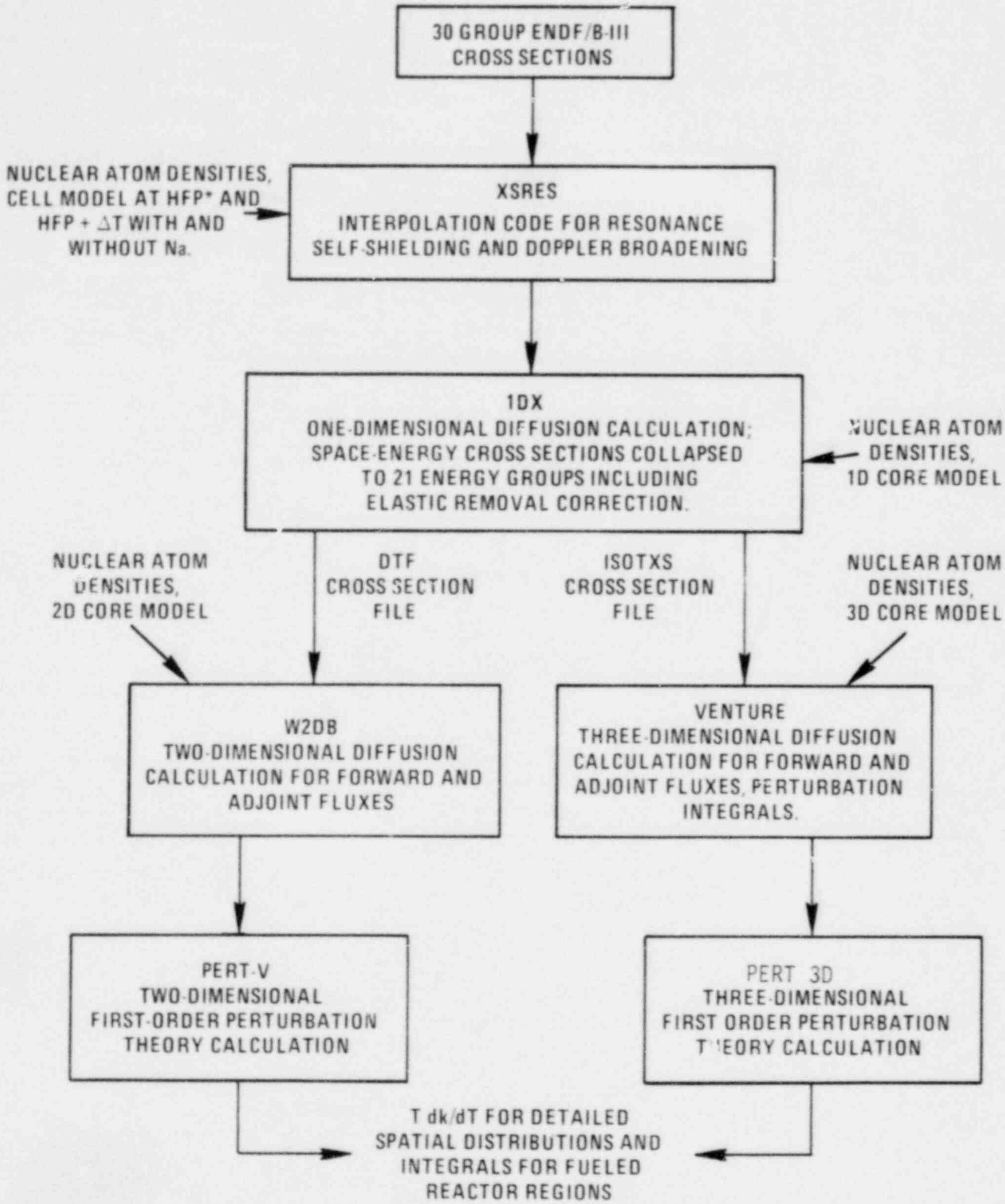

*HFP = HOT FULL POWER TEMPERATURE CONDITIONS

Figure 4.3-26. Flow Chart for Doppler Calculations

1544-26

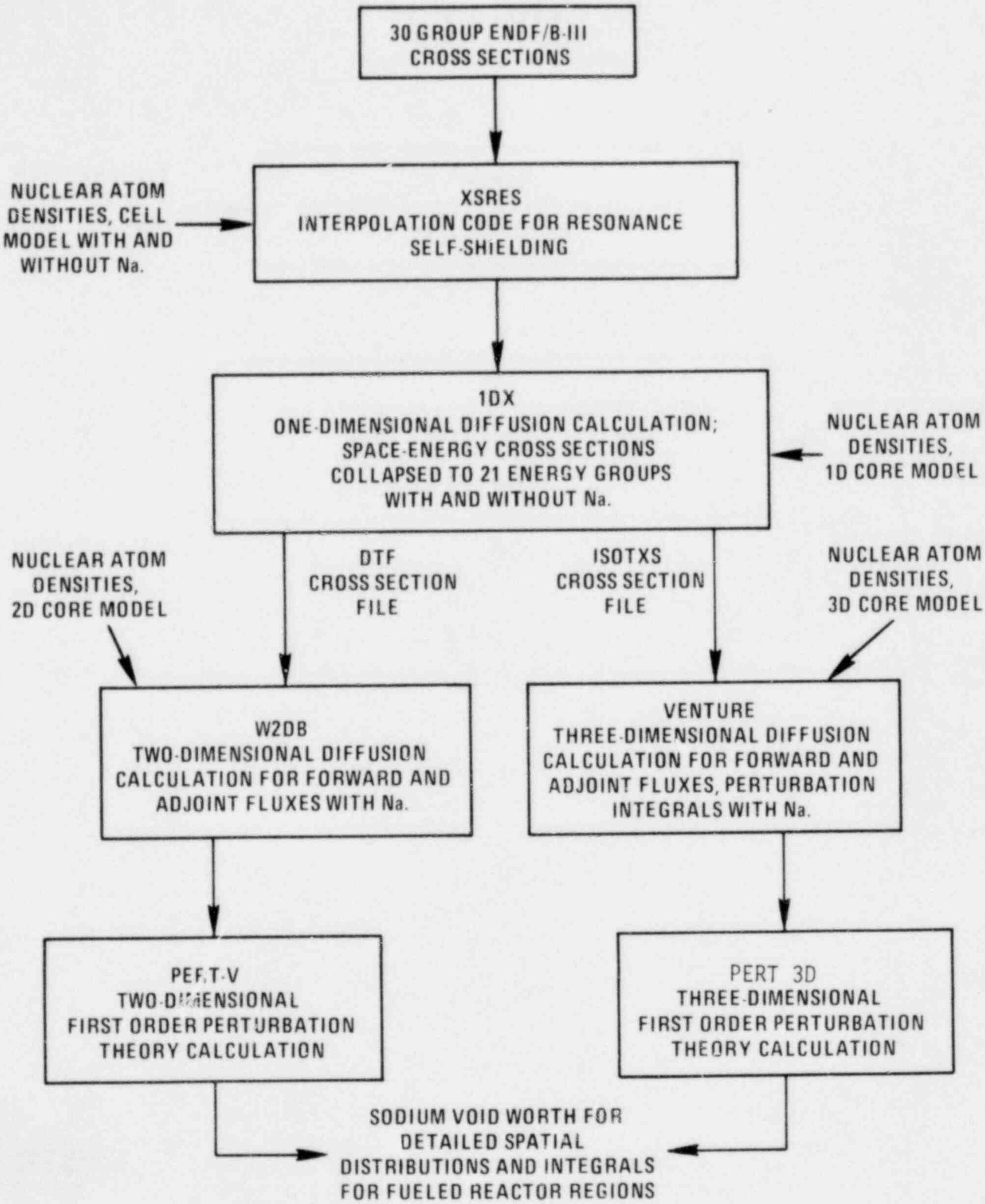

Figure 4.3-28. Flow Chart for Sodium Voiding Reactivity Worth Calculations

1544-29

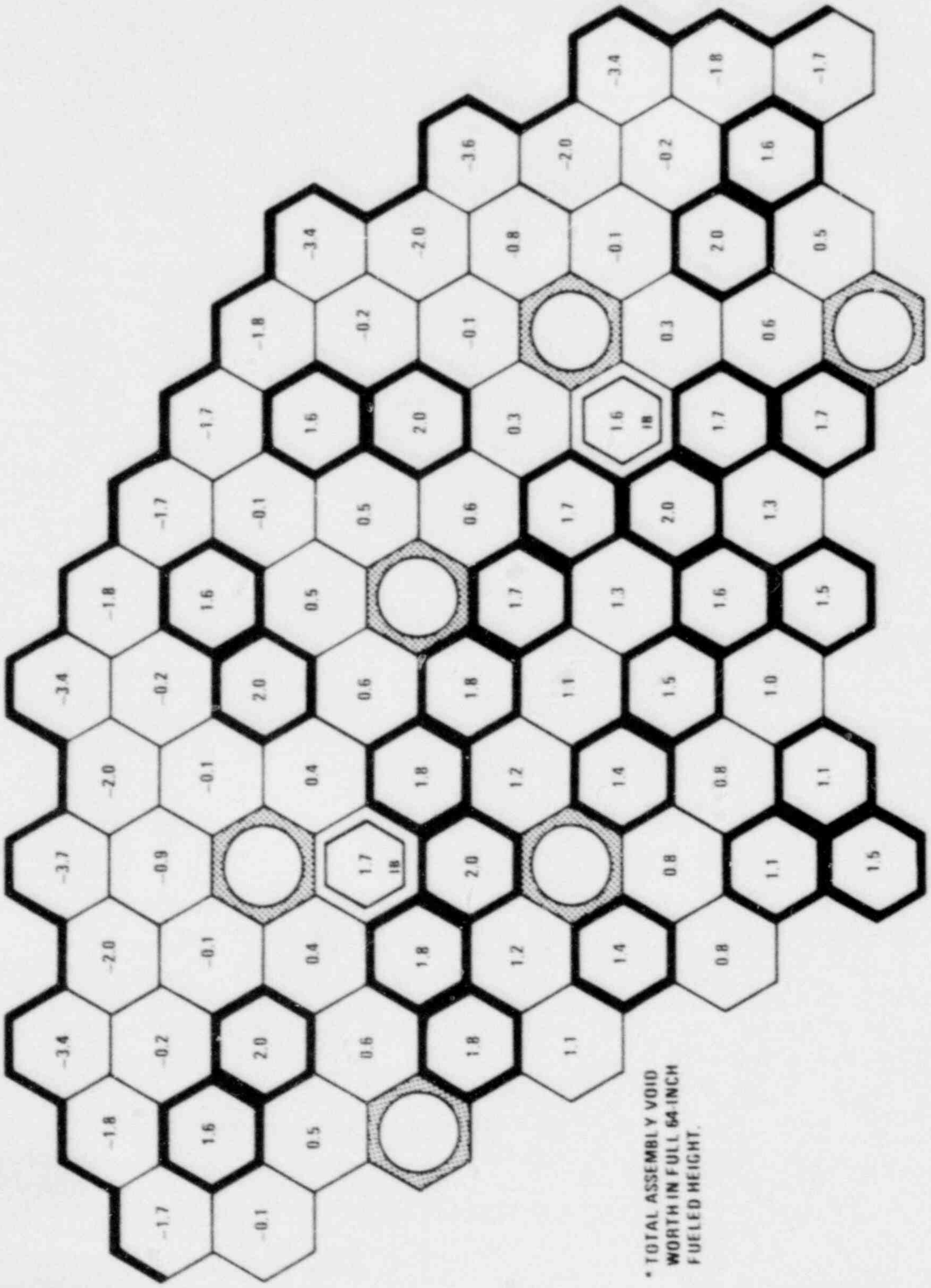

Figure 4.3-29a. CRBRP Sodium Void Worth By Assembly Beginning of Cycle One* (¢)

* TOTAL ASSEMBLY VOID WORTH IN FULL 64 INCH FUELED HEIGHT.

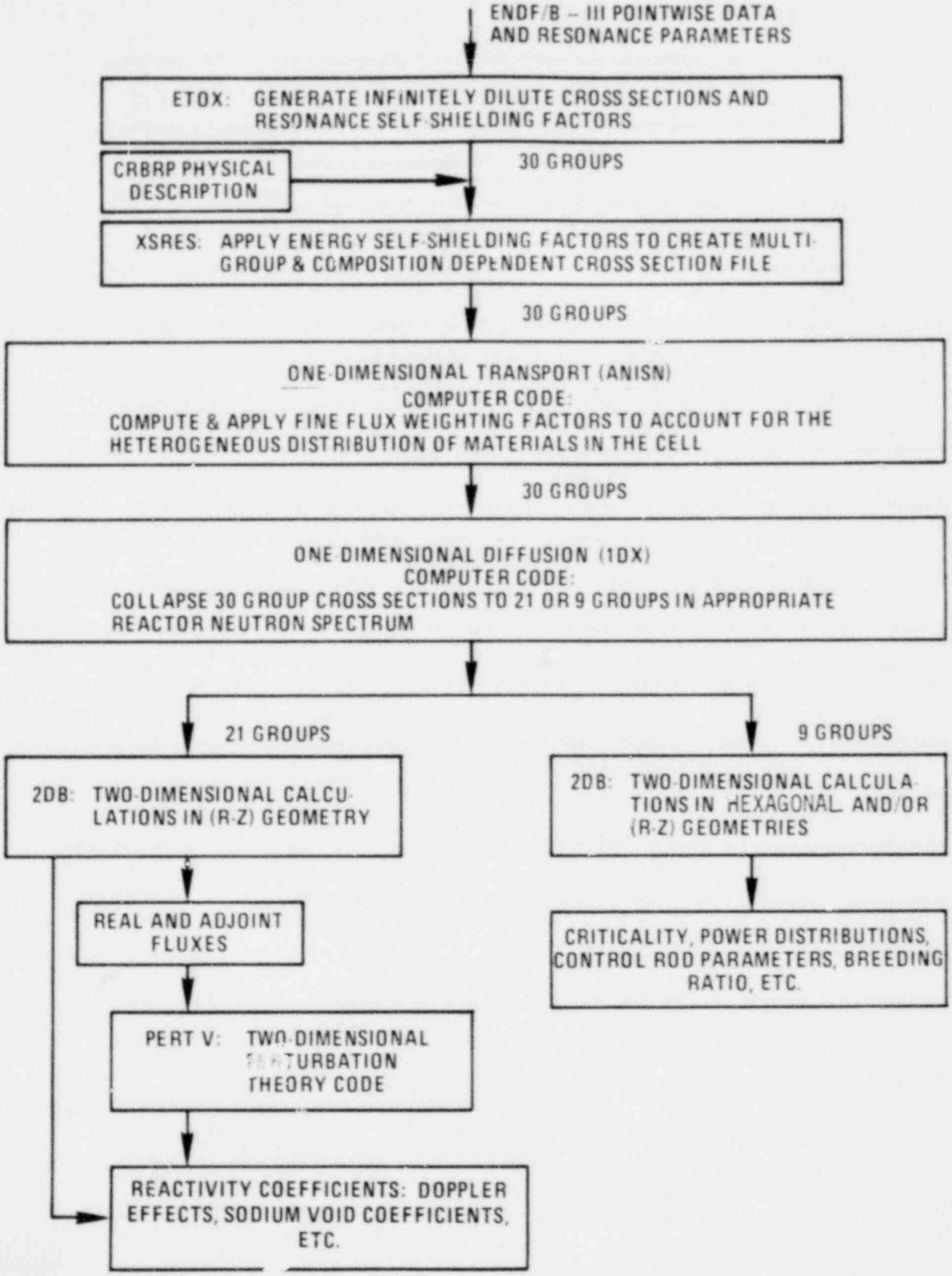

Figure 4.3-54. Calculational Scheme for Analysis of CRBRP

1544-53

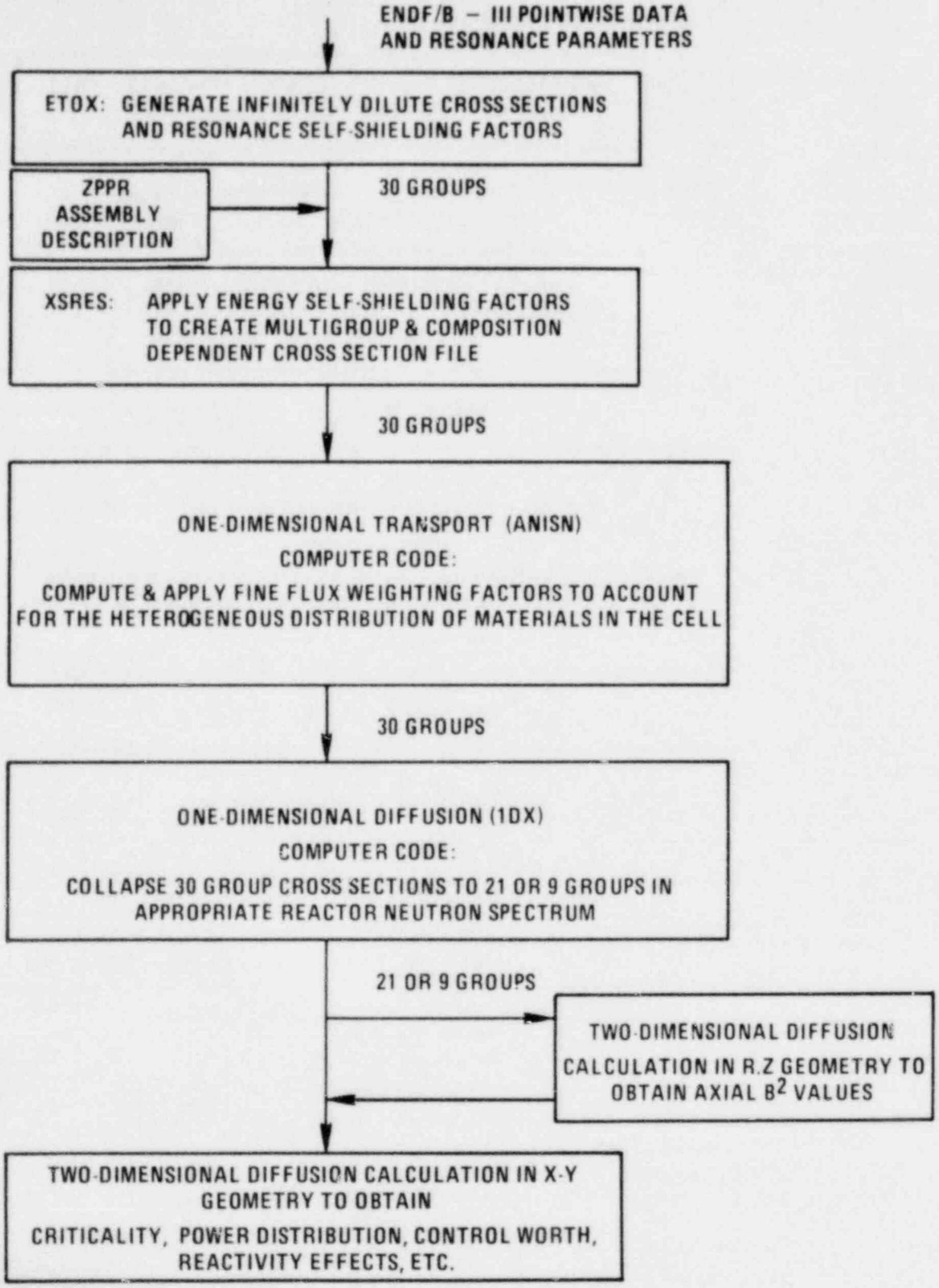

Figure 4.3-55. Calculational Scheme for Evaluation of ZPPR Critical Experiments

1544-54

Amend. 51
Sept. 1979

Since the absorber pellet centerline temperature ($T_{abs,\mathbb{C}}$)(*), is dependent on the absorber pellet surface temperature ($T_{abs,s}$) as a boundary condition, the iterative process on $T_{abs,\ avg}$ actually involves $T_{abs,s}$. Based on the heat transfer across the absorber pellet-to-cladding gap, considering the bond (helium) thermal conductivity and the (hot) gap size, the surface temperature can be expressed (under nominal rod operating conditions), as the following:

$$T_{abs,s} = T_{cl,\ i} + \frac{Q_{abs}}{2\pi\ K_{gap}\ \Delta Z} \ln \left(\frac{R_i}{R_p}\right) \qquad (4.4.2.8\text{-}11)$$

where $T_{cl,i}$ is the cladding inside temperature;

Q_{abs} is the absorber heat generation within a length ΔZ;

R_i is the hot cladding inside radius based on Equation (4.4.2.8-7);

R_p as indicated by Equations (4.4.2.8-9) and (4.4.2.8-10), is a function of $T_{abs,s}$;

K_{gap} is the gap (helium) thermal conductivity (see following Equation 4.4.2.8-14).

The gap thermal conductivity is again dependent on the absorber pellet surface temperature Tabs,s, since it is a function of the average gap temperature which can be defined as,

$$T_{gap,\ avg} = \frac{T_{abs,s} + T_{cl,i}}{2} \qquad (4.4.2.8\text{-}13)$$

---

*The absorber centerline temperature, $T_{abs,\mathbb{C}}$, is calculated based on the general differential equation representing the heat transfer through the absorber pellet,

56 $$K_{abs}\frac{d^2T}{dr^2} + \frac{K_{abs}}{r}\frac{dT}{dr} + q'''_{abs} = 0 \qquad (4.4.2.8\text{-}12)$$

where K_{abs} is the absorber (B_4C) thermal conductivity reported in Section 4.4.2.8.8; and

q'''_{abs} is the volumetric heat generation rate in the pellet.

51

Amend. 56
Aug. 1980

The iterative procedure on the hot pellet radius (R_p) is initiated by the first guestimate of $T_{abs,s}$ from Equation (4.4.2.8-11), assuming R_p = (R_p)cold and $T_{gap,avg} = T_{cl,i}$. This first guestimate value is used next to estimate values of R_p by Equations (4.4.2.8-9) and (4.4.2.8-10), and Tgap,avg by Equation (4.4.2.8-13). As mentioned previously, this process is repeated until the value R_p calculated in two successive iterations converges within a prefixed limit; with the established values of R_p and R_i (see Equation 4.4.2.8-7), the hot gap is obtained by Equation (4.4.2.8-6).

Experimental values of the control rods gap conductance have been determined (Reference 20) to be consistent with the method used.

The helium thermal conductivity is given by (Ref. 21).

$$K = 0.097 + 7 \times 10^{-5} T \qquad (4.4.2.8\text{-}14)$$

where K is in Btu/hr-ft-°F and T in °F.

The above equation is valid for T >700 °F.

4.4.2.8.7 Fuel Thermal Conductivity

The following equation (Ref. 18) is used in evaluating the fuel thermal conductivity in the fuel assemblies:

$$K = FP \left[\frac{1}{A+BT} + CT^3\right] \qquad (4.4.2.8\text{-}15)$$

where K = thermal conductivity, W/m°K;

T = temperature, °K;

$$FP = \frac{1.079\ (1-P)}{(1.0+0.5P+4.62P^2)}$$

P = fractional porosity (1-fraction of theoretical density);

55 $A = -6.0656 \times 10^{-4}$

$B = 3.04212 \times 10^{-4}$

$C = 0.75137 \times 10^{-10}$

A review of the effects of plutonium weight percent on conductivity revealed that for the range 0.12 $\leq$Pu $\leq$0.3, such effect was within the range of experimental uncertainties, and therefore, the thermal conductivity could be considered independent of plutonium content. No ex-
51 perimental conductivity data exist for a plutonium content corresponding

was in good agreement with ARD correlation. The root mean square deviation of the HEDL cubic fit was 0.2643. The arc-tangent curve had a much larger spread (0.418), while the hyperbolic relationship:

$$Q'_m = 19.5 \qquad G \leq 5 \text{ mils}$$
$$Q'_m = 13.60 + \frac{12.96}{G-3.11} \qquad G>5 \text{ mils} \tag{4.4.2.8-23}$$

had a root mean square deviation of 0.2953, i.e., comparable to the cubic fit. Finally the HEDL data were officially published (Reference 37), where the hyperbolic correlation (Equation 4.4.2.8-20) was selected as the most accurate fit while the numerical constants were slightly readjusted.

Figure 4.4-29 shows Equation 4.4.2.8-20 and the experimental data. The ±0.92 kw/ft band earlier determined for the cubic polynominal fit is superimposed. As evident from the figure, the uncertainty band is definitely overestimated when the optimum hyperbolic fit is adopted.

Subsequent to the P-19 test, additional power-to-melt data on very low burnup irradiated pins (P-20 test, Reference 38) indicated an improvement of about 20% in the value of the power-to-melt for pre-irradiated pins to 0.3% burnup, which can be achieved by initial operation at reduced power. Based on this experimental evidence, several programmed startups (combinations of reduced power and holding time) can be utilized to satisfy the no-melting criterion in the high power CRBRP fuel rods. A detailed power-to-melt analysis and preliminary suggestions for a startup procedure are reported in Section 5 of Reference 3. An optimum programmed startup will be selected following final analyses.

4.4.2.8.15 Fuel Restructuring Parameters

The LIFE-III code features a continuous pore migration model which supercedes the previous finite restructuring zones approach, and therefore no longer requires the definition of threshhold restructuring temperatures
56 or restructured zone densities.

4.4.2.8.16 Fission Gas Release and Fission Gas Yield

The model employed to predict fission gas release from the fuel pellets is basically an updating and refinement of the HEDL model (Reference 39).

The correlation for fission gas release from non-restructured fuel
51 as determined in Reference 39 is:

$$F_N = 1 - \frac{1 - \exp(-A_1 B)}{A_1 A_2 B \exp(A_3 Q)} \qquad (4.4.2.8\text{-}24)$$

where

F_N = fractional gas release from non-restructured fuel

B = local burnup (a/o)

Q = local linear heat generation rate (kw/ft)

$A_1 A_2 A_3$ = empirical constants.

The experimental data considered covered the following range of parameters (see Table 4.4-12):

Peak Burnup	0.87 - 5.8 a/o
Peak Linear Power	8.9 - 16 kw/ft
Fuel Density	0.895 - 0.956 theoretical pellet density
Beginning of Life Peak Cladding ID Temperature	837 - 1070°F
Diametral Gap Thickness	0.0022 - 0.008 inch (cold dimensions)

By fitting the correlation to experimental data, the values of the empirical constants were determined as follows:

$A_1 = 0.5748$
$A_2 = 0.3745$
$A_3 = 0.0911$

Subsequently, the model predictions of total gas release were compared with two sets of experimental data not used in the calibration and equation fitting, thus providing an independent check.

The first set (Reference 40) of data referred to high burnup (up to 12.7 a/o) fuel, the second set (Reference 41) to high cladding temperature (1160-1170°F) rods.

Tables 4.4-13 and 4.4-14 list the additional data for high burnup and high cladding temperature conditions, respectively, which were used
51 to verify the validity of the previously determined constants.

REFERENCES

1. M. D. Carelli, A.J. Friedland, C. W. Bach and R. A. Markley, "An Optimized Method for Orificing LMFBR Cores", Trans. Amer. Nucl. Soc., 26, pp. 437-438 (1977).

2. M. H. Fontana, R. E. MacPherson, P. A. Gnadt, and others, "Temperature Distribution in a 19-rod Simulated LMFBR Fuel Assembly in a Hexagonal Duct (Fuel Failure Mockup Bundle 2A): Record of Experimental Data", ORNL-TM-4113, September 1973. (Availability: US DOE Technical Information Center).

56 | 54 3. M. D. Carelli and C. W. Bach, "Predicted Steady State Thermal-Hydraulic Performance of the Fuel and Blanket Assemblies in the CRBRP Heterogeneous Core", WARD-D-0210, Rev. 1, January 1979.

4. "Covered Pressure Drop Flow Test/Crossflow Mixing Test", HEDL-TI-76049, November 1976. (Availability: US DOE Technical Information Center).

5. W. L. Thorne, "Pressure Drop Measurements in FFTF Fuel Vibration Tests", HEDL-TC-812, April 1977. (Availability: US DOE Technical Information Center).

6. W. L. Thorne, "Pressure Drop Measurements from Fuel Assembly Vibration Test II", HEDL-TC-824, April 1977. (Availability: US DOE Technical Information Center).

7. P. M. McConnell, "Clinch River Breeder Reactor Fuel Assembly Inlet/Outlet Nozzle Flow Tests", HEDL-TME-77-8, February 1977. (Availability: US DOE Technical Information Center).

8. H.M. Geiger, D.C. Mees, and D. K. Schmidt, "Radial Blanket Flow Orificing Testing: Calibration Tests", WARD-RB-3045-18, April 1977. (Availability: US DOE Technical Information Center).

9. F. C. Engel, R. A. Markley and A. A. Bishop, "Laminar, Transition and Turbulent Parallel Flow Pressure Drop Across Wire-Wrap-Spaced Rod Bundles", Nucl. Sci. Eng., 69, pp. 290-296 (1979).

10. M. R. Spiegel, Schaum's Outline of Theory and Problems of Statistics, p. 247, Schaum, New York, 1961.

54 | 51

11. I. E. Idel'chik, "Handbook of Hydraulic Resistance Coefficients of Local Resistance and of Friction", AEC-tr-6630 (1960).

12. L. F. Moody, "Friction Factors for Pipe Flow", Trans. Amer. Soc. Mech. Eng., pp. 671-684 (1944).

13. D. Y. Nee, "Clinch River Breeder Reactor Plant. Preliminary Thermal-Hydraulic Performance of CRBRP Primary Control Assemblies", CRBRP-ARD-0151, June 1977. (Availability: US DOE Technical Information Center).

14. Deleted.

15. G. H. Golden and J. V. Tokar, "Thermophysical Properties of Sodium", ANL-7323, August 1967.

16. M. S. Kazimi and M. D. Carelli, "Clinch River Breeder Reactor Plant. Heat Transfer Correlation for Analysis of CRBRP Assemblies", CRBRP-ARD-0034, November 1976. (Availability: US DOE Technical Information Center).

17. "Liquid Metal Fast Breeder Reactor Materials Handbook", HEDL-TME-71-32, June 1971.

18. "Nuclear Systems Materials Handbook", TID 26666. (Availability: Hanford Engineering Development Laboratory).

19. A. J. Friedland, "CRBRP Assemblies Hot Channel Factors Preliminary
56 Analysis", WARD-D-0050, Rev. 3, September 1979.

20. "A Compilation of Boron Carbide Design Support Data for LMFBR Control Elements", HEDL-TME-75-19, March 1975. (Availability: US DOE Technical Information Center).

21. J. F. Hogerten and R. C. Grass, "The Reactor Handbook, Vol. 2, Engineering", AECD-3646, Government Printing Office, Washington, D.C., May 1955.

22. A. Biancheria, "The Effect of Porosity on Thermal Conductivity of Ceramic Bodies", Trans. Amer. Nucl. Soc., 15, pp. 9-10 (1966).

23. G. P. Marino, "The Porosity Correction Factor for the Thermal Conductivity of Ceramic Fuels", J. Nucl. Matl., 38, pp. 178-190 (1971).

24. R. L. Gibby, "Fabrication Microstructure and Thermal Conductivity in UO_2- 25 Wt. Percent PuO_2 Sintered Pellets", HEDL-TME-72-88, May
51 1972.

Amend. 56
Aug. 1980

25. G. Ondracek and B. Schultz, "The Porosity Dependence of the Thermal Conductivity for Nuclear Fuels", J. Nucl. Matl., 46, pp. 253-258 (1973).

26. L. A. Lawrence and R. L. Gibby, "Effects of Pore Structure on the Melting Heat Rating of Oxide Fuels", HEDL-TME-72-81, May 1972.

27. R. B. Baker, R. D. Leggett and D. S. Dutt, "Effect of Burnup on Heat Rating-to-Incipient Fuel Melting: HEDL P-20 Interim Report", HEDL-TME-75-63 (1975). (US DOE Technical Information Center).

28. B. F. Rubin, "Summary of $(U,Pu)O_2$ Properties and Fabrication Methods", GEAP-13582, November 1970.

29. A. Biancheria, U. P. Nayak and M. S. Beck, "Effects of Burnup on Fuel Pin Thermal Performance", in Proceedings of the Conference on Fast Reactor Fuel Element Technology, pp. 361-381, American Nuclear Society, Hinsdale, IL. (1971).

30. U. P. Nayak and A. Biancheria, "Radial Blanket Power-to-Melt Analysis", Westinghouse Electric Corp., Advanced Reactors Division, Madison, PA, FMT-FI-AB-313, May 1973.

31a) E. A. Aitken and S. K. Evans, "Thermodynamic Data Program Involving Plutonia and Urania at High Temperatures. Quarterly Report No. 3", GEAP-5634, May, 1968.

31b) E. A. Aitken and S. K. Evans, "Thermodynamic Data Program Involving Plutonia and Urania at High Temperatures. Quarterly Report No. 4", GEAP-5672, October 1968.

32. J. L. Krankota and C. N. Craig, "Melting Point of Plutonia-Urania Mixed Oxides Irradiated to High Burnup", GEAP-13515, July 1969.

33. R. O. Meyer, E. M. Butler and D. R. O'Boyle, "Actinide Redistribution in Mixed-Oxide Fuels Irradiated in a Fast Flux", ANL-7929, May 1972.

34. R. O. Meyer, E. M. Butler and D. R. O'Boyle, "Actinide Redistribution in Mixed-Oxide Fuels Irradiated in a Fast Flux", ANL-7929 (Suppl. 1), July 1973.

35. R. O. Meyer, D. R. O'Boyle and E. M. Butler, "Effect of Oxygen-to-Metal Ratio on Plutonium Redistribution in Irradiated Mixed-Oxide Fuels", J. Nucl. Matl., 47, pp. 265-267 (1973).

51 36. M. Bober, C. Sari and G. Schumacher, "Redistribution of Uranium and Plutonium During Evaporation Processes in Mixed Oxide Fuel", J. Nucl. Matl., 40, pp. 341-345 (1971).

37. R. D. Leggett, E. O. Ballard, R. B. Baker and others, "Linear Heat Rating for Incipient Fuel Melting in UO_2-PuO_2 Fuel", Trans. Amer. Nucl. Soc., 15, pp. 752-753 (1972).

38. R. D. Legett, R. B. Baker, D. S. Dutt and S. A. Chastain, "Influence of Burnup on Heat Rating-to-Melt for UO_2-PuO_2 Fuel", Trans. Amer. Nucl. Soc., 19, pp. 136-137 (1974).

39. D. S. Dutt, D. C. Bullington, R. B. Baker and L. A. Pember, "A Correlated Fission Gas Release Model for Fast Reactor Fuels", Trans. Amer. Nucl. Soc., 15, pp. 198-199 (1972).

40. R. F. Hilbert, K. J. Perry, W. K. Appleby and others, "Performance of Mixed Oxide Fuel Rods Irradiated to 13 Atom Percent Burnup in EBR-II", GEAP-13538, April 1973.

41. R. F. Hilbert, T. J. Black, K. D. Challenger and W. K. Appleby, "Performance of LMFBR Fuel Rods at High Cladding Temperatures", GEAP-13971, June 1973. (Availability: US DOE Technical Information Center).

42. M. E. Meek and R. F. Rider, "Compilation of Fission Product Yields", NEDO-12154-1, January 1974. (Availability: US DOE Technical Information Center).

43. ASME Boiler and Pressure Vessel Code, "Section III - Division 1, Nuclear Power Plant Components, Subsection NB, Class 1 Components", American Society of Mechanical Engineers, New York, 1974.

44. RDT Standard RDT-C-16-1-T, "Supplementary Criteria and Requirements for RDT Reactor Plant Protection Systems", December 1969. (Availability: Reactor Standards Office, Oak Ridge National Laboratory).

45. A. S. Hanson and N. E. Todreas, "Fluid Mixing Studies in a Hexagonal 61-Pin Wire Wrapped Rod Bundle", COO-2245-51TR, August, 1977.

46. H. Hoffmann and E. Baumgartner, "Experimental Investigation of the Thermodynamic Behavior of Fast Breeder Reactor Fuel Elements with Different Spacer Types", in Fuel and Fuel Elements for Fast Reactors, Vol, 1, pp. 351-368, International Atomic Energy Agency, Vienna, 1974.

47. Deleted.

48. N. I. Buleev, K. N. Polosukhina and V. K. Ryshin, "Hydraulic Resistance and Heat Transfer in a Turbulent Liquid Stream in a Lattice of Rods",
51 High Temp., 2. pp. 673-681 (1964).

49. W. T. Sha and M. D. Carelli, "A Model for Predicting Turbulent Transport in Subchannel Analysis", Trans. Amer. Nucl. Soc., 21, pp. 380-382 (1975).

50. M. C. Chuang, M. D. Carelli, C. W. Bach and J. S. Killimayer, "Three-Dimensional Thermal-Hydraulic Analysis of Wire-Wrapped Rods in Liquid Metal Fast Breeder Reactor Core Assemblies", Nucl. Sci. Eng., 64, pp. 244-257 (1977).

51. M. C. Chuang, R. E. Kothmann, M. J. Pechersky and R. A. Markley, "Cladding Circumferential Hot Spot Factors for Fuel and Blanket Rods", Nucl. Eng. Design, 35, pp. 21-28 (1975).

52. R. Nijsing and W. Eifler, "Analysis of Liquid Metal Heat Transfer in Assemblies of Closely Spaced Fuel Rods", Nucl. Eng. Design, 10, pp. 21-54 (1969).

53. O. E. Dwyer and H. C. Berry, "Turbulent Flow Heat Transfer for In-Line Flow through Unbaffled Rod Bundles: Molecular Conduction Only", Nucl. Sci. Eng., 46, pp, 284-303 (1971).

54. R. M. Roidt, T. G. Bartholet and L. J. Harper, "Experimental Determination of Interior Subchannel Crossflow and Axial Flow in a Model of the Clinch River Breeder Reactor Fuel Assembly Rod Bundle with Wire-Wrap Spacers", ASME Paper 76-WA/HT-33, December 1976 (Also CRBRP-ARD-0108, January 1977).

55. T. G. Bartholet, R. M. Roidt and J. E. Romano, "Clinch River Breeder Reactor Plant. 11:1 Scale Wire Wrapped Rod Bundle Air Flow Test, Side Subchannels", CRBRP-ARD-0129, January 1977. (Availability: US DOE Technical Information Center).

56. E. H. Novendstern, "Turbulent Flow Pressure Drop Model for Fuel Rod Assemblies Utilizing a Helical Wire Wrap Spacer System", Nucl. Eng. Design, 22, pp. 218-219 (1973).

57. M. D. Carelli, C. W. Bach and R. A. Markley, "Hydraulic and Scram Dynamics Analysis of LMFBR Control Rod Assemblies", Trans. Amer. Nucl. Soc., 16, pp. 218-219 (1973).

58. M. D. Carelli, H. W. Brandt, C. W. Bach and H. D. Kulikowski, "LMFBR Control Rods Scram Dynamics", Trans. Amer. Nucl. Soc., 18, pp. 278-279 (1974).

51 59. D. S. Trent, "Application of Geometric Models for the FFTF Hydraulic Core Mockup", BNWL-575, November 1967.

60. M. D. Woods and T.S. Andreychek, "Clinch River Breeder Reactor Plant. Test Evaluation Report on the CRBR Outlet Plenum Flow Stratification Study", CRBRP-ARD-0125, September 1976. (Availability: US DOE Technical Information Center).

61. J. J. Lorenz and P. A. Howard, "A Study of CRBR Outlet Plenum Thermal Oscillations during Steady State Conditions", ANL-CT-76-36, July 1976. (Availability: US DOE Technical Information Center).

62. P. A. Howard, "Steady State CRBR Outlet Plenum Mixing with an AFMS Core", ANL-CT-77-14, April 1977. (Availability: US DOE Technical Information Center).

63. P. A. Howard and J. J. Lorenz, "CRBR Outlet Plenum Thermal Behavior during Transient Conditions", ANL-CT-76-49, September 1976. (Availability: US DOE Technical Information Center).

64. P. A. Howard and J. J. Lorenz, "CRBR Outlet Plenum Mixing Studies: Suppresor Plate and Shear Web Tests", ANL-CT-77-7, November 1976. (Availability: US DOE Technical Information Center).

65. J. J. Lorenz, R. D. Carlson and P. A. Howard, "An Investigation of LMFBR Outlet Plenum Thermal-Hydraulic Behavior during Reactor Scram Transients", ANL-CT-76-18, September 1975. (Availability: US DOE Technical Information Center).

66. M. L. Millburg, J. A. Hassberger and C. J. Boasso, "Natural Circulation Heat Transfer Testing With a Simulated Full Scale LMFBR 217-Pin Electrically Heated Fuel Assembly", HEDL-TME-77-3, June 1977.
51 (Availability: US DOE Technical Information Center).

67. M. D. Carelli, "Core Exit Instrumentation of the Clinch River Breeder Reactor Plant", Nuclear Technology, 37, pp. 261-273, 1978.

68. R. M. Singer and J. L. Gillette, "Measurements of Subassembly and Core Temperature Distributions in an LMFBR", AIChE Symposium Series, 73, p. 184, 1977.

69. A. K. Agrawal, et.al., "Dynamic Simulation of LMFBR Plant Under Natural Circulation", ASME Paper 79-HT-6, 1979.

70. M. Khatib-Rahbar and K. B. Cody, "Establishment of Buoyancy-Induced Natural Circulation in Loop-Type LMFBRs", ANS Transactions,
54 Vol. 28, pp. 432-433, June 1978.

TABLE 4.4-5

FUEL ASSEMBLY COMPONENT PRESSURE DROP DATA LINEAR REGRESSION ANALYSIS

COMPONENT	LINEAR REGRESSION FUNCTION	NO. OF DATA POINTS	MEAN OF ln(Re)	STANDARD DEVIATION ABOUT MEAN OF ln(Re)	MEAN OF ln(D)	STANDARD DEVIATION ABOUT MEAN OF ln(D) **	STANDARD ERROR OF ESTIMATE
Inlet Nozzle	ln(K) = 0.9177 - .05289 ln(Re)	222	13.64	0.3560			0.0841
Inlet Nozzle-Orifice-Shield:							
-- 1 Plate	ln(K)=2.352-.09211ln(Re)-1.452ln(D)	41	13.95	0.3763	-.1845	0.1256	0.0170
-- 2 Plates	ln(K)=1.708-.05022ln(Re)-3.293ln(D)	73	13.73	0.3684	-.3528	0.1057	0.0472
-- 3 Plates	ln(K)=2.240-.08226ln(Re)-3.891ln(D)	60	13.61	0.3560	-.4064	0.1165	0.0207
-- 4 Plates	ln(K)=2.293-.07141ln(Re)-4.032ln(D)	[illegible]3	13.52	0.2982	-.4454	0.1040	0.0136
-- 5 Plates	ln(K)=2.225-.03072ln(Re)-3.651ln(D)	42	13.45	0.2589	-.4484	0.0997	0.0165
Shield	ln(K)=0.3988-.03879ln(Re)	17	13.82	0.3768			0.0966
Rod Bundle:							
-- Inlet	K = 0.370	--					0.2(*)
-- Rod Friction	see Table 4.4-6	161 entire range					0.0524
		46 full flow					+0.0312,-0.0262
-- Outlet	K = 0.178	--					0.2(*)
Outlet Nozzle	ln(K) = .00495 - .04902 ln(Re)	16	13.67	0.7483			0.0450

(*) A 20% uncertainty was selected as a bounding value (not standard error), since no test data are available. This uncertainty is much greater than the values determined for other components, but the effect on flow rate calculations is negligible since the untested components account for only 1 to 2 psi of the 100 psi total assembly pressure drop.

51

** D is the hydraulic diameter of the plate flow area.

TABLE 4.4-6

FUEL ASSEMBLY COMPONENT HYDRAULIC CORRELATIONS

COMPONENT	CORRELATION	REFERENCE AREA (IN^2)	REFERENCE HYDRAULIC DIAMETER (IN)	REFERENCES
Inlet Nozzle	$K = 2.504\ Re^{-0.0529}$	3.976	2.250	7
Inlet Nozzle-Orifice-Shield:				
-- 1 Plate	$K = 10.50\ Re^{-0.0921}\ D^{-1.452}$	3.976	2.250	7
-- 2 Plates	$K = 5.519\ Re^{-0.0502}\ D^{-3.293}$			
-- 3 Plates	$K = 9.396\ Re^{-0.0823}\ D^{-3.891}$			
-- 4 Plates	$K = 9.909\ Re^{-0.0714}\ D^{-4.032}$			
-- 5 Plates	$K = 9.253\ Re^{-0.0307}\ D^{-3.651}$			
Shield	$K = 1.490\ Re^{-0.0388}$	3.976	2.250	7
Rod Bundle:				
-- Inlet	$K = 0.370$	6.724	0.1281	11
-- Rod Friction	$f = 84/Re$ for $Re \leq 1000$	6.724	0.1281	4 - 6
	$f = [1.080+0.0927*(1000/Re)^2+.1694*(1000/Re)^4]\ f_c$			
	where $f_c^{(*)} = 4Log_{10}(2.51/(Re\sqrt{f_c}))$			
-- Outlet	$K = 0.178$	6.724	0.1281	11
Outlet Nozzle	$K = 1.005\ Re^{-0.0490}$	5.899	2.116	7

51

(*) f_c is the Colebrook friction factor correlation[12] for a smooth tube.

TABLE 4.4-7

BLANKET ASSEMBLIES COMPONENT HYDRAULIC CORRELATIONS

COMPONENT	CORRELATION	REFERENCE AREA (IN^2)(*)	REFERENCE HYDRAULIC DIAMETER (IN)(*)	REFERENCES
Inlet Nozzle	$K = 2.504\ Re^{-0.0529}$	3.976 (1.767)	2.250 (1.500)	7
Inlet Nozzle Orifice Shield	$K = C\ Re^{-0.05}$	3.976 (1.767)	2.250 (1.500)	7,8
Shield	$K = 2.0$	2.405	1.750	11
Rod Bundle:				
-- Inlet	$K = 0.427$	3.956	0.1338	11
-- Rod Friction	$f = 110/Re$ for $Re \leq 400$ $f = (110/Re)\sqrt{1-\psi} + (.55/Re^{.25})\sqrt{\psi}$ where $\psi = (Re-400)/4600$ for $400 < Re < 5000$ $f = .55/Re^{.25}$ for $Re > 5000$	3.956	0.1338	9
-- Outlet	$K = 0.290$	3.956	0.1338	11
Outlet Nozzle	$K = 1.005\ Re^{-0.0490}$	3.976	2.250	7

51

(*) Number outside parentheses refers to inner blanket assemblies; inside parenthesis refers to radial blanket.

TABLE 4.4-8

BASES FOR REACTOR INTERNALS PRESSURE DROPS

COMPONENT	NOMINAL PRESSURE LOSS (psi)	LOSS COEFFICIENT	FLOW (lb/hr)10^6	FLOW AREA (ft^2)	BASIS - LIMITATIONS
1) Reactor Vessel Inlet Plenum	4.25	K=1.19	41.446	8.655	Loss coefficient obtained from the inlet plenum feature model test. $\pm$9% uncertainty used in design. $(\Delta P = K \bar{W}^2/2g\rho A_f^2)$
2) Lower Inlet Module	8.66	$(K+\frac{fL}{D})$=2.13	1.096	0.214	Calculated; to be confirmed by radial blanket orificing test. $\pm$20% uncertainty used in design. $(\Delta P = (K+\frac{fL}{D}) \bar{W}^2/2g\rho A_f^2)$
3) Reactor Vessel Outlet Plenum:					
a) UIS	1.78	$(K+\frac{fL}{D})$=2.01	33.986$^{(*)}$	14.51	Loss coefficient obtained from the integral reactor feature model test. $\pm$3% uncertainty used in design. $(\Delta P = (K+\frac{fL}{D}) \bar{W}^2/2g\rho A_f^2)$
b) Exit Nozzle	0.43	K=0.29	41.446	13.77	Loss coefficient obtained from the integral reactor feature model test. $\pm$7% uncertainty used in design. $(\Delta P = K \bar{W}^2/2g\rho A_f^2)$

(*)Based on a total reactor flow of 41.446 x 10^6 lb/hr with 82% flowing up the UIS chimneys.

A_f = flow area

f = friction factor

ρ = density ($\frac{g}{cc}$)

TABLE 4.4-27

CRBRP SECONDARY CONTROL ASSEMBLIES PIN TEMPERATURES HOT CHANNEL/SPOT FACTORS

		Coolant	Film	Cladding	Gap	Absorber	Heat Generation Absorber	Heat Generation Cladding	Heat Generation Coolant
DIRECT(+)									
Power Level Measurement and Control System Dead Band		1.03					1.03	1.03	1.03
Inlet Flow Maldistribution		1.05							
Subassembly Flow Maldistribution Calculational Uncertainties		1.10	--1.12						
Bundle/Bypass Flow Split		1.06							
Cladding Circumferential Temperature Variation			1.58 2.53(*)						
STATISTICAL (3σ)(o)									
Absorber Maldistribution and Conductivity		1.02				1.10	1.03		
Subchannel Flow Area		1.08							1.0
Film Heat Transfer Coefficient			1.40 1.37(*)	1.38(*)					
Pellet-Cladding Eccentricity									
Cladding Thickness and Conductivity		1.01		1.10	1.13			1.04	
Gap Thickness and Conductivity									
Coolant Properties		1.01							
TOTAL	2σ	1.54	2.25 3.85(*)	1.07 1.26(*)			1.05	1.06	1.03
	3σ	1.58	2.48 4.36(*)	1.10 1.39(*)	1.13	1.10	1.06	1.07	1.03

(+) Uncertainties due to physics analysis calculational methods (15% on coolant enthalpy rise and on absorber, cladding and coolant heat generation) are applied directly on nuclear radial peaking factors.

(o) In addition, the assembly inlet temperature will be increased by 16°F, to account for primary loop temperature control uncertainties.

(*) For maximum local cladding midwall temperature calculations only.

TABLE 4.4-28

CRBR EXPECTED OPERATING CONDITIONS DURING PLANT LIFETIME

Parameter	Clean & Unplugged Heat Exchangers (New Plant)				Estimated (2 Year Fouling)				Fouled & Plugged Heat Exchangers (30 Year Fouling)			
	Nominal	Mean	σ	$T_{97.7}$	Nominal	Mean	σ	$T_{97.7}$	Nominal	Mean	σ	$T_{97.7}$
Primary Hot Leg Temperature (°F)	943	946	13	968	950	954	13	976	960	964	13	987
Primary Cold Leg Temperature (°F)	698	697	13	722	705	704	11	725	714	714	12	735
Primary ΔT (°F)	245	249	12	273	245	250	12	274	246	250	12	275
Power (MWt)	975	975		1004	975	975		1004	975	975		1004

51

56 NOTE: Design and control uncertainties are included.

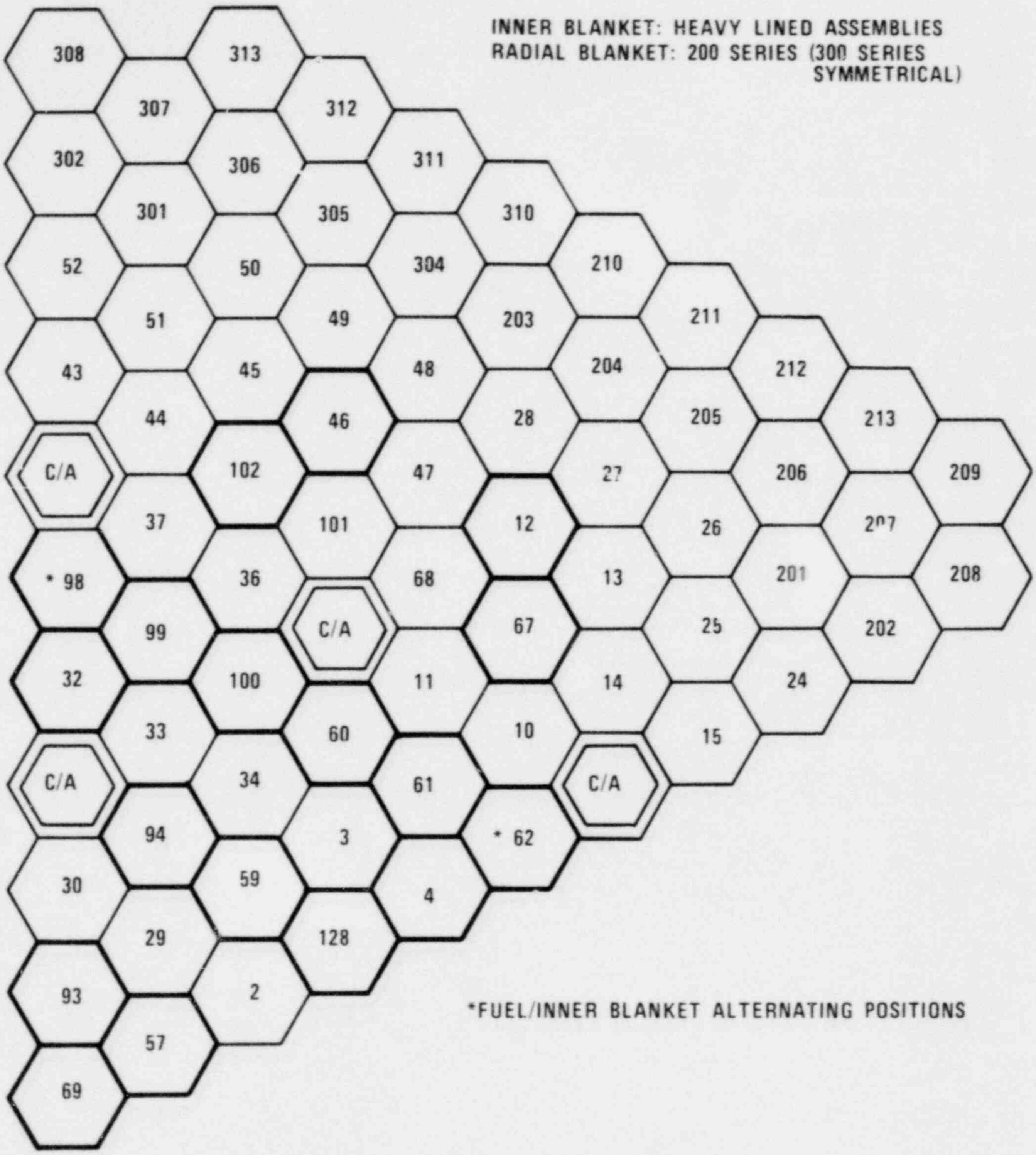

Figure 4.4-9 CRBRP Core 60° Symmetry Sector and Assemblies Numbering Scheme

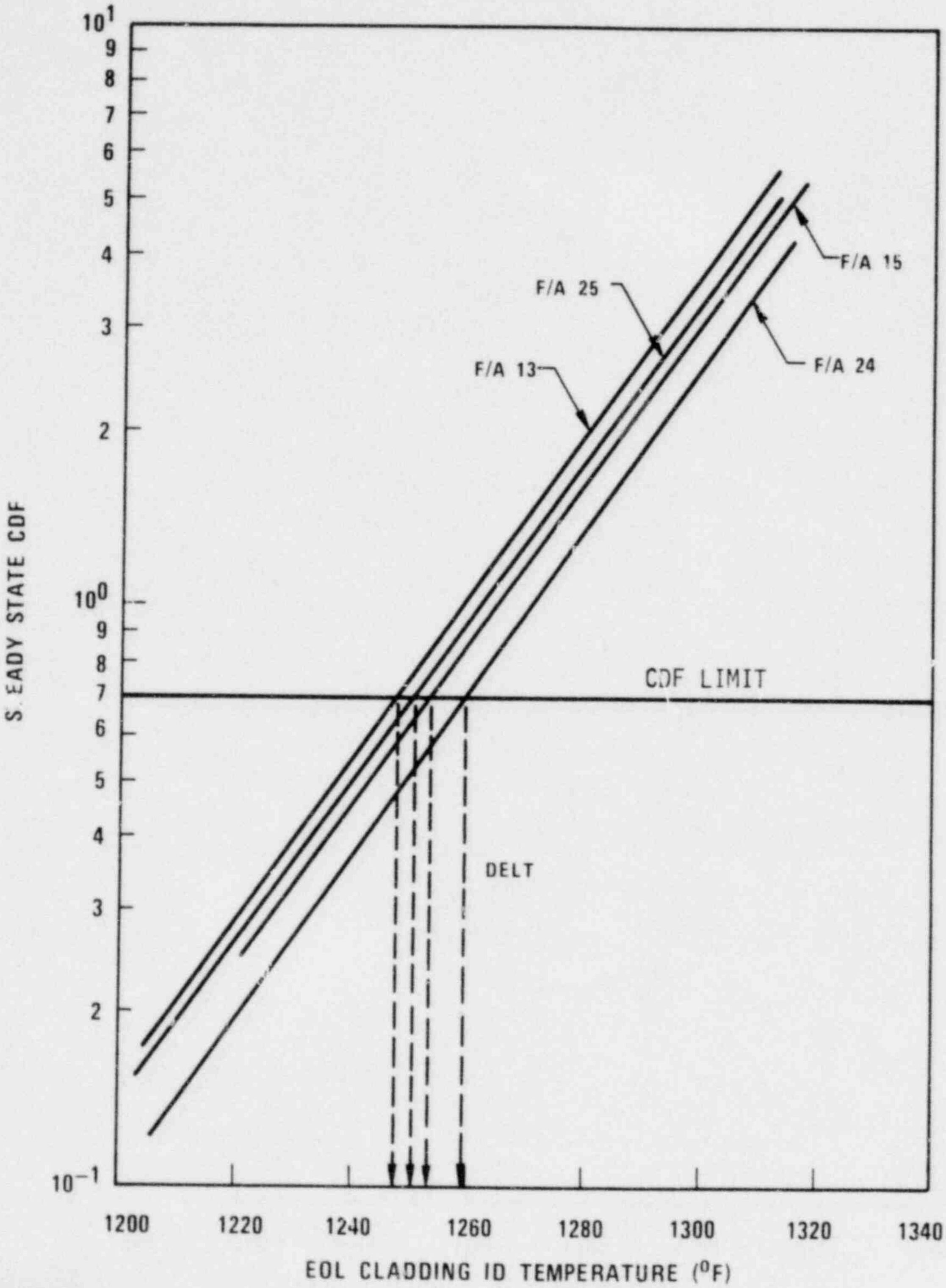

Figure 4.4-10 Typical DELT Determination for First Core Fuel Assemblies

1668-67

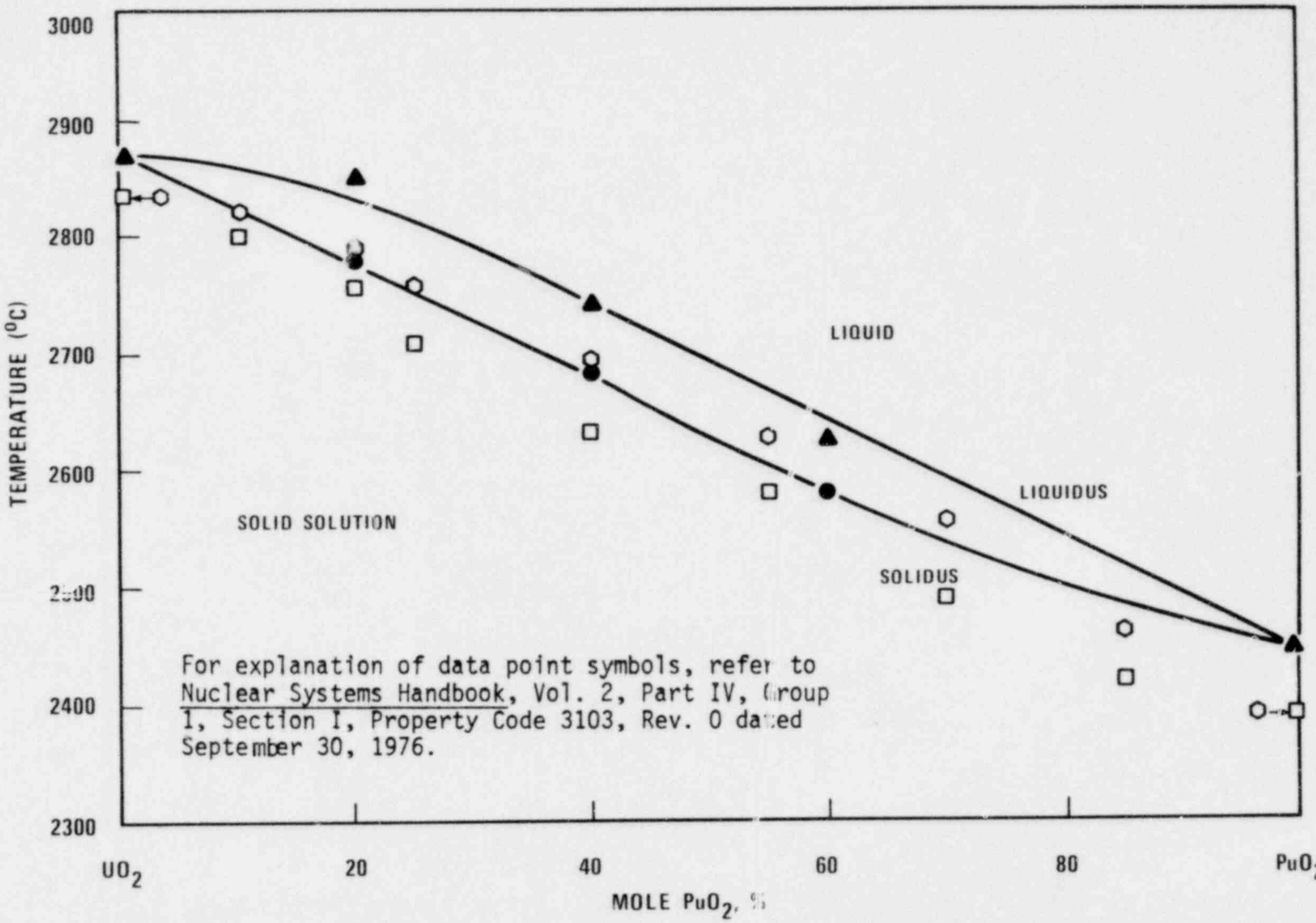

Figure 4.4-27 Phase Diagram for UO_2-PuO_2

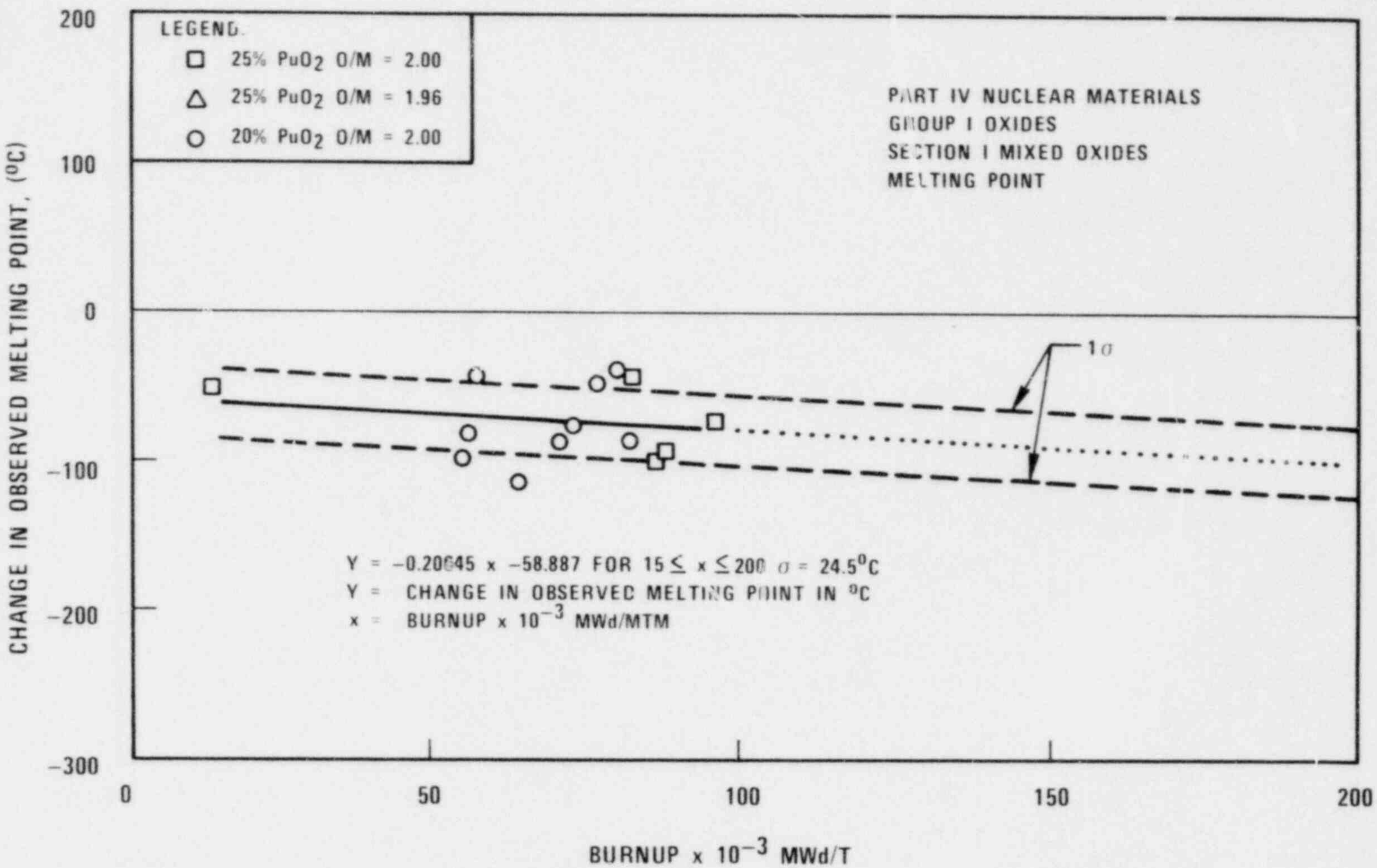

Figure 4.4-28 Effect of Burnup On Melting Point of (U,Pu) O_{2-x}

<u>LIST OF TABLES</u>

LIST OF FIGURES

LIST OF FIGURES (continued)

Amend. 44
April 1978

Amend. 56
Aug. 1980

TABLE 5.1-1

HEAT TRANSPORT SYSTEM THERMAL HYDRAULIC DESIGN CONDITIONS

	Parameter	Thermal Hydraulic Design Value	
	Thermal Power (MWt)	975	
	Primary System		
	Hot leg temperature (^{o}F)	995	
	Cold leg temperature (^{o}F)	730	
45	Flow (per loop) 10^6 lb/hr	13.8	
	Pump Flow (gpm @ 995^{o}F)	33,700	
45 36	Pump Head (Ft Na @ Design Flow and Temp)	450	33
	Intermediate System		
45 40	Hot leg temperature (^{o}F)	936	
	Cold leg temperature (^{o}F)	651	
45 40	Flow (per loop) 10^6 lb/hr	12.8	
	Pump Flow gpm @ 651^{o}F	29,500	
45	Pump Head (Ft Na @ Design Flow and Temp)	330	33

TABLE 5.1-2

PHTS VOLUMES AND VOLUME CHANGES*

Component	Sodium Containment Volume $(ft)^3$ at Room Temperature	Sodium Containment Volume at Thermal/ Hydraulic Design Conditions
Primary System		
45 Primary System o R.V. to Pump	725, 717, 728	746, 738, 749
o Pump to IHX	235	242
o IHX to R.V.	426, 435, 448	434, 444, 457
43 IHX (Shell Side)	1348	1381
Pump - Tank, Suction, and Discharge Nozzle at Normal Operating Level	367	378 33
Check Valve	88	90
Total Volume (Per Loop)	3189, 3190, 3214	3271, 3273, 3297
43 Three Loop Total	9593	9841
Reactor Vessel	13629	13961
45 44 43 Total Primary Volume	23222	23802

---

56 Note: Net sodium overflow volume from a system fill temperature of $400^{\circ}F$ to the thermal/hydraulic operating condition is 1439 FT^3 when corrected to an assumed $900^{\circ}F$ in the overflow tank.

* Where three volumes are given, they refer to loops #1, #2 and #3 respectively.

5.2 REACTOR VESSEL, CLOSURE HEAD, AND GUARD VESSEL

5.2.1 Design Basis

5.2.1.1 General - Reactor Enclosure System

The major components of the reactor enclosure system are the
reactor vessel, the closure head, and the guard vessel. The primary
safety related function of these components is to provide containment,
as appropriate, of coolant, cover gas, fuel, and associated thermal
17 and nuclear activities under all normal, upset, emergency and faulted
conditions. These components shall be designed, fabricated and erected
to quality standards that reflect the importance of this safety function.
Where generally recognized codes or standards for design, materials,
fabrication, and inspection are adequate, they shall be used. Where
a component is not covered by nationally recognized codes or standards,
specific and appropriate design requirements and acceptance criteria will
be defined and provided in component specifications. 1

The reactor enclosure system provides radiation shielding as well as access for insertion and removal of surveillance material, for in-service inspection and for controlling, monitoring and servicing the core and its associated components and structures. The design transients for each of the components are described in Appendix B of this PSAR. In all cases the expected or hypothesized condition, shall not be more severe than the selected design criteria and transients.

41 With regard to Regulatory Guide 1.87 (June 1974, Rev. 0),
"Construction Criteria for Class 1 Components in Elevated Temperature
Reactors" (Supplement to ASME Section III Code Cases 1592, 1593, 1594,
1595, and 1596), portions relevant to component design and manufacture
have been applied through the equipment specifications in the following
manner:

Regulatory Position C.I.a:

41 All five Code Cases should be invoked, where applicable, for
components in high-temperature gas-cooled reactors, gas-cooled fast
breeder reactors, and liquid metal fast breeder reactors.

Implementation

The subject Code Cases are imposed by the equipment specifications except the Code Case revision distributed at time of contract placement, or later, will be used. For example, Code Case 1592-2 was received at the time of reactor vessel contract placement (April 18, 1975). Hence, either Code Case 1592-2 or subsequent revisions will be applicable to the reactor vessel, in lieu of Code Case 1592 as specified in Regulatory Guide 1.87.

Regulatory Position C.I.b:

41 These Code Cases may be used in conjunction with Subsection NB
of Section III of the ASME Boiler and Pressure Vessel Code. Additional
justification, relative to elevated temperature applicability, should 25

be provided in the Stress Report when other portions of Section III such as Appendixes E and F and Subsections NF and NG are used with these Code Cases.

Implementation

Application of the subject Code Cases to Section III Appendix E and Subsections NF and NG is not relevant to elevated temperature portions of the reactor vessel, closure head, or guard vessel (guard vessel support design to NB in lieu of NF). Supplementary rules for application of Code Case 1592 to Appendix F are imposed via RDT Standard F9-4T required by the equipment specifications.

Regulatory Position C.I.c:

41 Component designs should accommodate any required inservice inspection and surveillance programs to monitor and alert for material or component degradation such as creep rupture, creep deformation, creep-fatigue interaction, profusion of microcracks, and buckling. Representative environmental factors of concern which should be considered are the effects of the cooling fluid such as sodium, helium, air, and/or impurities; irradiation effects such as aging and ductility loss; and aging resulting from prolonged exposure to elevated temperature.

Implementation

The Reactor Enclosure System and components (reactor vessel, guard vessel and closure head) are being designed to accomodate inservice inspection. A surveillance program is being planned. Each equipment specification contains detailed requirements necessary for implementation of the system programs for inservice inspection and surveillance. Environmental effects on material properties are specifically considered in design through definition of effects in the equipment specifications.

Regulatory Position C.I.d:

41 When a Code Case refers to an Article in Subsection NB or that Article in turn references another Article in Subsection NB, it should be ascertained that all referenced Articles in Subsection NB are consistent with all applicable elevated-temperature Code Cases and the corresponding supplements in Part C of this guide. 25

Implementation

The CRBRP requires full compliance with the precise provisions of the Code in regard to the requirement of this Regulatory Position. Consistency and/or applicability is determined in strict accordance with the detailed requirements defined in the Code, including the
41 applicable Code Cases.

Riser Elastomer Seals

The balance of the seals on the riser assembly operate at temperatures
41 below 125°F.

Upper Internals Structure Jacking Mechanism

The UIS jacking mechanism utilizes metal buffered seals in the 400°F areas. These seals are part of the mechanical assemblies. The seals will be removed with components at the appropriate maintenance period. Elastomer
41 seals are located in the cooler regions, 125°F maximum, and will be replaced using hands-on maintenance.

Liquid Level Monitor Ports

Four of these components, operating at 400°F, are located on the reactor vessel head. The double metal "O" rings which seal these components will remain attached to the liquid level plug during installation and removal. An inerted cask will be used to install and remove the liquid level monitor while at 400°F, requiring no hands-on operation. Because the liquid level plug remains stationary to the head assembly, the metal "O" rings beneath the plug are expected to require no maintenance. 25

5.2.1.4 Guard Vessel

The guard vessel provides for the retention of the primary sodium coolant in the event of a leak in the portion of the primary coolant boundary which it surrounds. The guard vessel geometry assures reactor vessel outlet nozzle submergence after such a leak which will maintain continuity in operating primary coolant loops to provide core cooling. The guard vessel also provides a uniform annulus for in-service inspection of the reactor vessel, with clearances that preclude contact with the reactor vessel and piping under accident conditions. Insulation for the reactor vessel and a heating system for the reactor vessel to be used prior to sodium fill and during prolonged shutdown are also mounted upon the guard vessel.

The maximum and minimum widths of the radial gap between the guard vessel and the reactor vessel have been conservatively calculated, taking into account all relevent factors such as tolerances on the diameters of the two vessels, permissible out-of-roundness of the two vessels, possible deviations from straightness due to manufacture and subsequent operation, thermal expansion, initial deviations in the alignment of the two vessels, etc. The transporter for the television camera will be designed to accommodate itself to this maximum possible range of gaps as it moves in the space between the two vessels. 25

5.2.1.5 Reactor Vessel Preheat

The Reactor Vessel Preheat System will control the dry heat-up and cool down of the Guard Vessel, Reactor Vessel and Internals between ambient (70°F) and 400°F and if required will provide make-up heat for that lost to the Reactor Cavity during prolonged shutdowns.

The heat will be provided by tubular electrical heaters mounted between the Guard Vessel and insulation. These heaters will be arranged circumferentially around the Guard Vessel and will be grouped and controlled in zones of uniform heat output. Temperature sensing devices will monitor the Guard Vessel temperature in each of these zones and provide the necessary feedback for power level adjustments in the heaters.

The heaters will be mounted to the same framework which supports the Guard Vessel insulation. Ceramic offsets will be used to offset the framework and heaters from the Guard Vessel surface. The heaters and framework will therefore be electrically isolated from the Guard Vessel. Convective barriers, reflective sheaths and the Guard Vessel insulation will be used to optimize heat input to the Guard Vessel and minimize losses to the Reactor Cavity.

Preliminary preheat, startup, and shutdown analyses have been performed on the Reactor Vessel and Guard Vessel to determine the temperature differences which will result in opening and/or closure of the annular gap between the two vessels. By necessity the preheat analysis is very preliminary since no firm preheat procedure has yet been developed. Figures 5.2-4 through 5.2-6 show the temperature differences between the Reactor Vessel and Guard Vessel in the inlet and outlet plenum regions for the three transients in question. As shown the largest positive temperature difference between the Reactor Vessel and the Guard Vessel occurs in the outlet plenum region during startup (335°F) while the largest negative temperature difference occurs in the outlet plenum region during shutdown (-214°F). The nominal radial gap between the reactor vessel and guard vessel is 8 inches at assembly and at the end of preheat. This gap decreases to approximately 7.6 inches minimum during start-up and increases to approximately 8.3 inches maximum during shutdown. During preheat the gap also increases but to a lesser value than during shutdown due to the smaller maximum temperature difference.

Variations in the axial gap between the bottom of the reactor vessel and the inner surface of the guard vessel are noted between the states shown in the table. Thus the largest axial gap is 11.0 inches at the dry cold condition and the smallest gap is 6.2 inches at the end of the heating phase of preheat. 9

5.2.2 Design Parameters

Overall schematic views of the reactor vessel, closure head assembly, inlet and outlet piping, and guard vessel are shown in
56 Figures 5.2-1, 1A and 1B. The top view is given in Figure 5.2-2.

41 17 load transmitted to the support ledge is reduced due to the large mass
presented by the spring-coupled closure head/reactor vessel system compared
to the mass of the postulated sodium slug.

36 5.2.2.2 Closure Head

The closure head consists of three rotating plugs which will be
constructed of SA 508 Class 2 steel. Each plug contains a major penetration
eccentric to its outside diameter. These rotating plugs are interconnected
17 by means of a series of plug risers. Sealing between the plugs is accomplished
by sodium dip seals and double inflatable seals of elastomer material. At
36 its top, the large rotating plug has an outer diameter of 257.38 in., and an
inner diameter of 176.50 in. The large rotating plug provides access to the
vessel interior for the ex-vessel transfer machine and the core coolant
liquid level monitors. The intermediate rotating plug (175.50 in. O.D. and
68.94 in. I.D.) provides access to the vessel interior for the control rod
41 drivelines, upper intervals support columns, and the liquid level monitors.
The small rotating plug (67.94 in. O.D.) provides access to the vessel interior
for the In-Vessel Transfer Machine. The thickness of each rotating plug is
41 22.0 in. Rotation of the plugs will be accomplished by a gearing and bearing
system attached to the plug risers. The nozzles for each penetration will
41 be constructed of an austenitic stainless steel.

Each rotating plug is provided with a system of mechanical locks and electrical interlocks which prevent plug rotation during reactor operation and refueling when plug rotation is not desired.

The mechanical locks include the following:

a. Each plug includes a separate positive lock to assure that the plug cannot be moved, and will not drift from its normal operating position during reactor operation. This lock will be installed to prevent relative rotation between each bull gear and its outer riser whenever the control rod drivelines are connected. The locks shall be manually installed at the end of each refueling cycle, and will be removed only during the refueling period when plug rotation is necessary.

b. The plug drives are designed to be self locking to react to any seismic torque occurring during refueling, which could rotate the plugs and thus damage a fuel or blanket assembly during removal from the core.

The electrical interlocks include the following:

a. During reactor operation, the plug drive and control system keyswitch is in the OFF position, the control system is deenergized, and there is no power to the plug drive motors.

24

b. Electrical interlocks are provided to prevent the plugs from being inadvertently rotated by their drive system unless the upper internals are raised and locked, and the IVTM and EVTM are in a safe condition.

56 24 c. An electrical interlock is also provided to prevent vertical operation of the IVTM or operation of the EVTM over the HAA during operation of the plug drive system.

Each rotating plug has attendant thermal and radiological shielding extended to a depth of 74.65 in. beneath the top of each plug forging. The shielding is composed of a series of plates fabricated from carbon steel,
17 and stainless steel. The cover gas between each set of plates attenuates thermal conduction and thereby acts to decrease the heat flux imparted to the rotating plug. A heating and cooling system is provided to maintain the closure head at 400°F (nominal) as well as providing heating and cool-
17 ing for other small head mounted subassemblies.

A gas entrainment suppressor plate assembly is positioned beneath
45 17 the head thermal and radiological shielding at a depth of 122.65 in. beneath the top of each rotating plug. It protects the head shielding from being contacted by the core coolant and minimizes the amount of cover gas entrained in the core coolant. The assembly is designed to accommodate all normal,
17 upset, emergency, and faulted conditions.

56 25

42 In plan view, the subassembly consists of 33 plates at the same elevation with horizontal gaps between them. (Fig. 5.2-3) These plates have penetrations in line with the head penetrations to allow the passage of the head mounted components into the outlet plenum. Each plate is supported by means of a central support column affixed to the lower shield plate and hanger rods, as needed, near the outer periphery of each plate. These central columns, when possible, consist of tubes which surround closure head penetrations. The number and location of the hanger rods will be determined such that harmful effects from seismic and flow induced vibrations are prevented. The support columns will be inserted through oversized penetrations in the lower shield plate, accurately positioned and then attached to the top surface of the lower plate by means of bolting. The support columns will be attached to the suppressor plate by means of welding. This attachment weld is located above the region of the suppressor plate where high thermal gradients occur by using a plate with an extruded weld neck. The use of a single support provides adequate support while lessening the thermal stresses by permitting the plates to flex
42 freely under the expected thermal gradient. 2

TABLE 5.2-3

MATERIALS FROM WHICH THE REACTOR VESSEL, CLOSURE HEAD AND GUARD VESSEL ARE FABRICATED

Reactor Vessel	Product Form	Material	Comment
Support Ring	Ring Forging	SA 508 Class 2	
Vessel Flange	Ring Forging	SA 508 Class 2	
1 Transition Shell	Plate	SB 168	Inconel 600
17 Shell Cources	Plate	SA 240, Type 304	Austenitic stainless steel
Core Support Ring	Forging	SA 182, Type F304	Austenitic stainless steel formed into arcs and welded
Core Support Cone	Plate	SA 240, Type 304	
Inlet Plenum	Plate	SA 240, Type 304	
Thermal Liner	Plate	SA 240, Type 316	Austenitic stainless steel
1 Thermal Liner Support Ring	Forging	SA 182, Type F304	Austenitic stainless, formed into segments and welded
Nozzles	Forging	SA 182, Type F304	
Closure Head			
Rotating Plugs	Forging	SA 508, Class 2	
Guard Vessel			
1 Vessel top flange	Bar, Plate, Forging	SA 479, SA 240, SA 182	Type 304
Vessel	Plate	SA 240	Type 304
Vessel to support skirt ring	Bar, Forging	SA 479, SA 182	Type 304
Support Skirt	Plate	SA 240	Type 304
Support Flange	Plate	SA 240	Type 304
Nozzles	Plate, Forging	SA 240, SA 182	Type 304
Guard Pipe Flanges	Bar, Plate	SA 479, SA 240	Type 304
Guard Pipe	Welded Pipe, Plate	SA 409, SA 240	Type 304
17 Guard Pipe Elbows	Welded Fitting, Plate	SA 403, SA 240	Type WP 304
Cleanout Nozzle	Forging	SA 182	Type F 304
41 Cleanout Nozzle Cap	Forging, Plate	SA 182, SA 240	Type F 304

56 | TABLE 5.2-4 HAS BEEN DELETED

b. After the second cycle or repair in welds that are heat treated after each repair cycle.

Purchaser approval is required for repair of crater cracks restricted to the crater of any weld pass if the third repair cycle results are not acceptable.

5.3.1.5 Leak Detection Requirement

The PHTS Leak Detection Subsystem, part of the Sodium/Gas Leak Detection System described in Section 7.5.5.1, will provide indication and location information to the operator in the event of a sodium leak from the primary sodium coolant boundary, in a timely manner in order that action may be taken
56 before a critical size crack in the primary boundary develops. (A critical size crack is a crack that would bulge open due to operating stresses. See Section 5.3.3.6.)

The detection system sensitivity requirements are discussed in Section 7.5.5.1.

5.3.1.6 Instrumentation Requirements

The primary system is provided with an instrumentation system which monitors the process variables within the PHTS and which provides signals for safety action and operational information. The measured variables and instrumentation provided are discussed in Section 7.5.2.

5.3.2 Design Description

5.3.2.1 Design Methods and Procedures

5.3.2.1.1 Identification of Active and Passive Components which Inhibit Leaks

In the primary heat transport system, the only active component which is considered a part of the PHTS is the primary pump (see Table 5.3-10 for a list of pumps and valves). In the event of pipe leaks, the primary pumps are reduced to pony motor flow following reactor shutdown.

40

In the unlikely event of a primary pipe or component boundary failure, the PHTS has been designed to limit the loss of reactor coolant and assure that for any boundary failure, continued reactor cooling is provided. The PHTS design features which limit loss of coolant and assure reactor cool-
56 ing are the combined use of elevated piping, use of a guard vessel around major equipment and a five foot pony motor shutoff head. The PHTS guard vessels have been designed such that the tops of the guard vessels are at an elevation which is approximately 9 feet above the tops of the reactor vessel discharge
56 nozzles. This level is based on the combination of the pony motor shut-off head of 5 feet and the minimum safe reactor vessel level which is two feet
40 above the top of the reactor discharge nozzle, plus an additional two feet to accommodate sodium shrinkage and hydraulic uncertainties.

The volume of the guard vessel and the volume of sodium above the minimum safe level of the reactor vessel have been sized to assure that the guard vessel's volume will be less than or equal to the volume loss from the reactor vessel for any leak condition plus contraction. The volume of sodium above the minimum safe level in the reactor is 3870 ft^3 and the PHTS guard vessels are sized at 2700 ft^3.

Continued reactor cooling is provided in the unlikely event of a pipe failure by the PHTS elevated piping arrangement. All PHTS piping is routed at an elevation above the tops of the PHTS guard vessels thereby limiting the loss of coolant in the unlikely event of a pipe failure.

The combination of guard vessel elevation, guard vessel volume, reactor vessel sodium inventory above the minimum safe level, pony motor shutdown head and elevated piping assures a limited loss of reactor coolant and continued reactor cooling capability.

Within the PHTS, there are two general types of failures of the pressure containing boundary. They are (1) failures which occur in a guard vessel and (2) failures in elevated piping outside of the PHTS guard vessels. Consideration of these cases has led to the conclusion that a rupture in a guard vessel represents the worst possible leak condition.

Leak in a Guard Vessel

To verify the consequences of a leak within a guard vessel, an analysis was conducted which made a number of assumptions to ensure conservatism. These assumptions are:

a. The leak occurs in the highest pressure point of the system, i.e., at the pump discharge.

b. The leak occurs when the plant is operating at the maximum temperature which will result in maximum sodium shrinkage following initiation of a leak. (Maximum temperature conditions are normal full power operation.)

c. The reactor vessel cover gas make-up is 100 SCFM. (The current design calls for a scram make-up rate of 25 SCFM.)

d. There is no reactor vessel sodium make-up.

e. Any sodium inleakage to a guard vessel will not flow back to the reactor vessel following sodium shrinkage.

f. There is no thermal shrinkage of components or piping; only sodium shrinkage.

The analysis based on the preceding indicated that for a very large leak, the reactor vessel cover gas make-up capacity limited the leak rate after a initial spill which would fill roughly 1/2 of a guard vessel. After

c. Pipe supports are located at points of concentration loads.

d. Pipe supports are located as close as practical to component nozzles to minimize the component deadweight nozzle loads.

The pipe supports for the Primary Piping System consist of assemblies made up of commercially available constant load pipe hangers, commercially available pipe vibration/seismic snubbers, and specially designed pipe clamps.

The load carrying capacity requirements of the constant load hangers will be determined by deadweight analysis and the travel requirements of the hanger will be determined from free thermal expansion analysis. The minimum travel to be accommodated by the constant load hangers will be the maximum free thermal expansion of the pipe at the hanger location plus 20 percent of that travel. The minimum travel must not be less than 1.0 inches. The constant load hangers will be provided with travel stops to limit the vertical travel of the pipe run when the pipe is empty.

The seismic snubbers are of the mechanical friction type (non hydraulic). The snubber allows the free movement of the pipe during normal expansion and contraction of the piping system, but will "lockup" before the pipe has moved farther than the design displacement along the axis of the snubber.

The pipe clamps which are located on the horizontal runs of piping will be of the "non-integral" type. Typically, the horizontal pipe clamps will consist of a segmented outer steel clamp ring, and a segmented steel sheathed load bearing insulation inner ring. The outer segments are held together by a system of bolts and belleville spring washers. The clamping loads exerted by the belleville spring washers are designed to prevent slippage of the clamp under a 3g acceleration, but will not cause any undue stress on the pipe wall or cause damage to the sheathed load bearing insulations. Reference Figure 5.3-36.

In order that the primary pipe in the vicinity of the reactor vessel maintain its integrity and to accommodate the deflections of the reactor vessel under third level margin design loads, the piping seismic restraints will be designed to fail at loads well beyond those of plant operating conditions but below those that could be generated by the reactor vessel movements. At support locations, where the seismic support must fail to accommodate the third level margin deflections of the reactor vessel, shear pin assemblies as shown in Figures 5.3-37A and 5.3-37B will be provided. An excessive load on the restraint will cause the shear pin to fail, releasing the load, and reducing stresses in the piping, thus preventing excessive yielding or precipitation of cracking in the piping. The pipe hanger assemblies will be designed to accommodate the increased pipe travel. 1

The pipe clamps which are located on the vertial runs of piping engage the horizontal surfaces of the transition pieces which are integral parts of the vertical piping to satisfactorily transmit the pipe loads to the pipe hangers without slippage. The vertical pipe clamp consists of three major components; the outer support ring, the steel-sheathed load-bearing insulation inner bands, and the pipe transistion section
56 which includes an axial support ledge. The transition piece is designed to be welded to the vertical run of the pipe line. It has the same inner diameter of the pipe, and the wall thickness is the same as the pipe line at the point of attachment to the pipe line, but gradually slopes to a larger wall thickness, thus forming a support ledge which contacts the load bearing insulation and transmits the pipe load to the clamp ring. The outer support ring is made up of two Type 304 stainless steel semi-circular rings which are bolted together to form a very stiff circular ring. The inside surface of the ring is machined to a "channel" shape to receive and capture the canned load-bearing insulation. Attachment lugs for snubbers and hangers are welded to the outer surface of the
56 15 ring (see Figure 5.3-38). 1

The constant load hangers being used for pipe support in the reactor cavity area are of "all metal" construction, and are designed to meet the requirements of the ASME Code subsection NF, components supports. Although there is no directly applicable experience with constant load pipe hangers in areas such as the CRBRP reactor cavity, it is expected that no material property degradation will take place due to the radiation and temperature environment because of the type of materials being used.

The radiation fluence in the vicinity of the hangers nearest the reactor core has been estimated to be a 5×10^{18} nvt when integrated over all energy neutrons essentially no neutrons have energy >1 MeV). For this type of neutron energy spectrum, a fluence of 10^{19} nvt corresponds to the onset of shift in nil-ductility temperature (Ref. 29). It is concluded that no significant material degradation will accrue from this phenomenon.

Access to the pipe hangers in the reactor cavity for maintenance and inspection is provided by removable access plugs located in the HAA ledge. There are no inaccessible pipe hangers. 16

speeds coincided with the synchronous speed of the drive motors and maximum (15 psig) cover gas pressure are less than the design pressure of the system (200 psig downstream of the pump, 30 psig upstream of the pump).

Code Case 1596, "Protection Against Overpressure of Elevated Temperature Components," Section III, Class 1, is complied with by the following method.

Specifications for components and piping in the reactor coolant boundary include off-normal dynamic and sustained overpressure loads resulting from:

- Check valve slams resulting from a primary pump seizure
- Dynamic loads associated with a sodium/water reaction (IHX)

41

The plant protection system trips the pumps on primary to intermediate flow mismatches. Therefore, any decrease in primary flow due to some flow blockage in one primary loop causing the pressure to increase as the pump approaches its shutoff head would be limited. The plant protection system also trips the reactor and pumps on a flux to flow mismatch, thereby providing protection against overpressure due to core blockage during power operation.

5.3.2.5 Leak Detection System

5.3.2.5.1 Leak Detection Methods

Leaks from the liquid metal circuits of the reactor coolant system can
be detected by measurement of changes in liquid metal inventory, detection of 28
radioactivity and a separate leak detection system. 28

40 The leak detection system will detect leaks, if they should occur,
in piping, and inside of major component guard vessels as well as below large
tanks such as the reactor overflow tank. Details of the methods for detection
40 of liquid metal to gas leaks are discussed in Section 7.5.5.1. 28

5.3.2.5.2 Indication in Control Room

Detection of a leak will activate an annunciator in the control room. As discussed in Section 7.5.5.1, leak location will be identifiable from either the Plant Data Handling and Display System or by reference to the leak monitoring
40 panels.

Since these loops do not contain isolation valves, isolation of the leaking loop is not possible; however, following shutdown, the affected loop may be partially or completely drained to limit the leak without jeopardizing the function of the other two loops.

5.3.2.5.3 PHTS Coolant Volume Monitoring

The total sodium inventory in the Primary Heat Transport System is monitored by the Data Handling and Display System, using sodium level detectors in the Reactor Vessel (see Section 7.5.3), in the Primary Sodium Pump Tank (see Section 7.5.2), and in the Auxiliary Liquid Metal Overflow Tank (see Section 9.3.5).

5.3.2.5.4 Critical Leaks

Reference 2 of Section 1.6 provides the results of the investigation of potential cracks in the PHTS and the capability to detect leakage from
45 such cracks.

5.3.2.5.5 Sensitivity and Operability Tests

The sodium-to-gas leak detection system, as described in Sec-
56 tion 7.5.5.1, is continuously self-monitoring for channel malfunction. Periodic maintenance procedures will provide for additional checking of operating characteristics. During installation and check-out, the correct electrical functioning of each contact and cable detector will be tested.

5.3.2.5.6 Confinement of Leaked Coolant

All cells and pipe chases within the Reactor Containment Building that house coolant (sodium) equipment and/or piping are operated with an inert atmosphere (nitrogen gas) containing a low oxygen concentration. Information concerning the design of these cells and pipeways is contained in Paragraph 3.A.1.1. The operation of these cells in an inerted atmosphere ensures that a minimum coolant fire will result from any spill or leak.

Inerting gas for individual cells or groups of cells is treated separately to prevent the spread of aerosol vapors beyond the confines of the area where the leakage or spill occurred. Separate cells are provided for redundant and/or safeguard equipment or systems to preclude the loss of that equipment or system in the event of a coolant leak or spill.

Provisions have been made for reducing any splash effect around coolant handling equipment or instrumentation by approximately locating such equipment within the cell to minimize such consequences.

The following design bases have been used to minimize the effects of leaks (including splash effects) from other components:

a) All piping and major components are suspended from the ceiling or side walls above the floor.

b) All piping and major components have an outer layer of metal sheathing over the insulation.

c) All instrumentation in general penetrates the top of the pipe and
56 is protected by metal guard boxes. 25

classified as faulted for the affected steam generator module. Differential pressure between the primary and intermediate sides during this event is conservatively evaluated by assuming that the primary side pressure is that resulting from pony motor speed (approximately 6 psig). For the rest of the loop, the occurrence is classified as an emergency event.

For the unaffected loops, the event is similar to the reactor trip from full power. Decay heat removal is maintained throughout the two remaining loops. The transient responses of temperature, flow and pressure on both the primary and intermediate side of the IHX in the
56 affected loop are presented in Figures 5.3-18A through 5.3-18G. Particular attention is directed to Figures 5.3-18F and G which show intermediate side short term and long term pressure effects.

In evaluating the structural adequacy of the IHX, with respect to the check valve slam, the dynamic nature of the primary sodium pressure history is being accounted for by using dynamic load factors. The factor will be applied to the maximum primary pressure, which in turn, is used to determine the pressure-induced primary stresses. These primary stresses are limited by the emergency condition allowables of Code Case 1592, Paragraph 3224, as modified by RDT F9-4T. The fatigue damage associated with the cyclic nature of the pressure history will be accounted for per Paragraph T-1400 of Code Case 1592. The description of the pressure pulses for the sodium-water reaction and check valve closure is included in the equipment specification. The curves define the amplitudes, duration and number of cycles.

Rapid check valve closure can only occur as a result of primary pump mechanical failure. The event involves a postulated instantaneous stoppage of the impeller of one primary pump, while the system is operating at 100% power. The failure may be a seizure or breakage of the shaft or impeller. Primary system sodium flow in the affected loop decreases rapidly to zero as the pumps in the unaffected loops seat the check valve (thereby causing a rapid check valve closure or slam). A reactor trip will be initiated by the primary intermediate flow ratio subsystem. Sodium flow in the intermediate circuit of the affected loop decays as in a reactor trip from full power, modified by changes in natural circulation head. The event is characterized by a down transient in the hot leg of the intermediate circuit of the affected loop. The transient responses of temperature, flow and pressure on both the primary and intermediate side of the IHX in the affected loop are presented in Figures 5.3-18H through 5.3-18M. Particular attention is directed to Figure 5.3-18J which shows primary pressure effects.

Both the sodium water reaction and check valve closure events are classified as emergency events for the IHX. As such, the IHX designer is required to determine which of the six emergency events is most severe to the IHX. The selected event is then applied with a periodicity of two consecutive occurrences during the first three years of operation, and thereafter five times over the remaining 27 years (or once every six year period). If vendor analysis indicate either as the most severe event, the occurrence of the two consecutive events will be moved to the most stringent time in the life for the event to occur. The IHX design has not progressed to the point where either the sodium water reaction or check valve closure can be defined as the most severe emergency event. Rather, preliminary analysis indicates that damage from either of these events will be insignificant. 16

Pump

Inelastic analyses of the pumps may be required to demonstrate con-
27 formance with ASME and RDT Standards. Paragraph 4 of RDT F9-5T, Sept. 1974 gives a description of acceptable methods for time-independent elastic-plastic analysis and time-dependent creep analysis. Some of the computer programs listed abovr have inelastic capabilities, and will be used where applicable.

For the purposes of loads and analysis the pump R-Spec divides the pump into four areas. These are: Subcomponent 1 which consists of the pump tank, Subcomponent 2 which is the upper inner structure including the pressure bulkhead, Subcomponent 3 which is the rotating machinery and Subcomponent 4 which is the static hydraulics.

Subcomponent 1 is designed to the ASME Boiler and Pressure Vessel Code Section III, Subsection NB Class 1 and Code Case 1592 where applicable. The cone and cylinder are designed mainly by dynamic stiffness requirements. These include seismic loads and the necessity of keeping the natural frequency of the structure above the operating speed of the impeller. SAP IV and the "CRISP" computer codes are used for this analysis. The analysis has been qualified by comparing the results of one analysis against the other. The sphere sealing ring and cone-sphere support ring are designed by sealing ring leakage which requires elastic response during normal and upset conditions. A failure will reduce pump efficiency below plant criteria. These areas are being analyzed by 3D global analysis using NASTRAN The nozzles are designed by pressure, pipe nozzle loads, and thermal transients. The failure modes associated will be creep and creep fatigue. 2D elastic analysis will be required. The design is being made with sufficient space for thermal baffles and liners to keep it elastic as much as is possible. But it may be necessary to qualify it using simple inelastic analysis. A hydraulic leakage test will be run to determine the relation of sealing gap to leakage rate.

Subcomponent 2 will conform to the same Code requirements as Subcomponent 1. The upper closure plate and radiation shield are designed by the design pressure and temperature requirements. Elastic failure is the predominant mode. The heat shield will have steady state thermal gradients which will be determined by a 2D axisymmetric model and stresses will be calculated with a 2D stress model. The motor stand will be designed by the stiffness requirements of the motor and seismic loads. The principle failure would be excess vibration leading to fatigue failures.

Subcomponent 3 can be removed and inspected after an emergency or faulted event and repaired before the plant is placed in service again. Therefore, this section will be designed and analyzed to the ASME Boiler and Pressure-Vessel Code, Section III, Subsection NB for Class 1 Components and Code Case 1592 where applicable. However for emergency events if Code Case 1592 is used the design rules for load controlled stresses (Section 3227) will apply. Strain deformation and fatigue analysis need only be performed up to the emergency event and the limits will apply only to the pumps ability to operate at pony motor speed after the event. This area will be designed by critical frequency requirements, inertial loads, torque and thermal transients. Failures associated will be fatigue, shear failure and creep fatigue. It will be analyzed with a 2D axisymmetric model. The loads caused by bearing misalignment will be accounted for. A general 1/2 scale model hydraulic performance test will be run using water as the pumped fluid. This test will give
26 a measure of pump performance and of internal leakage flows.

5.3.3.10.3.2 Mass Transfer of Radioactive Species

The radioactive aspects of mass transfer in the reactor coolant from the reactor to the Heat Transport System are discussed in detail in Section 11.1. These aspects, in themselves, do not affect the structural integrity of the HTS.

5.3.3.10.4 Compatibility with External Insulation and Environmental Atmosphere

Within the heat transport system the reactor vessel, pumps, and intermediate heat exchangers are enclosed by guard vessels. Between these components and the guard vessels a semi-inert gaseous atmosphere of 0.5-2% oxygen/nitrogen is maintained. The piping and the upper portions of the components containing sodium external to the guard vessels are also insulated to minimize heat loss to the PHTS cells. The thermal
53 insulation consists of alumina silicate blanket material manufactured under controlled conditions to minimize the pickup of halogens and/or moisture. The insulation is protected from halogen pickup during shipping, storage and installation. The insulation has an inner liner and is installed
53 on standoffs to provide a gap for heaters and leak detection equipment and, therefore, does not directly contact piping or components. No field compounded thermal insulation materials are used. This will minimize any potential contamination of the piping by corrosive elements in the insulation. Most piping is also exposed to the 0.5-2% oxygen/nitrogen atmosphere. 1

Sodium leaks into the guard vessels, should they occur, are unlikely to be self sealing in view of the low oxygen content. Small leakages will be contained within the guard vessel. With respect to the piping (except that which is situated within the guard vessels) any sodium leakage will react with oxygen, nitrogen, and thermal insulation. No comprehensive data appear to be available to evaluate the reaction in detail but available information from experimental sodium loops indicates that the leaking sodium will form a sodium oxide (and very likely sodium nitride) "growth" beneath the insulation at the point of leakage. For temperatures below about 1000°F no self sealing
53 of the leak is usually observed. Studies were conducted to evaluate the nature of sodium leakage through precracked austenitic stainless steel piping into a 1.2 v/o oxygen/98.7 v/o nitrogen atmosphere. Materials of Construction are listed in Tables 5.3-4 thru 5.3-9.

5.3.3.10.5 Chemistry of Reactor Coolant

The heat transport system sodium chemistry is selected to minimize corrosion. A periodic analysis of the coolant chemical composition is performed to verify that the coolant quality meets the specifications.

56

Sodium purification capability is provided through the use of cold traps.

Capabilities are provided both for "in-line" primary and
56| intermediate sodium purity determinations (sodium plugging temperature indicators) and for direct sampling and laboratory analysis to monitor impurities. The systems are described in Section 9.3.2.

1k. S. A. Shiels, C. Bagnall, and S. L. Schrock, "Interstitial Mass Transfer in Sodium Systems," in Chemical Aspects of Corrosion and Mass Transfer in Liquid Sodium, pp. 157-176, The Metallurgical Society of the American Institute of Mining, Metallurgical, and Petroleum Engineers, Inc., New York, 1973.

1m. M. C. Rowland, D. E. Plumlee, and R. S. Young, "Sodium Mass Transfer. XV. Behavior of Selected Steels Exposed in Flowing Sodium Test Loops," GEAP-4831, March 1965.

1n. "Investigation of Bi-Metallic Liquid Metal Systems, Progress Report February 1-May 31, 1966," GMAD-3643-5, June 1966.

1p. G. Hofer, "A Thermodynamic Analysis of Carbon Transport in Liquid Sodium," Trans. Amer. Nucl. Soc. 13, pp. 167-168 (1970).

1q. K. Natesan and T. F. Kassner, "Thermodynamics of Carbon Transfer in Sodium-Steel Systems," in Chemical Aspects of Corrosion and Mass Transfer in Liquid Sodium, pp. 130-155, The Metallurgical Society of the American Institute of Mining, Metallurgical, and Petroleum Engineers, Inc., New York 1973.

1r. "Carbon Equilibrium Loop Continuation, Sodium Technology Program Progress Report for the Period Ending November 30, 1970," WARD-4210 T1-1, January 1971.

1s. S. Shiels, C. Bagnall and S. L. Schrock, "Carbon Equilibrium Relationships for Austenitic Stainless Steels in a Sodium Environment," Nucl. Technol. 23 pp. 273-283 (1974).

1t. R. B. Snyder, K. Natesan and T. F. Kassner, "Kinetics of the Carburization-Decarburization Process of Austenitic Stainless Steels in Sodium," J. Nucl. Mater. 50, pp. 259-274 (1974).

1u. "Sodium Technology Program Progress Report for the Period Ending October 31, 1972," WARD-3045T1-7, January 1973. (Availability: USERDA Technical Information Center).

1v. A. Feduska, S. Orbon, S. L. Schrock and S. A. Shiels, "Interstitial Transfer Program Impact Assessment Report, Part I, Application of Data to FFTF Components," WARD-NA-3045-3, August 1973. (Availability: USERDA Technical Information Center).

1w. P. Soo, S. A. Shiels, S. J. Orbon, "Effects of Interstitial Transfer on the Mechanical Behavior of Fast Flux Test Facility Intermediate Heat Exchanger Tubing," WARD-NA-3045-14, 1974. 17
(Availability: USERDA Technical Information Center).

2. W. H. Yunker, "Standard FFTF Values for the Physical and Thermophysical Properties of Sodium," WHAN-D-3, July 1970.

2a. W. E. Ray, R. L. Miller, S. L. Schrock and G. A. Whitlow, "The Structure of Sodium Corrosion Deposits and Their Effect on Heat Transfer Coefficients," Nuclear Technology 16, pp. 249-262 (1972).

3. P. Shahinian, H. E. Watson, and H. H. Smith, "Fatigue Crack Growth in Selected Alloys for Reactor Applications," J. Mater. 7, pp. 527-535 (1972).

4. Deleted

5. Deleted

56

6. L. A. James, "Effect of Thermal Aging Upon the Fatigue Crack Propagation of Austenitic Stainless Steels," Met. Trans. 5, pp. 831-838 (1974).

7. L. A. James, "Crack Propagation Behavior in Type 304 Stainless Steel Weldments at Elevated Temperature," Weld J. Suppl. 52, pp. 173-s - 179-s.

8. Deleted

56

9. P. Shahinian, H. H. Smith and J. R. Hawthorne, "Fatigue Crack Propagation in Stainless Steel Weldments at High Temperature", Weld J. Suppl. 51, pp. 527-s - 532-s (1972).

10. L. A. James, "Fatigue-Crack Growth in Type 304 Stainless Steel Welements at Elevated Temperatures," J. Test. Eval. 1, pp. 52-57 (1973).

11. Deleted

12. Deleted

13. Deleted

56

References to Section 5.3 (Cont'd.)

14. Deleted

15. Deleted

16. Deleted

17. Deleted

18. Deleted

19. Deleted

20. Deleted

21. Deleted

22. Deleted

23. Deleted

24. Deleted

25. Deleted

26. Deleted

27. Deleted

6 | 56 28. Deleted 1

Amend. 56
Aug. 1980

29. C.Z. Serpan, Jr., "Engineering Damage Cross Sections for Neutron Embrittlement of an A302-B Pressure Vessel Steel", Nuclear Engineering and Design, Vol. 33, 1975, pgs. 10-29. 16

56 30. Deleted 19

*31. G.V. Smith, An Evaluation of the Yield, Tensile, Creep, and Rupture Strengths of Wrought 304, 316, 321 and 347 Stainless Steels at Elevated Temperatures, ASTM Data Series DS 552, 1969, p. 55.

*32. D. J. Wilson, The Influence of Simulated Service Exposure on the Rupture Strengths of Grade 11, Grade 22 and Type 304 Steels, Transactions of the ASME, January 1974, p. 10-21.

*33. M. Gold, W. E. Leyda and R. H. Zeisloft, The Effect of Varying Degrees of Cold Work on the Stress Rupture Properties of Type 304 Stainless Steel, Journal of Engineering Materials and Technology, October 1975, p. 305-312.

*34. R. A. Moen and G. V. Smith, "A Consideration on Limits of Cold Working in Nuclear Construction", Transactions of the ASME, April 1975, p. 162-170.

35. W. L. Matheys, WARD-LT-3045-1, "Sodium Leak Characterization Tests," June 1975.

36. W. L. Matheys, WARD-LT-3045-2, "Sodium Leak Characterization Tests, Series 2", April 1976. 23

37. R. R. Lowrie and W. J. Severson, "A Preliminary Evaluation of the CRBRP Natural Circulation Decay Heat Removal Capability", WARD-D-0132, Rev. 0, March 1976.

38. F. J. Loss and R. A. Gray, Jr., "Toughness of Type 316 Stainless Steel Weld Metal Using the J-Integral," in "Mechanical Properties Test Data for Structural Materials Quarterly Progress Report for Period Ending April 30, 1974," ORNL-4963, June 1974, pp. 55-59. (Availability: USERDA Technical Information Center).

39. F. J. Loss and R. A. Gray, Jr., "J-Integral Characterization of Irradiated Stainless Steels", NRL-Report 7565, April 1973.

40. F. J. Loss and R. A. Gray, "Toughness of Type 316 Stainless Steel Forging and Weld Metal Using the J-Integral", in Mechanical Properties Test Data for Structural Materials Quarterly Progress Report for Period Ending July 31, 1974", ORNL-4998, September 1974, pp. 110-117. (Availability: USERDA Technical Information Center).

41. Shahinian, P., "Fatigue Crack Propagation in Fast Neutron Irradiated Stainless Steels and Welds", in Special Technical Publication No. 570, American Society for Testing and Materials, 1975 (in press). 24

*References annotated with an asterisk support conclusions in the section. Other references are provided as background information. 23

References:

42. J. H. Driver, The Effect of Boundary Precipitates on the High-Temperature Fatigue Strength of Austenitic Stainless Steels, Metal Science Journal, Vol. 5, March 1971, p. 47.

43. K. Kanazawa and S. Yoshida, High-Temperature Rotating Beveling Fatigue Behavior of the Austenitic Stainless Steels, SUS 304-B and 316-B, Trans. Nat. Research Inst. Metals (Japan), June 1974, 16 (3) 90-98.

44. C. F. Cheng, C. Y. Cheng, D. R. Diercks, and R. W. Weeks, Low-Cycle Fatigue Behavior of Types 304 and 316 Stainless Steel at LMFBR Operating Temperature, Fatigue at Elevated Temperatures, STP 520, August 1973, p. 355-364.

45. C. R. Brinkman, G. E. Korth and R. R. Hobbins, Estimates of Creep-Fatigue Interaction in Irradiated Austenitic Stainless Steels, Nuclear Technology, Vol. 16, October 1972, p. 297.

46. L. A. James and R. L. Knecht, Fatigue-Crack Propagation in Fast-Neutron-Irradiated Types 304 and 316 Stainless Steels, Nuclear Technology, Vol. 19, Sept. 1973, p. 148.

47. M. W. Mahoney and N. E. Patton, The Effect of Carbide Precipitation on Fatigue Crack Propagation in Type 316 Stainless Steel, Nuclear Technology, Vol. 23, July 1974, p. 53.

48. B. Weiss and R. Stickler, "Phase Instabilities During High Temperature Exposure of 316 Austenitic Stainless Steel," Met. Trans., 3 April 1972, p. 851-866.

49. N. L. Mochel, C. W. Ahlman, G. C. Wiedersum and R. H. Zong, Performance of Type 316 Stainless Steel Piping at 5000 psi and 1200°F, Vol. XXVIII, Proceedings of the American Power Conference, 1966.

50. J. T. Barnby and F. M. Peace, The Effect of Carbides on the High Strain Fatigue Resistance of an Austenitic Steel; Acta Metallurgica, Vol. 19, Dec. 1971, p. 1351.

51. T. J. Daly and G. G. Elder, "Final Report of Clinch River Breeder Reactor Plant Piping and Valve Technical Support Team", Westinghouse Advanced Reactors Division, Madison, Pa., WARD-D-0051. September 27, 1974.

52. Deleted

53. Deleted

56 25

References:

54. P. Soo, "Selection of Coolant-Boundary Materials for the Clinch River Breeder Reactor Plant", WARD-D-0010, August 1974.

55. S.A. Shiels, S.L. Schrock, and L.L. France, "Interstitial Transfer Program Impact Assessment Report, Part II - Topical Report", WARD-NA-3045-3, September 1973.

56. G.V. Smith, "An Evaluation of Yield, Tensile, Creep and Rupture Strength of Wrought 304, 316, 321, and 347 Stainless Steels at Elevated Temperatures", ASTM Data Seri- . Publication DS 5S2, American Socie.y for Testing and .aterials, February 1969.

57. P.Soo (Compiler),"Analysis of Structural Materials for LMFBR Coolant-Boundary Components - Materials Property Evaluations", WARD-3045T3-5, November 1972.

56 58. Deleted 25

TABLE 5.3-13

COLD LEG CHECK VALVE CHARACTERISTICS

Requirement	Units	Design Value
Design Flow Rate (at 730°F)	lbs/hr	13.82×10^6
Flow Range at Normal Operating Conditions	% of Design Flow	40 - 100
Max. Shutoff, Δ P Imposed Across Seat		
Steady State	psi	160
Pressure Loss at Design Flow	psi	$\leq$10
Pressure Loss at Pony-Motor Flow Conditions of 2500 gpm at 600°F	psi	$\leq$0.20
Pressure Loss at Natural Circulation Flow Conditions of 670 gpm at 730°F	psi	$\leq$0.03
Temp. at Which Design Flow Pressure Loss is Calculated	°F	730
Allowable Leakage in Reverse Direction at Shutoff at 730°F	gpm	21
Pressure Difference for Allowable Leakage, Reverse Direction	psi	50

Closure Characteristics

The maximum steady state reverse flow allowed by the check valve shall be less than 1100 gpm. The valve shall not require a pressure differential across the disk greater than 1.0 psi to shut. Closing time shall be 5 seconds maximum (after flow reversal) with a resultant pressure surge of less than 50 psi under the specified reverse flow conditions.

56 53

TABLES 5.3-14 thru 5.3-22

HAVE BEEN DELETED

(next page is 5.3-97a)

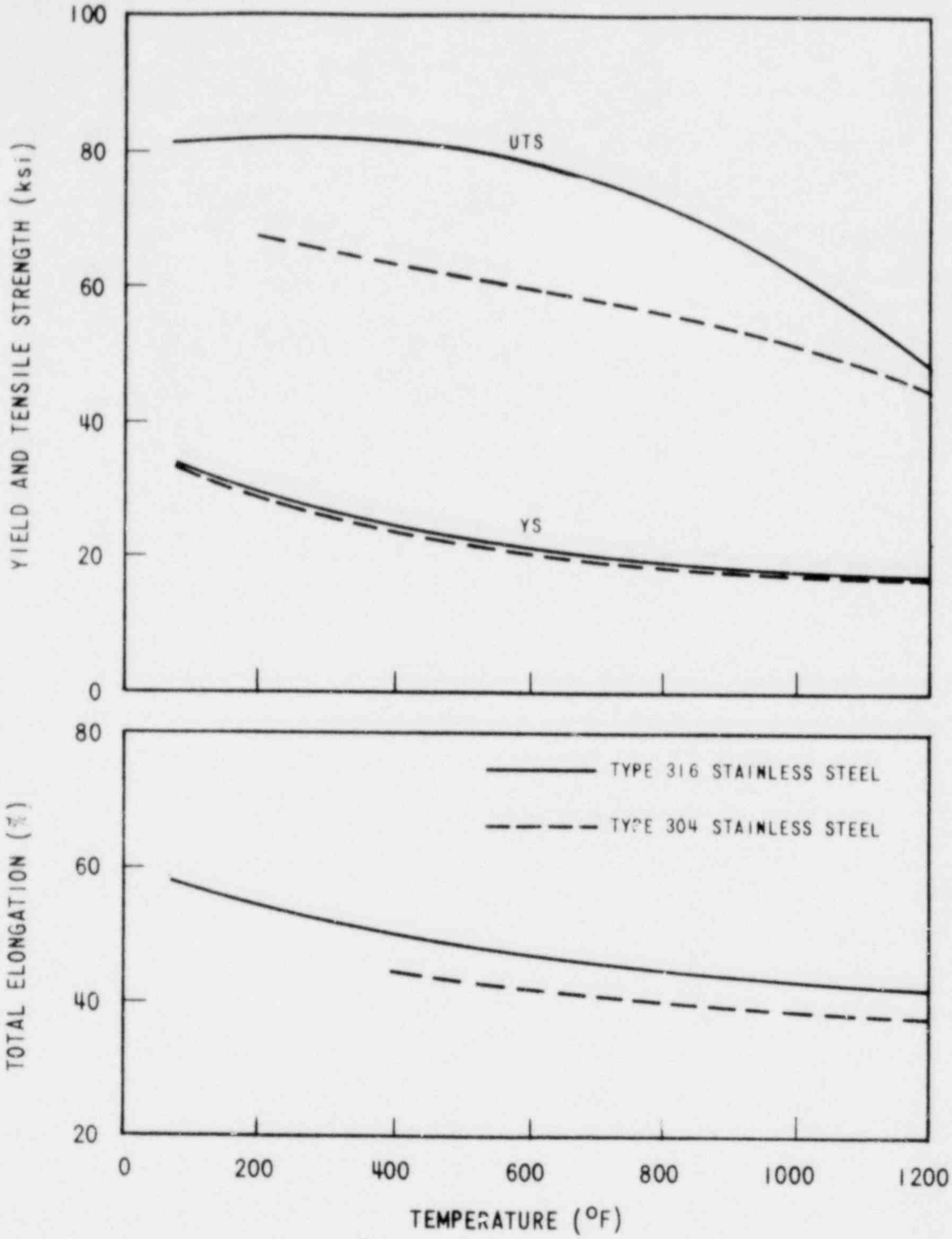

Figure 5.3-1. Comparison Between the Strengths and Ductilities of Solution Treated Types 304 and 316 Stainless Steel Containing 0.08 Weight Percent (C + N)

* Taken from Reference 54.

6669-17

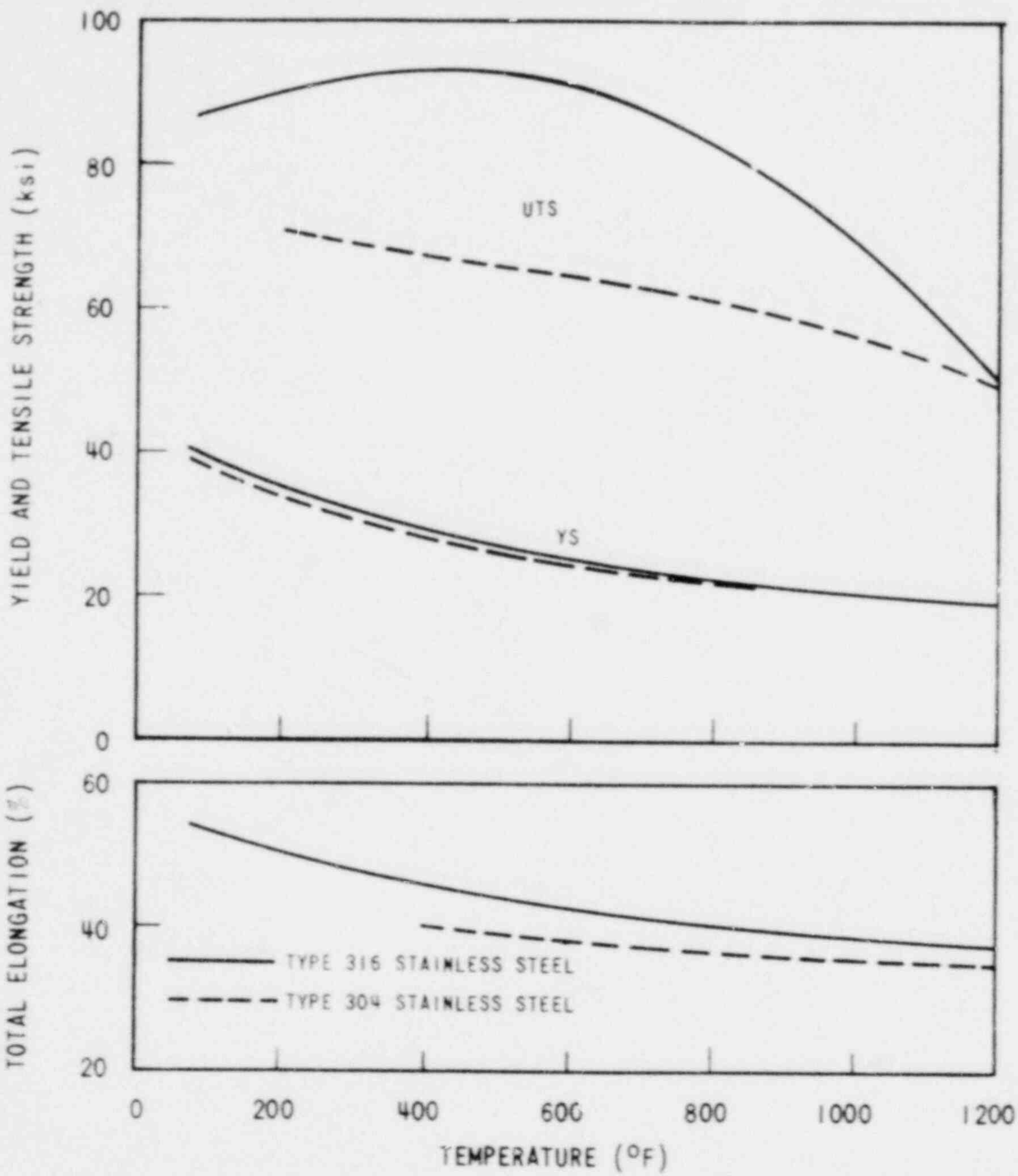

Figure 5.3-2. Comparison Between the Strengths a ³ Ductilities of Solution Treated Types 304 and 316 Stainless Steel Containing 0.12 Weight Percent (C + N)

* Taken from Reference 54.

6669-18

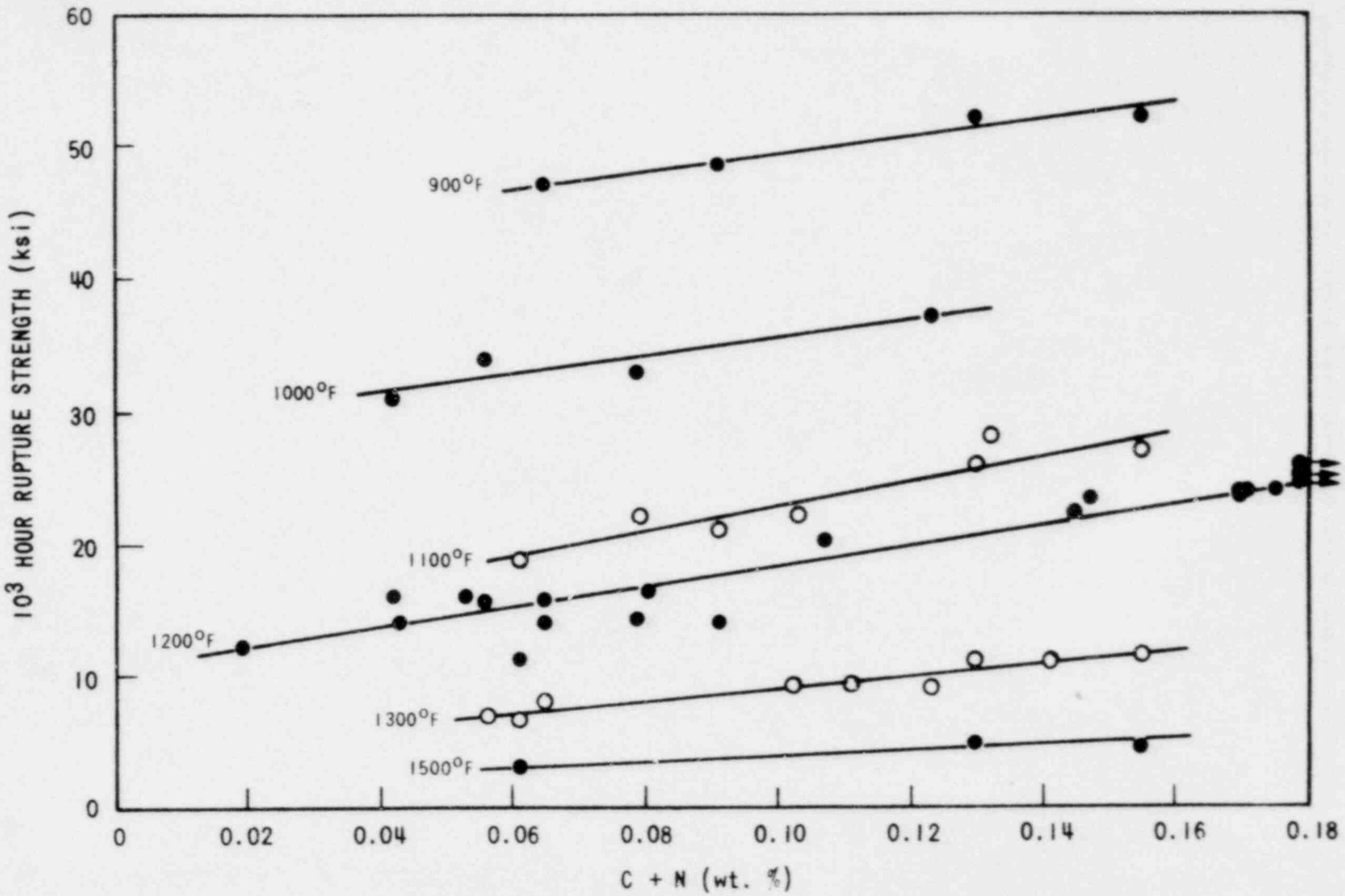

Figure 5.3-3. Effect of Interstitial Content on the 10^3 Hour Rupture Strength of Type 304 Stainless Steel Bar
* Taken from Reference 55.

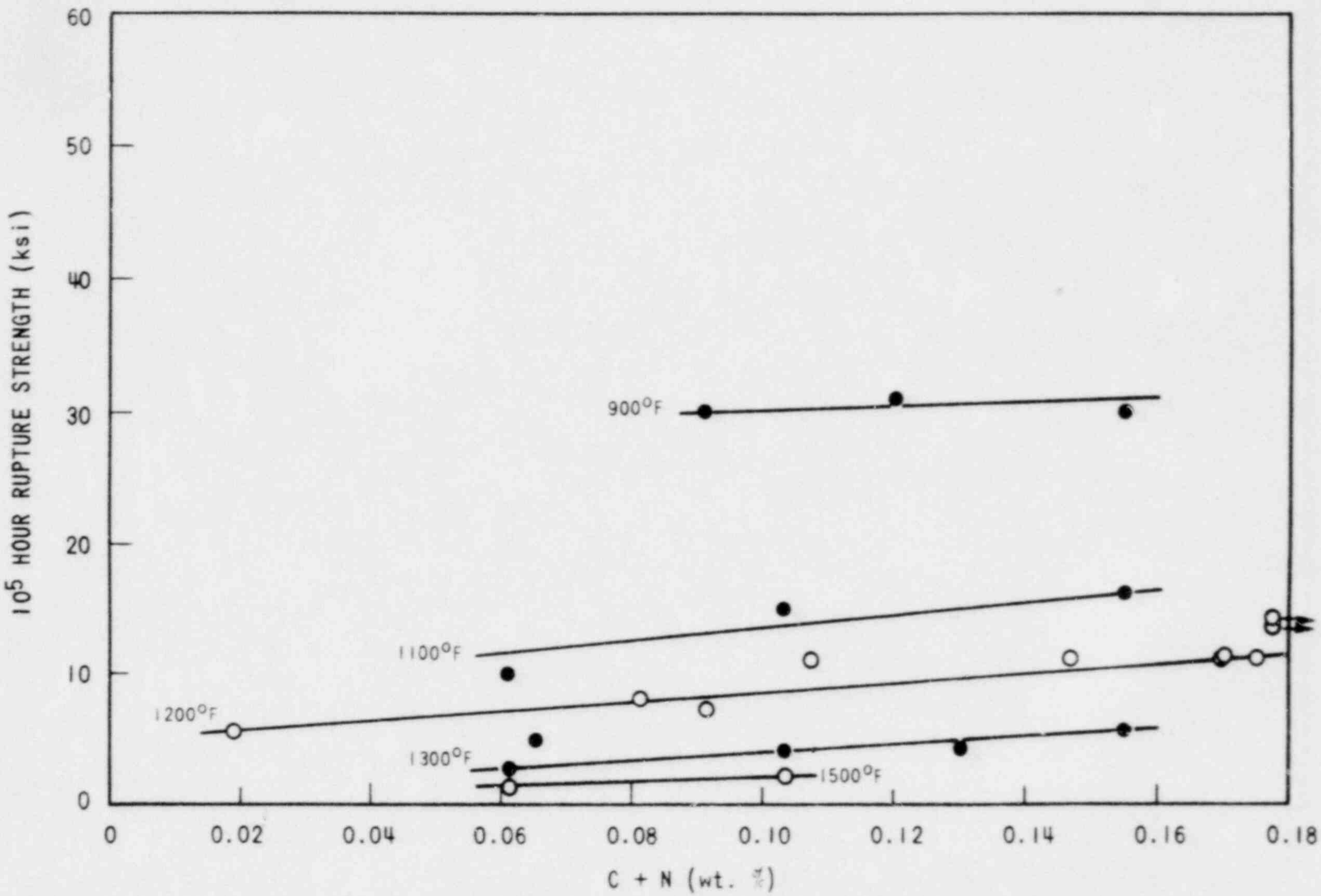

Figure 5.3-4. Effect of Interstitial Content on the 10^5 Hour Rupture Strength of Type 304 Stainless Steel Bar

* Taken from Reference 55.

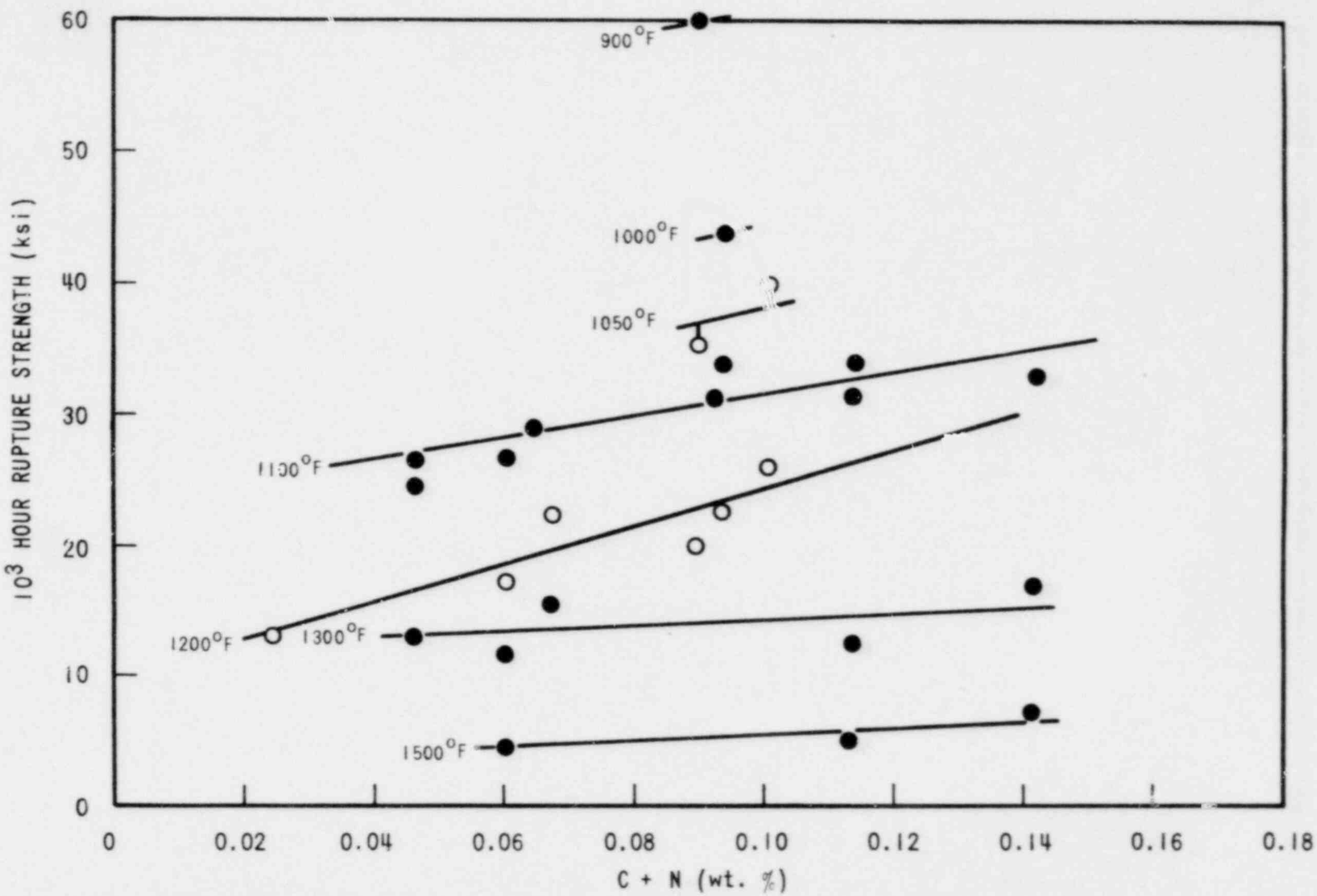

Figure 5.3-5. Effect of Interstitial Content on the 10^3 Hour Rupture Strength of Type 316 Stainless Steel Bar

* Taken from Reference 55.

6669-23

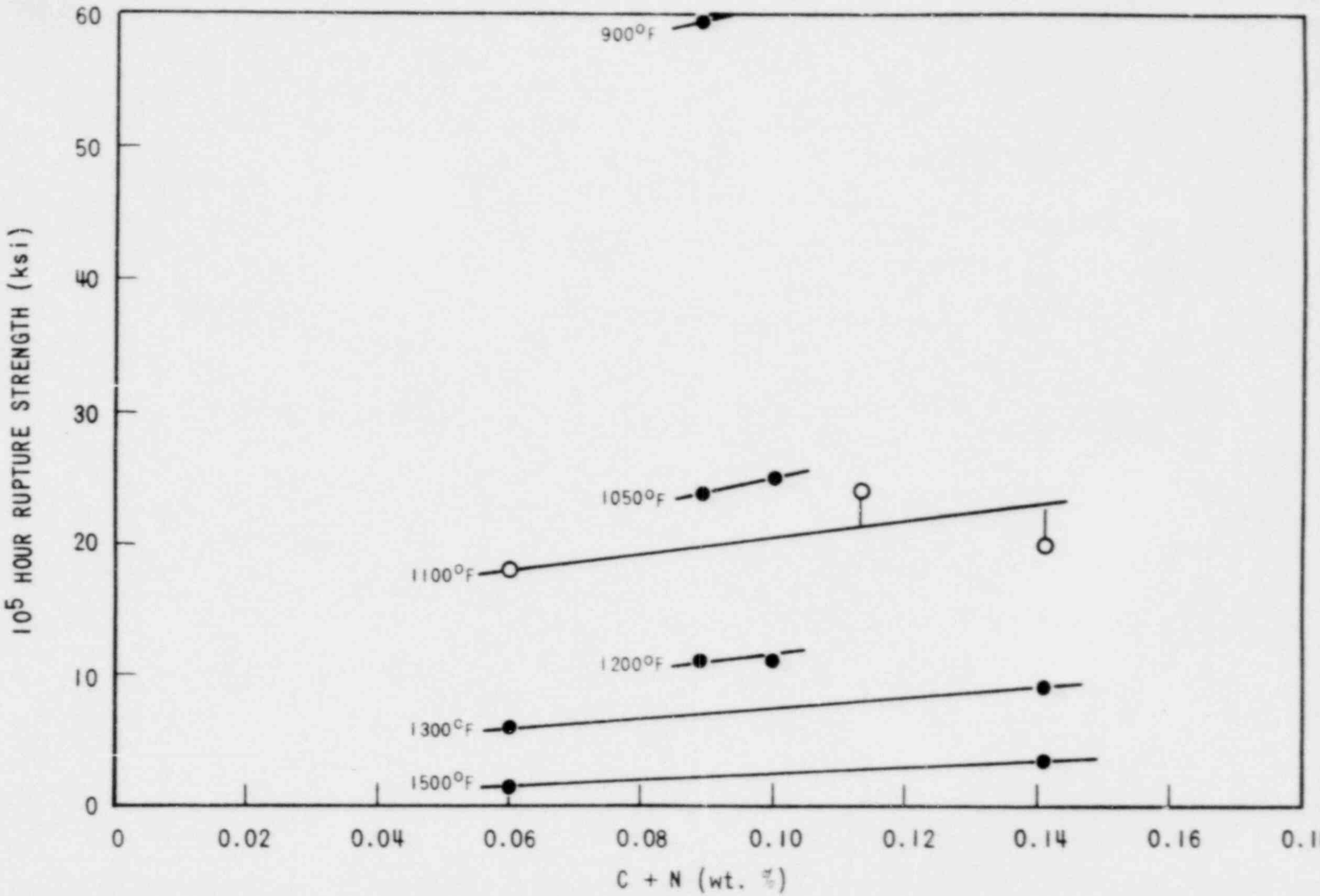

Figure 5.3-6. Effect of Interstitial Content on the 10^5 Hour Rupture Strength of Type 316 Stainless Steel Bar

* Taken from Reference 55.

6669-24

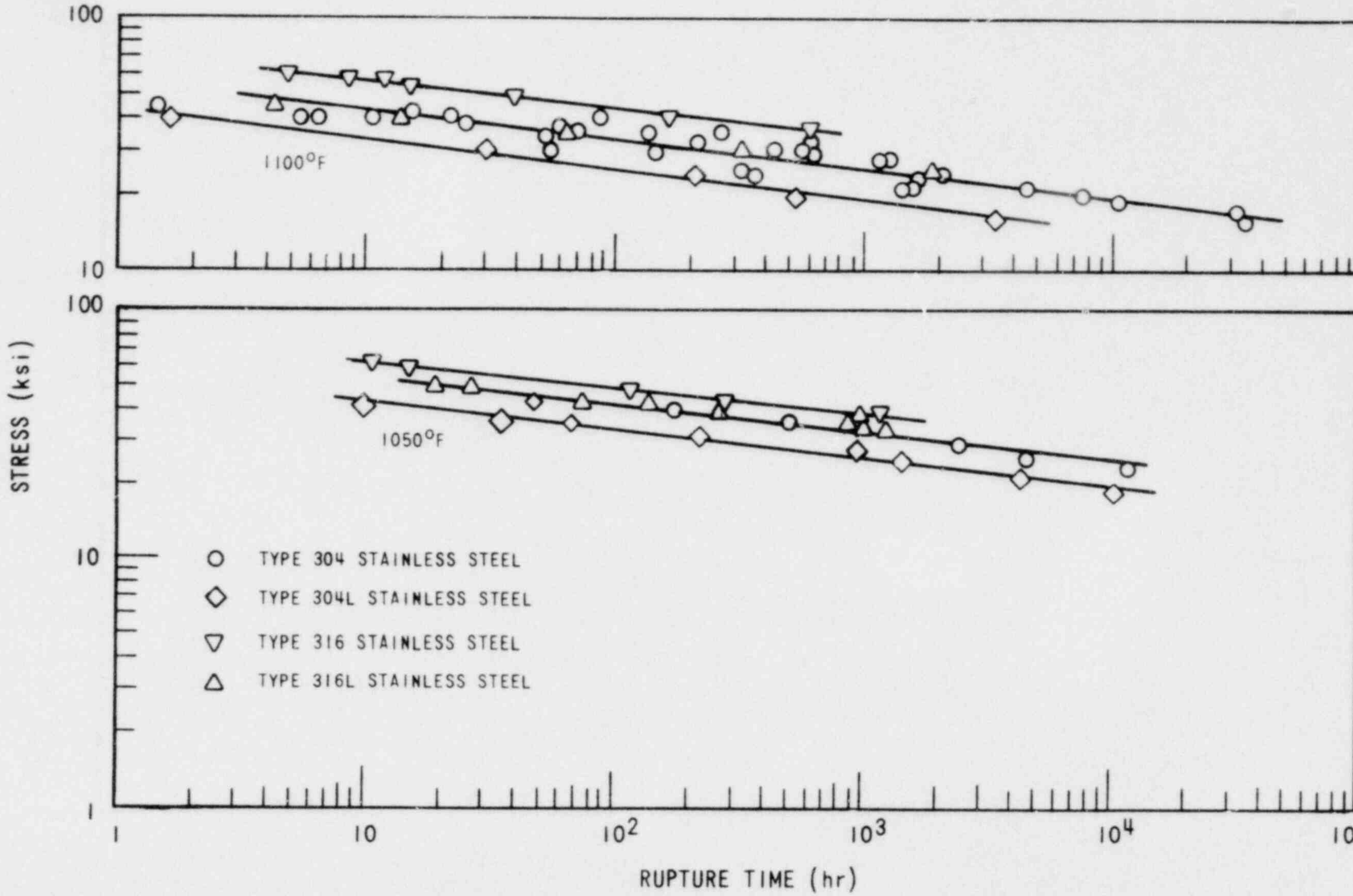

Figure 5.3-7. Stress-Rupture for Austenitic Stainless Steel Bar and Plate

* Taken from Reference 56.

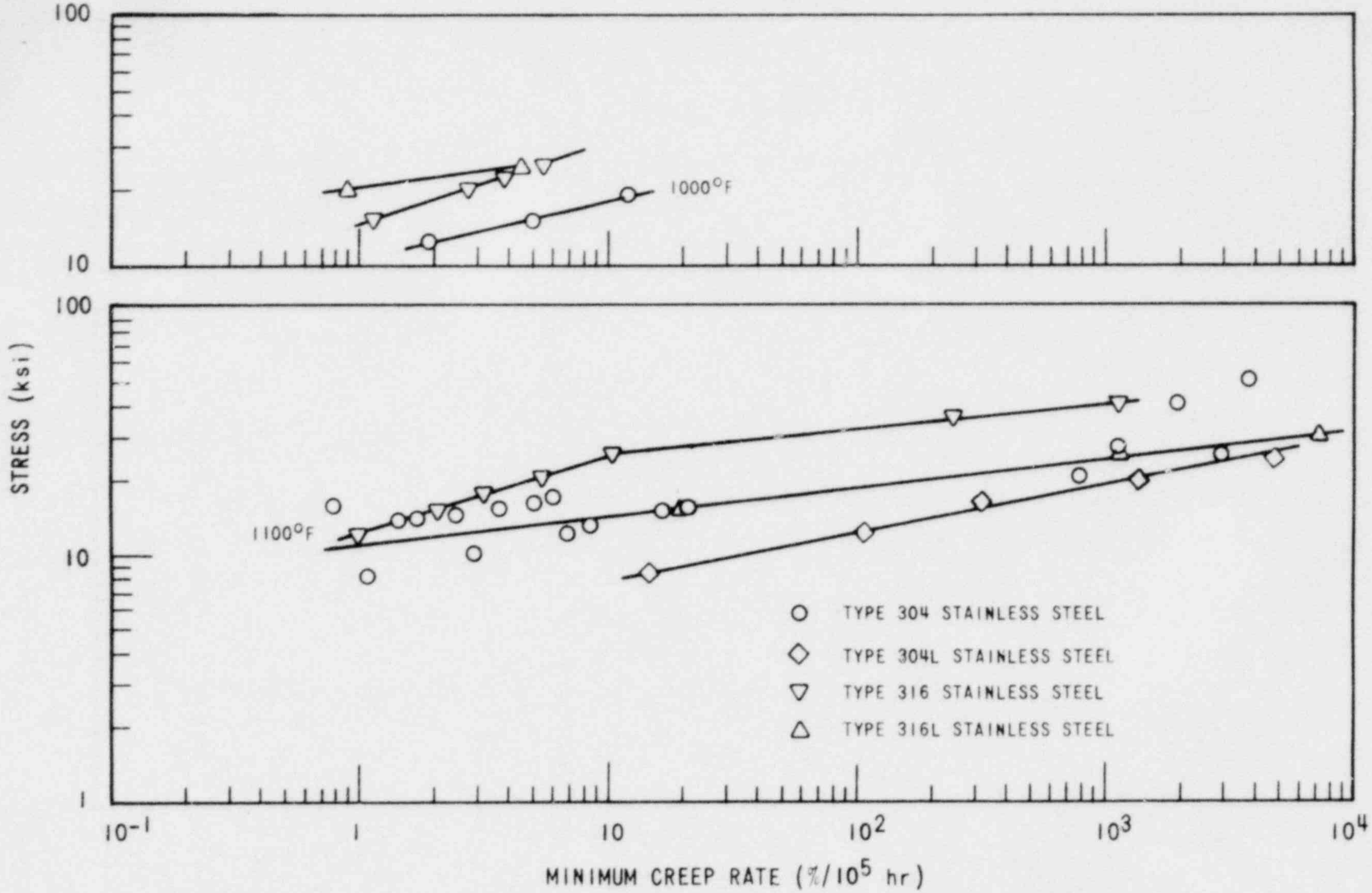

Figure 5.3-8. Minimum Creep Rates for Austenitic Stainless Steel Bar and Plate

* Taken from Reference 56.

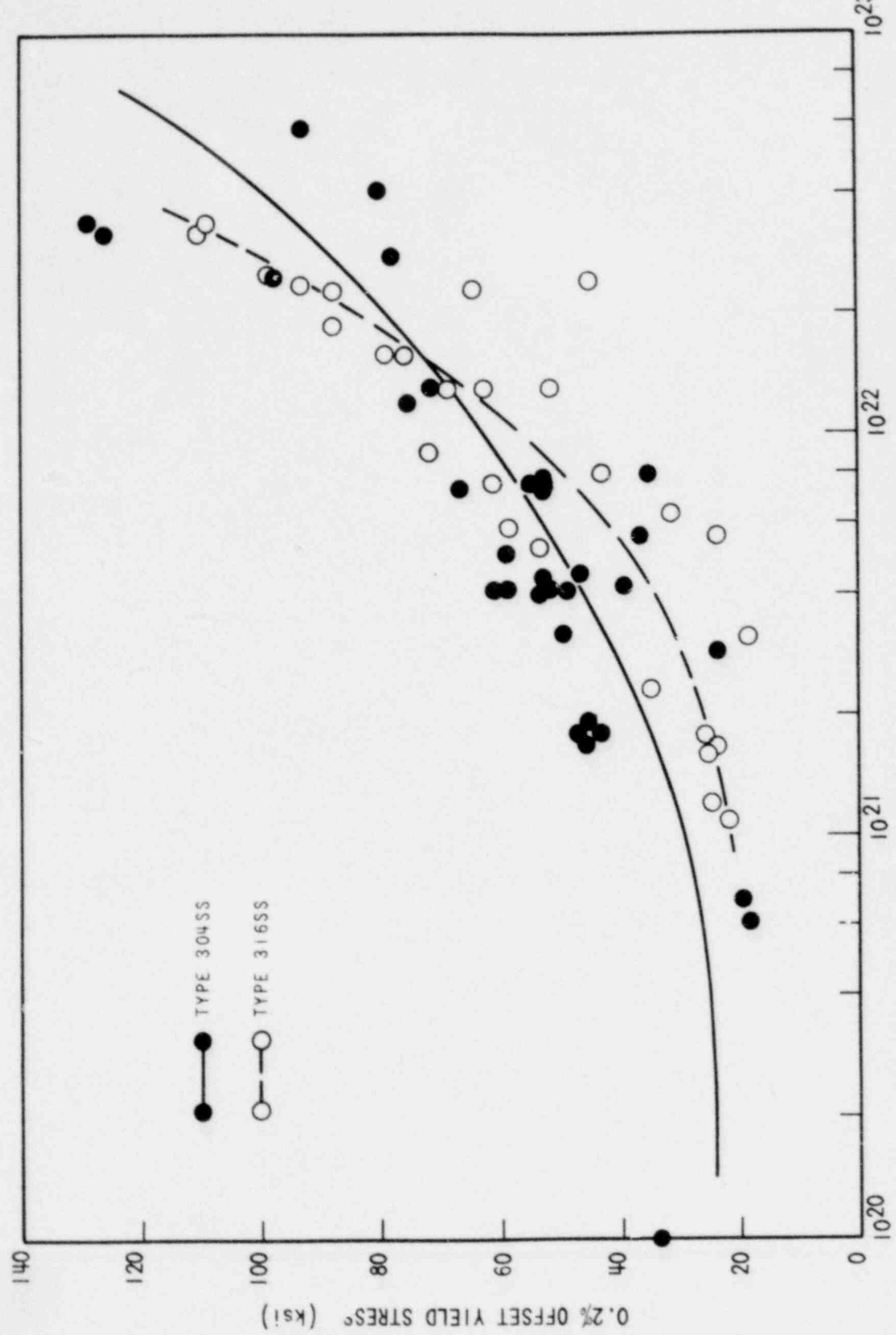

Figure 5.3-9. Yield Strength of Neutron Irradiated Austenitic Stainless Steel at 800°F

* Taken from Reference 57.

6669-12

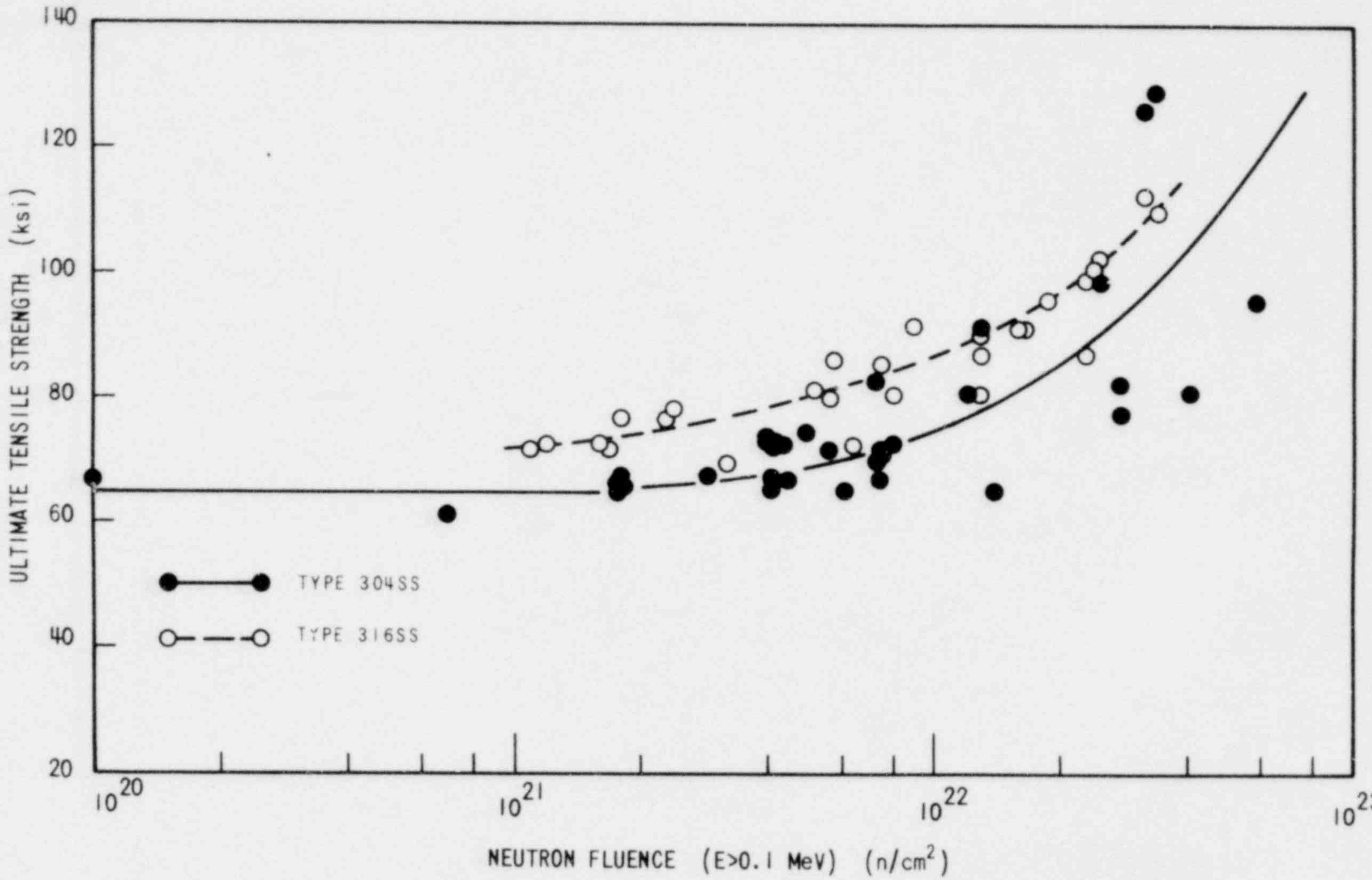

Figure 5.3-10. Ultimate Tensile Strength of Neutron Irradiated Austenitic Stainless Steel at 800°F

* Taken from Reference 57.

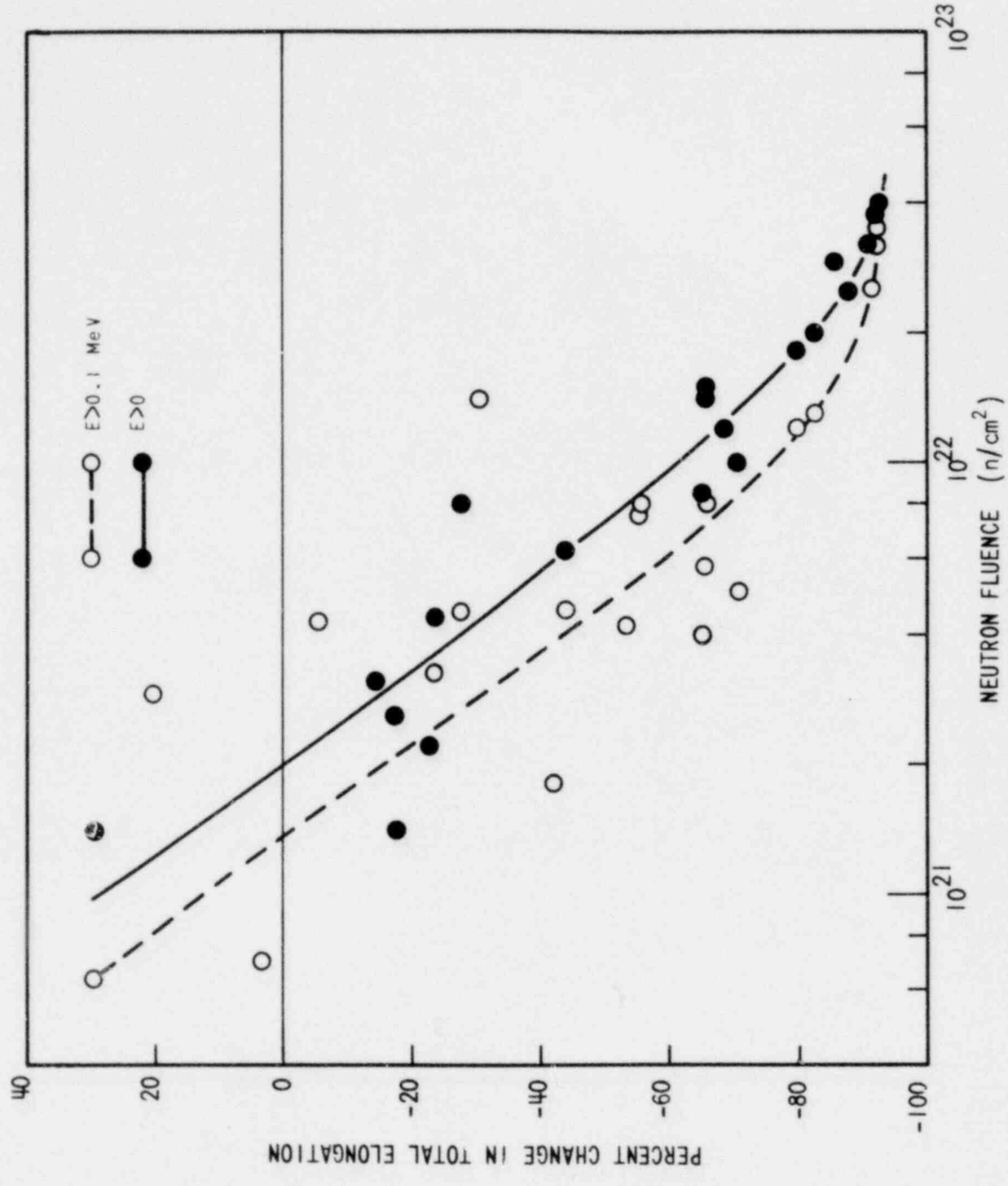

Figure 5.3-11. Irradiation-Induced Ductility Changes in Type 304SS at 800°F

* Taken from Reference 57.

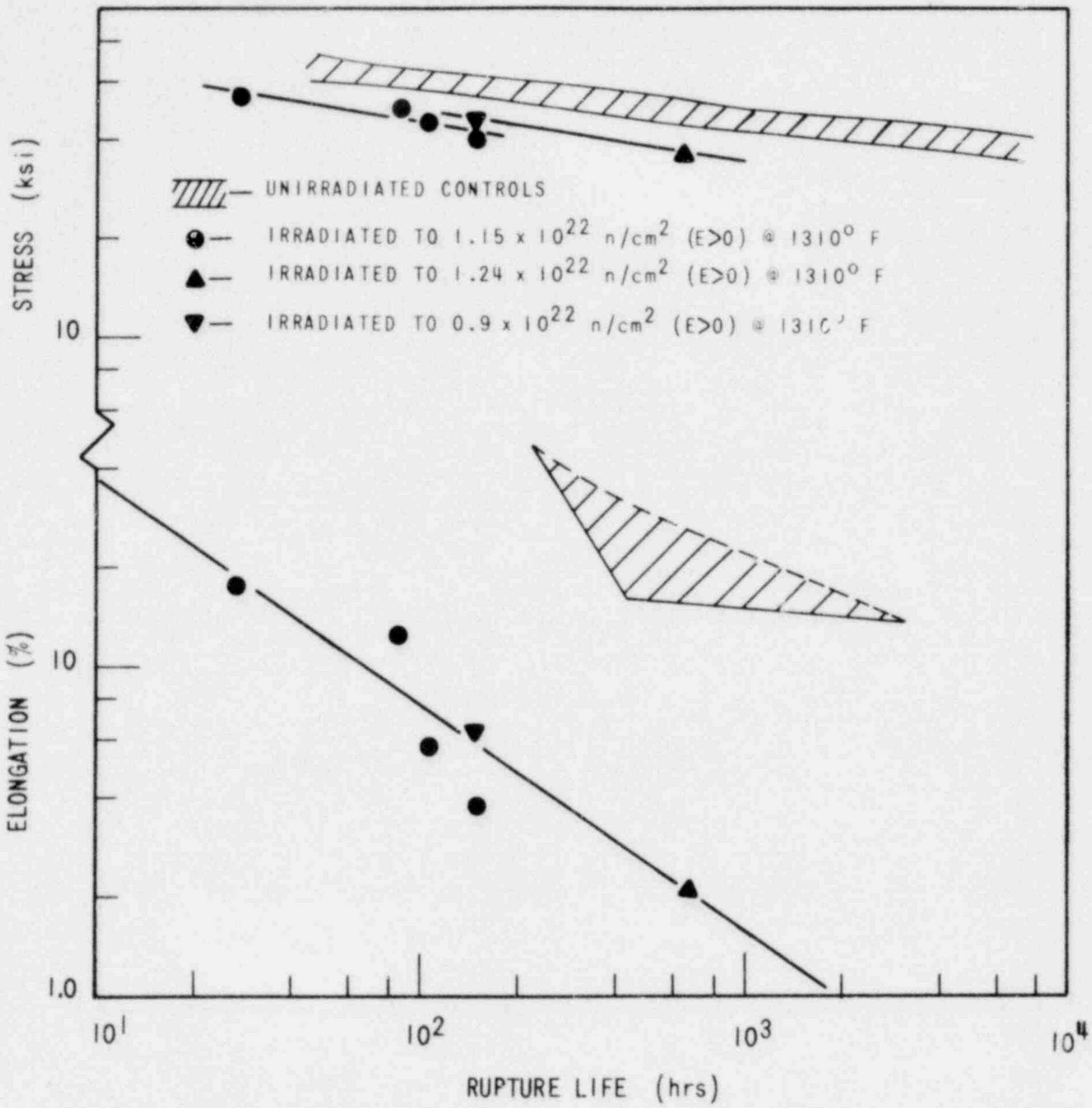

Figure 5.3-12. Creep-Rupture of Irradiated Type 316SS at 1000°F

* Taken from Reference 57.

6669-15

56 FIGURES 5.3-25 thru 5.3-35
HAVE BEEN DELETED

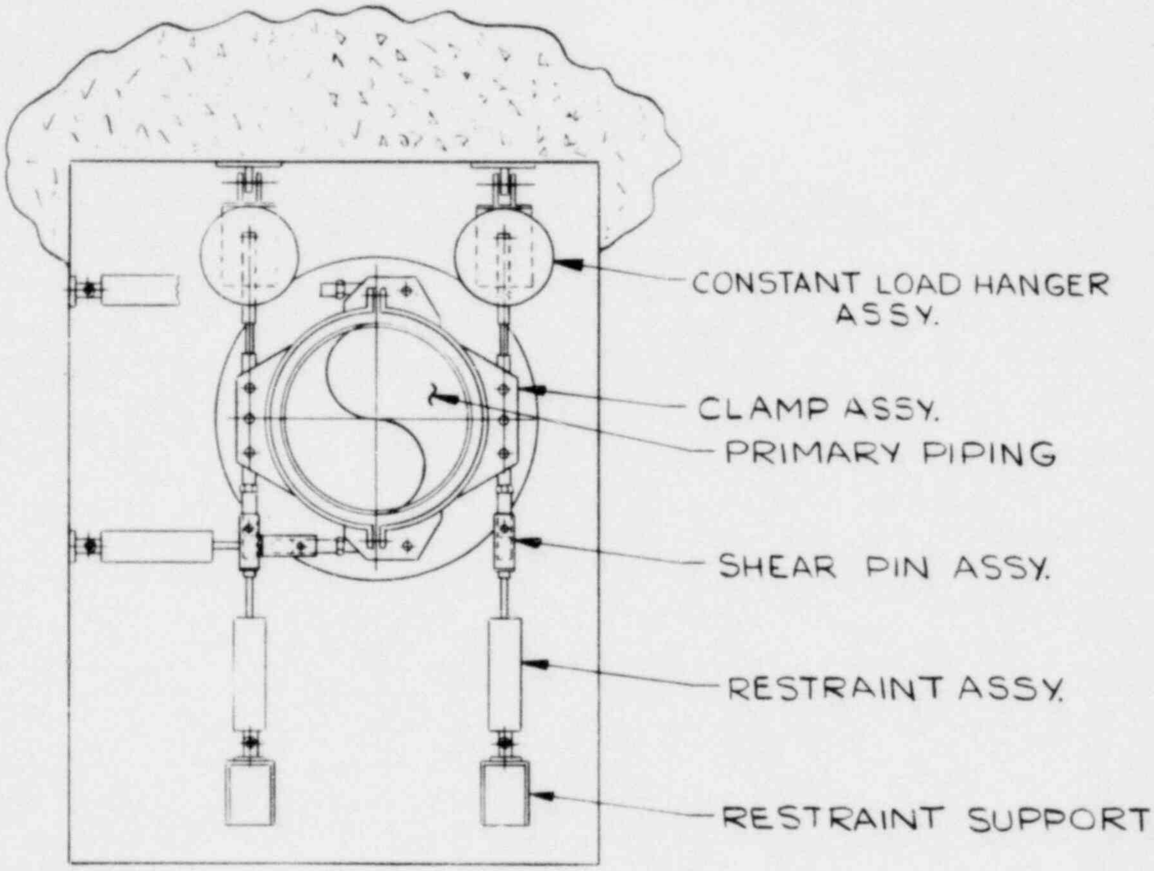

FIGURE 5.3-37B PIPE HANGER/SNUBBER ARRANGEMENT

7683-33

Amend. 56
Aug. 1980

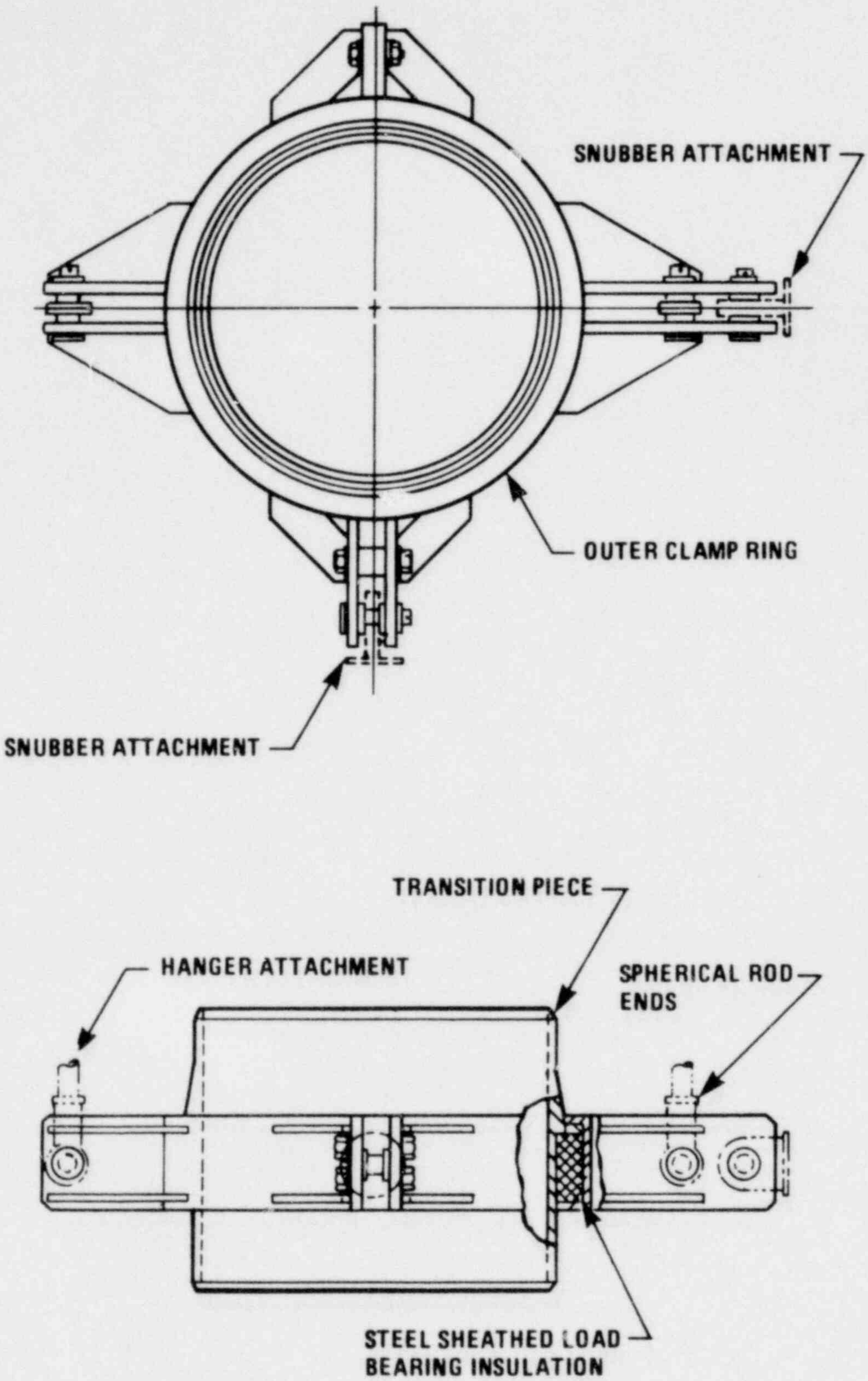

Figure 5.3-38. Vertical Pipe Clamp Assembly

1526-6

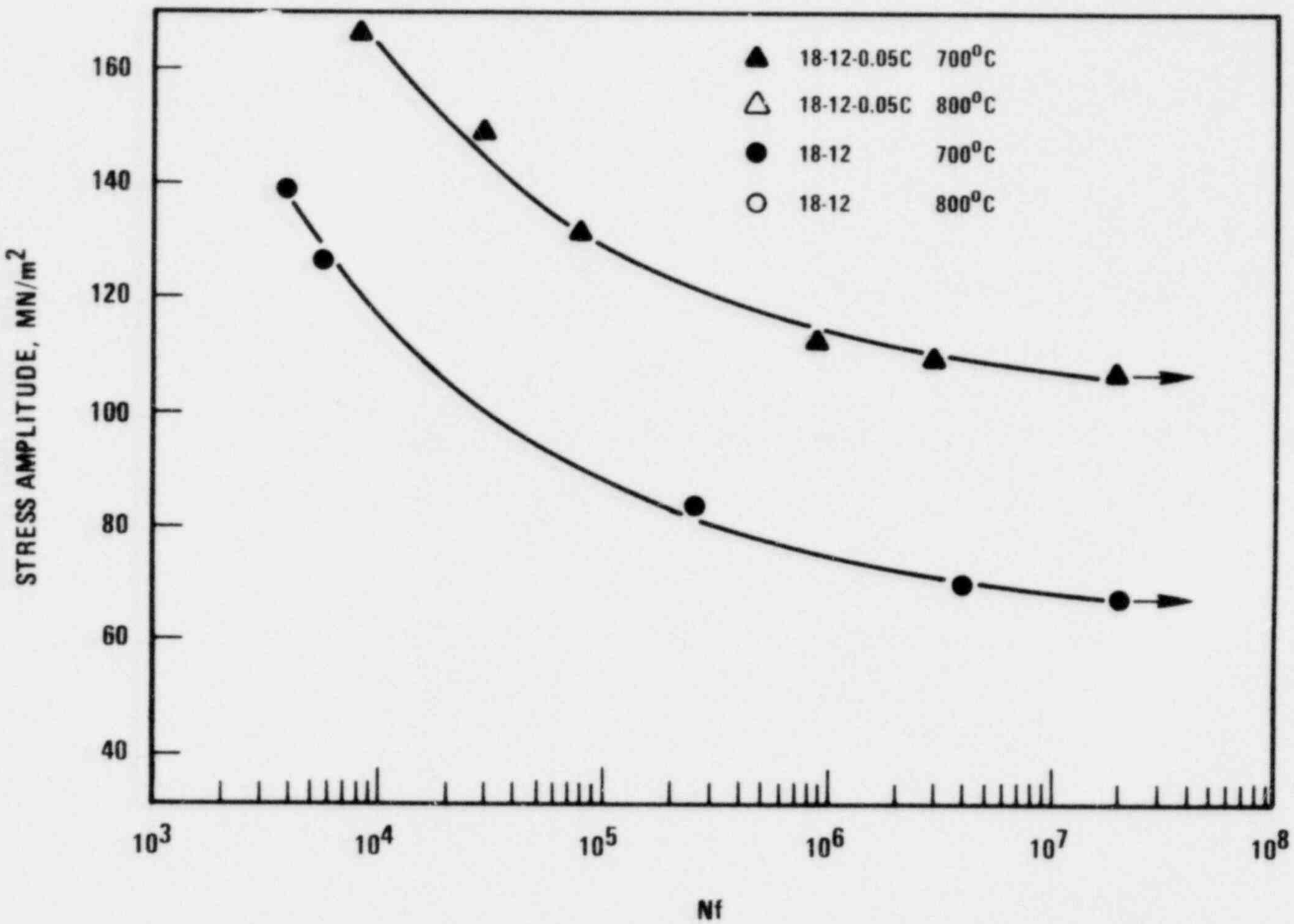

FIGURE 5.3-39 S/N Curves Of 18/12 And 18/12/0.05 C Alloys At 1292°F

56 FIGURE 5.3-40 HAS BEEN DELETED

56 FIGURE 5.3-41 HAS BEEN DELETED

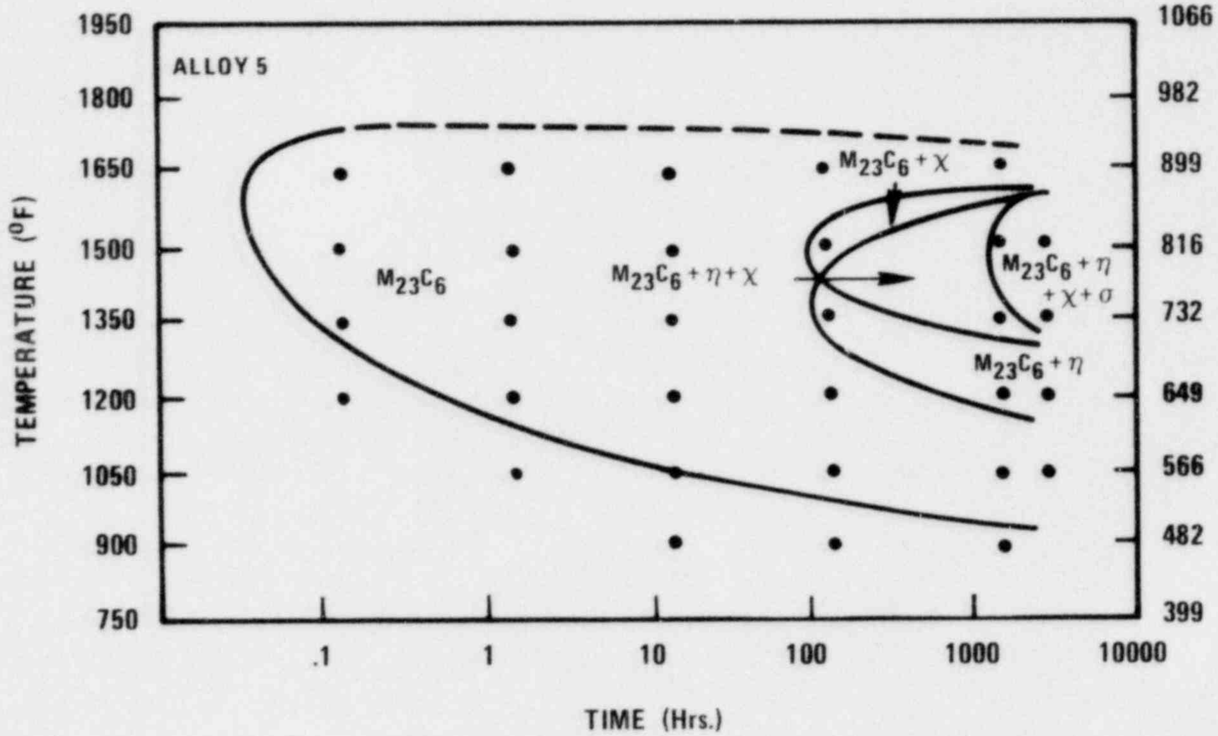

FIGURE 5.3-42 Precipitation Reactions In Type 316 Stainless Steel Solution Treated At 2300°F For 1.5 Hours And Water Quenched.

The IHTS piping will be supported from the building structure with constant load support hangers and will be restrained with seismic snubbers. Attachments to the piping for supports will be of the clamp type on the outside of load bearing insulation. If any attachment requires direct support to the pipe full penetration welds will be used.

Piping penetrations through the Reactor Containment will be a flued head, rigid type seal. Piping penetrations through the Steam Generator Building will not provide leak tight seals.

The piping within the IHTS consists of large sodium containing piping which must be installed per detailed drawings and rigid quality assurance requirements. There is no piping which can be field run.

5.4.2.3.4 Intermediate Heat Exchanger

The CRBRP Intermediate Heat Exchanger (IHX) serves to transfer reactor thermal energy from the radioactive primary sodium to the non-radioactive intermediate sodium. The IHX is a counterflow shell and tube type unit with a vertical orientation in the plant. The design arrangement provides for downflow of the cooled (primary) fluid and upflow of the heated (intermediate) fluid to enhance natural circulation for reactor decay heat removal. A detailed description of the IHX design is given in Section 5.3.2.3.2.

5.4.2.4 Overpressurization Protection

The IHTS has no isolation valves within the normal circulation path so that isolation of individual system pipe sections or components is not possible. If for some reason the system becomes blocked, the intermediate pump will not overpressurize the system as the IHTS structural design is sufficient to withstand the pump shutoff head. In the event of an argon supply valve failure, the system would not be overpressurized as the combination of argon supply pressure of 115 psi and pump shutoff head would not exceed the IHTS design pressure. This is true even if the pump shutoff head associated with the PHTS pump were reached instead of the IHTS pump shutoff head.

The system may be subjected to overpressure in the event of a water or steam leak in the Steam Generation System. For large or intermediate sodium-
40 water reactions, the resulting pressure increase due to the formation of reaction products in the faulted evaporator or superheater module is relieved through rupture disks. (See Section 5.5.2.4).

5.4.2.5 Leak Detection System

5.4.2.5.1 Leak Detection Methods

The methods used to detect Liquid Metal to gas leaks from pipes and components of the IHTS are aerosol detectors, cable detectors, contact detectors and visual inspection with back up from smoke detectors. See Section 7.5.5.1. 28

A sodium level monitoring system is provided to monitor any leakage
56 between reactor and intermediate coolant occurring in the IHX. The method is described in Section 7.5.5.2 in detail.

5.4.2.5.2 Indication in Control Room

Audible alarms will be sounded in the control room as described in Sections 7.5.5.1 and 7.5.5.2.

5.4.2.5.3 IHTS Coolant Volume Monitoring

The IHTS coolant volume is monitored by the level indicators in the IHTS pump tank and in the expansion tank. Details are discussed in Section 7.5.5.2. These monitors coupled with the sodium temperature measure-
56 ments allow monitoring of the total sodium in the IHTS loops. Small leakages of sodium from the IHTS can be replaced by use of the sodium fill system.

5.4.2.5.4 Critical Leaks

Critical leaks are discussed in Section 5.3.2.5.4. Detection
29 capability is discussed in Section 7.5.5.

5.4.2.5.5 Sensitivity and Operability Tests

56 Periodic maintenance will provide for checking the operational readiness of leak detectors. During installation and checkout, the correct electrical functioning of each leak detector and level detector will be tested.

5.4.2.5.6 Confinement of Leaked Coolant

If there is any leakage from the IHTS in the RCB it will be confined as described in 5.3.2.5.6. Any leakage from the IHTS in the SGB will be
29 contained in the catch pans and will be detected by the leak detection system. 28
Fires as a result of sodium spills are evaluated in Section 15.6. Leaks in the IHX are still contained in the passive coolant boundary, and no leakage
56 into the RCB will result.

5.4.2.5.7 Intermediate/Primary Coolant Leakage

Primary to Intermediate coolant leakage is very unlikely due to the higher operating pressure of the intermediate system. The IHTS pressure shall be maintained at a minimum of 10 psi higher than the PHTS pressure at
41 all points in the IHX during all normal modes of operation. Intermediate to primary coolant leakage detection is described in Section 7.5.5.2.

5.4.2.6 Coolant Purification (IHTS)

The IHTS coolant purification is accomplished by six cold traps, two in each of the three loops. One trap is in operation while the other is on
56 standby, except for a cleanup period after maintenance action. These cold

7.5.5.1.1 DESIGN BASES AND DESIGN CRITERIA FOR THE LIQUID METAL-TO-GAS LEAK DETECTION SYSTEM

The design bases of the Liquid Metal-to-Gas Leak Detection System arise from criteria needed to support the integrity of the PHTS boundary and from maintenance and plant availability considerations in the IHTS, SGS, and Auxiliary Systems.

The design bases are as follows:

1) The Liquid Metal-to-Gas Leak Detection System must provide diverse means for detecting and locating liquid metal to gas leaks throughout the plant at normal operating conditions.

2) The Liquid Metal-to-Gas Leak Detection System must operate at lower temperature conditions (<700° F), though its sensitivity may be reduced.

3, The Liquid Metal-to-Gas Leak Detection System must perform its function during and after an OBE (operating basis earthquake) even in the event of loss of offsite power.

The Design Criteria of the Liquid Metal-to-Gas Leak Detection
56 System for the Primary Heat Transport and Reactor Systems are outlined below:

1) The Leak Detection System must be able to detect "weeping" leaks which may have potential for long term growth.

2) The reference "weeping" leak is defined as a rate of approximately 100 gm/hr, or over, in pipes and components at
56 temperatures greater than 700°F.

3) The Leak Detection System must be capable of identifying within which cells the leak has occurred. Also, detection must be provided within each of the reactor vessel, IHX, and Pump Guard Vessels.

4) Each cell (and contained guard vessels) shall be monitored for
56 leaks by at least two diverse methods capable of providing the defined sensitivity. A confirmation method shall also be available in the event that conflicting information is provided by these systems. 28

56 5) Each of the two diverse methods shall have an individual response time of less than 250 hours for the reference 100 gm/hr leak size. Leaks of 30 gpm or larger shall be detected in less than 5 min. Leaks smaller than 30 gpm and larger than 100 gm/hr shall be detected prior to either a total spill volume of 150 gallons or 250 hours, whichever is less.

56 6) Indicators and alarms for leakage detection shall be provided in the main control room.

56 7) The leak detectors shall be equipped with provisions to readily permit testing for operability and calibration during plant operation.

Design Criteria Requirements for the Intermediate Heat Transport System, Steam Generator System, and Auxiliary Liquid Metal System are detection of a 30 gpm leak in five minutes.
45 Detection time requirements for a 100 gm/hr leak are up to 250 hours. 28

7.5.5.1.1.1 Design Description

General 28

A liquid metal-to-gas leak detection system is provided to protect 20 28 against economic losses and to support inservice inspection for CRBRP. Detection equipment is provided to monitor the primary and intermediate sodium coolant boundaries to identify comparatively small leaks when they occur.

45 A development program has provided the experimental data necessary 28 for the selection of the best method to satisfy these requirements. The data available from this program covers sensitivity, range, response time and overall performance of various detection. 28

The leak detection system selected for the following installations are:

1. Contact detectors in the space between the bellows and the stem packing of the bellows sealed sodium valves.

2. Cable detectors in guard vessels and under major liquid metal components.

3. Sodium Ionization Detectors (SIDs) which are aerosol detectors, for cell atmosphere monitoring.

4. Plugging filter aerosol detectors (PFADs) for Main Heat Transfer System piping and associated auxiliary piping; guard vessel and major components (e.g. Steam Generators, etc.).

The performance of these aerosol detectors for specific CRBRP applications have been demonstrated by verification tests (Reference 2).
45 28

The response of these detection methods has been determined for a wide range of environmental conditions, sodium temperatures and leak rates including:

Sodium Temperature	350 - 1000^{o}F
Atmosphere Moisture Content	300 - 30000 VPPM
Nitrogen Atmosphere	1 - 21% O_2
Sodium Leak Rate	0.4 - 243,000 gm/hr
Detection Sample Line Length	10 - 200 feet
Detection Sample Line Size	1/4 & 1/2 inch O.D.
Detection Sample Gas Flow Rate	0.3 - 7.0 liters/min.

28
56

Of the types of leak detection devices proposed for the Leak
Detection System, only sodium vapor/aerosol leak detection devices
56 show a difference in their response when operated in an air atmosphere
as opposed to an inert atmosphere. The electrical sensing types such as
56 cable and contact detectors show no difference in response due to operating
atmospheres. However, the potential for higher moisture content in air
56 31 can result in greater inhibition to sodium flow when the leak is very small.

The sodium vapor/aerosol detection devices sense the concentration of sodium vapor/aerosol from a leak and give a response. In air atmospheres, sodium burns more readily than in inert atmospheres and vapor/aerosol detection devices would be expected to respond faster in air atmospheres. However, because the reaction products tend to cover the leak, actual formation of aerosols tends to be inhibited by air atmospheres. The time for a detector to respond to a leak into an inert atmosphere tends to be
56 shorter than for leaks into air.

There are other considerations which affect detection devices response. These are: cell moisture content, sodium leak rate and temperature detection device location, and cell size. Test data indicates that sodium leaks of 2 gm to 100 gm per hour in an air atmosphere or inert
56 atmospheres can be detected by aerosol detection for sodium temperatures 25
as low as 350°F.

56

45

45

Results from tests that have been performed have verified that the
leak detection system will reliably and rapidly detect sodium-to-gas
56 leaks (Reference (2)). It is observed from the results that small 28
leaks (~100 gm/hr) of high temperature Na into an inert atmosphere (1% O_2)
can be detected in approximately 1 hour by most of the detection systems
under consideration. At lower temperatures (400°F) it will take up to
56 24 hours to detect the leak. For a 100 gm/hr leak rate of 640°F Na into an air
atmosphere the time to detection of leaks is in the range of four to six
hours. In the case of 100 gm/hr leaks from sodium pipes at 400°F into an air
atmosphere (as might occur in the case of the intermediate system) leak
detection levels are attained within about six hours by a majority of the
systems used. It will be noted that this is about one-fourth of the detection
time applicable to an equivalent sodium leak into an inert atmosphere. From
56 these test data it nas been shown that larger leaks (order of kg/min) will be
readily detected by two or more detection systems in minutes.

The increase in cell atmosphere temperature and pressure in the event
leaks of larger than 20 kg/min as detected by temperature and pressure sen- 28
sors can provide an additional source of leak detection. These detection
devices do not require development nor does the prediction of the cell
atmosphere temperature/pressure rise since extensive data is available
from the sodium burning experiments which were performed in support of FFTF.

The ability to detect small leaks (~100 gm/hr) by several methods
in hours plus the ability to detect large leaks (>kg/min) in minutes will
provide a highly reliable leak detection system that provides the operator
56 information and enable safe shutdown (see Section 15.6) to repair defects
without causing extensive time for cleanup operations.

Table 7.5-3 gives the candidate primary and possible back-up methods 28
of leak detection for the principal sodium systems and components in the
56 plant. These exact combinations were selected as a result of the
development program described above. The methods shown in the table are
related to the three sizes of leaks defined in Section 7.5.5.1.2. The
principal methods of leak detection are described below.

Contact Detectors (Spark-Plug)

56 Contact detectors consist of a stainless-steel-sheathed, mineral
oxide-insulated, two-wire probe with the sensing end open and the wire ends
exposed. Contact detectors are installed, for example, on bellows sealed
valves with the sensing end between the bellows and the mechanical backup
seal. A leak is detected by the reduction in circuit electrical resistance
caused by sodium contacting the wire ends.

Cable Detectors

Cable detectors consist of stainless-steel-sheathed, mineral-oxide-insulated, cable with holes penetrating the sheath to permit leaked liquid metal to come in contact with the conductors. Cable detectors will be placed, for example, in the bottom of guard vessels and below large tanks. The experimental results are presented in Reference 2. 28

Aerosol Monitoring

45 Aerosol monitoring will be performed by measuring the pressure drop across a membrane filter with a constant flow of gas sampled from the annular space between major piping and its insulation, from the space within guard vessels, and from cells containing liquid metal systems. Another aerosol monitoring method uses a sodium ionization
56 detector. Liquid Metal aerosols or vapor are ionized
by a hot filament and the ion current is measured. Increases in the
45 ion current indicate a leak. 28

Based upon the experimental results, these methods would allow detection of leaks of 100 gm/hr or less with a response time of several minutes for 1000°F sodium (Reference 2). 28

The major function of this instrumentation will be to provide indication of the presence of small leaks which do not present a significant contamination hazard, but which might result in undesirable long-term corrosion. The instrumentation will also provide backup signals for other leak detection methods.

45

56 Other Detection Methods

Pressure and temperature measurements available in the inerted cells (Section 9.5.1.5) will provide immediate indication of the presence of large leaks over the 20 kg/min size. In the case of systems containing radioactive sodium, the detection of airborne radioactivity
56 arising from Na-24 or Na-22 in the aerosols will be performed by particulate radiation monitoring equipment (Section 11.4.2) which provides a sensitive detection method for aerosol concentrations as low as 10^{-15} gm/cc. 28

Other Backup Detection Method

Liquid Sodium Level Sensors in the reactor, the EVST, the IHTS expansion tank, and sodium storage tanks will provide indications of
56 large leaks. Smoke detectors (Fire Protection System) will detect
43 combustion products originating from sodium leaks in air (See Section 9.13.2).

Indication in Control Room

56 An audible group alarm is sounded in the control room
upon indication of a leak or certain failures of contact, cable, or aerosol
channels. The channel number producing the alarm and the location of the
56 region covered by this channel are displayed on an annunciator
on a local panel. This information will identify the leak as occurring in
a specific major component or series of pipe sections, or specific bellow-
sealed valve, or the cell containing the leaking system. The leak detec-
tion system uses the Plant Data Handling System for channel failure monitor-
ing, data and trend logging; the sampling time interval will nominally be
56 approximately 30 seconds.

No automatic isolation functions or reactor scram are initiated by
the Liquid Metal-to-Gas Leak Detection System. Isolation or shutdown of a 28
system showing a leak will be performed manually, following verification
of the leak and review of the operating conditions.

7.5.5.1.2 Design Analysis

The Liquid Metal-to-Gas Leak Detection System will meet the
appropriate requirements of CRBRP Design Criterion 30, "Inspection and
Surveillance of Reactor Coolant Boundary" and Criterion 33, "Inspection
and Surveillance of Intermediate Coolant Boundary." Criterion 30 requires 28
that means be provided for detecting and identifying the location of the
source of reactor coolant leakage from the reactor coolant boundary to
the extent necessary to assure that timely discovery and correction of
leaks which could lead to accidents whose consequences could exceed the
limits prescribed for protection of the health and safety of the public.
Criterion 33 requires that means be provided for detecting intermediate 28
coolant leakage from the intermediate coolant boundary. In order to
demonstrate how the intent of the criteria will be satisfied, the instrumen-
tation requirements met by this system for three different ranges of leaks
56 are discussed. These ranges have been selected to analyze situations which
cover the complete range of the leak detection instruments. Section 15.6
discusses the consequences of leaks for the health and safety of the public.

Large Leaks

This category covers failures up to those resulting in a leak of 30 gpm or 100 kg/min. A significant physical characteristic of leaks of this size is that they would result in pressure and temperature changes in the primary cells if the leak occurs in PHTS pipe sections. This feature sets the lower boundary of the leak at about 20 kg/min; this being an estimate of the amount of sodium which would result in measurable changes in cell pressure and temperature. If the leak occurs in a guard vessel, continuity detectors will provide detection of these large leaks. Due to the nature of the physical parameters monitored, the response time of the instruments would be negligible compared with operator capabilities to react. It is inferred from Reference 2 that leaks of this magnitude would be detected in five minutes or less for the primary and intermediate heat transport system. The operator would then be abl to initiate and complete plant shutdown within ten minutes after the start of the leak. 28

The pressure and temperature measurements available in the inerted
56| cells will, in conjunction with the aerosol detectors, continuity detectors and radiation monitors, provide the response required for proper operator action in case of leaks of this magnitude.

Intermediate Leaks

Intermediate leaks were defined as those leaks which would not result in significant changes in cell pressures and temperatures but where the extent of the resulting contamination and plant maintenance makes plant shutdown desirable. The range of leak rates covered extends from the lower limit of the large leaks previously considered down to a leak of 100 gm/hr. The detection times for the wide range of leaks in this group would vary from a few minutes 28
56| to several hours depending on the rate of leakage. Based upon experimental results, it is concluded that several systems would detect a leak of this 28
magnitude in several hours at least and possibly in minutes.

Instrumentation capable of detecting leaks of this magnitude include radiation monitors, continuity detectors, and the different types of aerosol
56| detectors currently under long term performance evaluation.

Small Leaks

Small leaks at or below 100 gm/hr were defined as those events resulting in releases of sodium which do not pose a contamination or maintenance problem but might result in undesirable long-term corrosion (see Section 5.3.3). The methods for detecting leaks of this range are
56| aerosol detectors and radiation monitors in the case of the primary system.

In the course of test programs, aerosol concentrations produced by leaks of down to 5 gm/hr were found to be within the detection capability
56| of both a Sodium Ionization Detector and a Plugging Filter Aerosol Detector. The initial tests results show that leaks of this size can be detected in the range of one hour to 24 hours by annuli monitors depending upon the sodium temperature and gas environment. It is deduced from the test results 28
that very small

leaks (<1 gm/hr) will be detected by annuli monitors in several days. Tests during 1975 and 1976 showed that under environmental conditions
typical of LMFBR operation, small leaks from typical piping configura- 23
tions can be detected by both Sodium Ionization and Plugging Filter Aerosol Detectors. Continuity (cable or contact) detectors did not reliably detect small pipe leaks under these conditions. Testing in
56 1978 verified the performance of aerosol detectors using prototypic CRBRP cell atmosphere recirculation as well as pipe/insulation
45 design.

It is deduced from the test results that the sodium vapor/aerosol
56 systems will, in conjunction with existing radiation monitoring technology, provide adequate indication of the smallest sizes of leaks of interest.

Sodium Leaks into an Air Atmosphere

Test results (Reference 2) indicate that the methods applicable to
sodium leaks in inerted cells will also operate when applied in an air atmo- 28
sphere. The additional use of smoke detectors and the accessibility of piping located in an air atmosphere to visual inspection assist in the selection of an effective sodium-to-air leak detection system.

7.5.5.2 Intermediate to Primary Heat Transport System Leak Detection

7.5.5.2.1 Design Description

The IHTS pressure is maintained at least 10 psi higher than the Primary Heat Transport System at the IHX to prevent radioactive primary sodium from entering the IHTS in the event of a tube leak. Maintaining a positive pressure differential across the IHX is a limiting condition for operation of the plant (Chapter 16 - Technical Specifications). This provides assurance that a zero or negative differential will not exist during any extended interval. A loss of this pressure or a reversal of it is not expected to occur except during accident conditions. Such an occurance would necessitate an orderly plant shutdown to correct the problem. Since a reverse differential cannot occur for a significant interval, the potential leakage of primary sodium into the intermediate system, through an IHX tube leak, is small.

Leakage of primary sodium into the IHTS, should it occur, will be detected by radiation monitors provided on the IHTS piping within the SGB. The radiation monitor system will provide an indication of the radiation level and will provide alarms for conditions of excessive radiation indicative of ingress of primary sodium. Since the only activity expected in the IHTS is a low level of tritium, the radiation monitors will be very sensitive to the presence of significant amounts of radioactive primary sodium in the intermediate system. For accidents which involve a loss of IHTS boundary integrity the radiological effects have been evaluated. The results of these evaluations are presented in Sections 15.3.2.3, 15.3.3.3 and 16.6.1.5. 30

Maintaining a positive pressure differential across the IHX assures that the leakage across the IHX tube barrier will result in an inflow of sodium into the primary system causing a loss of sodium inventory in the IHTS. The sodium inventory in the IHTS is monitored by tracking the sodium levels and correcting for loop temperature effects. Alarms are provided in the control room to alert the operator upon detection of a large loss of IHTS sodium inventory.

7.5.5.2.2 Design Analysis

Intermediate to Primary Heat Transport System leak detection is provided to comply with CRBRP General Design Criterion 36 "Inspection and Surveillance of Intermediate Coolant Boundary". In order to demonstrate now the intent of this criterion will be satisfied, an analysis of the minimum detectable leaks in the IHX is provided below.

The minimum detectable level change of sodium in the IHTS pump and expansion tank is approximately 3 inches which corresponds to about 150 gallons. In the event of a full-circumferential break of an IHX tube, the leak rate of intermediate sodium to the primary side of the IHX would be approximately 150 gpm. At this leak rate, the detection time would be about one minute assuming steady state temperature conditions.

Based upon a 3-inch level change, leakage of as low as 6.25 gph would fall within the detection threshold. Over long time periods, the sensitivity of the detection system will be reduced by an insignificant amount due to other potential leakages from the system. If leakage occurs due to piping or component leaks, the external leak detection system will detect the leakage. A second potential source is leakage through the four sets of dump valves which has a maximum expected rate of one to two gallons per day. Since this leakage rate is essentially two orders of magnitude smaller than the leakage threshold, it will not have a consequential effect on the detection sensitivity. 30

7.5.5.3 Steam Generator Leak Detection System

A steam Generator Leak Detection System is provided to detect small (as low as 10^{-5} lb/sec) water-to-sodium and steam-to-sodium leaks in the steam generator modules, to identify the module in which the leak has occured, and to alert the control room operator enabling him to take manual corrective action to prevent the leak rate from increasing. Leak detection instrumentation is provided for:

47 1. Sodium exiting from the superheater.

47 2. Sodium filled vent lines from combined evaporator vents and the superheater vent.

47 3. Bulk sodium in the IHTS cold leg.

TABLE 7.5-3 28

SUMMARY OF SODIUM/GAS LEAK DETECTION METHODS

System	Equipment Monitored	Size of Leak (see Section 7.5.5.1.2)	Primary Method of Detection	Back-up Method of Detection
Reactor Enclosure	Reactor vessel and inlet, outlet, overflow nozzles	small	radiation monitoring aerosol monitoring	cable detector
		intermediate and large	aerosol monitoring radiation monitoring cable detector	sodium level in vessel cell temp. & pressure
PHTS	Major pipe sections	small	annuli aerosol monitoring, cell radiation monitoring, cell aerosol monitoring	sodium level in vessels
		intermediate and large	cell radiation monitoring, cell aerosol monitoring, annuli aerosol monitoring	cell temp. & pressure
	Pump housing, IHX shell, check valves	small	aerosol monitors and cell radiation monitoring	cable detectors
		intermediate and large	aerosol monitoring radiation monitoring cable detector	sodium level vessels cell temp & pressure

56 28

TABLE 7.5-3 (Continued)

System	Equipment Monitored	Size of Leak (see Section 7.5.5.1.2)	Primary Method of Detection	Back-up Method of Detection
IHTS and Steam Gen.	Major pipe sections, pump housing, expansions tank, steam generators distribution lines, steam generators	small	aerosol monitoring	visual inspection
		intermediate and large	cable detector aerosol monitoring	vault smoke detector
Aux. Liq. Metal, Impurity Monitoring and Analysis, and Reactor Refueling	EVST, overflow and storage tanks	small	cell radiation monitoring (RCB only) & aerosol monitoring	sodium levels in vessels cell temp. & pressure
		intermediate and large	cell radiation monitoring, aerosol monitoring, and cable detector	
	Cold traps, heat exchangers, impurity monitoring, and other small equipment	all	cell radiation monitoring, aerosol monitoring, and cable detector	cell temp. & pressure (large leaks)

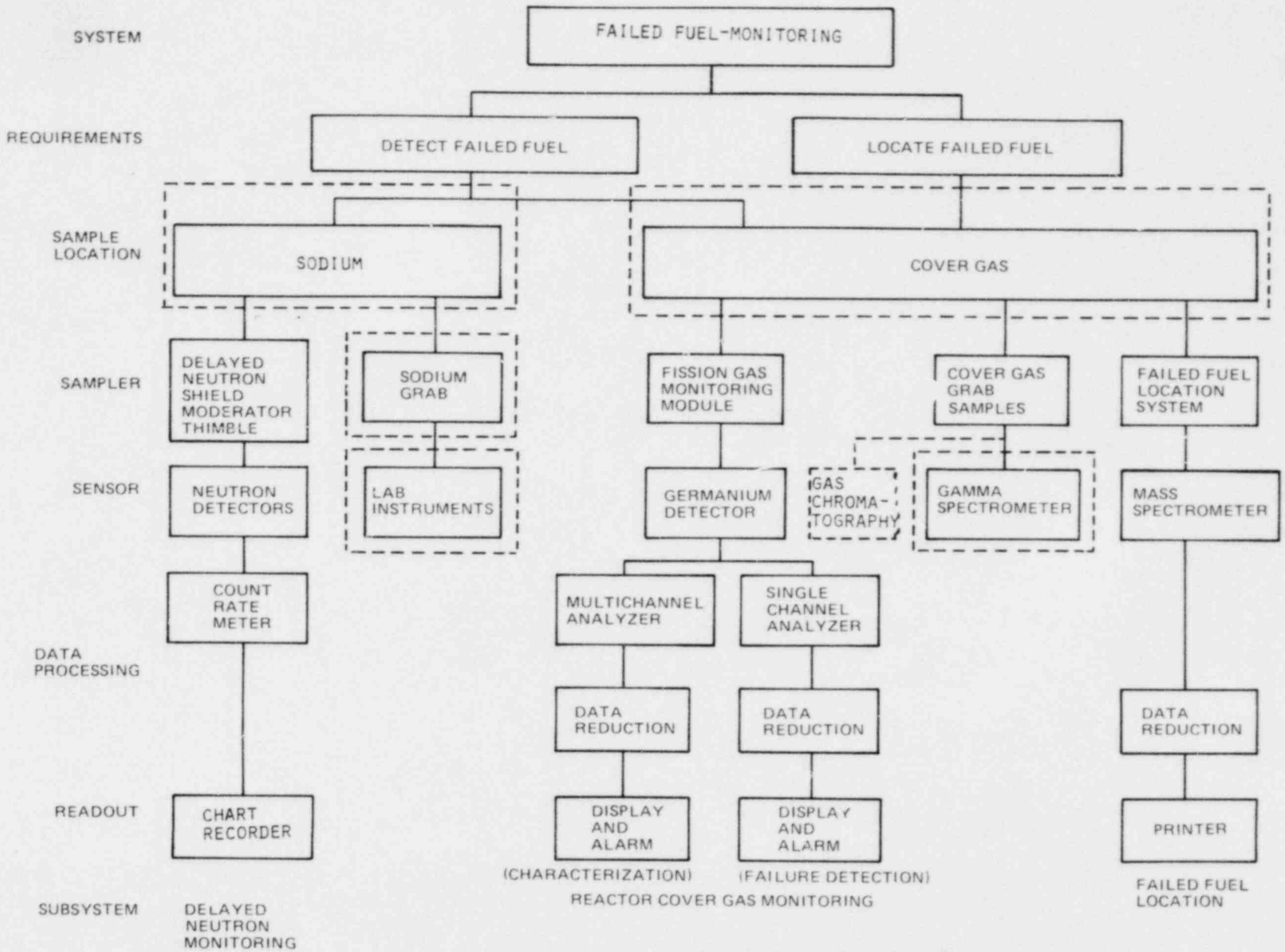

Figure 7.5-3. Fuel Failure Monitoring System

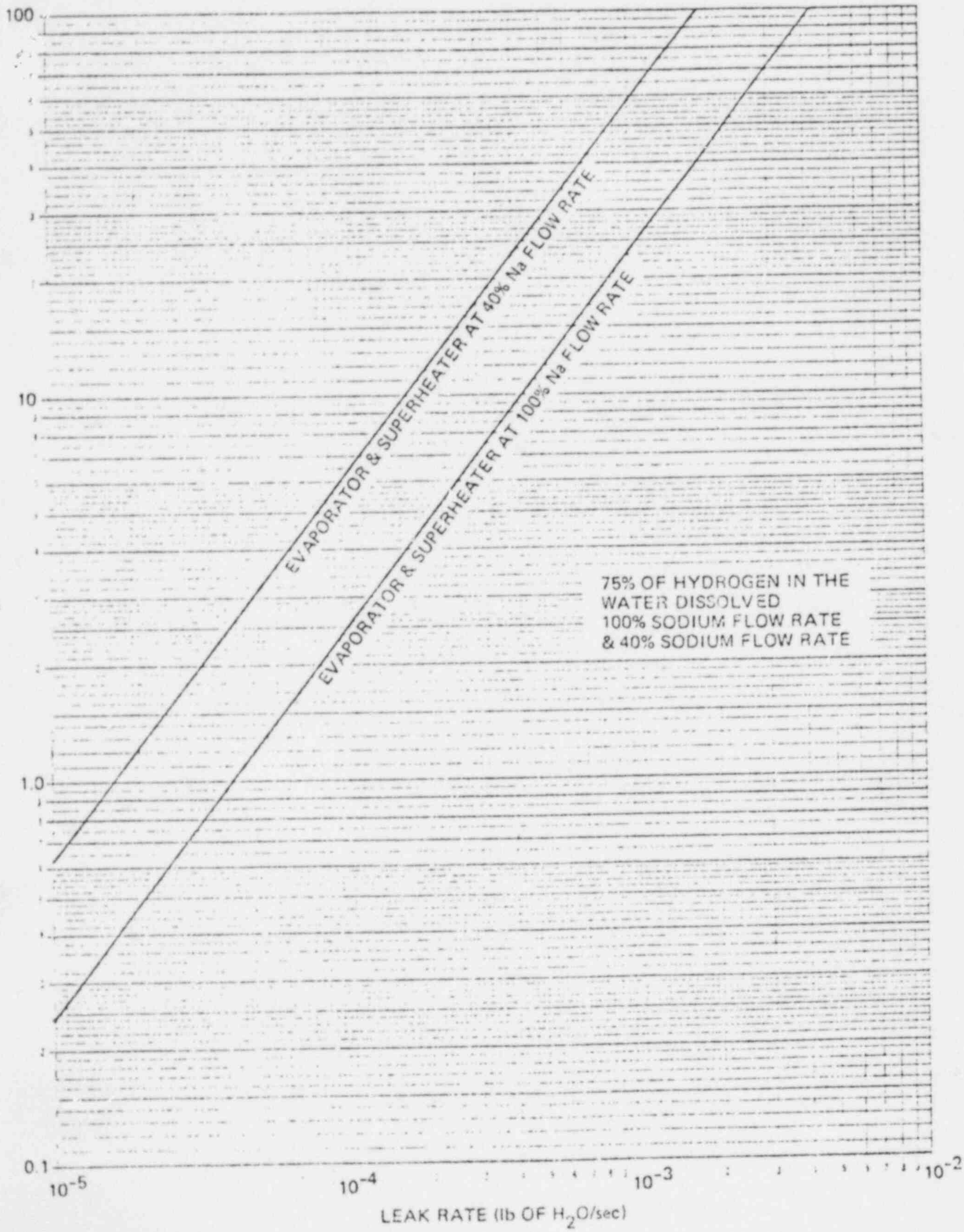

Figure 7.5-4 Main Sodium Stream First Pass Hydrogen Concentration Versus Leak Rate

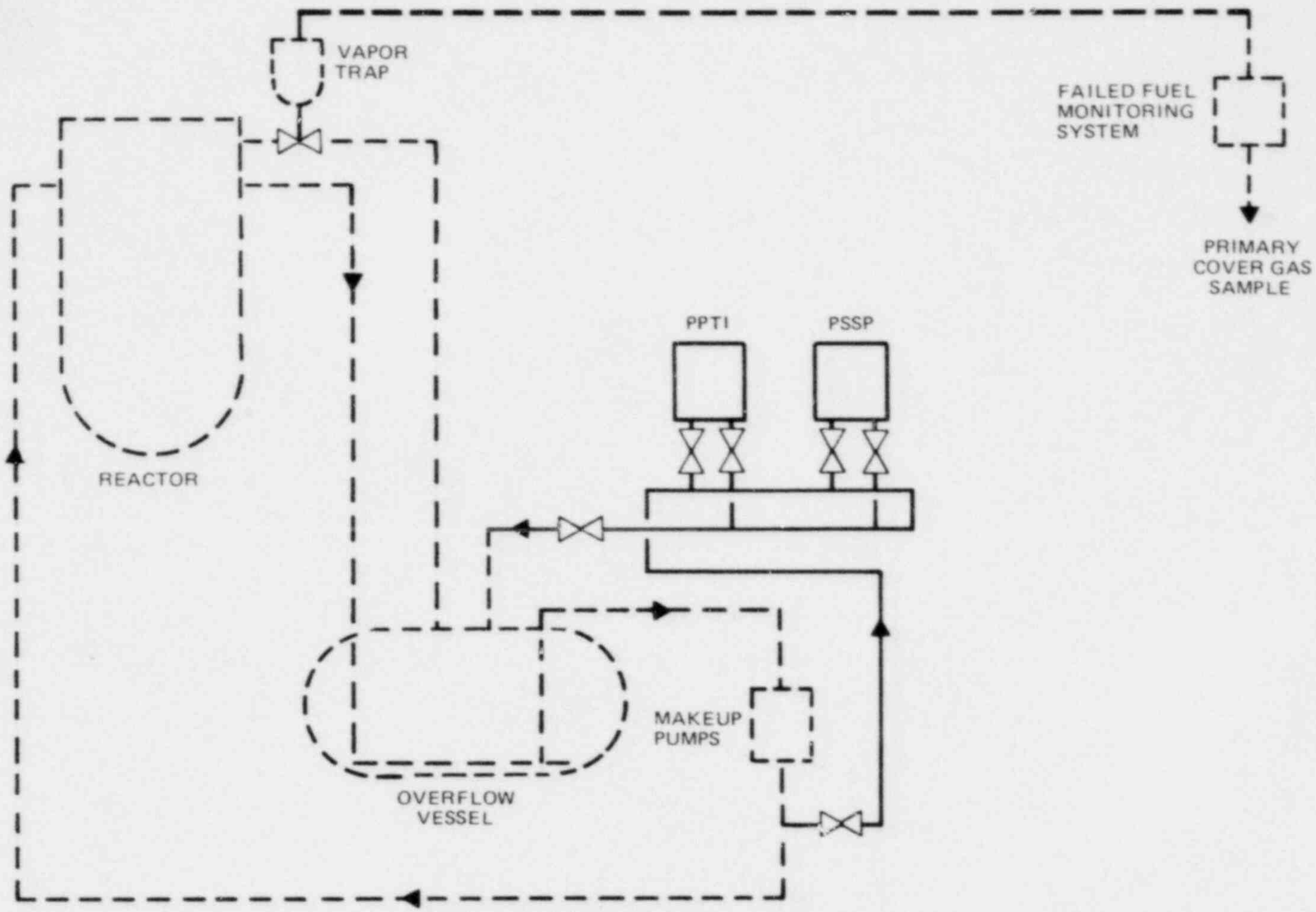

Figure 9.8-1. PHTS Sodium Characterization and Primary Cover Gas Sampling and Monitoring Subsystems

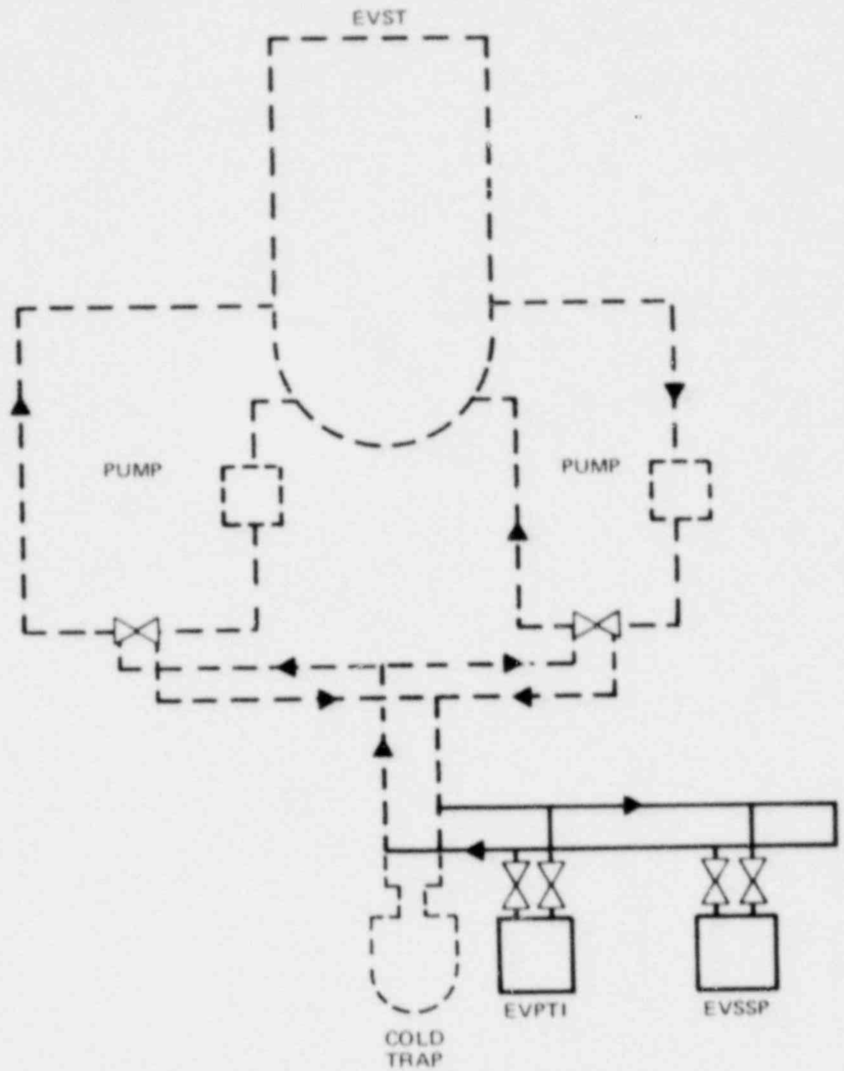

Figure 9.8-2 EVST Sodium Characterization Subsystem

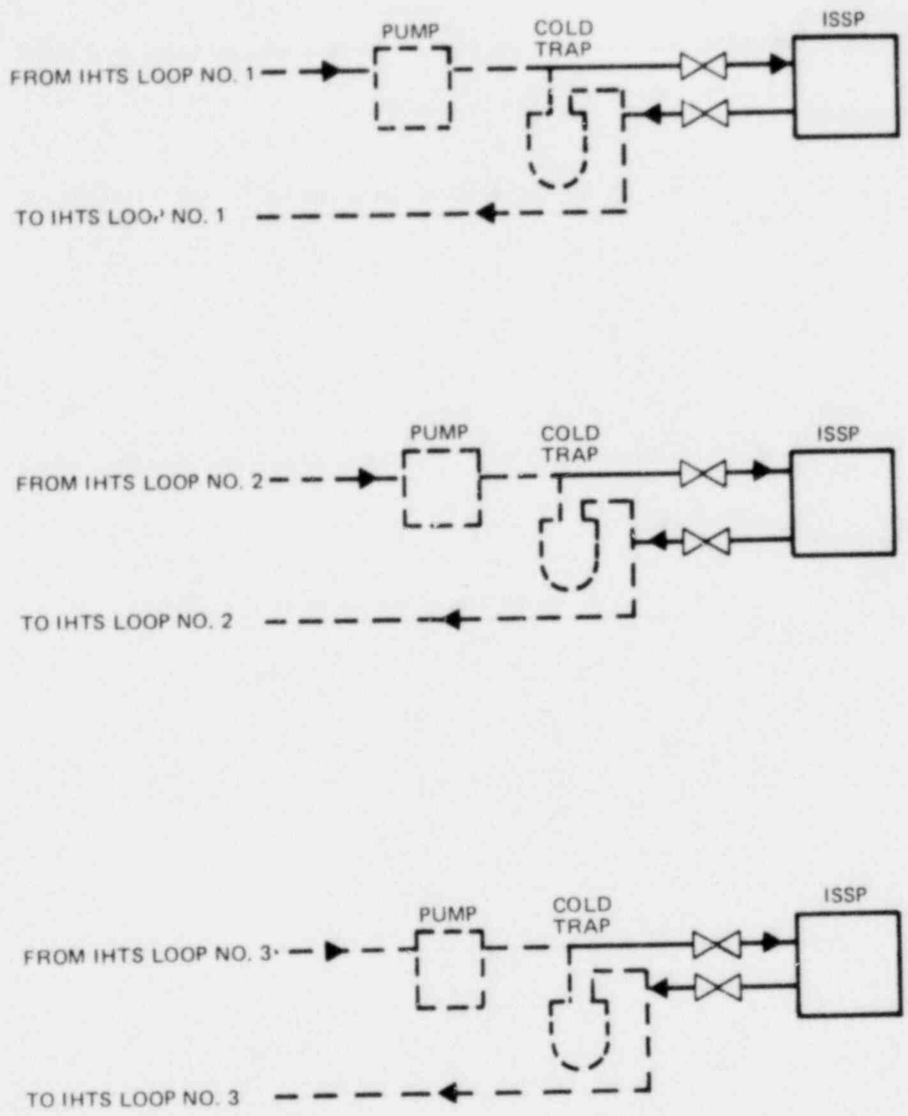

Figure 9.8-3 IHTS Sodium Characterization Subsystem

Amend. 56
Aug. 1980

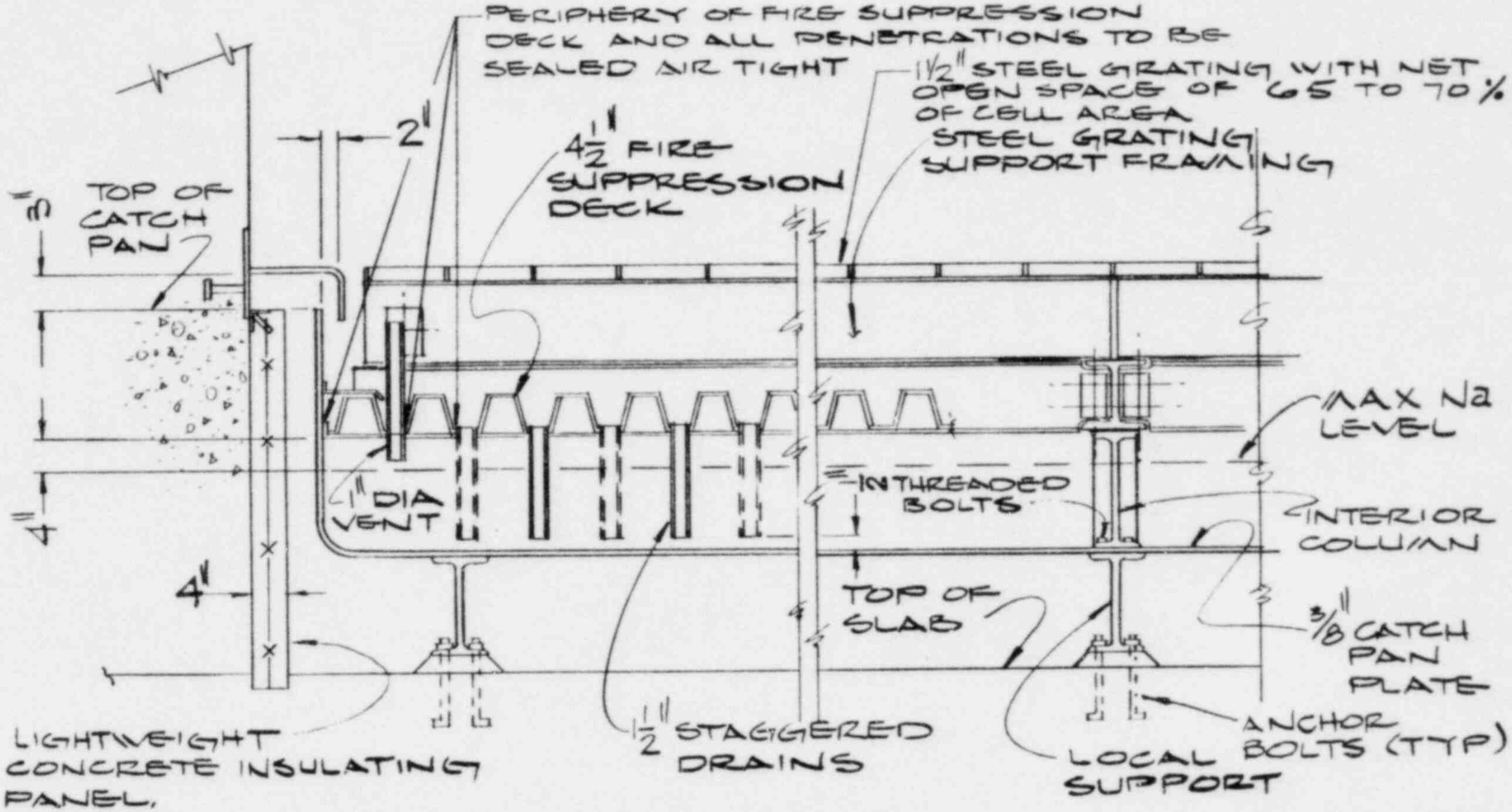

FIGURE 9.13-2

TYPICAL CATCH PAN

FIRE SUPPRESSION DECK ARRANGEMENT

Amend. 56
Aug. 1980

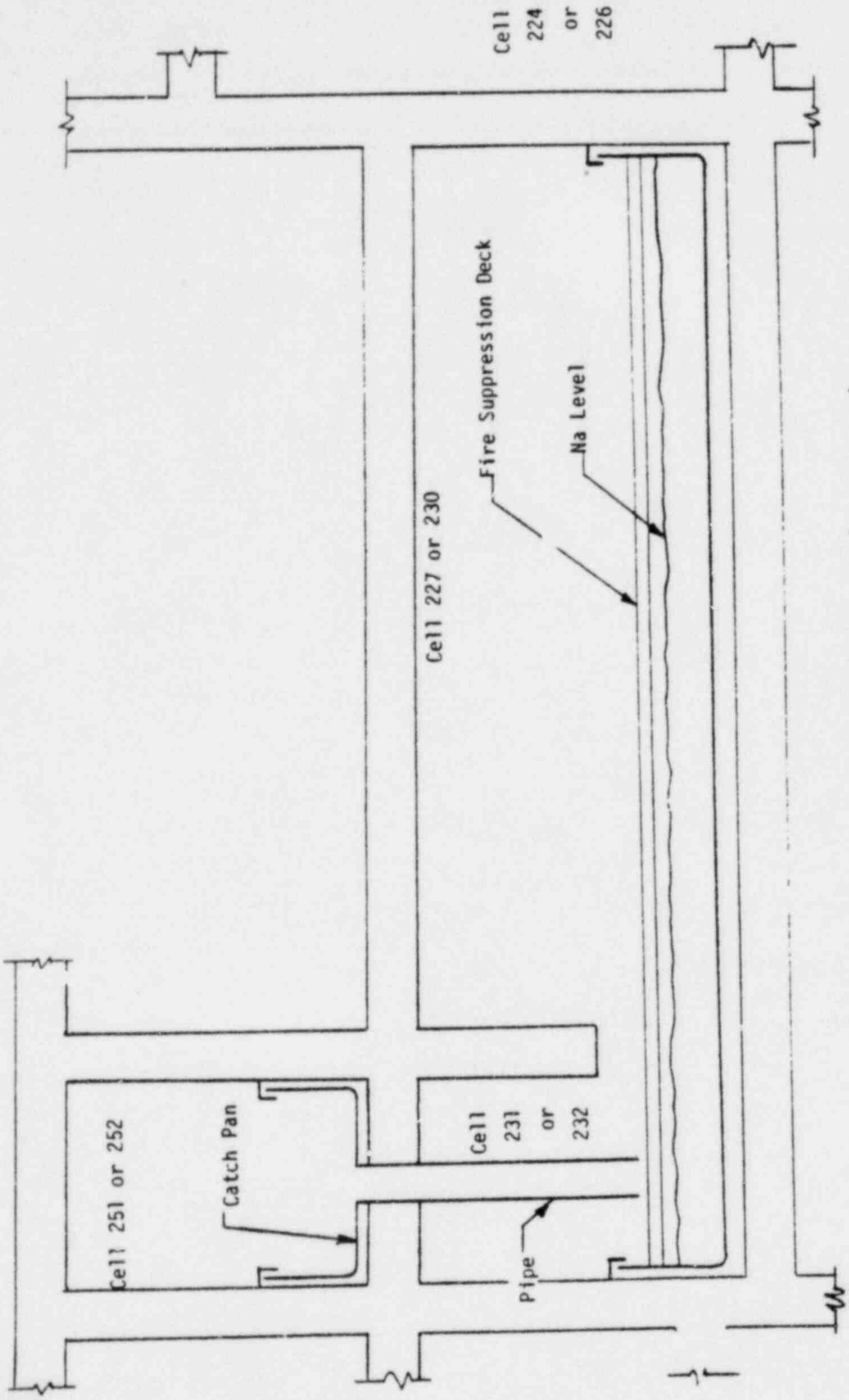

Figure 9.13-3. Catch Pan System Arrangement, Steam Generator Loops 1 and 3

15.3.3.4 Primary Heat Transport System Pipe Leak

15.3.3.4.1 Identification of Causes and Accident Description

Small sodium leaks have occurred several times in sodium testing facilities and in operating reactors. As a result, PHTS leaks are considered in the design and evaluation of the plant to assure that the design has adequate capabilities from the standpoint of core thermal transients. This particular section will address the PHTS pipe leak as an undercooling event while Section 15.6.1.4 provides a detailed discussion of the PHTS pipe leak and its consequences with regard to cell pressure and temperature transients and radiological effects.

Based on considerations of the leak detection system capabilities discussed in Section 7.5.1.5, and the fact that the leak detection systems
56 provide wide ranging coverage, it is considered that
leaks of approximately 3 gal/min will be easily detected. Therefore, to provide a wide margin between detectability and the leak rate selected for analysis purposes, a leak rate of 10 times the above value (i.e., 30 gal/min) for ten minutes was established as the leak that would result in assured detection and plant shutdown. With assurance that the leak rate of 30 gal/min is well above the detectable range of CRBRP instrumentation, a study was conducted to determine if this leak rate resulted in a significant core transient.

15.3.3.4.2 Analysis of Effects and Consequences

A 30 gal/min leak would not result in any measurable core transient. An automatic reactor trip would not be required. A normal reactor shutdown would be accomplished following indications from the leak detection system.

The magnitude of the 30 gal/min leak rate is orders of magnitude below the leak rate that could cause a significant core transient. Analysis indicates that for 3-loop operation, a transient maximum loss rate of approximately 75,000 gal/min would be required for the core sodium temperature to approach the saturation value, and this would require a rupture of about 1.7 square feet at the reactor inlet nozzle. At other postulated primary heat transport system locations, even larger rupture areas would have to be postulated for a peak loss rate of 75,000 gal/min.

Following an indication of a leak, the reactor would be shutdown and the coastdown of the pumps would reduce the system pressure. After pump coastdown (<1 minute), the leak rate would be reduced to a fraction of the 30 gal/min leak rate used for the event because of the pressure reduction and the system would then continue to drain until static equilibrium of the fluid in the system is reached, assuming no operator action to reduce the amount of sodium released. The quantity of sodium which could potentially leak from the system during this period is dependent on the location of the leak and the action that the operator takes. Once the plant is shutdown, the leakage rate becomes so small that the operator would have several days to select a method for further reducing the sodium leakage. Even if no further action were taken, the system design (guard vessels and elevated piping) would assure that long term core cooling would be provided.

15.3.3.4.3 Conclusions

The improbable occurrence of a leak, on the order of 30 gal/min in the PHTS piping would lead to an inconsequential transient in the reactor. Activation of several leak detection systems would result in corrective action including manual plant shutdown within minutes. The consequences would be limited to an economic penalty for plant downtime, sodium cleanup, and piping repair. Moreover, a leak over three orders of magnitude (70,000 GPM) would not cause hot channel coolant temperatures to approach saturation.

15.6.1.5 Intermediate Heat Transport System Pipe Leak

15.6.1.5.1 Identification of Causes and Accident Description

As in the discussion presented in Section 15.3.3.5, sodium leaks associated with Intermediate Heat Transport System (HTS) are being considered on a different basis from the Primary Heat Transport System (PHTS).

It is expected that results from development programs to be initiated
along with inservice inspection considerations, pipe fabrication quality
assurance measures, fracture mechanics analysis and tests, and leak detecta-
bility will lead to the conclusion that a large leak equivalent to the com-
plete severance of an IHTS pipe is not credible. In particular, data from tests
of leak detection capability indicate that the selected methods of leak detection
(filter plugging, ionization and cable detectors), insure early detection of small
IHTS leaks. However, since the data currently available on corrosion and mixing 28
tee behavior are insufficient at this time for PSAR purposes, it was determined
that a prudent approach to analyzing the potential programs associated with an
IHTS leak was to examine the limiting case, namely a large leak equivalent to the
complete severance of the pipe. As the necessary information becomes available
from the various development programs and analyses, it will be possible to analyze
56 this event based on specific leakage rather than on the limiting case approach.

Based on this discussion an evaluation of leaks equivalent to complete severance of the pipe in the 24-inch IHTS piping is evaluated as the limiting case transient for the IHTS (leaks in branch lines or thermo-wells are considered to fall within the scope of this limiting analysis). The break is assumed to occur at 781 ft. elevation in a horizontal run of piping between the pump and IHX in Loop No. 3 (each side of building) while the intermediate heat transport system is operating at full flow and heat load, and entire contents of the loop are assumed spilled into the sodium catch pans at the 765 ft. elevation.

The leak is assumed to result in a spray of sodium impinging on a flat surface causing splashing and breakup of the high velocity (22 fps) sodium stream, which increases the spill area. This increases the burning rate of sodium and produces consequences characteristic of a spray fire. As a result of the failure causing a sudden pressure reduction at the break, sodium flows from the expansion tank and pump tank to supply sodium to the pump inlet for several seconds. Then pump trip would be expected to result in reactor shutdown and flow coastdown with decreasing sodium velocities. Termination of the spray phase will occur within 30 seconds. The remainder of the loop contents are assumed to spill into the sodium catch pan during the next 30 to 60 minutes as the sodium drains under gravity head.

The spill volume utilized for this analysis is conservatively evaluated since portions of the superheater and evaporator are below the level of the 24-inch piping and these components would not be expected to be completely drained. The volume also assumes complete siphoning of the IHX tube bundle. This is a very conservative assumption because complete siphoning of the IHX tube bundle is not likely to happen because of the relative elevations of the IHX inlet and outlet nozzles with respect to the horizontal run of 24-inch piping. The area of the resultant sodium pool and therefore, the rate at which sodium is burned during the pool fire is maximized by selecting Loop No. 3.

Loop 3 is the largest of the three loops and this results in a spill quantity of 400,000 lbs. of sodium at a volume-average loop temperature of 800°F. The intermediate system would normally not contain radioactive primary sodium. However, it is postulated for this accident that the plant has been operating with a leak in the intermediate heat exchanger immediately prior to the pipe leak. Under normal operating conditions, the intermediate heat transport system sodium pressure is higher than the primary sodium pressure and any leak would flow from the intermediate to the primary system. A sudden leak in the intermediate system would cause the pressure to drop in the intermediate system and might reverse the direction of leakage. Primary sodium could possibly leak into the intermediate system until the primary pumps are shut off and the primary pressure decreased to the intermediate sodium pressure. Intermediate sodium which is mixed with this primary sodium could then drain out through the intermediate system pipe break and burn in the steam generator building. This is a very conservative assumption because the inert gas pressure on the intermediate system is maintained until after the reactor has been tripped, or until the gas is relieved through the leak.

The pertinent dimensions and ambient conditions of the Intermediate Bay are itemized in Table 15.6.1.5-1. The cell is ventilated at an air flow rate of 1000 cfm. The ventilation system is manually controlled and it is assumed for the evaluation of sodium burning rates and temperatures that the ventilation system is not shut off until five minutes after the spill. The ventilation rate is low enough so that the consequences of the fire are not strongly affected by the time of shutoff within approximately the first 30 minutes. Smoke detectors will alert the operators to the fire. An oxygen suppressing grating is installed above the sodium level in the catch pan which covers the floor area at the 765 ft. elevation. The internal recirculating air coolers are assumed inoperative. Nitrogen flooding is provided for in the event of a fire, and the nitrogen flow would be adjusted to maintain a slight positive pressure of a few inches of water to prevent inleakage during cooldown.

15.6.1.5.2 Analysis of Effects and Consequences

The spray is produced by impingement of sodium discharge from the break in the outlet pipe at the 781 ft. elevation. This leak location was selected since it is farthest from the pump suction and therefore maximizes

h. When an audit response has not been received in the allotted time.

i. When Nonconformance Review Board actions determine that a corrective action is required to obtain a specific corrective/preventive action.

8 The CAR identifies the requirement, the condition encountered, and requests
a proposed action from the recipient of the request. The required CAR response
contains the proposed corrective action to preclude repetition, the persons
responsible for implementation of the actions, and the schedule by which they
8 will be completed. This is reviewed for acceptability by Quality Assurance
and Engineering as may be applicable. Areas involved in corrective actions
40 are verified by Quality Assurance at the end of the scheduled period for imple-
mentation of the corrective action. When a CAR is issued, the fact is recorded
on a CAR summary. The summary identifies the originator of the request and the
date. It provides a description of the deficiency, identifies the organization
responsible for answering, the date a reply is required and the type of deficiency.
When an answer is received, the date of the required verification of the correction
is added to the summary. Frequent review of this summary defines that status of
all corrective action requests issued and provides a means for effective follow-up
until the request is closed.

40 16.3 DISTRIBUTION OF CORRECTIVE ACTION REQUESTS

Internal CARs are distributed to the responsible organization representative, the Cognizant Project Engineering Manager, and any others as may be required by the individual corrective action being requested. CARs for suppliers or contractors are transmitted via a transmittal letter to the concerned contractor or supplier through contractual channels.

40

17. QUALITY ASSURANCE RECORDS

40 17.1 QUALITY ASSURANCE RECORDS SYSTEM

The AE has established a Quality Records Management Plan providing
the general requirements for records identification and collection for
transfer to the Owner. The Quality Records Center (QRC) processes those
records resulting from activities that are necessary to define the overall
55 program quality and provide objective evidence of quality achievement. The
53 system includes provisions that ensure:

1. Records are processed to provide documentary evidence of the quality of items and activities affecting quality.

2. QA records include operating logs; results of reviews, inspections, tests, audits, and material analyses; monitoring of work performance; qualification of personnel, procedures, and equipment; and other documentation such as drawings, specifications, procurement documents, calibration procedures and reports, and deviations and corrective action reports.

3. 45 Records are readily identifiable and retrievable.

4. Requirements and responsibilities for record transmittals, retention, and maintenance subsequent to completion of work are consistent with applicable codes, standards, and procurement documents.

5. Inspection and test records contain the following:

   a. A description of the type of observation
   b. Evidence of completing and verifying a manufacturing, inspection, or test operation
   c. The date and results of the inspection or test
   d. Information related to deviations
   e. 45 Inspector or data recorder identification
   f. A statement as to the acceptability of the results

6. Record storage facilities provided by the owner are located and secured 55 to prevent destruction of the records by fire, flooding, theft, and deterioration by environmental conditions such as temperature or humidity.

The Quality Records Management Plan is executed using approved procedures which
40 address the following major elements:

o Declaring

o Filing

o Storage

53 o Retrieval

55

1) Maintaining and administering the Quality Program Audit
52 System by preparing and maintaining audit schedules.

55 2) Arranging for checklists; conducting or arranging for audit teams to conduct audits.

3) Insuring preparation of audit reports.

4) Follow-up to verify corrective action implementation.

5) Maintenance of audit case history files.

6) Development, issuance, control, and revision of Quality Assurance Manuals and procedures.

7) Review of operating procedures, and revisions thereto, prepared by other quality-affecting organizations, to assure compatibility with overall ESG Quality Assurance Program requirements.

55 8) Performing supplier quality surveys of procurement sources for materials and fabrication services and maintenance of the approved list of such supplies.

55 9) Administering a Material Review System for nonconforming items.

55 10) Administering a Corrective Action System to assure prompt and
52 effective correction of conditions causing nonconformance
to technical requirements/procedures.

Quality Assurance Engineering LMFBR Programs Manager - The
52 Quality Assurance Engineering LMFBR Programs Manager is responsible to the Quality Assurance Director and provides quality assurance engineers to support the CRBRP Quality Assurance Project Manager. The Quality Assurance Engineering LMFBR Programs Manager is responsible for performance
55 of the following activities:

1) Quality Assurance Program administration for specific portions of the CRBRP activities, to monitor and assure effective implementation of quality requirements, from design through procurement and fabrication.

2) Quality engineering support for change control boards, design reviews, and design document review and approval.

3) Nonconforming item review board coordination.

52 4) Develop and implement statistical test programs and analyses as required.

55 5) Provide source inspection, planning, and surveillance of suppliers of materials and fabrication services.

52 6) Review and evaluate bid invitations and returns for quality impact.

7) Participate on capability evaluation teams for prospective suppliers of major items.

8) Procurement document review and supplier quality surveys for materials and fabrication services and maintenance of the approved list of such suppliers.

9) Receiving inspection planning.

10) ESG fabrication inspection planning.

11) A quality data and records collection and storage system for procured and ESG-fabricated items.

12) Data packages for ESG-fabricated items.

Quality Assurance Engineering Utility and Energy Programs Manager - The Quality Assurance Engineering Utility and Energy Programs Manager is responsible to the Quality Assurance Director.

55 This function does not provide any services to the CRBRP Project Manager.

52

Appendix B Criterion	ESG Implementing Document or Procedure	
	Number	Title
I. Organization	SOP M-10	Program Management
	SOP Q-10	ESG Quality Assurance Program
	QAOP N1.21	Quality Assurance Plans
II. Quality Assurance	SOP A-01	ESG Policies and Procedures
	SOP M-10	Program Management
	SOP Q-10	ESG Quality Assurance Program
	SOP Q-16	Quality Assurance (QA) - Program Support Functions
	SOP Q-12	Quality Assurance Program Audits
	SOP Q-18	ESG Quality Records
	PMD No. 16	Quality Assurance Management Reviews
	PMD No. 11	CRBRP Document Hold Status System
	PMD No. 20	CRBRP Training and Indoctrination
	PMD No. 27	CRBRP Document Status System
	EMP 3-1	Engineering Documentation Process
	CMP 2.126	Case File Documentation
	QAOP N1.00	Preface to Quality Assurance Manual
	QAOP N1.01	Quality Assurance Department Functions
	QAOP N1.03	Vision Requirements for Quality Assurance Personnel
	QAOP N1.21	Quality Assurance Plans
	QAOP N1.23	Quality Status Reports
	QAOP N6.02	Qualification and Certification of Nondestructive Examination Personnel
	CS3M2.4	
	QAOP N7.02	Qualification and Certification of Visual and Dimensional Inspection Personnel
	QAOP N8.00	Statistical Quality Control Program
	QAOP N13.02	Quality Assurance Data Packages
	CS3M2.3	Training

Figure 17J-4. Quality Assurance Procedure Index vs Requirements of 10 CFR 50, Appendix B (Sheet 1 of 13)

Appendix B Criterion	ESG Implementing Document or Procedure	
	Number	Title
II. Quality Assurance Program (cont'd)	CS3M17	Quality Assurance Records
	PMD-13	CRBRP Licensing Administrator
III. Design Control	SOP M-10	Program Management
	SOP N-14	Configuration Summary Reports
	PMD No. 1	CRBRP Correspondence Control
	PMD No. 11	CRBRP Document Hold Status System
	PMD No. 15	Schedule Development and Control
	PMD No. 19	CRBRP SDD Preparation and Revision
	PMD No. 21	CRBRP Development Activities
	PMD No. 25	CRBRP Parts Standardization
	PMD No. 26	Use of Controlled Information Data Transmittal (CINDT)
	PMD No. 27	CRBRP Document Status System
	PMD No. 30	CRBRP Specifications
	PMD No. 32	CRBRP Design Reviews and Release
	PMD No. 34	Application of Additions to ASME Code Requirements
	PMD No. 36	Engineering Drawings
	PMD No. 40	Materials and Processes for CRBRP
	PMD No. 41	Baselining of Documents
	PMD No. 54	SHRS Reliability Program
	EMP 1-0	Preface to Engineering Management Procedures Manual
	EMP 2-8	Engineering Studies
	EMP 2-9	Design and Acceptance Criteria
	EMP 3-3	Limited Release System
	EMP 3-5	Standard Release System
	EMP 3-42	Engineering Management System for Specifications

Figure 17J-4. Quality Assurance Procedure Index vs Requirements of 10 CFR 50, Appendix B (Sheet 2 of 13)

AMENDMENT 56

LIST OF RESPONSES TO NRC QUESTIONS

There are no new NRC Questions in Amendment 56.